

**Proceedings of the 33rd Annual Meeting of
THE SOCIETY OF NUCLEAR MEDICINE
June 22–25, 1986 • Washington, D.C.**

The SNM 33rd Annual Meeting

Proceedings of the 33rd Annual Meeting of THE SOCIETY OF NUCLEAR MEDICINE June 22-25, 1986 • Washington, D.C.

1986 SCIENTIFIC PROGRAM COMMITTEE

Philip O. Alderson, M.D.
Scientific Program Chairman
Stephen L. Bacharach, Ph.D.
Vice Chairman
Daniel S. Berman, M.D.
Vice Chairman
R. Edward Coleman, M.D.
Vice Chairman
Edward A. Deutsch, Ph.D.
Vice Chairman
Robert J. English, CNMT
Subchairman
Alan Maurer, M.D.
*Scientific Exhibits
Subcommittee*
Paul H. Murphy, Ph.D.
Chairman Elect
C. Leon Partain, M.D., Ph.D.
Associate Chairman
Richard C. Reba, M.D.
General Program Chairman
Henry N. Wellman, M.D.
Vice Chairman

Ralph G. Robinson, M.D.
Heinrich R. Schelbert, M.D.
George N. Sfakianakis, M.D.
Aslam R. Siddiqui, M.D.
Suresh C. Srivastava, Ph.D.
Maria G. Straatmann, M.D.
Andrew Taylor, M.D.
Wynn A. Volkert, Ph.D.
Lynn R. Witherspoon, M.D.

REVIEWERS

Robert H. Ackerman, M.D.
Robert Akada, M.D.
Ajmod Ali, M.D.
William L. Ashburn, M.D.
Lew Becker, M.D.
George Beller, M.D.
Anthony R. Benedetto, Ph.D.
Harvey J. Berger, M.D.
Daniel S. Berman, M.D.
Hans J. Biersack, M.D.
M. W. Billinghamurst, Ph.D.
Elias Botvinik, M.D.
Charles Boucher, M.D.
Manuel L. Brown, M.D.

Robert W. Burt, M.D.
Ronald J. Callahan, Ph.D.
Jorge A. Carrasquillo, M.D.
Tuhin K. Chaudhuri, M.D.
John Clorius, M.D.
R. Edward Coleman, M.D.
David Collier, M.D.
Gary R. Conrad, M.D.
James J. Conway, M.D.
Barbara Y. Croft, Ph.D.
Frederick L. Datz, M.D.
Alan Davison, M.D.
Gerald L. DeNardo, M.D.
Jon J. Erickson, Ph.D.
Darlene M. Fink-Bennett,
M.D.
Keith Fox, M.D., Ch.B.
Robert P. Friedland, M.D.
J. James Frost, M.D., Ph.D.
Brian M. Gallagher, Ph.D.
Michael M. Graham, M.D.,
Ph.D.
Samuel E. Halpern, M.D.
Randall A. Hawkins, M.D.,
Ph.D.
Robert E. Henry, M.D.
Donald J. Hnatowich, Ph.D.

SUBCHAIRMEN

Abass Alavi, M.D.
A. Bertrand Brill, M.D.
Manuel B. Brown, M.D.
Robert Burt, M.D.
Henry M. Chilton, Pharm.D.
Gary R. Conrad, M.D.
Robert J. English, CNMT
Michael L. Goris, M.D., Ph.D.
Robert E. Henry, M.D.
William D. Kaplan, M.D.
Jonathan M. Links, Ph.D.
Jamshid Maddahi, M.D.

Contents

Matrix Schedule	874
Scientific Papers	876
Poster Sessions	986
Author Index	1056
Works-in-Progress	1067
Categorical Seminars	1078
Continuing Education	1081
Scientific Exhibits	1090

REVIEWERS *(continued)*

Edward J. Hoffman, Ph.D.
Lawrence E. Holder, M.D.
B. Leonard Holman, M.D.
Abdulmassih Iskandrian, M.D.
Ronald J. Jaszczak, Ph.D.
Robert H. Jones, M.D.
Avir Kagan, M.D.
John A. Katzenellenbogen, Ph.D.
Andrew Keenan, M.D.
Michael R. Kilbourn, Ph.D.
Michael A. King, Ph.D.
G.T. Krishnamurthy, M.D.
Kenneth A. Krohn, Ph.D.
Steven M. Larson, M.D.
James L. Lear, M.D.
Jeffrey Leppo, M.D.
Thomas K. Lewellen, Ph.D.
Merle K. Loken, M.D., Ph.D.
Gerd Muehlehner, Ph.D.
Massoud Majd, M.D.
Chester Mathis, Ph.D.
Leonard F. Mausner, Ph.D.
Linda Monroe, Ph.D.
John C. Mazziotta, M.D., Ph.D.
David McCarthy, M.D.
I. Ross McDougal, M.B., C.Ch.,
Ph.D.
Ismael Mena, M.D.
Kenneth Mido, M.D.
Harold Neely, M.D.
William O'Connell, M.D.
Chang H. Paik, Ph.D.
James A. Patton, Ph.D.
Dan G. Pavel, M.D.
Bertram Pitt, M.D.
James A. Ponto, M.S.
Steven Port, M.D.
David F. Preston, M.D.
Marcus E. Raichle, M.D.
Charles D. Russell, M.D.
Thomas R. Ruth, Ph.D.
Ung Yun Ryo, M.D., Ph.D.
Donald S. Schauwecker, M.D.,
Ph.D.
Carl Christian Schumichen, M.D.
Markus Schwaiger, M.D.
Andrew Selwyn, M.D.
Michael Shea, M.D.
Richard Shore, M.D.
Theodore R. Simon, M.D.
H. William Strauss, M.D.
Gopal Subramanian, Ph.D.
Andrew Taylor, Jr., M.D.

Mathew L. Thakur, Ph.D.
F. Deaver Thomas, M.D.
David E. Troutner, Ph.D.
Frans J. Wackers, M.D.
Heinz Wahner, M.D.
Denny D. Watson, Ph.D.
Alan D. Waxman, M.D.
Milo M. Weber, M.D.
Donald M. Wieland, Ph.D.
D. Scott Wilbur, Ph.D.
Gary G. Winzelberg, M.D.
Gerald Wisenberg, M.D.
Richard L. Witcofski, Ph.D.
Michal R. Zalutsky, Ph.D.

CATEGORICAL SEMINARS

William D. Kaplan, M.D.,
Chairman
Harvey J. Berger, M.D.
Alan Fritzberg, Ph.D.
Alan D. Waxman, M.D.

CE & COURSE APPROVAL SUBCOMMITTEE

William B. Kaplan, M.D.
C. Leon Partain, M.D., Ph.D.
Shankar Vallabhajosula, Ph.D.

CONTINUING EDUCATION COURSES

Harvey J. Berger, M.D.
William C. Eckelman, Ph.D.
L. Stephen Graham, Ph.D.
C. Leon Partain, M.D., Ph.D.,
Chairman

TECHNICAL EXHIBITS COMMITTEE

Thomas Anderson
Jessica Bede
Millard N. Croll, M.D.,
Chairman
Robert J. English, C.N.M.T.

Louis A. Perez, M.D.
Linda Pilgrim
Henry Prolog

1986 SCIENTIFIC EXHIBITS SUBCOMMITTEE

Gerald S. Johnston, M.D.
Robert D. Katz, M.D.
Alan H. Maurer, M.D.
Louis A. Perez, M.D.
Joseph J. Sanger, M.D.

1986 SCIENTIFIC EXHIBIT JUDGES

E. William Allen, M.D.
Russell C. Briggs, M.D.
Keith E. Britton, M.D.
John H. Clorius, M.D.
James J. Conway, M.D.
Homai DaCosta, M.D.
Ferruccio Fazio, M.D.
David L. Gilday, M.D.
David A. Goodwin, M.D.
Allan M. Green, M.D., Ph.D.
Shelley D. Hartnett, C.N.M.T.
Nilo E. Herrera, M.D.
Thomas C. Hill, M.D.
Schuyler V. Hiltz, M.D.
Gustav Hor, M.D.
Masahiro Iio, M.D.
Ervin Kaplan, M.D.
Ismael Mena, M.D.
Troels Munkner, M.D., Ph.D.
I.P.C. Murray, M.D.
Peter Paras, Ph.D.
Dan G. Pavel, M.D.
Peter Pfannenstil, M.D.
Malcolm R. Powell, M.D.
Dorothy Duffy Price, C.N.M.T.
Claude E. Raynaud, M.D.
Rex B. Schaefer, M.D.
Heinrich R. Schelbert, M.D.
George Sfakianakis, M.D.
Jon D. Shoop, M.D.
James E. Smith, Ph.D.
Robert C. Stadalnik, M.D.
Charles D. Teates, M.D.
Eduardo F. Touya, M.D.
David A. Turner, M.D.
Lawrence E. Williams, Ph.D.
Shin-Hwa Yeh, M.D.

The Society of Nuclear Medicine 33rd ANNUAL MEETING

Saturday, June 21 through Wednesday, June 25, 1986
WASHINGTON CONVENTION CENTER, WASHINGTON, DC

8:00-3:30/ROOM 40

SEMINAR I: CARDIOVASCULAR NUCLEAR MEDICINE 1986 Sponsored by the Cardiovascular Council. This seminar is a review of the current state of development in cardiovascular nuclear medicine.

- New Tc-99m perfusion tracers
- Dipyridamol stress imaging
- Progress in coronary artery disease
- Exercise left ventricular functions imaging methods
- Tl-201 SPECT
- Artificial intelligence
- Thrombolysis
- Intra-cardial scintigraphy

Admission is by ticket only. Pre-register on registration form before May 1, 1986. Early fee is \$50. Fee is \$70 if postmarked after May 1, 1986.

8:00-3:30/ROOM 39

SEMINAR II: NUCLEAR MEDICINE THE NEXT FIVE YEARS Sponsored by the SNM Correlative Imaging Council. This seminar is a review of the current state of the art and promising developments which may impact their clinical practice through 1990.

- Radiopharmaceuticals
- Brain imaging with single photon agents
- Positron tomography
- Monoclonal antibodies
- Clinical imaging
- Therapy
- Magnetic resonance
- Computers
- Instrumentation

Admission is by ticket only. Pre-register on registration form before May 1, 1986. Early fee is \$50. Fee is \$70 if postmarked after May 1, 1986.

8:10-4:30/ROOM 38

SEMINAR III: THE CHEMISTRY OF RADIOPHARMACEUTICALS: METHODS AND STRATEGIES FOR CHARACTERIZATION Sponsored by the Radiochemical Society. The objective of the seminar is to present the chemical state of radiopharmaceuticals *in vivo*, metabolism, tissue binding at the molecular level, and methodology of characterization.

- Brain perfusion agent
- Uptake of cations by the heart
- Organic cations
- Tc-99m cations
- Liver metabolism and binding
- Disposition and analogs
- Labeled fatty metabolism
- Abnormal metabolism

Admission is by ticket only. Pre-register on registration form before May 1, 1986. Early fee is \$50. Fee is \$70 if postmarked after May 1, 1986.

9:00-3:00/ROOM 35

SEMINAR IV: CURRENT ISSUES IN NUCLEAR MEDICINE A seminar on Marketing Nuclear Medicine Sponsored by the American College of Nuclear Physicians

Marketing Topics:

- The Importance of Marketing
- Identifying Market Segments
- Describing Your Product
- Marketing to the Referring Physician
- Marketing Strategies That Work
- Cost Analysis

Low-Level Waste Topics:

- The Low Level Waste Policy Act
- Amendments of 1985
- Alternative Approaches to an Approach
- Alternative Technologies

Admission is by ticket only. Pre-register on registration form before May 1, 1986. Early fee is \$50. Fee is \$70 if postmarked after May 1, 1986.

9:00-4:30/ROOM 36

SYMPOSIUM for the Referring Physician: Images for the Internist and the Surgeon

- How Nuclear Medicine Compares to X-ray, CT, NMR, Ultrasound
- How to Order
- What Works Better
- What's Cost-Effective
- How to Use the Information

Fee is \$15 (includes lunch)

5:30 to 7:30 Don't miss the Ice Cream Social Welcome Reception (and cash bar), sponsored in part by Mallinckrodt, Inc.—Diagnostic Products Division, at the J.W. MARRIOTT BALLROOM.

JUNE 22, 1986 EXHIBIT HALL, POSTERS, AND SCIENTIFIC EXHIBITS OPEN 10:00-6:00 TODAY *

8:45 to 10:00	FORMAL OPENING AND PLENARY SESSION/ ROOMS 38-40	followed by the GRAND OPENING OF THE EXPOSITION WHERE ALL MAJOR COMPANIES ARE REPRESENTED/HALL B1/P 87	
10:00 to 10:30	Coffee break sponsored by Konica Medical Corporation/EXHIBIT HALL		
10:30 to 12:00	ENDOCRINE Evaluation Using RIA & Multiple Imaging Modalities CE/ROOM 38/PG 38	SPECT vs PET vs MRI Relative Roles, Cost & Capability CE/ROOM 40/PG 38	NUCLEAR MEDICINE REVIEW COURSE ROOM 29/PG 60
12:00 to 1:30	Visit the Exhibits and have lunch/EXHIBIT HALL		
1:30 to 3:00	SOCIETAL Considerations in Nuclear Medicine CE/ROOM 31/PG 41	CARDIOVASCULAR I New Radiopharmaceuticals SP/ROOM 40/PG 69	ENDOCRINE I SP/ROOM 27/PG 75
3:00 to 5:00	NEUROLOGY II SPECT SP/ROOM 39/PG 76	ONCOLOGY II PET and Central Nervous System Metabolism SP/ROOM 38/PG 78	NUCLEAR MEDICINE REVIEW COURSE ROOM 29/PG 60
5:00 to 6:00	Presentation of Awards, SNM Business Meeting and Wine & Cheese Reception/ROOM 40/PG 42		
6:00	COMPUTERS FOR THE COMPUTER-SHY WORKSHOP (Sponsored by the SNM Computer Council) Please pre-register on the registration form. A \$5 fee is required. Buses leave from the Convention Center/Location to be announced /PG 42		

*Note: 10:30 to 12:00 FUNCTIONAL BRAIN IMAGING, New Radiopharmaceuticals ROOM 33

SATURDAY

SUNDAY

MONDAY

TUESDAY

WEDNESDAY

JUNE 23, 1986/EXHIBIT HALL OPEN 10:00-6:00 TODAY/POSTERS AND SCIENTIFIC EXHIBITS OPEN 8:00-6:00

8:30 to 10:00	CONSIDERATION OF IMAGING MODALITIES TO EVALUATE MYOCARDIAL ISCHEMIA DURING STRESS: The Potential Impact of Exercise Echnocardiography CE/ROOM 40/PG 43	ACCEPTANCE TESTING AND QUALITY CONTROL OF CAMERAS (including SPEC1) CE/ROOM 30/PG 45	KINETICS WITH SINGLE PHOTON EMITTING RADIOTRACERS I CE/ROOM 31/PG 45	DOSIMETRY SP/ROOM 27/PG 85
10:00 to 10:30	COFFEE BREAK sponsored by Mallinckrodt, Inc./Diagnostic Products Division/EXHIBIT HALL			
10:30 to 12:00	PEDIATRIC NUCLEAR MEDICINE UPDATE SP/ROOM 33/PG 46	CARDIOWASCULAR III SPECT Tl-201 SP/ROOM 40/PG 86	NEUROLOGY (II) RET Clinical (Part 1) P 900 SP/ROOM 30/PG 87	ONCOLOGY (III) Monoclonal Antibodies Routes of Administration and Therapy SP/ROOM 38/PG 88
12:00 to 1:30	VISIT EXHIBITS and have lunch/EXHIBIT HALL			
1:30 to 3:00	IN-VIVO APPLICATIONS OF MULTI-NUCLEAR NMR SPECTROSCOPY IMAGING CE/ROOM 32/PG 47	CARDIOWASCULAR IV Monoclonal Antibodies SP/ROOM 39/PG 93	CARDIOWASCULAR V Ventricular Function (Part 1) SP/ROOM 38/PG 94	NEUROLOGY IV Cerebral Blood Flow SP/ROOM 40/PG 96
3:30 to 5:00	POSTER SESSION All authors will be present in the Exhibit Hall to answer questions on their posterboard presentations SP/3:30-6:00 PM/PG 151	NEUROLOGY V PET Clinical (Part 2) SP/ROOM 39/PG 101	ONCOLOGY IV Monoclonal Antibodies: Metabolism Kinetics and Reactivity SP/ROOM 38/PG 102	PULMONARY I GASTROENTEROLOGY IV Hepatic Studies SP/ROOM 33 /PG 103
5:00 to 6:00	POSTER SESSION All authors will be present in the Exhibit Hall to answer questions on their posterboard presentations SP/3:30-6:00 PM/PG 151	NEUROLOGY VI PET Clinical (Part 2) SP/ROOM 39/PG 101	ONCOLOGY IV Monoclonal Antibodies: Metabolism Kinetics and Reactivity SP/ROOM 38/PG 102	PULMONARY I GASTROENTEROLOGY IV Hepatic Studies SP/ROOM 33 /PG 103

JUNE 24, 1986/EXHIBIT HALL OPEN 10:00-6:00 TODAY/POSTERS AND SCIENTIFIC EXHIBITS OPEN 8:00-6:00

8:30 to 10:00	STRATEGIES FOR A SUCCESSFUL NUCLEAR MEDICINE PRACTICE: Viewpoint of Clinical Practice CE/ROOM 40/PG 49	NEW CARDIOWASCULAR TRACERS & TECHNIQUES ON THE HORIZON CE/ROOM 39/PG 50	BONE DENSITOMETRY INSTRUMENTATION CE/ROOM 38/PG 51	SIMULTANEOUS IMAGING Measurements of Blood Flow and Receptor Concentration CE/ROOM 31/PG 52	INSTRUMENTATION I SPECT Collimation SP/ROOM 30/PG 110	PEDIATRICS II SP/ROOM 33/PG 110
10:30 to 12:00	FEDERAL REGULATORY Aspects Regarding the Use of Investigational Radiopharmaceuticals CE/ROOM 40/PG 53	CARDIOWASCULAR VII: Myocardial Metabolism SP/ROOM 39/PG 111	NEUROLOGY VII: Ventricular Function (Part 2) SP/ROOM 38/PG 113	CARDIOWASCULAR X Receptors & Biochemical Markers SP/ROOM 36/PG 123	COMPUTERS & DATA ANALYSIS V ECT Modeling SP/ROOM 30/PG 117	IMMUNOLOGY/ Infectious Disease SP/ROOM 27/PG 118
12:00 to 1:30	LUNCH/Visit the Exhibits/EXHIBIT HALL.					NUCLEAR MEDICINE REVIEW COURSE ROOM 29/PG 60
1:30 to 3:00	PET and SPECT: What are the things that will make a difference? CE/ROOM 40/PG 53	CARDIOWASCULAR IX Dipyridamoles Tl-201 SP/ROOM 31/PG 119	NEUROLOGY VIII: Data Analysis SP/ROOM 39/PG 120	ONCOLOGY V: MIBG, Bone, & Prostate SP/ROOM 32/PG 122	PULMONARY II BONE/Joint III SP/ROOM 30 /PG 124	NUCLEAR MEDICINE REVIEW COURSE ROOM 29/PG 60
3:30 to 5:00	STRATEGIES FOR A SUCCESSFUL NUCLEAR MEDICINE PRACTICE: The Customer's Perspective CE/ROOM 38/PG 55	CARDIOWASCULAR XI Planar Tl-201 SP/ROOM 40/PG 126	NEUROLOGY VIII: Modeling SP/ROOM 39/PG 127	GASTROENTEROLOGY VI: General Antibodies SP/ROOM 32/PG 129	RENAU/ELECTROLYTE/HYPERTENSION II SP/ROOM 33/PG 132	NUCLEAR MEDICINE REVIEW COURSE ROOM 29/PG 60
7:30 to 11:00	TECHNOLOGIST PARTY/Washington Hilton, 1915 Connecticut Avenue, N.W./Sponsored by all exhibitors/Buses depart all SNM hotels at 7:30 pm/Last bus returns at 11:30 pm /PG 24					ENDOCRINE III SP/ROOM 27

JUNE 25, 1986/EXHIBIT HALL OPEN 8:30-12:30/POSTERS AND SCIENTIFIC EXHIBITS OPEN SAME HOURS

8:30 to 10:00	RADIONUCLIDE FUNCTIONAL BRAIN IMAGING CE/ROOM 39/PG 56	CLINICAL APPLICATIONS OF BONE MINERAL Estimation by Single and Dual Photon Absorptiometry CE/ROOM 40/PG 57	KINETICS WITH POSITRON EMITTING RADIOTRACERS CE/ROOM 38/PG 58	HEMATOLOGY II Clinical SP/ROOM 27/PG 135
10:30 to 12:00	NUCLEAR MEDICINE MILESTONES-William G. Myers, Ph. D. M. D. ROOM 13/PG 59	CARDIOWASCULAR XII Acute Myocardial Infarction Tracer Kinetics SP/ROOM 38/PG 137	RADIOPHARMACEUTICAL CHEMISTRY VI Halogens SP/ROOM 31/PG 140	PERIPHERAL VASCULAR PET Technique P 913 SP/ROOM 30/PG 141
12:00 to 1:30	EXHIBITS CLOSE AT 12:30 TODAY. Lunch on the first level of the Washington Convention Center. Coat and baggage check available near the registration area all day today.			
1:30 to 3:00	CARDIOWASCULAR XIV PET Myocardial Perfusion SP/ROOM 40/PG 143	BONE/Joint IV Osteomyelitis SP/ROOM 39/PG 144	COMPUTERS & DATA ANALYSIS V ECT Modeling & Dynamics SP/ROOM 38/PG 145	RADIOPHARMACEUTICAL CHEMISTRY VII Positrons SP/ROOM 31/PG 147
3:00 to 4:30	SCIENTIFIC MEETING HIGHLIGHTS Henry N. Wagner, Jr., M. D. ROOM 40/PG 59	BONE/Joint V Osteomyelitis SP/ROOM 39/PG 144	DOSIMETRY: RADIOBIOLOGY SP/ROOM 30/PG 145	RENAU/ELECTROLYTES/HYPERTENSION III SP/ROOM 33/PG 148
				CARDIOWASCULAR XV Cardiac NMR SP/ROOM 27/PG 149
				NUCLEAR MEDICINE REVIEW COURSE ROOM 29/PG 60

SUNDAY, JUNE 22, 1986

FORMAL OPENING AND PLENARY

8:45-10:00 a.m. **Rooms 39 & 40**
Hall C is located on the second level of the Washington Convention Center.

- 8:45 Remarks. Stanley J. Goldsmith, M.D., President, The Society of Nuclear Medicine
Remarks. James J. Wirrell, CNMT, President, Technologist Section
Remarks. Philip O. Alderson, M.D., Chairman, Scientific Program Committee 1986
- 9:00 The Seventh Annual Georg Charles de Hevesy Nuclear Medicine Pioneer Award Presentation Honoring Rosalyn Yalow, Ph.D.
Solomon A. Berson Memorial Lab, Veterans Administration Hospital, Bronx, NY
Presenters. Stanley J. Goldsmith, M.D., Mount Sinai Medical Center, New York, NY, and William G. Myers, Ph.D., M.D., Ohio State University, Columbus, OH
- 9:15 The Third Annual SNM Lectureship
Images of the Brain: Past as Prologue, Henry N. Wagner, Jr., M.D., Johns Hopkins Medical Institutions, Baltimore, MD
- 10:00 Opening of the 1986 SNM Exposition in Hall B.

SUNDAY, JUNE 22, 1986

10:30-12:00 **Room 32**

GASTROENTEROLOGY I: GENERAL

Moderator: Ralph G. Robinson, MD
Comoderator: Tuhin K. Chaudhuri, MD

No. 1

GASTROINTESTINAL ULCERATION: DETECTION UTILIZING Tc-99m-HSA-SUCRALFATE AND POTASSIUM SUCROSE SULFATE (PSS). T.E. Vasquez, D.G. Evans, M.T. Hartman, P.L. Hagan and W.L. Ashburn. University of California Medical Center, San Diego, CA

The property of Sucralfate to selectively bind to ulcerated mucosa coupled with a gamma emitting isotope resulted in a new method of detecting gastrointestinal ulcerations: Tagged Ulcer-avid Material Imaging (TUMI).

The prolonged T- $\frac{1}{2}$ clearance of the radiolabeled Sucralfate allows unbound material to remain in the stomach, particularly the fundus, complicating the imaging of peptic ulcers. In order to solve this difficulty, we have radiolabeled a precursor of Sucralfate: sucrose sulfate. PSS (C12 H14 O35 S8 K8) is a small, water soluble, molecular weight compound with 8 sulfate groups and a protein interaction similar to Sucralfate.

TUMI scans utilizing Tc-99m-PSS were performed on six patients. Three patients had ulcer disease (duoden-

al, gastric, and pyloric channel) demonstrated by endoscopy. One patient's 2 mm duodenal ulcer was not visualized utilizing radiolabeled PSS. The gastric ulcer patient had an increased focal accumulation of PSS in the region of the known ulcer beginning at 15 minutes and lasting until 75 minutes post-ingestion. The pyloric channel ulcer patient had four ulcers measuring approximately 0.4 x 0.5 cm in a tight group near the pylorus. There was an increased focal accumulation of radiopharmaceutical in the region of the pylorus beginning at 5 minutes. Results were entirely negative in three healthy control cases.

No. 2

RELAXATION OF ACHALASIAIC ESOPHAGUS DUE TO FORCEFUL SWALLOWS WITH LIQUIDS - A NEW DIAGNOSTIC PROCEDURE. K. Gratz, H. Creutzig, E. Schalber, and H. Hundeshagen.
Medical School, Hannover, FRG

It is reported from patients with esophageal motor disorders and severe dysphagia that they help themselves by drinking a lot of liquids. The purpose of the study was to investigate the effect of such a maneuver by radionuclide transit studies (RTS).

51 patients with achalasia were entered into the study. Some patients were investigated before and after treatment. RTS was done in supine position with 15 ml Tc-99m-DTPA. No or minimal esophageal transit was detected after 25 dry swallows (every 15 s) in 34 of 58 examinations (59%). The patients drank through a blade of straw 150 ml water without changing the position. No change in esophageal transit occurred in 12 (35%), little change in 3 (9%) and a significant transit in 19 (56%) studies.

It is concluded that failure in lower esophageal sphincter (LES) relaxation in patients with achalasia is partial and that forceful swallowing with a greater volume of fluid is able to provoke relaxation. Total or partial failure of LES relaxation to swallowing is diagnostic for achalasia. The swallow effect must be excluded in studies testing drug interventions (i.e. glucagon).

No. 3

DYNAMIC RADIONUCLIDE SCINTIGRAPHY IN THE EVALUATION OF PNEUMATIC DILATATION TREATMENT OF ACHALASIA. G.W. Moskowitz, R.G. Schiff, M. Levine, B. Dorf, and S. Bank.
Long Island Jewish Medical Center, New Hyde Park, NY 11042

Sixteen patients with documented primary achalasia associated with marked esophageal obstruction were evaluated before and after pneumatic dilatation of the lower esophageal sphincter (LES). Each patient was studied with dynamic scintiphotos while swallowing liquid Tc-99m pertechnetate. Images of 5 seconds each were obtained for 20 frames of 64 x 64 pixels. Subsequent static images were obtained for 60 minutes. In contrast to other esophageal problems, patients with achalasia have as much difficulty with liquids as with solids.

Each of these patients had objective and quantitative delay in esophageal emptying by scintigraphic evaluation. These patients showed marked flattening of the time activity curves. Following the scintigraphic evaluation, each patient was subjected to esophageal dilatation using a 90-105 F balloon placed across the LES.

The success of the pneumatic dilatation was evaluated by comparing the pre- and post-dilatation radionuclide studies. In all pre-op cases, the scintigraphic studies showed qualitative and quantitative hold-up of passage of liquid radionuclide at the LES. The postoperative studies

demonstrated marked improvement of transit of Tc-99m across the LES. The scintigraphic studies did not reveal any perforations resulting from the procedure. Follow-up evaluations up to 1 year after the dilatation have shown sustained benefit from the procedure and none required redilatation or surgery. Radionuclide scintigraphy has been extremely useful in the assessment of the degree of obstruction in achalasia and the information correlated well with the clinical picture.

No. 4

A SCINTIGRAPHIC EVALUATION OF COLONIC TRANSIT IN NORMAL SUBJECTS: THE PROKINETIC EFFECTS OF CISAPRIDE. V. Caride, J. Petersen, E. Prokoff, R.W. McCallum, Depts. Medicine and Nuclear Medicine, and Hospital of St. Raphael, New Haven, CT, and Univ. Virginia, Charlottesville, VA.

Our purpose was to investigate the effect of Cisapride (C) on colonic transit in normal subjects utilizing a radionuclide method and a randomized double-blind study design. After a 12-hr fast and on 2 separate days normal subjects received C 10mg orally or placebo, and 10 minutes later a 100cc isotonic solution of the non-absorbable agent lactulose labeled with 500 microcuries of 99mTcDTPA. They had a standard breakfast and lay supine under a large field of view gamma camera. After 3 hrs they took another dose of C 10 mg or placebo, ate a standardized lunch and gamma counts were again continuously monitored. The total study time was up to 8 hrs. Regions of interest were selected over the cecum, transverse colon (TRANS), splenic flexure (SPLENIC), descending (DESC) and sigmoid (SIGM) colon and the rectum. Table 1 shows time of appearance in each segment.

Table 1. ORAL-COLONIC TRANSIT (min)

	Cecum	TRANS	SPLENIC	DESC.	SIGM.	Rectum
Placebo	77±19	94±12	234±134	190±92	255	255
Cisapride	65±23	108±37	146±77	159±71	150±46	186±86

Table 2. DISTRIBUTION OF COLONIC ACTIVITY AT 480 MIN.

	Cecum	TRANS	DESC	RECTO-SIGM
Placebo	53.8%	31.6%	3.8±4	0.8±2
Cisapride	31.3±20%	27.1±20%	17.6±6%	16.7±17%

4.6% isotope reached the left colon after placebo compared to 34.3% after C (p<0.05). We conclude that: 1) a noninvasive assessment of colonic transit can be achieved with a non-absorbable radiotracer, and 2) C significantly enhances colonic transit in normal subjects.

No. 5

CISAPRIDE ACCELERATES GASTRIC EMPTYING OF SOLID AND LIQUID MEAL COMPONENTS IN PATIENTS WITH GASTRIC STASIS. R.W. McCallum, J.M. Petersen, R. Lange. Depts. Med. and Nuclear Medicine, University of Virginia, Charlottesville, VA and Yale University, New Haven, CT.

Cisapride (C), a benzamide derivative, is a new prokinetic agent whose mechanism of action is thought to be through facilitation of acetylcholine release from the myenteric plexus. Our purpose was to investigate the effects of acute IV C on gastric emptying (GE) in patients with subjective and objective evidence of non-obstructive gastric stasis. 22 patients, 14 females and 8 males, mean age 41 yrs (range 20-62), with symptoms of gastric stasis attributed to diabetic neuropathy (N=8), idiopathic (N=7) and post-gastric surgery (N=7) underwent a GE study basally (B) and on a separate day 5 min after receiving 10mg IV C. The solid (S) component of the meal was chicken liver labeled in vivo with 99mTc-sulfur-colloid and mixed with beef stew. The liquid (L) was 4 oz water labeled with 111In-DTPA. GE was monitored for 2 hrs while patients lay supine under a gamma camera and results are below (* indicates p<0.05 after C versus baseline GE).

	30 min		60 min		90 min		120 min	
	B	C	B	C	B	C	B	C
% Isotope Retained	S 91.5	84.0	88.0	70.6*	86.0	63.4*	83.4*	54.7*
in Stomach	L 72.9	58.3*	61.8	34.3*	56.9	22.6*	52.9	15.4*

In 50% of patients the GE rate was actually returned to

normal. No side effects were noted. In summary: C significantly accelerated GE of solids and liquids in patients with gastric stasis associated with different etiologies. We conclude that C is a promising new gastric prokinetic agent and well controlled trials to establish its clinical efficacy are warranted.

No. 6

RESPIRATORY EFFECT IN RADIONUCLIDE ESOPHAGEAL TRANSIT TEST. H.A. Klein, T.O. Graham, and A. Wald. University of Pittsburgh School of Medicine, Pittsburgh, PA.

Tests with swallowing of aqueous Tc-99m sulfur colloid supine, analyzed by previously described methods (J Nucl Med 27: 947-964, 1984), revealed that some patients with severe esophageal motility disorders had a large esophageal residual component that underwent recurrent retrograde and antegrade motion at a frequency of about 10 cycles/min. This occurred in cases of achalasia, diffuse esophageal spasm, and systemic sclerosis. We sought to determine whether it was a passive phenomenon or the result of spasmodic contractions.

Condensed dynamic images having a spatial and a temporal dimension served to demonstrate the pattern and also provided the basis for an experiment that was applied in a case of achalasia and two of systemic sclerosis. At the completion of the routine test, imaging was continued as the patient swallowed ad lib and sequentially performed tidal breathing, breath-holding, and slow breathing. An investigator repeatedly introduced a radioactive source at the top of the imaging field to mark inspiration. The resulting images revealed that the distal and proximal excursions of the residual liquid were synchronized with inspiration and expiration, respectively.

We conclude that oscillations of this frequency generally represent a passive response to respiration rather than spasm, and that the pattern occurs in severe disease without specificity as to the type of motility disorder, but (based on our additional experience) that it is not the only pattern that may be observed.

1:30-3:00

Room 40

CARDIOVASCULAR I: NEW RADIOPHARMACEUTICALS

Moderator: Edward A. Deutsch, PhD
Comoderator: B. Leonard Holman, MD

1:30

**FEATURE PRESENTATION
Tc-99m-LABELED COMPOUNDS FOR
MYOCARDIAL IMAGING**

Edward A. Deutsch, PhD

No. 7

PHARMACOLOGY OF Tc-99m-ISONITRILES: AGENTS WITH FAVORABLE CHARACTERISTICS FOR HEART IMAGING. S.J. Williams, S.A. Mousa, R.A. Morgan, T.R. Carroll, and L.J. Maheu. E.I. DuPont de Nemours, Biomedical Products, N. Billerica, MA

Clinical studies by Holman et al. (1984) have shown Tc-99m-hexakis-t-butyl isonitrile (NEN-14) to be useful, although not ideal, for myocardial perfusion scintigraphy. Therefore, a number of structural analogs of isonitriles have been synthesized with the goal to retain the myo-

cardial specificity and rapid blood clearance of TBI but to circumvent its pharmacokinetic problems of early high lung and later high liver activity demonstrated clinically. The most promising structures which have been identified are the aliphatic (C-4 to C-5) ethers, 6 of which have been evaluated pharmacologically. Tc-99m-hexakis-2-methoxy-2-methyl propyl-1-isonitrile (NEN-30) and Tc-99m-hexakis-1-methoxypropyl-2-isonitrile (NEN-42) have the best overall characteristics. Both exhibit good heart extraction in guinea pigs (1.9 and 1.6% ID, $T_{1/2} = 4$ and 2 hours, respectively) rapid and complete blood clearance ($T_{1/2} = 1-2$ minutes), low lung activity (1.5 - 2.3% ID) and low peak liver activity (11% and 8% ID) with substantial hepatobiliary clearance ($T_{1/2}$ approximately 70 and 20 minutes, respectively). In comparison, 30-40% of TBI is extracted by the lung, initially. This activity clears with a $T_{1/2}$ of about 15 minutes and is sequestered by the liver from which there is little clearance. Imaging studies in miniature swine, monkeys, dogs and rabbits corroborate these results. In a rabbit coronary artery ligation-release model, neither agent redistributes measurably compared to TBI which shows up to 50% redistribution. Human imaging studies with NEN-30 confirm the biological characteristics predicted from animals. The potential clinical superiority of NEN-42 due to its lower peak liver activity and faster clearance kinetics is suggested.

No. 8

COMPARISON OF 3 TC99m ISONITRILES FOR DETECTION ISCHEMIC HEART DISEASE IN HUMANS. K. McKusick, Massachusetts General Hospital, B.L. Holman, A.G. Jones, Harvard Medical School, A. Davison, Massachusetts Institute Technology, Boston, MA., P. Rigo, Univ. Liege, B.V. Sporn, Hosp. Pravado "Luis Guemes", Buenos Aires, A., H. Vosberg, Univ. Dusseldorf, G., J. Moretti, Hosp. Henri Mondor, Creteil, F.

To select the Tc-isonitrile with best properties for myocardial imaging, results with Tc t-butyl isonitrile (TBI; 40 patients (P)), Tc carbomethoxyl isopropylisonitrile (CPI, 13P), and Tc methoxy methylpropyl isonitrile (MMI, 6P) were compared. For feasibility to diagnose CAD, correlative studies were done in those who had exercise induced Tl201 defects (ischemia); these were re-exercised within 1 month to same exercise level and imaged after injection of 4-10mCi Tc TBI(18P), CPI(6P), MMI(2); and again after injection at rest with same agent. Ant., 40° and 70° LAO digital data were acquired at preset timed frames. Each view was divided into 3 segments (S) and judged normal, ischemic, or scar.

Liver uptake obscured heart in 6/40 TBI, but in none of CPI or MMI P. Distribution of agents was (4+ most intense, and 0=none):

	HEART		LIVER		LUNG	
	init	lh	init	lh	init	lh
TBI	4+	4+	3+	4+	4+	1+
CPI	4+	2+	3+	2+	1+	0
MMI	4+	3+	2+	1+	0	0

TBI/Tl agreed in 125/162 S (77%); CPI/Tl agreement in 43/54 S (80%). There was complete agreement in MMI/Tl.

Ischemic heart disease was detected by all 3 agents, but because of good heart uptake and lung and liver parameters, MMI displayed highest initial contrast and has best potential.

No. 9

MYOCARDIAL IMAGING WITH Tc-99m TBI AT REST AND AFTER DIPYRIDAMOL (DPM) STRESS. R. Vikydal, R. Dudczak, R. Schmoliner, P. Angelberger, A.G. Jones*, J. Lister - James* 1st Medical Clinic, University of Vienna, Austria, and *Harvard Medical School, Boston, MA

The feasibility of Tc-99m TBI for diagnosing CAD was evaluated in 14 patients (St.p.MI/12) in comparison to Tl-201. Imaging (APEX 215M) was done 10, 60, 120, 240 and 360 minutes after injection of 5-10 mCi Tc-99m TBI in the LAO 45°, ANT and LAO 70° view. DPM (0.5mg/kg/5 min) stress (n=9) and rest (n=14) studies were done 3 days apart.

Initially high lung activity prevented an adequate interpretation of scintigrams. Images of sufficient quality could be obtained later, with highest heart / non-target ratios

at 240 min p.i. ($p < 0.025$). Myocardial TBI extraction was higher at stress than at rest. Heart activity retention was constant and not different for rest and stress studies.

RATIO at 240 min p.i.:	REST	DPM-STRESS	
heart/lung	1.76±0.42	2.05±0.34	$p < 0.01$
heart/mediastinum	2.47±0.65	2.76±0.53	$p < 0.01$
heart/liver	0.39±0.07	0.43±0.12	n.s.

In contrast to Tl-201, interpolative background correction did not improve the diagnostic information, mainly because of high liver activity. Yet, interpretation of analog images equaled the global and regional sensitivity as seen in Tl-201 studies, delineating infarcted and ischemic tissue.

We conclude: Tc-99m TBI is a reliable imaging agent for evaluation of patients with CAD. However, it has the disadvantage of prominent liver uptake, which may pose eventually problems in the interpretation of the inferior apical region, and at least one hour waiting time for lung clearance. Also stress and rest studies have to be done on separate days.

No. 10

MYOCARDIAL IMAGING WITH Tc-99m CPI: INITIAL EXPERIENCE IN THE HUMAN. V. Sporn, N. Perez-Balino, B.L. Holman, A.G. Jones, A. Davison, L. Camin, A.S. Liprandi, O. Masoli, J.F. Kronauge, J. Lister-James, A.E.A. Mitta, B.S.T. Sia, S. Campbell. Brigham and Women's Hospital, Harvard Medical School, Boston, MA, Hospital Privado "Luis Guemes, Buenos Aires, Argentina.

The hexakis(isonitrile)technetium(I) complex of the analog Tc(carbomethoxyisopropyl isonitrile) (CPI) has high myocardial uptake and rapid lung and liver clearance in most animal species, but poor myocardial uptake in the rat and mouse. To evaluate Tc-99m CPI as a myocardial imaging agent in the human, we administered this tracer in 2 normals and in 4 patients with coronary artery disease. In normals, Tc-99m CPI cleared quickly from the lungs and accumulated in the liver and heart. Planar images were of excellent technical quality with high myocardial to background ratios as early as 10 min after injection. The heart to lung activity ratio was 1.7:1, 2.2:1, and 2.0 at 10, 30 and 60 min after iv injection of 5mCi Tc-99m CPI. The liver activity peaked at 10-15 min and cleared the hepatobiliary system. Myocardial activity fell gradually with a $T_{1/2}$ of 87 minutes based on the 10-60 minute activity profile. In 4 patients with CAD, defects corresponding to those seen with Tl-201 imaging were present on planar images obtained immediately and at 1 hour after exercise and injection. In 1/4 patients redistribution had occurred by 3 hours. In all four patients normal perfusion patterns were observed one hour after reinjection of Tc-99m CPI at rest (4 hours after the initial injection). Tc-99m labeled CPI appears to have excellent physical and biological properties for use in association with myocardial imaging with exercise.

No. 11

FIRST PASS EJECTION FRACTION AND MYOCARDIAL PERFUSION WITH SINGLE INJECTION OF A Tc-99m ISONITRILE. N. Perez-Balino*, V. Sporn*, B.G. Holman, A. Sosa-Liprandi*, O. Masoli*, A. Mitta* and L.L. Camin*. Hospital L. Guemes, Buenos Aires, Argentina*, CNEA, Argentina*, Harvard Medical School, Boston, MA* and E.I. du Pont de Nemours, Biomedical Products, Billerica, MA*.

One attribute of a Tc-99m labeled myocardial agent is the possibility to measure both ventricular function and myocardial perfusion with a single injection. To assess this, 5 normal volunteers and 14 symptomatic patients were injected with 8-10 mCi Tc-99m carbomethoxy isopropyl isonitrile (Tc-CPI) at peak semi-recumbent bicycle exercise and again at rest. Thirty msec per frame first pass data, and 5 min. static anterior, 40° and 70° LAO images were obtained using an APEX computer interfaced to an Elscint LFOV gamma camera in zoom mode.

Standard Tl-201 stress tests were also done within one month, and were at the same level of exercise.

The left ventricular ejection fraction (EF) increased with exercise (69-76%) in 4/5 normals; perfusion was normal in all five including the one with an abnormal EF response, who also had a normal arteriogram. The EF increased in 4/14 patients, decreased in 6/14 patients, and remained unchanged in 4/14 patients of whom 2 had ischemia and 2 had scar on perfusion imaging. The interpretation of patient Tc-CPI perfusion studies generally correlated with the Tl studies.

The results support the concept of dual ventricular function and perfusion studies using a single Tc-99m labeled myocardial agent, and suggest that this could become the standard radionuclide stress test in the future.

1:30-3:00

Room 39

NEUROLOGY I: RECEPTOR IMAGING (Part 1)

Moderator: Michael J. Welch, PhD
Comoderator: Dean F. Wong, MD

No. 12

3-(2'-[F-18]FLUOROETHYL)SPIPERONE: TOMOGRAPHIC DOPAMINE RECEPTOR CHARACTERIZATION IN LIVING PRIMATES. J.R. Barrio, N. Satyamurthy, R.E. Keen, R.A. Hawkins, G.T. Bida, E.J. Hoffman, S.C. Huang, J.C. Mazziotto and M.E. Phelps. UCLA School of Medicine, Los Angeles, CA.

3-(2'-[F-18]Fluoroethyl)spiperone (FESP), a new positron emitting-labeled neuroleptic tracer, was synthesized in multimillicurie amounts and used for dynamic characterization of dopamine receptor binding in living primates with positron emission tomography. When non-carrier added FESP (measured specific activity >500 Ci/mmol) was administered IV to nemistrina monkeys and serial PET scans obtained, radioactivity rapidly accumulated in the striatum. The striatum (rich in dopamine receptors)/cerebellum (low dopamine receptor concentration) ratio increased linearly over time at a rate of 0.02/min. By the end of 4 hrs, the radioactivity ratio striatum/cerebellum was about 5.0. In conjunction with the tomographic studies, arterial input function and temporal sequence of radiotracer metabolism were measured in monkey plasma. Chromatographic analyses of plasma extracts showed that FESP metabolites steadily increased with time, with only 5% measured in the FESP fraction 3 hr after IV injection. Temporal activity in striata analyzed by the Patlak plot shows that results are consistent with a two-compartmental model with small efflux of tracer from tissue. Rectilinear scans for a 3 hr period also permitted evaluation of the time course of radioactivity in various organs as well as the excretion mode of the drug. These tomographic studies were preceded by ex-vivo experiments in rats followed for several F-18 half-lives. Similar striatum/cerebellum ratios were observed after a 4 hr period.

No. 13

DOPAMINE D-1 AND D-2 RECEPTORS IN THE LIVING HUMAN BRAIN STUDIED WITH THE SELECTIVE LIGANDS C-11 SCH 23390 AND C-11 RACLOPRIDE. L. Farde, S. Stone-Elander, C. Halldin and G. Sedvall. Dept of Psychiatry and Psychology, Karolinska Institute, S-104 01 Stockholm, Sweden
SCH 23390 is a compound with high affinity and selectivity for binding to dopamine-D1 receptors. PET-scan experiments with C-11 labelled SCH 23390 were performed in healthy volunteers (1). The radioactivity in the dopamine rich caudate putamen was threefold higher than in the dopamine poor cerebellum 35 min after injection. There was also more radioactivity in neocortical areas than in the

cerebellum. The conspicuous accumulation of radioactivity in the caudate putamen was similar to the accumulation of C-11 raclopride, a ligand selective for dopamine-D2 receptors (2). Experiments were also performed in a schizophrenic patient treated with sulpiride, a neuroleptic with high affinity for D2 receptors. The regional uptake of C-11 raclopride in the striatum was reduced to about 15% whereas the uptake of C-11 SCH 23390 was about the same as in the healthy volunteers. These experiments demonstrate that C-11 SCH 23390 and C-11 raclopride are useful as selective ligands for clinical PET-scan studies on central dopamine-D1 and D2 receptors in patients with neuropsychiatric disorders and to examine how pharmacological agents interfere with these receptors.

1. Sedvall, G., Farde, S. Stone-Elander & C. Halldin: Dopamine D1-receptor binding in the living human brain. In: *Biochem. Funct. Studies of D1 Dopamine*. Eds: GR. Breese & I. Creese. 1986. In press.
2. Farde, L., Hall, H., Ehrin, E. & Sedvall, G., Quantitative analysis of dopamine-D2 receptor binding in the living human brain. *Science*, 1985. In press.

No. 14

BRAIN UPTAKE OF ALKYLATED AND FLUOROALKYLATED DERIVATIVES OF SPIROPERIDOL; LIGANDS FOR STUDYING DOPAMINE RECEPTORS IN VIVO. M.J.Welch, C.J.Mathias, D.Y.Chi, J.A.Katzenellenbogen, M.R.Kilbourn, J.W.Brodack. Department of Radiology, Washington University, St. Louis, MO and Department of Chemistry, University of Illinois, Urbana, IL

There is great interest in the application of positron labeled ligands to map the dopamine receptor in vivo. To prepare the commonly used ligands, spiroperidol (SP) and N-methyl-spiroperidol, requires either a multistep low yield synthesis with fluorine-18 or else uses carbon-11 whose 20 minute half-life limits the time of a study. We have prepared a series of fluorine-18 labeled N-alkyl and N-fluoroalkyl spiroperidol derivatives (F-18-methyl-SP; F-18-N-ethyl-SP; N-2-fluoroethyl-F-18-SP; F-18-N-propyl-SP; F-18-N-3-fluoropropyl-SP; N-3-fluoropropyl-F-18-SP; N-2-fluorobutyl-F-18-SP; N-2-fluoropentyl-F-18-SP; and N-2-fluorohexyl-SP). The lipophilicity of these ligands (log octanol/water partition coefficient) varies from 2.7 to 5.5 and the initial brain uptake in rats, measured at 2 minutes, was greatest with the methyl, ethyl, and propyl derivatives. (1) The highest striatum/cerebellum values 1 hour after administration were obtained with the N-methyl, N-propyl, and N-3-fluoropropyl derivatives, while that N-2-fluoroethyl showed the greatest uptake of total activity in the brain at this time. The uptake of all these ligands in the striatum could be blocked by cold SP showing the striatal uptake to be by the dopamine receptors. This work suggests that other ligands more readily prepared than those currently in use may be substituted for in vivo studies.

No. 15

IMAGING OF MPTP-INDUCED CHANGE IN TURNOVER AND DAMAGE TO STRIATAL DOPAMINE. C.C. Chiueh and G. Firnau. Clinical Brain Imaging Section, Natl Inst of Mental Health, Bethesda, MD and Dept of Nuclear Medicine, McMaster Univ Medical Centre, Hamilton, Ontario, Canada.

1-Methyl-4-phenyl-1,2,3,6-tetrahydropyridine (MPTP) is a specific dopamine neurotoxin to the nigrostriatal system. It produces a parkinsonian syndrome in man and monkey. MPTP acutely decreases the turnover of striatal dopamine while two to three weeks later it causes an irreversible lesion of the dopaminergic system. In these studies, the MPTP-induced damage was determined either neurochemically or histologically at autopsy. In the present study, we employed a PET brain dopamine imaging procedure (Garnett et al., 1983) by using 6-¹⁸F-

L-dopa (Firnau et al., 1984) and McMaster PET scanner (Nahmias, 1984) to visualize the effect of MPTP in anesthetized rhesus monkeys.

The PET procedure was used to monitor repeatedly the changes in dopaminergic activities in an MPTP-treated monkey for 10 days. The accumulation of 6-¹⁸F-dopamine increased three days after MPTP and then declined sharply ten days later. Furthermore, we compared in tandem the ¹⁸F-PET activity in the basal ganglia measured *in vivo* with the striatal content of endogenous dopamine assayed postmortem in control, subclinical, clinical and severely affected parkinsonian monkeys. There was a linear relationship between the logarithm of the percent decrease in the content of endogenous dopamine and the decrease in specific ¹⁸F-dopamine PET activity in these parkinsonian monkeys. This preclinical trial has demonstrated that the degree of brain damage and/or turnover in living parkinsonian monkeys appears to be quantifiable by the PET imaging procedure.

No. 16

THE EFFECT OF LITHIUM ON DOPAMINE RECEPTOR BINDING OF C11-3-N-METHYLSPERONE IN THE LIVING HUMAN BRAIN. D.F. Wong, C. Ross, G. Pearson, L. O'Tuama, J. Williams E. Broussolle, G. Fanaras, J.M. Links, R.F. Dannals, H.N. Wagner, Jr. The Johns Hopkins Medical Institutions, Baltimore, MD.

Lithium is widely used in the treatment of bipolar affective disorders. In the study of dopamine receptors in depressed patients, it is maybe undesirable to risk cessation of lithium therapy. Animal studies of the effect of lithium on dopamine receptors have been inconclusive, some suggesting a decrease in receptors and others no change. Therefore, we examined the effect of lithium administration on normal volunteers, who had C11-N-methylspiperone (NMSP) PET studies of D2 dopamine receptors before and following administration of therapeutic doses of oral lithium. Each subject was maintained on a plasma level of least 0.7mEq/l of lithium for at least 1 month before the second study. In 5 of 6 subjects there was an increase in the index of the rate of binding of NMSP to the dopamine receptors in the caudate nucleus, i.e. the slope of the straight line relating the caudate/cerebellum ratio to time. The slope averaged 0.0114 + .0072/min., which represents an increase of 7-30%. In the 6th subject the slope fell 0.00016/min., a 0.24% decrease. The increase was statistically significant (p<.05) on the basis of a paired t test. Reproducibility studies in normal subjects, have shown changes of less than 5-10% in the slope.

No. 17

SERIAL [¹⁸F]-N-METHYLSPEROPERIDOL (¹⁸F-NMS) PET STUDIES MEASURE CHANGES IN ANTIPSYCHOTIC DRUG D₂ RECEPTOR OCCUPANCY IN SCHIZOPHRENICS. M. Smith, Psychiatry Dept., SUNY at Stony Brook, Stony Brook, NY; A.P. Wolf, C.-Y. Shue, J.S. Fowler, J.A.G. Russell, R. MacGregor, C. Arnett, J. Logan, Chemistry Dept., Brookhaven National Laboratory, Upton, NY; A. Wolkin, J. Rotrosen, J.D. Brodie, Psychiatry Dept., NYU Medical Center, NY

Using [¹⁸F]-N-methylspiperoperidol, a potent butyrophenone neuroleptic, and PET, we have developed a method for probing the effects of antipsychotic drugs at their presumed locus of action. Six schizophrenic subjects taking haloperidol or chlorpromazine underwent two ¹⁸F-NMS PET studies, the first 2 hours after receiving their usual dosage of antipsychotic medication and the second after a 24 hour drug-free interval. Plasma samples were obtained for therapeutic drug levels. Cerebral radioactivity distribution and plasma ¹⁸F-NMS concentration were measured for up to 5 hours from time of injection. The relative rate of dopamine receptor binding was estimated by the slope of

the basal ganglia/cerebellum activity ratio versus time. Therapeutic drug dose and plasma level were highly correlated with this measure. The 24 hour therapeutic drug withdrawal resulted in a significant increase of tracer uptake in the basal ganglia reflecting appreciable clearance of the antipsychotic drug from the D-2 receptor. This is the first report of a PET method which measures the effect of alterations in antipsychotic drug plasma level on central D-2 receptor blockade. A further evaluation of the clinical management of schizophrenia relative to therapeutic drug dosage and dosing interval is now feasible. Research supported by DOE, OHER, and NIH Grant NS-15638.

1:30-3:00

Room 38

ONCOLOGY I: MONOCLONAL ANTIBODIES, CLINICAL

Moderator: William D. Kaplan, MD
Comoderator: Jorge A. Carrasquillo, MD

No. 18

RESULTS OF RADIOIMMUNOSCINTIGRAPHY USING ECT COMPARED TO TCT IN PATIENTS WITH LOCAL RECURRENCIES OF COLORECTAL CANCER. K. Scheidhauer, H. Dennecke, E. Moser, L. Schmid and G. Wehmeyer. Depts. of Radiology and Surgery, Klinikum Grosshadern, Tumorzentrum, Univ. of Munich, Munich, FRG

62 patients (pts) with colorectal cancer (CRC) were investigated by radioimmunoscintigraphy (RIS). 20 out of these 62 pts had a history of CRC with suspicion of local recurrence (LC). Tumor markers (CEA and/or CA 19-9) were elevated. After second-look surgery (within 4 months), 15/20 pts had a histologically proven LC, the remainder: 1 ovarian cyst, 2 granulomatous necrosis and 2 unspecific tissue alterations. RIS was performed using radioiodinated F(ab')₂-fragments of different monoclonal antibodies: a) anti-CEA, b) anti-CA 19-9, c) cocktail of a) and b). 0.5 - 2 mg proteine labelled with 55 - 125 MBq I-131 were injected intravenously without any side effects. All pts were examined by X-ray CT (TCT) and RIS applying ECT (RIS-ECT). RIS-ECT was performed twice, 3 - 7 days p.i., using a rotating gamma camera with a 1/2 inch crystal. For anatomical landmarking, a second study with Tc-99m sulfur colloid or Tc-99m DTPA followed the RIS without moving the patient. TCT and RIS-ECT were evaluated by 2 unbiased observers.

	true pos.	true neg.	false pos.	false neg.
RIS-ECT	14	0	5	1
TCT	8	2	3	7

The data show, that RIS-ECT has a much higher sensitivity compared to TCT (94 vs 54%) in detecting LC of CRC in pts with elevated tumor markers. False positive results may be caused by CEA and/or CA 19-9 antigens in ovarian cysts or necrotic tissue.

No. 19

CLINICAL USE AND LIMITATION OF I-123 LABELED MONOCLONAL ANTI-CEA FRAGMENTS FOR THE ECT DETECTION OF COLORECTAL CARCINOMA. B. Delaloye, A. Bischof-Delaloye, F. Buchegger, V. von Fluedner, J.C. Volant, S. Curchod, B. Johner, F. Mosimann, J. Pettavel and J.P. Mach. Nuclear Medicine Dpt, Surgery Dpt, CHUV and Ludwig Institute, Lausanne, Switzerland

As previously shown in a retrospective study of 31 patients with colorectal cancer ECT with I-123 labeled fragments (F(ab')₂ and Fab) of monoclonal anti-CEA antibodies (MAB) allows the visualization of the majority of primary, recurrent or secondary tumors [JCI 77:301-311, 1986] For the present study 34 patients (13F, 50-82y, x61.5y,

21M, 39-77y, x60.5y) suffering from colorectal cancer were examined without knowledge of the results of other investigations. Serum CEA ranged from 1.3 to 2000 ng/ml. 3 MABs (35, 25, 19) were used either as F(ab')₂ (n=14) or Fab (n=20) fragments. 5 patients were excluded from evaluation because of lacking further work-up. 2/2 primary and 8/9 recurrent tumors were correctly diagnosed with 1 false positive (FP) and 1 false negative (FN). 18/21 liver involvements suspected by immunotomoscintigraphy were subsequently confirmed (0 FN, 3 FP). Correct diagnosis of peritoneal involvement was made in 1/2. There were two true positive (TP), 5 FP and 1 FN lung, 4 TP, 1 FP and 1 FN bone metastases.

These preliminary prospective data show that immunotomoscintigraphy gives satisfying results in the detection of local recurrences and liver metastases of colon carcinoma. In the lungs several FP were observed and not enough data are yet available to assess its value for the diagnosis of peritoneal and node involvement.

No. 20

RADIOIMMUNOSCINTIGRAPHY, RIS: PRACTICE AND TUMOUR UPTAKE IN COLORECTAL AND OVARIAN CANCER. M. Granowska, J.R. Jass, J.M.A. Northover, K.E. Britton, J. Bomanji, C.C. Nimmon, L. Bingham, I.P. Todd. St Bartholomew's Hospital, London, UK.

RIS should now be past the stage of anecdotal success yet there are few prospective studies or definitions of its clinical purpose. RIS in colorectal cancer is accurate but of little use in detecting primary tumours because endoscopy and radiology are reliable. Uptake in excised tumour specimens taken 24-96h after the patient received iv 3.5 mCi In-111 C46 anti-CEA (Amersham International) as % administered dose per gram was Mean 7.0 x 10⁻³%/G (range 0.03-206 x 10⁻³%/G for tumour weights between 3.93 and 23.55G). Tumour to mucosa uptake ratio was Mean 4.95 (range 2.04-9.54). Lymph node uptake was mean 4.7 x 10⁻³%/G (range 0.7-13.3 x 10⁻³%/G) and node to mucosa ratio was mean 6.92 (range 0.4-21.9). Tumour to node ratio was mean 3.93 (range 0.36-7.73). These results, taken with pathological findings, may have implications for prognosis as well as in vivo staging. RIS was most clinical use in follow-up, identifying whether pelvic x-ray CT masses were due to tumour recurrence (positive uptake) or fibrosis (no uptake).

A prospective study in ovarian cancer showed RIS cannot distinguish whether or not a pelvic mass is due to ovarian cancer. A single blind, biopsy controlled study (54 sites) showed that RIS, with kinetic analysis and probability mapping, has a role in identifying peritoneal seedlings, clinically negative recurrences and in evaluating chemotherapy.

Efforts should now be directed in controlled trials at the clinically important or difficult problems and not in imaging the obvious.

No. 21

RADIOIMMUNODETECTION OF LUNG CANCER BY MEANS OF AN ANTICEA MONOCLONAL ANTIBODY. P. RIVA, G. PAGANELLI, G. RICEPUTI, G. CACCIAGUERRA, V. TISON, G. MOSCATELLI. Nuclear Medicine Dept. "M. BUFALINI" Hospital and Istituto Oncologico Romagnolo - CESENA - ITALY

12 patients with oat cell carcinoma and 28 patients with epidermoidal carcinoma of the lung, have been studied using the fragments F(ab')₂ of a monoclonal antibody raised against CEA (FO23C5-SORIN BIOMEDICA) labelled with ¹³¹I or ¹¹¹In. We succeeded in imaging all primary tumours and, in the field of metastatic lesions, we were able to detect 4 out of 7 bone metastases and all the recurrences in brain, liver, lymph nodes and skin.

Furthermore, 30 unexpected "hot spots" of the chest and other areas of the body were investigated; of these, 23 have been confirmed as neoplastic lesions in the follow-up. In 5 patients already submitted to operation we found neoplastic spreading when other radiological investigations were negative. 3 patients with chronic pulmonary disease were studied with immunoscintigraphy because of their doubtful X-Ray findings and resulted true negative. In four patients with positive scans an equal amount of a non specific MoAb raised against melanoma has been injected as negative control: no positive scans have been obtained in any cases.

No. 22

THE POTENTIAL UTILITY OF IN-111 LABELED OC-125 ANTIBODY IN PATIENTS WITH GYNECOLOGICAL TUMORS. P.W. Doherty, T. Griffin, M. Rusckowski, M. Gionet, R. Hunter, D.J. Hnatowich. University of Massachusetts Medical Center, Worcester, MA.

Monitoring the response to therapy of these tumors, particularly ovarian cancer, is difficult; frequently requiring surgical re-staging. The finding of elevated levels of the antigen (CA-125) in the majority of these patients with recurrences lead us to evaluate the utility of using the antibody (OC-125) to this antigenic determinant for radioimmunodetection. We studied 11 patients (ovarian n=8) whose tumor status was documented by surgery (n=8) or biopsy (n=3) and correlated the results of imaging with their CA-125 levels and other studies (CT scans). Following the infusion of 1 mg of the F(ab')₂ fragments (1-2 mCi In-111) quantitative SPECT and planar imaging was obtained daily for 72 hours along with analysis of serum. Mean doses to the liver and kidneys of 2.8 and 1.8 Rads/mCi were lower than we observed with other antibodies and this was associated with a slower blood clearance (T 1/2 24 hours). The images of sites of tumor recurrence were of surprisingly good quality and correlated well with surgical and CT scan findings. There were 6 true positives, 3 of whom had normal CA-125 levels, with one false positive and one false negative. Those with multiple small metastatic nodules showed a pattern of diffuse uptake which increased with time, whereas those with nodal or larger recurrences showed more focal uptake. The combination of favorable biodistribution and positive images, especially in patients with normal antigen levels, suggest a role for OC-125 imaging in their management.

No. 23

IMAGING OF MELANOMA, OSTEOGENIC SARCOMA, AND NEUROBLASTOMA USING GD2 SPECIFIC I-131 LABELLED MONOCLONAL ANTIBODY. F. Miraldi, A.D. Nelson, S. Ellery, R. Adams, B. Landmeier, S. Kallick, C. Kraly, N. Berger, and N.K. Cheung. University Hospitals of Cleveland, Cleveland, OH.

We have shown in previous studies that I-131 labelled monoclonal antibody (MAB) 3F8 can image human neuroblastoma tumors. 3F8 is an IgG3 murine monoclonal antibody specific for the ganglioside GD2. The GD2 is known to be present on neuroblastoma, melanoma and osteogenic sarcoma, but does not appear on normal human tissue except neurons. We report here our experience with 20 patients (11 neuroblastoma, 7 melanoma and 2 osteogenic sarcoma). Three to 5mCi of I-131 labelled MAB was administered intravenously and the patients imaged daily for 3 to 5 days. Strong focal accumulations were seen in neuroblastoma tumors with tumor-to-non-tumor ratios ranging from 10:1 to 20:1. Osteogenic sarcoma tumors also

showed strong uptake, but the uptake by melanoma was not as strong and in addition showed wide heterogeneity. No non-specific uptake in normal bone, liver, spleen, or brain was observed. Time-activity curves showed activity half-times of approximately 10-20 hours for blood, 30 hours for normal tissue, and 60 hours for tumors. Our results indicate that the 3F8 MAB is a good agent for imaging of neuroblastoma, osteogenic sarcoma and some melanomas, and has potential for therapy.

1:30-3:00

Room 32

GASTROENTEROLOGY II: HEPATOBILIARY (Part 1)

Moderator: Darlene M. Fink-Bennett, PhD
Comoderator: Aldo N. Serafini, MD

No. 24

INCREASED VOLUME AND IMPAIRED EMPTYING OF THE GALLBLADDER IN MORBID OBESITY. W.C. Vezina, R.L. Paradis, D.M. Grace, R.A. Zimmer, L.C. Hutton, G.W. Chamberlain, K.M. Rycroft, W.Y. Chey. University Hospital, London, ON, Canada and The Genesee Hospital, Rochester, N.Y.

The increased incidence of cholelithiasis in morbid obesity may not be entirely explained by abnormalities in bile composition as a functioning gallbladder (GB) could theoretically evacuate cholesterol crystals prior to stone formation.

Fasting GB volumes (vol) were determined ultrasonographically (U/S) and 90-minute postprandial radionuclide GB emptying studies using Tc-99m DTPA and In-113m DTPA in 10% cream, were performed in 18 morbidly obese subjects (9 M and 9 F) and in 18 age and sex-matched volunteers (+ 20% of ideal weight).

Gastric emptying of cream was similar in the two groups $t_{1/2}$ 57 + 20 (min) (SD) for the obese and 75 + 20 for the normals ($p > .05$).

The integrals of the increase of cholecystokinin were similar in the obese, 625 + 187 (pmol/L min) and in the normals, 617 + 192 ($p > .05$).

The obese had lower GB ejection fractions (EF), EF 60 min after onset of GB emptying 50 + 22% than normals, EF 74 + 14% ($p < .02$).

Fasting GB vol were greater in the obese, 71 + 14 mL than in normals, 28 + 14 mL ($p < .005$). Calculated postprandial GB vol $\{(\text{fasting vol} \times \text{EF})/100\}$, were greater in the obese, 36 (+ 22) mL than in normals, 7 (+ 6) mL ($p < .01$). U/S GB were acalculus.

Bile stasis may be a factor contributing to the increased risk of cholelithiasis in morbid obesity.

No. 25

Gd-DISIDA - A POTENTIAL CONTRAST AGENT FOR MR IMAGING OF HEPATOBILIARY SYSTEM. G.B. Saha, B. Bateson, T. Meaney, R.T. Go, W.J. MacIntyre, J.K. O'Donnell, D.H.I. Feiglin. Cleveland Clinic Foundation, Cleveland, OH.

The objective of this study was to prepare and evaluate gadolinium-diisopropyl iminodiacetic acid (Gd-DISIDA) complex as a potential paramagnetic contrast agent for magnetic resonance imaging (MRI) of the hepatobiliary system. Gd-DISIDA was prepared by mixing Gd and DISIDA solutions at appropriate chemical conditions and adjusting pH to 7.5. The yield was determined by thin layer chromatography (TLC) using Gd-153 as the radio-tracer and found to be 97 + 3%. The complex was found to be stable both in vivo for 24 hrs, determined by dialysis of the plasma sample, and in vitro over a period of 4 days determined by TLC. Approximately 0.05 mmol/kg of Gd-

DISIDA was injected intravenously into each of a group of 5 Swiss mice. Normal and injected mice were sacrificed 30-35 min after injection and different organs were removed and wiped. T1 and T2 values of all tissue samples were measured at 20 MHz on an IBM PC-20 spectrometer. T2 values did not change significantly with Gd-DISIDA. T1 values of the normal liver were reduced by almost 56%. No significant change in T1 was observed in kidneys, lungs, heart and spleen with this agent. The T1 values of blood decreased by almost 55%. MRI of the liver obtained in rabbits on a 1.5 Tesla MR machine prior to and 30-35 min after injection of 0.05 mmol/kg of Gd-DISIDA. Excellent contrast enhancement was observed. Nearly 50-60% decrease was obtained in T1 values calculated from the pre- and post-injection images. These results indicate that Gd-DISIDA may be a potential contrast agent for MRI of the liver.

No. 26

CHOLECYSTOKININ (CCK) CHOLESCINTIGRAPHY (C) IN ACALCULOUS BILIARY DISEASE (ABD). D. Fink-Bennett, P. DeRidder, W. Kolozsi, R. Gordon, J. Rapp. William Beaumont Hospital, Royal Oak MI and Northern Columbiana County Hospital, Salem OH.

We retrospectively analyzed the max. gallbladder (GB) ejection fraction response (EFR) to CCK in 374 symptomatic (neg. GB US) pts. and 27 "normal" (asymptomatic) volunteers (NV).

Pts. received 5 mCi of Tc-99m Disofenin. Post-max. GB filling, 0.02 ug/kg CCK was infused. GB EFs were determined q.5 min. X 4 by pre-CCK - post-CCK/pre-CCK GB cts.

	Symptomatic Patients			
	EF < 35%		EF > 35%	
	Surg.Dx.	Med.Dx.	Surg.Dx.	Med.Dx.
CC	108	69	7	9
Normal GB	7	13	4	130
Lost to FU		18		9

Predictive Value Surg. pts. 94%; All pts. 90% (CC - Chronic Cholecystitis; FU - Followup)

In 9/27 NVs max. GB EFs were > 35%; unexpectedly, 16/27 < 35%, 2 non-calculable. 2 NVs have stones, 5 delayed GB filling or biliary-to-bowel transit (B-B-T) 1 symptoms (Surg. scheduled), 1 NV no EF obtained has stones, 1 delayed B-B-T.

CCK C can reliably confirm the clinical impression of ABD. It detects GB disease whether symptomatic or asymptomatic.

No. 27

SENSITIVITY (SENS), SPECIFICITY (SPEC), AND ACCURACY (ACC) OF CCK CHOLESCINTIGRAPHY (CCK-C) IN ACALCULOUS BILIARY DISEASE (ABD).

L. Swayne, F. Palace, J. Rothenberg, D. Heitner, and J. Trivino. Morristown Memorial Hospital, Morristown, NJ.

87 patients (pts.) were prospectively studied with CCK-C to determine the SENS, SPEC, and ACC of this modality in the detection of ABD. All patients had symptomatology suggestive of gallbladder disease of at least six months duration, and each had an ultrasound study demonstrating no stones. After an overnight fast, each pt. was administered 5 mCi of technetium-99m Hepatolite. At maximal gallbladder filling (60-90 min.), .02ug/kg CCK was infused IV over 5 min. followed by a 40 min. computer acquisition. A latent period, ejection period, ejection rate, and gallbladder ejection fraction (GBEF) were calculated from background subtracted images. A GBEF \leq 35% was considered indicative of ABD.

30 pts. with a GBEP \leq 35% underwent cholecystectomy (Cx); all had pathologic evidence of ABD, and all but one improved clinically. 2 pts. with a GBEP $>$ 35% had Cx; a false - improved, a true - did not. 8 pts. had sonographically demonstrable polyps (SDP). 5 pts. with SDP had a GBEP \leq 35%; 3 with Cx improved, 2 without Cx did not. 3 pts. with SDP had a GBEP $>$ 35%, did not have Cx and did not improve.

Thus, the SENS, SPEC and ACC for pts. with Cx and/or SDP is 89%, 100%, and 89%.

No. 28

EMERGENT Tc-99m DISOFENIN HEPATOBILIARY SCINTIGRAPHY: CLINICAL EFFICACY AND COST-EFFECTIVENESS. P. Gagliardi, J. Sulzer, C. MacDonald and P. Hoffer, Yale University School of Medicine, New Haven, CT.

This study investigated whether hepatobiliary scintigraphy performed outside of regular hours influenced patient care during the time interval before a scheduled study would have been available and whether the cost savings generated offset costs of providing the service. Charts of all 38 patients having off-hours hepatobiliary during a 17 week period were reviewed. Of the 28 scans on outpatients 13 were normal; 5 of these patients were not hospitalized. Admitting these patients for scanning during the next working day would have cost at least \$2142, compared to a cost of \$1964 attributable to providing the scans emergently. 23 patients were admitted; 9 with normal scans were admitted with diagnoses other than biliary disease. Of 14 outpatients with abnormal scans, 10 had confirmed cholecystitis (mean time to surgery 4.6 days), 2 elected for later surgery, and 2 had non-diagnostic scans due to fasting. 2 patients not admitted in spite of scans diagnostic of acute cholecystitis had gangrenous cholecystitis confirmed at 7 and 10 days. In the 10 inpatients studied no diagnosis of biliary disease was made (8 normal, 2 non-diagnostic scans). Emergent hepatobiliary scans expedite outpatient management: cost savings generated offset the cost of providing the service. Although surgery followed diagnostic scans by several days, non-diagnostic scans due to post-admission fasting were probably minimized. The most efficacious use of emergency scans was in determining whether to admit patients who did not require admission on clinical grounds alone.

No. 29

THE SENSITIVITY AND POSITIVE PREDICTIVE INDEX OF BILIARY NONVISUALIZATION IN TOTAL BILIARY OBSTRUCTION. M.L. Lecklitner* **, A.R. Austin*, A.R. Benedetto**, and G.W. Growcock**. *University of South Alabama Medical Center, Mobile, AL and **University of Texas Health Science Center, San Antonio, TX.

Hepatobiliary findings demonstrating concurrent nonvisualization of gallbladder, common bile duct, and intestinal activities have been considered to be inconclusive, indicating an uncertainty as to whether a medical or a surgical disease caused the nonvisualization. The sole purpose of our study was to determine the sensitivity and positive predictive index of hepatobiliary scintigraphy in diagnosing total biliary obstruction (TBO), using Tc-99m DISIDA, 8 mCi, in 401 adult patients and continuing the acquisition to 4 hrs, given the nonvisualization of the aforementioned structures. All patients had been fasting for a minimum of 3-4 hrs prior to the study, and no patient was receiving perenteral nutrition at the time of imaging.

We identified 26 patients who fulfilled the above criteria. One patient was removed from the study, because he departed the emergency service against medical advice following his study. Twenty three of the remaining 25 patients had surgically-documented evidence of TBO. Two false-positive studies were encountered.

We conclude that the criteria of hepatic uptake with no biliary excretion is sensitive [100% (23/23 patients)] and positively predictive [92% (23/25 patients)] of total biliary obstruction, if imaging is acquired to 4 hrs.

1:30-3:00

Room 30

COMPUTERS & DATA ANALYSIS I: ECT SCATTER & ATTENUATION CORRECTION

Moderator: Andrew E. Todd-Pokropek, MD, PhD
Comoderator: Guy Simmons, PhD

No. 30

USE OF A GERMANIUM DETECTOR TO STUDY SCATTER CORRECTION IN SPECT. M.Singh and C.Horne. University of Southern California, Los Angeles, CA.

A collimated 5mmx5mmx6mm high purity germanium (Ge) detector with energy resolution of 1 keV at 140keV was used to study and correct for the scatter fraction emanating from a 26cm diamx26cm tall cylindrical test-object containing an asymmetrical distribution of Tc-99m and non-uniform attenuation. Spectra containing 40Kcnts each in a 140±1 keV window were acquired from 8 angular views around 360° and 2 linear offsets(±5cm) per view(total 24 samples). After normalizing for Ge efficiency, the spectra were convolved with gaussians corresponding to energy resolutions of 7,12(typical Anger camera) or 15%, and the mean and std dev of the scatter fraction within prescribed energy windows were determined in conjunction with a scatter-free reference spectrum. Statistical effects were included by adding Poisson noise to scaled spectra(100 or 1000 photopeak counts after convolution). Using the expression T=P-aB where P and B are photopeak and background counts in variable windows, the factor 'a' was optimized to produce a mean value of T equal to the scatter-free reference with minimal dispersion among samples. Results at 12% energy resolution show an average scatter fraction of 37.7% before correction. After optimal subtraction, the mean peak cnt/std dev degrades from 9.3 to 7.1 for 100 cnts, but improves from 19.8 to 20.5 for 1000 cnts. Thus, a germanium detector enables experimental evaluation and optimization of a scatter correction technique.

No. 31

SCATTER MEASUREMENTS USING DUAL ENERGY WINDOWING IN PET. W.H. Wong. University of Texas Graduate School of Biomedical Sciences, Houston, Tx.

The scatter events in PET quantitation has been the most difficult error to correct. One has to understand the scatter distribution for the object to be imaged in order to devise method to correct the scatters. An obvious way to measure the scatter is to image with a high energy-acceptance-window to reject the scatters and then image with a lower or regular energy window. This paper studies the accuracy and practicality of this method.

This study found that to reject most of the scatters in a 20 cm phantom, the energy window will have to be set at about 500 KeV. Since the energy detection response of the detector for true 511 KeV gamma is constant and can be measured on the bench, the counts collected at the high window setting can be normalized to that of the lower/normal window to estimate the true counts in the normal window run. The difference between the extrapolated true count and the total counts collected at

the normal energy window will be the scatters. Error analysis based on the detector photopeak efficiency for BGO scintillators, 20 cm phantom, and 5 millions events per image with the normal window, the scatter measurement error is about 20% for each 6x6mm pixel. The data collection period can be extended longer than normal to lower the error, but the distribution of activity should remain fixed in the extended period. This dual-energy technique can only be used for directly measuring scatters but cannot directly improve the accuracy of extracting the true events with the normal window in routine studies. This method can be used as a gold standard to judge the accuracy of other scatter correction methods which can be easier to use in routine clinical studies.

No. 32

EVALUATION OF SCATTER CORRECTION METHODS IN SPECT. M.C. Gilardi, V. Bettinardi, C. Pantalone, A. Todd-Pokropek, P. Gerundini, and F. Fazio. CNR, University of Milan, Istituto S.Raffaiele, Milano-Italy, and University College London, UK.

The detection of Compton scattered radiations results in qualitative degradation and quantitative inaccuracy of images in SPECT. Aim of this study was to evaluate and compare three scatter correction methods. The first, proposed by Axelsson et al., consists in a convolution and subtraction of scattered events from the measured projection data. The second, by Jaszczak et al., is based on the subtraction of a fraction of Compton events (92-125 KeV) from the photopeak data (140 KeV, 20% for Tc-99m), after reconstruction. The third, developed by Todd-Pokropek et al., is based on a weighted subtraction of the filtered Compton events from the photopeak data, before reconstruction. Line spread functions were measured at various distances (d) of the source from the center of rotation in air and scattering medium. A slight improvement in spatial resolution (2.5% reduction in FWHM) was found after scatter correction for all three methods. Ratio between corrected and measured counts (d=0) was 0.81, 0.80, 0.76 for the 1st, 2nd and 3rd method respectively; these results agreed with the theoretical expected scatter fraction of 0.78 evaluated by Monte Carlo technique. A 25% increase of contrast, calculated on cold lesions, was found for all three techniques. Recovery on hot lesions ($\beta=4$ cm), for various lesion to background radioactivity concentration ratios, was measured to be within 10%, 5%, 4% from the expected value (100%) for the 1st, 2nd, 3rd method respectively. Clinical cerebral perfusion studies show improvement of image quality following scatter correction.

No. 33

The use of 1-D and 2-D scatter deconvolution techniques for contrast enhancement and quantification in SPECT. S.A. Larsson, B. Axelsson, C.M. Dahl and P. Msaki Karolinska Hospital, Stockholm, Sweden

Introduction. A major part of photon interactions with body-tissue in most nuclear medicine applications is due to Compton scattering. In SPECT, the loss of primary photons may be compensated for by some accurate attenuation correction algorithm but large fractions (20-40%) of falsely positioned events may still be present due to insufficient scatter rejection capability of the detectors presently used. In this paper, we present the use of 1-D and 2-D post-acquisition scatter correction techniques for SPECT.

Method. Both methods are based on deconvolution of projections with a scatter distribution function before image reconstruction. The 1-D scatter distribution function is obtained from measurements of a line-source in water (and the ordinary energy discriminator window). This function operates pixel by pixel along each 1-D projection of a section. Axial variations of radioactivity is not taken into account by this method. This is done with the 2-D correction method which is based on

measurements of a point-source in water. A 2-D convolution kernel is calculated recursively from these data into a 31x31 matrix for subsequent 2-D convolution of the projected views (64x64 pixels).

Results and conclusions. Phantom measurements and patient studies show that both techniques improve image contrast and quantification in SPECT. The 2-D correction technique seems to produce slightly better results than the 1-D technique, but the latter may be preferable in routine applications due to shorter reconstruction time.

No. 34

AREA WEIGHTED APPROACH TO ATTENUATION CORRECTION IN SPECT USING ARBITRARILY SHAPED NON-UNIFORM ATTENUATION MAPS. R.B. Schwinger, S.L. Cool, and M.A. King. University of Massachusetts Medical Center, Worcester, MA, and Analogic Corporation, Wakefield, MA.

A different approach has been considered in the development of an attenuation correction algorithm for use in SPECT. This new algorithm takes advantage of the fact that any one pixel in a transverse section image to be corrected is incrementally attenuated by at most, three of its nearest neighbors at any projection angle. Therefore, an area weighted sum of these three neighboring pixels (attenuation coefficients) can be performed. Also assumed is that a pixel will attenuate one half its own activity. These properties are incorporated into an efficient row by row or column by column summation to calculate a correction matrix at each projection angle for an iterative correction or for all projection angles in a post-reconstruction correction. Since the algorithm is not based on an analytic definition of the attenuation border, an arbitrarily shaped attenuation map with non-uniform coefficients determined from a SPECT transmission scan can be easily included. The algorithm is flexible in that it can be used in either an intrinsic correction or a post-reconstruction correction. The relative speed of this algorithm in Fortran is approximately 4 times that of a typical post-reconstruction correction algorithm that is based on analytically solving for an elliptically shaped uniform attenuator. Preliminary results show that the performance of this algorithm with uniform attenuation data is equivalent to currently used algorithms. An added benefit is the suitability of this algorithm for implementation on parallel processing hardware.

No. 35

IMPROVED SPECT USING SIMULTANEOUS TRANSMISSION AND EMISSION TOMOGRAPHY. B.F. Hutton, D.L. Bailey, P.J. Walker, Royal Prince Alfred Hospital and NSW Institute of Technology, Sydney, N.S.W. 2050, Australia.

The accuracy of attenuation correction, essential for SPECT quantitation, can be improved by determination of a valid body outline and map of attenuation coefficients (μ) for each tomographic slice. A method has been developed for simultaneous recording of transmission and emission tomography to provide this information in a practical time.

A dual radionuclide SPECT acquisition is performed with a transmission source attached to a rotating gamma camera, of lower energy than the emission radionuclide. A suitable source for Tc-99m studies is Ga-153 (103 keV). The lower energy window includes scatter from the emission source which must be removed prior to reconstruction. The geometric mean is formed for each conjugate pair of images in both energy windows. The scatter can be predicted by convolving each upper energy image pair with an experimentally determined biexponential scatter function and scaling by the appropriate fraction ($k=0.60$). Both the scatter function and fraction must be determined for the particular pair of radionuclides and can be shown to be relatively independent of activity distribution. After scatter correction the transmission data are

transformed then reconstructed to provide an attenuation map for Gd-153 which is proportional to the μ values for Tc-99m ($\mu_{Tc} = 0.97 \mu_{Gd} - 0.009$). The method allows body outline and attenuation coefficients to be estimated without extending the normal SPECT study time.

1:30-3:00

Room 33

BONE/JOINT I: BONE MINERAL ANALYSIS (Part 1)

Moderator: Heinz W. Wahner, MD, MS
 Comoderator: C. Robert Appledorn, MS

No. 36

BONE MINERAL DENSITOMETRIC ANALYSIS OF DISUSE OSTEOPOROSIS IN PARAPLEGICS. E.B. Silberstein, University of Cincinnati Medical Center, Cincinnati, OH.

The paraplegic patient is at risk for lower extremity fracture not only because of loss of sensation but because of a reported high prevalence of disuse osteoporosis. We have attempted to provide early detection of tibial osteoporosis, quantitate its progression and evaluate the effect of computerized electrical muscle stimulation on the disorder using dual photon bone mineral densitometry (BMD).

Appropriate patient positioning for high precision measurements of tibial trabecular bone density was first developed using conventional femoral head software on normal volunteers in various positions and then employing new prototype software (Lunar Corp., Madison, WI).

Normal values for the target population (15-40 yrs) were:

		Mean BMD	Range
Male	Tibia	0.97	0.72-1.11
	Central	0.99	0.70-1.10
Female	Tibia	0.80	0.72-0.85
	Central	0.78	0.67-0.89

Studies on ten paraplegic osteoporotic patients have shown a bone mineral loss exceeding 3% in 6 months in the majority, with higher BMD levels in patients involved in the electrically stimulated exercise program.

We conclude that BMD can detect early disuse osteoporotic in the tibia of paraplegics and evaluate the effect of exercise on this process.

No. 37

BONE MINERAL DENSITY IN OSTEOPOROSIS. R.B. Mazess, M. Ettinger, and E. Schulz. University of Wisconsin, Madison, WI, Osteoporosis Bone Diagnostic Laboratories, Stuart, FL and Loma Linda University, Loma Linda, CA.

Bone mineral density (BMD) was measured in 158 normal young women, 244 normal older females and 28 women with hip fractures. Density of the lumbar spine and proximal femur was measured using dual-photon absorptiometry (Gd-153) and the radius shaft was measured using single-photon absorptiometry (I-125). The BMD in the older women with no fractures was about 20% below young normal women (age 20-39) for the radius and spine, and 30% below for the femur. The BMD in hip fracture cases was 8% below the age-matched controls (Z-score = 0.4) for the radius and 10% for the spine (Z-score = 0.6). The BMD for the neck and trochanter regions of the femur was 25% lower (Z-score = 1.4) while the Ward's triangle region was 35% lower (Z-score = 1.6). Measurement of the proximal femur affords excellent discrimination of early fracture risk of the hip compared to either the radius or the spine.

BONE MINERAL DENSITY (mg/cm²) AT SEVERAL LOCATIONS

	CONTROL		HIP FRACTURE	
	YOUNG	OLD	FLORIDA	CALIFORNIA
n =	158	244	18	10
age	30	68	70	72
FEMORAL NECK	1020	746	575	564
WARD'S TRIANGLE	946	599	407	369
TROCHANTER	803	643	491	427
SPINE L2-L4	1267	982	889	-
RADIUS SHAFT	700	566	519	-

No. 38

AGE-SPECIFIC, LONGITUDINAL BONE LOSS RATES AT MULTIPLE CORTICAL AND TRABECULAR SKELETAL SITES. R.D. Wasnich, J.M. Vogel, P.D. Ross, and L.K. Heilbrun. Kuakini Medical Center and John A. Burns School of Medicine, Honolulu, HI.

Serial bone mineral content (BMC) measurements were obtained at yearly intervals, over a 4.5 year followup, in 1098 women ranging in age from 43 to 81 years. Lumbar spine (LS) BMC was measured by dual photon absorptiometry, and os calcis (OC), distal radius (DR), and proximal radius (PR) BMC by single photon absorptiometry. For the entire cohort, the greatest yearly, mean loss rates were observed for the OC (-1.7%), followed by DR (-1.3%) and PR (-1.0%). These results were lower, but proportionate to, the rates predicted by cross-sectional data on the same cohort. However LS BMC, instead of showing the expected loss, showed a consistent positive change of (+5-6%), probably related to technical factors.

By 5 year age groups, OC BMC loss rates were -2.3% (under age 54), -1.7% (age 55-59), -1.4% (age 60-65), -1.7% (age 65-69), and -2.4% (over age 70). This heterogeneity of loss rates was also mirrored at the other appendicular sites. These findings suggest that rapid bone loss may occur in the older (> 70 yrs) female, equal to that seen in the immediate postmenopausal years. The results also confirm marked heterogeneity of loss rates not only between individuals, but also in the same individual on a year-to-year basis. Loss rates also appear to be proportionate to the trabecular bone content of the measurement site.

No. 39

SPONTANEOUS AND OESTROGEN CAUSED BONE CHANGES IN EARLY POSTMENOPAUSAL WOMEN: A LOCAL OR GENERALIZED PHENOMENON? C. Christiansen, A. Gotfredsen, L. Nilas, B.J. Riis, K. Thomsen. Glostrup Hospital, Glostrup, Denmark.

Regional values of bone mineral content (BMC) and bone mineral density (BMD) from a total body dual photon absorptiometry (DPA) scan were calculated in fifty-two early postmenopausal women treated one year with oestrogen, and in fifty-two similar placebo treated women. The six regions were head, arms, chest, spine, pelvis, and legs. Moreover values of lumbar spine BMD by DPA and forearm BMC by single photon absorptiometry were obtained from separate special-purpose scanners. All regions were unchanged after one years oestrogen treatment excluding the lumbar spine which rose. All regions excluding the lumbar spine fell significantly during the year of observation in the placebo group. The rates of loss ranged from 2 per cent to 8 per cent with no significant differences between the regions. It is concluded that bone loss in the early menopause is a generalized phenomenon including all parts of the skeleton. Furthermore, oestrogen prophylaxis of bone-loss is effective in all parts of the skeleton. Finally it is suggested that the forearm BMC measurement be used for clinical follow-up of bone changes in the single patient as the performance of this method in terms of change/precision ratio is superior to other measurements.

No. 40

EVALUATION OF BONE MINERAL LOSS IN HYPERPARATHYROIDISM BY SINGLE AND DUAL PHOTON ABSORPTIOMETRY. B. Greenspan, A. Strashun, D. Bergman, M. DaCosta, M. DeLaney and S. J. Goldsmith. Mount Sinai Medical Center, New York, NY.

The purpose of this study is to evaluate the differential effect of primary hyperparathyroidism (HP) on cortical (CB) and trabecular bone (TB) with the use of single and dual photon absorptiometry (SPA and DPA) in 13 patients (pts) with HP confirmed by parathormone-RIA Tl-201 scintigraphy, and surgical localization of parathyroid adenomata. Two males and 11 females, ages 36 to 76 years, mean 61, were examined with SPA and DPA utilizing standard methodology validated in our laboratory. Paired t test analysis was performed to determine significant differences from age matched normal group data.

The result reveal significant reduction in 11 of 13 patients (with the mean approx. 2 standard deviation (SD) below the age matched normal mean) in bone mineral (BM) content of the radius, as measured by SPA. The mean value was 0.511 G/cm (SD 0.127), range 0.346-0.720 G/cm, versus (VS) 0.611 G/cm (predicted normal mean (PNM)). There was a significant decrease in BM density of the lumbar spine (> 2 SD) as measured by DPA in 11 of 13 pts, mean 0.851 G/cm² (SD 0.156), range 0.668-1.044 G/cm² vs 1.048 G/cm² (PNM).

Whereas it has been reported that midradius BM content is insensitive to the effects of HP, our population demonstrated significant reduction of BM of both lumbar spine and midradius sites suggesting active resorption of both TB and CB.

No. 41

RESPONSE OF OSTEOPOROSIS TO MEDICAL THERAPY. M.R. Powell, F.O. Kolb, K.A. Meier, P. Bowsher AND C.J. Peterson Nuclear Medicine Consultants, San Francisco, CA.

Re-analysis of our spine mineral measurement by dual photon absorptiometry (DPA) data base was performed for the osteoporosis patients under the management of one bone endocrinologist (FOK). There are now 77 patients with serial measurements of L-2 through L-4 by DPA using uniform data reduction by the same analysis software and edge finder. Patients were categorized as 32 Normal Menopause (NM), 11 Premature Spontaneous Menopause (PM), 4 Surgical Menopause (SM), and 30 Idiopathic Osteoporosis (IO) that was not hypogonadal or due to other obvious medical disease. Average followup was 19.5±18.5 months for NM, 17.5±9.7 months for PM, 14.3±17.7 months for SM, and 19.9±18.4 months for IO. Mean change of spine mineral was +8.4±8.8% for NM, -0.15±5.4% for PM, +6.0±6.8% for SM and +2.9±11.1% for IO. Our data show significant average increases of several times the 2% measurement precision for the method for both NM and SM. The large standard deviations within these groups continue to demonstrate the importance of using DPA estimation of bone mineral to identify need for modification of therapy in those who do not respond to the initial therapy approach.

1:30-3:00

Room 27

ENDOCRINE I

Moderator: Aslam R. Siddiqui, MD

Comoderator: Amjad Ali, MD

No. 42

I-131 STAGING OF THYROID CANCER: EFFECT OF TOTAL THYROIDECTOMY AND I-131 ABLATION ON DETECTION OF METASTASES. W.H. Beierwaltes, C. Dmuchowski, R. Rabanni. University of Michigan Hospitals, Ann Arbor, MI.

We reported (J Nucl Med 23:561, 1982) that in 103 patients with well-differentiated thyroid carcinoma (WDTC) with metastases detected outside the neck, 41 patients (39%) had distant metastases first detected an average of 7.44 years (1-25 yrs) after the primary surgery. We now report an update through 6-30-85 with a cumulative incidence curve of detection of metastases.

Six-hundred ninety patients were treated for (WDTC) during the period of 1-1-47 to 6-30-85 with an attempted total thyroidectomy, then off all thyroid hormone for 6 weeks, a 2 mCi tracer dose of I-131, radioiodine uptake at 24 hours, pin-hole images of neck and chest, complete history, physical examination and chest x-ray. Patients were rechecked at 1, 3 and 5 years, then every 5 years permanently.

The cumulative incidence of detection of thyroid cancer after the first symptom was plotted on 690 patients. Thirty-one % of the patients had their carcinoma detected 0-1.4 yrs after the first symptom, 3%/yr at 1.4-6.17 yrs, and 0.2%/yr at 6.17-52 yrs. Of the 167 who had metastases detected, 160 (95%) had metastases detected outside the neck. Eight (5%) had metastases confined to the neck. Seventy-six % had metastases detected at the initial surgery or initial postsurgical scan. The yearly cumulative incidence curve of detection of metastases after the primary surgery and scan was 16%/yr at 0-0.6 yrs, 1.5%/yr from 0.6-7.3 yrs, and 0.17%/yr from 7.3-23.5 yrs.

If the follow-up % uptake and scan show no significant remnant at 1 year and 3 years, patients should be asked to return every 5 years as long as they live.

No. 43

DETERMINATION OF TRACER DOSE OF I-131 FOR DETECTION AND FOLLOW-UP OF METASTATIC THYROID CANCER USING A SMALL-SOURCE PHANTOM. N.B. Arnstein, J.C. Sisson, S.A. Spaulding, and J.E. Carey. University of Michigan Medical Center, Ann Arbor, MI.

The dose of radioiodine (I-131) used to survey patients for metastatic thyroid cancer varies from 0.2 mCi to 30 mCi, and has not been based on experimental data. Higher doses occasionally reveal smaller lesions, but deliver more radiation to the patient. We asked which dose would be sufficient to detect metastatic deposits. Using a 13 liter water tank with small-source phantoms and two gamma cameras, we sought to determine: 1) the minimum imageable activity and volume of I-131, 2) effects of background and source depth on detectability, and 3) a practical I-131 tracer dose based on these findings. In volumes of 10 to 300 ul, the lowest activity detectable at the surface (without background) was 0.03 uCi, and at 10 cm depth, 0.10 uCi. Background activity at 0.01 uCi/ml resulted in a three to tenfold loss of detectability; computer subtraction of background did not improve results.

Assuming uptake of 0.05%/gram and T_{1/2} effective of 3 days, 200 mCi is sufficient to impart 5000 rad to a 30 ug tumor, the smallest that can be efficiently treated by the β particles of I-131. At an uptake of 0.05%/gram, the above results indicate that a 2 mCi tracer dose would detect a 30 ug lesion, but only at the surface and without background radioactivity. With patient motion and background activity, some potentially treatable lesions may not be detected even with 30 mCi. Our data show that no reasonable tracer dose can detect all potentially treatable disease. Acknowledging these limitations, we have chosen a routine dose of 2 mCi to minimize the cumulative radiation burden to the patient from repeated studies.

No. 44

THYROGLOBULIN AND I-131 UPTAKE OF REMAINING TISSUE IN PATIENTS WITH DIFFERENTIATED CARCINOMA AFTER THYROIDECTOMY. E. Moser, S. Fritsch and S. Braun. Dept. of Radiology, Klinikum Grosshadern, Univ. of Munich, Munich, FRG

I-131 uptake values are commonly used to document the success of ablation of the thyroid gland in patients (pts) with differentiated carcinoma. Measuring Thyroglo-

bulin- (Tg) levels is an additional component employed with increasing frequency in follow up. The relationship between Tg and I-131 uptake was studied after thyroidectomy before radioiodine treatment to test the reliability of Tg in assessing the mass of functioning thyroid tissue. 158 pts with nonmetastatic disease were included in this study. Uptake tests with 18-74 MBq were started 14 to 29 days (19±3; mean + SD) after thyroidectomy. Blood samples for measuring Tg and TSH were taken immediately before. The indication for therapy with radioiodine is an uptake >2% of the administered dose in the neck. Tg was measured with a double antibody RIA (Sensitivity: 6 ng/ml). Sera with Tg-antibodies were excluded. In 133 pts, Tg was >6 ng/ml and I-131 uptake >2% (Tg: 29 + 18 ng/ml; I-131: 23.1 + 13.2%). In 11 pts Tg was undetectable (<6 ng/ml) and I-131 uptake <2%. In 34 pts, however, with undetectable Tg, I-131 uptake values varied between 3 and 46% (12.4 + 10.5%). Only in 4 of these 34 pts TSH was not maximal (50 µU/ml) because of a shorter (9,10,11,13 days) period from thyroidectomy. In conclusion, a minimum of remaining thyroid tissue highly stimulated by TSH can trap a remarkable amount of radioiodine, but is unable to produce detectable Tg-levels. Therefore, in contrast to I-131, measuring Tg is insufficient to document the success of thyroid ablation.

No. 45

DIAGNOSIS AND STAGING OF DIFFERENTIATED THYROID CARCINOMA IN THE EUTHYROID PATIENT WITH THALLIUM-201. M. Ling, M. Okerlund, A. Holly. University of California Medical Center, San Francisco, California.

Thallium-201 imaging was evaluated in the diagnosis of differentiated thyroid carcinoma. We performed 41 studies in 38 patients, including 23 with papillary and 13 with medullary carcinoma. Each was given 3-4 mCi of Tl-201 chloride and neck and body images were obtained at 0.5 and 4 hours with an LFOV camera/LEAP and pinhole collimator.

In 23 cases of papillary carcinoma, 3 of 3 (100%) of pre-op cases correlated with surgically proven disease and predicted presence or absence of cervical node involvement. Of 21 post-op studies, 11 were positive with 18 of 19 (95%) tumor sites detected. 5 negative Tl studies were also negative by all modalities. 2 Tl studies (8% of total) were negative but later positive on I-131 scan. 28 of 32 total known tumor sites (88%) as detected by all modalities were successfully localized with Tl. Of 13 medullary cancer patients (all post-op), 4 studies were abnormal in 5 total sites and this was later confirmed by other studies. 8 others were negative despite detectable calcitonin levels in 6 of these.

Thallium-201 imaging is a highly sensitive method of detection of residual, recurrent or metastatic differentiated thyroid carcinoma. One Hurthle cell tumor was also localized. One "false positive" occurred in a giant cell tumor of bone. It is of definite, though lesser utility in medullary carcinoma. The studies correlated highly with other imaging modalities and required no withdrawal from thyroid medication. Tl-201 imaging can be of major clinical utility in the lifelong follow-up of thyroid cancer and in selecting patients for withdrawal from thyroid medication for specific I-131 imaging and treatment.

No. 46

EFFICACY OF RADIONUCLIDE THYROID SCAN IN EVALUATION OF UPPER MEDIASTINAL MASS FOR INTRATHORACIC GOITER. H.M. Park, R.D. Tarver, A. Siddiqui, D.S. Schauwecker, Indiana University, Indianapolis, Indiana.

Some chest radiology textbooks state that "many retrosternal goiters are not hormonally active" or "are seldom functioning" without adequate supportive data. We reviewed 54 (32F, 22M) consecutive cases that had a suspected upper mediastinal mass on CXR or CT and had a radionuclide thyroid scan between 1972-1985.

The mass was found to be a substernal goiter (SSG) in 42 patients and non-thyroidal in 12. In 93% (39/42) the thyroid scan correctly identified the SSG (26 with

I-131, 14 with I-123, 2 with Tc04). In 7% (3/42) the scan missed the SSG. Two of the three had posterior mediastinal goiters and one had a large intrathoracic thyroid cyst. Of the patients with SSG, 2 were hyperthyroid, 4 were hypothyroid and 36 euthyroid (mean T4 8.4ug). The average radioiodine uptake was 20% (nl 10-35%). The average TSH level was 2.9 uIU (nl 0-4.4uIU). In 21 patients the substernal portion was equal to or greater than the uptake in the normal thyroid and in 21 it was less. In two patients the SSG was completely separated from the remaining thyroid in the normal position. We observed parallax error in 40% (8/20) of the cases who had pinhole thyroid imaging studies. Many SSGs may be missed if this technical error is overlooked.

In summary, most of the SSGs are hormonally active and can be accurately diagnosed by radionuclide scan. SSGs can be better identified by centering the pinhole collimator at the suprasternal notch to avoid parallax or by using an "old fashioned" rectilinear scanner.

No. 47

CORRELATIVE MR AND SCINTIGRAPHIC THYROID IMAGING. B. Eisenberg, M.G. Velchik, W.B. Geffter, C.E. Spritzer, F.H. Sterling, H.Y. Kressel and A. Alavi. Hospital of the University of Pennsylvania, Philadelphia, PA

Eighteen thyroid patients (12F, 6M) ranging in age from 20-80 (x̄ = 49) were studied with MR and scintigraphy to evaluate clinical utility. Disorders evaluated included multinodular goiter (toxic and nontoxic) (pre- and post-therapy), Hashimoto's thyroiditis and solitary cold nodules.

T1 weighted (TR 600/TE 25 msec) and T2 weighted (TR 2500/TE 80 msec) spin echo pulse sequence MR images of the neck and upper mediastinum were performed with a 1.5 T superconducting magnet equipped with a surface coil. Pinhole images and RAIU values were obtained 24 hours after 200-300 uCi of I-123.

The MR signal intensity of normal thyroid tissue was slightly higher than surrounding neck muscle on both T1 and T2 weighted images. Cold (nonfunctioning) nodules had a signal intensity ≥ normal gland on T1 weighted images and markedly increased signal intensity on T2 weighted images. MR revealed excellent anatomic detail of tracheal deviation and/or compression and substernal thyroid extension. Colloid and hemorrhage had very high signal intensity with both T1 and T2 weighted images.

Scintigraphy accurately detected palpable nodules, though MRI frequently detected additional smaller lesions of uncertain clinical significance. Surface coil MR is more sensitive in detecting lesions not evident on scintigraphic images though specificity has yet to be ascertained. MR provided superior anatomic detail in multiple imaging planes without any radiation exposure.

3:30-5:00

Room 39

NEUROLOGY II: SPECT

Moderator: Richard A. Holmes, MD
Comoderator: Thomas C. Hill, Jr., MD, BS

No. 48

INITIAL EXPERIENCE WITH Tc-99m-HEXAMETHYLPROPYLENEAMINE OXIME (Tc-99m-HMPAO) BRAIN SPECT. I. Podreka, E. Suess, G. Goldenberg, M. Steiner, Th. Brücke, Ch. Müller, L. Deecke. Neurologische Universitätsklinik Wien, Austria

This study was undertaken to prove the clinical reliability of Tc-99m-HMPAO SPECT. 120 patients with various neurological disorders (seizures n=25, stroke n=31, migraine n=10, Parkinson's syndrome n=7, Alzheimer's disease and dementia n=10, psychiatric disorders n=12, others

n=25) and 5 normal volunteers were investigated. Additionally 20 stimulation studies (employment of imagery, VEP, SSEP) were performed. CT-scan of all patients was available. SPECT was performed with a Dual-Rota scintillation camera 15 min after i.v. injection of 12-20 mCi Tc-99m-HMPAO. During 30 min 60 projections have been acquired. Transversal sections were obtained after filtering of projections and correction for tissue absorption, by filtered back projection (128x128 matrices). SPECT-studies revealed regional hypoperfusion in 90% of seizure patients. Ischemic areas were detected in all stroke patients, in one case luxury perfusion was observed 5 days after onset of symptoms. Regional flow patterns allowed good differentiation of cases of Alzheimer's disease and other forms of dementia. All patients with Parkinson's syndrome showed low tracer uptake in the anterior basal ganglia and cortex. During an attack 4 migraine patients showed regional hypoperfusion. Stimulation studies showed relatively increased rCBF compared to resting state in various brain regions corresponding to the stimulus. In our experience excellent image quality is obtained by brain SPECT with the new compound Tc-99m-HMPAO. This technique allows detection of rCBF changes caused by different pathological and physiological mechanisms in the brain.

No. 49

BRAIN SPECT IMAGING WITH Tc-99m-HM-PAO IN THE EARLY DETECTION OF CEREBRAL INFARCTION: COMPARISON WITH TRANSMISSION COMPUTED TOMOGRAPHY. S.H. Yeh, R.S. Liu, H.H. Hu, W.J. Wong, Y.K. Lo, Z.Y. Lai, J.C. Huang, S.L. Chang, S.J. Wang, and F.L. Chu. Veterans General Hospital and National Yang-Ming Medical College, Taipei, Taiwan.

This study evaluated a new cerebral blood flow agent, Tc-99m-hexamethylpropyleneamine oxime (HM-PAO), in early detecting acute cerebral infarction, in conjunction with the transmission computed tomographic (CT) studies.

Brain SPECT imaging was performed within 24 hr after the initial CT scan in patients (pts) with acute stroke without CT evidence of hemorrhage after IV injection of 10 mCi of Tc-99m-HM-PAO. Diagnosis of cerebral infarction (CI) was confirmed by the initial and/or sequential late CT scans. Individuals without evidence of cerebral diseases served as controls.

In 8 controls, no perfusion defects were seen in the cortex, basal ganglia and thalami. Of 15 pts with acute stroke due to CI, 14 (93%) were detected within 48 hr of onset by HM-PAO scans in contrast to only 5 (33%) by CT. Discordance of HM-PAO perfusion defect with initial negative CT scans occurred in 60% (9/15) of pts. One pt had both negative HM-PAO and CT studies. In 3 of 5 pts with abnormal CT scans as well, the perfusion defect with HM-PAO was much larger than edema seen on CT. In the other two, both SPECT and CT were equal in the extent of abnormalities.

In summary, Tc-99m-HM-PAO is able to early detect acute cerebral infarction prior to CT with rather proper depiction of its extent in the majority of pts. This plus no logistical problems will make it a useful and practical agent for diagnosing and managing acute cerebral infarction.

No. 50

TC-99m HEXAMETHYLPROPYLENEAMINE OXIME (HMPAO) SPECT IN CEREBROVASCULAR DISEASE (CVD). A COMPARISON TO TRANSMISSION CT. A. Berberich, U. Buell, A. Eilles, W. Gerhards, A. Jaeger, A. Ferbert, E. Moser, W. Krappel. Univ. of Aachen, Homburg, Munich, Wuerzburg, Fed. Rep. Germany

Tc-99m HMPAO has shown considerable promise for imaging cerebral blood flow. Thus, it was employed in patients (pts) with CVD to experience changes of relative regional cerebral uptake in diseased (di) and undiseased (un) areas with time after injection and to compare sizes of low flow areas (LFA) to low density areas (LDA) in TCT. 46 pts with completed stroke (CS, n=31) or reversible neurological deficit (RND, n=15) were examined 15, 60 and 300

min after iv injection of 400 MBq Tc-99m HMPAO using rotating gamma cameras and 360° rotation. Transversal slices of 20 mm thickness were reconstructed and regional interhemispherical ratios of di-to-un (DUR) were computed by ROI programs. All pts had TCT, angiography or Doppler sonography within the same week.

DUR in pts with visible LFA was .754+.15 (15min), .762+.12 (60min) and .842+.12 (300min) (mean+SD). Size of LFA did not decrease within this period. In pts with RND, DUR (15 min) was .84+.10 (p<.025 vs CS). With HMPAO SPECT, 69 LFA were detected. Of these, 48 were found in the hemispherical periphery, 21 in the basal ganglia or the internal capsule. In 53% of the pts, HMPAO defects were more extended than LDA in TCT, in 38%, sizes were equal and in 9%, LDA were larger. A cerebellar diachisis occurred in 8 pts with a timely interval to the ictus of 9+5 days.

We conclude that Tc-99m HMPAO SPECT is a safe and reliable method to evaluate rCBF in CVD without critical time schedules of imaging after iv injection. It provides a powerful means in assessing the true size of low flow areas adjacent to morphological changes.

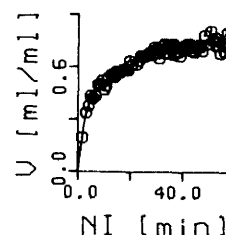
No. 51

BLOOD-BRAIN TRANSFER OF [^{99m}Tc]HMPAO IN HUMAN PARIETAL CORTEX IN VIVO. N. Rossing¹, H. Diemer¹, F. Pedersen¹, S. Holm³, D.F. Wong⁴, and A. Gjedde². ¹Finsen and ²Panum Institutes, Copenhagen University, ³NOVO Diagnostic Systems, Copenhagen, and ⁴Johns Hopkins Medical Institutions, Baltimore, MD.

Blood-brain transfer and binding constants of [^{99m}Tc]HMPAO were measured in normal, young male volunteers who received 20 mCi of this putative CBF indicator i.v. Arterial and parietal cortex radioactivities were monitored continuously for 45 minutes, using the NOVO Tomograph 810 (SPECT). The calculated virtual volumes of distribution (V, unit ml/ml) as function of the normalized arterial time-radioactivity integral (NI, unit minutes) are represented in the graph shown below:

The differential equations governing the transfer between plasma, free and bound HMPAO were solved for the four parameters K₁ (clearance), k₂ (efflux), k₃ (binding), and k₄ (release from binding):

Constant	Estimate ± SD
K ₁ (ml/ml/min)	0.215 ± 0.032
k ₂ (per min)	0.518 ± 0.111
k ₃ (per min)	0.049 ± 0.014
k ₄ (per min)	0.056 ± 0.009



Thus, the partition coefficient of HMPAO is only 0.42 ml/ml and the initial extraction no more than 40%. We conclude that HMPAO is not irreversibly bound and that full description of the uptake, using all four constants, is necessary to calculate CBF with this agent.

No. 52

STUDY OF CHRONIC CEREBRAL INFARCTS BY 123-I-iodo AMPHETAMINE (IMP) AND 133-Xe SPECT AND BY PET, SIGNIFICANCE OF THE PERIPHERAL AREA. C. Raynaud, G. Rancurel, J.P. Soucy, J.C. Baron, Y. Samson, N.A. Lassen, E. Cabanis, A. Majdalani, M. Bourdoiseau, S. Ricard, M. Bourguignon and A. Syrota. Service F. Joliot, CEA, Orsay. Hôpital La Salpêtrière, Paris, France.

Chronic cerebral infarcts are known to present a larger IMP hypofixation area than the infarct zone defined by the X ray CT hypodense (CT+) image. The existence of a functionally depressed peri-infarct zone suggested by these results was studied in 17 chronic cerebral infarcts with IMP at 10th min and 5th hour and with 133-Xe for rCBF, using a highly sensitive SPECT system, TOMOMATIC 64. Two types of decreased IMP uptake areas were differentiated.

One presented a marked hypofixation at 10th min and 5th hour, with respective mean of -35 and -26 %. This CT + area corresponded to the infarct zone and was characterized by a decrease of rCBF, mean : -46 %, and of rCMRO₂ and rOER in 4 cases studied by PET.

The other, the peripheral area, surrounded the infarct area and presented a slight hypofixation at 10 min, mean -16 %. It was also characterized by a normal Xray CT image, subnormal IMP5H uptake, mean -8 %, and a slight rCBF decrease, mean -23 % ; rCMRO₂ were subnormal or normal. The size of this area ranged from 2 to 72 % of a hemisphere and appeared to correlate to the neurological status of the patient, the largest peripheral areas being found in patients with severe sequelae, the smallest in patients with complete remission. This area persisted for months and was still seen once in the 3rd year ; it may be explained by deafferentation or selective neuronal loss.

No. 53

ASSESSMENT OF I-123 IMP SPECT IN MILD/MODERATE AND SEVERE ALZHEIMER'S DISEASE. S.P. Mueller, K.A. Johnson, D. Hamil, R.J. English, S.J. Nagel, M. Ichise, B.L. Holman. Harvard Medical School, Boston, MA.

We studied the potential of I-123 N-isopropyl p-iodoamphetamine (IMP) SPECT in the diagnosis of Alzheimer's disease (AD). All 27 AD patients (pts) underwent detailed neurological examination laboratory tests and CT scans and matched research criteria for AD (McKhann); 17 had severe dementia (Blessed dementia scale BDS > 25) and were institutionalized; 10 pts were mildly to moderately demented (BDS < 25). The pts were compared to 9 age-matched normal controls (nl) who were all gainfully employed or living independently. None of the pts or nl had any history or neurological sign of stroke (Hachinski score < 4). SPECT imaging was performed 15 min after iv. injection of 5 mCi IMP using a rotating gamma camera with a long bore collimator. The reconstructed resolution after prefiltering of the projection data with a 2D Butterworth filter (cutoff .4 cm, order 20) was 1.8 cm FWHM. The IMP activity measured in 1.2x2.4 cm ROIs over frontal, temporal, parietal and visual cortex was normalized to the cerebellar uptake. While there was considerable overlap between AD and nl for the ratios of frontal, temporal, and visual cortex, the parietal ratio ranged from .71 to .90 in nl and from .31 to .75 in AD pts. With a cutoff of .71, all 17 pts with severe dementia and 8/10 pts with mild to moderate disease were correctly classified. The characteristic pattern of IMP SPECT scans in AD shows a promising ability to identify AD even in earlier stages of the disease.

3:30-5:00

Room 38

ONCOLOGY II: PET AND CENTRAL NERVOUS SYSTEM METABOLISM

Moderator: Frank H. DeLand, MD
Comoderator: Thomas P. Haynie, MD

No. 54

METABOLIC AND HEMODYNAMIC STUDIES OF GLIOMAS USING POSITRON EMISSION TOMOGRAPHY (PET).

J.L. Tyler, M. Diksic, J-G. Villemure, A.C. Evans, Y.L. Yamamoto, W. Feindel, Montreal Neurological Institute
PET was used to evaluate 15 patients suspected of having high grade cerebral gliomas. All patients were studied before any intervention was undertaken. Measurements of cerebral glucose and oxygen metabolism, oxygen extraction, and blood flow and volume were done in all patients. In addition, pH values were obtained in 6 cases. These patients were later proven by biopsy to have gliomas; 3 were Grade II, one was Grade III, and 12 were Grade IV.

Compared to homologous regions in the contralateral hemisphere, tumor tissue demonstrated decreased oxygen extraction and oxygen metabolism, and increased blood volume. Compared to Grade II tumors, Grade IV tumors demonstrated higher relative oxygen extraction and utilization, and higher blood volumes. Tumor blood flow was variable, but tended to be higher in the higher grade tumors. Rates of glucose utilization in tumor, using individually calculated rate constants, were variable, and did not correlate with tumor size or tumor grade. These findings differ from results obtained from studies of gliomas after radiation and/or chemotherapy. Parietal tumors (N = 6) tended to have higher relative glucose utilization and blood flow, and lower relative oxygen extraction, when compared to frontal tumors (N = 4). Tumor pH differed significantly from the pH in contralateral brain (p .005); despite uncoupling of oxygen and glucose metabolism consistent with anaerobic glycolysis, alkalotic pH values were consistently seen. Primary cerebral gliomas and surrounding cerebral tissue studied before intervention are different metabolically and hemodynamically from similar tissues after exposure to radiation or chemotherapy.
This research is supported by NIH and MRC grants.

No. 55

SERIAL PET STUDIES OF HUMAN CEREBRAL MALIGNANCY WITH [1-¹¹C]PUTRESCINE (¹¹C-PUT) AND [1-¹¹C]2-DEOXY-D-GLUCOSE (¹¹C-2DG). E. Hiesiger¹, J. Logan², A.P. Wolf², J.D. Brodie³, D. McPherson², R.R. MacGregor², J.S. Fowler², D.R. Christman², and E. Flamm⁴. ²Chemistry Department, Brookhaven National Laboratory, Upton, NY; ¹Neurology, ³Psychiatry, ⁴Neurosurgery Departments, NYU Medical Center, NY, NY

Serial PET measurements of ¹¹C-PUT uptake and GMR (using ¹¹C-2DG) were made on eight human subjects with a radiological and, in most cases, pathological diagnosis of primary or metastatic brain tumor. Tumor uptake of ¹¹C after ¹¹C-PUT injection was unidirectional peaking at 15 minutes. Time-activity data for tumor and plasma were used to calculate blood-to-brain influx constants (K_i) (Patlak, et al, J. Cereb. Blood Flow Metab. 3:1, 1983). The mean K_i's for ¹¹C-PUT for tumor and normal brain tissue were 0.078 ± 0.045 and 0.024 ± 0.007 ml g⁻¹ min⁻¹ respectively (ratio:3.25) whereas the ratio of GMR for tumor and normal brain tissue was 1.2 ± 0.5. The mean K_i for high grade astrocytomas was 0.098 ± 0.030 (n=4) in contrast to 0.027 ± 0.008 ml g⁻¹ min⁻¹ (n=2) for low grade astrocytoma. Active, high grade astrocytomas also showed marked CT contrast enhancement and regional glucose hypermetabolism. In one subject, both ¹¹C-PUT and GMR correlated with declining clinical pictures in repeated studies over a 4 month period. These results support the contention that PET studies with ¹¹C-PUT are useful for locating small hypometabolic tumors providing a far better signal:noise ratio than GMR measurements and also an index of degree of malignancy when used in longitudinal studies in a single subject.
Research supported by DOE, OHER and NIH Grant NS-15638.

No. 56

METABOLIC AND STRUCTURAL FINDINGS RELATED TO WHITE MATTER DISORDERS AS SHOWN BY PET, MRI AND CT. J.B. Alavi, A. Alavi, J. Powe, D. Hackney, M. Reivich. Hospital of the University of Pennsylvania, Philadelphia, PA. 19104

We and others have observed locally decreased cortical metabolism in areas adjacent and remote from brain tumors. We have analyzed 18F-FDG PET scans of 28 pts with cerebral astrocytomas, to look for possible correlations with other brain disorders. All pts had CAT scans and most had MRI scans. A Laterality Index (L.I.) was calculated from the PET studies. The L.I. is the percent difference in metabolism between the two hemispheres at certain areas of interest. When quantitative data were not available, the PET visual images were examined for areas of cortex which showed suppression of metabolism.

In 19 cases, there was at least 1 area of depressed metabolism ipsilateral to the tumor, with L.I. of 20-84%. Most of these pts had "hot" tumors; all but 1 of these pts had CAT or MRI evidence of probable peritumoral edema or extensive tumor in the white matter. In 9 cases with no suppression or less than 20% L.I., the CAT and MRI showed no white matter disease or else white matter change which was more compatible with radiation leukoencephalopathy than edema. Only 1 of these 9 patients had a "hot" tumor, all others were low grade tumors or clinically indolent grade III astrocytomas, with low or normal metabolic activity.

We have observed that ipsilateral cerebral glucose metabolism is often suppressed in patients with brain tumors. We suggest that this may be a remote effect of edema. It appears that white matter damage from radiation therapy, when it does not induce edema, is not associated with the same degree of metabolic suppression.

No. 57

C11-METHIONINE AND F18-DEOXYGLUCOSE (FDG) IN THE POST-OPERATIVE MANAGEMENT OF PATIENTS WITH BRAIN TUMORS WITH POSITRON EMISSION TOMOGRAPHY. N.D. LaFrance, J. Links, J. Williams, H. Holcomb, R. Dannals, H. Ravert, A. Wilson, H. Drew, S. Herda, D. Wong, H. Brem, D. Long, H. Wagner, Jr. The Johns Hopkins Medical Institutions, Baltimore, MD.

C11-methionine and FDG studies were performed in patients with known brain tumors who had had a recurrence of neurological symptoms. Prior to the PET study, there was uncertainty about the persistence or recurrence of the tumor or the presence of radiation necrosis. Most patients had CT and NMR as well as PET. Before each PET scan, the neurosurgeons described their proposed course of treatment based on clinical, CT and NMR evidence alone. They then recorded how the PET data affected their management plan. In 5/5 patients the surgeons concluded that the data from the PET scan modified their approach to the solution of the patient's problem. As reported by Lilja and others, the extent of the tumor was predicted better with C11-methionine than with FDG. With FDG, the size of the affected areas of brain was usually larger than the tumor itself, reflecting the secondary effects on regional brain metabolism. The decision to operate, the surgical approach, and the extent of surgery were influenced by the PET results.

Our preliminary data suggest that PET imaging: 1) influences the neurosurgeons' management of brain tumor patients; 2) helps differentiate tumor from radiation necrosis; 3) helps delineate the extent of tumor; and, 4) provide information about the metabolic effects of the tumor.

No. 58

GRADING OF BRAIN TUMORS BY C-11-L-METHIONINE PET O. Schober, G.-J. Meyer, M.R. Geab, J.A. Müller, and H. Hundeshagen. Medical School Hannover, D-3000 Hannover 61, West Germany.

MRI and CT give a high accuracy in the detection and differential diagnosis of brain tumors, but an exact delineation and grading of malign tumors are not always met. It is the purpose of the study to evaluate uptake of C-11-methyl-L-methionine in tumors to non-tumor ratios (T/NT) for the clinical need for differential diagnosis.

Methionine uptake was measured in 32 pts (F-18-FDG: 12/36 pts) with brain tumors prior to surgery, and in 6 patients with strokes, using PET. The diagnosis was ascertained by CT, MRI, angiography, histologically and in 8/36 pts by Tc-99m-scan.

A penetrable blood brain barrier (BBB) is not a prerequisite for methionine accumulation. Relevant details are given in the table.

Pts	Diagnosis	C-11-L-Methionine T/NT
8	astro/glio IV	2.5 (1.8-3.1)
5	astro/glio II-III	1.8 (1.6-2.8)
9	astro/glio II	1.3 (0.9-1.6)

4	metastasis	1.7 (1.3-2.1)
4	meningeoma	2.3 (1.9-2.7)
6	stroke	0.6 (0.4-0.8)

PET, MRI and CT are complementary with regard to extent of tumor tissue, necrotic areas and edema. It is concluded that the uptake reflects metabolic activity in brain tumor tissue rather than a diffuse uptake due to BBB damage. PET with glucose has limitations with regard to delineation of low-grade astrocytomas, while PET with C-11-L-methionine usually reflects the extent of tumors better.

No. 59

GALLIUM-68 COLLOID TOMOGRAPHIC LIVER IMAGING WITH A POSITRON CAMERA. P. Frey, G. Schaller, D. Townsend, R. Egeli, H. Tochon, A. Christin, O. Huber, A. Rohner, G. Reich, B. Ody, R. De Gautard, G. Banna, A. Jeavons, A. Donath; University Hospital of Geneva, Switzerland.

A high resolution positron camera has been used for positron emission tomography (PET) of the diseased human liver in-vivo. The patients included in this on-going study present with primary and metastatic liver malignancy, the clinical diagnosis confirmed by histological examination from a liver biopsy obtained prior to the PET study. Tomographic images are made 20 min. after i.v. administration of the positron emitting radionuclide Ga-68 (physical half-life: 68 min.) in the form of Ga-68 labelled colloids, with activities varying between 2 and 4 mCi to patients scheduled for intraarterial, loco-regional chemotherapy of their liver disease.

The preliminary results obtained from a small patient group show clearly the superiority of PET liver imaging for the detection and precise localisation of liver malignancies, when compared to planar scintigraphy and to SPECT imaging using Tc-99m labelled colloids. The PET results are also in good agreement with the results obtained from CT and Ultrasound liver imaging. Calculations of the total and regional functional liver volume from both the initial PET study and a follow-up study provide new insight into tumour tissue replacement, which reflects the effectiveness of loco-regional chemotherapy. It is hoped to display PET data of individual cases as a three-dimensional (liver) object using shaded graphics techniques, offering a global view of the diseased liver before and following chemotherapy. This approach has already proved successful for the display of tomographic images of the thyroid.

3:30-5:00

Room 40

CARDIOVASCULAR II: MYOCARDIAL METABOLISM & VIABILITY

Moderator: Heinrich R. Schelbert, MD, PhD
Comoderator: R. Edward Coleman, MD

FEATURE PRESENTATION

Radionuclide Radius of Myocardial Metabolism
Heinrich R. Schelbert, MD, PhD

No. 60

GLUCOSE METABOLISM IN POST-ISCHEMIC CANINE MYOCARDIUM. M. Schwaiger, R. Neese, W. Wijns, J. Wisneski, M. Grover-McKay, M.E. Phelps, H.R. Schelbert, and E. Gertz. UCLA School of Medicine, Los Angeles, CA and UCSF School of Medicine, San Francisco, CA.

F-18 deoxyglucose (FDG) uptake is frequently increased in ischemic and in reperfused myocardium and indicates tissue viability. Because FDG traces only the initial uptake and phosphorylation of glucose, the meta-

bolic fate of glucose was studied with [6-¹⁴C] glucose, infused intravenously in 8 dogs 24 hrs after a 3-hr balloon occlusion of the left anterior descending artery (LAD). Blood samples were withdrawn simultaneously from the left atrium (art), LAD vein and coronary sinus (CS) and plasma concentrations of chemical and labeled glucose, CO₂ and lactate determined. Compared to the entire heart (art.-CS), glucose extraction by reperfused myocardium (art.-LAD vein) was 68% higher and averaged 0.37±0.15 μmol/mL. Of the extracted glucose, 72±15% was metabolized to C-14 CO₂ (43%) or C-14 lactate (57%). The remaining 28% entered an undefined storage pool. The CO₂ fraction of extracted glucose was inversely related to plasma free fatty acid levels (r=-0.86). Thus, increased FDG uptake in reperfused myocardium reflects increased glucose extraction. Glucose is largely metabolized anaerobically as indicated by lactate release. Residual glucose oxidation occurs probably in cells responsive to normal regulatory mechanisms as shown by the relationship to plasma free fatty acid levels. Thus, reperfused myocardium contains myocytes in which anaerobic glycolysis persists for prolonged time periods after restoration of blood flow. The persistence of anaerobic glycolysis can be demonstrated noninvasively with PET and FDG.

No. 61

SEVERITY OF SEGMENTAL MYOCARDIAL BLOOD FLOW REDUCTION AND PERSISTENCE OF METABOLIC ACTIVITY IN PATIENTS WITH CHRONIC ISCHEMIC HEART DISEASE. R. Brunken, M. Schwaiger, J. Tillisch, R. Marshall, M. Phelps, and H. Schelbert. UCLA School of Medicine, Los Angeles, CA

Persistence of glucose metabolism in hypoperfused myocardial segments on PET distinguishes viable from infarcted myocardium. We hypothesized a relationship between persistence of metabolic activity and the severity of the blood flow deficit. Thus, 13 patients with chronic ischemic heart disease were studied with PET using tracers of blood flow (N-13 ammonia, NH₃) and glucose metabolism (F-18 deoxyglucose, FDG). Five ventricular segments were analyzed: septal, anterior, lateral, apical and inferior. Normalized tracer concentrations were calculated for each of 12, 30° sectors on circumferential activity profiles of each cross-sectional image. Relative concentrations were corrected for partial volume effect by use of ratios derived from the study of normals. Using previously reported criteria, 34 segments with depressed NH₃ were identified. In 20 segments with depressed FDG activity (PET infarct), mean relative NH₃ activity was 44.7±10.8%. In contrast, in the 14 segments with preserved FDG activity (PET ischemia), mean relative NH₃ activity was 61.2±20.0% (p<0.01). In PET infarction, the decrease of FDG activity paralleled that of NH₃ (44.0±9.1%, FDG/NH₃=0.99), while in PET ischemia FDG activity was augmented relative to NH₃ (83.8±10.7% FDG/NH₃=1.37). Thus, residual metabolic activity can persist and glucose utilization is accelerated relative to blood flow when myocardial perfusion is moderately severely depressed. More severe flow reductions are associated with concordant decreases in glucose utilization, suggesting tissue necrosis.

No. 62

METABOLIC STUDIES OF 15-(ORTHO-I-123-PHENYL) PENTADECANOIC ACID IN CORONARY ARTERY DISEASE. M.A. Antar*, G. Spohr, H. Herzog, H.-J. Machulla, E. Vester, B. Schwartzkopf, B. Lössle and L.E. Feinendegen. Institute of Medicine Nuclear Research Center, Jülich, Jülich, FRG, and *Univ. of Conn. and V. A. Medical Center, Newington, CT.

We have reported that in coronary artery disease (CAD) patients, 15-(Ortho-I-123-phenyl pentadecanoic acid) (o-IPPA) was avidly incorporated by the normal myocardium and retained for several hours suggesting some "trapping" mechanism. This is in contrast to findings in rodents. In vivo kinetics of o-IPPA were investigated in 15 fasting stressed male patients with CAD for 70-90 min. Radiobio-

chemical analyses were performed on blood samples up to 60 min. using Folch et al method, and radiochromatography. After the initial perfusion phase, myocardial radioactivity was retained for several hours with long T_{1/2} (>200 min). The elimination of the radioactivity from the blood was rapid (an initial component with T_{1/2} of 0.73±.23 min, followed by another with T_{1/2} 219±47 min). The activity in the aqueous phase (including iodides, hippuric and benzoic acids) remained at less than 10% of the initial organic activity, even at 30 minutes, suggesting either slow catabolism or minimal accumulation of the aqueous metabolites in the blood. These findings are in contrast to those with p-IPPA where at 20 minutes the water soluble catabolites in the plasma had reached 80% of the initial activity. Chromatography of the organic phase showed only one major peak (95%) of the original tracer (o-IPPA) and some minimal activity in the triglyceride band. These findings suggest that o-IPPA is not or very slowly, converted to final labelled organic catabolites in the plasma.

No. 63

MYOCARDIAL IMAGING WITH IODINE-123 PHENYLPENTADECANOIC ACID IN ISCHEMIC HEART DISEASE. CL Hansen, PV Kulkarni, JT Willerson, V Ugolini, PL Kennedy, DE Jansen, LM Buja, KW Parkey, JR Corbett. Univ. Texas Health Science Center at Dallas, TX.

In this study, we tested the hypothesis that I-123 phenylpentadecanoic acid (IPPA) imaging with single photon emission tomography (SPECT) is useful in the identification of patients (Pts) with ischemic heart disease (IHD). Nine normal volunteers (age 27.2 ± 2.0 yrs) (± SD) and 15 Pts (age 53.3 ± 9.3 yrs) with IHD were studied with symptom limited treadmill exercise. IPPA (4-8 mCi) was injected 1 minute (m) prior to termination of exercise, and SPECT imaging was performed at 9 m and repeated at 40 m following injection. Normals showed uniform segmental IPPA activity and washout. Pts showed a maximal variation (MxV) in IPPA activity on 9 m images of 35.5 ± 14.2%, on 40 m images of 32 ± 14%, and a MxV in washout rate of 21.6 ± 7.1%. Fourteen of 15 Pts had MxV in IPPA activity >2SD outside the normal range, and 14 of 15 had variations in IPPA washout >2 SD outside the normal range. Thirteen of 15 Pts had a least 1 segment with IPPA washout >2 SD below the normal range. All Pts had abnormalities (>2SD) in at least 2 of the variables measured. There was excellent agreement between coronary anatomy and IPPA, 19 of 25 vessels stenosed ≥ 70% showed corresponding areas of abnormality. Nine Pts with myocardial infarcts (MI) were studied at rest. All Pts demonstrated marked reductions in activity (46.4 ± 11.9%) and washout (2.4 ± 4.5%) in MI segments. We conclude that IPPA imaging with SPECT and exercise is a highly sensitive means to detect significant IHD noninvasively. *p > 0.001.

No. 64

N13 GLUTAMATE AS A MYOCARDIAL IMAGING AGENT IN MAN. P. Rigo, J. Beckers, C. De Landsheere, V. Mahaux, G. Delfiore, J.M. Peters, L. Quaglia, D. Lamotte, H. Kulbertus, University of Liege, Cyclotron Research Centre and Malvoz Institute, Liege, Belgium.

Myocardial uptake of N13 glutamate (G) is high and related to regional flow and to metabolic extraction. It has been suggested that the uptake of G could be increased in patients (pts) with ischemia.

In this study, we have analysed data in 17 pts. Three control subjects (CS) and 11 pts with CAD underwent rest and stress G positron emission tomograms at 3 levels of the myocardium. Three additional pts had tomograms before and after dipyridamole infusion with isometric exercise. Comparative rest-stress tomograms were also obtained with N13 ammonia as a reference flow tracer. Pts were divided into 2 groups : 6 pts with myocardial infarction and 8pts with exercise-induced ischemia. Data were normalized to

the region of maximum uptake. Normal regional myocardial uptake (RMU) was defined in CS and averaged 96.2±5% at exercise. G resulted in a high target to background ratio with little lung uptake. RMU in infarct regions was decreased to 41.1±8.6% at rest and 37.3±6.6% during exercise (NS). In pts with ischemic response RMU decreased from 84.3±3.1% at rest to 75.1±3.8% (p<.02) after exercise and from 76.4±8.5% at rest to 47.3±5.7% (p<.01) during dipyrindamole infusion. N13 ammonia scans when performed showed similar directional changes in the ischemic and non ischemic regions.

We conclude that N13 G gives excellent definition of the myocardium with high target to background ratio. G myocardial uptake appears to decrease in ischemic regions as compared to normal tissue illustrating the flow dependence of the uptake mechanism.

3:30-5:00

Room 27

RADIOASSAY

Moderator: Howard J. Dworkin, MD
Comoderator: Avir Kagan, MD

No. 65

ASSOCIATION OF CYCLOSPORIN A WITH HUMAN SERUM PROTEINS. C.A. Pickering and D.E. Drum, Radioassay Laboratory, Department of Radiology, Harvard Medical School and Brigham and Women's Hospital, Boston, MA

Cyclosporin A (CsA) is a neutral, highly lipophilic, cyclic endecapeptide proven to be a very effective immunosuppressant. Because its nephrotoxicity is a major side effect, post-dose trough levels in serum are measured by RIA. As in evaluating other therapeutic drugs, we examined the binding of CsA to serum proteins in an initial step toward identifying nephrotoxic moieties.

At 200 ng/mL, less than 10% of H-3-labeled CsA or unlabeled CsA or CsA added to serum and filtered immediately passes through 30,000 MW cutoff membrane ultrafilters as measured by RIA. By this method the "free" CsA found in serum from 9 renal transplant patients varied from 0 to 35% and for 9 heart transplant patients from 0 to 31%. Although "free" CsA varied widely from patient to patient, individuals exhibited approximately the same fraction when studied weekly for 12 week periods.

Diversity of binding proteins and/or metabolites was exhibited by Sephadex G-25 filtration in 0.9% saline, a solvent in which CsA behaved as expected for its size. For all samples studied, several peaks of CsA eluted between totally excluded (Vo) and totally diffusible (Vt) solutes. The major CsA peaks for a given patient tended to occur at the same elution volume on different sampling days, whereas there was greater interpatient variation.

Jointly these simple techniques provide a convenient means for studying laboratory correlates of both nephrotoxicity and successful immunosuppression. Whether our data are consistent with hypotheses that all serum CsA is associated with lipoproteins remains to be established.

No. 66

CLINICAL PERFORMANCE OF A NEW DIRECT CEA ASSAY. L.R. Witherspoon, S.E. Shuler, H.R. Neely, K. Aleya. Ochsner Medical Institutions, New Orleans, LA 70121.

We evaluated a CEA assay requiring no sample pretreatment (Diagnostic Products Corporation (DPC)) employing antisera raised against CEA in goats. This assay and the Abbott polyclonal (A-P) and monoclonal (A-M) RIAs yield essentially equivalent results (*Clin Chem* 31:981, 1985). DPC-CEA between assay CVs (8 assays) were 7.3-10%. We measured CEA in 88 normal subjects (19 smokers), 91 ill patients, and in 473 samples from 193 patients with colon or rectal CA (27

preoperatively, 111 followed 6-20 mo.). Metastatic or recurrent CA was present at the time of 120 samplings. CEA-DPC was <3.5 in 90% and <5.0 ng/ml in 100% of normal non-smokers. It was 5.0-8.5 in 21% of smokers and 5-9.5 ng/ml in 19% of ill patients. In bowel CA patients, sensitivity/specificity was:

For 3.5 ng/ml:
True + 67%, False - 23%
True - 83%, False + 17%
For 5.0 ng/ml:
True + 52%, False - 48%
True - 94%, False - 6%

CEA-DPC remained normal in 3 patients, was elevated before (2-8 mo) in 4, and coincident with clinical recurrence in 5; and paralleled disease course in 29 patients. Discrepant results occurred in 10 of 193 patients. CEA was elevated, no mets (A-M 5, DPC 1, A-P 1) or normal, mets (A-M 1, DPC 3, A-P 1). DPC provides a clinically effective measure of CEA.

No. 67

CAN THE SCHILLING TEST BE REPLACED BY A RESORPTION TEST WITH COLD VITAMIN B12 ? E. HENZE, S. MANNER, W.E. ADAM, UNIVERSITY OF ULM, GERMANY

It was the purpose of this study to evaluate the diagnostic usefulness of an oral resorption test using non-labeled B12 as suggested by a commercial distributor as an alternative for the more expensive Schilling test (ST). Plasma levels of cold B12 were measured with a commercial kit before and 4 hrs after oral administration of 1 mg B12 in 36 normals, in 16 pts with normal ST (group 1) and in 11 pts with abnormal ST (group 2) for determination of sensitivity (SE) and specificity (SP) with the ST as golden standard. In normals, a mean±SD of 767.4±404.3 pg/ml before and 1095.8±775.8 pg/ml after oral B12 with a mean increase due to resorption of 331.4±452.8 pg/ml was measured. Because of the obvious large variation and a non-Gaussian distribution of the mean increase, no meaningful value of normal resorption by using +2SD of normal could be established. Assuming a minimum increase required in normal resorption of 100 pg/ml as suggested by the kit distributor, only a SE of 27% and a SP of 75 % was calculated from the results in pts groups 1 and 2, whereas an assumed minimum increase of 200 pg/ml resulted in a SE of 55% and a SP of 50%. There was also no correlation in the 27 pts between ST and the resorption test with r=0.0075. The lack of any diagnostic value of this approach might be caused due to the known passive resorption of approximately 1% of any B12 given orally even in complete absence of intrinsic factor and due to the relatively large amount of orally administered B12 (at least 1 mg) needed for a "cold" resorption test. The latter can thus, in conclusion, not replace the Schilling test.

No. 68

RACIAL DEPENDENCE OF SERUM VITAMIN B12 LEVELS. I-W Chen, E.B. Silberstein, C.P. Volle, L.A. Heminger, H.R. Maxon. E.L. Saenger Radioisotope Laboratory, University of Cincinnati Medical Center, Cincinnati, Ohio 45267.

Higher B12 levels have been reported in black (compared with white) adults living in the United States, and the use of separate reference ranges for these two populations has been suggested (*J. Nucl. Med.* 26:790, 1985). In order to gain further insight into this difference, we measured B12 levels and unsaturated Vitamin B12 binding capacity (UBBC) in 59 black (42 males and 17 females) and 65 white (44 males and 21 females) blood donors, ranging in age from 17 to 66 years. A liquid-phase no-boil radioassay kit from Diagnostic Products Corp. (Los Angeles, California) was used for B12 measurements and ⁵⁷Co-labeled Vitamin B12

obtained from the same company was used for UBBC measurements. The following mean values \pm 1SD were obtained:

Race	B ₁₂ (pg/ml)	UBBC (pg/ml)
Black	504 \pm 205*	722 \pm 190*
White	385 \pm 146	520 \pm 175

* Significant race difference at $p < 0.001$

Blacks had higher mean serum Vitamin B₁₂ levels than whites. The reference ranges calculated from mean and standard deviation values were 94-914 and 93-677 pg/ml, respectively. Although elevated Vitamin B₁₂ levels were accompanied by higher UBBC among blacks, there was no statistically significant correlation between these two values, suggesting that elevation of Vitamin B₁₂ and UBBC among blacks was probably attributable to different causes.

No. 69

ADAPTATION OF AN AFP RADIOASSAY METHOD FOR OPTIMAL CLINICAL USE AT LOW LEVELS. K. Najpauer and D.E. Drum, Radioassay Laboratory, Department of Radiology, Harvard Medical School and Brigham and Women's Hospital, Boston, MA

Recent reports suggesting an association of Down's syndrome with low values for maternal serum AFP (MSAFP) have led to application of methods designed originally for high value analytical and statistical evaluation. Low-end performance of these methods has not been well documented.

In order to avoid low-end errors we investigated practical modifications to a well established FDA-approved vendor's materials and procedures for a standard double antibody radioimmunoassay using I-125 readout. By extending a recommended incubation time from 4 to 18 hours at 37°C and by changing the diluent for standards from "low AFP" serum to 0.5% HSA-saline, we find a technically improved assay. The low-end sensitivity is less than 1 IU/mL ($p < .05$). Dilution linearity is observed from 1 to 180 IU/mL, intersecting the origin. Intraassay precision (as \pm 1 S.D.) at 3 and 9 IU/mL is 20% and 5%, respectively, and recovery is 100 \pm 10% at 5 IU/mL. Over the range 5 to 98 IU/mL our relation to the CDC Biological Standard is linear, with [WHO value] = 1.00 [BWH value] + 0.47 IU/mL ($p < .01$).

Measurements of 500 consecutive MSAFP values, like those done in paired fashion with our reference laboratory, exhibit closely log-normal distributions at each gestational week, thus obviating the need to employ "multiples of the median" for defining normality at either high or low values.

No. 70

THE DEVELOPMENT OF A RADIOENZYMATIC ASSAY FOR URINARY SALSOLINOL. V.M. Camp, J.D. Lenton, T.W. Stammers, S.R. Lee, and B.A. Faraj, Emory University School of Medicine and Veterans Administration Medical Center, Atlanta, GA.

In vivo formation of a mammalian morphine-like alkaloid, salsolinol (SAL), a condensation product of dopamine and acetaldehyde, may play a role in alcoholism. This hypothesis, which has been controversial, has been difficult to test because of a lack of assays sufficiently specific or sensitive to detect the formation of this putative mammalian alkaloid. The present study reports the development of a single-isotope radioenzymatic assay for the simultaneous measurement of SAL and D in diluted urine. The technique involved the conversion of SAL and D in the sample to their respective radioactive O-methylated metabolites by the enzyme catechol-O-methyltransferase and (methyl-3-H)-S-adenosyl-methionine (5 μ Ci). A rapid thin-layer chromatographic separation of the formed tritiated metabolites contributed to the specificity of the differential assay of SAL and D. With the availability of this assay, we were able to study urinary SAL and D in hospitalized male alcoholics at

admission (group A, n=20) and recovering male alcoholics (group B, n=7) with 2-5 years of abstinence. The results of this study demonstrated that alcoholics (group A, 6.11 + 3.21 ng/ml; group B, 6.20 + 5.5 ng/ml) excreted significantly ($p < 0.045$) higher levels of SAL as compared to controls (1.0 + 1.5 ng/ml). In contrast, high D output was noted only in active alcoholics. These preliminary findings demonstrate the prevalence of high endogenous output of SAL in alcoholics.

3:30-5:00

Room 31

RADIOPHARMACEUTICALS I: Tc-99m CHEMISTRY

Moderator: Alun G. Jones, PhD

Comoderator: Gopal Subramanian, PhD, MD, MS

No. 71

BORONIC ACID ADDUCTS OF TECHNETIUM OXIME COMPLEXES (BATOes) A NEW CLASS OF NEUTRAL COMPLEXES WITH MYOCARDIAL IMAGING CAPABILITIES. A.D. Nunn, E.N. Treher, T. Feld. Squibb Institute for Medical Research, New Brunswick, NJ.

A new technetium labelled myocardial imaging agent has been developed. The compound is Chloro (Methylboron(1-)-tris[1,2-Cyclohexanedionedioxime]N,N',N'',N''',N'''' ,N''''') Technetium (SQ 30217).

SQ 30217 is a member of a totally new class of neutral, seven coordinate technetium complexes (the BATO complexes) where the oximes, boron R groups or capping ligand can be varied together or independently. These complexes represent a major departure from preceding radiopharmaceutical chemistry because the selectivity and chelating portions of the molecule are separated until the final complex is synthesized. This is done in quantitative yield at the no-carrier-added level via template synthesis around the technetium atom upon reconstitution and heating of a lyophilized kit. The complexes can also be made at the carrier level starting from pertechnetate plus reducing agent or TcOCl₄⁻ and TcCl₆³⁻.

SQ 30217 has been fully characterized by x-ray crystallography, FAB- FD-, DCI- and LC-MS, conductivity, IR, UV-VIS, elemental analysis, photoelectron spectroscopy and chromatography. The coordination sphere of the technetium atom consists of three (N bonded) cyclohexanedionedioxime molecules and one chlorine atom. The technetium has a mono capped distorted trigonal prismatic geometry. The dioxime molecules are held together at one end of the molecule via a proton bridge in which only two hydrogen atoms are shared by three oxygen atoms. The other end of the molecule is held together by a methylboron cap through the remaining three oxygen atoms of the oxime groups.

No. 72

IMAGING OF MYOCARDIAL PERFUSION WITH TC-99M SQ 30217: DOG AND HUMAN STUDIES. R.E. Coleman, M. Maturi, A.D. Nunn, W.C. Eckelman, P.N. Juri, F.R. Cobb. Duke University Medical Center, Durham, NC, and Squibb Institute for Medical Research, New Brunswick, NJ.

This study evaluates Tc-99m labeled Chloro(methylboron(1-)-tris[1,2-cyclohexanedionedioxime(1-)]-N,N',N'',N''',N'''' ,N''''')Technetium (SQ 30217), a new Tc-99m myocardial imaging agent. Planar images were obtained in 8 normal dogs and in 13 dogs with infarction (4 of these also had TI-201 injections and 3 had a second Tc-99m SQ 30217 injection). In 9 volunteers and one patient with remote infarction, serial chest images were obtained following the administration of Tc-99m SQ 30217.

With Tc-99m SQ 30217, good myocardial images occur in the dog from 2-20 minutes. The radioactivity cleared rapidly from the lungs such that they were not visible

after one minute. Hepatic activity peaks between 4.5 and 7.0 minutes. The infarcts were seen as areas of decreased or absent activity in all 13 dogs. Tl-201 was used to confirm areas of decreased perfusion in 4 of the dogs given Tc-99m SQ 30217. The infarction could also be seen after a repeat injection of Tc-99m SQ 30217 given 30 minutes after the first.

In the 9 volunteers, the myocardium is visualized at 60 seconds and good visualization continuing through 20 minutes. One patient with remote myocardial infarction and abnormal resting Tl-201 images had abnormal Tc-99m SQ 30217 images.

Tc-99m SQ 30217 is a new myocardial perfusion imaging agent which gives good images of the myocardium. The normal clearance from the myocardium permits a second injection within thirty minutes which would allow stress/rest studies.

No. 73

DEVELOPMENT OF NONREDUCIBLE 99m-TECHNETIUM(III) CATIONS AS MYOCARDIAL PERFUSION IMAGING AGENTS. E. Deutsch, J.-L. Vanderheyden, P. Gerundini, K. Libson, W. Hirth, A. Savi, L. Zecca and F. Fazio. University of Cincinnati, Cincinnati, OH and Instituto San Raffaele, Milano, ITALY

This study was initiated in order to test the hypothesis that a nonreducible 99m-Tc(III) cation would not suffer myocardial washout in humans. One of the reasons that the Tc(III) cation $\text{tr-[}^{99\text{m}}\text{Tc}(\text{DMPE})_2\text{Cl}_2]^+$ fails as a myocardial perfusion imaging agent in humans is that it suffers in vivo reduction to the neutral Tc(II) form. This leads to washout of the Tc(III) complex from the myocardium and an unacceptably low heart/liver ratio. A new class of 99m-Tc(III) cations, containing a tetradentate- O_2N_2 Schiff base ligand and two monodentate tertiary phosphine ligands, has been developed. These complexes are not reducible in vivo, and correspondingly they do not suffer washout from the heart. Variations in the structures and properties of the Schiff base and phosphine ligands lead to a range of mixed ligand complexes which exhibit different biodistributions in test animals. The prototype for this new class of agents, $\text{tr-[}^{99\text{m}}\text{Tc}(\text{acac}_2\text{en})(\text{P}(\text{O}i\text{Pr})_3)_2]^+$, where acac₂en represents N,N'-ethylenebis(acetylacetonate iminato), has been evaluated in human volunteers at both rest and exercise. The resulting myocardial images are superior to those obtained with $\text{tr-[}^{99\text{m}}\text{Tc}(\text{DMPE})_2\text{Cl}_2]^+$ and no myocardial washout is observed. However, blood clearance is relatively slow and myocardial perfusion images are obtained only ca. one hour after injection. Chemical variations in the Schiff base ligand are likely to lead to other nonreducible Tc(III) agents that undergo more rapid blood clearance and yet do not suffer myocardial washout.

No. 74

ISONITRILE ESTER COMPLEXES OF TECHNETIUM. JF Kronauge, AC Jones, A Davison, J Lister-James, SJ Williams, SA Mousa. Harvard Medical School and Brigham and Women's Hospital, Boston, MA, Massachusetts Institute of Technology, Cambridge, MA and EI DuPont de Nemours & Company Biomedical Products, N. Billerica, MA.

A new group of technetium complexes containing isonitrile ligands bearing ester functionalities are being tested as improvements over the cation hexakis(*t*-butylisonitrile)technetium(+1) (Tc-99m TBI) for cardiac perfusion imaging. Among these, the cation hexakis(carbomethoxyisopropylisonitrile)technetium(+1) (Tc-99m CPI) shows much promise. In the guinea pig, cardiac uptake peaks at 0.5 min (2.1 ± 0.2 %ID/organ; mean \pm sd) clearing with a Tl/2 of 90 min. Tc-99m TBI peaks at 2 min (1.6 ± 0.3) and a Tl/2 of 9 h. Peak liver uptake is at 2 min (17.4 ± 0.8) with a Tl/2 of 35 min, but Tc-99m TBI levels continue rising to 2 h (24.9 ± 0.1). Lung uptake of Tc-99m CPI is 2.3 ± 0.4 at 0.5 min (Tc-99m TBI = 43.5 ± 7.6). Scanning in swine and rabbits gave heart images immediately after injection. Experiments in rabbits using

Tc-99m CPI, Tl-201 and Nb-95 microspheres show a linear distribution with blood flow: for CPI, slope 0.92, intercept 6.9%; for Tl-201, 0.9 and 5.9%. In a rabbit model of reperfusion, the slope and intercept for Tc-99m CPI became 0.76 and 18%, indicating a slight filling upon release of the ligation. For Tl-201 and Tc-99m TBI, the intercepts were 42% and 45%. The low initial lung uptake reflects the more hydrophilic nature of these ester complexes and the rapid liver clearance the hydrolysis of the ester groups to species more readily excreted, as intended. Tc-99m CPI is a promising agent for investigation in humans for myocardial stress studies.

No. 75

NEW Tc-99m MYOCARDIAL AGENT WITH LOW PLASMA BINDING AND FAST BLOOD CLEARANCE. D.W.Wester*, D.L.Nosco*, J.R.Coveney*, R.T.Dean*, P.Gerundini, L.Zecca, A.Savi and F.Fazio, *Mallinckrodt, Inc., St. Louis, MO and Hospital San Raffaele, Milan, Italy.

A series of bis- π -arene technetium(I) cations has been prepared by reaction of sodium pertechnetate, aluminum, aluminum chloride and suitable arenes. The cationic Tc(arene)₂⁺ complexes are purified by HPLC and characterized on the Tc-99 level by exact mass measurements using FABMS. Biodistribution studies show a number of complexes that have substantial myocardial uptake. For the methyl-substituted benzene derivatives, trends toward higher myocardial uptake, higher plasma binding and higher octanol-buffer extraction ratio with increasing number of methyl groups are observed, suggesting a relation between lipophilicity, myocardial uptake and plasma binding.

Gamma scintigraphy using trimethyl- and tetramethylbenzene complexes in dogs show that excellent myocardial images can be obtained after ten minutes, no doubt facilitated by rapid blood clearance and low plasma binding. In normal human volunteers, the same complexes show rapid clearance from the blood, relatively low plasma binding, and myocardial uptake.

No. 76

RELATION BETWEEN STRUCTURE AND RENAL TRANSPORT OF ISOMERIC METHYLDERIVATIVES OF Tc-99m MERCAPTOACETYLTRIGLYCINE A. Verbruggen, P. Dekempeneer, B. Cleynhens, M. Hoogmartens, M. De Roo. U.Z. Gasthuisberg, Nuclear Medicine, Leuven, BELGIUM.

Tc-99m MAG₃ (R) has been described (JNM 1986, 27:111) as a useful alternative to I-131 Hippuran. To study the structural requirements for optimal renal tubular transport we have synthesized the D-, L- and DL- isomers of the 3 possible derivatives of MAG₃ in which glycyl (G) is replaced by alanyl (ala): MAG₃-ala (A), MAG-ala-G (B) and MA-ala-G₂ (C). The compounds were labeled with Tc-99m by the dithionite reduction method and biodistribution was studied in mice 10 min after injection.

DL-, D- and L-Tc-99m-(A) did show a similar biological behaviour, nearly the same as that of (R). The diastereomers were also isolated but their renal excretion characteristics were not different.

L-Tc-99m-(B) is accumulated and retained mainly in the kidneys (70%), whereas the D-isomer is efficiently transported to the urine (69%). The properties of the DL-compound are intermediate.

A similar difference is observed for the isomers of Tc-99m-(C): the D-isomer is rapidly excreted into the urine, the L-isomer is retained in the kidneys.

It appears that methylsubstitution in the terminal carbonylglycine of (R) does not impair the efficiency of tubular transport, as has also been reported for Hippuran. Introduction of a methyl substituent in one of the other glycyl moieties can drastically alter renal handling, depending on the orientation (D or L) of the substituent.

3:30-5:00

Room 30

COMPUTERS & DATA ANALYSIS II: ECT RECONSTRUCTION TECHNIQUES

Moderator: Bernard E. Oppenheim, MD
 Comoderator: Michael A. King, PhD

No. 77

THE CIRCULAR HARMONIC TRANSFORM ALGORITHM FOR SPECT RECONSTRUCTION. W.G. Hawkins, P.K. Lechner, N.C. Yang, T.L. Frenkel, and D.M. Loudenslager. The Johns Hopkins Hospital, Baltimore, MD.

The purpose of this study is to demonstrate the potential for SPECT reconstruction by use of the circular harmonic transform (CHT) solution of the exponential Radon transform. The CHT algorithm is based on both the 2-D Fourier transform of the projection sinogram and the intrinsic solution for uniform attenuation. Accurate patient contours and correction for table attenuation are required for quantitative studies. Mathematical simulations, SPECT scans of an anthropomorphic phantom, the Jaszczak phantom and patients are used to compare the algorithm with the intrinsic algorithm based on ordinary backprojection and commercial software based on the precorrective method. The simulations and line source studies demonstrate improved resistance to streaking and a better signal-to-noise ratio for the CHT algorithm when compared to either of the other two methods. A volumetric study with the anthropomorphic phantom shows that the CHT algorithm provides better estimates of organ volume over a wide range, from pancreas (145 ml) to liver (1950 ml). The correlation coefficient from a least-squares fit of the volumes was 0.9997 (CHT) and 0.9991 (commercial software). The CHT algorithm is much less prone to nonfocal geometric distortion when compared to the commercial software. The CHT algorithm is also computationally efficient, with processing times generally less than ordinary backprojection. For SPECT protocols in which the assumption of uniform attenuation is reasonable, the CHT algorithm is preferable to the algebraic-iterative methods which require long processing times.

No. 78

INVERSE MONTE CARLO IMAGE RECONSTRUCTION FOR SPECT WITH MAXIMUM LIKELIHOOD ESTIMATION. C.E. Floyd, R.J. Jaszczak, S.H. Manglos, K.L. Greer, R.E. Coleman. Duke University Medical Center, Durham, NC.

The Inverse Monte Carlo (IMOC) algorithm has been applied to reconstruct SPECT images from projection data including quantitative compensation for scatter, attenuation, and depth dependent collimator effects. Monte Carlo simulation of photon transport through the SPECT acquisition apparatus (including scatter and attenuation interactions) forms a detection probability used in an EM maximum likelihood algorithm to estimate the source distribution. Scatter and attenuation compensation was achieved for studies with three isotopes: Tc-99m, Tl-201, and I-123 for several phantom geometries as well as for clinical acquisitions. For line sources immersed in an interacting water bath containing background activity, ROI comparison showed agreement between the image of sources in air (without scatter and attenuation) and in water (with scatter and attenuation) to better than 1% for large ROI regions. Comparison between IMOC and filtered back projection revealed IMOC to simultaneously provide superior resolution and noise for this phantom. Reconstructions with compensation for scatter and attenuation were achieved for SPECT acquisitions which included only 180 degrees of projection data. Asymptotic behavior of the EM esti-

imator was investigated out to 1000 iterations. For some projection sets, divergence in the chi-squared convergence criteria was noted at ~500 iterations. These preliminary results indicate the IMOC can provide quantitative SPECT reconstruction including simultaneous compensation for scatter and attenuation.

No. 79

EVALUATION OF A FAST MAXIMUM LIKELIHOOD METHOD FOR ESTIMATION OF REGION-OF-INTEREST VALUES IN EMISSION TOMOGRAPHY. R.E. Carson, G.W. Berg, M.V. Green, S.M. Larson, National Institutes of Health, Bethesda, MD.

A maximum likelihood (ML) method for the unbiased estimation of region-of-interest (ROI) values and their variances for emission tomography has previously been developed. This study presents a significantly faster version of the algorithm and evaluates its performance against filtered backprojection (FBP) with a realistic brain simulation. Processing time has been reduced 8-10 times with the Fisher scoring algorithm instead of the EM algorithm, with convergence in 4-6 iterations. 100 ROI values can be estimated in 20 minutes on a PDP-11. The ML method requires ROIs defined over all radioactive portions of the field and assumes activity is uniform in each region. To evaluate the algorithm's sensitivity to violations of its assumptions, a simulated brain slice was constructed. FBP reconstructions were performed and ROIs were drawn covering the gray matter, with white matter filled automatically. 30 simulations of 3 million and 300 thousand count scans with resolutions of 10 and 6 mm FWHM were performed to calculate the bias and variability of ML and FBP estimators.

The ML estimates did not show the partial volume bias of FBP (0.8%+7.1% versus 12.4%+3.6% for 1 cm resolution). ML showed a greater range of bias due to its sensitivity to placement and size of the ROIs. The variability of the ML estimates was accurately predicted by the algorithm and was slightly greater than FBP (3.7% versus 2.8%). ML variability and FBP bias increase with smaller ROI size or increasing FWHM. These studies demonstrate that ML can remove the partial volume bias without significant noise increase in reasonable computation time.

No. 80

MAXIMUM-LIKELIHOOD ESTIMATION OF REGIONAL ACTIVITY. S.P. Mueller, M.F. Kijewski, S.C. Moore, B.L. Holman. Harvard Medical School and Brigham and Women's Hospital, Boston, MA.

We have compared the accuracy and precision of a maximum-likelihood (ML) method of estimating regional activity to that of two currently used estimators: the peak (PROI) and the average (AROI) reconstructed activity over a region of interest. We simulated images of discs superimposed on a uniform background, convolved them with a Gaussian point-spread function (PSF) and added white noise. Using the ML criterion and a mathematical model, we estimated the activity, size, and location of the discs and the activity of the background using a non-linear fitting algorithm.

For disc diameters from 1.25 to 3.25 times the FWHM of the PSF, the accuracy of the ML method ranged from 0.1% for the largest disc to 0.5% for the smallest. For a ROI corresponding in size and position to the disc, the AROI underestimated activity, with errors ranging from 10% for the largest disc to 24% for the smallest. The peak method underestimated disc activity by up to 10% for discs smaller than 2 times the FWHM, and overestimated activity by up to 16% for larger discs. The standard deviation of the ML estimates over 50 images ranged from 1.1% for the largest disc to 2.3% for the smallest. For the AROI method, the standard deviation ranged from 0.7% to 1.3%, while the standard deviation of the PROI estimates ranged from 3.4% to 3.9%.

The performance of the ML estimator was superior to

averages (1-4) and data matrix size (interpolated 128 pixel/noninterpolated 256 pixel in the signal phase axis).

The selection and application of the ECG leads was most critical in the higher field strength as adverse effects of RF interference and aortic flow pulses were common. Small children presented less difficulty in this regard than adults. Problems were minimized using 0.6T imager. With the body coil, or infants in the head coil, single signal average data appeared anatomically sufficient using the 1.5T imager. No significant differences in cardiac anatomy were noted on either imager using similar acquisition parameters. Improvement in image contrast on the 1.5T imager can be obtained on T1 weighted images by gating on alternate cardiac cycles. Prolongation of imaging time using a higher order acquisition matrix often was associated with greater patient motion; resulted in data similar to lower order matrix acquisition.

Surface coil data provides high anatomic resolution on both images but is extremely sensitive to patient or respiratory motion. Variation of other acquisition parameters for anatomic imaging plays a minor role in this circumstance.

No. 447

OBLIQUE MAGNETIC RESONANCE IMAGING FOR MYOCARDIAL INFARCT EVALUATION. R.F. Johnson, Jr., M. Ahmad, E.G. Amparo, D.J. Dornfest, W.J. Prevost. University of Texas Medical Branch, Galveston, TX 77550.

NMR imaging of the heart has been described in the literature illustrating the combination of patient positioning and oblique slice selection gradients to present images of the heart in an orientation that provides short and long axis views. These images are similar to the anatomic presentations seen in T1-201 and 2-D echocardiography techniques. This paper describes an electronic technique that results in the same oblique views without patient rotation or other complicated positioning. The NMR imager has the capability of pulsing the gradient coils in a manner that will produce complex gradient angles that correspond to the precise orientation of the heart. The clinical result is an uncomplicated but tailored presentation of the heart in short and long axis views. Advantages include a clear view of wall thickness for a detailed analysis of all segments of the myocardium. Clinical comparisons of the short axis NMR images were made in 11 patients in which T1-201 and 2-D echocardiography imaging had been

performed. There was close correlation of the anatomic orientation and pathologic findings of the heart. In 2 patients with recent myocardial infarction, wall motion evaluation by echocardiography and perfusion deficits by T1-201 corresponded with observed wall thinning of the left ventricle in the NMR images. Nine patients without recent myocardial infarction demonstrated similar cardiac anatomy by NMR imaging to that seen by T1-201 and 2-D echocardiography. Thus, oblique NMR imaging has been determined to provide the best method of presenting the myocardium for infarct evaluation.

No. 448

QUANTITATION OF CANINE MYOCARDIAL INFARCT SIZE USING CONTRAST ENHANCED MAGNETIC RESONANCE AND Tc-99m-PYP, SPECT IMAGING TECHNIQUES. J.A. Clanton, C.J. Wehr, D.S. Freeland, G.E. Holburn, S.S. Oyog, R.R. Price and M.P. Sandler. Vanderbilt University, Nashville, TN.

To evaluate current methods of quantitating infarct size and the "volume at risk", we studied nine canines with surgically induced myocardial infarct (ligation of LAD beyond second diagonal) 24 hours after surgery with MRI and SPECT. Radiolabeled microspheres were administered into the left atrium immediately prior to and post ligation for flow determination.

MR imaging was performed pre and post administration of Gd-DTPA (0.25 mM/Kg) using ECG gated short spin-echo techniques (TE=30mSec, TR=350mSec). SPECT scans were performed 2 hours post-administration of 25mCi of Tc-99m PYP. On completion of the in-vivo SPECT scan, a third set of microspheres were injected into the left atrium and the dog sacrificed by the left atrial injection of monastral blue dye ("volume at risk" determination).

The SPECT and MRI scans were repeated on the heart ex-vivo, the heart sectioned and stained with TTC (infarct size determination) after the "volume at risk" had been determined. Each section was divided into four regions, ischemic and perfused endo and epicardium and counted in a well counter for Tc-PYP uptake and microsphere distribution.

Analysis of these data indicate that Gd-DTPA and Tc-PYP localize in areas that exhibit less than 20% of the normal blood flow. Both techniques consistently overestimated the "volume at risk" and the infarcted volume when compared to pathological specimens.

Poster Sessions

Monday, 3:30-6:00

Exhibit Hall

BONE AND JOINT**No. 449**

Sm-153 EDTMP TREATMENT OF SPONTANEOUS CANINE BONE TUMORS. L.A. Corwin, Jr., J.C. Lattimer, W.F. Goeckeler*, J. Stapleton, B.E. Edwards, L. Stringham,

J. Simon*, A.R. Ketring, W.A. Volkert, and R.A. Holmes, University of Missouri-Columbia, MO and Dow Chemical Co.*

Dogs with primary bone tumors were used to evaluate the efficacy of Sm-153 ethylenediaminetetramethylene-phosphonic acid (EDTMP) complex for its potential use in treatment of metastatic bone neoplasia in man. Skeletal images obtained with this complex were similar to the Tc-99m MDP images and show selective concen-

tration in osteoblastic lesions giving high target to non-target ratios. To date, 23 dogs with primary bone tumors have been treated and progressively evaluated with radiographs, scintigraphy, bone marrow aspirates, hematology and serum chemistries. Most dogs received a single intravenous dose of 1.0 mCi of the complex/kg body weight producing a calculated dose to the lesion between 25 to 50 Gy. Most dogs demonstrated an early reduction in pain as judged by improved locomotor function. None of the dogs demonstrated significant clinical problems from the treatment. Hematological abnormalities were limited to dose related reduction in platelets and white blood cells two to three weeks post-injection which returned to normal by six weeks. Of the 23 dogs treated to date, eleven are still alive with apparent clinical and radiographic arrest of the disease. One dog died of unrelated disease 1 year post treatment and had no evidence of active neoplastic disease at necropsy. Sm-153-EDTMP appears to be an effective therapeutic agent for treatment of neoplastic bone disease.

No. 450

DEVELOPMENT OF INSTRUMENT SYSTEM OF DUAL PHOTON ABSORPTIOMETRY USING A GAMMA CAMERA. M. Fukunaga, T. Tomomitsu, N. Otsuka, T. Sone, K. Nagai, A. Muranaka, S. Yanagimoto, K. Torizuka, K. Masuda, H. Atsumi and R. Morita. Kawasaki Medical School, Kurashiki, Hamamatsu Photonics, Hamamatsu and Kyoto University, Kyoto, Japan.

Dual photon absorptiometry (DPA) with the rectilinear scanning has been widely used to measure the bone mineral content (BMC) in axial skeleton. In this study, we have developed a new instrument system of DPA using a gamma camera.

The system consisted of 50 mCi ¹⁵³Gd (44 and 100 keV) as an emitting source, NaI crystal for a detector, 19 photomultiplier tubes and a computer.

Fundamental studies were made, and the results were evaluated. The intrinsic spatial resolution (FWHM) was 9.2 mm at 44 keV and 5.5 mm at 100 keV. The intrinsic flood field uniformity was 8.1% at 44 keV and 3.7% at 100 keV. The count rate performance was 2.3 usec. The precision error for triplicate determinations on pig femoral bone *in vitro* was 1.6% for 9 min. and 1.2% for 15 min. of acquisition time. BMC, derived from this DPA system, on phantom immersed in K₂HPO₄ solution (bone equivalent material) correlated highly to actual density ($r=0.99$, $p<0.001$). Furthermore, high correlation between BMC determinations obtained from DPA and those from SPA was observed ($r=0.98$, $p<0.005$). Irradiation dose of 50 mCi ¹⁵³Gd was 16.3 ± 4.5 mR at skin surface.

Thus, it was shown that DPA system using a gamma camera was reliable in evaluation of bone mass, and that the amount of ¹⁵³Gd used in a gamma camera system was less than one tenth of that required for the scanning system. DPA using a gamma camera could be thought to hold the great promise as an investigative tool in quantifying bone mass.

No. 451

INTRA-ARTICULAR YTTRIUM-90 THERAPY OF CHRONIC HEMOPHILIC SYNOVITIS. M. Heim, U. Martinowitz, H. Horosowsky and L.M. Lieberman. Sheba Medical Center, Tel Aviv University Sackler School of Medicine, Tel Aviv, Israel.

Recurrent hemarthrosis in patients with hemophilia often results in severe joint deformity, limitation of movement, and bony ankylosis. Surgical synovectomy is associated with marked morbidity, is costly, and the results are disappointing. Synoviorthesis represents an improved treatment method and recent reports suggest that the undesirable side effect of chromosome damage seen with Au-198 colloid is greatly reduced with Y-90 silicate colloid (Y-90 SC).

We treated 18 joints (9 knees, 5 elbows, 4 ankles) in 15 severe classical hemophiliacs with Y-90 SC. An

arthrogram was performed prior to treatment to ensure intra-articular injection of the radioactive colloid. After withdrawal of contrast material 2-5 mCi of Y-90 SC and 80 mg Depomedrol were injected. Joint scintigraphy was done within 1 hour and repeated approximately 24 hours later by detection of bremsstrahlung radiation.

Patients with high titers of antibodies to Factor VIII received a single dose of Autoplex 100u/kg prior to treatment and were immobilized in a cast for 3 days. Factor VIII levels were controlled at 30% for 48 hours.

We observed an 80% reduction of bleeding episodes during an average follow-up of 4.8 months. There were no complications and no loss of movement range was noted. We find that this therapeutic modality is effective, simple, inexpensive and results in a low morbidity.

No. 452

DIFFUSE INTRATHORACIC ACCUMULATION OF TECHNETIUM-99m MDP: EXPERIENCE IN 40 CASES. S. Kosuda, T. Hashimoto, A. Kubo, I. Nishiguchi, E. Kunieda, S. Hashimoto. Okura National Hospital and Keio University Hospital, Tokyo, Japan.

Diffuse intrathoracic uptake of technetium-99m bone seeking agents is uncommon, and the incidence and details of the causative diseases have not been reported.

We reviewed the records of 8021 patients who were referred to us for bone scanning during the past four years. There were 3120 males and 4901 females, age range 1 to 91 yr, mean 55. Forty out of 8021 patients (0.50%) had bone scintigram revealing diffuse intrathoracic uptake of technetium-99m methylene diphosphonate (MDP). 37 out of 40 cases (93%) showed unilateral diffuse intrathoracic uptake. All those cases with diffuse intrathoracic uptake were classified as strongly positive (2 cases, 5%), moderately positive (7 cases, 18%), and weakly positive (31 cases, 78%).

The causative diseases were malignant pleural effusion, diffuse pulmonary metastases, primary pulmonary carcinoma, pulmonary tuberculosis, radiation pneumonitis, fibrothorax. Diffuse intrathoracic uptake due to unknown origin was seen in 8 cases (20%). Only two cases (tuberculosis, fibrothorax) showed calcification on the chest roentgenograms.

Nineteen out of 40 cases underwent sequential gallium-67 citrate scan. Of those, 14 cases (74%) revealed diffuse intrathoracic uptake of Ga-67 in the same side.

In conclusion, these observations stress the need for careful correlation in the interpretation of technetium bone scan, whereas the exact mechanism of localization of Tc-99m MDP remains undefined.

No. 453

SEMI-QUANTITATIVE Tc-99m HYDROXYMETHYLENE-DIPHOSPHONATE (HM DP) SERIAL BONE SCANS DURING CHEMOTHERAPY IN OSTEOGENIC SARCOMA (OS): CORRELATION WITH HISTOLOGICAL GRADING. J. Lumbroso, C. Kalifa, C. Tainturier, Y. Rabarison, A. Boddart. Institut G. Roussy and INSERM U66, Villejuif, France.

Twenty five children aged from 7 to 18 years with histologically proved OS were treated in our institution according to the T10 protocol (Rosen et al, Cancer, 1982, 49: 1221-30). Bone scans were carried out before preoperative chemotherapy 3 hours after injection of 10MBq/kg of Tc-99m-HM DP. The tumour to contralateral uptake ratio (R) was determined by the ROI method. A second scan was done at half course (6 weeks) of the chemotherapy and the ROI were drawn with reference to the previous scan. The procedure was repeated at the end of the chemotherapy. After surgical resection of the tumour, the pathologist classified the specimens in 2 categories: good response (GR: less than 10% of viable cells) and poor response (PR).

Eleven values of R were determined at the level of femoral and tibial metaphyses of 9 control patients whose bone scans were definitely classified as normal. The normal R was 1.01 ± 0.06 . The values of R in OS patients are

listed below (mean \pm SD):

	first scan	second scan	last scan
GR (12 cases)	6.3 \pm 3.8	3.2 \pm 1.6	1.9 \pm 0.6
PR (13 cases)	5.0 \pm 3.2	6.5 \pm 5.3	4.6 \pm 3.3

All the patients of the GR group had a scintigraphic response (decrease of R more than 20% on consecutive scans). In the PR group, 4 patients had a scintigraphic response and 9 had a stable or worsening R. This parameter has a predictive value when stable or increasing and should be routinely used since the tumour response may be difficult to assess on clinical examination and radiography.

No. 454

ACCURACY AND RELIABILITY OF In-WBCs IN OSTEOMYELITIS. K. E. McCarthy, M.G. Velchik, A. Alavi, G.A. Mandell, J. Esterhai, and S. Goll. Hospital of the University of Pennsylvania, Philadelphia, PA.

46 patients (23M, 23F) ranging in age from 19 to 79 with a clinical history of a non-union fracture, surgery, diabetes, or a soft tissue infection were studied with In-111-oxine WBCs to detect osteomyelitis. There were 27 TP, 9 TN, 2 FP, and 1 FN. The TPs and the FN occurred in patients with soft tissue infections overlying the area of interest. All diagnoses were confirmed by intraoperative bone biopsies and cultures. Seven patients were excluded because of nonconcurrent indium scans and bone biopsies. Bone biopsy and scan were performed within 2 days of each other in the remaining 39 patients.

The overall sensitivity was 97% (27/28), specificity 82% (9/11), and the diagnostic accuracy 92% (36/39). The remaining 7 patients had negative indium scans several months after positive bone biopsies and definitive antibiotic treatment. This suggests that In-WBC scans become negative after appropriate therapy is undertaken.

Interobserver data was obtained from 4 nuclear physicians of varying experience blinded to clinical information. A high degree of agreement was found in over 90% of the cases. This study demonstrates the utility of In-WBC scans in the diagnosis and follow-up of complicated osteomyelitis and a high level of interobserver agreement in scan interpretation.

No. 455

IMPORTANCE OF DETERMINING BMC IN LOCAL POPULATION FOR CLINICAL USE. D. Picard, L. Carrier, R. Chartrand, G. Breton, L-G. Ste-Marie, P. D'Amour. Hôpital St-Luc, Montréal, Québec.

We measured bone mineral content (BMC) of the proximal femur and lumbar spine (L2 to L4) by dual photon absorptiometry in 79 normal Canadian volunteer white women aged from 20 to 67 years. Were included in this study women with normal lumbar spine x-ray, without back pain, fracture of the spine or femur, no endocrinological, gastroenterological or hepatic disease, and no intake of thyroid hormones, steroids or diuretics. Results were expressed in grams of hydroxyapatite per cm² (1g ash bone equals 1.26 gHA/cm²). The regression of BMC on age was linear and equal to:

$$y = 1.15 - .00630 \text{ gHA/cm}^2 * \text{age for lumbar spine}$$

$$y = 0.89 - .00376 \text{ gHA/cm}^2 * \text{age for femoral neck}$$

There is no significant difference between our results and the ones published by Riggs et al. (1) for lumbar spine. However, the BMC of proximal femur is lower than the normal white American published data, but the annual rate of loss is slower. This discrepancy could be due to multiple factors such as geography (sun exposure), diet (calcium, protein intake, etc), social and occupational status. Further studies are warranted to determine their respective importance. Meanwhile, normal local BMC values should be obtained before using dual photon absorptiometry clinically.

(1) Riggs BL, Wahner HW, Seeman E et al: J.Clin.Invest. 70: 716-723, 1982.

No. 456

WEIGHTED ACQUISITION: A METHOD FOR IMPROVING BONE AND GALLIUM IMAGES. M.E. Siegel, K.H. Lee, R.P. DeVito, O. Chen, D.C.P. Chen, USC School of Medicine, Los Angeles, CA and Siemens Gammasonics, Des Plaines, IL.

The pulse height analyzer is unable to reject scattered photons of similar energy as primary photons. We compensated for scatter contribution by weighting the importance of each photon according to its energy.

One image with conventional window and one using an energy weighted protocol were simultaneously collected using special acquisition hardware in the processor of the camera. Each event was modified by a weighting factor (WF) before adding to matrix. The WF's were determined according to energy, contrast, and signal/noise ratios desired and were stored in ROM.

51 procedures, 39 of bone, and 12 gallium scans were performed as described. Images were evaluated by comparing the weighted (WI) to non-weighted images. Quantitative analysis of image contrast over the ribs (bone) or lesion (gallium) were computed by the ratio of counts in ROI to adjacent background. The contrast from weighting protocols was correlated with visual assessment.

Ribs were better defined in 64%, vertebra in 65%, and pedicles in 59% of bone scans using the WI. In every gallium scan, the anatomy was better defined using WI. The mean contrast ratio for ribs increased from 1.5 to 2.2. For gallium the lesion contrast increased by 30%. The best images were found using WF maximizing signal/noise ratio and altering slightly the contrast ratio.

For the same number of counts and scanning time, the weighted acquisition method appears to yield better quality images by suppressing the expression of the scatter contribution in the final image.

No. 457

DOES THE "THREE PHASE" BONE SCAN ADD DIAGNOSTIC INFORMATION IN BONE SCINTIGRAPHY? E.B. Silberstein, A. Elgazzar. The University of Cincinnati Medical Center, Cincinnati, OH 45267.

The use of a nuclear scintiangiogram or flow study as a routine part of bone imaging is said to add additional diagnostic information. *A priori* the blood pool image obtained shortly after injection also provides information on the vascularity of a lesion however, without the requirements of additional camera time or special injection technique. We examined the additional information provided by the flow study in 19 consecutive patients referred for bone imaging to rule out osteomyelitis where a flow study was technically feasible.

Each patient received a flow study employing 20-25 mCi of ^{99m}Tc-MDP injected as a bolus with four second frames over the area of interest acquired for forty seconds. A blood pool study was then obtained with delayed skeletal imaging 3 hours later. Each study was read at least twice by two different nuclear physicians.

Osteomyelitis was confirmed by culture on 17 of 19 patients. In each case the blood pool and delayed skeletal scintigraph of the focus showed the abnormality. However there were three falsely negative flow studies (18%).

One patient with arthritis and one with phlebitis had normal flow and blood pool studies. The latter also had a normal delayed bone scan.

We conclude that the flow study contributes no new information to a bone scan which includes a blood pool image obtained shortly after injection and yielded almost 20% false negative results.

No. 458

TC-99m MDP UPTAKE BY NORMAL LYMPH NODES ON BONE SCANS: CLINICAL AND LABORATORY EVALUATION. J.W. Wallis, S. Fisher, R.L. Wahl. University of Michigan Hospitals, Ann Arbor, MI.

Uptake of bone scanning agents in non-osseous sites has been described in a variety of pathologic conditions including tumor metastases. Recently we have seen several patients in which such uptake was proximal and ipsilateral to the injection site of Tc-99m MDP, apparently in normal lymph nodes. To further investigate this phenomenon, it was studied in a rat model. Nine rats were injected with 100 μ Ci of Tc-99m MDP, four using an intravenous (IV) femoral vein injection and five by a single subcutaneous (SQ) footpad injection. Two hours post injection, the animals were sacrificed and samples taken from popliteal and femoral lymph nodes ipsilateral (IL) and contralateral (CL) to the site of injection, and from liver, spleen and muscle. Tissue samples were weighed and counted using a 140KEV Tc99m 20% window. Tc99m MDP purity was assayed by silica gel thin layer chromatography to be 99.4% colloid free.

Activity (expressed as time corrected kg % dose/gm) in popliteal nodes IL to the injection site was over 60-fold greater in the animals that received SQ injection compared to IV injection (SQ .58 \pm .18, IV .009 \pm .006; p<.0004). This difference in the SQ group was not simply due to extension into local tissues by dissection of injected radionuclide along tissue planes, as the activity in leg muscle sampled between the SQ injection site and popliteal region (SQ .003 \pm .003, IV .001 \pm .0004; N.S.) was significantly lower than the IL popliteal node activity (p<.002). IL popliteal node activity in the SQ group was 159 times that of CL popliteal nodes, with an IL node to liver ratio of 184:1. Popliteal nodes in the IV group exhibited no significant difference between the two sides, with a node to liver ratio of 1.7:1.

In summary, dramatically increased uptake of Tc-99m MDP in normal lymph nodes IL and proximal to an extravasated injection has been demonstrated. An awareness of this phenomenon in the clinical setting can avoid confusion with pathologic forms of soft tissue uptake.

No. 459

GALLIUM-67 SUPRAPATELLAR/THIGH RATIO IN RHEUMATOID ARTHRITIS AND OSTEOARTHRITIS OF KNEES. S.H. Yeh, R.S. Liu, L.C. Wu, S.J. Wang, S.Q. Liao, Y.K. Chu, H.Y. Lin, and J.L. Lan. Veterans General Hospital, Taipei and Taichung, and National Yang-Ming Medical College, Taipei, Taiwan.

In view of its location and the different degree of synovial involvement by various diseases, the suprapatellar bursa may have Ga-67 uptake dependent on the diseases. A quantitative method is described below.

Data were acquired in the lateral view of the knees with the equally time-exposed technique at 48 hr after IV injection of 5 mCi of Ga-67 citrate. A computer routine was used to calculate the right and left suprapatellar/thigh ratio (RS/T for right; LS/T for left). Twenty-three patients (pts) were studied. RS/T and LS/T were also determined in 15 normal subjects. The mean ratio \pm s.d. was 1.35 \pm 0.15 for LS/T and 1.17 \pm 0.18 for RS/T.

In all 23 proven pts with noninfectious disorders of the knees, 13 had rheumatoid arthritis (RA; unilateral in 5 and bilateral in 8) and 10 had osteoarthritis (OA; unilateral in 5 and bilateral in 5). RA increased greatly the suprapatellar/thigh ratio (2.49 \pm 0.70 for LS/T and 2.35 \pm 0.60 for RS/T vs N, p < 0.005), and so did OA in a moderate degree (1.71 \pm 0.33 for LS/T and 1.49 \pm 0.19 for RS/T vs N, p < 0.005). Furthermore, S/T was significantly higher in RA than in OA (p < 0.005 for RS/T and p < 0.025 for LS/T). RA and OA had their respective sensitivity of 90% and 86% and specificity of 97% and 87% at their respective cutoff value of 1.60 and 1.40.

Our preliminary results indicate that the suprapatellar/thigh ratio may be a useful index for diagnosing the arthritic disorders of the knees. It can separate RA from OA in this study.

No. 460

THE VALUE OF SKULL SCINTIGRAPHY IN ACUTE MASTOID AND EAR INFECTIONS IN CHILDREN. S.T. Zwas and D. Millet. Sheba Medical Center, Sackler School of Medicine, Tel Aviv University, Tel Aviv, Israel.

The correct clinical diagnosis of acute mastoiditis in pediatrics is crucial due to possible complications. Recurrent acute otitis media and acute external otitis with local soft tissue reaction often mimic acute mastoiditis.

Clinical diagnosis and radiographs can be inconclusive and the utility of bone scintigraphies for this purpose has not yet been established.

We employed Tc-99m MDP bone scans for evaluation of mastoidal involvement in acute ear infections. Twenty-one consecutive patients, age range 0.5-11 years, mean 2.5 years, suspected of acute mastoiditis, were referred by their pediatricians for bone scintigraphy within 2 weeks from the onset of symptoms. Patients' scintigraphies were carefully compared with normal skull anatomy and scintigraphies of children without ear infections. Thus, patient scan abnormalities were defined and correlated with their final clinical diagnoses independently made by an otolaryngology specialist. Consequently, several distinctive patterns of image abnormalities corresponding to acute otitis media (in 11 cases) or acute external otitis (in 2 cases), acute mastoiditis (in 6 cases) and occipital periostitis (in 1 case) were observed and were found to be highly correlated with the final diagnoses.

We conclude that skull scintigraphy is highly efficient in assessing mastoidal involvement and periauricular tissue reaction in recurrent acute ear infections in children.

Monday, 3:30-6:00

Exhibit Hall

CARDIOVASCULAR: BLOOD POOL IMAGING AND VENTRICULAR FUNCTION

No. 461

THE SCINTIGRAPHIC EVALUATION OF MULTIPLE VENTRICULAR TACHYCARDIA (VT) FOCI. E. Botvinick, M. Dae, J. Davis, J. Herre, J. Abbott, M. Scheinman, J. Griffin, D. Faulkner, W. O'Connell. University of California, San Francisco.

During blood pool scintigraphy of 31 patients (pts) in sustained VT, 5 pts revealed multiple ECG patterns suggesting 12 VT foci, 2 or 3 in each case. The site of earliest phase angle was taken as the VT focus and the phase pattern was compared to the surface ECG in all cases, and to endocardial maps (M), which owing to rapid focus transition or pt intolerance, were performed in association with only 7 foci.

Phase analysis localized the VT focus to septal, lateral or inferior left ventricular (LV) regions. The focus and phase pattern correlated with the ECG in 10/12 and with M in 7/7, in spite of severe resting LV dysfunction (LVEF=.31), deteriorating with VT (LVEF=.19). In 2 pts, ECG patterns thought to originate from divergent foci were localized to the same region with differing "conduction". Three different VT foci were reproducibly localized in a third pt, studied twice, months apart. In this pt, a third study, during induced VT, after clinically successful septal focus ablation, indicated VT origin from a secondary, lateral focus, supporting electrophysiologic impressions. Image foci were adjacent to contraction abnormalities and in 3 pts localized to different aspects of an aneurysm perimeter.

Scintigraphic localization of multiple VT foci is feasible, correlates with and complements ECG and M, and promises to aid differentiation of independent from identical foci. It can be important in evaluating pts prior to and after focus ablation or resection, since multiple, disparate VT foci can have an adverse influence on the efficacy of such management.

No. 462

PRESERVATION OF REST (R) AND EXERCISE (E) SYSTOLIC AND DIASTOLIC VENTRICULAR FUNCTION IN CHRONIC ALCOHOLICS (CA). M. Cerqueira, G. Harp, J. Ritchie, R. Dale Walker, VA Medical Center, Seattle, WA.

Autopsy studies have suggested that prolonged excessive alcohol consumption causes myocardial damage

even in the absence of clinical cardiac symptoms. Echocardiography and phonocardiography have provided mixed results on the existence of a preclinical alcoholic cardiomyopathy. These studies measure resting systolic function and maybe insensitive to early signs of myocardial damage. We used list mode acquired gated blood pool scans at R and E to study systolic and diastolic function in 18 CA (drinking 5 days/wk, >5/yr) and 12 age matched normals (N1). Following arrhythmia rejection (+10% mean RR interval), filtering, and 20msec interval forward and backward reformatting, time activity curves were generated using a variable region of interest. The 4th harmonic derivative was used to calculate EF, peak ejection time (PET, msec) peak ejection rate (PER, EDV/sec), peak filling time (PFT, msec) and peak filling rate (PFR, EDV/sec). There were no significant differences between groups, see below. (Mean + S.D.)

	R-N1	R-CA	E-N1	E-CA
PET	183±28	179±21	85±39	81±19
PER	3.6±.5	3.8±.5	6.9±1.3	7.2±1.3
PFT	158±18	147±30	85±39	81±19
PFR	3.3±.6	3.4±.5	8.7±2.1	9.5±2.1

Thus, evaluation of systolic and diastolic function at R and E by sensitive radionuclide techniques fail to show evidence for the existence of a preclinical alcoholic cardiomyopathy in CA.

No. 463

SCINTIGRAPHIC PATTERNS OF ENDOMYOCARDIAL FIBROSIS. M.C.P.Giorgi, J.Soaes Jr., F.H.Hironaka, D.Daaur, J.C.Menegueti, A.C.P.Barreto F.Pileggi, E.E.Camargo.- The Heart Institute, São Paulo, Brazil.

Endomyocardial fibrosis (EMF) is characterized by collagen deposition in the apical endocardium of either ventricle with extension to the inflow tract and progressive impairment of ventricular diastolic and systolic functions. To determine scintigraphic patterns and their meaning in this disease we retrospectively correlated catheterization data with first pass (FP) and gated blood pool (GBP) studies of 14 patients (pts) with biopsy-proven EMF (12 female; 23-60 years).

Two scintigraphic patterns were recognized: I) Obliterative (n=9) with prolonged pulmonary transit time (PTT); marked RA dilatation; markedly reduced RV volume with hypo-or akinesis; normal or dilated PA usually tilted to the left; normal, dilated or thickened LV, usually normokinetic; equalization of mean pressures with RA, RV and PA hypertension; marked anatomic ventricular changes, with disappearance of the apex. II) Restrictive (n=5) with prolonged PTT; slight to moderate dilatation of RA, RV, PA and LV and normal mean pressure gradients in the right chambers.

FP and GBP imaging distinguished two scintigraphic patterns in EMF, which correlated well with catheterization data. These techniques seem promising as new tool for a non-invasive classification of these pts.

No. 464

EFFECTS OF SPONTANEOUS RESPIRATION ON BOTH VENTRICULAR FUNCTION: EVALUATION BY RESPIRATORY GATED RADIONUCLIDE VENTRICULOGRAPHY. BH.Kim, M.Inoue, H.Takeda, Y.Ishida, Y.Tsuneoka, N.Matsubara, K.Kimura, T.Kozuka, and T.Kamada Osaka University Medical School. Osaka, Japan.

To clarify the mechanism of inspiratory reduction of left ventricular (LV) stroke volume (SV) during spontaneous respiration (SR), we measured both ventricular volume changes from expiration (exp) to inspiration (insp) using radionuclide ventriculography with respiratory gating

technique. In this method, scintigraphic data were acquired in a list mode with ECG R waves and respiratory volume curve derived from respiratory flowmeter. Cardiac cycles occurring during the second halves of inspiratory and expiratory phases were separately selected and used to produce multi-gated images. Twelve patients with normal LVEF (>50%) and RVEF (>40%) and without pulmonary diseases were studied. In this study, both ventricular volume changes during SR were determined as percent changes from exp to insp. LV end-diastolic volume (EDV) decreased in all subjects and the percent decrease was 11 ± 5 % (mean±SD). LV end-systolic volume (ESV) showed no significant change. Then, LVSV decreased during insp in all subjects and the percent decrease was 17±7 %. LVEF decreased from 64±6 % during exp to 60±6 % during insp (p>0.001). Right ventricular (RV) EDV and SV increased by 13±11 % and 22±18 %, respectively. RVEF also increased from 48±6 % during exp to 52±5 % during insp (p>0.05).

These results indicate that inspiratory reduction of LVSV during SR is due to a decrease in LVEDV (preload) and that this reduction of LV preload may be partly due to an increase in RV volume during insp through the mechanism of ventricular interdependence.

No. 465

A NEW METHOD FOR LABELLING PLASMA PROTEINS WITH A TECHNETIUM-99M LABELLED AGENT FOR RADIONUCLIDE VENTRICULOGRAPHY IN MAN. A. Lahiri, G.D. Zanelli, N.M. Patel, J.C.W. Crawley, T. Smith and E.B. Raftery. Department of Cardiology and Radioisotope Division, Northwick Park Hospital and Clinical Research Centre, Harrow, Middx.

Radionuclide ventriculography with in-vivo Tc-99m labelled red blood cells (RBC) is limited because: 2 injections; the label is unstable; the count rate obtained from the ventricles are low due to poor labelling efficiency. We have developed phosphine ligands which can be labelled to Tc-99m: [TcD₂X₂]⁺; D = bis diethyl phosphino ethane and X = tert-butyl isocyanide. Five volunteers were studied (age range 37-58 years) with both the phosphine and the standard in-vivo RBC method. A gated RNV study was performed with both methods. The counts over the LV were 3 times higher with the phosphine. The LV ejection fraction (%) were closely correlated (r=0.98) and the background counts were lower. The blood pool half-life was 4 hours. The label was bonded to plasma proteins and was excreted via the gall bladder. [TcD₂X₂]⁺ has advantages over the red cell labelling method: a higher blood pool concentration is achieved, there is less background activity and a single injection is required. This technique has advantages over the RBC labelling method and a simple 'kit' may be prepared for hospital usage.

No. 466

DETECTION OF CORONARY ARTERY DISEASE BY ANALYSIS OF DIASTOLIC FUNCTION: THE EFFECT OF AGE. T.R. Miller, A. Fountos, D.R. Biello, S.J. Grossman, K.B. Schechtman, P.A. Ludbrook, and A.A. Ehsani. Washington University School of Medicine, St. Louis, MO.

Analysis of cardiac diastolic function by radionuclide ventriculography is reportedly useful in detecting coronary artery disease (CAD) in patients with normal left-ventricular ejection fractions (LVEF). Since the effect of age has not previously been considered, we determined the left-ventricular peak filling rate (PFR) in 30 normal subjects (age 48 ± 18) and in 25 patients with catheterization-proven CAD and normal LVEF (>50%) with ages between 40 and 65 yr. Regional wall motion was normal in 11 patients (CADN) and abnormal in 14 (CADA). In the normal subjects, PFR (in units of end-diastolic volumes/sec) is strongly correlated with age (r=-0.82, p<0.0001).

To evaluate the effect of this age dependence, the CAD patients were compared with two separate control groups, one a

set of 10 young normal volunteers (N1), the other a group of 12 age-matched normals (age 40-65) (N2). Sensitivity (SENS) for detection of CAD was determined using the 95% confidence limit for the normal controls. Specificity was 100% in all cases.

	N1	N2	CADN	CADA
PFR	3.64±0.65	2.12±0.53	2.00±0.59*	2.01±0.66*
SENS(N1)	-	-	58%	57%
SENS(N2)	-	-	0	0
AGE	29±4	59±6	57±5	53±6

*p<0.001 vs N1, p=N.S. vs N2

Thus, using an inappropriate, but commonly employed, young group of normal controls, PFR appears to detect CAD in patients with normal LVEF. In fact, PFR cannot identify this group when the proper age-matched controls are used because of the strong age dependence of PFR.

No. 467

THE CORRELATION OF RIGHT VENTRICULAR AND LEFT VENTRICULAR EJECTION FRACTION AND VOLUME MEASUREMENTS. M.L. Nusynowitz, A.R. Benedetto, M.R. Starling, and R.A. Walsh, UTMB, Galveston and UTHSC, San Antonio, TX.

Right and left ventricular EF, SV, EDV, and ESV were determined by first pass radiocardiography in 13 patients with left-sided regurgitant valvular disease (R+) and 7 patients without regurgitation (R-) but with suspected coronary artery disease or cardiomyopathy. In the R- group, corresponding RV and LV parameters correlated highly with each other: r=.86-.89; p=.01 for EF, SV, EDV, and ESV. The correlation of EF in R+ was fair (r=.64, p<.05) because total SV correlation was excellent (r=.93, p<.001) but EDV (and ESV) showed no significant correlation. In both R+ and R-, EDV and ESV were increased, and RVEF correlated with mean pulmonary artery pressure (PAP), r=-.76. The PAP was significantly higher in R+ than in R- and the RVEF significantly lower, but there was no correlation between PAP and RVEDV. Similar EF results are found in other reports of patients with CAD; furthermore, the correlation of volume measurements indicates either direct interdependence of ventricular function or common causes of abnormalities in both ventricles. Proposed mechanisms include increased RV afterload as a result of LV failure, biventricular ischemia, and mechanical interference of RV by LV enlargement. Since there is a lack of correlation of EDV and ESV in the R+ group, our results suggest that mechanical factors are not of major importance. Since there is no correlation of PAP and RVEDV, afterload itself may not be critical. Thus, ischemia may be the major factor in the R- group, and multiple factors may be responsible for the changes seen in R+.

No. 468

ASSESSMENT OF VENTRICULAR PERFORMANCE AND ITS FOLLOW UP AFTER AN ACUTE MYOCARDIAL INFARCTION BY RADIONUCLIDE ANGIOGRAPHY.

Osman RATIB, Alberto RIGHETTI, Vivianne STUCKI, Alex F. MULLER. Cardiology Center and Internal Medicine Dep., University Hospital, Geneva, SWITZERLAND.

A radionuclide angiogram (RNA) was performed in 98 patients (pts) within 24 hours after an acute myocardial infarction (MI). None of the pts had a previous MI. Early death occurred in 10 pts and 8 pts underwent a bypass surgery or coronary angioplasty during the first 10 days after MI. The remaining 80 pts had a RNA at rest (R) and during submaximal exercise (Ex) just before hospital discharge (12.3 ± 4 days). During a follow up period of 1 year, 13 pts experienced a major clinical event (cardiac death n=8, recurrent MI n=2 or bypass surgery n=3). A coronary angiography was performed in 58 pts and showed a single vessel disease (1vx) in 36 pts and a multiple vessel disease (Mvx) in 22. The 18 pts who died during the total followup period had a significantly lower initial ejection fraction (EF) than the pts who survived (35±16% vs 53±11%, p<0.0001). During Ex RNA in 1vx pts EF increased from 46±6% at R to 51±8% (p<0.01) but did not change significantly in Mvx pts (52±8% vs 51±11%).

During Ex16/33 (48%) pts with 1vx and 15/22 (68%) of the pts with Mvx failed to normally increase their EF (p<0.05). Ischemic ECG changes were observed at Ex in only 6/22 Mvx pts and in 4/33 of the 1vx pts. 62 pts had RNA 3 months after MI and mean R EF was comparable to initial R value.

In conclusion: RNA provides a noninvasive means to assess ventricular function in acute MI and to depict pts with high mortality risks. Furthermore a failure to increase EF during early submaximal Ex RNA is a more sensitive means than Ex ECG for the detection of Mvx pts with residual ischemia.

No. 469

SUPERIORITY OF FACTOR ANALYSIS OF RADIONUCLIDE EQUILIBRIUM GATED STUDIES FOR EVALUATION OF REGIONAL WALL MOTION ABNORMALITIES (RWMA). D.G. Pavel, E. Olea, J. Sychra, K. Zolnierczyk, C. Kahn, J. Shanes, University of Illinois Hospital, Chicago, IL.

Factor analysis (FA) has been suggested as a superior method for detection of RWMA because of its ability to separate anatomically and functionally superimposed areas.

Material and method: A detailed evaluation based on 8 segments (SEG) in LAO was performed by comparing 14 normals to 54 patients (Pt) who underwent biplane contrast angiography (CA) and also phase analysis. The standard algorithm was optimized for ventricular RWMA detection. Comparison was based on number of abnormal SEG detected by CA, FA and phase image (PhI). In addition, based on CA findings, the results obtained by FA and PhI were compared to each other in each patient, for number of SEG and for type of abnormality detected. Four categories were used: better (B), much better (BB), equal (E), worse (W).

Results: the 14 normals generated a consistent pattern of reference. For the 432 SEG (54 Pt), CA detected 261 as being abnormal versus 222 for FA and 114 for PhI. Thus, FA detects 85% or abnormal SEG versus only 44% for PhI. On a Pt by Pt basis, FA versus PhI is B or BB in 43/54 (80%) for number of SEG detected and is B or BB in 40/54 (74%), for type of abnormality detected. The only 2 cases (4%) in which FA was W than PhI, had LVH and filling rate abnormality; FA indicated abnormality not seen on either PhI or CA.

Conclusion: FA improves significantly the detection and characterization of RWMA, by noninvasive means.

No. 470

EVALUATION OF LEFT VENTRICULAR REGURGITATION BY FACTOR ANALYSIS AND DECONVOLUTION OF FIRST-PASS RADIONUCLIDE ANGIOGRAPHY. COMPARISON WITH INVASIVE TECHNIQUES. L. Philippe, I. Mena, J. Darcourt, W.J. French. Div. of Nuclear Medicine and Cardiology, Harbor-UCLA Medical Center, Torrance, Ca.

New deconvolution techniques of curves gathered by factor analysis have permitted Tc-99m DTPA First-Pass Radionuclide Angiography (FPRNA) to produce a reliable evaluation of Regurgitant Fraction (RF) in aortic and mitral insufficiency. RF was computed in 26 patients: 13 Valvular (V), 8 mitral- 3 aortic- 2 mitro-aortic, and 13 Controls (C). FPRNA was performed within 1 hour prior to the Contrast Ventriculography (CV). In 19 patients, CV was preceded by determination of the cardiac output by green-dye dilution (n=16) or thermodilution (n=3), in order to calculate the catheterization RF (CATH RF).

FPRNA RF was assessed by a lagged normal deconvolution of LV and pulmonary curves gathered by factor analysis. The appearance of a long transit time component in the left heart transfer function was observed in V patients, and then quantified. The presence of regurgitation was determined from CV.

FPRNA RF was different between C and V patients CV graded 1+ or 2+ (p<.001), and between V graded 1+ or 2+ and V graded 3+ or 4+ (p<.025).

FPRNA RF (m±sd) .39 ± .19 (n=13 V) .01 ± .03 (n=13 C)
 CATH RF (m±sd) .34 ± .24 (n=11 V) .13 ± .12 (n= 8 C)
 The coefficient of interobserver variability was 9.2% (r=.92). A 10% RF threshold between V and non-V patients

yielded 1 false negative and 0 false positive.

FPRNA allows an accurate and reproducible quantification of aortic and mitral regurgitation.

No. 471

A NEW METHOD FOR DETERMINING PRESSURE-VOLUME LOOPS IN THE CLINICAL SETTING. C.M. Purut, T.L. Sell, R.H. Jones. Duke University Medical Center, Durham, NC.

Left ventricular stroke work (LVSW) as calculated from left ventricular pressure-volume (P-V) loops accurately defines cardiac function but is difficult to obtain in most clinical settings. Using the Scinticor, a portable multicrystal gamma camera, and high fidelity micromanometer catheters placed in the left ventricle during coronary artery bypass grafting, we acquired simultaneous dynamic intraventricular volume and pressure data during and immediately after surgery. Radionuclide left ventricular volumes and pressures were beat-matched to generate P-V loops for calculation of LVSW. A potentially less accurate, but more simple, method for calculating stroke work multiplies radionuclide stroke volume by the mean arterial pressure. We compared these two methods for calculating stroke work in 12 pairs of measurements. The two methods did not differ significantly by analysis of variance ($N = 12$, mean differences = $0.072 \text{ erg} \cdot 10^6 \cdot \text{m}^{-2}$, $SD = 0.35 \text{ erg} \cdot 10^6 \cdot \text{m}^{-2}$). We conclude that accurate measurement of LVSW is possible from radionuclide calculated stroke volume and mean radial artery pressure. However, a more complete assessment of ventricular performance throughout the cardiac cycle is obtained only when left ventricular pressure is recorded and P-V loops constructed. Clinical application of this method of assessing cardiac function both during and after coronary artery bypass surgery appears promising for assessing the adequacy of revascularization and for use as a guide in postoperative patient management.

No. 472

PROGNOSTIC IMPORTANCE OF CHANGE IN WALL MOTION IN PATIENTS WITH ACUTE MYOCARDIAL INFARCTION. N. Tamaki, J.B. Newell, T. Yasuda, R.C. Leinbach, H.K. Gold, K.A. McKusick, H.W. Strauss. Massachusetts General Hospital, Boston, MA.

To determine the prognostic significance of changes in regional wall motion in the first 10 days following acute myocardial infarction, a series of 109 patients who received standard medical therapy were studied by serial radionuclide gated blood pool scans. The scans were recorded in the anterior and LAO views on admission and at 10 days after infarction. Regional wall motion was quantitatively assessed as percent shortening (ZS) in 8 segments in two views. Abnormal segments were divided into akinetic segments (ZS < 15%) and hypokinetic segments (16-29%). When more than one akinetic or hypokinetic segment was present, values were averaged for ZS. Cardiac death occurred in 15 patients during a follow-up period of 2.9 ± 1.9 years (range 1-6 years). Stepwise Cox regression analysis of ejection fraction (EF), change in EF (1-10 days), ZS change of akinetic and hypokinetic segments, and number of akinetic segments were performed. Univariate analysis revealed that ZS change of hypokinetic segments was the strongest predictor ($X^2=10.12$; $p=0.002$), followed by number of akinetic segments at 10 days ($X^2=8.85$; $p=0.003$). Multivariate analysis showed that once ZS change of hypokinetic segments was known, no other variables contribute independent prognostic information. All 8 patients who died within one year after infarction showed decrease in ZS of hypokinetic segments.

These data suggest that serial evaluation of regional wall motion can offer prognostic information in patients with acute myocardial infarction.

No. 473

RIGHT ATRIAL TIME-ACTIVITY CURVE ANALYSIS FOR THE DETECTION OF TRICUSPID REGURGITATION: A COMPARISON WITH DOPPLER ECHOCARDIOGRAPHY. K.A. Williams, P.E. Wolenski, P.J. Gaddis, J.W. Ryan, A. Neumann, and K.M. Borow. University of Chicago, Chicago, IL.

Doppler echocardiography (DE) has recently become the non-invasive standard for detection of tricuspid regurgitation (TR). Using Tc-99m DTPA and a multicrystal camera we examined the ability of first pass radionuclide angiography (RNA) to detect TR in an unselected population of 44 patients (pts) who underwent pulsed DE during routine echocardiography. During inflow of the bolus we examined the right atrial (RA) time-activity curve (TAC), using a region of interest drawn just above the tricuspid valve plane. In normal pts, once the tracer has passed the vena cava, the RA TAC falls during right ventricular (RV) diastole, and remains static during RV systole. With mild to moderate TR, the regurgitant stream of tracer increases the RA TAC during RV systole. With more significant TR, the RA and RV TAC's oscillate out of phase with one another, and prolonged RA and RV transit times occur.

When this RNA algorithm was applied to the pts in this study, significant TR was found in 13 of the 44 pts. DE and RNA agreed upon the absence of TR in 29 pts. 3 pts were graded mild to moderate for TR by RNA in whom no significant TR was found by DE, however, each of these pts had normal RA and RV by both RNA and echocardiography. Only 2 pts had TR by DE that was undetected by RNA.

We conclude that RA TAC analysis during RNA detects TR with results similar to pulsed DE. Since TR can prolong RA and RV transit times and degrade left ventricular imaging, we suggest that the RA TAC be examined prior to RNA ejection fraction determination.

Monday, 3:30-6:00

Exhibit Hall

CARDIOVASCULAR GENERAL

No. 474

REGIONAL PHASE MAPPING USING GATED NUCLEAR ANGIOGRAPHY OR TOMOGRAPHY DURING VENTRICULAR TACHYCARDIA. D. Casset, R. Itti, L. Philippe, P. Cosnay and J.P. Fauchier, Trousseau University Hospital, Tours, France.

18 patients (10 M and 8 F) presenting ventricular tachycardia (VT) of various origin: 12 cases of primary cardiomyopathy including 8 patients with angiographically confirmed arrhythmogenic right ventricular dysplasia, 2 VT of ischemic origin and 4 VT of undefined (idiopathic) origin, have been studied during a prolonged episode of VT.

During recording, VT was spontaneous in 2 cases and provoked in the others. Acquisition time could be long enough to record one projection (LAO = 5 min) in 9 patients; for 7 patients two projections could be registered and for 2 patients gated tomography (32 projections over 360 degrees = 32 min) could be performed. In a second time all the patients were explored in sinus rhythm with the same technique.

Data processing was mainly the mapping of biventricular contraction using the Fourier method, and the site of earliest activation was defined both in VT and sinus rhythm.

A good correlation was found regarding the site of ectopic foci when compared with invasive procedures and, in 5 patients, with epicardial mapping during surgery. Advantage of tomography over single LAO projection imaging was a better approach of VT localization, allowing a distinction between anterior and posterior regions.

No. 475

SKELETAL MUSCLE BLOOD FLOW DURING MAXIMUM AND SUBMAXIMUM EXERCISE IN PATIENTS WITH HEART FAILURE. L. Davis, J. Mexler, D. Mancini, B. Chadwick, T. LeJemtel. Albert Einstein College of Medicine and Montefiore Medical Center, Bronx, N.Y.

In normals, skeletal muscle blood flow (SMBF) increases linearly with workload during graded exercise (Ex). Changes in SMBF during Ex were studied in 7 patients (Pts) with symptomatic heart failure (HF) despite therapy to determine if SMBF increased during graded Ex in these Pts. The Pts underwent treadmill Ex at submaximum workloads (Submax Ex) of 50-70% of a predetermined Max O₂ uptake (V_{O₂}) and maximum workloads (Max Ex) of 97-100% of Max V_{O₂}. For each Pt, SMBF was determined at rest and Ex using I33-Xenon washout and a Cd/Te detector interfaced to a micro-computer. Heart rate (HR), V_{O₂}, femoral vein lactate (FVL) and pH (FVph) were determined throughout Ex as follows:

	SMBF	V _{O₂}	FVL	FVph	HR
	cc/min/100gm	ml/kg/min	mg/100ml		beats/min
Submax					
Rest					
Ex	2.27	4.58	9.6	14.5	7.34
Max Ex	2.21	4.66	15.7	38.2	7.25
	NS	NS	P<.005	P<.01	P<.01
					P<.005

A significant (P<.01) increase in SMBF occurred between rest and Ex. No significant increase in SMBF occurred between Submax and Max Ex. Therefore, in Pts with HF, Max SMBF was obtained at Submax Ex. Further increases in workload beyond 60% V_{O₂} were achieved by increasing O₂ extraction with lactate accumulation and severe acidosis. This pattern is different from what is seen in normals who increase SMBF during graded Ex. This may reflect abnormalities in either the peripheral or central circulatory system.

No. 476

TOMOGRAPHIC LENGTH-BASED FOURIER ANALYSIS (LFA) AND EPICARDIAL PACING IN THE WOLFF-PARKINSON-WHITE SYNDROME. K. Nakajima, H. Bunko, J. Taki, I. Nanbu, Y. Shiire, M. Taniguchi, N. Tonami, K. Hisada, T. Misaki, and T. Iwa. Kanazawa University School of Medicine, Kanazawa, Japan.

The purpose of this study was to validate the tomographic LFA in patients (pts) with Wolff-Parkinson-White syndrome (WPW). Forty-four pts with WPW who underwent both surgical division of accessory conduction pathway (ACP) and gated blood-pool emission CT were studied. Thirty-three pts showed WPW patterns on ECG during radionuclide studies. In 3 pts, pacing studies were performed post-operatively using pacing wires placed on the epicardium. The degree of fusion was changed using atrio-ventricular sequential pacing or ventricular pacing with atrial trigger. In one pt, simultaneous pacings were performed at two sites simulating multiple antegrade ACPs. We have previously described the algorithm of LFA (J Nucl Med 25: 917, 1984). The time-length curves from a center to ventricular edges were generated and Fourier transform was applied to calculate length-based phase (LP). The segment of minimal LP was compared with surgically confirmed site of ACP. The detectability of ACPs was as follows:

ACP (R)	ant	lat	post	sep.	(L)	ant	lat	post	(Multiple)
	2/2	0/0	4/5	3/3		3/4	10/11	3/4	3/4
total	9/10				16/19				(4/8 ACPs)

Sensitivity of LFA for detecting ACPs was 28/33 (85%). The epicardial pacing site closely correlated with the segment of minimal LP. Two simultaneous pacing sites were identified. However, in the WPW with multiple ACPs, there was a limitation to estimate multiple ACPs prospectively only by Fourier analysis. We concluded that tomographic LFA can be an effective adjunctive method in the WPW.

No. 477

THE UTILITY OF GALLIUM SCINTIGRAPHY IN AMIODARONE PULMONARY TOXICITY. Y. Zhu, E. Botvinick, J. Golden, M. Stul-

barg, R. Hattner, M. Dae, M. Scheinman. University of California San Francisco.

We sought to determine the utility of gallium scintigraphy (Ga) in the assessment of Amiodarone (A) pulmonary toxicity (PT). Symptoms (S), chest X-rays, pulmonary function tests (PFT) and lung biopsies were studied where available in 57 patients (pts) on A, 25 with clinical PT (Group I), 20 with S without PT (Group II) and 12 without S or PT (Group III). All had Ga with S and/or PT or while on A without S or PT. Fourteen pts with S and/or PT had Ga and 22 had PFT before starting A. Treatment duration and total A dose was not different among groups.

All studies in Group III were normal. S could not differentiate between Group I, 3 without S, and Group II. X-ray was normal in only one Group I pt, but neither X-ray pattern or serial change could separate Group I from Group II pts. Biopsies in 13 Group I and 4 Group II pts were abnormal but non-specific. Serial reduction in diffusion capacity was greater among Group I than Group II pts (p<.05). Ga, graded 1-4+, were more abnormal in Group I than in Group II pts (p<.001). Although Ga was normal in 2 Group I pts with APT pts, serial Ga revealed impressive increases in grade only in Group I (p<.01). Ga at the time of APT looked benign in 3 pts, but was abnormal compared to Ga before A or compared with current X-ray.

Although S, X-ray, PFT and biopsy were sensitive for APT, diffusion capacity measured serially and Ga at the time of APT provided specificity. Most specific for APT was serial worsening of Ga, which was best appreciated when compared with a Ga performed before A or with a concurrent X-ray.

Monday, 3:30-6:00

Exhibit Hall

CARDIOVASCULAR: MYOCARDIAL IMAGING

No. 478

DEMONSTRATION OF Tc-99m PYROPHOSPHATE UPTAKE IN REVERSIBLY INJURED NEONATAL MYOCYTES. A.J. Fischman, J.A. Scott, C. Rabito, H.W. Strauss, E. Haber, B.A. Khaw. Massachusetts General Hospital, Boston, MA.

The effect of ischemic injury to myocardium on Tc-99m pyrophosphate (PYP) uptake by neonatal rat myocytes was investigated in primary cultures at 37 °C. One to 2 day old neonatal rat hearts were dispersed by trypsinization. After 48 hr in culture, the cells were beating at a rate of about 150/min. Three days later, culture plates were exposed to an atmosphere of 95% N₂/5% CO₂ for 4 hr in an anaerobic chamber to produce ischemic injury. Myocytes stopped beating in these cultures. The cultures were divided into 2 parallel groups; Group I was recultured under normoxia (95% O₂/5% CO₂). After 24 hr, the cells were beating normally. Then 10⁶ cpm PYP were added and incubated for 3 hr. Group II had PYP (10⁵ cpm) added immediately followed by exposure to the tracer under normoxia for 3 hr. Controls (Group III) were grown under normoxia and treated identically for PYP and reculture conditions. The myocytes were dissociated by mild trypsinization, washed with cold media, centrifuged and then counted in a gamma counter. The counts were then normalized to 5x10³ cells. PYP uptake in the three groups is as follows:

Group	PYP (CPM ± SEM)	Function	P	N
I	827 ± 37	Normal beating	> 0.5*	6
II	2424 ± 128	No beating	< 0.01*	6
III	862 ± 31	Normal beating		6

* = P values relative to control Group III.

Uptake of PYP in anoxic cultures also paralleled the uptake of propidium iodide, an indicator of increased cellular permeability. The results suggest that PYP is sequestered during reversible injury but not by neonatal rat myocytes which had recovered.

No. 479

MYOCARDIAL IMAGING WITH Tc-99m TERTIARY BUTYL ISONITRILE (T-BIN), MN Khalil, KM Patel, JV Thornback, MY Early, G Hartley, DN Taylor, JM Berry, PJB Hubner. Cardiology Department, Groby Road Hospital, Leicester, U.K.

We report our clinical experience with a new myocardial imaging agent; Tc-99m T-BIN in 15 patients with myocardial infarction (M.I.) and 45 with angina due to angiographically proven coronary artery disease.

Imaging was performed in 3 projections after the administration of 200-400 MBq of Tc-99m T-BIN using a gamma camera with a converging collimator. In patients with M.I. defects in myocardial uptake were clearly shown at rest. The patients with angina showed reversible perfusion defects following intravenous injection at maximal treadmill exercise. Optimal images were obtained at 30 minutes for post exercise scans and at 4 hours for the delayed views. Hepatic to myocardial uptake ratios were approximately 4:1 at rest and 2:1 after exercise. Separation between the liver and the heart was best demonstrated on the 45° LAO projection with 20° cranial tilt. 5 patients with M.I. and 15 with angina also had Tl-201 scans. T-BIN images were superior to those obtained with Tl-201 and perfusion defects were better seen on the T-BIN scans.

24 patients in the same study had ECG gated T-BIN cardiac scintigraphy. Regional wall motion could be seen and assessed using a cine display and defects in myocardial uptake were best seen in diastole.

In conclusion, besides its use as a myocardial perfusion imaging agent, Tc-99m T-BIN scan allowed assessment of L.V. contraction when gated studies were performed. The results with T-BIN have been favourable and in our experience, superior to thallium-201.

No. 480

CORRELATION OF Tc-99m-STANNOUS PYROPHOSPHATE MYOCARDIAL SCINTIGRAMS WITH SERUM MB-CREATININE KINASE (CPK-MB) AND CLINICAL COURSE IN EVALUATION OF PERIOPERATIVE MYOCARDIAL INFARCTION (M.I.). A. R. Khan, J. M. Gona, R. Tymm, J. Aldridge, S. Gutman, J. J. Steinbach. VA Medical Center, Buffalo, NY.

We corroborated scintigraphic findings with CPK-MB levels and clinical course in 152 patients who underwent coronary artery bypass surgery (CABG) between 1981-1985. No patients with concomitant valvular surgery or L.V. aneurysmectomy were included. The imaging was performed 1-4 days prior and 3-8 days after the surgery. The scintigrams were read by two observers and graded 0-4+, diffuse or focal, without knowing clinical details about the patients. A 2+ focal, 3+ or 4+ myocardial scintigram was considered positive for M.I.

Blood for analysis of cardiac enzymes was obtained the day prior to surgery and serially at 8, 12, 24, 48, and 72 hours after surgery.

130 patients had peak CPK-MB below 50 IU L. 128 of them had negative scintigrams. Of the two patients who had positive scintigrams with CPK-MB below 50 IU L, one had M.I. clinically, and the other had uneventful recovery. 22 patients had peak CPK-MB above 50 IU L. 12 of them had positive and 10 had negative scintigrams. The post-operative course was uneventful in all the ten patients who had negative scintigrams.

We conclude that in our institution, patients with peak CPK-MB level below 50 IU L are unlikely to have perioperative M.I. The CPK-MB can be falsely elevated as was in our ten patients with negative scintigrams and uneventful clinical course. Scintigrams thus add specificity to the patients with elevated CPK-MB levels and are useful in diagnosing perioperative M.I.

No. 481

IN-111-ANTIMYOSIN MONOCLONAL ANTIBODY IN THE DETECTION OF DOXORUBICIN INDUCED CARDIOTOXICITY. M.C. Lee, N.D. LaFrance, K. Takeda, S. Tanada, U. Scheffel, H.T. Ravert and H.N. Wagner, Jr. The Johns Hopkins Medical Institutions, Baltimore, MD.

Doxorubicin hydrochloride causes severe cardiotoxicity often discovered by ventricular function studies only after irreversible cardiac damage has occurred. In-111 antimyosin antibody (AMAb) and Tc-99m-pyrophosphate (PYP) have been used to detect myocardial necrosis in patients with myocardial infarction. In the present study our goal was to determine whether myocardial necrosis that accompanied doxorubicin toxicity could be detected by In-111-AMAb.

Organ distribution of In-111 AMAb was measured in mature rabbits (12: control, 9: doxorubicin) that received weekly 2.5 mg/kg of doxorubicin intravenously for 4-8 weeks. At this dose, 70% of the animals could be expected to become cardiotoxic. All animals were injected with 40-50 uCi of In-111-AMAb 24 hr before sacrifice and the radioactivity in the heart and other organs was expressed as % injected dose/gm (%ID/gm). For In-111-AMAb the control myocardial uptake (mean ± 1SD) was 0.033 ± 0.021 and 0.022 ± 0.012 for the left and right ventricles, respectively, while in the doxorubicin treated group their values increased to 0.063 ± 0.035 and 0.082 ± 0.036 with a range of 0.027 to 0.126 %ID/gm (p<0.025). Similar results were obtained in septum and atrium.

We conclude: 1) In-111-AMAb myocardial uptake accumulates to a high degree in doxorubicin cardiotoxicity, and 2) the amount of uptake may reflect the degree of myocardial damage.

No. 482

GALLIUM-67 IMAGING IN HEART TRANSPLANTS (HT) J.C.Meneguetti, J.Soaes Jr., G.Bellotti, E.Bocchi, M.L.Higuchi, N.Stolf, F.Hironaka, C.Buchpiguel, F.Pileggi, A.Jatene, E.E.Camargo.- Instituto do Coração, São Paulo, Brazil.

Acute rejection (AR) is the most important complication in HT. Endomyocardial biopsy (EB) is considered the most reliable study for AR monitoring. The purpose of our investigation was to correlate a non-invasive procedure, Ga-67 imaging, with EB data in HT patients (pts). Seven male pts (41-54 years) were sequentially submitted to 41 Ga-67 studies between one week and 8 months after surgery. Images and EB were obtained 48 hr after Ga-67 injection. Pathological findings were graded as 0=absent; 1=non-specific reaction; 2=AR in remission; 3=mild AR; 4=moderate AR; 5=severe AR. Cardiac Ga-67 uptake was graded as absent, mild, moderate and severe AR, the latter not found in our pts.

Ga-67 Imaging	Biopsy				
	0	1	2	3	4
Absent (n=15)	8	3	1	3	0
Mild (n=19)	0	6	5	7	1
Moderate (n=7)	0	1	0	1	5

Imaging sensitivity was 83% (19/23), with 27% false-negatives which included one AR in remission previously treated and 3 mild AR (pts not treated with uneventful course). Out of 7 studies with moderate Ga-67 uptake, 5 EB showed moderate AR and the pts were submitted to therapy. It is conceivable that Ga-67 imaging may play an important role as a screening procedure for EB in heart transplanted pts.

No. 483

REGIONAL DISTRIBUTION OF Tc-99m HEXAKIS-ALIPHATIC ISONITRILES IN ISCHEMIC HEARTS WITH AND WITHOUT REPERFUSION. S.A. Mousa, S.J. Stevens, and S.J. Williams. E.I. DuPont de Nemours, Biomedical Products, N. Billerica, MA

Many derivatives of Tc-99m-hexakis-aliphatic isonitriles show potential as agents for myocardial perfusion scintigraphy. Three derivatives, [isonitrile = t-butyl (NEN-14); 2-isonitrilo-2-methyl isobutyrate (NEN-26); 2-

methoxy-2-methylpropyl-1-isonitrile (NEN-30)] have been studied to determine their distribution relative to regional myocardial blood flow (RMBF) and their potential for redistribution in coronary artery ligation and ligation-release models. The initial distribution of all 3 isonitriles and Tl-201 is proportional to RMBF in normal swine or rabbit hearts and in hyperemic hearts following dipyrindamole infusion (4-5x normal blood flow). In ligation-release studies, Tl-201 and NEN-14 both redistribute 40-45% during 1 hr of reperfusion following a ligation which is released 5 min. after intravenous injection (protocol A). If the ligation is maintained for 15 min post-injection, or if NEN-14 is injected in the left ventricle, only 20% redistribution of NEN-14 is observed. Therefore, redistribution of NEN-14 is a result of its high residual lung pool (30-40% ID) and minimal myocardial clearance. In contrast, NEN-26 and NEN-30 exhibit much lower initial lung extraction (6.8 and 2.3% ID, respectively). Under protocol A, NEN-26 redistributes only 18%, while no measurable redistribution of NEN-30 is detected. Some ischemic to normal zone activity normalization with NEN-26 likely is due to moderate normal-zone clearance ($T_{1/2} = 1.5-2$ hr) compared to NEN-30 which does not clear substantially from normal heart tissue ($T_{1/2} = 4-5$ hr). These results show the regional distribution of NEN-30 in the heart to be the most stable of any Tc-99m-isonitrile yet evaluated and suggest it to be a promising agent for diagnosis of ischemic heart disease in humans.

No. 484

MYOCARDIAL UPTAKE AND RETENTION OF Tc-99m-HEXAKIS-ALIPHATIC ISONITRILES: EVIDENCE FOR SPECIFICITY.
S.A. Mousa and S.J. Williams. E.I. DuPont de Nemours, Biomedical Products, N. Billerica, MA

The Tc-99m-hexakis-aliphatic isonitriles are a promising class of agents for myocardial perfusion scintigraphy (Holman, et al. 1984). A definition of the mechanism of extraction and retention of Tc-99m-isonitriles by the heart will be valuable in understanding the diagnostic information these agents can provide. Studies in guinea pig heart slices demonstrate the uptake of Tc-99m-hexakis-t-butylisonitrile (NEN-14) to be sensitive to pH and temperature, insensitive to ouabain, and inhibited by Tc-99 labeled complex. The uptake of Tl-201 in this preparation is inhibited 50% by ouabain but unaffected by the Tc-99 labeled complex. In isolated buffer-perfused guinea pig hearts, the first-pass extraction of NEN-14 is 95%. The uptake of NEN-14 approaches saturation after 50 min of continuous infusion of a solution containing 5 mCi/L. A less lipophilic isonitrile derivative, 2-methoxy-2-methylpropyl-1-isonitrile (NEN-30), is 40% extracted on first-pass but shows rates of uptake and saturation similar to NEN-14 during continuous infusion. When hypoxia is induced by pre-equilibration of the perfusate with N₂:CO₂ (95:5), the rates of uptake and the levels of saturation are greatly reduced. Moreover, the subcellular distribution of the extracted activity is different in normal and hypoxic heart preparations. The membrane to cytosol ratios of NEN-14 and 30 are 5.0 and 0.04 respectively in normal hearts, but for NEN-30 this increases to 0.4 in hypoxic hearts. Gel filtration HPLC of the cytosolic extracts show both NEN-14 and 30 to be bound to a fraction which co-elutes with a protein standard of 5-8 x 10³ MW. Binding of NEN-14 is inhibited by the Tc-99 labeled complex. These studies demonstrate the uptake and retention of Tc-99m isonitriles in the heart to be specific, different than Tl-201, and potentially related to physiological parameters in addition to blood flow.

No. 485

PLANAR AND TOMOGRAPHIC EVALUATION OF Tc-99m TERTIARY BUTYL ISONITRILE (Tc-99m TBI) AS A MYOCARDIAL IMAGING AGENT. P. Rigo, F. Gilis, R. Cantineau, University of Liege, Institute of Medicine, Liege, Belgium.

Development of technetium labeled myocardial (M) blood flow agents should enhance the clinical role of M imaging. This procedure will indeed benefit from the higher photon flux, improved energy range and availability of technetium.

Tc-99m TBI is such a compound. Preliminary experience in animals and patients (pts) with M infarction has demonstrated good M-uptake in relation to blood flow and

definition of regional M infarction. In this study, we have evaluated its ability to document stress-induced regional M perfusion deficits in pts with CAD. Ten pts with stress-induced thallium (Tl) defects and CAD defined by angiography were studied (mean age : 53, range 51-72) at rest and stress. Exercise load and duration were comparable in all pts (mean 8.1 min and 106 watts on Tl and 8.3 min and 112 watts on TBI). Heart rate on TBI was slightly lower as 2 pts were treated by beta-blocking agents in the interval (Tl 130/min, TBI 126/min N.S.). Tl defined ischemic or necrotic defects in 14 arterial territories (3 MI, 11 ischemia). TBI demonstrated 11 of these, although in 2 cases the defect disappeared before one hour. Missed segments occurred twice in pts with multivessel defects and once because of hepatic superimposition. Tomography in 3 pts provided better M to background ratio in the thorax allowing early scanning (<30min). Liver uptake remained a problem however.

We conclude that Tc-99m TBI is a promising new agent allowing definition of transient M ischemia. Early scanning with tomography and an analog with less hepatic uptake should be developed.

No. 486

VALUE OF INTERPOLATING SCAN AND OBLIQUE-ANGLE TOMOGRAMS FOR EVALUATION OF CORONARY ARTERY DISEASES IN MYOCARDIAL POSITRON TOMOGRAPHY USING N-13 AMMONIA. M.Senda, Y.Yonekura, N.Tamaki, H.Saji, H.Koide and K.Torizuka. Kyoto University School of Medicine, Kyoto, Japan.

We recently pointed out the presence of low sensitivity areas or gaps between adjacent slices of the multislice positron emission tomography (PET) and introduced the "interpolating scan", which was performed as the object was moved half the slice interval, to fill them out and reconstruct oblique-angle tomograms (IEEE Trans Med Imag MI-4:44-51, 1985). The goal of the present study is to evaluate clinical usefulness of the interpolating scan and the oblique-angle tomograms for detection of diseased coronary vessels. Stress myocardial perfusion studies using N-13 labeled ammonia were performed in 20 patients with coronary disease. The detectability of the diseased vessel observed as segmental perfusion defects for the right coronary artery (RCA) and the left anterior descending artery (LAD) was 57 and 89%, respectively, in single-position scans. The false negative defects were often located in the inferior and apico-inferior walls, which were almost tangential to the image plane and were considered to have fallen into the gaps. When the interpolating scan was utilized and the two sets of images were interlaced with each other, the detectability was 71% for RCA and 94% for LAD lesions. The interpolating scan also allowed to reconstruct long-axis and short-axis tomograms in high quality, which further improved the detectability (100% for RCA or LAD and 75% for LCX lesion) and helped understand the anatomical relationships to the coronary territories.

No. 487

KINETICS AND BIODISTRIBUTION OF LOW DENSITY LIPOPROTEIN: ^{99m}Tc-LDL vs ¹³¹I-TYRAMINE CELLOBIOSE-LDL.

S. Vallabhajosula, M. Paidi, H. Lipszyc, J.J. Badimon, Anh-Le, S.J. Goldsmith, V. Fuster and H.N. Ginsberg. Mount Sinai Medical Center, New York, NY.

We have previously demonstrated that ^{99m}Tc-LDL (Tc-LDL) was removed from plasma with kinetics that were identical to radioiodinated native-LDL. To further validate the utility of Tc-LDL, we have compared the kinetics and biodistribution of Tc-LDL with ¹³¹I-Tyramine Cellobiose-LDL (I-TYC-LDL), an intracellularly trapped ligand in normal rabbits (NR) and rabbits fed on a high cholesterol diet (HCR). Tc-LDL and I-TYC-LDL were administered simultaneously into NR and HCR. The fractional catabolic rate calculated from the plasma time-activity curves of Tc-LDL

($2.97 \pm 1.78 \text{ d}^{-1}$) is higher than that of I-TYC-LDL ($1.0 \pm 0.15 \text{ d}^{-1}$) suggesting that the plasma turnover of LDL is faster with Tc-99m than with ^{131}I -TYC. The rabbits were sacrificed at 24 hours and the % injected dose/gram of tissue was determined.

Organ	NR (n=4)		ATR (n=3)	
	Tc-LDL	I-TYC-LDL	Tc-LDL	I-TYC-LDL
Adrenal	2.02 ± 1.03	1.23 ± 0.56	0.12 ± 0.05	0.09 ± 0.05
Spleen	0.74 ± 0.50	0.62 ± 0.20	0.25 ± 0.14	0.27 ± 0.16
Liver	0.46 ± 0.08	0.22 ± 0.03	0.24 ± 0.05	0.17 ± 0.08

The uptake of both tracers was similar with adrenals, spleen and liver accumulating the greatest activity per gram of tissue. The specific uptake of Tc-LDL and I-TYC-LDL in adrenals and liver of HCR is significantly reduced compared to NR. This may be due to the down regulation of LDL receptors in HCR. These results show that Tc-LDL could be used as a "trapped ligand" to image and quantitate LDL distribution in vivo.

No. 488

RADIOANTIBODY DETECTION OF CARDIAC ALLOGRAFT REJECTION. R.L. Wahl, M. Liebert, R. Pierson, D. DaFoe. University of Michigan Medical Center, Ann Arbor, MI.

Rejection represents a major cause of transplanted organ loss. The accurate early diagnosis of rejection is essential to initiating appropriate therapy. We have shown that radiolabeled monoclonal antibodies (MoAbs) reactive with T-cell subsets are capable of localizing preferentially to rejecting non-vascularized allografts in the mouse (Transplantation 40:451, 1985). The ability of anti T-cell MoAbs to localize to rejecting vascularized grafts has not, however, been evaluated.

Hearts from Lewis (RT1) rats when transplanted to Brown Norway (BN)(RTn) will be rejected in approximately 1 week. Five male BN rats received Lewis hearts grafted to the abdominal aorta. Four days after transplantation these rats were injected intravenously with I-131 W3/13W (anti-rat pan T-cell MoAb) or I-131 OX-8 MoAb (anti cytotoxic-suppressor). Animals were imaged at two and four days post-injection, and sacrificed after imaging.

Both the W3/13 and OX-8 antibodies accumulated preferentially in the rejecting hearts with a 2.92 and 2.44 fold radioantibody excess respectively, over the control native hearts ($P < .05$). Images of the animals showed activity in the region of the rejecting transplant, however it was not obviously more intense than the activity seen in the region of the native heart. The blood pool activity at sacrifice was twice the rejecting heart's activity, and this likely degraded image quality.

While refinements in technique will be necessary, possibly including blood pool subtraction, to produce diagnostic images, these preliminary experiments demonstrate the potential of MoAbs to T-cells as specific scintigraphic probes for the diagnosis of transplant rejection.

Monday, 3:30-6:00

Exhibit Hall

CARDIOVASCULAR: Tl-201

No. 489

SERIAL 201-Tl SPECT : INTEREST IN THE ASSESSMENT OF THERAPY IN ACUTE MYOCARDIAL INFARCTION (MI). A. Bertrand, M. Amor, G. Karcher, F. Zannad, N. Danchin, F. Aug, P. Maurin, J.M. Gilgenkrantz. CHU Nancy-Brabois France

Increasing developments in therapy (beta-blockers, calcium-antagonists, thrombolysis...), aimed at the reduction in infarct size (IS), necessitate more adaptable methods than the conventional ones (ECG, cardiac enzymes...). Analysis of Tl-SPECT allows a good assessment of Thallium defect size (TDS) to be made, as well as of its evolution over time and thus the evolution of pathological zones.

34 patients, admitted within 6 hrs of the first MI symptoms, were randomized, double-blind to placebo (PCB), or calcium-antagonist drug : Diltiazem (DTZ) for 21 days. I.S. was assessed by plasma CK and MB-CK curves (Peak level, time to-peak, area under curves, cumulative release) and by serial rest-Tl-SPECT, performed at admission, 48 hrs and 21 days later and analyzed semi-quantitatively by two independent observers grading 13 myocardial sectors from 0 (normal) to 2 (no fixation) and calculating a Thallium defect size varying from 0 to 26. Groups were comparable in terms of age, sex, infarct location, rate of acute complications, and inclusion time ($4.4 \pm 1 \text{ VS } 4.6 \pm 0.9 \text{ hrs}$). Results showed no differences in CK and MB-CK data, although a decrease in TDS was observed, which was significantly greater in the DTZ group than in the PCB group ($- 2.2 \pm 1.93 \text{ VS } - 0.7 \pm 3. \text{ p} < 0.02$).

This study shows that the serial quantitation of perfusion defect by 201-Tl SPECT reveals a significant reduction in infarct size, undetectable by conventional methods in such small groups of patients. Serial 201-Tl SPECT is a valuable tool for studying changes in myocardial infarct size and thus for assessing therapy.

No. 490

THALLIUM "REDISTRIBUTION" - AN EXPLANATION. T.F. Budinger and G.M. Pohost*, Donner Lab, University of California, Berkeley, CA and *University of Alabama Medical Center, Birmingham, AL

The change in the pattern of thallium-201 myocardial distribution observed after exercise and that observed an hour or more later without reinjection has led to a number of explanations (Seminars Nucl Med X,70, 1980). Based on observations of transient hyperemia involving separate injections in dogs using Rb-82 and positron tomography at Donner Laboratory before and after coronary occlusions, and recent observations of prolonged hyperemia in ischemic zones in patient studies post-exercise (at rest), we hypothesize that the simple explanation is that the heart physiology changes such that the ischemic zone maintains its metabolic signals for maximum perfusion after exercise whereas the normal myocardial tissue returns to a low flow state at rest.

To test whether circulating Tl-201 amounts would be sufficient for an effective "endogenous reinjection" to reflect this new flow status in the ischemic heart when at rest, we evaluated the Tl-201 blood activity in 38 patients. Multiple exponential fits were made to blood sample data. Using the fit equation as the model we calculated the available activity for uniform time intervals. Below are shown some of the ratios of available activity.

Minutes	Relative Available Activity
0 - 5	1.0
5 - 20	2.1
20 - 120	5.0

These analyses give plausibility to our hypothesis.

No. 491

QUANTITATION OF THE DISTRIBUTION PATTERN OF Tl-201 SPECT IN NORMAL MALES AT STRESS AND REDISTRIBUTION. R.D. Burow and C.R. Corn. University of Oklahoma Health Sciences Center, Oklahoma City, Ok.

A technique is presented which characterizes the variation in regional Tl-201 distribution of the entire myocardium. SPECT imaging using 2.0 millicuries of Tl-201 was performed within five minutes of maximal exercise on fourteen male volunteers with a low a priori probability of coronary artery disease. Sixty four 64x64 word mode images were acquired for 30 seconds at 2.8° intervals from the RAO 40° to the LAO 50° projection using a single head camera equipped with a low energy all purpose parallel hole collimator. Short axis slices (0.6mm thick) of the myocardium were constructed from apex to base using a standard filtered back-

projection algorithm. Circumferential profiles of the slices were used in the construction of a 2 dimensional map of the 3 dimensional myocardium. Identical acquisition and processing procedures were employed for stress (S) and 4 hour redistribution (R) studies. The mean normalized S activity varied from a maximum of 90% in the mid-lateral wall to a minimum of 50% in the basal septum and apical regions. The mean R varied from a maximum of 91% to a minimum 49% in the same respective areas. The largest variance in the S images (11%) was in the inferoapical region. In the R images the largest variance (14%) occurred in the high septum with a high (9%) variance in the inferoapical region. Maximal per cent change from redistribution to stress (15%) occurred in the basal area, with minimum values in the apex. We conclude: 1) in normals, there is no difference between S and R patterns of Tl-201 distribution although there is significant regional variation in Tl-201 distribution and 2) quantitative techniques are required for proper interpretation of SPECT studies.

No. 492

REDISTRIBUTION ABNORMALITIES IN EXERCISE THALLIUM IMAGES: UNRESOLVED ISCHEMIA VS INFARCTION? KG Cloninger, EG DePuey, EV Garcia, GS Roubin, WL Robbins, HJ Berger, A Nody, EE DePasquale. Emory Univ, Atlanta, GA

To determine if incomplete redistribution (RD) at 4 hrs in exercise tomographic thallium-201 (TL) studies is always due to scar, 154 patients (pts) were evaluated before and after a total of 162 successful percutaneous transluminal coronary angioplasty (PTCA) procedures. TL studies were analyzed using polar bullseye maps. For both immediate and delayed (DL) images, abnormalities were quantified as a TL score by calculating a standard deviation (SD) weighted sum of pixels > 2.5 SD below gender-matched normal limits. 146 of 162 studies were abnormal pre-PTCA. Of these 146, incomplete RD occurred in 113 (77%): 16 (12%) in pts with prior myocardial infarction (MI) and 97 (88%) in pts without MI. Post-PTCA improvement in DL image score occurred in 8/16 (50%) with MI and 72/97 (89%) without MI (p < .05). Post-PTCA, DL images were normal in 1/16 (6%) with MI and 32/97 (33%) without MI (p < .05). Pre-PTCA, DL image scores were positively correlated with scores in the immediate post-exercise images in pts with MI (r=.78) and those without MI (r=.65).

To determine if additional DL images could help differentiate scar from ischemia, an 8-24 hr DL image was obtained in each of 40 other pts with incomplete RD at 4 hrs. Of 28 pts with prior MI, 15 had no RD, and 13 had further RD at 8-24 hrs. In 12 pts without MI, 1 had no RD, 7 had further RD, and 4 had complete RD.

Thus, 4 hr DL image defects frequently do not signify MI. Their severity is proportional to immediate post-stress abnormalities. Additional imaging at 8-24 hrs is recommended in pts with incomplete RD and no prior MI.

No. 493

A COMPARISON OF FATTY ACID AND Tl-201 UPTAKE IN A CANINE MODEL OF MYOCARDIAL ISCHEMIA AND REPERFUSION. M.D. Devous, Sr., J.K. Payne. Nuclear Medicine Center. The University of Texas Health Science Center at Dallas, TX.

Relationships among the distributions of Tl-201, l-125-15(4-iodo-phenyl)-9-methyl pentadecanoic acid* (l-125-9-MPDA) and regional myocardial blood flow (RMBF, tracer microspheres) were compared in anesthetized open chest dogs following 90 min of left anterior descending coronary artery occlusion and 3.5 hr of reperfusion (REP; N=8). RMBF was assessed during control, ischemic, and early and late REP. Tl-201 and l-125-9-MPDA were injected 15 min prior to sacrifice. In 3 animals RMBF was restored to both epi- and endocardium throughout REP, in 3 animals REP was maintained only in epi, and in 2 animals REP was not

maintained. Correlations among uptake in ischemic and non-ischemic zones, area of decreased uptake, and RMBF were compared. The area of decreased fatty acid uptake (FAU) was significantly smaller than that for Tl-201 (TLU) (area ratio l/TL:epi 0.65; endo 0.89). When expressed as percent of uptake in non-ischemic zones, then FAU was 40±7% in epi and 19±4% in endo, while TLU was 33±5% in epi, and 31±8% in endo. Endo had more severe flow reductions than epi both early and late, and therefore suffered the most severe ischemic insult. Thus, FAU correlated with the severity of ischemia while TLU did not. FAU was correlated with RMBF at the end of REP (r=.83, slope=.89) while the correlation for TLU was not as strong (r=.63, slope=.38). FAU is a more sensitive indicator of ischemic injury in the setting of myocardial REP and FAU but not TLU correlates with residual RMBF. *Mallinckrodt Nuclear, Inc.

No. 494

THE VARIABILITY OF THALLIUM HALF LIFE AT REST AS COMPARED TO EXERCISE. M.R. Freeman, N. Kanwar, P.W. Armstrong. St. Michael's Hospital, University of Toronto, Toronto, Ontario, CANADA.

The half life (t1/2) of thallium(Tl) after resting (RE) injection has not been fully characterized in man and not compared to similar data after exercise(EX). Accordingly, we injected IV Tl at RE in 30(43±11 yrs) normal male subjects and during EX in 28(45±9 yrs) normal male subjects. Tl imaging in the anterior, 45° LAO, and 70°LAO views for 10 minutes each was begun 20 min and 4 hrs post injection, and in addition, at 24 hrs post RE injection. After interpolative background subtraction with an irregular ROI, we generated circumferential profiles from the mean of 3 maximum pixels along 60 radii at 6° intervals from the center of the LV. The t1/2 data for 0 to 4 hrs are shown in the table:

	ANTERIOR	45°LAO	70°LAO	ALL VIEWS
REST	11.4±1.0	10.6±1.0	8.8±0.7	10.3±1.0
EXERCISE	3.6±0.1*	3.9±0.3*	4.2±0.3*	3.9±0.3*

*p<.001 vs REST, each view t1/2 value different from all other views (ANOVA, p<.01).

The t1/2 at RE of all views from 4 to 24 hrs was 19.7±1.1 hrs, different than 0 to 4 hrs (p<.01). Total myocardial counts of 1.6±.5x10⁵ at RE in the 45°LAO view were greater than 1.3±.3x10⁵ at EX(p<.05).

We conclude that the t1/2 of Tl is dependent upon status at injection and is multiexponential at RE. The variability of t1/2 between views suggests that 20 min. after injection, maximum Tl uptake had not occurred at RE, but washout of Tl had already commenced after EX. The differences in t1/2 after rest and exercise injections must be considered in quantification and is not explained by less myocardial thallium at rest.

No. 495

QUANTITATIVE STRESS-REDISTRIBUTION Tl-201 SINGLE-PHOTON EMISSION TOMOGRAPHY (SPECT): DEVELOPMENT OF A SCHEME FOR LOCALIZATION OF CORONARY ARTERY DISEASE. F Prigent, J Maddahi, DS Berman. Cedars-Sinai Med Ctr, Los Angeles, CA

To define the vascular territories (VT) on SPECT images, we studied 19 patients (pts) with angiographic single-vessel (SV) coronary artery disease (CAD) and positive exercise Tl-201 SPECT, of whom 7 had left anterior descending (LAD), 6 had left circumflex (LCX), and 6 had dominant right (R) CAD. Maximal-count stress circumferential profiles (CP) were generated from the LV short-axis tomograms and the apical part of the vertical long-axis tomograms. Perfusion defects, defined by the % CPs falling below normal limits, were plotted onto a polar coordinate map, which was divided into the apex and 48 equal sectors. The probability (pr) of a sector to represent a particular VT was defined by the relative frequency by which it was involved in pts with CAD of the corresponding vessel. The 3 VT were defined by the sectors in which

the pr for the corresponding vessel was $>.80$. Defects in these regions were assigned to the given VT, whereas defects in the remaining regions of the myocardium ($pr < .80$) were considered nonspecific for VT but positive for CAD and were assigned to the VT from which they originated. Of the 19 pts, 16 (84%) were classified as SVD (all in the correct VT), while the remaining 3 were classified as double-vessel CAD due to extension of defect into another VT. The true negative rate for absence of CAD in the 3 coronary arteries was 92% for the LAD, LCX, and RCA. Conclusion: a scheme for localization of CAD perfusion defects to specific coronary arteries on SPECT images has been developed that 1) accounts for inter-individual anatomic variation and 2) offers promise for clinical characterization of patients with CAD.

No. 496

IN PATIENTS WITH HIGH-RISK CORONARY ARTERY DISEASE AND Tl-201 ISCHEMIA, IS EXERTIONAL ANGINA MEANINGFUL? S Reisman, J Maddahi, D Berman. VA Medical Center, Long Beach, and Cedars-Sinai Medical Center, Los Angeles, CA

In light of recent reports suggesting a high frequency of asymptomatic ("silent") ischemia in patients with coronary artery disease (CAD), increasing attention is being focused on the clinical importance of chest pain symptomatology in patients with "high-risk" CAD, defined as left-main and/or triple-vessel CAD. Since the results of testing influence clinical decisions in this group, we analyzed the relationship between the presence or absence of exertional angina during treadmill testing and the extent and severity of exercise-induced ischemia, by evaluating 55 consecutive patients (pts) with Tl-201 exercise-induced ischemia (>1 reversible segment) and left-main and/or triple-vessel stenosis ($>50\%$). Three-view Tl-201 scintigrams were divided into 15 segments. Severity of exercise-induced ischemia was represented by a Tl-201 ischemic severity score (ISS) and extent of ischemia by # reversible Tl-201 segments. Exertional angina during treadmill testing was present in 34 pts (62%) (GpI) and absent in 21 pts (38%) (GpII).

	ISS	# R Segs	Ex Dur	HR	Max ST+
GpI	7.1+4.6	4.2+2.5	6.8+2.5	134.7+22.9	2.0+1.5
GpII	6.7+4.0	4.0+2.0	7.9+3.3	137.4+18.4	2.4+1.1

R segs=reversible segments; Ex=exercise; Dur=duration (minutes); HR=peak heart rate; Max ST+= maximum ST depression (mm). No significant differences were noted between the two groups. We conclude that in pts with high-risk CAD and Tl-201 ischemia, silent exertional ischemia is common and does not indicate a less ischemic group. Thus, the presence or absence of angina during treadmill testing may not be reliable for guiding medical or surgical intervention in this patient group.

No. 497

THALLIUM SCINTIGRAPHIC AND CORONARY ARTERIOGRAPHIC CORRELATES OF PROLONGED POSTEXERCISE ST SEGMENT DEPRESSION. S Reisman, A Rozanski, J Maddahi, D Berman. VA Med Ctr, Long Beach, & Cedars-Sinai Med Ctr, Los Angeles, CA

To determine the significance of prolonged post (p) exercise (Ex) ST depression (ST+), we studied 81 patients with >1 mm ST+ during Bruce protocol treadmill Ex who underwent Ex Tl-201 scintigraphy and coronary angiography. Three-view Tl scintigrams were divided into 15 segments (segs). The extent of myocardium with Tl ischemia was determined by the number (#) of reversible segs. Forty-six patients had "normalization" of ST+ to <1 mm within the first 5 min pEx (GpI) and 35 patients had prolonged >1 mm ST+ for >5 min pEx (GpII). Results:

	Ex Dur	# Rev Segs	Sig V	Cr V	Max Ex ST+
GpI	9.0+3.4	2.1+2.1	2.0+1.1	1.2+1.1	2.0+0.9
GpII	6.9+2.5*	3.5+3.1*	2.5+0.9*	1.7+1.1*	2.7+1.3*

* $p < 0.05$ vs GpI, Dur=duration (minutes), Rev=reversible, Sig V=# vessels with $>50\%$ stenosis, Cr V=# vessels with $>90\%$ stenosis. Max=maximum. Triple-vessel stenosis ($>50\%$) was more common in GpII vs GpI (69% vs 41%, $p < .05$). Sev-

ere exertional hypotension (drop below resting BP) was also more common in GpII vs GpI (29% vs 9%, $p < .05$). Onset of 1mm ST+ was earlier in GpII vs GpI (3.3 ± 1.9 min vs 6.2 ± 3.3 , $p = .0001$). Thus, compared to patients with early pEx ST normalization, those with prolonged pEx ST manifest more extensive and severe: 1) anatomic coronary artery disease (CAD), 2) Tl and Ex ECG ischemia, and 3) physiologic and hemodynamic abnormalities. These data suggest that assessment of the duration of postexercise ST depression aids in identifying the extent and severity of CAD and of exercise-induced ischemia by Tl-201 scintigraphy.

No. 498

THALLIUM-201 SPECT IMAGING OF MYOCARDIAL CONTUSION. G. Strich, P. Braunstein, R. Bridges, A. Cohen, H. Solomon, K. Waxman. University of California Irvine Medical Center, Orange, CA.

There is no specific diagnostic test for traumatic myocardial contusion, an injury associated with cardiac conduction abnormalities and a risk of life-threatening arrhythmias. Therefore, the current standard practice at our institution is to admit all patients with significant blunt chest trauma to a cardiac monitoring bed for three days of observation.

The current study evaluates Tl-201 single photon emission computed tomography (SPECT) in the diagnosis of cardiac contusion. Forty-eight patients admitted to our institution with a diagnosis of possible myocardial contusion were prospectively studied with Tl-201 SPECT scans, serial cardiac isoenzymes, and continuous EKG monitoring. Twenty-five patients had clearly abnormal or equivocal scans, most of these having a characteristic perfusion deficit in the apex and anterior wall and/or adjacent septum. Of these, five developed serious arrhythmias and seven had conduction abnormalities. Of the 23 patients with clearly normal scans, none had serious arrhythmias and only three had conduction abnormalities. A larger percentage of patients with positive scans had elevated cardiac isoenzymes.

Our study demonstrates that Tl-201 SPECT scanning may prospectively identify that subgroup of trauma patients at risk for developing serious arrhythmias from cardiac contusion, and may therefore obviate the need for expensive continuous cardiac monitoring in a significant number of trauma patients.

No. 499

THALLIUM-201 TESTING OF ASYMPTOMATIC SUBJECTS WHO HAVE POSITIVE EKG TESTS. D.D. Watson, V.J. Patrone, T.A. Kelly, R.S. Gibson, G.A. Beller, C.D. Teates. University of Virginia, Charlottesville, VA.

Physical fitness awareness has resulted in more graded exercise EKG tests (GXT) on relatively young asymptomatic subjects. Since the incidence of significant coronary artery disease in this group is well below the false-positive (FP) rate of 10-12%, most positive tests will be FP and a back-up test is essential to separate true-positive (TP) from FP. We prospectively performed GXT on 88 healthy asymptomatic volunteers. No positive GXT occurred in 34 who were less than 40 years old. In 53 between ages 40 and 70 there were 7 positive GXT with average ST segment depression of 2.6 mm. Pre-test probability of CAD based on age and sex was $8.5 \pm 2\%$ with post GXT probability increased to $33 \pm 6\%$ using Bayes' analysis with sensitivity of 0.65 and specificity of 0.88. Normal Tl-201 exercise studies were subsequently found in patients with positive GXT. A normal Tl-201 test reduced likelihood of CAD back to $8.0 \pm 2\%$ based on sensitivity of 0.85, specificity of 0.90. We conclude that: 1) Tl-201 is useful applied to asymptomatic positive GXT responders. 2) GXT and Tl-201 tests should be sequential, not simultaneous (which would double the FP probability). 3) Routine GXT appears to be

of insignificant value below age 30 since post test probability of CAD is less than 10% even after positive GXT result. 4) Statistical calculations for this subgroup should be based on data obtained from asymptomatic populations rather than data obtained from patients referred for symptoms.

No. 499.5

COMPARISON OF Tl-201 SINGLE PHOTON EMISSION COMPUTERIZED TOMOGRAPHY (SPECT) AND PLANAR IMAGING FOR EVALUATION OF CORONARY ARTERY DISEASE. J Maddahi, KF Van Train, C Wong, J Gurewitz, F Prigent, C Youngkin, J Friedman, D Berman. Cedars-Sinai Medical Center, Los Angeles, CA

Although Tl-201 SPECT offers theoretical advantages over conventional planar (PL) imaging, systematic comparison of optimized quantitative SPECT and PL for assessment of disease in individual coronary arteries is not available. Thus, in 33 patients with angiographic coronary artery disease (>50% stenosis), 2-3 mCi of Tl-201 was administered at peak treadmill exercise. Sequential SPECT and PL images were obtained in all pts alternating the order of imaging. With SPECT, 30-32 projections (30 seconds each) were obtained over 180°. Circumferential count profiles of all short-axis and apical portion of vertical long-axis tomograms were plotted onto a polar coordinate map, were compared to a previously established normal SPECT data base. Defects in various vascular territories were automatically determined. With PL, 3-view images were obtained and quantitatively analysed for presence of perfusion defects and/or Tl-201 slow washout. Sensitivity and specificity of SPECT and PL for identification of disease in each of the three coronary arteries were as follows: (*p<.01 vs. PL)

	LAD		LCX		RCA	
	SPECT	PL	SPECT	PL	SPECT	PL
Sensitivity	72%	69%	76%*	41%	88%	84%
Specificity	75%	75%	100%	100%	62%	75%

In the 14 pts in whom PL preceded SPECT, the superiority of SPECT for detection of LCX disease was maintained (.83 vs. .50). We conclude that SPECT is superior to conventional planar imaging for detection of disease in the LCX territory.

No. 500

HIGH DIAGNOSTIC ACCURACY OF 180° EXERCISE THALLIUM TOMOGRAPHY IN EIGHTY CONSECUTIVE PATIENTS EVALUATED FOR CHEST PAIN SYNDROME. M.F. Wilson, C.P. Herbst, R.D. Burow, D.J. Brackett, B.H. Sung, C.R. Corn, and E.W. Allen. VAMC and Oklahoma University Health Sciences Center, Oklahoma City, OK.

Due to recent controversy about reliability of 180° emission computerized tomography (ECT) we evaluated this technique by calculating sensitivity (SEN), specificity (SPEC) and diagnostic accuracy (DA) for the detection of coronary disease (CD) in both women (W) and men (M). We studied 82 consecutive patients (PTS), 21 W and 61 M, with history of chest pain (CP) by symptom limited treadmill exercise, electrocardiography (ECG), stress and 4 hr redistribution 180° ECT PL imaging. CD was documented in 68 PTS; 51 by coronary angiography (CA) and 17 by myocardial infarction. Fourteen were normal (6W, 8M) either by CA (2W, 3M) or low probability profile. Results in percent for each diagnostic modality, plus mean age, peak rate pressure product (RPP) and treadmill time (TMT) were:

	SEN	SPEC	DA	AGE	RPP/100	TMTsec
Women	93	67	86	48	213	459
Men	96	75	93	53	203	399

Three CD PTS were not detected by ECT; 2 had 50% single vessel disease, one anterior and one posterior; one had 2 vessel disease. There were 4 (2W, 2M) false positives; locations were 3 inferior and 1 anterior. Conclusions: 1) Reliability of 180° data sampling ECT to detect CD in W and M was comparable, 2) Both had high sensitivity and diagnostic accuracy, 3) In our hands this technique has

proven to be a reliable tool for diagnosis of coronary artery disease.

No. 501

DYNAMIC SINGLE PHOTON EMISSION COMPUTED TOMOGRAPHY OF Tl-201 WITH EXERCISE LOADING. Y. Yonekura, H. Koide, T. Mukai, N. Tamaki, Y. Konishi, T. Fudo, and K. Torizuka. Kyoto University School of Medicine, Kyoto, Japan.

Single photon emission computed tomography (SPECT) with Tl-201 has been reported to provide accurate means for diagnosis of coronary artery disease (CAD). The purpose of this study is to examine the serial changes in regional myocardial activity of Tl-201 injected during exercise loading in CAD using a multidetector SPECT system.

Four cases without coronary stenosis (N) and 17 patients with CAD including 9 cases with prior myocardial infarction (MI) were studied. Tl-201 was injected during submaximal exercise loading with a bicycle ergometer. Serial dynamic SPECT scan was performed every 5 min until 30 min after injection, followed by additional 3 scans for 10 min at 1 hr, 2 hr and 3 hr after injection. These SPECT images were corrected for the acquisition time, but no corrections were made for photon attenuation and scattering. N revealed uniform distribution throughout the study, and rapid washout was observed from the early period in 3/4 cases (10 to 24 % for initial 25 min). CAD showed various patterns of abnormal distribution and washout. In addition, the changes in regional distribution of Tl-201 were observed during the early period.

These preliminary results indicate the significance of the early washout during the 30 min after injection of Tl-201, and careful consideration should be taken in calculating the washout rate by a conventional SPECT system with a rotating gamma camera.

Monday, 3:30-6:00

Exhibit Hall

COMPUTERS AND DATA ANALYSIS

No. 502

THE INFLUENCE OF PLASMA SAMPLING TIMES ON ACCURACY OF ESTIMATION OF THE INPUT FUNCTION IN THE DEOXYGLUCOSE METHOD. S. Jovkar, H. Nakai, A. Evans, M. Diksic, and Y.L. Yamamoto, Montreal Neurological Institute.

The accurate estimation of the input function, C(t), is essential in the quantitative determination of the rate constants in the deoxyglucose method. The conventional strategy for designing the plasma sampling times in the deoxyglucose method is based on the intuitive notion of taking more samples when the rate of change of the input function is large and less when the rate is small. In this work a plasma sampling schedule is designed based on achieving the maximum possible accuracy of the input function parameters in the presence of measurement noise.

The sampling schedule which minimizes the variance-covariance of the estimated parameters of the input function is deemed to be the optimal sampling schedule. The optimal sampling time schedule designed was found to be sample clusters focused at specific times. The validation of this optimal sampling schedule was tested in simulation. It was found that this sampling schedule allows a more accurate characterization of the parameters of C(t) than the conventional sampling schedule; an improvement of up to 33 percent in the average standard deviation of a parameter (1 - SD(optimal)/SD(intuitive)) was observed in the estimation of the parameters of C(t). This optimal sampling schedule was used in rats to validate its practicality. Using a similar

strategy we are presently studying the influence of tissue sampling times on the accuracy of determination of the rate constants by Positron Emission Tomography.

No. 503

EVALUATION OF ROUTINE TELEPHONE TRANSMISSION OF NUCLEAR MEDICINE STUDIES. G.M. Kolodny, I. Tal, J.A. Parker, H.D. Royal and J.A. Orlin. Beth Israel Hospital, Boston, MA.

We have developed software to send nuclear medicine studies via telephone. We can rapidly review studies from satellite hospitals, arrange joint conferences with widely separated medical centers and take call from home. We use IBM PC/XT based computers with 512x512 pixel displays, 16 bits deep, which can read 8" floppy disks from either our Technicare, Elscint or DEC computers. We communicate at 9600 bps with synchronous half duplex modems over regular dial up telephone lines. A special long training sequence is used for each turn around of the line and fallback to 7200 or 4800 bps is automatically performed if line quality deterioration occurs. The line is turned around only every 30 seconds and any blocks showing a CRC error are again sent with the next 30 second transmission. The software protocol is optimized for speed of transmission. Each study is sent in 512 byte blocks and only those blocks having non-zero data are sent. A baseline can be set on each image to eliminate stray counts and thus reduce the blocks having non-zero data. Data compression by a log function over a range only up to the maximum counts per pixel is performed automatically. Transmission time for 12 view (128x128) bone scan is 90 secs. and for a four view 32 frame (64x64) gated cardiac study is 180 secs.

Transmission is used on a routine basis to take call at home and to communicate with a sister center in Haifa, Israel. Comparison of data before and after compression, transmission and expansion of 100 studies by three observers showed no discernible differences in any of the studies both by direct image comparison or ROC curves.

No. 504

DESIGN, DEVELOPMENT, AND TESTING OF A HIGH PERFORMANCE, MICROCOMPUTER BASED, SOLID STATE AUTORADIOGRAPHIC IMAGE ANALYZER.

J. L. Lear, J. S. Plotnick, and S. Rumley. Stanford University School of Medicine & VA Medical Center, Palo Alto, CA

We designed and developed from the ground up, a microcomputer based, solid state, digital image analyzer for quantitative autoradiography. We measured dynamic ranges and signal/noise characteristics of detectors used in existing digitizers, video camera systems (VC) and scanning microdensitometers (SM), and found them to be less than optimal for the gray scale ranges typically found in autoradiographs. We then tested two types of solid state arrays, linear silicon diode arrays and charge coupled device (CCD) arrays and found that CCD arrays had the most appropriate sensitivity for fast scanning.

We next developed control circuits which could move a 1024 element linear CCD array so as to digitize an image into 1024 x 1024 pixel elements. Amplification circuits were developed to match the CCD sensitivity to autoradiography so as to obtain 256 true intensity levels and interfaces were developed to transmit the data through a standard bus to an IBM AT central microcomputer. Programs were written in C for processing requirements of single and multiple tracer quantitative autoradiography and a video controller was programmed for high resolution pseudocolor display of the 256 levels.

The complete system was used to scan autoradiographs and results were compared with those of the other systems. The microcomputer based CCD system was significantly more precise and accurate for tracer concentration measurement.

	<i>Scan Time</i>	<i>Precision</i>	<i>Accuracy</i>
VC	5 seconds	Within 3%	Within 6%
SM	300 seconds	Within 4%	Within 12%
CCD	3 seconds	Within 1%	Within 2%

No. 505

DESIGNING A COMPUTER SYSTEM FOR A TIME OF FLIGHT POSITRON EMISSION TOMOGRAPH. T.K. Lewellen, R.H. Harrison, University of Washington, Seattle, WA.

The University of Washington is installing a Scanditronix time-of-flight PET gantry. However, the data processing portion of the system has been developed in our laboratories. The basic design is a distributed computer network using 32 bit minicomputers instead of "hardwired" electronics. The use of a network of 32 bit processors was chosen to allow the full use of the distributed computing power for data analysis and display when acquisition was not in progress. Three performance benchmarks were developed and tested on many processors including Data General MV series, DEC VAX and microVAX systems, Perkin Elmer, and a variety of 68000 processors. The benchmarks were 1) a list mode acquisition simulation with a bit register tested for a status bit, the 32 bit event put into a list mode buffer, and the buffer transferred to disk when full; 2) an on-the-fly simulation with a 32 bit register tested for a status bit, the event read and 16 bits isolated and used for a table look up followed by an add one cycle to a matrix element; and 3) a Bessel function optimizer written in Fortran. The benchmark results favored the Data General processor by factors of 2 to 4, particularly for the on-the-fly application. However by packing the list mode data from 32 bits/event to 24 bits/event, it was possible to achieve >90,000 events/second for essentially all of the processors tested. For our application, we selected a network of Data General MV series processors based on the benchmark performance and the general software tools provided with the system.

No. 506

HIGH QUALITY SCINTIGRAPHIC IMAGE RECORDING ON PAPER USING A LOW COST LASER PRINTER. B.R. Line, J.C. Goble, J.A. Cooper. Albany Medical Center, Albany, NY.

Reports of nuclear medicine studies may be greatly enhanced by using line graphics and image data to visually transmit clinical findings and analysis results. Low cost, 300 dot per inch resolution laser printers can be used to achieve this end, but software to merge text and graphic data is not currently available, and procedures to provide an acceptable gray scale from single intensity laser dots are poorly defined.

We have developed a software driver for an inexpensive laser printer that is controlled by high level command protocols. It formats text, line graphics and gray scale images into a single report. We have also investigated the factors influencing perceived gray in laser generated paper based images. Gray levels were generated by varying the position and number of dots written into 2 by 2 up to 8 by 8 dot matrices. Perceived gray is found to be related to both dot packing density and dot pattern. Best packing strategies are produced by maximizing distance between dots and by using similar dot patterns for neighboring gray levels. Despite the greater number of patterns possible with larger matrix sizes, 4 by 4 matrices with 16 gray levels provide the best compromise between required processing time and image appearance. A sigmoid relationship is evident between perceived gray and dot density which vary in proportion to the square of the difference between the number of dots written and unwritten in a given matrix. Image appearance is noticeably improved by correcting for this relationship and by assigning image values falling between defined gray levels according to distance weighted random probability.

This type of report generation system will provide an inexpensive means of transmitting high quality images and graphic results to referring clinicians.

No. 507

TEMPORAL WIENER FILTERING OF GATED BLOOD POOL STUDIES FOR THE IDENTIFICATION OF THE SITE OF ELECTRICAL ACTIVATION. J.M. Links, M.A. King, and H.N. Wagner Jr. The Johns Hopkins Medical Institutions, Baltimore, MD. and University of Massachusetts, Worcester, MA.

We have previously described the use of first

harmonic Fourier analysis for the identification of the site of electrical activation by gated blood pool imaging. One potential limitation of the method is the use of a single harmonic (cosine) to represent the time-activity curve of each pixel. Accordingly, we have now used first derivative analysis after non-stationary temporal Wiener filtering of gated blood pool studies. The Wiener filter is a low pass filter whose cut-off frequency is dependent on a given pixel's signal-to-noise ratio. In our studies, the filter passed 2-5 harmonics (typically 2-3).

We applied both single harmonic Fourier analysis and first derivative analysis after Wiener filtering to 21 studies acquired during pacing in 8 patients with coronary artery disease and episodes of sustained ventricular tachycardia. Both single harmonic Fourier analysis and first derivative analysis resulted in a 71% accuracy in predicting the site of the pacing electrode. We conclude that factors other than the cosine approximation, such as anatomic overlap and patient pathology, limit the accuracy of activation site identification.

No. 508

MAPPING OF RATE CONSTANTS IN THE KINETIC MODEL OF FDG: VALIDITY OF THE DATA. T.Mukai, S.Tanada, S.Nishizawa, M.Senda, Y.Yonekura, H.Saji, K.Minato, T.Fujita, and K.Torizuka. Kyoto Univ. School of Med., Kyoto, Japan.

Estimation of rate constants of glucose metabolism pixel by pixel from serial PET images at 4 min intervals for 60~120 min scan of FDG was studied. The kinetic model of FDG is based on the three compartments with four parameters. PETs were reconstructed employing corrections for attenuation, scatter and dead time of counting. Curve fitting was performed by Newton-Raphson method providing the mapping of each parameter with the relative accuracy (95% confidence limit). Arterial blood sample curve was approximated by one straight line and sum of three exponential curves. Estimation of all rate constants and cerebral metabolic rate for glucose (CMRG) of each pixel could be performed in a few seconds on PDP 11/60 computer. Correction of blood volume (BV) effect was done by subtracting BV image by CO-15 from serial FDG images. While the rate constant maps were quite noisy because of random fluctuation of data, the accuracy of the parameters increased remarkably by using average values of a few pixels. The dephosphorylation rate (k_4) could not be estimated sufficiently from 1 hr measurement. Estimation of k_4 required 2 hr scan data. The values of all constants decreased slightly for 3-parameter fitting both for 2 hr and for 1 hr measurement, and k_1 and k_2 values decreased 15~50% by BV correction. In healthy subject, each constant almost coincided with the normal value. These maps provide a useful mean for studying the glucose transport system in various organs and diseases.

No. 509

MEASUREMENT OF ARTERIAL TIME-ACTIVITY CURVES BY MONITORING CONTINUOUSLY DRAWN ARTERIAL BLOOD: ERRORS AND CORRECTIONS. M.Senda, S.Nishizawa, Y.Yonekura, T.Mukai, H.Saji, K.Yamamoto and K.Torizuka. Kyoto University School of Medicine, Kyoto, Japan.

Accurate description of the arterial time-activity curve (ATAC) is of paramount importance in quantitative determination of the regional cerebral blood flow (CBF) using positron tomography and one-shot intravenous injection of 0-15 labeled water. Frequent manual sampling from the arterial catheter does not permit sampling in less than 5 sec interval and runs the risk of missing the arrival time or the peak count, which may induce errors of 5-10% in CBF values. The present study deals with the accuracy of an ATAC monitoring system.

This system consists of a single bismuth germanate (BGO) detector contained in a lead shield and a constant-flow aspirator. The arterial blood was drawn continuously from a catheter in the brachial artery into an extended tube and its activity was monitored by the detector as the detector time-activity curve (DTAC). Comparison with manual sampling from the contralateral brachial artery in the same run revealed that the DTAC differed from the manual sampling not only in delayed arrival but also the shape of the curve was blunted because of viscosity of the blood and the width of detector field of view. However, deconvolution of DTAC using experimentally acquired system step response provided accurate arterial time course, which successfully filled out the gaps of the manual sampling. Moreover, water and blood showed different viscosity effect on the step response, suggesting that the system characteristics should be acquired using blood or fluid of similar viscosity.

No. 510

CORRELATION WITH FINAL DIAGNOSIS
NUCLEAR MEDICINE SPECT, CT, AND MR

D. Bruce Sodde, S.A. Cook, Hillcrest Hospital, Mayfield Heights, OH.

In accordance with the Quality Assurance Program of the Division of Medical Imaging, the hospital quality assurance department performed a study assessing the correlation or non-correlation with the final diagnosis of Nuclear Medicine SPECT, CT scanning, Ultrasound imaging and MR imaging performed on inhouse patients.

The Quality Assurance Department utilized the entire hospital chart, final diagnosis, and results of biopsy and/or surgery in arriving at their correlation and non-correlation results.

Liver SPECT was compared with CT and Ultrasound while Brain SPECT utilizing glucoheptonate, was compared with CT scanning and MR imaging.

Nuclear Medicine SPECT imaging of the liver/spleen had an interpretation correlation with final diagnosis in 106 patients and non-correlation in 5 patients. CT scanning with and without contrast correlated in 20 patients and did not correlate in 12 patients. Real time Ultrasound imaging correlated in 33 patients and had non-correlation in 6 patients.

Nuclear Medicine SPECT brain imaging utilizing glucoheptonate had an interpretive correlation in 111 patients and there was non-correlation in 15 patients. CT imaging had correlation in 94 patients and non-correlation in 35 patients. In a separate group of patients that had Nuclear Medicine SPECT, CT scanning and MR imaging, CT imaging with and without contrast had a correlation in 7 patients and non-correlation in 5 patients. Nuclear Medicine SPECT correlated in 9 patients with non-correlation in 3. MR imaging correlated in 9 patients and there was non-correlation in 3 patients.

Routine SPECT imaging of the brain and liver has been performed in our Department of Nuclear Medicine since late 1983, and the present study was completed in mid 1985. The above results reveal that Nuclear Medicine SPECT imaging of the liver and spleen is more sensitive than CT imaging or Ultrasound in evaluating parenchymal liver disease and space-occupying lesions of the liver.

Nuclear Medicine SPECT imaging of the brain utilizing glucoheptonate has proven to be more sensitive in establishing the abnormalities related to stroke at an earlier time than CT imaging and in evaluating space-occupying lesions is more sensitive than CT, dramatically so in the posterior fossa and has been as sensitive as MR without the interference of edema as visualized on T2 MR imaging. Thus SPECT imaging of the liver/spleen and the brain is a cost effective modality.

No. 511

EFFECTS OF INCREASING PET SCANNER RESOLUTION ON NEUROLOGICAL DATA VARIABILITY. S.C. Strother[†], T. Peters[†], C.J. Thompson[†], [†]Montreal Neurological Institute, Montreal, Canada, and ^{*}Memorial Sloan-Kettering Cancer Center, New York, NY, USA.

Increased image resolution is assumed to be advantageous for PET studies of the brain. This may not be true because most brain structures are not simple homogeneous objects, but multiple, randomly oriented substructures repeatedly packed into larger heterogeneous regions (e.g. 1 cm-2 cm wide cortical rim delimiting the gyri and sulci). We studied the contrast recovery coefficient (CRC) behavior of simple repeat structures, different object profiles and region-of-interest analysis techniques with a range of image resolutions. The resultant curves show the importance of the number of dimensions for which structural variations are considered

and suggest two important analysis regions for the delimiting region size (S)/resolution (FWHM) ratio: S/FWHM < 1 (R1) and S/FWHM > 1 (R2). As PET resolution volumes (RV) move from > 10 mm³ towards 5 mm³, the low but stable CRC's of R1, which are relatively insensitive to the arrangement and shape of the underlying anatomical structures, become the higher but more variable values of R2.

The increased variability of regional values, due to sensitivity to the underlying anatomical variation with smaller RV's, may decrease our ability to identify consistent functional activation patterns in all but test retest scanning protocols. We suggest that RV's ≈ 10 mm³ may be nearly optimal for some tasks: in particular, for establishing activity distributions that best reflect functional, and not anatomical, normal range variations in populations.

No. 512

CONTINUOUS MEASUREMENT OF LEFT VENTRICULAR FUNCTION BY AN AMBULATORY VENTRICULAR FUNCTION MONITOR (VEST): ITS VALIDATION AND VARIABILITY. N. Tamaki, J.B. Gill, R.H. Moore, T. Yasuda, H.W. Strauss, M.N. Suzuki, A. Suzuki. Massachusetts General Hospital, Boston, MA and Capintec, Inc., Ramsey, NJ.

We have tested a new portable non-imaging device (VEST) which continuously records a beat-to-beat left ventricular (LV) time activity curve and ECG signal. To validate the measurement of LV function in ambulatory subjects with the VEST, 7 normals and 26 cardiac patients were studied with sequential gamma camera and VEST measurements. The VEST detector was placed over the region of LV. Serial beat-to-beat data were averaged over 15 seconds with the VEST and the following parameters derived: ejection fraction (EF), relative end-diastolic volume (ZEDV), cardiac output (ZCO) and heart rate. The variability of the averaged EF over 2 minutes sitting quietly was < 3.5% (1SD) in all patients. EF calculated by the VEST (v) was compared with that by the gamma camera (g) both at rest and during each stage of bicycle exercise.

(rest) EF(v)=0.87xEF(g)+3.59; r=0.92, SEE=3.3, n=33
(exercise) EF(v)=0.99xEF(g)+0.85; r=0.80, SEE=9.0, n=29

Repeated VEST study after complete removal and repositioning of the device resulted in a correlation of 0.98 for resting EF. ZEDV change from lying to sitting calculated by the VEST was correlated with that by the gamma camera (r=0.84).

We conclude that the VEST provides reproducible and accurate measurement of LV function in ambulatory subjects.

No. 513

COMPUTER SYSTEM FOR LONG TERM STORAGE OF NUCLEAR MEDICINE DATA. J. Weber, V. Savant, M. DeLaney, S.J. Goldsmith. Mount Sinai Medical Center, New York, NY.

A single large computer system was developed to provide simultaneous viewing, acquisition and processing of patient (pt) data, pt data base management, pt image archival, pt scheduling (automated and manual), report generation, word processing and general ledger operations.

The department consists of 11 imaging devices and a pharmacy lab. Average daily imaging of 58-65 pts generates about 2 Gb/annum of data.

A local area network was developed, consisting of a DEC VAX 11/750 as a central node and 12 stand-alone micro-processors for acquisition, processing and display.

The VMS Operating System is adequate for system management. An in house software package written for the VAX is used for pt data base management, scheduling, and report generation. A software package developed by the

microprocessor manufacturer is effective for image processing.

All pt data and demographics are stored. With data compression techniques, an 8 week image data base is available on-line. Older studies are purged to mag tape and a tape index file is maintained. Demographic data is available on-line and is key in the location of pt studies.

An optical disk subsystem will permit a 24 month image data base to be available on-line. Scheduling software will provide the automatic retrieval of all previous studies on scheduled pts and VMS utilities permit operator retrievals.

Monday, 3:30-6:00

Exhibit Hall

COMPUTERS AND DATA ANALYSIS: ECT**No. 514**

FULLY AUTOMATED DATA PROCESSING OF PET STUDIES OF DOPAMINE (D2) RECEPTORS. M. Clausen, A.N. Bice, M.J. Stumpf, J.M. Links, H.N. Wagner, Jr. The Johns Hopkins Medical Institutions, Baltimore, MD.

Data processing and quantification in PET studies of neuroreceptors is time consuming. To minimize this problem we have developed a fully automated, operator independent computer program for use in analysis of 11-C-N-methylspiperone (NMSP) PET images.

With the NMSP tracer, dopamine (D2) receptor rich areas of the brain yield a linear relationship between ROI/cerebellar ratios and time, reflecting the nearly irreversible binding of the tracer. This fact serves as a basis for the functional images produced by our program.

11-C-NMSP tracer specific characteristics were used to define sequences of automatic program actions. First the program determined cerebellar ROIs in the early (post-injection) PET frames. This was performed by multiplying vertical profiles of the appropriate transaxial image with a ramp function that increased progressively from the anterior to the posterior part of the brain. The image row corresponding to the maximum value of the weighted vertical profile was used together with an edge detection method to define the cerebellar ROI. Automatic ROI definition also was performed for caudate, putamen, frontal and temporal lobe regions.

Functional images of the slope of ROI/cerebellar ratios versus time, intercepts and linear correlation coefficients of such plots were produced. These images are convenient for quick assessment of approximate basal ganglia D2 receptor density, left-right receptor asymmetries and deviations from normal receptor binding kinetics.

No. 515

DETERMINATION OF OPTIMUM FILTER FUNCTION FOR SPECT IMAGING. D.R. Gilland^{*}, B.M.W. Tsui^{*}, J. Berg⁺, D.J. Nowak⁺, E.R. Edgerton^{*}, J.R. Perry^{*}, W.H. McCartney^{*}. ^{*}University of North Carolina, Chapel Hill, NC, ⁺General Electric Medical Systems Group, Milwaukee, WI.

An observer study was performed to determine the optimum filter function for SPECT image processing. The images used in the study were reconstructed from simulated projection data. The simulated object was a cylinder of uniform activity distribution containing a cold, spherical lesion, 2 cm in diameter. The data was simulated in a manner which closely approximates acquired data, incorporating the effects of attenuation, collimator and scatter response functions, and noise characteristics typical of clinical SPECT studies. The projections were processed before reconstruction with either the Hanning or Butterworth filters with varying

cut-off frequency, or the Metz filter with varying power factor. The observers were tested on their ability to detect the lesion in a 2AFC paradigm.

For each filter we have plotted percent correct responses vs. cut-off frequency (vs. power factor for the Metz filter). The results indicate a broad optimum for the Hanning and Metz filters. The Butterworth filter, however, displayed a well-defined optimum near 0.15 cycles/pixel at a pixel size of 6.4 mm. At its optimum, the Butterworth scored higher than either Hanning or Metz. All filters scored significantly better than no filter. We have proposed a model to explain the results based on the frequency response of the filter functions.

No. 516

AXIAL SAMPLING DENSITY REQUIREMENTS IN POSITRON EMISSION TOMOGRAPHY. E.W. Grochowski, M.R. Palmer, S. Pelletier, and B.D. Pate. UBC/TRIUMF PET Program, Vancouver, B.C., Canada.

This study was directed at evaluating the effects of increased spatial sampling density in the axial direction on the accuracy of inter-plane interpolated data in positron emission tomography. With multislice PET scanners, arbitrary slices in the imaged volume (e.g. coronal and sagittal sections) can be calculated by interpolating interleaved transverse section images which are in turn acquired by translating the subject axially between scans. It is important to consider the accuracy of such interpolated data.

Simulation studies were performed using the parameters of the UBC/TRIUMF PET VI tomograph which collects 7 axial slices simultaneously, with a center-to-center separation of 14.2 mm and a central slice thickness of 11 mm FWHM. The simulations involved the reconstruction of data along the axial direction from computer generated random signals, filtered, and sampled at densities corresponding to data taken at 2, 3, and 4 chair positions. Using a cubic spline interpolation kernel, the reconstruction error was found to be 12.2%, 3.3%, and 1.3% RMS for 2, 3, and 4 chair positions respectively.

The costs of sampling at a higher axial densities are: 1) increased dead time as the chair is being moved; 2) lower statistics per acquired image slice, given the same number of counts in the study; and, 3) increased data storage requirements. The simulations indicate that a satisfactory trade-off between increased clinical scanning complexity and reconstruction accuracy occurs at 3 chair positions.

No. 517

A NUMERICALLY STABLE CIRCULAR HARMONIC TRANSFORM ALGORITHM FOR APPLICATION TO PET AND X-RAY CT. W.G. Hawkins, P.K. Lechner, N.C. Yang, T.L. Frenkel, and D.M. Loudenslager. The Johns Hopkins Hospital, Baltimore, MD.

The circular harmonic transform (CHT) solution of the 2-D Radon transform has only recently emerged as a computationally efficient method of image reconstruction. The algorithm is based on finding the fundamental solution of a system of non-homogeneous difference equations, and overcomes the poor spatial and contrast resolution associated with CHT algorithms. When compared to ramp-filtered backprojection or fan-beam convolution, the CHT algorithm is more robust to ringing and systematic errors in the projection data. The CHT algorithm can be applied to positron ring data without interpolation. For fan-beam data, a wide variety of geometries can be accommodated by interpolation of the projection sinogram in the angular direction only, with exact matching in the radial coordinate. For narrow-angle fan-beam data, however, the condition of exact matching requires that the dimension of the Tschebyshev radial

transform become excessively large. Using Mellin transforms, we show that the signal energy of the 2-D Fourier-Tschebyshev transform of the sinogram is concentrated in well-defined sectors in transform space. The angle defining the sectors depends in a simple way on the fan-beam angle of the field-of-view. This result is used to reduce the dimension of the Tschebyshev radial transform, and to optimize the calculation of the series of orthogonal functions that constitute the reconstructed object. Simulations with the SNARK-77 x-ray CT phantom and narrow-angle fan-beam geometry are used to support these results.

No. 518

OBJECT DEPENDENT INTERACTIVE VISUAL OPTIMIZATION OF SPECT PRE-RECONSTRUCTION FILTERING. M.A. King, S.J. Glick, B.C. Penney, R.B. Schwinger, and P.W. Doherty. University of Massachusetts Medical Center, Worcester, MA.

Starting with images of a liver/spleen phantom, a count-dependent Metz filter has been developed for use in two-dimensional pre-reconstruction filtering of single photon emission computed tomographic (SPECT) studies. However, it has been noted that alteration of the filter parameters from those determined for the liver/spleen phantom was required to obtain the most visually pleasing images for different organ systems (objects). Through implementation on a hardware configuration which includes an array processor (AP400), a "real-time" interactive visual optimization of the Metz filter for the image of interest has been achieved. The program filters the first SPECT acquisition image according to the Metz filter formed for its count level. This filtered image, and the Metz filter employed in filtering it overlaid on a plot of the logarithm of the image power spectrum, are then displayed. The user is then allowed to interactively vary the filter parameters of the Metz filter by changing the position of a "joystick." The "joystick" is set so that when it is centered in its X and Y range, the initial Metz filter is formed. Visual feedback from the filtered image, and plots of the filter and the image power spectrum are used to obtain an "optimal" filter. Preliminary results have indicated that pre-reconstruction filtering with this method produces visually superior SPECT images. It also allows for adapting the filter to the preferences of the individual reader, and serves as a useful teaching tool for the effects of filtering.

No. 519

EXAMINATION OF ASSUMPTIONS FOR LOCAL CEREBRAL BLOOD FLOW STUDIES IN POSITRON EMISSION TOMOGRAPHY. R.A. Koeppe, G.D. Hutchins, R.D. Hichwa. Cyclotron/PET Facility, University of Michigan, Ann Arbor, MI.

We have examined the validity of two common assumptions of the Kety-Schmidt model for ICBF estimation as it is applied to positron emission tomography (PET). These assumptions are: 1) since an ICBF tracer must be freely diffusible, there is no effect due to blood-borne radioactivity, and 2) the arrival time of the arterial input function is homogeneous throughout the brain. Both theoretical computer simulations and actual PET studies using 0-15 water indicate these assumptions can sometimes cause significant errors in the estimated flow values.

Even though complete equilibration between tissue and venous blood occurs, arterial blood remains at a different concentration. Thus, the early PET data following a bolus injection will have a considerable contribution from arterial-borne radioactivity. The effect of this blood-borne radioactivity is readily observed in the vicinity of the carotid arteries during the first 40 sec following injection. Blood flow images calculated using a dynamic protocol are noticeably

changed when the first 40 sec of data are omitted from the calculation. Flow estimates in cortical regions not near major arteries were decreased by ~5% which is in agreement with theoretical predictions.

The temporal shift of the arterial input curve was incorporated as an additional parameter in the model. Results indicate that arterial arrival times can differ by as much as 3 sec to various regions of the brain. This translates to changes in flow values of approximately 4-8%.

No. 520

ITERATIVE ATTENUATION CORRECTION IN SPECT USING ATTENUATION COEFFICIENTS OBTAINED FROM TRANSMISSION MEASUREMENTS. M Ljungberg, S-E Strand, B Jonson*. Dept of Radiation Physics and *Dept of Clinical Physiology, Univ of Lund, Lund, Sweden.

Purpose: To perform quantitative measurements of distribution of radioactivity in SPECT by correcting for attenuation and using the method for dose planning for internal radiotherapy with radionuclides. The method is not depending on the contour of the object or the distribution of attenuating tissue.

Method: An algorithm for correction of attenuation has been developed and quantitative emission images from SPECT have been obtained. The algorithm is based on an iterative method where measured projections are individually corrected for attenuation by calculating projections from the emission image that are corrected for attenuation. The attenuation map is obtained from transmission studies using a flat radioactive source or from Computed Tomography. Using attenuation maps obtained from reference patients stored in a computer library, the method can be efficient and fast and will be useful for the clinical routine.

Conclusion: The code has been developed and has shown an improvement in quantification of radioactivity in a human inhomogeneous phantom. The relative distribution of pixels in a region of uniform radioactivity has been reduced from about 17% for the un-corrected image to 5% for the corrected image. The time required for correcting an image has been reduced from 12 minutes to about 1.5 minutes, for a PDP 11/34 computer with Floating Point Processor. This indicates the possibility of obtaining corrected sections other than transversal.

No. 521

A COMPARISON OF PET IMAGES OF CBF ESTIMATED BY THE INTEGRATED PROJECTION TECHNIQUE WITHOUT VS. WITH FIXED DISTRIBUTION VOLUME. DK Mahoney, SC Huang, ME Phelps. UCLA School of Medicine, Los Angeles, CA.

The integrated projection technique (IP) yields estimate images of both CBF and distribution volume (Vd) from algebraic formulas based on reconstructed images of decay- and non-decay-corrected tissue activity time-integrals. Although IP executes faster than nonlinear regression, the speed of CBF estimation could be increased by modifying IP so that Vd is fixed to a globally uniform value beforehand and only CBF is estimated. This study examined the effect of fixing Vd on the estimation of CBF with IP.

We processed central-brain-slice data from four adult patients injected with 0-15 water and scanned with the NeuroECAT. After computing by IP a CBF and a Vd image for each patient, we calculated the mean value within the tissue in each Vd image. We re-processed the data twice using IP with two fixed global Vd values: the mean Vd value described above; and, a commonly cited value of 0.8 ml/g. To compare each fixed-Vd CBF image to its corresponding variable-Vd CBF image, we computed the mean and standard deviation of the tissue values in each image.

CBF images calculated from IP with fixed Vd gave lower mean values than corresponding images with variable Vd. Paired t-tests for the differences between means for any patient implied that the differences were significant at the 0.05 level of significance. This result, along with other reports

that the original IP underestimates CBF on boundaries between gray and white matter, suggests that fixing Vd in the integrated projection technique will lead to significant underestimation of CBF.

No. 522

BAYES REGRESSION COMPUTATION (BR) OF LOCAL CEREBRAL METABOLIC RATE OF GLUCOSE (LCMRG) IN STROKE. PD Wilson, RA Hawkins, SC Huang. Univ. of Maryland, Baltimore, MD. and University of California, Los Angeles, CA.

LCMRG is typically estimated from FDC PET scans using a single scan (SS Method) which is cheaper and easier to conduct than the accurate computation via individual rate constants estimated from dynamic scans repeated up to 3 hours (Direct Method). But Hawkins et al showed that in ischemic tissue the SS Method produces estimates about 50% too low. Earlier we reported simulation studies indicating that BR should give more accurate estimates than SS in ischemic tissue.

We now report comparison of BR and SS to Direct Method in ischemic and contralateral normal regions of 5 stroke patients. We used BR with repeat scans up to T, and SS with scan at T, for T=30,45,60,90,120 min. The table gives mean and (RMSE) of % errors relative to Direct.

	T	30	45	60	90	120
normal	BR	13(21)	4(10)	-1(7)	-6(9)	-8(10)
	SS	-39(41)	-31(34)	-22(23)	-29(29)	-21(21)
ischemic	BR	64(98)	15(18)	5(9)	-5(11)	-7(15)
	SS	-76(86)	-70(82)	-65(75)	-60(60)	-45(51)

For ischemic tissue the individual 60 min. % errors are: (Direct (N/I) = ratio of normal to ischemic LCMRG).

Patient	1	2	3	4	5
DIRECT(N/I)	3.76	3.14	1.21	1.55	1.82
BR	2	-6	15	6	7
SS	-100	-84	-11	-43	-88

We conclude that BR may be superior to SS in normal tissue and should be markedly superior in ischemic tissue. BR should be useful in other LCMRG abnormalities and also in studies where the scanner is repositioned for additional slices, resulting in missing dynamic scans.

Monday, 3:30-6:00

Exhibit Hall

COMPUTERS AND DATA ANALYSIS: QUANTITATION

No. 523

ABSOLUTE QUANTITATION FROM NUCLEAR MEDICINE IMAGES FOR RADIOIMMUNOTHERAPY. L.T. Chang, H.H. Hines, J.T. Davidson, R.K. Roberts. ADAC Laboratories, San Jose, Ca. W.F. Butler. Hybritech Incorporated, San Diego, Ca.

Radioimmunotherapy requires accurate quantitation of source activities and volumes. Correction for internal photon absorption, elimination of scattered radiation, and normalization of camera collimator spread with depth are the 3 most important aspects in quantitation of nuclear medicine images. Most existing methods for image quantitation do not address all of these problems. Our procedures handle these aspects effectively.

Experimentally derived image files are used to produce point spread functions (PSFs) of scattered and unscattered photons in water at various distances from the camera. These PSFs are then used to compute the scatter fractions in images. Both scatter removal and collimator spread normalization are done by deconvolution of camera images with functions generated from these PSFs. After scattered radiation is removed we simply apply a factor, $\exp(-u*d)$, to each pixel in the region of interest for attenuation correction; with u given as the linear attenuation coefficient of the primary photons in water and d given as the mean

attenuation distance. For dual energy gamma emitters such as ^{111}In the value of u is a weighted average. Normalization of collimator spread with depth is necessary for source volume determination. Equal sized images are produced from sources of the same size, irrespective of the source-to-detector distance.

Our experiments with the liver, spleen and kidneys in an Alderson Torso Phantom resulted in errors $< 9\%$ in absolute quantitation of ^{111}In activities. Thus, these procedures allow effective absolute quantitation.

No. 524

AN ARTIFICIAL INTELLIGENCE APPROACH TO INTERPRETING THALLIUM-201 3-DIMENSIONAL MYOCARDIAL DISTRIBUTIONS. EV Garcia, NF Ezquerria, EG DePuey, WL Robbins, and HJ Berger, Emory Univ. and Georgia Tech., Atlanta, GA

To overcome the subjectivity associated with identifying the presence and location of coronary artery disease (CAD) from stress Tl-201 myocardial distributions, we developed an expert system based on artificial intelligence (AI) tools to totally objectify this interpretation. After reviewing 291 patient (pt) studies with coronary angiography, we developed heuristic rules which best correlated the presence and location of perfusion defects (PDs) on 180° SPECT studies with documented CAD. The PDs were identified from polar bullseye maps as pixels below gender-matched normal limits. Using AI tools, we structured 30 rules as the knowledge base of this expert system. This LISP driven, microprocessor-based expert system, tailored after MYCIN, acts as an inference engine where the location, size and shape of each of the PDs identified from bullseye maps, as well as pt-related information, is used to "fire" the rules to produce new facts or draw inferences. For each input parameter and for each rule, a certainty factor is assigned which is traced to infer the certainty of the identification and location of CAD. The entire interpretation takes place in less than 10 secs. This system is being tested and refined using a training set of 25 pts and will be validated against a prospective group of pts with angiographic correlates.

This expert system, which has the ability to learn new rules and justify its interpretations, offers a tool for totally objectifying the interpretation of Tl-201 distributions. Importantly, this is the first report of the use of AI tools for interpreting medical images.

No. 525

A NEW TECHNIQUE FOR THE ANALYSIS OF DUAL RADIONUCLIDE STUDIES. B.F.Hutton, M.A.C. Jayasinghe, D.L.Bailey, R.R.Fulton, G.J. Bautovich, Royal Prince Alfred Hospital, Sydney, NSW 2050, Australia.

Images of two radionuclides recorded simultaneously demonstrate differences in resolution, sensitivity and attenuation at the two energies. Also one image will include scatter from the second higher energy radionuclide. A technique has been developed to compensate for these differences and minimize the resultant artifacts.

The geometric mean of conjugate views has been previously demonstrated to have several depth independent properties. This was further investigated using sources placed at various depths in a water tank. The geometric mean energy spectrum was shown to be independent of source location and as a result the fraction (k) of scattered events in any window could be predicted from the photopeak counts ($k=0.57$ for Tc-99m in Tl-201 window, $SD=0.03$). A function (s) relating the spatial distribution of scattered events to photopeak events was determined experimentally for geometric mean images and was demonstrated to be depth independent. The solution was well approximated by a biexponential function ($s=10\exp(-1.6r)+\exp(-0.07r)$ for

Tc-99m scatter in a Tl-201 window, r is radial distance in cms). A similar relationship was established for the compensation necessary to correct for differences in resolution at the two energies.

The technique has been applied in both phantom and clinical studies involving dual radionuclide subtraction and demonstrated excellent scatter prediction with significantly reduced artifacts.

No. 526

QUANTITATION OF PERFUSION DEFECTS BY 201-TL SPECT. PRELIMINARY RESULTS IN PATIENTS WITH ACUTE MYOCARDIAL INFARCTION.

G. Karcher, M. Amor, A. Bertrand, F. Zannad, P. Maurin, F. Aug, G. Ethevenot - C.H.U. Nancy-Brabois - France

Since 201-Tl myocardial distribution could only be assessed on a relative basis and since it is non homogeneous even in normal subjects (relative hypofixation in inferior and basal septal walls), we developed a quantitative analysis by 201-Tl SPECT which allows the myocardial distribution to be studied with respect to the myocardial distribution in normals. From short-axis, long axis and 4-chambers slices, both the volume containing the heart and the long axis are determined. A radial analysis of each short-axis slice is performed by calculating the maximum count value along 64 radii. The distribution of 201-Tl is expressed according to the mean distribution of a normal series (45 NaI subjects). The Tl-Defect Size (TDS) is calculated from the points differing from the normal distribution.

To validate this quantitative analysis, a cardiac phantom with defects varying from 2 to 80 ml, was used. A good correlation ($n = 40$, $r = 0.97$) was obtained between TDS and the real sizes of the defects. To assess this method in man, the reproducibility was tested on 30 diseased patients (mean relative error 11%), and the comparison between this method and cardiac-enzymes (MB-CK) was made in 24 patients with very acute myocardial infarction ($r = 0.81$).

These preliminary results allow this quantitative analysis to be proposed for the assessment of the defect size and thus for the follow-up of therapy.

No. 527

RECOVERY COEFFICIENTS FOR QUANTITATIVE IMAGING OF SMALL OBJECTS BY 180° and 360° SPECT. S. Loncaric, A.N. Bice, M. Clausen, and H.N. Wagner Jr. The Johns Hopkins Medical Institutions, Baltimore, MD.

For quantitative analysis of SPECT images it is important to estimate the loss of quantitation (recovery coeff., RC) for objects comparable in size or smaller than the system resolution. A computer program was developed to simulate 180° and 360° SPECT acquisitions of long cylindrical sources in air to investigate the behavior of the RC as a function of acquisition parameters and source position in the field-of-view (FoV). The simulation involved randomly selecting point sources within the object and calculating each point source's contribution to every angular projection. This contribution was estimated from measured gaussian point spread functions (PSF) of the Toshiba GCA-90B rotating camera with a LEAP collimator. PSFs were measured for source-detector distances of 0-50 cm. Cylindrical objects, 1-6 cm in diam., were simulated using a radius of rotation of 25 cm and 4° sampling. For the 360° acquisition the RC depends primarily on object size, not on FoV location. For 180° acquisition, the RC changes significantly with object location and acquisition starting angle. For a 2 cm diam. rod located 9 cm off the axis-of-rotation (AoR) in the LAO direction, the RC is 39% larger than that at the AoR for an RAO-LPO acquisition. Other 180° sampling arcs can produce a loss of quantitation that is greater off the AoR than on the AoR. This is due to the camera response dependence

on source distance. The simulation method is extendable to arbitrary source shapes in attenuating medium. The method is also useful for investigating inherent SPECT volume estimation inaccuracies and object distortions.

No. 528

PURE TUBULAR RENOGRAM CURVES OBTAINED BY FACTOR ANALYSIS OF I-131 HIPPIRAN STUDIES.

D.G. Pavel, E. Olca, K. Zolnierczyk, J. Sychra, University of Illinois Hospital, Chicago, IL.

Pure tubular renogram (R) curves can not be obtained in routine, due to simplistic, empirical, background (B) subtraction. This is due to complexity of surrounding structures and to kidney anatomy. Factor Analysis (FA) provides theoretically the ideal solution but only for single kidney (K) patients. In order to prove the theory and feasibility for 2 K patients we studied bilaterally normal renal cases, using LFOV camera and 20 (1 min) frames. After delineation in a classic fashion of ROI-s for each K and of 2 B areas, standard R-s were obtained and used for comparison. FA by Bazin-Di Paola algorithm, on whole field of view, by requesting 3 and 4 factor (F) searches. The results were used to reconstruct sequences of 20 frames based on all 3 or respectively 4 F and then, separately, based only on the typical tubular factor found. The same ROI-s were used on all sequences. Results: 1) The reconstructed series based on all factors preserve the original image information while showing a filtering effect and a slight loss in B; the total count loss within the ROI-s is negligible; 2) the isolated tubular factors show significant change in shape, characterized by sharper peak and steeper rate of decline; these changes are more pronounced than the effect of standard B subtraction on the original curves; 3) the best tubular R appears to be the one resulting from a 4 factor search and shows that it has been cleaned up of surrounding B as well as of intrinsic vascular B and of pelvis interference; 4) normal kidneys generate perfectly superimposable curves; 5) factor images also enable easy and accurate ROI delineation. Conclusion: Pure renogram curves can be obtained from each kidney without a priori bias, B subtraction and interoperator variability. The method is simple and reasonably fast on standard computers.

No. 529

ESTIMATION OF RENAL VOLUME WITH SPECT; PHANTOM STUDY VALIDATION. W. Robeson, I. Zanzi, M. Lesser, P. Loy, and D. Margouloff. North Shore University Hospital, Cornell University Medical College, Manhasset, N.Y.

Kawamura et. al. have shown (Eur J Nucl Med 9:168,1984) that renal volume can be accurately computed from addition of voxels in multiple transaxial sections of a SPECT Tc-99m-DMSA scan. The accuracy of the results depends on the method used for outlining the kidneys on each transaxial section. An isocontour method based on a percentage of the maximum renal counts from all sections (threshold) has been shown to work well by Kawamura. The calculation of renal volume depends on the threshold value chosen as well as the amount of background activity in the vicinity of the kidneys, a factor not considered by Kawamura. A hollow lucite trunk phantom containing two hollow kidneys was used. Each chamber was filled separately with different concentrations of Tc-99m pertechnetate. Background varied from 9% to 41% of renal counts (measured as the geometric mean of count ratios from anterior and posterior planar projections). Our results indicate that the linear model based on threshold used by Kawamura explained 91% of the variability observed in our data using multiple regression analysis. The use of a cubic model improved the fit to 94%. Adding background variation to the cubic model slightly improved the fit to 95%. Threshold values which predict the most accurate volumes are shown below and are in excellent agreement with results obtained by others. Using a Goris background correction on each transaxial section to compensate for background effects altered the corresponding threshold value but did not significantly reduce the background dependence of the model.

Optimal Threshold Values (%)

Bkgd. Correction	Background		
	Low (10%)	Medium (20%)	High (50%)
None	50	53	54
Goris	47	50	51

These results demonstrate that kidney volume can be accurately determined in humans using a renal parenchymal imaging agent such as Tc-99m-DMSA.

No. 530

TARGET DETECTION USING SINGLE PHOTON EMISSION COMPUTED TOMOGRAPHY. T.R. Simon, B.S. Walker, J. Triebel, J.E. Dowdey. Univ. TX, Dallas VAMC, Dallas, TX.

Getting the best data for a given acquisition time and tracer dose becomes progressively challenging with more acquisition options. The type of filter (F) and number of projections (P) were analyzed for ability to identify hot and cold targets in images of a specially constructed set of phantoms with targets arranged in either a circular or rectangular array.

The phantoms were charged with technetium-99m pertechnetate. Two observers independently graded images acquired with 15 to 120P over 360 degrees in imaging series with 3-24 million total counts back-projected with Ramp, Hamming, Hann, Parzen and various Butterworth F. The targets were hot crosses and cold bars 3-9 mm in diameter. Targets were considered "detected" if not >2 contiguous pixels were missing in the processed image.

Hot and cold target detection showed opposite trends: Cold targets were better recognized with more counts per P while hot targets benefitted from more P. Hot target detection at 15P was unacceptable. As expected more total counts in a series uniformly improves both hot and cold target detection through the range studied. We conclude that for the studied variables: (1) targets in a rectangular array are easier to detect than those in a circular array; (2) the type of back-projection filter is important with the best results obtained using a Hann, Hamming or high order Butterworth and (3) the number of P should be traded off against the number of counts per P with careful consideration toward purpose since hot object detection benefits from a different strategy than cold target detection.

No. 531

QUANTITATIVE SINGLE-PHOTON EMISSION TOMOGRAPHY. D. Snyder, M. Miller, T. Miller, and C.-J. Chen. Washington University, St. Louis, MO.

A mathematical model for data acquired in single-photon emission computed tomography (SPECT) is derived for the quantitative reconstruction of radioactivity distributions. The model accurately accounts for: (1), the nonuniform attenuation of photons in body tissue; (2), the depth-dependent point-spread function of gamma-ray cameras used as a radiation detector; and (3), the statistics of radioactive decay. The algorithm for reconstruction of radioactivity distributions is based on the maximum-likelihood method of statistics and incorporates all three of the aforementioned effects; photon attenuation, measurement errors due to the point-spread function of the gamma camera, and the statistics of the measurements themselves. The algorithm has been implemented using the iterative, expectation-maximization procedure of Dempster, Laird, and Rubin. Our treatment of the effects of attenuation and point-spread is fundamentally different from methods used in other published SPECT algorithms in that it arises from analysis of an accurate physical model rather than from an ad hoc averaging of data acquired in opposing views.

We also describe how a "noise-like" artifact, which has been seen in positron-emission tomography as a series of randomly distributed peaks and valleys distributed through the image field when maximum-likelihood approaches have been used, is an intrinsic effect that may be removed via the use of Grenander's method of sieves. We discuss the often advocated policy of avoiding this "noise" artifact by arbitrarily terminating the iterative maximum-likelihood procedure after 30-50 steps.

No. 532

A RENAL VASCULAR TRANSIT TIME DISTRIBUTION METHOD FOR USE WITH TECHNETIUM-99m COMPOUNDS. C.A. Wesolowski, G.R. Conrad, and P.T. Kirchner. University of Western

Ontario, London, Ontario, and University of Iowa, Iowa City, Iowa.

An integral method has been developed for the analysis of the early or vascular portion of the renal time activity curve generated from scintillation camera frame file data produced after peripheral venous injection of Tc-99m chelates. The kidney is modeled as three parallel capillary channel networks. A background subtracted aortic input function is produced and this curve along with the renal curve data are noise reduced by an appropriate asymmetric smooth. The integral from 0 to t of this input function is related to the earliest portion of the renal curve to determine the renal arterial delay time and a signal proportionately constant. This information is then used to synthesize the cumulative renal feed function which differs from the renal function only when tracer begins to leave the kidney. The difference between these latter two functions is the renal vascular output function. The output function is stripped of renal compartmental information by comparison of the early linear portion of this function with the identical portion of the cumulative feed function. The mean of the transit time distribution of the renal vascular output function is isolated for each of the first two compartments (mean \pm 1SD = 6.8 \pm 2.4 and 12.8 \pm 3.2 sec. respectively for 40 normal kidneys studied with Tc-99m MDP). The magnitude of the renal plasma flow is derived for all three compartments (mean \pm 1SD 67 \pm 9%, 17 \pm 10%, 16 \pm 9% respectively) where the third compartment contains tracer which resides in the kidney for an extended period of time.

No. 533

MASS ATTENUATION AND MASS ENERGY ABSORPTION COEFFICIENTS OF HUMAN TISSUES AT GAMMA RAY ENERGIES OF SEVERAL RADIOISOTOPES FROM 93 TO 1332 KEV. N.C. Yang, P.K. Leichner, W.G. Hawkins, D.M. Loudenslager, and T.L. Frenkel. The Johns Hopkins Hospital, Baltimore, MD.

Mass attenuation and mass energy absorption coefficients of human tissues are important in dosimetry calculations. They can be calculated with a sum rule by weighting the same coefficients of the individual elements with percentage chemical compositions and adding them together. For energies greater than 10 Kev, the molecular binding effect causes errors of less than a few percent. For certain energies, the coefficients of the individual elements have been published and tabulated. But for energies in-between (gamma ray energies of most clinically used radionuclides), we used a cubic spline interpolation method to calculate the coefficients of blood, bone, brain, fat, heart, kidney, liver, lung, muscle, pancreas, and spleen for Co-57, Co-60, Ga-67, Se-75, Tc-99m, In-111, In-113m, I-123, I-131 and Cs-137. Compared with some existing experimental values, our values agreed with them from 0.9% to 4.5%. Different values of chemical compositions of the same tissue from different reports were compiled and compared, and the resulting coefficients agreed within 2%. Therefore, the coefficients are insensitive to the chemical compositions at these gamma ray energies.

Monday, 3:30-6:00

Exhibit Hall

DOSIMETRY/RADIOBIOLOGY

No. 534

ABSORBED DOSE IN SKIN FROM CONTAMINATION OF ¹¹¹IN-OXINATE WHEN WORKING WITH CF¹¹¹ LABELING. Gustav Grafström, Bo-Anders Jönsson and Sven-Erik Strand, Radiation Physics Department, University of Lund, Lund, Sweden.

The radioisotope ¹¹¹In-oxinate is used in labeling of leukocytes, granulocytes, platelets and antibodies. Be-

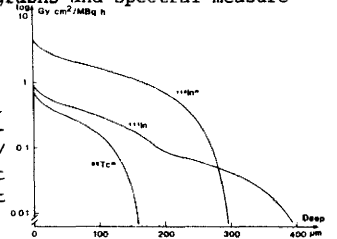
cause of its liquid state there is always a risk of contamination during the handling procedure. As the oxinate is soluble in fat, the contamination may penetrate the skin. Emission of low-energetic electrons during the decay would cause high absorbed dose. The aim with this investigation was to evaluate the "normal" grade of contamination and the absorbed dose enclosed.

The degree of contamination during different operations of handling was investigated by determination of the activity on protection gloves used by personnel at isotope-laboratories. Measurable activity remained after all handling procedures, ranging from 0,1 to 100 kBq.

Leakage in different latex protection gloves, with or without simulation of excessive sweating, showed fractions up to one percent of contaminated activity.

penetration in skin was evaluated with two different methods. In both autoradiographs and spectral measurements with surface barrier detector it was found that the main activity stays on or near the surface, not exceeding a depth of 10 μ m.

The figure shows theoretical absorbed dose rate (Gy/h per MBq/cm²) at different deep, from contamination at the surface



No. 535

SPATIAL DISTRIBUTION OF ABSORBED DOSE FOR Y-90 IN SMALL SOURCES. H.H. Hines, L.T. Chang, ADAC Labs, San Jose, Ca. J.M. Frincke. Hybritech Incorporated, San Diego, Ca.

It is important in radiation therapy to deliver cell killing doses to all of the cancer cells. In therapy using beta emitters, the equilibrium dose rate does not apply to small sources or at the edges of tumors due to the finite range of the beta rays. The purpose of this paper is to present the spatial distribution of the absorbed dose per microcurie hour (AD/uCiH) for Y-90.

Computer simulations were performed to calculate the spatial distribution of the AD/uCiH for Y-90 sources of different volumes and spatial distribution. The sources were placed in a uniform absorbing media. The AD/uCiH was calculated using convolutional techniques and the absorbed-dose distribution from Berger (MIRD # 5).

For spherical sources containing homogeneously distributed Y-90 the maximum AD/uCiH, the AD/uCiH at the edge of the source, and the average in the object are

OBJ. VOL. (ml)	MAXIMUM (rad/uCiH)	EDGE (rad/uCiH)	AVERAGE (rad/uCiH)
0.1	1.11	0.46	0.76
0.2	1.38	0.59	0.95
0.4	1.64	0.69	1.12
1.0	1.88	0.75	1.32
2.0	1.96	0.83	1.45
4.0	1.97	0.88	1.56

The above calculations show that the absorbed rad dose for small sources can be significantly less than the equilibrium dose rate suggests (1.98 for Y-90). Thus, it is important to calculate the dose for representative small tumors or at the edge of large tumors to insure that a sufficient absorbed radiation dose is delivered to all of the tumor cells to achieve a cure.

No. 536

FETAL DOSIMETRY FROM IODINE-131 DURING THE FIRST MONTH OF PREGNANCY. F. Hosain, R.P. Spencer, L.A. Spitznagle, M.K. Karimeddini, and V.T. Penikas. The University of Connecticut Health Center, Farmington, CT.

Despite careful history taking and pregnancy testing, therapeutic radioiodine is occasionally administered to a woman who turns out to be in the earliest stages of pregnancy. Because of concerns about fetal radiation,

genetic counseling, and possible therapeutic abortion, reliable dose estimates are needed. Iodine-131 iodide therapy has been one of the most widely accepted nuclear medicine procedures, but radiation dose estimation (with any degree of accuracy) for the fetus, during the early stage of pregnancy, appeared to be difficult. Dosimetry for a two week old fetus by several experienced investigators varied widely between 2.7 and 54 cGy/GBq (maternal thyroid uptake was 24% at 24 hour, and total body retention was 25% and 15% after 1 and 2 days). This led to the present reevaluation of fetal dosimetry. A 1-3 week old fetus was expected to be implanted in the uterus with a mass less than 10 grams. Calculations were based on MIRD recommendations, other relevant publications, available experimental data, and kinetic considerations for iodine-131. Fetal radiation dose was mainly contributed from circulating hormone, whole body iodide level, and concentrations of radioactivity in the urinary bladder and the GI tract. Calculations were also made for uterus as a reasonable equivalent organ. Fetal dose in the above case, with the present approach, was approximately 12 cGy/GBq (0.43 Rad/mCi), narrowing down the wide range of 2.7-54 cGy/GBq. This dosimetry model employs a dynamic system with limited data, but offers higher accuracy.

No. 537

DOSIMETRY IN METABOLIC RADIOTHERAPY USING I-131 META-IO-DOBENZYLGUANIDINE (mIBG) FOR NEUROBLASTOMA AND PHEOCHROMOCYTOMA. J.Lumbroso, B.Aubert, M.Ricard, M.Di Paola, M.Schlumberger, C.Parmentier, R.Di Paola. Institut G. Roussy and INSERM U66, Villejuif, France.

We assessed radiation doses to tumours in order to evaluate new metabolic radiotherapeutic agents.

Seven children aged from 4 to 18 years received 14 therapeutic doses of I-131-mIBG for metastatic neuroblastoma; 2 adults received 4 treatments for malignant pheochromocytoma. The 18 infused doses ranged from 1.1 to 5.5 GBq bound to 1 to 5mg of mIBG. A dual-probe digitized whole body scanner with 5"x4" NaI(Tl) crystals and high sensitivity collimators was used, linked to a computer system (Sopha Medical). We obtained the activity present in a tumour using manually drawn ROI on the image representing the geometrical mean of the anterior and posterior views. Whole body scans were recorded from 1 to 14 days after injection. CT and NMR images were used to determine the volume of tumoral targets. The effective half-life of mIBG after the last scan was extrapolated exponentially.

After calibration with I-131 sources (0.2 to 740MBq) placed at various depths in a phantom filled with water at a height of 10, 15 and 20cm, estimated error was $\pm 15\%$. Computed tumour doses varied from 3 to 105Gy. We report here the results in 2 cases. In a case of an orbital metastase of a neuroblastoma, the biological half-life was 9.3 days, the uptake represented 11% of the injected dose for a tumour volume of 50 cm³; the resulting radiation dose was 105Gy. In a case of hepatic metastases of malignant pheochromocytoma, the biological half-life was 9 days with an initial uptake of 15%, and one third of the liver was estimated to be involved by the tumour: the dose was 24Gy.

No. 538

THERMAL EFFECTS OF HIGH-FIELD (1.5 TELS) MAGNETIC RESONANCE IMAGING: CLINICAL EXPERIENCE BELOW AND ABOVE A SPECIFIC ABSORPTION RATE OF 0.4W/kg. F.G. Shelllock, D.J. Schaefer and J.V. Crues. Department of Diagnostic Radiology, Cedars-Sinai Medical Center, Los Angeles, CA and General Electric Company, Milwaukee, WI

The U.S. Food and Drug Administration has issued guidelines to ensure the safe operation of magnetic resonance imaging (MRI) systems which include limiting the radiofrequency (RF) radiation exposure to a whole body average specific absorption rate (SAR) of 0.4 W/kg. This recommendation may be unnecessarily restrictive, therefore we determined the thermal

effects of MRI in patients subjected to RF exposures below (SAR ≤ 0.4 W/kg, range 0.1 to 0.4 W/kg, N=23, Group I) and above (SAR > 0.4 W/kg, range 0.5 to 1.3 W/kg, N=28, Group II) the suggested SAR. Body and skin temperatures were obtained immediately before and after MRI. A high-field MRI device (Signa MR System, General Electric) was used in this study and scans were obtained with conventional RF pulse sequences.

	Tb(°C)	Tf(°C)	Th(°C)	Ti(°C)
Group I Before	36.5 \pm 0.4	32.7 \pm 0.7	30.1 \pm 1.3	31.0 \pm 1.9
After	36.6 \pm 0.3	32.8 \pm 0.6	30.7 \pm 1.7*	31.7 \pm 1.9*
Group II Before	36.5 \pm 0.4	32.7 \pm 0.9	30.3 \pm 1.5	32.0 \pm 1.6
After	36.7 \pm 0.3*	32.7 \pm 0.6	31.0 \pm 1.4*	33.0 \pm 1.4*

(Tb - body temperature, Tf - forehead temperature, Th - hand temperature, Ti - positioning isocenter temperature, *p<0.05 before compared to after). Skin temperatures increased a statistically significant amount in both Groups I and II after MRI. Body temperature increased a statistically significant amount in Group II. Although there were elevations in temperatures measured in these patients, the absolute temperatures were well below levels believed capable of producing adverse biological effects.

No. 539

BIOLOGICAL DISTRIBUTION AND DOSIMETRY OF Tc-99m-MAA. G.H. Simmons, J.J. Coupal, F.H. DeLand, J.S. Blake. Veterans Administration and University of Kentucky Medical Centers, Lexington, KY.

Tc-99m-MAA is used extensively for lung perfusion studies, yet existing human data are insufficient to accurately calculate the absorbed dose to individual organs. The objective of this study is to gather bio-distribution data sufficient to enable the calculation of average organ doses in humans with normal lung function to an accuracy of 15%. Two approaches for quantitating the data were investigated. Absolute efficiency measurements were performed on 10 volunteer subjects using Tc-99m-HAM which is trapped in the lung capillaries with greater than 98% efficiency on the first pass. Efficiency factors for other organs of interest were measured using the REMCAL phantom. This method was judged unsatisfactory because of the large dispersion in the measured lung efficiencies, especially among females (51% rms). In the other method conjugate counts were performed over a 24 hour period on 20 subjects following injection of Tc-99m-MAA. Quantitation was achieved by assuming 100% of the injected activity to be in the lungs on the first count. Blood was drawn at the time of each count, and urine was collected for 48 hours, enabling a balance determination to account for all injected activity. Particle size, tagging efficiency and integrity, radiochemical purity, and the number of MAA particles injected were measured for each subject. The average lung dose was determined to be 0.23 \pm 0.024 (rms) rads/mCi. Doses to other organs as well as biological rate constants were also calculated.

No. 540

RADIATION DOSE CHARACTERISTICS OF AN IMPROVED Os-191/ Ir-191m GENERATOR SYSTEM. M.G. Stabin and E.E. Watson, Oak Ridge Associated Universities, Oak Ridge, TN; F.F. Knapp and T.A. Butler, Oak Ridge National Laboratory, Oak Ridge, TN; C. Brihaye and M. Guillaume, Universite de Liege, Belgium.

Short-lived radionuclides have great potential for use in radionuclide angiography because studies can be repeated frequently with little interference from previous studies and with low radiation doses to patients. An Os-191/Ir-191m generator system, developed at ORNL and the Universite de Liege in Belgium, shows Ir-191m yields of up to 20% with Os-191 breakthrough of around 0.0002%. Detailed distribution studies were performed in female Fisher rats for extrapolating radiation dose

estimates to humans. Organ distribution, retention, and excretion data were collected for up to eight days; results were fit to one or two compartment exponential ingrowth and elimination curves, using linear and non-linear least squares techniques. The Ir-191m radiation dose estimates were on the order of 10^{-6} mGy/MBq. The Ir-192 and Os-191 contaminants contributed most of the radiation dose to the major organs. The highest dose estimate to any organ, including contaminants, for an administered activity of 5300 MBq of Ir-191m was near 100 μ Gy (representative of the dose to the liver, kidneys, spleen, and thyroid). Most of the estimates were less than 50 μ Gy. The dose estimates for this generator system will be compared to estimates for other agents currently used in radionuclide angiography.

Work was performed for the USDOE under contract DE-AC0576OR00033 and Interagency Agreement No. FDA 224-75-3016.

No. 541

DOSIMETRY OF TANTALUM-178 AND TUNGSTEN-178 IN ADULTS AND CHILDREN. R.E. Zimmerman, R.L. Holman, and R.D. Neirinckx. Joint Program in Nuclear Medicine, Department of Radiology, Harvard Medical School and Brigham and Women's Hospital, Boston, MA.

Dosimetry calculations have been performed for the isotope Ta-178 and its parent W-178. Tantalum-178 is a short half-life (9.3 min) generator-produced, low energy radionuclide for imaging heart function in first pass studies using gas imaging detectors. It decays from the parent W-178 ($T_{1/2}=22d$) by complex electron capture with subsequent gamma emission and internal conversion. Approximately 1% of the decays are by positron emission. The principal radiations for dosimetry considerations are the Auger electrons, L-x-rays, positrons and K-x-rays. The number of internal conversion electrons, x-ray abundances and Auger electron yields were calculated from nuclear data for Ta-178 and W-178. Biodistribution data were obtained from phosphate buffered Ta-178 eluant and for the W-178 breakthrough product by injection into rats. The dosimetry calculations were performed for adults by using the MIRD schema and tables and for children using the MIRD data on geometric objects for all significant organs. The critical organ is the kidney which in the adult receives 2.9 mrad/mCi from Ta-178 and 1.9 mrad/ μ Ci from W-178. Photon yield per mCi is 70% that of Tc-99m in similar imaging situations in the adult. The total reduction in dose to the kidney compared to a Tc-99m study with equal number of photons is 28. This suggests that Ta-178 could be utilized for low dose pediatric imaging, for high statistics imaging of first pass heart function and interventional studies requiring repeated heart imaging procedures.

Monday, 3:30-6:00

Exhibit Hall

ENDOCRINE

No. 542

MIBG UPTAKE IN MEDULLARY THYROID CANCER (MTC) : A FEATURE OF MULTIPLE ENDOCRINE NEOPLASIA (MEN) J.L. Baulieu*, D. Guilloteau, C. Calmette, G. Coutris, M.J. Delisle, D. Gardet, F. Baulieu, N. Delepine, R. Itti, L. Pourcelot, J.C. Besnard and the French Medullary Cancer Study Group.
* Univ. Hosp. Tours, France.

It was recently reported that MIBG could accumulate into various tumors growing from the APUD system, especially MTC. The aim of this cooperative study was to assess MIBG as a scintigraphic marker for MTC.

After thyroid blockage by Lugol's solution, 18.5 MBq I-131-MIBG were injected to 35 patients for detection or follow up of MTC. Whole body scintiscan and 10 to 20 mn activity recording of the neck, chest and abdomen were obtained at 24 and 48 hr.

MIBG scintigraphy was negative in patients with normal calcitonin levels ($<0.1ng/ml-n=9$). It was negative in patients with sporadic and isolated MTC ($n=15$), despite elevated calcitonin and obvious tumor masses. It was positive in 2 patients with isolated MTC and unsatisfying familial screening. In familial or MEN cases ($n=9$), 3 patients with calcitonin between 1 and 6 ng/ml had negative scan, 6 patients with higher calcitonin level had positive scan, demonstrating uptake in thyroid tumors (4 cases) and liver metastases (2 cases).

In conclusion, MIBG uptake in MTC is essentially detectable in familial disease or MEN syndrome with markedly elevated calcitonin. It could be a specific feature of MEN syndrome.

No. 543

QUANTITATIVE ASSESSMENT OF SECRETION OF Tc-99m PERTECHNETATE IN SALIVARY GLAND DISEASE. L. Drubach, N.D. LaFrance, H. Kashima, D. Koller, W. Kasecamp, P. Cole, H.N. Wagner, Jr. The Johns Hopkins Medical Institutions, Baltimore, MD.

Salivary gland function was studied in 20 patients with tumor, stone or other afflictions of the major salivary glands.

Ten mCi of Tc-99m pertechnetate was administered intravenously and the patient was imaged beginning immediately in the anterior position for 60 minutes. Salivary gland evacuation was stimulated 40 minutes after injection by administering the patient granular citric acid. The entire study was acquired by computer in list mode with 60 one minute frames. The time to maximum uptake and excretion fraction of the tracer were calculated for the parotid and submandibular glands. Contralateral glands and normal volunteers were used as controls.

The excretion fraction after citric acid stimulation for normal parotid and submandibular glands was greater than 75% and 55% respectively. Radiotracer excretion after citric acid stimulation was rapid, and peak excretion effect (defined as minimum counts in the ROI following stimulation) was achieved by 4 minutes. Obstruction of salivary ducts by tumor or stones resulted in a greatly diminished excretion fraction (range 3% to 45%).

We conclude that quantitative assessment of Tc-99m pertechnetate kinetics before and after stimulation of salivary glands aids in the assessment of gland function and in detection of duct obstruction.

No. 544

SCINTIGRAPHIC EVALUATION OF GASTRIC EMPTYING IN DIABETIC PATIENTS WITH CARDIAC AUTONOMIC NEUROPATHY. J.L. Urbain, M. Moulart, M. Buyschaert & S. Pauwels, University of Louvain Medical School, Brussels, Belgium.

The radionuclide technique was used to assess whether, in diabetic patients, cardiac autonomic neuropathy (C.A.N.) is associated with delayed gastric emptying. Twelve patients with CAN (CAN+) were compared to 9 patients without CAN (CAN-). Nine healthy subjects matched for age were used as controls (N). All patients and subjects were asymptomatic and without any organic gastrointestinal disease. Measurement of variation in heart rate during deep breathing was used as index of CAN.

Gastric emptying of solids (GES) was determined after ingestion of Tc-99m-SC scrambled eggs. Anterior and posterior images were obtained every 20 min for a 120 min period and data were corrected for radioactive decay and changes in depth.

Percentages of activity retained in the stomach over the test are summarized below for each group (Mean ± SEM).

Group	N	20	40	60	80	100	120
N	9	96 ± 1	90 ± 3	73 ± 2	59 ± 4	42 ± 4	29 ± 4
CAN(-)	9	91 ± 2	84 ± 3	74 ± 4	60 ± 3	48 ± 4	41 ± 8
CAN(+)	12	99 ± 3	92 ± 3	82 ± 4	73 ± 4*	60 ± 5°	50 ± 5°

* p < 0.05; ° p < 0.02

GES was significantly lower in CAN(+) compared to CAN(-) and controls. No statistical difference was found between CAN(-) and controls. Six patients with CAN presented a delayed emptying at 100 and 120 min whereas patients without CAN were all in the normal range.

We conclude that GES is delayed in diabetic patients with CAN suggesting an impairment of the neurovegetative control of gastric motility due to diabetic autonomic dysfunction.

No. 545

DETECTION OF PHEOCHROMOCYTOMA: I131-MIBG, CT, MRI CORRELATION. M.G. Velchik, K. Engelman, H.Y. Kressel, and A. Alavi. Hospital of the University of Pennsylvania, Philadelphia, PA.

Ten patients (7M, 3F) ranging in age from 18-64 years old (x=46) with clinically suspected (n=3) or surgically proven (n=7) pheochromocytoma were evaluated with I131 MIBG scintigraphy, CT, and MRI.

MRI scans were performed with a 1.5 T superconducting magnet with spinecho pulse sequences to provide T1 weighted and T2 weighted images.

All three imaging modalities were negative in two of the cases. MIBG scintigraphy was negative in one case, although bilateral adrenal enlargement was demonstrated by both CT and MRI. Four adrenal lesions and 3 extraadrenal lesions (1 perivesical) were detected by all three modalities and confirmed pathologically. Three patients had metastasis (liver 2, bone 1). Pheochromocytomas were found to be of low signal intensity (=muscle, liver, or spleen) on T1 weighted images and of high signal intensity (>muscle, liver and spleen) on T2 weighted images. Precise localization of lesions was sometimes difficult by MIBG scan.

We conclude that MIBG, CT, and MRI are complementary procedures with the former providing more functional and specific information and the latter two superior anatomic detail and localization. MIBG scans are recommended as the screening study of choice, particularly for the detection of extraadrenal disease, direction of CT and MRI and specific confirmation of their findings. Although MRI provides images in multiple planes without any radiation exposure, it has not demonstrated increased specificity over CT which is the current anatomic adrenal imaging study of choice.

No. 546

THE EFFECT OF THE MENSTRUAL CYCLE ON DOPAMINE RECEPTOR BINDING OF C11-3-N-METHYLSPERONE. D.F. Wong, G. Wand, H. Zacur, D.S. Goldberg, J. Williams, L. O'Tuama, E. Broussolle (*), R.F. Dannals, J.M. Links, H.N. Wagner, Jr. The Johns Hopkins Medical Institutions, Baltimore, MD.

In a previous report of the decline of dopamine receptor binding of C11-3-N-methylspiperone in the caudate nucleus as a function of age, the decrease was statistically different in men than in women. (Science 226:1393-1396,1984.) To determine whether hormonal effects could be important, we examined women at different stages of the menstrual cycle. All had normal menstrual cycles, were not receiving exogenous estrogens, and had a normal gynecologic history. The phase of the menstrual cycle was assessed by history, basal body temperature and serum and urine hormonal values. Each subject was studied with C11-3-N-methylspiperone at two

different phases of the menstrual cycle. In 6 subjects in whom there was no more than 1 cycle between the two PET studies, there was a significant increase in the rate of binding of the C11-3-N-methylspiperone to the dopamine receptors during the pre-ovulatory period. The increase in receptor binding correlated with increasing serum estrogen levels. Previous studies in animals have suggested that estrogen administration can increase dopamine receptor density. The percent differences in each study was on an average 20±6%, and was significant at p < .05 using a sign test.

*ADAMHA visiting NIDA Addiction Research Fellow.

Monday, 3:30-6:00

Exhibit Hall

GASTROENTEROLOGY: ESOPHAGEAL AND LOWER GI

No. 547

RADIONUCLIDE ASSESSMENT OF ILEO-ANAL ANASTOMOSIS EMPTYING: PRELIMINARY RESULTS. R. Taillefer, J. Heppell, V. Derbeyan, P. Belliveau, S. Dubé. Hôpital Hôtel-Dieu and Royal Victoria Hospital, Montréal, Canada.

The aim of this study was to assess and compare with a radionuclide enema the emptying of two types of reservoir constructed with an ileo-anal anastomosis. Reservoirs were made of either two ("J" shaped pouch) or three limbs of ileum ("S" pouch). This prospective study includes 24 patients (11 with "J" pouch and 13 with "S" pouch) and 10 subjects with normal ano-rectal function as controls. One mCi of 99mTc-sulfur colloid was added to 300-350 cc of beaten eggs. The mixture was then cooked until firm in consistency. With a syringe and rectal tube, the semi-solid marker was instilled per anum in the neo-rectum until a sensation of fullness was reached. Ileal pouch counts (posterior view) were measured (2 min. acquisition) using a scintillation camera and computer pre and post spontaneous evacuation. The emptying was defined as the difference in counts divided by pre-evacuation counts. The results are as follows:

	nb	emptying (mean ± SE)	range
controls	10	90 ± 4%	67-99%
"J" pouch	11	70 ± 6%	20-93%
"S" pouch	13	60 ± 7%	21-89%

The "J" and "S" pouches empty less than controls. There appears no significant difference in the reservoir emptying of both pouches. More data is necessary however to confirm this latter finding.

The radionuclide study provides quantitative evaluation of ileo-anal reservoir emptying. As well, it helps in the follow-up and identification of patients who would benefit from rectal intubation.

No. 548

TL-201 PER-RECTAL ADMINISTRATION: OBSERVATION OF CHANGES IN PORTAL-SYSTEMIC CIRCULATION AFTER TREATMENT. N.Tonami, K.Nakajima, N.Watanabe, K.Yokoyama, Y.Seki, S.Kawabata, Y.Shiire, N.Shuke, K.Koizumi and K.Hisada. Kanazawa University, Kanazawa, Japan.

A noninvasive method of Tl-201 per-rectal administration was performed to observe the changes in portal-systemic circulation after sclerosing therapy (ST) and/or splenic artery embolization therapy (SAET) in patients with esophageal varices. One mCi of Tl-201 chloride was given rectally and scintigram and heart/liver uptake ratio (H/L) at 60 min. after administration were investigated before and after ST (22 studies in 16 patients) and SAET (8 studies in 8 patients). After successful ST there was 5.1% of decrease as the mean change rate of H/L, but many of the studies showed little

or no change in H/L. A marked decrease of k/L together with marked scintigraphic change was observed in two cases. One of them showed the recurrence of esophageal varices later. A marked increase of H/L was observed in one case in which the recurrence of esophageal varices was not found for two years. After SAET H/L dropped in most of the cases. We conclude 1) In cases showing highly decreased H/L after ST, portal-systemic shunting greatly depended on esophageal varices and they have a high risk of the recurrence of esophageal varices. 2) In cases showing little change or increase in H/L after ST, portal-systemic shunting did not depend on esophageal varices, but other shunting routes. 3) Reduction of splenic blood flow decreased H/L. This method was found to be useful in evaluating the pathophysiological changes of portal circulation after treatment.

No. 549

ESOPHAGEAL DYSMOTILITY IN PYLORIC OBSTRUCTION BEFORE AND AFTER GASTRIC DECOMPRESSION. S.H. Yeh, R.S. Liu, T.C. Yen, S.C. Hu, and L.C. Wu. Veterans General Hospital and National Yang-Ming Medical College, Taipei, Taiwan.

This study assessed esophageal dysmotility in pyloric obstruction and the effect of gastric decompression on such a dysfunction by radionuclide transit (RT) studies.

Data were acquired in list mode after an oral dose of 0.5 mCi Tc-99m sulfur colloid in 10 ml of water in the supine position. A computer routine modified from Klein (J Nucl Med 25:957, 1984) was used to calculate: (A) total mean transit time (TMTT) in sec, (B) residual fraction after the first swallow (RF), (C) retrograde index (RI), and (D) regional transit times (RTT).

Ten patients with pyloric obstruction (secondary to longstanding chronic duodenal ulcer in 8, gastric erosion in 1 and stricture after surgery in 1) underwent RT studies before and 7.1 ± 4.5 days following gastric decompression (GD). GD decreased both TMTT (mean ± s.d., 9.7 ± 1.9 sec to 7.7 ± 1.9 sec, p < 0.05) and RF (0.41 ± 0.19 to 0.19 ± 0.18, p < 0.02). RTT's also significantly decreased, especially for the proximal third (5.8 ± 2.1 sec to 3.6 ± 1.9 sec, p < 0.05). However, TMTT and RTT's (mid and distal) were still significantly higher after GD than in normal subjects (n = 25; TMTT = 5.8 ± 0.6 sec, p < 0.001). In contrast, proximal RTT and RF did not differ in pts after GD and in normal subjects (p < 0.2 in both). RI was unchanged by GD. In 10 pts of this study, 9 had moderate to severe symptoms of esophageal dysfunction, and all of them after GD were symptomatically improved or relieved together with improved motility.

In summary, symptomatic esophageal dysmotility occurs in the great majority of pts with pyloric obstruction, and can be mitigated by gastric decompression.

Monday, 3:30-6:00

Exhibit Hall

GASTROENTEROLOGY: GASTRIC

No. 550

DUAL RADIONUCLIDE STUDIES OF BILE AND FOOD FLOWS IN THE PATIENTS WITH UPPER ABDOMINAL RECONSTRUCTIVE SURGERY. T. Aburano, A. Tada, N. Tonami, K. Hisada, I. Konishi, Y. Takeshita, I. Miyazaki, and M. Matsudaira. Kanazawa University Hospital, Kanazawa, Japan.

The presence of bile is necessary in the digestion and absorption of fat. The dual nuclide studies of bile (Tc-99m IDA) and food (In-111 DTPA) flows were done in 28 patients with upper abdominal reconstructive surgery, such as gastroenterostomy and/or biliary enteric anastomoses, in order to evaluate the relation between bile and food flows. Five hundreds microcuries of In-111 DTPA dissolved into 200 ml of fat-rich liquid meal was orally administered 20 to 30 min. after intravenous

injection of 5 mCi of Tc-99m diethyl IDA. Both images of Tc-99m and In-111 over upper abdomen were simultaneously taken every 5 min. for 2 hours.

In 21 patients with Billroth II reconstruction, only five (24%) showed the good mixture of bile and food. The remained sixteen showed the poor mixture of those, mostly due to the prolonged retention of bile in the afferent loop and the rapid transit of food into the efferent loop (14 patients). Moreover, five showed the enterogastric reflux of bile. On the other hand, in 7 patients with Billroth I reconstruction, six (86%) showed the good mixture of bile and food, although one showed the poor mixture of those due to the markedly prolonged transit of food.

These findings suggest that the reconstruction with Billroth I method may be better than the one with Billroth II method in order to keep the good physiologic relation between bile and food flows in the patients following upper abdominal surgery.

No. 551

IN-111 LABELED SOLID MEAL FOR GASTRIC EMPTYING STUDIES. M. K. Dewanjee, S. C. Chowdhury, G. Thomforde, J. Malagelada, M. L. Brown. Mayo Clinic and Foundation, Rochester, MN

A new In-111 labeled solid meal (ILSM) was prepared by chelation with chelex resin bead (CRB). The effect of grinding of normal chelex resin bead (NCRB) on In-111 chelation and retention in solid meal with and without microencapsulation with silicone was evaluated in an in vitro system. NCRB (30-70 µm) was ground in a mortar-pestle to form ground chelex resin bead (GCRB). Fine particles were removed by resuspension in distilled water and centrifugation (1750 g). 100-150 µCi of In-111 Chloride was diluted with 0.1 N HCl and mixed with 1 gm of NCRB and GCRB in triplicate. Unbound In-111 was removed by centrifugation (1750 g). Some samples were coated with 0.5 ml of silicone oil (SO) and heated for 30 minutes. The In-111 labeled control and SO coated NCRB and GCRB were mixed with eggbeater (Fleischmann) and ILSM was prepared by heating until solid. The meals were digested with HCl-pepsin (1.2 mg/ml of 0.1 N HCl) for four hours in a stirrer-bath (37°C). Aliquots were collected at intervals for determination of In-111 loss from ILSM. The CRB labeling efficiency and In-111 loss at 4 hours are tabulated:

	Labeling efficiency(%)	¹¹¹ In-loss(%)
In-111 NCRB	98 ± 1	8 ± 2
In-111 NCRB (SO)	96 ± 2	7 ± 1
In-111 GCRB	92 ± 2	5 ± 1
In-111 GCRB (SO)	96 ± 1	5 ± 1

These results suggest that In-111 GCRB was retained in solid meal at higher level than NCRB and coating does not significantly increase retention.

No. 552

pH DEPENDENCE OF In-111 ALGINIC ACID ANTIGASTROESOPHAGEAL REFLUX BARRIER. L.C. Knight, A.H. Maurer, I.A. Ammar, J.A. Siegel, B. Krevsky, R.S. Fisher, L.S. Malmud. Temple University Hospital, Philadelphia, PA.

Alginic acid (AA) combined with antacid is used for the treatment of symptomatic gastroesophageal reflux. Prior studies with strontium-87m-labeled AA demonstrated that one mechanism of action involves the formation of a barrier (raft) which floats on the surface of gastric contents. In this study a new In-111 AA was used to study the effect of gastric pH on raft formation. In-AA was prepared by adding In Cl₃ to a suspension of Mg alginate in 0.04 N HCL. After centrifugation and washing 85% of the In-111 was bound to AA. The In-AA was combined with MgCO₃, dried Al(OH)₃ and NaHCO₃. In vitro studies in 0.2 N HCL showed formation of a thick raft which contained 70% of the In-AA. Two groups of human

subjects were studied. Group I received In-AA and 300 ml of H₂O with 150 uCi Tc-99m sulfur colloid (n=5) and Group II received In-AA with 150 ml of 0.1 N HCL + 150 ml of apple juice (n=5):

	5 min		30 min		60 min	
	Tc	In	Tc	In	Tc	In
Group I	51/49	47/53	30/33	34/41	15/16	29/30
Group II	47/54	61/39	24/18	56/34	15/16	48/37

For Group I a significant raft could be demonstrated in only 1/5 subjects. For Group II rafts were present in 4/5. In-AA activity in the upper stomach was significantly higher than Tc-99m (p<0.05). We conclude that gastric pH must be acidic to form an AA antireflux barrier.

Monday, 3:30-6:00

Exhibit Hall

GASTROENTEROLOGY: HEPATIC

No. 553

DIFFERENTIATION OF PRIMARY SCLEROSING CHOLANGITIS (PSC) FROM PRIMARY BILIARY CIRRHOSIS (PBC) BY Tc-99m-IDA SCINTIGRAPHY. S. Krishnamurthy, G.T. Krishnamurthy, E.B. Keefe, and D.A. Lieberman. VA Medical Center and Oregon Health Sciences University, Portland, OR.

PSC and PBC are chronic cholestatic diseases that share many clinical and biochemical features. This study was undertaken to test if these two diseases could be differentiated reliably from each other by Tc-99m-IDA scintigraphy. Thirteen patients with documented PSC and 10 with PBC were studied with Tc-99m-DISIDA. Analogue images were obtained at 2 minute intervals for 60 minutes with simultaneous computer data collection at 1 frame/min. Clearance t-1/2 was calculated for 3 regions of the liver. Single photon tomographic images (SPECT) were obtained between 60 and 90 minutes. The regional retention of radiotracer was noted on the SPECT images. The analogue and SPECT images were interpreted independently by 2 physicians who were unaware of the specific diagnosis.

Scintigraphically PSC was characterized by single or multiple band constriction of CBD, beaded appearance of RHD or LHD, cystic duct obstruction, and marked variation in regional hepatic clearance time. The anterior segment of the right and medial segment of the left lobe were involved more frequently than others in the SPECT images. PBC was characterized by hepatomegaly (predominantly left lobe); normal RHD, LHD, CBD, and cystic duct with diffuse retention of isotope in the liver. It is concluded that the distinct morphologic and physiologic alterations of PSC and PBC can be differentiated reliably by scintigraphy.

No. 554

MEASUREMENT OF REGIONAL LIVER BLOOD FLOW BY INHALATION OF XENON-133. A. Kroiss, K. Herholz, L. Peschl, H. Benko, Ch. Kölbl, and A. Neumayr. KA Rudolfstiftung, Vienna, Austria.

Liver blood flow was measured by the Xe-133 inhalation technique with an Anger camera and an on-line computer system. In the same position Tc-99m colloid was then applied for edge detection of liver and spleen and to exclude overlapping areas from calculation. The activity of expiratory air (expiration-tube) was used as the arterial input function and a ROI was placed over the spleen representing the portal vein input function. Liver blood flow was estimated with a modification of Obrist's algorithms.

Liver blood flow was found to be 63.1±10 in 27 patients with compensated cirrhosis; 43.1±5 in 13 patients with decompensated cirrhosis (p<0.001); 48.1, 59.3 and 35.6 in 3 patients with hepatoma; and 60.3 and 76.1 ml/100 gm/min in 2 patients with liver secondaries. The flow data agreed well with values recorded with an invasive method (Szintisplenoportography; r=0.88) in 12 patients in a direct comparison and also with invasive methods in earlier investigations of our group and with those reported in literature.

The method is suitable for estimation of the recent status of the liver and controls, for prognosis of surgical procedures in shunt operations and liver transplantations.

No. 555

IS RADIONUCLIDE LIVER SCAN ALREADY UNNECESSARY FOR DIAGNOSIS OF HEPATOCELLULAR CARCINOMA? M. Kudo, H. Kashida, M. Hirasa, H. Takakuwa, Y. Ibuki, K. Fujimi, S. Tomita, H. Komori, A. Orino, A. Todo, Y. Saiki, H. Ito, M. Hino and K. Ikekubo, Kobe General Hospital, Kobe; and K. Torizuka, Kyoto University, School of Medicine, Kyoto, Japan.

Rapid progress of several imaging modalities, especially ultrasound (US), has simplified the diagnosis of hepatocellular carcinomas (HCCs). Concerning the imaging modalities, some investigators insist that radionuclide liver scan (RN) is already unnecessary because of the following reasons: 1) The detectability of RN is much more inferior to that of US, 2) RN cannot differentiate HCCs from other tumors, 3) The ability of resolution is much more inferior to that of US, and 4) RN is comparatively more expensive. The purpose of this study is to clarify whether or not RN is truly necessary for the diagnosis of HCCs.

From 1981 to 1985, RN was performed on 383 cases out of a total of 486 of which all had HCCs. These 383 cases were studied and graded into 3 categories according to the usefulness of RN. These categories are 1) HIGHLY USEFUL, 2) MODERATELY USEFUL and 3) NOT USEFUL. The results, using single photon emission computed tomography, were also evaluated separately.

The cases categorized into the HIGHLY USEFUL group had 2 types of HCCs; one which were a macroscopically diffuse type and another which were located in the subdiaphragmatic portion of the liver. In conclusion, RN is definitely still necessary in these cases for the diagnosis of HCCs.

No. 556

IDENTIFYING HEPATOCELLULAR DISEASE BY MEASURING SPLEEN/LIVER RATIOS. D.F. Preston, M.A. Smith, D. Hayes, H. Lindsley, K. Gerald, N.L. Martin, R.G. Robinson, A.V. Wegst. Kansas University Medical Center, Kansas City, Kansas

Our purpose is to determine the numeric parameters from digitized Tc-99m sulfur colloid (TSC) liver spleen scans which are of value in identifying hepatocellular disease.

Eighty TSC liver spleen scans requested for routine clinical purposes were recorded on a 64x64 array by an MDS computer. Measurements of total activity from the anterior liver (AL), anterior spleen (AS), average counts/pixel from the anterior liver (MAL), average counts/pixel from the anterior spleen (MAS) and comparable posterior values (PL), (AS), (MAS), (MPS) were obtained. Ratios of MPS/MPL, geometric mean (GM S/L), PS/PL, PS/AL, MPS/MAL were made. After 6 months, patients were classified by chart review into normal (51), hepatocellular disease (9), normal but receiving methotrexate (7), cancer metastatic to liver (7) and myeloproliferative disease (6) groups. Duncan's Multiple Range Test searched for significant (P<.05 differences between the groups

PS/AL, GMS/L and PS/PL identified hepatocellular disease as a group distinct from other groups. Use of the total organ count produced parameters of better discrimination to detect hepatocellular disease than did parameters which used the mean count of the organ.

PS/AL >1.00, GM S/L >1.10 or PS/PL >1.00 are strong numeric indicators of hepatocellular disease.

No. 557

QUANTITATIVE ASSESSMENT OF LIVER TRANSPLANT FUNCTION BY DECONVOLUTIONAL ANALYSIS. R. Reichle, D. Campbell, E. Tagge, S. Warber, J. Juni. University of Michigan Medical Center, Ann Arbor, MI.

A quantitative non-invasive technique to determine hepatic function in liver transplant patients is desirable. We have assessed liver function by deconvolutional analysis (DCA) of disofenin scans in an acute swine transplant model and in human liver transplants. By correcting for the effects of systemic circulation of a bolus injection, DCA simulates a bolus injected directly into the hepatic vascular supply.

Three normal and 11 unrelated donor transplant (within 1 hour at transplantation) were imaged with 5 mCi Tc-disofenin. All, except 1 of the transplants, had normal extraction efficiencies (XE's) of 100%. The average disofenin mean transit time (MTT) of the normals, however, was 8.60 min (range 5.7-10.5) compared to 15.5 min (range 10.5-24.8) of the transplants (p<0.008).

The 4 chronic transplant patients were studied serially (2-60 days post-transplant) for a total of 16 studies. Changes in XE's showed a striking inverse relationship and generally preceded changes in bilirubin levels, bile volumes, and clinical status. MTT's, however, showed no such relationship.

Quantitative measurement of liver transplant function by DCA clearly identified acute liver dysfunction associated with transplantation and appears to correlate with and predict clinical course in preliminary patient studies.

Monday, 3:30-6:00

Exhibit Hall

GASTROENTEROLOGY: PANCREAS

No. 558

IMAGING OF HUMAN PANCREAS WITH I-123 LABELED HIPDM AND SINGLE PHOTON EMISSION COMPUTED TOMOGRAPHY (SPECT). K. Yamamoto, Y. Kuge, H. Saji, E. Aoki, N. Hayashi, Y. Fujibayashi, Y. Yonekura, H. Adachi, K. Torizuka. Kyoto University, Kyoto, Japan.

The pancreas accumulation of radioiodinated HIPDM (N,N,N'-trimethyl-N'-(2-hydroxy-3-methyl-5-iodobenzyl)-1,3-propanediamine) in mice and rats has been reported (J Nucl Med 26:765-9,1985). In this study, we have tried to assess the localization of I-123 labeled HIPDM in the human pancreas.

2-3 mCi of I-123 labeled HIPDM was given to the normal volunteers intravenously. The planar scintigram was obtained at 1, 3, 5 and 20 hours later. SPECT was performed at 1, 3 and 5 hours after injection using the rotating gamma camera with medium energy collimator and it took 32 min to get projection data over 360°.

The pancreas was visible in the planar image from 3 hours and more clearly visualized at 20 hours later, but the radioactivity ratio of pancreas to liver was much lower than those of mice and rats. Only a little activity was seen in the kidneys and the intestinal tracts throughout the study.

SPECT could avoid overlapping the radioactivity in the liver and the spleen with that in the pancreas, and thus good positive images of pancreas could be obtained at 3 hours after injection of I-123 HIPDM in spite of

slightly lower radioactivity in the pancreas as compared with in the liver and the spleen.

In conclusion, I-123 labeled HIPDM was expected to have the clinical usefulness as the pancreas imaging agent, especially if imaged using a SPECT system.

Monday, 3:30-6:00

Exhibit Hall

HEMATOLOGY

No. 559

EFFECT OF SPLENO-RENAL ANASTOMOSIS ON SPLENIC SIZE IN HEPATOSPLENIC SCHISTOSOMIASIS. M. Abdel-Razzak, A. Nasef, and A. El-Aggan. Kasr El-Aini Faculty of Medicine and A.C. Medical Center, Cairo, Egypt.

Shunt operations have been used in the management of portal hypertension that ultimately develops secondary to periportal fibrosis characteristic of hepatosplenic schistosomiasis. Out of the shunt operations, splenorenal anastomosis is considered the procedure of choice since it selectively decompresses the portal bed without draining the mesenteric blood from the liver. Because of its decompressing effect, splenorenal anastomosis is expected to diminish the splenic size.

To test the validity of this assumption, the size of the spleen was determined from the anterior, left lateral and posterior projections of hepatosplenic radiocolloid scans obtained before and after splenorenal anastomosis in 5 patients suffering from hepatosplenic schistosomiasis. Postoperative scans were obtained at periods ranging from 2 to 80 weeks.

Following the operation, the clearance rate of radiocolloid from the circulation became faster. However, the size of the spleen did not change significantly. Accordingly, splenic enlargement in schistosomiasis should be due to cellular hyperplasia, rather than venous congestion.

No. 560

RED BLOOD CELL VOLUME (RBCV) AND BLOOD VOLUME (BV) IN THE MALE ALBINO (NZW) RABBITS. N.D. Karatzas, K.I. Kalaras. University of Miami, Miami, Florida and Aristotelion University of Thessaloniki, Greece.

The estimation of RBCV and BV in experimental animals is important in studies of pharmaceuticals distribution. Since the standard values of them with Tc-99m in the rabbit has not yet been published we measure RBCV and BV in 64 male albino New Zealand rabbits 2.0-4.0 kg body weight (BW) (x±sd: 3.12 ± 0.37 kg). Two ml heparinized (20 µl) venous blood from the rabbit's ear was added to 10 ml saline and centrifuged. The supernatant was removed and 0.015 µg of Sn⁺⁺/ml was added. Five min later 15 µCi Tc-99m pertechnetate (in 0.3 ml normal saline) was added, incubated for 5 min washed with 5 ml saline twice and resuspended in 2 ml saline for injection and the standard. Blood was drawn 10 min after injection from the other ear (2ml) and duplicate samples of 0.5 ml were counted. Venous hematocrit was 38.2 ± 0.24 (sd.) The RBCV was calculated according to the formula RBCV = S.R.Vs. Hct./B (ICSH 1980) and the BV by RBCV (BV = RBCV x 100/Hct.%) x 0.97. The labeling efficiency was 96.4 ± 3.8 (sd.) The RBCV (ml/kg) was found to be: 0.021 x (BW^{gr}) - 8.13 (r² = 0.62, p < 0.001). The RBCV were 18.52 ± 1.96 (sd) ml/kg BW or 57.87 ± 9.90 (sd.) ml. The correlation with hematocrit has shown RBCV (ml/kg) = -144.55 (Hct.)² + 164.87 (Hct.) - 23.28 (r² = 0.382, p < 0.001). The BV (ml) = 42.60 x (BW)^{1.14} (r² = 0.69 p < 0.001). The BV were 156.12 ± 24.27 (sd.) or

5.00% +0.43% (sd.) ml/kg of the BW of the rabbits. The above values with Tc-99m do not differ significantly from those of the standard Cr-51 procedure and permit repeating RBCV measurements in shorter intervals as compared to Cr-51.

No. 561

KINETICS OF EOSINOPHILS IN THE HUMAN BODY. S. Kariyone, M. Konno, Y. Takagi, T. Yui, S. Matsuda and T. Uchida. Fukushima Medical College, Fukushima, Japan.

Kinetic observations were done in two patients with eosinophilia and the kinetic patterns were compared with those of neutrophils. About one hundred million of cells of eosinophils or neutrophils were collected and they were labelled by In-111-oxine or -tropolone with 300-500µCi of radioactivity.

Two cases of reactive eosinophilia with the count of 56,700 and 41,500/µl of blood were used for this study. The disappearance of labelled eosinophils from the circulation formed single exponential curve after the initial fluctuation. The pool sizes and turnover rate were calculated from the recovery and disappearance rate according to the formula of Mauer for granulocyte kinetics study. Various indices of eosinophils kinetics were compared to those of neutrophils in neutrophilia (DFP-32 study) and in chronic myeloid leukemia with almost same sizes of circulating pool.

Disappearance rate of eosinophils was slower than that of neutrophils in CML and was fastest in neutrophilia. Size of total blood pool of eosinophils was much smaller than that of neutrophils in CML and was almost equal in neutrophilia. Turnover rate of eosinophils was smaller than that in neutrophilia and was remarkably larger in CML. Migratory pattern of labelled eosinophils in the body was observed by scintillation camera. Radioactivity accumulated in the spleen and it gradually increased until 24 hours while there were no change of radioactivity in the lung, liver and bone marrow. Specificity of eosinophils kinetics were clearly demonstrated from these findings.

No. 562

IN VIVO KINETICS OF AUTOLOGOUS RED CELLS PRESERVED 49 DAYS AT 4°C IN PAGGSS AND IN ADSOL-A1. O. Messian, L. Noel, G. Fabre, J. Saint-Blancard, B. Saint-Paul. Centre de Transfusion, Le Chesnay, France.

Extending the storage period of red blood cells (RBC) at 4°C will help to improve the supply and simplify the development of autologous transfusion programs. Measurement of the in vivo recirculation of preserved RBC has been a controversial subject over the last years.

In order to give an accurate 24 hours recirculation percentage we used a double label technique with 51 Chrome preserved RBC and 99m Technetium fresh RBC. The ratio of the RBC volume, simultaneously measured by the two methods, is used to take into account the number of non viable red cells removed from the circulation within the first five minutes after transfusion. Furthermore, we studied the stored RBC survival beyond 24 hours and measured the half life of this population (T50-24 H) and the time where fifty percent of the total injected activity disappeared (T 50 %).

In ADSOL-A1 (n=5) the 24 hours survival percentage was 75 ± 8.5 % with Chrome only and 72 ± 6.5 % after correction. The T 50 % was 16.9 ± 3 days and the T50-24 H was 32.2 ± 4.7 days. In PAGGSS these values were 79.5 ± 8 % and 78.2 ± 8.5 % (n=10); T 50 % was 18.6 ± 3 and T50-24 H was 30.9 ± 5.8 days (n=7).

The double label technique appeared to be easy to use and demonstrated some degrees of early exaggerated post transfusion destruction after 49 days of storage (11 % for two patients in ADSOL-A1). PAGGSS appeared to maintain the viability of stored RBC at a satisfactory level by present standards. From our results, we believe that

further studies should be done including late kinetics measurements for evaluation of new RBC products.

No. 563

IN VITRO EVALUATION OF GRANULOCYTE LABELING WITH In 111 CHELATED TO THREE DIFFERENT AGENTS. L. Mortelmans, A. Verbruggen, M. Bogaerts, C. De Bakker, M. De Roo, U.Z. Gasthuisberg, Leuven, BELGIUM

We have studied the influence of granulocyte labeling with commercially available In 111-Oxine or- Tropolone (Trop) or home made In 111-Merc (JNM 26: 518-523, 1985) on the cell structure by electron microscopy (EM) and on the cell function by measuring myeloperoxidase content and release, superoxide production, random migration (RM), chemotaxis (CHEM), phagocytosis (PHAG) and bactericidal activity (BACT).

(i) The granulocytes were labeled with 400 µCi of In 111-Oxine in saline or In 111-Trop or- Merc in plasma. (ii) The influence of the chelating agents without addition of the tracer was tested (n=4) in the following range (µg/ml final solution): 5-10 (Oxine), 10-160 (Trop), 1-4 (Merc). (iii) The test was repeated for the same concentration range with addition of In 111.

(i) CHEM and RM were not affected by Trop and clearly suppressed by Oxine and Merc. The results of the other tests were normal. The cell structure was disturbed by Merc (EM). The labeling efficiency was excellent with Oxine (>90%), acceptable with Trop (30-80%) and poor with Merc (10-25%). (ii) Without In 111, CHEM and RM were normal up to a concentration of 80µg/ml (Trop), 8.5 µg/ml (Oxine) and 1µg/ml (Merc). PHAG and BACT were normal in the full range. (iii) With addition of In 111, CHEM and RM were unaffected up to 80µg/ml by Trop and markedly suppressed by Merc and Oxine.

In our experience, only labeling with In 111-tropolone assures morphologically and functionally intact cells with a reasonable labeling efficiency.

Monday, 3:30-6:00

Exhibit Hall

IMMUNOLOGY/INFECTIOUS DISEASE

No. 564

COMPARISON OF INDIUM-111-TROPOLONE AND INDIUM-111-OXINE LABELED LEUKOCYTES SEPARATED BY THREE TECHNIQUES. S. Chowdhury, M.K. Dewanjee, M.L. Brown, L.A. Forstrom, J.A. Katzmann. Mayo Clinic and Foundation, Rochester, MN.

Leukocytes were separated by three techniques: Ficoll-Hypaque (FH), volax sedimentation (VS), and VS-hypotonic lysis (VSHL)(method of Karesh et al JNM 26:97, 1985). The cells were labeled with Indium-111-oxine containing Tween-80 (INO) and Indium-111-tropolone (INT). All studies were done on normal volunteers. The harvested granulocyte (PMN), platelets (PLT), and red blood cells (RBC) per ml of whole blood and the ratio of Chemotactic migration to Random migration (CM/RM) (using the granulocyte chemotaxis response to E. coli in agarose plates) are tabulated below (mean ± SD):

METHOD	PMNX10 ⁶	PLTX10 ⁶	RBCX10 ⁶	CM/RM
INT FH	2.0±0.8	0.7±0.3	1.3±0.7	1.7±0.8
INT VS	2.4±0.7	5.6±2.4	6.2±2.3	1.3±0.3
INT VSHL	2.8±0.9	1.5±0.9	1.1±0.5	1.4±0.3
INO VS	2.1±0.4	6.4±4.0	4.5±1.0	1.4±0.2
INO VSHL	2.2±0.4	1.3±0.6	0.9±1.4	1.4±0.2

In a separate animal study, the leukocyte survival times were found similar among all techniques.

With VSHL there were significantly fewer RBCs and PLTs approaching the results of FH. CM/RM response is not significantly changed by hypotonic lysis. Trypan-

blue exclusion testing showed 100 percent cell viability in all experiments.

In conclusion, VSHL separation technique is a simple method of obtaining a relatively pure granulocyte preparation with no sacrifice of viability or function.

No. 565

GASTROINTESTINAL ACTIVITY IN In-111 LEUKOCYTE IMAGING: CLINICAL SIGNIFICANCE IN PATIENTS WITH FEVER OF UNKNOWN ORIGIN. F.L. Datz, D. A. Thorne, P. E. Christian. University of Utah School of Medicine, Salt Lake City, UT.

We undertook a study to determine the frequency and clinical significance of In-111 labeled leukocyte activity in the GI tract of patients with fevers of unknown origin. 312 In-111 studies involving 271 patients were retrospectively reviewed. A total of 59 cases (19%) showed bowel activity. These scans were correlated with necropsy findings, laboratory data, radiographic studies and clinical course.

Of the 59 cases with gastrointestinal uptake, only 45% (27 studies) were due to infectious or inflammatory causes which caused the patient's fever (true positives). 55% (32 studies) were false positives. True positives included abscesses communicating with the bowel (8), pseudomembranous colitis (6), inflammatory bowel disease (6), GI infections (2), necrotic bowel (2), vasculitis (2), and typhilitis (1). The false positives included swallowed leukocytes secondary to endotracheal, Dobhoff, and other tubes (10), pneumonia and empyema (5), sinusitis (2), esophagitis (1), pharyngitis (1) and parotitis (1). Other causes were related to bleeding and included ulcers (3), diverticuli (2), gastric leiomyosarcoma (1), aortoduodenal fistula (1), and other causes (3). No cause for bowel uptake was found in 2 patients.

Gastrointestinal activity on In-111 leukocyte scan in patients with fever of unknown origin correlates with true causes of the patient's fever in only 45%. The remaining 55% are false positives due primarily to swallowed leukocytes and GI bleeding.

No. 566

GALLIUM-67 IMAGING IN THE DIAGNOSIS AND FOLLOW-UP OF BLASTOMYCOSIS. M.C.P.Giorgi; W.P.Pinto; G. Del Negro; E.E.Camargo.- Centro de Medicina Nuclear, Sao Paulo, Brazil.

Gallium-67 imaging is very sensitive for detection of active granulomatous diseases. The purpose of our study was to investigate the usefulness of Ga-67 imaging to evaluate the extent of blastomycosis, a granulomatous disease, and to follow its response to therapy. Twelve patients (pts) with active blastomycosis (11 male; 4-57 years) were studied. Clinical and laboratory data indicated lesions in the lungs (11 pts), lymph nodes (6), skin (5), subcutaneous layer (1), bone (1) and rectum (1). Pts were imaged at 24 and 48 hr after intravenous injection of 111 MBq of Ga-67 citrate. All of the above lesions were detected in all pts. Moreover, hepatic (3 pts) and cerebral (1) lesions were also found but not demonstrated by other studies. Abnormal parotid uptake was found in 5 pts without clinical evidence of parotitis. Bony lesions were found in 2 pts and confirmed in one of them on bone scintigraphy but not on X-ray. Chest X-ray (CXR) and Ga-67 imaging correlated well, except for 2 pts in whom CXR underestimated the extent of the disease. Follow-up imaging on 3 pts after therapy showed decreased uptake in the lungs and other sites, despite an equivocal CXR in one pt.

Gallium-67 imaging is a useful tool for detection and follow-up of blastomycotic lesions, particularly those non-detectable by other diagnostic modalities.

No. 567

IN VIVO TUMOR LOCALIZATION, BIODISTRIBUTION, AND PHARMACOKINETIC ANALYSIS OF Tc-99m-METALLOTHIONEIN CONJUGATED MOUSE MONOCLONAL ANTIBODY B72.3. R.A. Hadjian, C.L. Tolman, C.A. Drozynski, M.E. Malone, S.A. Shah, and H. Sands, E.I. duPont de Nemours, Co., Inc., No. Billerica, MA 01862

Using preparative scale technologies which minimize polymer content and maximize Tc-99m specific activity, metallothionein (MT) conjugates of a mouse monoclonal antibody (B72.3) reactive with human breast and colorectal adenocarcinomas have been prepared in a lyophilized instant-kit format. After reconstitution and transchelation via Tc-99m glucoheptonate, the Tc-99m-MT-IgG or F(ab')₂ conjugates were purified by gel permeation HPLC. Radiolabeled conjugates retained full immunoreactivity compared to radioiodinated MAb in a direct tumor membrane microtiter plate binding assay. Athymic mice bearing subcutaneous target LS174T, or non-target HCT-15, human colon tumors were injected with either Tc-99m-MT-IgG or MT-F(ab')₂ conjugate and the corresponding radioiodinated control. Biodistribution and imaging were evaluated between 1-24 hours. The blood clearance of I-131 B72.3 and Tc-99m-MT-B72.3 were similar. The ratio of Tc-99m-MT-B72.3 to I-131-B72.3 in the liver was 1.4 at 24 hours. Tc-99m-MT.B72.3 imaged all LS174T tumors between 375-835 mg at 4-6 hours post injection. Comparable studies with Tc-99m-MT-F(ab')₂ are in progress. Biodistribution, pharmacokinetics, tumor targeting, and imaging for both conjugates will be presented and compared.

No. 568

THE LABELING OF MONOCLONAL ANTITUMOR ANTIBODIES (MoAb) WITH 113M-In. S.E. Halpern, J. KAO, C. Lallo J.M. Frincke, R.M. Bartholomew, J.K. Poggenburg, P.L. Hagan, and D.J. Carlo; VA Medical Center and Hybritech, Inc., San Diego, CA.

Radiolabeling with 111In using bifunctional chelation methodology is now an accomplished fact. Attempts to label MoAbs with eluate from a 113-Sn generator has met with poor labeling efficiency and high liver uptake. Since a 113M-In MoAb would prove useful in double tracer studies of MoAbs, the current work was undertaken.

Eluate from an aging 113-Sn generator resulted in very low labeling efficiency. Eluate from a new 100mCi (Amersham Corp.) generator which had been eluted 24 hours prior to the experiment was then reacted with approximately 100ug of conjugated MoAb using a modification of the Krejcarek technique. This preparation was administered intravenously to Balb/C mice and total body distribution performed at multiple time points up to 4 hours. Labeling efficiencies as high as 60 uCi per ug were achieved. The distribution of the 113M-In radio-pharmaceutical and the same MoAb labeled with 111In were nearly identical.

We conclude that 113M-In labeling of MoAbs can be achieved with high specific activity provided competing ions are removed from the eluent. The resultant 113M-In MoAb will have the same distribution in mice as 111In labeled MoAb.

No. 569

EFFECT OF LOCAL HYPERTHERMIA ON THE INVIVO DISTRIBUTION OF INDIUM-111 MACROPHAGES IN TUMOR BEARING RATS. L.P. Kasi, A.W. Boddie, J.W. Frazer. The University of Texas M. D. Anderson Hospital, Houston, Texas.

The relationship between hyperthermia and the immune system is complex, and it has been reported that Macrophage-T-cell interactions play an important role in the destruction of tumors by hyperthermia. To evaluate the effect of hyperthermia on the uptake of macrophages in tumors and other tissues, we labeled purified resident peritoneal

macrophages obtained from a Fisher 344 rat with In-111 oxine, and evaluated their in vivo distribution patterns in rats bearing transplanted mammary adenocarcinoma (upper flank). A group of the tumor bearing rats was treated with focal hyperthermia (FH) of 43°C for 20 mins at the tumor site. For controls, groups of untreated tumor bearing rats (UTB) and sham-heated (SH) tumor bearing rats were used. At 1 hr after hyperthermia treatment, a dose of 2×10^6 In-111 macrophages per 100 g weight was injected i.v. in each rat and distribution calculated as %ID/g tissue was evaluated at 2, 24, 48 and 72 hours post injection. Significantly different uptake patterns were observed in the FH group when compared to the control groups. At 2 hrs the lung uptake of the labeled macrophages was higher in the UTB controls than in the FH and SH groups. Splenic uptake at 24 hrs and hepatic uptake at 72 hrs was higher in the FH rats than in the SH and UTB controls. Uptakes in the tumor tissue was higher in the FH rats than in the SH group but lower than in UTB controls from 24 to 72 hrs post injection. The differences in tissue distribution of the In-111 macrophages in the FH group, especially in the spleen, liver and tumor indicates functional effects exerted by hyperthermia, probably caused by splenic processing of macrophages prior to redistribution.

No. 570

LOCALIZATION OF Tc-99m MULTILAMELLAR LIPOSOMES AT SITES OF FUNGAL INFECTION: POTENTIAL USE IN AMPHOTERICIN B THERAPY. L.M. Lamki, G. Lopez-Berestein, L.P. Kasi, T.P. Haynie, H.J. Glenn. University of Texas, M.D. Anderson Hospital and Tumor Institute, Houston, TX.

Multilamellar liposomes (MLV) are lipid vesicles prepared from a 7:3 mixture of Dimyristoyl phosphatidylcholine and Dimyristoyl phosphatidylglycerol. The MLV's were labeled with Tc-99m pertechnetate reduced with stannous chloride. A dose of 150 mg/m² labeled with 8-10mCi Tc-99m was injected intravenously. These liposomes are normally cleared by the reticulo-endothelial system (RES) and may be used for delivery of certain drugs to areas of increased localization. We used Tc-99m labeled liposomes to study the distribution in four patients with malignancy and systemic fungal infection including candidiasis and aspergillosis with the intention of using liposomes encapsulated amphotericin B in their therapy. Images were recorded immediately, at 4 and 24 hours post intravenous injection of Tc-99m MLV. Regions of interest over the areas of infection and the liver, spleen, kidney, bone and cardiac blood pool were taken from the digital images. There was increased localization of the labeled liposomes in the nasopharynx and in the lungs of the two patients with fungal infection in these areas respectively. In the patients with liver infection, there was nonuniform distribution of radioactivity in the liver of one patient and in the other there was general increased liver uptake when compared to the normal values which we had established on other patients with cancer and with Hodgkin's disease. This study suggests that Tc-99m liposomes may be useful in the investigation of patients with severe systemic fungal infection requiring bold anti-fungal therapy.

No. 571

RADIOLOCALIZING MONOCLONAL ANTIBODIES AGAINST CONCEALED EPITOPES ON CARCINOEMBRYONIC ANTIGEN (CEA) F. J. Primus, R. M. Sharkey, C. Ballance, E. Kelley, D. Varga, and D. M. Goldenberg. Center for Molecular Medicine and Immunology, Newark, NJ

Soluble tumor-associated antigens may be less desirable targets for antibody-directed tumor imaging or therapeutic agents due to combination of antibody with circulating antigen. We have prepared monoclonal antibodies to CEA that have different binding activities in immunoassay in which incubation buffer ionic strength was varied. The activity of one antibody, NP-2, was markedly reduced when ionic strength was raised whereas the activity of another, NP-3, remained unaltered. Radioiodinated NP-2 and NP-3 were similar in their localization of

human colonic tumor xenografts growing in hamsters which had undetectable circulating antigen. Injection of radiolabeled NP-2 into cancer patients having CEA titers exceeding 200 ng/ml did not result in the formation of antibody-CEA complexes as measured by molecular sieve chromatography. However, CEA-containing NP-3 radioantibody complexes appeared in patients injected with NP-3 antibody. The amount of complex formed was related to circulating CEA titer, with levels around 200 ng/ml producing complexes consisting of up to 70% of the circulating radioantibody. Enhanced clearance of the NP-3 radioantibody was also observed in some patients, especially those having elevated levels of immune complexes. These results suggest that certain monoclonal antibodies to CEA that have the unique property of reacting with a site on this antigen that is hidden while in the blood, such as NP-2, could be more useful for tumor imaging and therapy since they would avoid neutralization and altered metabolism by circulating antigen.

No. 572

TC-SULFUR AND ANTIMONY COLLOIDS AND IN-OXINE LABELED GRANULOCYTES: ARE THERE FUNCTIONAL DIFFERENCES? E.B. Silberstein, P.G. Mayfield, M. Sperling, R. Harris, P. Hook, Univer. of Cincinnati Medical Center, Cincinnati, OH.

Indium-111 (In) has been employed as a leukocyte label has potential drawbacks: special conditions for labeling not easily achieved in every nuclear medicine laboratory; labeling of and damaging lymphocytes when granulocytes are labeled. Several attempts have been made to employ granulocyte phagocytosis to specifically "self-label" with a commercially available technetium sulfur colloid (TcSC) and technetium antimony colloid (TcSbC).

Granulocytes labeled with technetium-99m-antimony colloid had such poor chemotaxis that further testing was not warranted. Chemotaxis with TcSC cells was mildly to moderately decreased. TcSC cells killed *S. aureus* less well than In-wbc which performed this normally. Complement mediated phagocytosis was stimulated by In labeling, while it was subnormal in the TcSC experiments although stimulated by TcSbC. Peroxide production by In-wbc and TcSC cells was normal except for some stimulation in the resting phase at higher doses by In. Cells with both labels ingested uncoated latex particles and reduced NBT normally.

It is concluded that granulocytes labeled with indium with activities from 1-500 uCi have essentially normal function in a series of tests not all of which have been heretofore reported. Larger activity (2 mCi) of TcSC reduces some but not all of these functions. At the doses employed a major advantage of In is the 75% av. labeling efficiency while specific TcSC labeling was 12%.

Monday, 3:30-6:00

Exhibit Hall

INSTRUMENTATION**No. 573**

COMPARISON OF SPATIAL RESOLUTION IN 180° VERSUS 360° SPECT IMAGING. A.N. Bice, M. Clausen, S. Loncaric, H.N. Wagner, Jr. The Johns Hopkins Medical Institutions, Baltimore, MD.

Arguments favoring 180° SPECT data acquisition (acq.) over 360° sampling for 201-thallium myocardial imaging include improved resolution in the former.

Using circular 180° and 360° SPECT acq. modes the resolution of line sources in air and in water were measured at different positions in the field-of-view.

With the 180° acq. mode, the line sources in air, located 5, 7.5 and 10 cm off the axis of camera rotation (AOR) showed an oval distortion, with a difference of the full width at half maximum of up to 30 % between the long and the short axes of the ovally distorted image. The angles between the semi-axes of the ovally shaped images and the plane containing the line sources (in air) showed a systematic relation to the starting point of the detector for the 180° acq. All central line sources (on the AOR) in air were undistorted, regardless of the 180° acq. starting angle.

The 360° acq. images of the line sources in air showed similar effects but in a very mild form. Transaxial reconstructions of line sources off the AOR in water for both the 180° and 360° acq. showed an enhancement of the line source oval distortion. Computer simulations of line source measurement were performed for comparison with experimental data.

Although 180° sampling can provide improved resolution it also accentuates the inherent non-uniformity in spatial resolution across the transaxial plane. This will contribute to the difficulties with 180° SPECT quantification.

No. 574

MRI: Importance of Surface Coil Geometry for Field Size and Uniformity.

Clarke LP, Pidick G, Cullen J, Schnitzlein N, Brown K, Murtagh R, and Silbiger M.
University of South Florida College of Medicine,
Tampa, Florida.

MRI surface coils are required to obtain good spatial resolution, signal to noise and realistic imaging times. A major limitation of small surface coils is their limited sensitive area and fall off in response in all imaging planes. A more realistic compromise between optimum physical characteristics of the coils and field size and uniformity is required, particularly in oblique views i.e. paraxial. A variety of coils were designed for a Siemens MRI system (15 MHz) (a) flat circular coils of 18 cm diameter, (b) flat elliptical coils with a major axis of 30 cm, (c) opposed elliptical coils in parallel and (d) curved elliptical coils that followed the cervical lordosis at the expense of field inhomogeneity. Loaded and unloaded Q values were respectively 180(130), 150(120), 100(80) and 125(60).

Remote electronic tuning facilitated ease of coil positioning and tuning circuit was modified to reduce capacitive loading effects. Despite the loss of Q for the larger coil geometrics, comparable images of the lumbar and cervical spine were obtained (estimated spatial resolution 0.5-0.7mm) with the added advantage of a larger and more uniform field size.

No. 575

DESIGN CONSIDERATIONS AND SIMULATIONS FOR RING SPECT SYSTEMS WITH A MODULAR FOCUSED COLLIMATOR. W. Chang, C. Tian, S. Li, B.M.W. Tsui, K. Rezai, J.J. Williams, J.E. Ehrhardt, and P.T. Kirchner. Univ. of Iowa, Iowa City, IA and Univ. of North Carolina, Chapel Hill, NC.

The ability of focused collimators to achieve high sensitivity at depth while preserving resolution makes them highly desirable for SPECT imaging. Tomographic systems with fixed detector rings are known to have the advantages of simplicity, reliability and tolerance to variations in detector response. We have combined these two desirable features in the design of a multidetector ring SPECT system with a unique modular focused collimator. To optimize the design and verify performance predictions, preliminary hardware and software simulations were performed.

Collimator modules similar to the proposed design were evaluated to provide a reference for overall sensitivity of the system. A mathematical model was developed to simulate the projection data acquired in our proposed system for controlled studies of various parameters which include ring radius, number of detectors, collimator response, quarter ray offset, photon attenuation, and noise. Tomograms were reconstructed from the projection data with standard fan beam algorithm. Several variations of system design were evaluated based on their input collimator resolution and output tomographic resolution.

From the simulations we conclude that a system with 72 or 80 detectors on a 34 cm diameter ring will be needed to achieve 8 mm FWHM resolution at the center of the reconstruction volume. The corresponding sensitivity should be about 2.5 to 3K cps/uCi/ml for a 13 mm thick tomographic slice.

No. 576

PORTABLE, CEREBRAL BLOOD FLOW MEASUREMENT SYSTEM FOR REAL DIAGNOSTICS. G. Entine and T. Tiernan, Radiation Monitoring Devices, Inc., Watertown, MA; D. Stump, L. Hinshelwood, Bowman Gray School of Medicine, Winston Salem, NC.

It is becoming widely recognized that in situ analysis of regional cerebral blood flow (rCBF) patients undergoing surgery or in intensive care can provide important diagnostic information needed to decrease the potential of brain damage in these critical situations.

Under an NIH sponsored program, we have conducted research to construct a very portable rCBF diagnostic system which uses miniature, solid state radiation detectors and sophisticated high speed microprocessor systems to provide real time analysis. The instrument can be brought directly to a patient and perform safe, rapid, evaluation in the often cramped confines of the neurosurgical and cardiac bypass operating room, the intensive care unit and the emergency room.

Preliminary clinical studies have been done in these arenas on a variety of patients. In particular, measurements taken on twenty patients undergoing bypass surgery indicated that, contrary to expectations, the cerebral vascular system is not completely autoregulating the blood flow during these procedures. The data suggests that the flow is almost entirely dependent on the setting of the external pump and the general body vascular chemistry and condition. This situation may relate to the significant fraction of bypass patients which experience a post-operative brain deficit.

No. 577

EVALUATION OF THE USE OF THE NEMA STANDARD FOR IN-FIELD ACCEPTANCE TESTING OF SCINTILLATION CAMERAS--EXPERIENCE OVER FIVE YEAR PERIOD. C. Finney, B. Horn, H. Mak, R. McDermott, D. Loo, K. Luk. Medical Physics Department, Southern Calif. Permanente Medical Grp. Los Angeles, CA.

In-field acceptance testing using the protocol adopted by the National Electrical Manufacturers Association (NEMA, U.S.A.) Standards Publication NUL-1980 was initiated five years ago. Of the first 23 cameras to undergo on-site acceptance testing using our implementation of the NEMA standard, 22 failed to meet the manufacturers' specifications. Four manufacturers are represented in those cameras tested to date. Parameters found to depart from the specified performance were field uniformity, energy resolution, intrinsic spatial resolution, system resolution, multiple window spatial registration, intrinsic count rate performance, and system sensitivity. Most problems were rectified by subsequent adjustment

by the manufacturer, although several required a number of months to correct.

Even though each of the manufacturers represented by the cameras tested subscribed to the test procedures of the NEMA standard, we found different interpretations being applied by the various manufacturers to specific measurements. Due to these differences the prospective purchaser should use caution when intercomparing the published NEMA performance measurements for scintillation cameras.

Our experience over the last 5 years has proven the practicality and value of performing in-field NEMA testing on scintillation cameras. It has also shown that very few cameras initially meet all of the published NEMA performance specifications after installation by the manufacturer.

No. 578

DESIGN AND PERFORMANCE OF A SMALL CLINICAL CYCLOTRON
G.O. Hendry, M.G. Straatmann, L.R. Carroll, F.A. Ramsey,
and B. Wieland (CTI, Inc. Berkeley, California)

A clinic-based cyclotron system for delivery of short-lived positron-emitting isotopes has been designed to meet the following objectives: 1) Automated, unattended operation. 2) Compact, self-shielded configuration for minimum facility requirement. 3) Economical, high-yield target reactions.

Tests on the completed cyclotron have demonstrated that it easily and stably delivers 50 μ A protons through a 1 cm collimator at the target entrance. This is more than enough beam to produce required quantities of positron-emitting isotopes and allows for simultaneous irradiation of two separate targets.

Carbon-11, Nitrogen-13, Oxygen-15, and Fluorine-18 have been economically produced in clinically useful quantities. For example, continuous flow Oxygen-15 is produced at a rate of 20 mCi per minute at a cost of \$1 per minute for enriched target material.

Initial test of the prototype system shield have demonstrated that the cyclotron can be installed in a facility without additional shield construction.

No. 579

IMPROVEMENT OF SPATIAL RESOLUTION AND VARIANCE OF rCBF IMAGE BY A RING DETECTOR SPECT (HEADTOME II).
A. Komatani, K. Yamaguchi, N. Yamaoka*. Yamagata Univ., School of Medicine, Yamagata, *Shimadzu Corp., Japan.

Dynamic SPECT with inhaled Xe-133 has been used to map regional cerebral blood flow (rCBF). This method, however, has several problems such as uncertainty of rCBF value and poor spatial resolution, especially in deep region of the brain. The rCBF images are influenced by Compton scattered photons, the timing to start data acquisition, and inhalation techniques. The image quality is mostly affected by the energy window of the pulse height analyzer (PHA). The amount of scattered radiation is approximately proportional to both the depth of radiation source and the width of energy window. Fraction of scattered radiation is, for example, 4% for 2cm source depth/73-110KeV (-10~+35%) window and 63% for 12cm depth/57-110KeV (-30~+35%). This fraction is severely affected by lower level of the energy window. Therefore, an asymmetric window should be adopted for Xe-133 rCBF study. According to our experiences, the window of -10~+35% was the best for this purpose. The time difference between the start of inhalation and the start of data acquisition also affects the rCBF. The best results are obtained when the effective data acquisition starts at 6 seconds after the rising point of the end-tidal curve. Mouth-piece inhalation had less effects of nasal activity on rCBF than

with an inhalation mask. Before these improvements were adopted, rCBF values of normal volunteers were 51.2 \pm 7.1. By improvement of data acquisition timing, adopting a narrower window, and inhalation with a mouth-piece, rCBF values were improved to 50.0 \pm 1.7. The authors have obtained also superior images using Tc-99m and I-123 IMP.

No. 580

QUANTITATIVE DIGITAL AUTORADIOGRAPHY J. L. Lear, K. Mido, J. P. Plotnick, and R. A. Muth. Stanford University School of Medicine / V. A. Medical Center, Palo Alto, CA

Quantitative autoradiography requires a method of obtaining precise and accurate densitometric measurements of the images created by exposure from tissue sections. Existing image analysis systems, such as scanning densitometers or video cameras interfaced to microcomputers, use detectors which were designed for purposes other than autoradiography and their performance is therefore not optimal for digitizing the gray scales typically found in autoradiographs.

We therefore developed a solid state, digital image analyzer from the ground up specifically optimized for quantitative autoradiography of tracers used in cerebral blood flow and metabolism studies. The system uses a linear array of charge coupled devices (CCDs) which scan the images under the control of a DEC PDP 11/23+ computer and create a digitized matrix of 512 by 512 pixels with 256 true gray levels. Data is directly mapped into random access memory for processing and video memory for display on a monochrome monitor. Software was written in Fortran for conversion of densitometric images to blood flow or metabolism images using appropriate kinetic equations. Cross contamination between different images obtained in multiple tracer studies can be subtracted on a pixel by pixel basis to yield pure tracer concentration images. Ratio images can be generated for detailed comparison of tracer uptake mechanisms.

Autoradiographs of brain sections containing I-123 isopropyl-iodoamphetamine, C-14 iodoantipyrine, F-18 deoxyglucose, C-14 glucose, and Tl-201 diethyldithiocarbamate were digitized with this scanner as well as with previously reported video and rotating drum densitometers. The CCD scanner provided 2-3 times the precision and 1.5-2.0 times the accuracy of the other systems for autoradiographic determination of tissue tracer concentration.

No. 581

AN AUTOMATED HIGH-RESOLUTION SCANNER FOR COLLIMATOR PERFORMANCE EVALUATION. K. Rezai, W. Chang, S. Li, J.C. Ehrhardt, P.T. Kirchner. University of Iowa College of Medicine, Iowa City, IA.

Collimator sensitivity and resolution values derived directly from gamma camera-computer data are often too imprecise. We have developed a microprocessor-based scanning device capable of 3-dimensional mapping of a collimator's sensitivity and resolution at spatial sampling of 0.4 mm/pixel. The system runs automatically under software control and special display techniques facilitate global assessments of collimator performance vs depth or detailed analyses at a given depth.

A scanner, bearing a point source of activity, is driven by 2 precision motors in the X and Z directions within any number of planes (y axis) perpendicular to the face of the collimator. Positioning is accurate to 0.1 mm. Counts are recorded via a single channel detector in a 6502-based microcomputer, decay corrected, and stored in 2 bytes/pixel. The pixel X-Z dimensions in a plane are independently software selectable in the range of 0.4-10 mm. Output includes: 1) Color-coded display of counts/pixel in the entire field of view with highlighting of FWHM points. 2) Color-coded isoresponse contours at 5,10,50,90, and 100%. 3) Pseudo 3-D display of line-spread functions. 4) Count profile at a given depth with FWHM and FWTM. 5) Numerical printout or input to image simulation routines.

Software implementation makes the system versatile and upgradable. The scanner can be constructed from inexpensive hardware and interfaced to available detectors and computers in any nuclear medicine department. The system is a powerful tool in the design and testing of high-performance collimators for SPECT imaging.

No. 582

IAEA STUDY OF THE QUALITY OF NUCLEAR MEDICINE IMAGING IN DEVELOPING COUNTRIES - PRELIMINARY RESULTS. A. V. Wegst, University of Kansas Health Sciences & Hospital, Kansas City, Kansas, H. Bergmann, II. Medizinische Universitätsklinik, Vienna, Austria, R. Ganatra, M. Nofal, International Atomic Energy Agency, Vienna, Austria and G. Souchkewitch, World Health Organization, Geneva, Switzerland

The International Atomic Energy Agency (IAEA), in cooperation with the World Health Organization (WHO), initiated an imaging performance survey including countries in Latin America and Asia and the Pacific to gather information concerning the quantity and state of nuclear medicine imaging in those countries. The methodology was similar to that used by the College of American Pathologists and permits analysis by receiver operating characteristic (ROC) indices.

Identical transmission phantoms whose images resemble an anterior liver containing space occupying lesions were designed and built by the IAEA. Fifty phantoms were distributed with instructions for image acquisition for scintillation camera or rectilinear scanner to approximately 30 countries. Each laboratory was asked to complete a questionnaire concerning equipment, procedures and quality control (QC) to be returned with the image evaluation form and QC and phantom images. A coordinator was chosen in each country to direct the project.

One hundred fifty questionnaires from 10 countries have been analyzed to date. The ROC curves, area under the curves and other statistical parameters will be presented. Strict anonymity with regard to country and laboratory will be maintained. Lesion detectability, though variable, was generally quite good with no difference between the scanners and cameras. There were significant country-to-country differences. The images suggested many instruments are not being properly maintained. The study is being continued.

Monday, 3:30-6:00

Exhibit Hall

MONOCLONAL ANTIBODIES

No. 583

RADIOIMMUNOTHERAPY WITH I-131 LABELED MONOCLONAL ANTIBODIES 19-9/ANTI-CEA AND OC 125. R.P. Baum, J.F. Chatal, J.C. Saccavini, R. Senekowitsch, J. Happ, K. Manegold, F. Berthold, and G. Hör. University Clinics, Frankfurt, FRG.

The potential of I-131 labeled monoclonal antibodies (MoAbs) as therapeutic agents was evaluated in 2 patients (3 treatment courses). After permission of the BGA for phase one clinical trial, 2.33 GBq of a cocktail of anti-CEA and 19-9 F(ab')₂ fragments were administered iv within 1 h to a 13-year old girl with incurable mucinous colon carcinoma. Preliminary immunoscintigraphy (IS) and immunohistochemistry demonstrated tumor targeting of MoAbs. No toxicity was observed. Radiation doses between 5.60 and 20 Gy were delivered to the tumor (radiation burden for whole body and liver was 0.46 and 2.90 Gy respectively (T1/2 2.2 d). 3.70 GBq (specific activity: 296 MBq/mg) of OC 125 F(ab')₂ fragments were administered as 1 h infusion to a 39-year old patient with incurable adenocarcinoma of the lung. Diagnostic IS had shown excellent antibody uptake by the malignant lesions. Therapeutic application resulted in tumor irradiation of 11.0 Gy (whole body 0.15 Gy, liver 2.0 Gy, T1/2 1.8 d). A clinical improvement was noted for at least 8 wks. A 2nd therapy (4.63 GBq, specific activity: 370 MBq/mg) had no influence on progression of disease.

Palliative but no curative effects and tumor doses of about 20 Gy can be achieved by antibody guided irradiation with I-131 labeled MoAbs. Repetitive treatments with high doses can be used.

No. 584

RADIOIMMUNOTHERAPY OF HUMAN COLON CARCINOMA XENOGRAFTS USING MONOCLONAL ANTIBODY B72.3. D. Colcher, F. Mornex, J. Esteban, M.F. Minelli, J. Schlom. National Cancer Institute, National Institutes of Health, Bethesda, MD.

Monoclonal antibody B72.3 is a murine IgG1 that was generated using a membrane-enriched fraction from a human carcinoma metastases. Mab B72.3 binds to a novel high molecular weight glycoprotein (termed TAG-72) with characteristics of a mucin. Immunohistochemical studies demonstrated that TAG-72 is expressed in approximately 85% of colon carcinomas, while it is not expressed or expressed in only trace amounts in normal adult tissue. I-131 B72.3 IgG has proven useful for the radioimmunodetection of human colon carcinomas, both in athymic mice bearing xenografts and in clinical trials.

I-131 labeled B72.3 IgG was injected i.p. into athymic mice bearing established human colon carcinomas (LS-174T; TAG-72 positive). Increasing dose levels resulted in decreased growth rates with 500 µCi causing a complete cessation of growth. There was, however, bone marrow toxicity resulting in death after 3 weeks. The dose was therefore fractionated and mice were given 2 doses of approximately 250 µCi at a 1 week interval. There was no long-term toxicity while the tumor growth was stopped in most animals (85%). The therapeutic effect of the I-131 B72.3 was shown to be specific; unlabeled IgG at levels of up to 1 mg per mouse did not affect the tumor growth rate. While I-131 labeled control antibody had some effect on the tumor growth rate, due to the circulating radioactivity, there was clearly a specific enhanced effect with the I-131 B72.3 IgG. These studies along with the successful use of radiolabeled B72.3 for the detection of metastatic colon carcinomas suggests the potential of Mab B72.3 IgG as a radiotherapeutic agent.

No. 585

RADIODETECTION OF METASTATIC MELANOMA (MM) USING IN-111-DTPA-ZME-018 MONOCLONAL ANTIBODY (MoAb). E. Cornelius, R. Neumann, S. Zoghbi, M. Ernstoff, J. Kirkwood and M. Unger, Yale University School of Medicine, New Haven, CT & Hybritech, Inc., San Diego, CA.

This was a phase I study of ZME-018 to assess safety, kinetics and imaging sensitivity over a dosage of 1-40 mg. 1.0 mg of MoAb was labeled with 5.0 mCi In-111, then mixed with a variable amount of "cold" MoAb. Kinetics are reported separately. 1/26 patients (pts) had mild wheezing and urticaria. Scans were done at 1 & 3 dys with computer storage. Blood activity was high at 1 dy; at 3 dys it was less but still present. Blood, liver, spleen, marrow & bowel activity interfered with tumor detection. 109/149 known metastases (mets) ≥ 1 cm were detected (73%). Sensitivity related to MoAb dosage was: 1 mg, 2 pts, 3/11 (27%); 2.5 mg, 4 pts 2/2 (100%); 5.0 mg, 5 pts, 2/12 (17%); 10 mg, 5 pts, 18/27 (67%); 20 mg, 5 pts, 59/65 (91%); 40 mg, 5 pts, 25/32 (78%). 4 pts had previously undetected foci. In 2 pts with widespread mets, 55/55 (100%) & 20/24 (83%) of mets ≥ 1 cm were detected, respectively; 19/19 & 15/15 additional mets seen on Ga-67 scans were also detected; and 2 & 32 previously unknown foci were seen. 11 pts had a Ga-67 scan within 1 mo; Ga-67 sensitivity was 78%, and for MoAb, 80%. 7/46 extracerebral mets < 1 cm were detected. Major false positives were axillae (17/21 pts) and female breast (3/9 pts). ZME-018 scintigraphy is safe as a 1 dose procedure. Results complement current imaging tests.

No. 586

I-123 - F(ab')₂ AND Fab FRAGMENTS OF ANTI-CEA LABELED MONOCLONAL ANTIBODIES:BIOKINETICS IN PATIENTS WITH COLORECTAL CARCINOMA. B. Delaloye, A. Bischof-Delaloye, F. Buchegger, V.von Fluedner and J.P. Mach. Nuclear Medicine Dpt, CHUV and Ludwig Institute, Lausanne, Switzerland.

In 31 patients (11F, 48-82, \bar{x} 62y, 20M, 39-82, \bar{x} 62y) plasma disappearance and in vivo distribution of I-123-F(ab')₂ (n=17) and Fab (n=14) fragments of 2 monoclonal antibodies (MAB) were studied. 4 of each group were pretreated by iv perfusion of cold MAB. Thyroid and gastric mucosa were blocked. 6 and 24h after injection organ distribution was measured with respect to the remaining whole body (WB) activity by the ROI technique in averaging simultaneously obtained anterior and posterior data Dual head camera, WB attachment.

Plasma disappearance curves were bi-exponential with effective plasma T_{1/2} (\bar{x} ± SD) of 18 ± 3.6h for MAB25 F(ab')₂, 30.9 ± 14.8h for MAB35 F(ab')₂ and 9.5 ± 1.9h for MAB35 Fab. These T_{1/2} were not influenced by serum CEA (1.0-2500ng/ml) or pretreatment with cold MAB.

Organ distribution in % of remaining activity (\bar{x} ± SD)

		F(ab') ₂ 25	F(ab') ₂ 35	Fab 35
Heart	6h	8.8 ± 0.8	12.5 ± 2.4	8.0 ± 1.7
	24h	8.0 ± 0.5	13.7 ± 1.9	5.6 ± 1.3
Lungs	6h	10.8 ± 2.4	9.6 ± 1.8	10.3 ± 1.3
	24h	9.7 ± 1.8	8.0 ± 0.7	10.8 ± 1.6
Liver/ spleen	6h	15.2 ± 4.4	13.9 ± 3.1	14.8 ± 2.8
	24h	15.9 ± 2.0	16.1 ± 3.7	14.9 ± 2.0
Kidneys	6h	7.3 ± 1.6	8.3 ± 0.8	11.6 ± 3.9
	24h	7.5 ± 1.7	6.1 ± 2.1	9.1 ± 1.5

24h urinary elimination was 20.1 ± 11.6% for F(ab')₂ and 44.5 ± 12.1% for Fab. Because of low background Fab seem preferable for the use with I-123.

No. 587

CLINICAL TRIALS WITH INTRAVENOUS (IV) AND SUBCUTANEOUS (SQ) IN-111 ANTIMELANOMA MONOCLONAL RADIOIMMUNOIMAGING. B. Engelstad, A. Khentigan, M. Del Rio, L. Rosendorf, E. Ramos, C. Reinhold, R. Hattner, M. Okerlund, L. Spittler, P. Scannon. University of California, San Francisco and XOMA Corporation, Berkeley, CA.

To assess preliminary safety and efficacy of In-111 antimelanoma whole IgG2a monoclonal murine antibody: a) six patients with Stage III melanoma were administered 5 mCi in protein dose groups (1, 5, 20 mg) as an IV infusion; and b) six patients with Stages I or II melanoma undergoing lymph node exploration were administered 1 mCi in 1 mg protein as a SQ interdigital injection. Following IV administration: a) no major adverse effects were detected; b) unsuspected and CT-negative lesions were detected; c) detection was improved with delayed (1 week) images, emission computed tomography, and correlation with other radiopharmaceuticals; d) 6/6 > 3 cm, 6/8 1.5-3.0 cm, and few < 1.5 cm lesions were detected; e) clearance, distribution, dosimetry and antimurine Ig response varied with protein dose. Following SQ administration: a) no major adverse effects were observed; b) tumor-negative and tumor-positive lymph nodes exhibited uptake and were scintigraphically indistinguishable; c) autoradiograms showed histiocyte binding in tumor-negative lymph nodes; d) antimurine Ig titers rose in 3 patients; and e) available data are inconclusive regarding relative well-counts of tumor-positive and tumor-negative lymph nodes.

Using SQ administration, attempts will be required to improve scintigraphic distinction between tumor-negative and tumor-positive nodes. Further assessment of diagnostic utility using IV administration is warranted.

No. 588

COMPARISON OF TWO I111n LABELED MONOCLONAL ANTITUMOR ANTIBODIES (I111n MoAb) IN THE DETECTION OF MELANOMA. S.E. Halpern, R.O. Dillman, J. Dillman, P.L. Hagan, M. Clutter, and D. Amox. Departments of Nuclear Medicine and Oncology, VA Medical Center, San Diego, CA.

Radioimmunodetection of melanoma using I111n MoAbs has been studied in the United States for 3 years. The following are the results of our experience in 42 patients employing an anti-P97 MoAb and an anti-KD240 MoAb. The patients were studied without knowledge of the presence or absence of antigen on their tumors.

Both antibodies were labeled with I111n using the bifunctional chelation technique. 3-5 mCi (1-21 mg) of the I111n labeled 96.5 (anti-P97) and ZME-018 (anti-KD-240) were administered and scanning performed at the end of infusion, 4, 24, 48, 72, and 144 hours postadministration. Serum was taken to observe the disappearance rate of I111n from the vascular compartment.

Compartmentalization was different for the 2 MoAbs with a greater concentration of ZME-018 in the liver, spleen, gastrointestinal tract, and testicles than was seen for 96.5. Seventy-four out of 113 lesions were noted in the 42 patients (65%). Sixty-two of the lesions were detected for 96.5 and 73% for ZME-018. The distribution of both I111n MoAbs was dramatically affected by the MoAb mass administered. Fourteen lesions were detected by the 2 MoAbs that were not known prior to the study. Presumed false positive lesions occurred with ZME-018.

In conclusion, I111n MoAbs targeted against melanoma associated antigens appear to have clinical utility in the detection of metastatic melanoma.

No. 589

IN-111 MONOCLONAL ANTIBODY (MOAB) PAY-276 IMAGING AND KINETICS IN PROSTATIC CANCER. R.E. Henry, F.R. Ahmann, J.A. Kotler, M.E. Ahmann, K.A. Green and M. Unger*. V.A. Medical Center and University of Arizona, Tucson, AZ and Hybritech Inc.*, San Diego, CA.

21 patients (pts) with prostatic carcinoma (19 with metastases) were infused with 5 mCi In-111 labeled murine MoAb to prostatic acid phosphatase (PAP) in doses of 1(5pts), 5(3pts), 10(4pts), 20(5pts) and 40(4pts) mg over 1 h without significant side effects. Planar whole body and spot imaging was performed at 24 and 72 h post infusion. Liver and spleen activity was high at 24 h and bone marrow activity increased with time. The prostate imaged at 24 h in 9/15 pts with palpable mass. Abnormalities were seen best at 72 h when vascular activity had declined. In 17 pts with current bone scans, MoAb identified lesions as prostatic metastases in 46% of abnormal regions. Identification increased with dose: 22% with ≤ 5 mg and 58% with ≥ 10 mg. Bone lesion detection was difficult due to prominent marrow activity or small size of lesions as in ribs. MoAb identified pulmonary metastasis in 1 pt and unsuspected malignant pleural effusion in another. CT-confirmed pelvic adenopathy was not identified in 3/3 pts. Blood clearance was biphasic with T/2 of 24.3 ± 10.5 h for all antibody doses. Urine clearance was 29.1 ± 15.8% in 24 h and 38.8 ± 16.5% by 72 h. Anti-PAP MoAb has low sensitivity for imaging bone metastases compared to phosphates but is highly specific with potential to differentiate benign bone lesions in selected patients. Its potential for detection of soft-tissue metastases appears promising and merits further evaluation.

No. 590

LACK OF CORRELATION BETWEEN IN VITRO CELL BINDING AND ACCUMULATION IN TUMOR XENOGRAFTS OF RADIOLABELED MONOCLONAL ANTIBODY (MAB). P.L. Jones, B.A. Brown, and H. Sands. Dupont, No. Billerica, MA 01862

In order to determine if the *in vitro* evaluation of a radiolabeled MAB reflects its utility for tumor imaging, *in vitro* and *in vivo* studies were performed using two human tumor cell lines, LS174T (colorectal) and A549 (lung), and the tumor specific MAB B6.2. FACS analysis showed that FITC-labeled MAB B6.2 bound to both LS174T (49.0% positive) and A549 (85.2% positive) cells. Further, 3X10⁷ of LS174T or A549 cells maximally bound 59.4% and 88.2% of I-125-B6.2, respectively. After a 24 hr. *in vitro* incubation of either In-111 or I-125 labeled B6.2 with cells, HPLC analysis of the culture media showed minimal antibody degradation and no evidence for the formation of soluble immune complex.

Gamma scintillation images of athymic mice bearing s.c. LS174T xenografts showed significant tumor uptake

of B6.2 labeled with either isotope. In contrast, A549 tumors imaged poorly or not at all. Biodistribution data indicated that In-111 and I-125-B6.2 cleared more rapidly from A549 mice than from LS174T animals. Thyroids of A549 mice accumulated I-125 rapidly. Abnormally elevated % I.D./g values of In-111 in both liver (35.25) and spleen (11.22) resulted after In-111-B6.2 injection into A549 mice. These contrasting findings between A549 and LS174T mice may be the result of more shed antigen or catabolism of antibody by A549 tumor. The prediction from the *in vitro* data that A549 tumors would be an excellent *in vivo* target for labeled B6.2 was not fulfilled. The striking differences between distributions of isotopes observed in mice bearing tumors antigenic for the same antibody may have important implications for future *in vivo* studies.

No. 591

RADIOIMMUNOIMAGING WITH Ga-67 LABELED MONOCLONAL ANTI-BODY TO HUMAN OSTEOSARCOMA. M. Koizumi, K. Endo, H. Sakahara, T. Nakashima, M. Kunimatsu, Y. Kawamura, H. Ohta, Y. Ohmomo, T. Nakamura, H. Tanaka, Y. Kotoura, T. Yamamuro, S. Hosoi, S. Toyama, A. Yokoyama and K. Torizuka. Kyoto University, Kyoto, Japan.

This study was taken to evaluate Ga-67 labeled monoclonal antibody (MoAb) for the tumor imaging using human osteosarcoma as a tumor model. MoAb was efficiently labeled with Ga-67 through the chelation of deferoxamine (DFO) employing three methods for the coupling of DFO and MoAb; glutaraldehyde method, pyridyl disulphide method and maleimide method, which introduced Schiff's base, disulphide bond and thioether bond, respectively.

All Ga-67 labeled and radioiodinated MoAb showed similar specific binding reactivity *in vitro* to osteosarcoma cells. Transplanted tumors in nude mice were clearly visualized at 24 and 48 hours after the administration of Ga-67 labeled MoAb prepared by the three methods as well as with I-131 labeled ones, while the coupling method between MoAb and bifunctional chelates influenced the localization of MoAb in tumor tissues and liver. Highest tumor-to-liver ratio and *in vivo* stability was observed by using labeled MoAb with thioether bonds, which was considered a choice of coupling procedure. Ga-67 labeled irrelevant MoAb or free Ga-67 did not localize in tumors.

Present study demonstrated that Ga-67 labeled anti-tumor MoAb appeared promising for the radioimmunology. These methods would be also applicable to the preparation of immunoconjugates for the selective and specific transport of anti-cancer drugs.

No. 592

THE EFFECT OF INCREASING "COLD" ANTIBODY DOSE ON PROSTATIC CANCER METASTASES DETECTION AND ON BODY DISTRIBUTION OF PAY-276 MONOCLONAL ANTIBODY (MOAB). L.A. Lamki, R. Babayan, J.L. Murray, T.P. Haynie, A.C. Von Eschenback, E. Hersh, M. Unger, D.J. Carlo. Univ. Texas M.D. Anderson Hospital, Houston, TX and Hybritech Inc, San Diego, CA.

PAY-276 is an anti-prostatic acid phosphatase murine MoAb. 1 mg was labeled with 5mCi ¹¹¹Indium using bifunctional DTPA. Twenty-five patients were studied divided into 5 groups of 5 patients each (Groups I-V). Each group was given "cold" MoAb, 5, 10, 20, 40 or 80 mg intravenous with the labeled PAY-276. Images were recorded analog and digital at 24, 72 hours and in some patients at 120 or 144 hours. Relative non-tumor body distribution of the labeled PAY-276 was analyzed by regions of interests (ROI) over liver (L), Blood pool (H), spleen (S), kidney (K) and bones (B). Lesion detection was compared with clinical, radiographic and scintigraphic bone scan findings. Increasing the amount of "cold" antibody resulted in a higher detection rate. Bone lesions detected were 29% at 20 mg and 53% at 40 mg and it approached 70% at 80 mg. Lymph nodes

metastases were not detected up to 80 mg. Liver metastasis appeared "cold" compared to normal liver uptake. The body distribution of labeled PAY-276 changed significantly with the dose of "cold" PAY-276. The liver uptake diminished while other organs uptake increased with increasing dose of "cold" antibody e.g. B/L ratio was 0.15 ± 0.03 at 10 mg and 0.42 ± 0.09 with a P = 0.025 at 40 mg. Similar P values were observed for K/L and H/L ratios from 10 to 40 mg and continued to rise at 80 mg. Nonspecific localization in areas of inflammation e.g. pneumonia was occasionally seen. PAY-276 in conjunction with a high dose of unlabeled MoAb has potential for diagnosis of metastatic cancer of the prostate.

No. 593

SCINTIGRAPHIC FINDINGS OF COLONIC CANCER USING INDIUM-111 LABELED ANTI-CEA MONOCLONAL ANTIBODY (ZCE-025) COMBINED WITH UNLABELED ANTIBODY. L.M. Lamki, Y.Z. Patt, J.L. Murray, T.P. Haynie, H.J. Glenn, E.M. Hersh, M.W. Unger, and D.J. Carlo. U.T. M.D. Anderson Hospital, Houston, TX and Hybritech Inc., San Diego CA.

One mg of ZCE-025 monoclonal antibody (MoAb) directed against carcino-embryonic antigen (CEA) was labeled with 5 mCi of Indium-111 using bifunctional DTPA, and administered intravenously to 16 patients with metastatic carcinoma of the colon. Patients were divided into 4 groups (I to IV) and each group was given 2.5, 5, 10, or 20 mg of unlabeled MoAb with the labeled ZCE-025. Images were recorded at 24, 48, and 72 hours (h) and occasionally at 144h. Regions of interests over the liver, blood pool, spleen, bone, and kidney were used to analyze relative body distribution. Lesion detection was compared with clinical, CT, and other nuclear studies. Detection of metastatic lesions in the lungs improved with increased dose of unlabeled MoAb. No lung metastases were detected at less than 10 mg. Lymph node lesions were readily detected even with less than 10 mg of "cold" antibody. Liver lesions appeared "cold" indicating the metastatic lesions take up less labeled ZCE-025 than normal liver. There was uptake in 2 sites of previous disease but no disease at the time of the study. Two other positive areas were not substantiated by other tests (occult disease?). Non-tumor body distribution of the labeled MoAb showed greater liver concentration at doses below 10 mg than at higher doses of unlabeled antibody. Occasional uptake in breasts and lungs was observed with the higher doses.

ZCE-025 is a promising MoAb for imaging metastatic colonic cancer, when used in conjunction with blocking MoAb. However, liver metastases are overshadowed by the normal liver uptake.

No. 594

CONSIDERATIONS FOR RADIOTHERAPY OF PSEUDOMYXOMA PERITONEI WITH IP I-131 B72.3, A MONOCLONAL ANTIBODY. SM Larson, JA Carrasquillo, D Colcher, JR Reynolds, P Sugarbaker, J Schlom. National Institutes of Health, Bethesda, MD.

Adenocarcinomas of the GI tract may spread within the peritoneal cavity and cause death of the patient by bowel obstruction or perforation. We biopsied tumor implants at surgery to measure targeting of I-131 labeled B72.3 after the radiolabeled antibody was instilled into the peritoneal cavity via a Tenckhoff catheter. In 2 patients with diffuse tumor spread throughout the peritoneum, binding of antibody to tumor was rapid, as shown by gamma camera images. Localization of radioactivity ranged from .04% to .184% injected dose per gram, (extrapolated back to time of injection) with half-life of clearance of 5 days. Calculations were performed using the MIRD schema. For tumor, RAD doses were 1732 to 7998 Rads per 100 mCi administered. Marrow and small intestinal dose, were 31-51 Rad and 84-114 RAD respectively, doses which would be expected to be well tolerated by the normal tissues. As a comparison, it was possible to calculate the RAD dose which was delivered by I-131 B72.3 to the LS 174T tumor growing in nude mice. Tumoricidal doses were computed to be 7864-

9652 RADS. Thus, dosimetry calculations predict that IP I-131 B72.3 may be used to treat intraperitoneal cancer with minimal risk to normal radiosensitive tissues.

No. 595

DOUBLE ISOTOPE EMISSION TOMOGRAPHY FOR DETECTING HUMAN HEPATOCELLULAR CARCINOMA BY IMMUNOSCINTIGRAPHY. J. Lumbroso, J.F. Bergmann¹, L. Manil¹, J.C. Saccavini², P. Rouquier³, D. Bellet¹, C. Bohuon¹ and C. Parmentier. Nuclear Medicine, Clinical Biology¹ and Gastroenterology³ Dpts of Institut G. Roussy, Villejuif, France; CEA-ORIS², Gif-sur-Yvette, France.

We used anti- α -fetoprotein (AFP) monoclonal antibodies (MAbs) for imaging hepatocellular carcinoma (HCC).

Two anti-AFP MAbs (AF01 and AF04) were produced (Bellet et al., Proc Natl Acad USA, 1984, 81:3869-73). Isotope and affinity constants were respectively IgG2a and $1.6 \cdot 10^{10} M^{-1}$, IgG1 and $0.8 \cdot 10^{10} M^{-1}$. After I-131 labeling the bound fraction of AFP ranged between 70 and 85%. Informed consent was obtained from 18 patients bearing HCC. After control, 0.27 to 0.50 mg of intact MAbs (AF01, 7 cases; AF04, 5 cases) or Fab fragments (AF04, 6 cases) labelled with 70 to 118 MBq of I-131 were intravenously infused after thyroid protection. Emission tomography (SPET) was performed 1 day and 2 or 3 days later and after a complementary injection of Tc-99m sulfur colloid (74 MBq), providing comparative distribution of I-131 and Tc-99m in each transverse slice.

We obtained 3 negative results, 5 were doubtful (no contrast to normal liver), 5 positive (weak contrast to normal liver) and 5 strongly positive (tumour uptake without I-131 uptake on normal liver). The MAbs uptake was higher around the tumour than in its center. There was no correlation between the outcome of SPET and the blood AFP level which ranged from 25 to 147000 ng/ml. Patients receiving Fab fragments seemed to have better results. The sensitivity of immunoscintigraphy for HCC is not sufficient for widespread clinical use, but the method provides valuable information for the practicability of therapeutic use of radiolabelled anti-AFP MAbs in HCC.

No. 596

IMAGING OF MELANOMA WITH MONOCLONAL F(ab')₂ and THALLIUM-201 CHLORIDE. L. Mansi, M. Salvatore, S. Del Vecchio and L. Lapenta. 2nd Med. School and Cancer Inst., Naples, Italy.

28 patients (pts) with melanoma were studied after an i.v. bolus injection of radiolabelled F(ab')₂ of 225.28S, a Monoclonal Antibody (MAB) reacting against an High Molecular Weight Melanoma Associated Antigen. Pts were studied during a 96 hr period using 2-3 mCi (30-50 mCi/mg) for In-111 and during a 24 hr period with 4-10 mCi (30-100 mCi/mg) using Tc-99m. 24/28 pts (85.7%) showed at least one pathological uptake. 32/52 (61.5%) tumor sites were clearly visualized. Using a retrospective approach a further 7 locations were evidenced. False negatives were connected with the organ, absence of antigen, and the tumor size and location with the lowest number of positives in skin lesions. 8 pts were studied one month from immunoscintigraphy after i.v. injection of 2 mCi of Thallium-201 Chloride (Tl), whose uptake in malignant tumors has been related to the pathophysiological state (blood flow, cellularity, growth rate, transformation). 11/17 melanoma sites were clearly positive. In addition 3 pts underwent a 2nd Tl scan six months after the first one. A disagreement with previous data was demonstrated with uptake only in sites with a disease progression. The comparison Tl/MAB showed substantially overlapping results. These data suggest that the "in vivo" lack of arrival of the MAB to the Antigen could determine some false negatives in Immunoscintigraphy.

No. 597

DOSE-DEPENDENT DIFFERENCES IN BIODISTRIBUTION OF IN-111 LABELED MONOCLONAL ANTIBODIES (MoAb) D Munz, JA Carrasquillo, RD Neumann, JC Reynolds, P Abrams, K Foon, PA Bunn, JL Mulshine, R Schroff, C Morgan and SM Larson. National Institutes of Health, Bethesda, MD.

This study was done to determine whether increasing doses of MoAb result in biodistribution changes. All MoAb were labeled by a modification of the Krejcarek method (Hybritech, Inc.) with approximately 5 mCi of In-111 on 1 mg of MoAb. Dose escalation studies were done by adding increasing amounts of the same MoAb, unconjugated and unlabeled to provide total mg doses listed. Three MoAbs (IgG2a) were evaluated: 9.2.27 directed at a high molecular weight antigen (Ag) of melanoma, 96.5 directed at p97 a melanoma associated Ag and T101 directed at a pan T-cell Ag present on cutaneous T-cell lymphoma (CTCL). 11 patients were studied with 1 to 100 mg of 9.2.27, 7 pts were studied with 1 to 3 mg of 96.5 and 11 pts were studied with 1 to 50 mg of T101. Digital acquisition of patient images up to 1 week post-injection had ROI analysis (CPM per pixel, geometric mean) performed. Pts receiving higher total doses had the least "nonspecific" organ uptake (liver, spleen and marrow). Ratios of blood pool to organ were significantly different at the various dose levels. Higher doses of 9.2.27 showed decreased activity in the spleen and marrow. Higher doses of 96.5 showed predominantly less activity in the liver. Higher doses of T101 showed decreased activity in the liver, spleen and marrow. In conclusion, 1) each MoAb has a characteristic pattern of distribution; 2) this distribution can be altered by increasing "carrier" amounts of the MoAb.

No. 598

RADIOIMMUNODETECTION OF HUMAN COLON AND GASTRIC CANCERS XENOGRAFTS BY IGM MONOCLONAL ANTIBODIES. K. Nakamura, T. Ohishi, M. Watanabe, S. Hirohashi*, A. Kubo, S. Kodaira, Y. Shimamoto*, S. Hashimoto, and O. Abe. School of Medicine Keio University, and *National Cancer Research Institute, Tokyo, Japan.

The aim of this study was to evaluate monoclonal antibodies (IgM), ST-439 and ST-433, raised against a gastric cancer (ST-4), xenografts, in the radioimmunodetection for human colon and gastric carcinoma xenografts in nude mice.

Label-imaging and localization experiments were performed by IV injecting approximately 40 μ Ci of I-125 labelled antibodies into nude mice bearing Co-4 (poorly differentiated colon carcinoma), and H-111 (well differentiated gastric carcinoma).

There was uptake of ST-439 (polymer) into the Co-4 at day 8, with tumor to blood ratio (T/B) 3.0, but tumors were not clearly visualized until 4 days post injection. By injecting ST-439 (monomer), tumors were better seen at day 3 (T/B=1.7), while average accumulation into the tumors equaled to 0.33% of the total injection dose (ID). Uptake into liver was 0.74% of the ID, probably due to the immunocomplex with the antigen in the blood. On the other hand, ST-433 was selectively accumulated into the H-111 with T/B as high as 7.8 at day 7, with no significant uptake into liver, spleen and kidney as well as stomach itself. Excellent images were obtained 1 day after the injection.

The efficacy of IgM antibodies for in vivo diagnosis and therapy has been questioned. ST-433 holds promise for the radioimmunodetection of colon and gastric cancer.

No. 599

HUMAN ANTI-MURINE ANTIBODIES FOLLOWING IMMUNOSCINTIGRAPHY OR THERAPY WITH RADIOLABELED MONOCLONAL ANTIBODIES. J.C. Reynolds, J.A. Carrasquillo, A. M. Keenan, M.E. Lora, P. Sugarbaker, P. Abrams, K. Foon,

J.L. Mulshine, J. Roth, D. Colcher, J. Schlom, S.M. Larson, National Institutes of Health, Bethesda, Md.

A potential impediment to repeat immunoscintigraphy or radioimmunotherapy is the development in patients of human antimurine antibodies (HAMA). To assess for the presence of circulating HAMA a simple screening assay was developed using I-125 B72.3 monoclonal antibody (MoAb) as tracer and protein A for separation of the HAMA. Patients evaluated for HAMA were those that had been studied under one of 8 imaging or therapy studies using MoAb B72.3 (IgG₁), T101 (IgG_{2a}), 9.2.27 (IgG_{2a}), 791T/36 (IgG_{2b}) and Fab fragments of antibodies 96.3 and 48.7 (IgG_{2a} and IgG₁, respectively). 23 of 50 patients who received one IV injection of IgG developed HAMA whereas none of the 12 patients who received a single Fab injection became positive. However, four of 7 patients who received multiple injections of Fab did develop HAMA. 6 of 20 patients who received IgG_{2a} developed HAMA compared to 15 of 30 patients receiving IgG₁. With subcutaneous (SC) injections 3 of 10 IgG_{2a} patients and 1 of 6 Fab patients became HAMA positive. We conclude 1) that murine IgG is more immunogenic than Fab fragment, 2) but that repeat administration of murine Fab fragment will lead to a high frequency of HAMA positivity, 3) both SC and IV injections of MoAb are immunogenic, 4) that HAMA frequently occurs after IV injection of murine IgG or Fab and is a significant problem in the use of these agents for immunoscintigraphy or radioimmunotherapy.

No. 600

A PROSPECTIVE STUDY OF RECURRENCE IN COLON CANCER WITH I-131 B72.3 MONOCLONAL ANTIBODY. M. Salvatore, S. Lastoria, L. Mansi, A. Renda, D. Colcher, J. Schlom, S.M. Larson, L. Callegaro. 2nd Medical School, Naples, Italy, NIH, Bethesda, MD, SORIN Biomedica, Saluggia, Italy.

23 patients (pts) that underwent a total resection of a colon cancer were prospectively analysed using I-131 labelled monoclonal antibody B72.3 (IgG₁) reacting against a tumor associated glycoprotein present in more than 80% of Human Colon Carcinoma. B72.3 was labelled via the Chloramine-T method (Specific Activity 5mCi/mg). Pts were studied at .6mg and 3 mCi at different times (24-48-72-96 hours) after an i.v. bolus injection. A very low activity was seen in the liver. Nor other organs neither blood cells accumulated the radiotracers. Blood Pool activity was present at all times. Tumor sites were demonstrated by surgery or by conventional methods (Endoscopy, CT, US, Radio nuclides). Scans were negatives in 3 pts free of disease. 16/19 (84%) recurrences were positives. Tumor uptake was evident starting 48 hrs after injection. Using an analogical analysis only 4/8 (50%) liver metastases were detected. A worst Tumor/not Tumor uptake ratio could explain this data. The possibility of a basal membrane surrounding the tumor site has also to be taken in account. Two unexpected lesions, a 1.2cm left paramediastinal lung metastasis and an inguinal lymphnode involvement were also demonstrated.

Supported by CNR grant Special Project Oncologia.

No. 601

PHARMACOKINETICS AND IMAGING USING MUTANT MONOCLONAL ANTI-ARS ANTIBODIES. S.A. Shah*, R.R. Pollock⁺, B.A. Brown*, B.M. Gallagher*, M.D. Scharff⁺, and H. Sands*, Dupont*, N. Billerica, MA 01862 and Albert Einstein College of Medicine⁺, New York 10461

Selective modification in antibody structure and may provide better diagnostic and therapeutic reagents. We compared the blood clearance, whole organ distribution, and *in vivo* targeting of two mutant IgG_{2b} immunoglobulins (ArM16, -CH₂ domain deficient; ArM1, -CH₃ domain deficient) and the parent Ar13.4 antibody all

specific for azophenylarsonate (ARS). The ArM1 was purified by size exclusion chromatography to separate H₂L₂ (47%) from HL (53%). Micropore diffusion chambers containing immobilized ARS antigen on 75 mg of Sepharose beads were implanted s.c. in CD1 mice to serve as "model tumors". Immunoreactivities of the ¹²⁵I/¹³¹I (iodogen method) and ³⁵S-methionine labeled antibodies *in vitro* were comparable. The blood clearance of all ARS antibodies in mice was biphasic, an initial rapid decrease followed by a slower rate of disappearance. Blood and whole organ (liver, kidney, spleen, G.I.) clearance of ¹²⁵I-ArM1 (H₂L₂) > ¹²⁵I-ArM16 > ¹³¹I-Ar13.4. At 13 days, the ratios of antibody accumulation in ARS beads/blood were 1680, 80, and 65 for ArM1, ArM16, and Ar13.4, respectively. Percent I.D./gm ± S.E.M. were:

	5 Days		13 Days	
	ARS-Beads	Blood	ARS-Beads	Blood
¹³¹ I-Ar13.4	43.7±4.0	4.1±0.5	39.4±3.4	0.60±0.1
¹²⁵ I-ArM16	9.0±3.8	0.5±0.0	8.0±1.0	0.10±0.0
¹²⁵ I-ArM1	11.8±1.7	0.1±0.3	16.8±2.3	0.01±0.0

Specific images of the ARS chambers were observed with all the ARS antibodies 2-5 days after injection. These results suggest that CH₃ deficient antibodies may prove useful for tumor localization.

No. 602

CORRELATION OF TUMOR IMAGING AND SURGICAL SAMPLES FOLLOWING IN-111-ANTI-CEA INJECTION IN HUMANS. L.E. Williams, V.J. Philben, J.G. Jakowatz, R.J. Paxton, J.E. Shively, B.G. Beatty, W.G. Vlahos, J.L. Werner, K. Sheibani, M.M. Kemeny, W.A. Kokal, D.U. Rihimaki, J.J. Terz, and J.D. Beatty. City of Hope Medical Center, Los Angeles, CA.

The correlation between monoclonal antibody (MoAb) imaging and surgical specimens was studied in a group of 21 colorectal cancer patients. A high affinity MoAb to carcinoembryonic antigen (CEA) was used - each patient receiving 200 µgm of protein labeled with 2.0 mCi of In-111. Scans were obtained at 24 and 48 h and laparotomy was performed within 17 days of injection. Surgical specimens were assayed for CEA content, weighed and counted for activity. By immunoperoxidase staining, all tumors were CEA-positive. Of the 10 primaries, 3 scans were positive (30%), 4 were equivocal (40%) and 3 were false negative (30%). 13 patients had hepatic metastatic disease, but only 5 scans (38%) were positive; i.e. showed an elevated count rate at the rim of the lesions and/or a cold nodule. Correlations of scan result, lesion site, CEA content (µgm/gm) and tissue uptake in % injected dose (ID) per kgm were as follows:

Site	Scan	Fraction	CEA (µgm/gm)	% ID/Kgm (at 7d)
Colon	+	3/10	7.3	6.4
	±	4/10	10.2	5.5
	-	3/10	0.3	4.5
Liver	+ rim	2/13	9.5	16.4
Mets	-nodule(s)	3/13	3.7	3.6
	-	8/13	0.9	8.9

We conclude that an In-111 labeled anti-CEA MoAb permits correct localization of those colorectal lesions having high CEA content. Uptake by normal liver remains an appreciable problem, however.

No. 603

IMMUNOSCINTIGRAPHY OF COLON METASTASES WITH MONOCLONAL ANTIBODY HT 29-15. S.D.J. Yeh, K. Cohn, T. Allen-Merish, J. Sakamoto, C. Gordon-Cardo, S. Welt, J. Daly, N. Kemeny, C. Mies, K. Lloyd, J. DeCosse, H. Oettgen, R.S. Benua, and L. Old. Memorial Sloan-Kettering Cancer Center, Cornell Medical College, New York, N.Y.

Mouse monoclonal IgG₁ antibody (Ab) HT-29-15 reacts with 76% colon Ca, but not to most normal tissues. Tumor uptake was shown in human colon Ca heterotransplants in nude mice. Studies were done in 14 patients with metastatic colon Ca. I-131 labeled Ab (1-2 mCi, 1-6 mg, about 40% immunoreactivity) was given. Images of thorax and abdomen were quantified 4 hrs to 3-5 days

later with a gamma camera. In 12 patients, liver metastases were clearly shown in the liver scans. Large lesions in general appeared as cold defects in the early Ab images but lesions became equal to or higher than liver later. Clear delineation of liver involvement occurred in all lesions after subtraction of ^{99m}Tc sulfur colloid but not after human serum albumin. In surgical specimens from 5 patients 3 to 5 days after injection of labeled Ab, the tumor to liver ratio was 2.87 ± 0.51 and tumor to blood ratio was 0.66 ± 0.10 . Patients excreted $12.32 \pm 1.53\%$ of the dose in the 1st day and $40.84 \pm 4.35\%$ in 3 days. One patient had liver biopsy on the 3rd day and resection on the 23rd day. The tumor to liver ratio was 2.37 in the early specimen but 88 in the resected specimen.

This preliminary study suggest that mouse monoclonal Ab HT 29-15 is potentially useful for radioimmuno-detection of metastases from colon Ca.

Monday, 3:30-6:00

Exhibit Hall

NEUROLOGY: GENERAL

No. 604

ERROR IN PARAMETER ESTIMATES OBTAINED FROM Rb-82/PET STUDIES OF BLOOD-BRAIN BARRIER PERMEABILITY (BBB) EFFECT OF TISSUE HETEROGENEITY AND COUNT RATE. V. Dhawan. Memorial Sloan-Kettering Cancer Center, New York, NY.

Rb-82 bolus infusion in conjunction with dynamic positron emission tomography (PET) has been used to estimate the blood-to-brain and blood-to-tumor transport constants (K_1) for Rb. The accuracy of these estimates depends primarily upon PET measurements of regional tissue radioactivity. We have extended our previous error analysis for homogeneous regions (J Cereb Blood Flow Metabol 5 [Suppl 1]: S85-S86, 1985) to regions containing a varying mix of tumor and normal tissue. Effects of count rate were studied by changing the magnitude of the arterial brain input function, $C_p(t)$. Brain radioactivity (A_m) was calculated at one-minute intervals for 6 min for 8 different tumor-tissue mixes. The blood curve simulated a "slow" bolus infusion of 120 mCi of Rb-82. Appropriate noise was added to A_m , and the operational equation was then solved for K_1 and blood water volume, V_b . Our analysis suggests that for a 10% error in A_m , K_1 and V_b can be estimated with an accuracy of 5% for all tissue mixes. The error in K_1 and V_b increased marginally (<5%) vs that for equivalent homogeneous regions. Substantially decreased count rate (one-half injected radioactivity) increased the error in K_1 to >40% for small regions (<2.5 cm³). Based on this error analysis we conclude that accurate estimates of K_1 and V_b can be obtained for heterogeneous tissue regions using our bolus injection protocol for Rb-82/PET studies.

No. 605

THE RATE OF VENTRICULAR ENLARGEMENT IN DEMENTIA OF THE ALZHEIMER TYPE (DAT) CORRELATES WITH RATE OF NEUROPSYCHOLOGICAL DETERIORATION J. Luxenberg, H. Creasey, J. Haxby, M. Sundaram, S.I. Rapoport. Laboratory of Neurosciences, National Institute on Aging, National Institutes of Health, Bethesda, MD; Lidcombe Hospital, Lidcombe, New South Wales, Australia

Twelve men with DAT (age 63 ± 2 yrs, interscan interval 508 ± 47 days) and twelve healthy male control subjects (age 65 ± 4 yrs, interscan interval 1196 ± 108 days) were studied with serial brain X-ray CT scanning. Ventricular volumes were calculated by summing ventricular areas outlined with a light-pen on an image analysis system, and multiplying by the interslice distance (7 mm). The DAT patients had a mean third ventricular (1.20 ± 0.32 cc/yr) and lateral ventricular

(13.3 ± 2.0 cc/yr) enlargement; both values differed from controls ($p < 0.02$). The controls had significant third ventricle enlargement (0.3 ± 0.1 cc/yr, $p < 0.01$) but not lateral ventricular enlargement.

A composite neuropsychologic score was obtained utilizing the Syntax Comprehension Test, Extended Range Drawing Test, Porteus mazes, and verbal and visual immediate memory from the Wechsler Memory Scale. In men with DAT, the rate of decline in neuropsychological scores correlated with both rate of third ventricular enlargement ($r = 0.67$, $p < 0.05$), and right lateral ventricular enlargement ($r = 0.83$, $p < 0.003$).

There was no overlap between the rates of lateral ventricular enlargement in controls and DAT subjects. Serial CT differentiates between normal aging change and pathological ventricular enlargement in DAT. The rate of ventricular enlargement in DAT correlates with the rate of neuropsychological deterioration.

No. 606

NON INVASIVE METHOD FOR BLOOD-BRAIN BARRIER (BBB) PERMEABILITY MEASUREMENT USING Ga-68 EDTA and PET. L.Mansi, B. Alfano, M.Salvatore, F.Iannotti, P.Picozzi, C.Pozzilli, G.Del Vecchio, A.Punzo, F.Fazio, G.L.Lenzi, P.Conforti and C.Fieschi. PET Center, Universities of Naples and Rome "La Sapienza", Italy.

BBB permeability to Ga-68 EDTA was measured using NeuroECAT in 11 patients (pts) with primary or metastatic brain tumors and in 4 normal volunteers. 6-8 mCi of 68-Ga EDTA were injected as an i.v. bolus and 16 consecutive 300 sec scans were performed. Arterial blood samples were collected throughout the procedure. A 20 ml venous blood sample was obtained at 10-15 min and a PET scan of the syringe was performed later. Using Multiple Time Graphical Analysis (Patlak, 1983) K_1 : unidirectional blood to brain transfer constant and V_p : estimate of cerebral blood volume were calculated. We used as input function both the arterial concentrations of the tracer and values obtained from a ROI taken on the superior sagittal sinus, using a correction factor derived from the scan of the syringe. Values of K_1 were corrected for V_p . Full agreement was found between both methods ($R = 0.997$). In normal subjects K_1 was 0.0003 ± 0.00008 ml/g/min and $V_p = 3.4 \pm 0.7$ ml/100g. Similar values were found in areas contralateral to a tumor. Tumor regions presented a net variability in K_1 . While low grade astrocytomas did not show alteration of K_1 and V_p , K_1 was increased in malignant tumors up to twenty-folds.

No. 607

USING FLOOD PHANTOMS TO EVALUATE QUANTIFICATION IN PET: OBJECT SIZE EFFECTS. S.C. Strother*, A.C. Evans, C.J. Thompson. Montreal Neurological Institute, Montreal, Canada.

Typically a series of images from a decaying flood phantom (FP) are analyzed as plots of reconstructed image activity vs true activity (RIA/TA) to establish the linear operating range of a given scanner. However, random coincidence and deadline errors may compensate for each other, and an independent measurement of one or the other is required [e.g. randoms (true activity)²].

Such FP linearity of mean RIA/TA can be achieved without FP spatial uniformity when errors due to incorrect scatter and/or attenuation corrections remain. A sensitive test of any spatial non-uniformity may be developed by noting that all the relevant error effects are circularly symmetric about the center of a centrally placed FP. By averaging circumferentially around annuli a few pixels wide we obtained radial uniformity profiles. The F-statistic from a one-way ANOVA of these

profiles is a sensitive measure of spatial uniformity. It was used to adjust an analytic scatter deconvolution filter. In particular we measured the filter parameters required to optimally flatten images from 20 cm and 15 cm FP's using a narrow beam attenuation coefficient for water of .096. Applying the scatter filter, derived for a 15 cm FP, to a 20 cm FP produced systematic spatial variations of > 10%. In addition, the 15 cm FP scatter filter increased the mean image values from the 20 cm FP, to +19% of those obtained with the 20 cm FP scatter filter. This demonstrates the need to explicitly adjust scatter corrections for object size effects.

*Memorial Sloan-Kettering Cancer Center, New York, NY.

No. 608

ASSESSMENT OF CEREBROSPINAL FLUID SHUNT FLOW RATES BY COMPUTERIZED SEMICONDUCTOR DETECTOR SYSTEM. Y. Suzuki, M. Matsumae, T. Murakami, M. Ueda and O. Sato. Tokai University School of Medicine, Isehara-city, Japan.

Nuclear medicine techniques have been widely used for measurement of cerebrospinal fluid shunt flow rates (CSFSFR), however, the measurements are only feasible when the patients (pts) are in their supine position in most of the cases and real CSFSFR are hardly available during changing position, while CSFSFR will be greatly influenced by it. The purpose of this paper is to describe a new flexible method of assessing CSFSFR with a computerized cadmium telluride (CdTe) probe system. The size of CdTe detector is 16mm in diameter and 2mm in thickness, and a small straight bore collimator; 5mm in length, is attached to it. Total weight of the detector is less than 100g so that it can be easily attached to the patient's head. With this system, experimental measurements were carried out on a shunt device connected to an infusion pump and correlation between flow rates (F) and clearance half time ($T_{1/2}$) was determined in the wide range of flow rates. An equation of $\log F = 3.66 - 1.01 \log T_{1/2}$ was obtained, which was used to calculate the CSFSFR in the pts. In 40 pts, CSFSFR were measured in supine position. The CSFSFR were varied from nearly zero to 0.85ml/min. In the 16 pts whose CSFSFR were less than 0.01ml/min in supine position, the measurements were carried out continuously as the head being raised 5 degree (dg) each at 2min intervals. The CSFSFR greater than 0.1ml/min were obtained at 10dg in 10 pts, at 15dg in 2pts, at 25dg in one pt and in 3 pts no CSFSFR was demonstrated at any head positions. In conclusion, with this new system continuous assessment of CSFSFR can be made at any patient's head positions.

Monday, 3:30-6:00

Exhibit Hall

NEUROLOGY: PET

No. 609

REPRODUCIBILITY OF METABOLIC PATTERN FOR BEHAVIORAL STATES STUDIED REPEATEDLY IN A SINGLE PET/FDG PROCEDURE. J.Y. Chang, R. Duara, W. Barker, A. Apicella, and F. Yoshii. Mount Sinai Medical Center, Miami Beach, FL.

Using a single PET/FDG procedure to study two behavioral states (J.Nucl. Med. 26:P103, 1985), the reproducibility of cerebral metabolic rates of glucose (CMR_{glc}) for a specific behavioral state was examined. The Word Fluency Test (WFT) which is simple to administer and requires constant attention from the subject was chosen as the specific task. Starting immediately prior to the first injection of FDG, the subject was required to say as many words as possible starting with a given letter, one minute per letter for 30 min. After the first administration of WFT, a 20 min. scan was obtained, followed by a second administration of WFT and a second scan.

Percent differences ($\Delta\%$) in the ratio, regional CMR_{glc}/whole brain CMR_{glc} (Y ratios), were used to examine any changes of metabolic pattern in the repeated scans. $\Delta\%$ of Y ratios among 20 brain regions for four subjects who had WFT/WFT were generally under 5% (mean $\Delta\% \pm$ S.D. = 2.4 ± 2.0). In 3 out of 4 subjects $\Delta\%$ for some regions was greater than 5%, namely two regions in subject 1 (5.4%, -5.2%), 1 region in subject 2 (-6.6%), and 3 regions in subject 3 (7.3%, 5.5%, 12.2%) (subject 3 had to urinate during the procedure).

We conclude that the reproducibility of CMR_{glc} values for a specific activation state is very good using this method and that it is likely to be equally reliable for identifying differences when dissimilar activation states are used.

No. 610

THE USE OF A BEHAVIORAL "STRESS" TEST TO ENHANCE METABOLIC ABNORMALITIES IN ALZHEIMER'S DISEASE (AD). R. Duara, W. Barker, J.Y. Chang, F. Yoshii and A. Apicella. Mount Sinai Medical Center, Miami Beach, FL.

PET/FDG studies in AD have shown hypometabolic areas and asymmetries in metabolism in temporo-parietal regions. Normal subjects also show these features but to a lesser extent. The purpose of this study was to effectively distinguish normal subjects from mild cases of AD by using a behavioral task which would activate unaffected brain regions and increase the contrast between normal and abnormal regions. Six patients with mild AD and 3 normal controls were studied in the resting state and while performing a verbal memory test. The studies, in each subject, were performed in one extended procedure, using 2 injections of FDG and 2 PET scans in a 100 min. period (Chang, et al. J. Nucl. Med. 26, P103, 1985). The orbito-frontal and inferior temporal regions were activated maximally in normals, with global glucose metabolic rates (mg/100g-min) from 7.52 to 8.34; only the left inferior frontal cortex and cerebellum were activated in demented subjects with metabolic rates increasing from 7.4 to 7.55. Hypometabolic deficits were generally more apparent during activation than rest in demented subjects. Mean % asymmetry during rest and activation were 5.1 ± 0.3 and 5.5 ± 2.0 in normals and 11.0 ± 7.9 and 11.1 ± 6.1 in demented subjects. Only in demented subjects were there any regions that showed significant increases in asymmetry during activation relative to rest (eg. medial temporal asymmetry was $4.6 \pm 4.0\%$ at rest and $8.6 \pm 0.6\%$ during activation, $t = 3.0$, $p = 0.04$).

We conclude that behavioral activation may be a useful way to enhance metabolic abnormalities in AD.

No. 611

DISCRIMINATION OF FUNCTIONAL BRAIN RESPONSES BENEATH IMAGE RESOLUTION WITH POSITRON EMISSION TOMOGRAPHY. M.A. Mintun, P.T. Fox, and M.E. Raichle, Washington University School of Medicine, St. Louis, MO.

As positron-emission tomography (PET) is safely performed on normal subjects engaged in controlled sensory, motor or cognitive activities, it has unique potential for studying structure: function relations of the in vivo human brain. A major hindrance, however, to the utility of PET for functional brain mapping has been the limited spatial resolution of emission imaging relative to the size of brain structures. PET images typically have spatial resolution greater than 1.0 cm full-width at half-maximum (FWHM), prompting the inference that PET cannot establish structure: function relationships with accuracy better than one cm. We have now demonstrated, using both simulated and actual PET brain images, that a conventional PET device (PETT VI, 18 mm FWHM images) can specify the location of a region of functionally activated brain to within 1 mm and, similarly, can discriminate activated foci separated by less than 3 mm. The fundamental constraint of this technique is that at least two studies (resting-state and

activated-state) must be acquired for each subject during a single scanning session. To enable a brief interval between studies we have chosen the measurement of cerebral blood flow using bolus, intravenous administrations of oxygen-15-labeled water. This allows a measurement time of less than one minute, and an inter-measurement time of 8-10 minutes. Subtraction of the resting-state image from the activated-state image results in a difference image which is used to find the locale of the activated focus. Such functional brain mapping beneath the image resolution, therefore, is achieved by experimental strategy alone and does not require any physical modifications of the PET device.

No. 612

COMPARATIVE STUDY OF POSITRON EMISSION TOMOGRAPHY AND MAGNETIC RESONANCE IMAGING IN CEREBROVASCULAR DISEASE. S.Nishizawa, M.Senda, Y.Yonekura, K.Nishimura, I.Fujisawa, H.Fukuyama, M.Ishikawa, W.Taki, M.Kameyama, H.Handa, and K.Torizuka. Kyoto University School of Medicine, Kyoto, Japan.

X-ray computed tomography (CT) frequently fails to diagnose cerebrovascular disease (CVD) without major stroke. In order to evaluate the clinical role of positron emission tomography (PET) and magnetic resonance imaging (MRI) in CVD, we studied the patients with occlusion of internal carotid artery (IC) using PET, CT and MRI. Regional cerebral blood flow (rCBF), cerebral blood volume (CBV), oxygen extraction fraction (OEF) and cerebral metabolic rate of oxygen (CMRO₂) were measured with inhalation of O-15 labeled gases. For MRI, superconducting high magnetic field device, SIGMA, was used with pulse sequence of spin echo 2000/20-60 or 2000/40-80.

In all cases, MRI revealed small multiple high intensity lesions in the white matter with higher contrast and detectability than CT. On the other hand, PET demonstrated decreased CBF with increased CBV and OEF not only in the white matter but also in the extensive cortical area.

MRI is superior in detecting small organic lesions, while PET shows hemodynamic and metabolic aspect of brain function. In addition, PET is valuable in predicting prognosis and determining operative indication in cases with such CVD.

No. 613

ASSESSMENT OF 11-C-L-METHIONINE TRANSPORT INTO THE HUMAN BRAIN WITH A SIMPLE DUAL-PROBE DETECTION SYSTEM. L.A. O'Tuama, T.R. Guilarte, R.F. Dannals, A.N. Bice, M.C. Lee, J. Williams, D. Valle, H.N. Wagner, Jr. The Johns Hopkins Medical Institutions, Baltimore, MD.

Decreased transport into the brain of large neutral amino acids (LNAA) may be a major factor in the pathogenesis of certain neurodegenerative disorders (Ratzmann, *Biochim. Biophys. Acta.* 43:197, 1984). We have used a simple, inexpensive, high efficiency detection system (HEADS) to quantify LNAA uptake by the human brain. In studies of normal, fasted volunteer subjects, 360-410 uCi (1.5-24 ug) 11-C-L-methionine (MET) was injected i.v. and a 40 minute time activity curve of brain 11-C-L-MET uptake was acquired. All studies showed a rapid initial accumulation of brain 11-C-L-MET, which plateaued after 5 mins. A second study was performed 1 hour after the oral administration of 100 mg/kg L-phenylalanine (L-PHE). These studies showed a decreased 11-C-L-MET accumulation after the L-PHE challenge: mean \pm S.D. Δ = -32.5 \pm 14.7%. Total serum LNAA levels (except L-tryptophan) were analysed before and after each 11-C-L-MET injection and showed: a) a greater than 12-fold elevation of serum PHE after loading; b) no change in other LNAA levels.

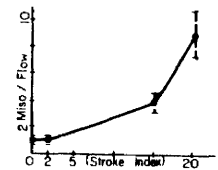
The HEADS system needs approximately 1/40th the tracer dose needed for PET imaging, thus allowing multiple studies without excessive radiation. Our results

indicate that this simple detector system may play a useful role in the study of neurometabolic diseases such as phenylketonuria or other conditions where brain amino acid transport is altered.

No. 614

BLOOD FLOW AND BBB INTEGRITY AS FACTORS IN MISONIDAZOLE UPTAKE IN CEREBRAL ISCHEMIA. D.W. Shaw, J.S. Rasey, A.M. Spence and K.A. Krohn. Univ. of Wash., Seattle, WA.

Our recent work (JNM 26:P25, 1985) with misonidazole (MISO) in the gerbil stroke model was consistent with its preferential uptake by hypoxic tissue. However the pharmacology of drugs in the brain is complicated by factors in addition to specific metabolism by cells. Studies have been done to delineate the relationship between MISO uptake in cerebral ischemia and the concurrent regional cerebral blood flow (rCBF) and BBB integrity. The production of cerebral ischemia in the gerbil stroke model is linked with alterations in rCBF, blood volume and ultimately disruption of the BBB, any of which potentially alter tissue delivery and retention of MISO. MISO uptake appears relatively unaffected by changes in the BBB. Gross disruption with mannitol produced only small increases in MISO uptake, thought to represent relative ischemia produced with the transient increase in local cerebral glucose utilization, uncompensated by flow changes. In contrast there was 2-3 fold increased MISO uptake in the stroke model at 4 hours when there was only minor alterations in the BBB. This is consistent with MISO's octanol:water partition coefficient of 0.43. Studies in the gerbil stroke model utilizing IAP as a flow tracer demonstrated a variable correlation between MISO uptake rCBF, depending on the degree of stroke. Consequently MISO uptake per unit of flow was assessed and provided a more useful measure of hypoxia than MISO uptake alone. Tracer delivery in the most severely affected animals is limited by flow.



Monday, 3:30-6:00

Exhibit Hall

NEUROLOGY: RECEPTOR IMAGING**No. 615**

DIFFERENTIATION OF DOPAMINE RECEPTOR SUBTYPES IN THE PRIMATE BRAIN USING PET. O.T. De Jesus, W.L. Woolverton, G.J.C. Van Moffaert, A.M. Friedman, N.J. Yassilo, C. Ortega, and M.D. Cooper. University of Chicago, IL and Argonne National Laboratory, Argonne, IL.

CNS dopamine (DA) receptors have been classified into D₁ and D₂ subtypes based on their coupling to the enzyme adenylate cyclase. We recently reported the visualization, *in vivo*, of D₁ receptors in a monkey brain with Br-75-SCH 23390 analog and PET (*Eur. J. Pharmacol.* 108:327, 1985). Here we report the preparation of C-11-SCH 23390, presently the most potent and selective D₁ antagonist, and evaluation of its utility for PET studies. In experiments involving two anesthetized rhesus monkeys each scanned twice on separate occasions after receiving 2-4 mCi C-11-SCH 23390 (dose=4-34 ug/kg), this drug entered the brain rapidly and was taken up, distributed, and cleared in a manner consistent with mediation by DA receptors. Fifteen minutes after injection, mean striatum/cerebellum (S/C) uptake ratio was 2.51 \pm 0.54. Blocking experiments to characterize the localization of D₁ receptors in the monkey brain and saturation experiments to assess receptor parameters were done. Preliminary results show that pretreatment with 56 ug/kg unlabelled SCH 23390 reduced the S/C ratio to 1.10 while after pretreatment with 10 ug/kg p-bromospiperidol,

S/C ratio measured was not significantly different from control. These results demonstrate that PET, involving both C-11-SCH 23390 and current D₂ radioligands, is a useful non-invasive tool in distinguishing subtypes of CNS DA receptors and may provide insights into the role of multiple DA receptors in normal and diseased physiology.

No. 616

MULTICOMPARTMENTAL ANALYSIS OF C-11 CARFENTANIL BINDING TO OPIATE RECEPTORS IN MAN BY POSITRON EMISSION TOMOGRAPHY. J.J. Frost, K. Douglass, H. Mayberg, R.F. Dannals, J. Links, A. Wilson, H. Ravert, H.N. Wagner, Jr. Johns Hopkins Medical Institutions, Baltimore, MD.

C-11 carfentanil (CAR) can be used to measure opiate receptor (OR) binding in man by the use of PET (Frost, et al. JCAT, 1985). Three compartment (vascular, extravascular and receptor) analysis similar to that described by Mintun, et al. (Ann. Neurol., 1984). was carried out using CAR binding in the thalami (TH) and unmetabolized CAR in arterial plasma [$C_p(t)$] determined by HPLC. Four males and 1 female (ages 21 to 44) were studied with (w.) and without (w/o) 1 mg/kg naloxone (NAL). The maximum occupancy of OR was \leq ca. 8%. The average percent CAR of total arterial plasma activity was 69 ± 14 (1 σ), 47 ± 9 and 28 ± 9 at 15, 30 and 60 minutes after injection w/o NAL; w. NAL the percent CAR was ca. 20% lower. There was a good fit to the data by the 3 compartment model to TH CAR binding and $C_p(t)$ using nonlinear least square analysis w. and w/o NAL. The fit was significantly worse when the data w. NAL was fit to 2 compartments and when total plasma radioactivity was used in place of $C_p(t)$. The binding potential ($BP = B_{max}/K_D$) ranged from 12 to 34 (mean 21) in this group of normal subjects who were heterogeneous with respect to age and sex. BP was >0 w. 1 mg/kg NAL indicating that not all OR are occupied at this dose.

These findings demonstrate that compartmental analysis can be used to obtain quantitative estimates of OR binding when plasma radioactivity is corrected for CAR metabolism.

No. 617

RELATIONSHIP OF OPIATE RECEPTOR BINDING AND TEMPORAL LOBE EPILEPSY USING C-11 CARFENTANIL. J.J. Frost, H.S. Mayberg, J. Fisher, R.F. Dannals, J.M. Links, A. Wilson, H. Ravert, H.N. Wagner, Jr. The Johns Hopkins Medical Institutions, Baltimore, MD.

Seizure activity produces an increased release of endogenous opioid peptides and may result in an increased threshold for immediate repetition of a seizure. In laboratory animals chronic seizures produce an increase in opiate receptors in the brain, further enhancing the anti-seizure effect of endogenous opioids. C-11 carfentanil can be used to measure opiate receptor (OR) binding and was employed in the study of 3 patients with temporal lobe epilepsy.

Three male patients were identified who had a predominantly unilateral temporal lobe seizure focus based on EEG criteria and were candidates for temporal lobe resection. CAR binding was measured in the amygdala (AM), caudate, thalamus (TH), temporal cortex (TCX) and frontal cortex. Activity in the calcarine cortex, an area very low in OR, was subtracted from that in the other regions to estimate left and right specific OR binding 15-45 min. after CAR injection.

There was a mean increase of 26% in specific CAR binding in AM on the side of the temporal lobe focus (range 21-33%). By contrast, specific OR binding in AM in 8 normal volunteers showed a mean asymmetry of 9%. Elevation of OR binding on the side ipsilateral to the seizure focus was also observed in TH and TCX in some patients. These results support the hypothesis that chronic seizures result in increased OR in AM and

possibly in additional brain regions. The study of OR in epilepsy may provide new insights into the brain's adaptive responses to seizures.

No. 618

ALTERATION IN BRAIN OPIATE RECEPTOR BINDING IN MAN FOLLOWING SEXUAL AROUSAL USING C-11 CARFENTANIL AND POSITRON EMISSION TOMOGRAPHY. J.J. Frost, H.S. Mayberg, F. Berlin, R. Behal, R.F. Dannals, J.M. Links, H.T. Ravert, A.A. Wilson, H.N. Wagner, Jr. The Johns Hopkins Medical Institutions, Baltimore, MD.

The opiate receptor (OR) and endogenous opiate peptides have been implicated as mediators of sexual behavior in laboratory animals and in man. C-11 carfentanil (CAR) was used to measure regional OR binding in 3 normal male volunteers and 4 patients with a history of deviant sexual behavior during a control resting state and following sexual self arousal. Arousal was initiated 10 min. prior to receiving CAR and continued for 15 min thereafter. Activity was measured in the amygdala (AM), caudate (CD), thalamus (TH), and frontal, temporal, cingulate and calcarine cortex (FCX, TCX, CNG, and CCX). Activity in CCX, which contains very few OR, was subtracted from activity in the other regions to obtain estimates of average specific OR binding 15-45 min. after CAR injection. The ratio (R) of OR binding during arousal to that in the control state was then computed. In 6/7 subjects $R \leq 1$ in most regions whereas in 1/7 R was uniformly >1 . The largest individual deviations of R from 1 tended to occur in AM, TH and CNG and ranged from 1.41 to 1.72 and 0.27 to 0.83. Activity was not significantly different 0-6 min. after injection indicating that blood flow and diffusion effects are not producing the observed changes in R at 15-45 min.

These results support the hypothesis that sexual arousal predominantly results in release of endogenous opioids which increase the occupancy of OR ($R < 1$). However, there is evidence for decreased OR occupancy following arousal in some regions ($R > 1$).

No. 619

ASSESSMENT OF D1 AND D2 DOPAMINE RECEPTORS IN LESCH-NYHAN SYNDROME BY POSITRON TOMOGRAPHY. DF Wong, C Braestrup, J Harris, RF Dannals, H Ravert, A Wilson, J Williams, J Links, U Scheffel, L O'Tuama, G Fanaras, H Moser, S Naidu, W Nyhan, HN Wagner, Jr., A Gjedde. Johns Hopkins Medical Inst., Kennedy Inst., Baltimore, MD. UCSD, San Diego CA. Panum Inst. Novo Ind. Copenhagen, Dk

Lesch-Nyhan Syndrome is an X-linked metabolic disorder associated with compulsive self-injury in which there is autopsy evidence of reduced striatal dopamine and its metabolites. Experiments in monkeys suggest that D1 blockade may reduce the self-injury. We have examined D1 and D2 dopamine receptors in the brain of a 21 year old male patient, using C-11 SCH 23390 and C-11 3-N-methylspiperone, respectively.

We have radiolabelled the D1 antagonist SCH 23390 and our animal studies have shown that C-11 SCH 23390 (SCH) is specifically bound to D1 receptors. In vivo rodent binding studies indicated that uptake of SCH was reduced by 77% in caudate by the D1 antagonist cis-flupentixol, but only 6% by the S2 antagonist cinanserin, and 27% by the D2 antagonist haloperidol. Similar blockade was demonstrated in baboon PET studies. The ligand localizes in striatum and dissociates after 90 min. in mice and 50 min. in baboon.

NMSP PET studies were conducted before and after a bone marrow transplant. Both studies showed low D2 binding. A D1 study done concurrently with the 2nd NMSP scan suggested the relative D1/D2 ratio of the rate of binding to the receptors (k_3) maybe as high as 3:1. The D1 ligand equilibrated with the receptor during the scan. Hence receptor density measurements are possible for both ligands. Autopsy studies at this age indicates a 1:1 ratio of D1/D2 receptor densities.

No. 620

IMAGING METASTATIC BRAIN TUMORS USING MONOCLONAL ANTIBODIES. D.V. Woo, C. Koprowski, L.W. Brady, S. Dadparvar, Z. Steplewski*, H. Koprowski*. Hahnemann University and Wistar Institute*, Philadelphia, PA.

The monoclonal antibody, 17-1A, to human colorectal carcinoma antigens is also immunoreactive to metastatic adenocarcinoma. Since it was uncertain whether this antibody would localize in brain metastases, radiolabeled 17-1A was intravenously administered to patients with confirmed metastatic adenocarcinoma of the brain. A bifunctional chelating group, DTPA, was attached to 17-1A, IgG using its cyclic anhydride. Approximately .8-1.0 DTPAs per molecule of IgG were attached. In-111 was then complexed to the DTPA conjugate in citrate buffer. Free uncomplexed In-111 was removed using gel chromatography. Immunoreactivity was determined to be greater than 75% from in vitro binding studies. Patients were initially skin tested and then received intravenously 1.0 millicurie of In-111 labeled antibody containing about 10-20% In-111 DTPA. Imaging was initiated at 4-6 hours postinjection with later images obtained at 24-48 hours. The resulting scans indicated positive In-111 uptake in metastatic tumors from 24 through 48 hours. All tumors in the brain were clearly delineated in multiple spot images and correlated well with CT scanning. Other metastatic sites in the rest of the body were also visualized and confirmed by CT scans. These preliminary results suggest that certain monoclonal antibodies will selectively concentrate in brain tumors after crossing the blood-brain-barrier as demonstrated by imaging.

No. 622

DOES IMP MEASURE CEREBRAL BLOOD FLOW IN ISCHEMIA? J.H. Greenberg, S. Komatsumoto, C. Arost, G.R. Robinson. University of Pennsylvania, Philadelphia, PA.

Although isopropylidoamphetamine (IMP) labeled with I-123 has been suggested as an agent for measuring cerebral blood flow (CBF) and is currently being used in patients in combination with SPECT, its behavior has not been adequately investigated in pathological situations. In a series of rats (n=5) in which the middle cerebral artery (MCA) has been occluded we have compared local CBF using 14-C-iodoantipyrine (IAP) with 123-I IMP uptake utilizing a double label autoradiographic technique. 123-I IMP was injected 30 minutes following MCA occlusion. At variable times up to 30 min later, CBF was measured with IAP. Although CBF calculated using IMP was highly correlated with CBF using IAP in most of the brain tissue, there were regions in which a mismatch occurred. In the ischemic territory, blood flow measured with IAP dropped to 15-20% of control, whereas the corresponding IMP uptake was 40-50% of control. Therefore IMP is an inaccurate measure of local cerebral blood flow in ischemia. Very dramatic mismatches between IMP and IAP were also observed in regions remote from the ischemic tissue, primarily in the white matter where the uptake of IMP was greater than in the surrounding grey matter even though blood flow with IAP showed a 1:3.5 white:grey flow ratio. The uptake mechanism for IMP is presumably different in ischemic tissue as well as in the white matter.

Monday, 3:30-6:00

Exhibit Hall

NEUROLOGY: SPECT

No. 621

BRAIN IMAGING WITH ^{99m}Tc-HMPAO SPECT, CT, and NMR-RESULTS IN EPILEPSY. H.J.Biersack, H.Stefan, K.Reichmann, B.Hünermann, K.Kühnen, A.Bockisch, H.Penin, F.F.Knapp, C.Winkler Institute for Nuclear Medicine, Dpt.of Epileptology, University of Bonn, FRG, and Oak Ridge Nat.Lab., Tennessee, USA

This investigation was undertaken to compare brain SPECT by means of the d,l-isomer of Tc-99m labeled HMPAO with results of CT and NMR in patients (pts) with epilepsy. 18 pts were studied with ECT according to phase II and III protocols. Blood clearance was determined in 12 pts, and urinary excretion in 8 pts. EEG and CT results were available in all pts and NMR in 15 pts. Brain SPECT was performed with a rotating gamma camera 15, 60, and 180 min after iv injection of 10 mCi ^{99m}Tc-HMPAO.

No adverse reactions were observed in any of the pts. There were no significant changes in vital signs, blood count, blood chemistry, and urine analysis before and after injection. Blood clearance showed a rapid decrease (T/2 = 2,5 hrs). Urinary excretion amounted to 20 - 40 % within 24 hrs. The clinical results are summarized as follows:

CT + SPECT normal	CT + SPECT abnormal	CT normal/ SPECT abnormal	CT abnormal/ SPECT normal
4	4	10	0
NMR + SPECT normal	NMR + SPECT abnormal	NMR normal/ SPECT abnormal	NMR abnormal/ SPECT normal
1	10	2	2

In the group of 15 pts who underwent SPECT, CT, and NMR the sensitivity for epileptic foci was: SPECT = 12/15, NMR = 12/15, and CT 4/15. Our data suggest that ^{99m}Tc-HMPAO SPECT and NMR are likewise useful for the evaluation of pts with seizures.

No. 623

ECT BRAIN IMAGING USING Tc-99m-HEXAMETHYL PROPYLENEAMINE OXIME (d,l-HM-PAO); CLINICAL STUDIES. R.A. Holmes, K.W. Logan, W.A. Volkert, A. Singh, W.H. Olive, T.A. Lairmore. Nuclear Medicine Division, University of Missouri, Columbia, MO.

Tc-99m-d,l-HM-PAO, a new radiopharmaceutical developed by Amersham International in collaboration with our laboratory is a lipophilic chelate that efficiently crosses the intact blood-brain-barrier and maintains a high concentration in the brain tissue for an extended period. Its distribution reflects cerebral blood flow and we have studied its ECT imaging characteristics in more than 30 patients with neurologic diseases. Counts for the ECT images were recorded stepwise (64 angles) around the circumference of the head after the IV administration of 20 mCi Tc-99m-d,l-HM-PAO starting at 15 min and repeating the study 180-240 min post-injection. Tomographic images (1.5 cm thick) are reconstructed for transverse coronal and sagittal projections using commercial computer software. The highest regional activity is seen in the grey matter, cerebellum and basal ganglia. Three stroke patients with fluent aphasia demonstrated large focal defects in the right fronto-thalamic (Broca's) area that were not as clearly seen on their x-ray CT's. Two of 7 TIA patients demonstrated focal decreased perfusion at the brain base without concomitant changes on the CT. Three of 25 stroke patients with post-infarction "luxury perfusion" demonstrated greater CT lesion discordance with the hyperperfused area. Like iodoamphetamine a cerebellar medulloblastoma showed fixed reduced tumor uptake. Our results should provide additional impetus for wider application of this agent clinically.

No. 624

DISPARITY BETWEEN CEREBRAL BLOOD FLOW (CBF) AND UPTAKE OF LABELED AMINE PERFUSION AGENTS IN CEREBELLUM. S.C. Jones, H.T. Friel, J.H. Greenberg, D. Lu, C.H. Block, G. Saha, A.R. Furlan, J.R. Little. Cleveland Clinic Foundation, Cleveland, OH and University of Pennsylvania, Philadelphia, PA

This study was performed to investigate the spatial and quantitative relation between CBF and the I-123 labeled amines, isopropylidoamphetamine (IMP) and the diamine, HIPDM.

The brain distribution in rats of I-123 HIPDM (N=5) and I-123 IMP (N=4) was compared to CBF determined with C-14 iodoantipyrine using quantitative double label autoradiography. Forty minutes after a bolus injection of I-123 amine, a CBF study with C-14 IAP was performed. The ratio of CBF between gray and white matter was 4 to 1. In the cortex, thalamus and brain stem, the distribution of the two agents is similar. However, in the cerebellum, the high contrast distribution of the I-123 amines is not related to the CBF pattern and is suggestive of the distribution of aminergic neurons.

The use of the I-123 amines for the investigation of cerebral perfusion with SPECT has rested on the assumption that the distribution of their uptake is proportional to CBF. Both SPECT and techniques using tissue sampling to compare CBF with the uptake of the I-123 amines do not possess the spatial resolution of autoradiography and would not reveal this disparity. This observation emphasizes that the binding mechanism of the I-123 amines is not completely understood.

No. 625

ASSESSMENT OF CEREBRAL PERFUSION RESERVE IN PATIENTS WITH CEREBRO-VASCULAR DISEASE BY SINGLE-PHOTON EMISSION TOMOGRAPHY. W.H.Knapp, R.von Kummer, W.K.Kübler, H.Ostertag. German Research Center and Neurologic Department; University of Heidelberg, Heart Center NRW, Bad Oeynhausen, FRG.

The ratio between cerebral blood flow (CBF) and cerebral blood volume (CBV) determined by positron-emission tomography has been proposed as a parameter for the perfusion reserve in cerebro-vascular disease (CVD), but its assessment with SPECT is not yet established. We have chosen N-isopropyl-(I-123)-p-iodoamphetamine for CBF and Tc-99m erythrocytes for CBV imaging. The distribution of both nuclides was investigated in succession using corrections for the contamination of the Tc-99m tomograms by I-123. The ratio between I-123 and Tc-99m tomograms yielded the CBF/CBV distribution. Quantitation was obtained by side-to-side comparison of both hemispheres and of segments containing the territories affected by CVD. In 16 patients with CVD, CBF of the affected territories was 85±19% (SD) when related to the non-symptomatic contralateral side (=100%). When the regions of interest defined within one slice encompassed the whole affected hemisphere, the average CBF was 95±9%, again related to the non-symptomatic side. The corresponding CBF/CBV data in 15% out of these patients differed significantly ($p < 0.001$) from CBF with 60±32% and 81±16%. In unilateral stenoses > 50% (N=10), segmental CBF averaged 81.1±10.1% and CBV/CBF 49.6±15.5 ($p < 0.001$) relative to the contralateral side. The figures for the hemispheres were 92.8± 5.8 and 75.8±12.6 ($p < 0.001$), respectively. These clinical findings mirror the characteristics of cerebral blood flow autoregulation in decreased arterial perfusion pressure, namely the vasodilation of arteriolar resistance vessels and small veins. They thus substantiate the adequacy of the concept to determine CBF/CBV for the assessment of cerebral perfusion reserve in CVD and of the procedure chosen for imaging this parameter with SPECT.

No. 626

CORRELATIVE STUDIES OF THE BRAIN WITH I-123 IMP-SPECT, MRI AND XCT. T. Momose, J. Nishikawa, N. Kosaka, K. Yoshikawa, T. Ohtake, T. Shimizu, M. Iio. University of Tokyo, Tokyo.

Fourteen patients with a variety of central nervous system disorders were examined with N-Isopropyl I-123 p-Iodoamphetamine (IMP) SPECT, MRI and XCT. SPECT images were obtained using GE 400AC/T and MRI was performed with 0.35 or 1.5 Tesla super-conductive magnet. Regional IMP uptake was determined in 1.2x1.2cm regions of interest and the ratio of each cortical region to mean whole brain IMP uptake was calculated; ratios for frontal, parietal, temporal, occipital, rolandic, thalamic, striate and cerebellar regions.

SPECT was most sensitive for the detection of lesions in all five cases with cerebral infarction. Crossed cerebellar diaschisis was only detected by SPECT in cerebral infarction (2/5), multiple sclerosis (1/1) and Alzheimer's disease (AD) (1/7). In AD patients, MRI and XCT showed cerebral atrophy (3/7) and periventricular change (4/7), whereas SPECT revealed severe cerebral asymmetry (2/7) between right and left hemisphere and decreased activity of several cortical regions; parietal (6/7), frontal (4/7) and temporal (4/7) cortex. These findings suggest that SPECT can detect earlier change of Alzheimer's disease than MRI or XCT. In one case of Creutzfeldt-Jakob disease, SPECT showed diffuse decrease of activity in the cerebral cortex, although MRI and XCT suggested minimal atrophy of the cerebrum.

In conclusion, SPECT appears valuable for the detection of the disturbed perfusion area and remote effect in cerebral infarction and the early focal change in dementia.

No. 627

DETECTION OF rCBF CHANGES IN PARTIAL COMPLEX SEIZURES OR HALLUCINATIONS BY N-ISOPROPYL-(I-123)-p-iodoamphetamine (IMP) SPECT. I. Podreka, B. Mamoli, O. Lesch, E. Suess, D. Wimberger, N. Mayr, Ch. Müller, M. Steiner, L. Deecke. Neurologische Universitätsklinik Wien, Austria.

14 normal volunteers (mean age: 24.9 y), 30 patients with partial complex seizures (mean age: 31.3 years) and 12 patients with acoustic or visual hallucinations (mean age: 41.8 years) were investigated by IMP-SPECT. Studies were performed with occluded eyes and without ear plugs in a silent dim lightened room. 18 ROI's in each hemisphere were drawn on 5 adjacent transversal SPECT slices. For evaluation of relatively hypo- or hyperperfused ROI's a regional index=RI (=ratio between cts/voxel of one ROI and mean cts/voxel of all ROI's) was calculated. If the RI of a ROI exceeded the value of the corresponding normal RI± 2 standard deviation hypo- or hyperperfusion was assumed. Patients with seizures showed in 98.8% relatively hypo- or hyperperfused brain regions compared to the control group, while all patients with hallucinations had abnormal rCBF patterns. Statistical analysis was performed by unidirectional ANOVA and Keuls-Newman test. For both patient groups significantly higher RI's were found in the hippocampus (left $p < 0.001$, right $p < 0.01$) and right basal ganglia. Patients with hallucinations had additionally higher RI's in both inferior occipital regions (left $p < 0.01$, right $p < 0.001$) and significantly lower RI's in both frontal lobes (left $p < 0.01$, right $p < 0.05$). The study shows that in seizure and hallucinating patients rCBF is relatively increased in limbic structures reflecting their importance in the generation of seizures or hallucinations. Since all psychotic patients had hallucinations during IMP-SPECT relatively increased rCBF in the visual cortex can be related to this phenomena.

No. 628

RADIOACTIVE THALLIUM DISTRIBUTION IN THE BRAIN AFTER CSF INJECTION. D.V. Woo, J. Rubertone, J. Emrich. Hahnemann University, Philadelphia, PA.

The cerebral spinal fluid (CSF) which bathes the brain and spinal cord may be used to permit entry of drugs that do not readily cross the blood brain barrier. However, the actual circulation of such exogenous substances via the CSF is uncertain and unpredictable. Although cisternography with radioactive tracers is commonly used to evaluate CSF space, no radioactive drugs designed to be taken up by specific neurons after injection directly into the CSF have been recently studied and used in nuclear medicine procedures. We report preliminary studies which examine the uptake and distribution of selected radioactive cations in the brain and spinal cord after direct intrathecal injection. Radioactive Thallium-201 (Tl-201) was stereotaxically administered into either the lateral or fourth ventricle

of adult rats. From 2 to 6 hours after injection, the brains were lightly fixed, sectioned on a freezing microtome, and apposed to autoradiographic film. The developed autoradiograms of brain sections indicated uptake correlating to specific nuclei. Significant uptake was also observed in the spinal gray matter. Increased uptake was seen in specific nuclear regions of the thalamus, hypothalamus, periaqueductal gray, and deep cerebellar and vestibular nuclei. Movement of tracer throughout the neuropil with time appeared to correlate well to known patterns of CSF circulation. Thallium uptake in specific neurons may reflect CSF flow as well as active transport processes. Therefore, these data suggest that Tl-201 may be useful in delineating specific neuronal function via CSF circulation.

Monday, 3:30-6:00

Exhibit Hall

ONCOLOGY: GENERAL**No. 629**

THE EFFECT OF RADIOTHERAPY ON Tc-99m-HMPAO DISTRIBUTION IN BRAIN TUMORS: INITIAL RESULTS. JW Babich, MA Flower, F Keeling, S Fielding, S Chittenden, L Repetto, A Whitton, VR McCready. The Royal Marsden Hospital, Surrey, England.

Regional cerebral blood flow imaging has been shown to be useful as an aid in the diagnosis of neurological and cerebral vascular disorders. As yet its role in the study of brain tumors is uncertain. Tc-99m-HMPAO (a neutral, lipophilic complex) crosses the blood brain barrier and is fixed in brain tissue proportional to blood flow. We have studied the uptake and distribution of HMPAO in patients with various types of brain tumor, undergoing radiotherapy (RT). 4 patients have been studied and 16 scans performed to date. Each patient received a HMPAO/SPECT scan pre-, mid- and post-RT. X-ray CT scans were also performed and when possible Glucoheptonate(GH)/SPECT scans. All patients received ~ 750MBq Tc-99m-HMPAO per study. Dynamic images were acquired for 4 min. post-injection, followed 10 min. later by a SPECT scan using the GE STARCAM system. For each study brain uptake curves were generated, tumor uptake was studied using ROI analysis and global HMPAO uptake was determined using a thresholding technique to exclude extracerebral activity. 4/5 lesions, verified by CT and exhibiting positive GH uptake, demonstrated decreased HMPAO uptake pre-RT compared with normal brain. Over the course of RT significant changes in HMPAO uptake were noted corresponding to tumor areas and were quantified using ROI analysis. In 1 patient the tumor/normal brain uptake ratio increased from 0.73±0.02 pre-RT to 1.00±0.02 post-RT. Global HMPAO uptake measurements in 2 patients indicate 44±4% increase by the end of RT.

No. 630

PAIRED-STUDY COMPARISON OF N-13 L-VALINE AND L-GLUTAMATE IN HUMAN SARCOMAS. J.R. Bading, A.S. Gelbard, G.B. Magill, P.P. Sordillo, M. Rossleigh, R.S. Benua. Memorial Sloan-Kettering Cancer Center, New York, NY.

Radiolabel uptake by human sarcomas after i.v. injection of N-13 L-glutamate (Glu) reflects tumor viability (Reiman et al., Cancer 1981;48:1976). To investigate specificity of tumor uptake of amino acid nitrogen, 11 patients with sarcomas of soft tissue or bone were studied >4 hr post-prandial by quantitative 2-D imaging both with N-13 L-valine (Val) and Glu, injected about 1 hr apart. Five patients had recurrence; 6 were newly diagnosed. None were being treated at the time. Kinetic studies showed equilibration of tumor activity within 10 min; tumors were imaged at >10 min. Three other patients were studied twice in <2 hr with Val to assess precision of the tumor uptake measurements (including blood flow

variability). The mean (±sd) paired-study variation was 5(±4)%; hence same-session differences >10% were deemed significant. In patients studied with both compounds, N-13 uptake was greater from Val in 5, greater from Glu in 2, and not significantly different in 4. Differences were as large as 50% and not accountable by tissue background. No relationship with histologic type or prior treatment was seen. Venous sampling in 2 patients and "arterialized" (heated hand) sampling in 2 normal subjects consistently showed N-13 to be cleared more rapidly with Glu than Val. Thus, in a situation of constant flow, the variation seen among individual tumors implies that relative N-13 uptake from Val and Glu depends on processes (transport and/or metabolism) intrinsic to the tumors, different for the two amino acids, and different among individual tumors. Hence use of more than one amino acid can add information about tumor function.

No. 631

Sr-89 THERAPY:- STRONTIUM KINETICS IN METASTATIC BONE DISEASE. G.M.Blake, M.A.Zivanovic, A.J.McEwan & D.M.Ackery. Southampton General Hospital, Southampton, U.K.

Strontium kinetics were investigated in a group of 14 patients receiving Sr-89 palliation for metastatic bone disease secondary to prostatic malignancy.

Using Sr-85 as a tracer, whole body strontium retention was monitored for a three month period following Sr-89 administration, and at 90 days was found to vary from 11 to 88 percent and to correlate closely with the fraction of the skeleton showing scintigraphic evidence of osteoblastic metastatic involvement. Strontium renal plasma clearance varied from 1.6 to 11.6 litres/day, and was significantly reduced compared with normal controls due to increased tubular reabsorption associated with the disturbance of calcium homeostasis.

Gamma camera studies of strontium turnover in individual metastases gave retention curves that typically rose to a plateau at 10 days after therapy and then decreased very slowly. In contrast, retention curves for adjacent normal trabecular bone showed more rapid turnover, peaking at 1 day and subsequently decreasing following a power law function in time with index -0.2. Preliminary estimates of absorbed dose to spinal metastases following Sr-89 therapy administered at 2.2 MBq/kg body weight gave values between 1000 and 3000 cGy, with dose depending on the total extent of skeletal involvement and strontium renal plasma clearance amongst other factors.

No. 632

GALLIUM TUMOR SCANNING: HOW MANY DAYS BETWEEN INJECTION AND IMAGING? M.B. Brachman, L. Ramanna, D.E. Tanasescu, and A.D. Waxman. Cedars-Sinai Medical Center, Los Angeles, CA.

The purpose of this study was to determine the "ideal" time between gallium injection (inj) and imaging in patients (pts) with malignant tumors. Imaging, with computer acquisition, was performed on at least two different days in a total of 17 pts. The pts were scanned an average of 2.9 times. Analog images were based on a 500,000 count technique centered over the chest. Computer acquisitions were all for a set time of 6 minutes. Regions of interest were selected over lesions and adjacent background areas. Target to non-target ratios (T/NT) were measured. The T/NT were normalized to the two day post inj values.

In 5 of 12 pts the T/NT at five days was greater than at three days. The T/NT was greater at six days than at two days in eight of eight pts. We grouped two and three day measurements and compared them to four and five day, as well as six and seven day measurements. Results are shown in the following table.

Days	2&3	4&5	6&7
Lesions Measured	32	21	18
Average T/NT	2.00	2.04	2.24

There was a 10% increase in contrast between baseline and late imaging, which was significant at the .05 level. Using both subjective evaluation of images and measurement of T/NT, we have found that many tumors are more clearly visualized beyond three days post inj. Late imaging may not be practical as a routine, but should be considered in selected cases.

No. 633

CORRELATION OF GALLIUM UPTAKE AND DEGREE OF MALIGNANCY IN NON-HODGKIN'S LYMPHOMA. D.C.P. Chen, G.L. Hung, A. Levine, and M.E. Siegel. LAC/USC Medical Center, Los Angeles, CA.

The gallium (Ga) uptake in the Non-Hodgkin's Lymphoma (NHL) is variable. With the new pathologic classification of NHL, the degree of malignancy can be determined. We performed a retrospective study to investigate the relationship between the grade of Ga uptake and degree of malignancy of NHL.

47 patients (29 male, 18 female, age range: 16-77 with mean age 44) with NHL had total body Ga scans 24-48, and/or 72 hrs. post IV injection of 3 mCi of Ga-67 citrate. The Ga activity was classified as grade 0: normal, grade 1: < sternum activity, grade 2: equal to sternum activity, grade 3: < liver activity, and grade 4: ≥ liver activity. Function classification of these 47 NHL shows 25 high degree of malignancy, 5 medium degree, 12 low degree, and 5 miscellaneous.

In the high degree NHL, 20/25 (80%) had grade 4 gallium uptake, 2 (8%) had grade 3, 2 (8%) had grade 2, and 1 (4%) had normal activity. In contrast, low grade uptake (grade 0 through 2) was noted in 8/12 patients (75%) with low degree malignancy. Using the criteria of Ga activity above grade 2 as high uptake, we found that the positive predictive value of high Ga uptake for NHL classified as highly malignant was 85% and negative predictive value for low degree NHL is 73%.

In conclusion based on this preliminary data, there appears to be good correlation between Ga uptake and degree of malignancy of NHL. Further investigation is progressing to evaluate the potential clinical application of this finding.

No. 634

RADIONUCLIDE ASSESSMENT OF HEPATIC ARTERY INFUSION PUMP (HAIP) FUNCTION. A.C. Civelek, N.D. LaFrance, L. Grochow, P. Cole. The Johns Hopkins Medical Institutions. Baltimore, MD

Metastatic carcinoma commonly involves the liver which has spurred the development of selective intra-hepatic artery chemotherapy. We studied 28 consecutive patients referred for routine evaluation of hepatic artery infusion pump function. Most of the patients had no pre-test diagnosis of pump dysfunction or aberrant catheter placement.

One to three mCi of 99m Tc microspheres were administered per pump port, via trans abdominal injection, after the sterile cleansing of the abdominal skin site. A dedicated camera/computer acquisition began immediately post injection for 60 seconds (3 second frames) followed by an immediate hepatic view (500K counts). Next, multiple abdominal, thoracic and pelvic images with appropriate markers were obtained. We found 15 out of 57 studies in 28 patients were abnormal. These abnormalities included unexpected catheter migration, anomalous anatomy, arterial thrombosis, pump and / or catheter malfunction and other organ perfusion.

We conclude that routine hepatic artery infusion studies should 1) be done on every hepatic artery catheter to confirm proper placement and 2) should be

performed serially in patients to identify potential problems. These studies 1) discovered catheter or pump related abnormalities in 15 of 57 studies 2) can be performed simply and safely in a routine nuclear medicine laboratory and 3) can be done with 99m Tc microspheres as well as MAA.

No. 635

POTENTIAL USE OF C-11 LABELED ALPHA-AMINOISOBUTYRIC ACID (AIB) FOR STUDYING ALTERATIONS IN AMINO ACID UPTAKE IN TUMOR ASSOCIATED CACHEXIA. P.S. Conti, H.F. Starnes, E.L. Kleinert, and M.F. Brennan. Memorial Sloan-Kettering Cancer Center, New York, N.Y. 10021.

Alterations in host metabolism associated with progressive tumor growth may be attributed to anorexia or some unknown direct effect on the host tissues not related to reduced dietary intake. Changes in amino acid uptake in tissues of rats bearing the Dunning R3327G prostate tumor from 2-5 weeks post-implantation, in non-tumor bearing rats starved for 7 days, and in fed control rats were studied with C-14 AIB at 45 minutes after injection (6 rats per group):

	MEAN RELATIVE CONCENTRATION (RC)*					Starved
	Control	2wks	3wks	4wks	5wks	
LIVER	1.96	2.80	2.14	2.57	3.49	14.4
MUSCLE	0.32	0.45	0.43	0.36	0.34	0.15
BLOOD	0.64	0.93	0.87	0.73	0.82	0.54
TUMOR	-	1.55	1.35	0.96	1.09	-

*RC = dpm found/gm tissue ÷ dpm injected/gm animal mass
During the period 2-5 weeks, uptake of AIB increased in liver and decreased in muscle and viable tumor tissue. Between 5-6 weeks animal mortality approached 50% with tumors accounting for 25-33% of total body weight. The starved animals showed significantly higher levels of AIB in liver tissue compared to 5 week rats (p<0.005) and controls (p<0.001). The RC of AIB in the muscle of starved rats was significantly lower compared to 5 week tumor rats (p<0.001). Carbon-11 labeled amino acids such as C-11 AIB may be useful as *in vivo* tracers of amino acid transport in tumor associated cachexia using positron emission tomography.

No. 636

TC-99m HMPAO AS A TUMOR AND TISSUE BLOOD FLOW AGENT. P.A.G. Hammersley and V.R. McCready, Royal Marsden Hospital, Sutton, U.K.

The lipophilic radiopharmaceutical, Tc-99m hexamethylpropyleneamine oxime (HMPAO) has been introduced as an agent for imaging regional cerebral blood flow (1). We have investigated the use of this compound as an indicator of blood flow to subcutaneously implanted tumors and other tissues in mice. The distribution of Tc-99m HMPAO has been compared with that of Rb-86, an established marker of blood flow.

There was a good correlation (P 0.001) between the concentrations of Tc-99m and Rb-86 in tumor (sarcoma PM), muscle, spleen and small intestine. This correlation was maintained when the blood flow was altered by propranolol and anaesthetics. Uptakes $\bar{x} \pm SD$ (n=6) in tumor: Tc 2.19 \pm .11, Rb 2.59 \pm .31; muscle Tc 1.37 \pm .44, Rb 1.44 \pm .40. After propranolol (10mg/kg), tumor Tc 2.64 \pm .27, Rb 3.14 \pm .60; muscle Tc 1.07 \pm .24, Rb 1.15 \pm .41. Thus, the effect of propranolol is to increase both Tc and Rb in tumor by 21% with a concomitant reduction in muscle of 21%.

We conclude that Tc-99m HMPAO may be useful as a general indicator of blood flow for tumors as well as normal tissues.

Reference. (1) Nowotnik DP et al. Nucl Med Comm 6: 499-506, 1985

No. 637

GALLIUM-67 SCINTIGRAPHY IN GARDNER'S SYNDROME. R. Hardoff, D. Ben-Dov, and A. Front. Lady Davis Carmel Hospital, Haifa, Israel.

Gardner's syndrome was described in 1953 as a disease entity associating familial polyposis with extracolonic manifestations. The latter consists of cutaneous and subcutaneous lesions, desmoid tumors, as well as osteomas and dental abnormalities. Desmoid tumors differ from most fibrous growth by their tendency to infiltrate into surrounding tissues, therefore difficult to treat surgically or medically. We used GA-67 scintigraphy as an additional imaging modality in patients with Gardner's syndrome in order to evaluate its contribution to the management of these patients. Their extracolonic manifestations consisted of desmoid tumors, small bowel polyps and skull osteomas. Four patients were considered to be clinically disease-free. Two of them had a normal GA-67 scintigraphy and two patients demonstrated abnormal uptake. One of them had an abdominal uptake which was subsequently found to be a desmoid tumor on an ultrasound study, and the second patient showed bilateral diffuse maxillary and mandibular uptake, which was thought to be due to osteomas, in spite of normal skull radiology. In two patients who had known desmoid tumors, an additional abnormality was found on GA-67 scintigraphy. One patient with a giant abdominal desmoid tumor medically treated had three consecutive C-T and GA-67 studies, which demonstrated a decrease in tumor size and uptake. It is concluded that GA-67 uptake can differentiate between viable tumor cells and post treatment fibrosis, and is therefore a useful adjunct to the clinical and radiological follow-up of patients with Gardner's syndrome.

No. 638

IMMUNOSCIINTIGRAPHY (IS) OF MALIGNANT TUMORS. INTRA-INDIVIDUAL COMPARISON OF EMISSION COMPUTER TOMOGRAPHY (ECT) AND PLANAR SCINTIGRAPHY (PS). J. Happ, R.P. Baum, F.D. Maul, I. Loose-Wagenbach, T. Schmitt-Bylandt, and G. Hör. Dept. of Radiology, University of Frankfurt, and Dept. of Radiology, St. Mary's Hospital, Frankfurt, FRG

I-131 labeled monoclonal antibodies (MAB) or its fragments are widely used for planar IS and high sensitivity is reported. High quality of images is obtained with I-125 labeled MAB or its fragments and ECT. In the present paper, sensitivity of PS and ECT was compared intraindividually with the use of I-131 MAB fragments.

Twelve patients with malignant tumors or its metastases (colorectal carcinoma (CR) (n=4), ovarian carcinoma (OV) (n=4), breast cancer (MA) (n=2), and lung cancer (LU) (n=2) were submitted to ECT gamma camera (Apex, Elscint) IS as well as to PS (Searle, LFOV) 2 (ECT) or about 5 (Ps) days after the administration of I-131 labeled F(ab')₂ fragments of MAB ("cocktail" of anti-CEA and anti-²CA19-9 for CR and LU, anti-CA125 for OV and MA; tracers purchased by Isotopen Diagnostik CIS). For anatomical land marking double-nuclide double-compound scintigraphy was performed for simultaneous imaging of RES, bone and urinary tract.

Planar IS was positive in all patients whereas IS with ECT was positive in 5 patients, only. In 1 case, marked paravesical tracer accumulation was found by ECT while PS could not clearly differentiate between intra- and extravesical tracer. Thus, with I-131 labeled MAB fragments, ECT gives lower sensitivity but has an advantage in localizing paravesical tumor.

No. 639

CLINICAL ASSESSMENT OF TECHNETIUM-99m DMSA ABNORMAL UPTAKE BY MALIGNANT TUMORS. S. Kosuda, T. Gokan, K.

Tamura, A. Kubo, S. Hashimoto. Okura National Hospital and Keio University Hospital, Tokyo, Japan.

In our concern for the diagnostic study of malignant tumors by Technetium-99m dimercaptosuccinic acid (Tc-99m DMSA), tumor scanning by Tc-99m DMSA was examined in 39 patients (50 lesions) with miscellaneous malignant tumors. All of the patients (23 males, 16 females) had histologically or cytologically proven diagnoses. The median age of the patient population was 64.6 (range, 29-89). The patients were scanned 2 to 6 hr following i.v. administration of 25 mCi (925 MBq) of Tc-99m DMSA. Six out of 39 cases had four-phase study, including radionuclide angiogram, blood-pool image, delayed 2-6 and 24 hr images. Further, in 33 out of 39 cases, we performed sequential gallium-67 citrate scintigraphy which was compared with Tc-99m DMSA tumor imaging.

Besides localization of Tc-99m DMSA within the normal renal cortex, Tc-99m DMSA accumulated in 29 of 50 malignant tumors (58%). The true positive rate of Tc-99m DMSA was lower than that of Ga-67 citrate, 84% (28/33). Ga-67 citrate more avidly accumulated than Tc-99m DMSA, except one case with ovarian cancer. The visualization of malignant tumors appeared to be much better in the late Tc-99m DMSA image (3-6 hr).

In conclusion, our findings suggest that persistence of activity in the tumors cannot be ascribed to increased vascularity alone, but Tc-99m DMSA possibly has affinity for malignant tumor cells. The details of tumor affinity mechanism of Tc-99m DMSA still must be studied.

No. 640

UNILATERAL BONE AGENT ACCUMULATION IN THE THORAX IN LUNG CANCER. Howard A. Levy and Chan H. Park. Thomas Jefferson University Hospital, Philadelphia, PA.

Soft tissue accumulation of bone imaging agents has been reported in lung cancer and in malignant effusions, but the incidence of this finding is unknown. The bone scans of 130 patients with proven lung cancer and available clinical and laboratory data were studied. 59/130, or 45% of these patients showed unilateral thoracic soft tissue accumulation (UTS) of MDP, and in every case, this was in the hemithorax in which the tumor was located. The remaining 70/130 or 55%, did not have UTS. There was no significant difference between the two groups as to age, sex, tumor cell type, use of chemotherapy, or performance of a thoracotomy. Pleural effusion (PEF) noted on chest radiographs or computed tomography was seen in 41% of patients with UTS, but only in 18% of those without this finding. 46/59, or 78% of the patients with UTS had received Radiation Therapy (RT) prior to the bone scan, compared to 6/71, or 8% who received RT but did not have UTS. 8/59, or 14% of patients demonstrated UTS but had not received RT, while 57/70, or 80% did not have UTS and were not treated with RT. The bone scans of 14 patients showed no UTS prior to RT, but did so after RT. 5/59, or 8.5% of patients with UTS had received RT to other parts of the body but not to the lung, as compared to 7/71, or 10% of those without UTS who received the same therapy. Of 47 patients with UTS who received RT, there were about as many patients without PEF, 27, as those with this finding 20. UTS was seen in almost half of treated lung cancer patients, most commonly in patients with prior RT to the tumor.

No. 641

GALLIUM IMAGING IN OAT CELL BRONCHIAL CARCINOMA. R. Milroy, M L Smith, S W Banham and J H McKillop. Departments of Respiratory Medicine and Nuclear Medicine, Royal Infirmary, Glasgow, Scotland.

Gallium scanning has been extensively investigated as a means of pre-operative mediastinal staging in lung cancer. However, there have been few studies of Gallium scanning specifically in oat cell bronchial carcinoma.

We have studied 39 such patients.

All patients underwent Gallium scanning as part of pretreatment staging. Gallium scan was positive for primary tumour in 38 patients (97%) and suggested mediastinal spread in 31 patients (79%). In 20 patients (all with positive pretreatment scan) Gallium scan was repeated after induction chemotherapy (6 complete responders (CR), 8 good partial responders (good PR), 3 modest partial responders (modest PR) and 3 non-responders). Following chemotherapy Gallium scan returned to normal in all 6 CRs and in 7 of 8 good PRs. In 2 of 3 modest PRs and in all 3 non-responders there was no improvement in scan appearances following chemotherapy. Thus Gallium scan changes following chemotherapy correlate well with response to chemotherapy as assessed by conventional measures (restaging radiology and bronchoscopy). In 5 patients Gallium scan has been repeated 3 monthly up to 1 year. In 3 patients the scan remains negative and these patients continue in remission. In 2 cases the scan indicated relapse confirmed clinically.

Gallium is taken up avidly by oat cell tumours. Gallium activity appears to mirror clinical disease activity and may prove useful in the evaluation of response to chemotherapy.

No. 642

IMAGING OF SOFT TISSUE TUMORS WITH TECHNETIUM(V)-99m DIMERCAPTOSUCCINIC ACID, SECOND REPORT. H. Ohta, Tamatsuo Hospital, Kobe, Japan, K. Endo, H. Sakahara, T. Nakashima, K. Torizuka, Kyoto University, Faculty of Medicine, Kyoto, Japan.

We have previously reported the usefulness of Tc(V)-99m dimercaptosuccinic acid (Tc(V)-DMS) in the diagnosis of soft tissue tumors. But the amount of the cases is not so large and no case is followed. This time, we examined 150 cases (64 malignant cases and 86 benign cases) and 15 cases were followed with Tc(V)-DMS. And in some cases, time course study was also performed.

Tc(V)-DMS was found to have a sensitivity of 94% for malignant tumors and a specificity of 70%. Therefore the accuracy of Tc(V)-DMS scintigrams in soft tissue tumors was 80%. False-negative 4 cases occurred in clear cell sarcoma, hemangiosarcoma and 2 cases of malignant fibrous histiocytoma, and failure to image could be due to the small size of tumors. False-positive cases were observed in some inflammatory lesions, operation scar, neurogenic tumors and hemangioma. And whether the recurrence of the tumor is present or not was correctly diagnosed in 12 cases. 3 misdiagnosis cases were false positive uptake to the operation scar.

Usually we take scintigrams 120 min after i.v. administration to decrease the background radioactivity. But only 30 min after i.v. administration, we could obtain good images as clear as those of 120 min and enough to make correct diagnosis.

Tc(V)-DMS scintigraphy is early and cheap examination and would be surely useful in the diagnosis and follow-up of the soft tissue tumors.

No. 643

THALLIUM-201 KINETICS IN MALIGNANT TUMOURS.

A. Sahweil, M. El-Sayed, G. Ziada, F. Al-Huda, L. Mobarak, Y.T. Omar, H.M. Abdel-Dayem, J.H. McKillop. Depts. of Nucl. Medicine and Radiation Oncology, Ministry of Public Health and Kuwait University, and Glasgow University.

Tl-201 uptake in malignant tumors has been previously reported but kinetics were not carefully investigated. The aim of this study is to find the best time for imaging malignant tumours (TRS) after I.V. injection of 2 mCi of Tl-201 by determining the time of the highest Tl uptake and best TR to background (BKGD) ratio. Forty six patients with malignant TRS [Ca Breast (18), Ca lung (18) and malignant lymphoma (10)]

were examined. After I.V. injection of 2 mCi Tl-201 while under a LFOV gamma camera two dynamic acquisitions were recorded. The first was every 5 sec. for 5 min. and the second followed immediately every minute for 60 min. The FOV covered the TR area and the heart. Normalised time activity curves over the TR, surrounding BKGD area and the myocardium were generated for both dynamic acquisitions. TR curve was subtracted by BKGD curve in order to determine the TR to BKGD ratio. Forty four patients had two positive Tl uptake (18 Ca breast, 17 Ca lungs and 9 lymphoma) only two patients had true negative Tl uptake (1 lung and 1 lymphoma). The max. TR uptake and the best TR/BKGD ratio was obtained at $13m + 2.5 m$ in Ca breast, $17.5 + 2.5m$ in lymphoma and $18.8 + 2.2$ in lymphoma. This study indicates that an average waiting period of 15 m is needed after I.V. Tl injection for imaging malignant tumours. This observation suggests that the mechanism of Tl uptake in malignant lesions is similar to the myocardium.

No. 644

DEVELOPMENT OF C-11 THYMIDINE AS A PET IMAGING AGENT: BIOCHEMISTRY OF ITS SYNTHESIS, DEGRADATION, AND REUTILIZATION. A.F. Shields, R.C. Quackenbush, D.V. Coonrod, J.M. Link, K.A. Krohn, M.M. Graham, and T.K. Lewellen. Fred Hutchinson Cancer Center and University of Washington, Seattle, WA.

The interpretation of images obtained using thymidine (TdR) labeled with C-11 will require a detailed knowledge of the biochemistry of TdR utilization. The first problem is that cells may utilize either endogenously synthesized or exogenously supplied TdR. We measured these two sources in a number of mammalian cell lines, tissues and tumors by incubating them in the presence of the TdR analog H-3-bromodeoxyuridine (BUdR). After extraction of the DNA the degree of substitution of the TdR by BUdR was determined on density gradients. All the cell lines and tissues tested utilized both TdR sources to a similar extent. With this information the effective specific activity of intracellular TdR can be calculated.

Reutilization of TdR is important since TdR released from the DNA of dead cells may be taken up and compete with labeled TdR. Previous investigators have estimated the rate of reutilization of TdR as up to 60%, by comparing the rate of loss of H-3-TdR to the TdR analog I-125-iododeoxyuridine (IUdR) (Myers et al., Cell Tiss. Kinetics 9:215, 1976). Our data indicates that IUdR is being deiodinated in vivo giving spurious reutilization rates. 6-H-3-IUdR has similar retention to C-14-TdR indicating that little reutilization is occurring. This will greatly simplify the modeling of TdR metabolism.

Finally, we have synthesized C-11-methyl-TdR and using BaF probes in coincidence have measured its uptake in exteriorized rat intestine. This uptake was compared with H-3- and C-14-methyl-labeled-TdR. As TdR was degraded there was preferential retention of the methyl carbon, probably in proteins. This previously unrecognized problem will need further study.

No. 645

I-123-IMP AS A NEW TUMOR AFFINITY AGENT FOR MALIGNANT TUMOR. N.Watanabe, K.Yokoyama, T.Aburano, S.Kawabata, K.Mukai, H.Ishida, H.Sumiya, H.Seki, H.Matsuda, N.Tonami, and K.Hisada. Kanazawa University, Kanazawa, Japan.

It is reported that N-isopropyl-p-[I-123]-iodoamphetamine (IMP) is incorporated into melanocyte producing melanin. In our institution, four out of eight patients with malignant melanoma were clearly visualized at 24 hours after injection of 0.5-1 mCi of I-123 IMP. The purpose of this study was to evaluate the specificity of I-123 IMP in the diagnosis of malignant melanoma, using animal models.

As animal models of tumor, B-16 melanoma, Lewis lung cancer, Hepatoma Ah109A, Ehrlich ascites tumor and Yoshida sarcoma were used. And as an inflammation model the drug-induced abscess was used. Serial images were obtained at 6, 12 and 24 hours following IV injection of 0.1 mCi of IMP. For biodistribution, mice beared with

B-16 melanoma and Lewis lung cancer were sacrificed periodically. The tumor and other organs were assayed for radioactivity. As a result, the tumor tissues of B-16 melanoma and Lewis lung cancer were clearly visualized at 12 hours after injection. On the other hand, the tumor tissues of other three models were not well visualized. And the turpentine oil-induced abscess also showed good visualization. The mean tumor to blood ratio of B-16 melanoma and that of Lewis lung cancer at 12 hours after injection were 9.8 and 13.3 respectively.

In conclusion, our data suggest that I-123-IMP may not be a specific agent for the diagnosis of malignant melanoma, although I-123-IMP is useful to localize the metastatic as well as primary lesion of melanoma.

No. 646

Tc-99m ANTIMONY SULFIDE COLLOID (SbSC) LYMPHOSCINTIGRAPHY OF THE PROSTATE BY DIRECT TRANSRECTAL INJECTION. L.S. Zuckier, M. Finkelstein, P. Stone, S.Z. Freed, R. Bard, M.D. Blafox and L.M. Freeman. Montefiore Hospital Medical Center / Albert Einstein College of Medicine, Bronx N.Y.

Bilateral pelvic lymphadenectomy, utilized in the staging and treatment of carcinoma of the prostate, is an extensive procedure with significant morbidity. Unilateral dissection would significantly reduce this morbidity if clinically justified. Lymphatic drainage of the prostate gland was studied to delineate drainage routes after direct prostate lobe injections.

8 patients with aspiration-biopsy proven or clinically suspected prostate carcinoma were studied. Tc-99m SbSC (0.25 mCi) was administered directly into the prostate by Franzen needle via a transrectal approach. Injection was directed into an involved lobe in all 8 subjects. A contralateral injection was additionally performed in 1 patient at a subsequent date. Anger-camera imaging with a LEAP collimator was performed at 1 and 4 hours in anterior, posterior and lateral projections. In 1 patient injection was unsuccessful (having entered the intraprostatic venous plexus). Drainage in 4 studies was confined to the ipsilateral chain of lymph nodes, in 3 studies was bilateral and in 1 patient only contralateral nodes were imaged.

These studies with direct intraprostatic injection in patients with prostatic carcinoma suggest that lymphatic drainage may be ipsilateral, contralateral or bilateral and cannot be predicted from the site of tumor. This should be considered in the determination of appropriate staging and treatment of patients with this condition.

Monday, 3:30-6:00

Exhibit Hall

PEDIATRICS**No. 647**

SCINTIGRAPHY IN GASTROINTESTINAL BLEEDING IN THE PEDIATRIC POPULATION. T.R. Hall, J.H. Miller. (Childrens Hospital of Los Angeles, Los Angeles, CA), J.R. Sty (Milwaukee Childrens Hospital, Milwaukee, MI)

Gastrointestinal (GI) bleeding in the pediatric population is a common problem in chronically ill patients. A total of 29 patients with GI bleeding were studied by scintigraphy using Technetium (Tc)-99m labeled red blood cells (RBC) or sulfur colloid at two major pediatric medical centers. The age range was from three weeks old to 20 years old with an equal sex distribution. Of the 19 patients studied with the labeled red cells using an in vitro labeling technique, evidence of GI bleeding was documented scintigraphically in 15 of the patients. Tc-99m labeled sulfur colloid scans in the remaining ten

patients were positive for GI bleeding in six of the cases. A variety of bleeding abnormalities were detected by scintigraphy including stress and stomal ulcers, erosive gastritis, a duodenal hemangioma, bleeding esophageal and duodenal varices, and a case of retroperitoneal hemangioma. Both Tc-99m labeled RBC and sulfur colloid are equally sensitive for the detection of active bleeding. However, Tc-99m labeled RBCs offer the advantage of detection of GI bleeding without competition from the liver and spleen and delayed imaging up to 18-24 hours following initiation of the study. We will illustrate the ease of performance and the value of this procedure in children, which makes this the method of choice for initial examination of older children with acute GI bleeding.

No. 648

ANGULAR DEFORMITY OF THE LOWER EXTREMITY: EVALUATION BY BONE SCINTIGRAPHY. H.T. Harcke, G.A. Mandell, C.A. Sharkey, L.A. Cooley. A.I. duPont Institute, Wilmington, DE.

Angular deformity of an extremity is known to occur following trauma or infection near the growth plate. It is hypothesized that this results from alteration of plate function. Bone-seeking tracers, which actively localize in the physis of the immature skeleton, accurately reflect the physiologic status of the plate and should be of assistance in assessing deformity.

The two- or three-phase bone scintigrams of 16 patients with growth plate abnormalities were analyzed for patterns of physal uptake. Patients ranged in age from 4-15 years. Etiologies included fracture (7), surgery (4), infection (3), and other (2). In 11/16, there was a clinically significant angular deformity: varus (6), valgus (5). All 6 patients with varus deformity had physal activity in the involved bone which was appreciably greater in the lateral aspect of the plate than in the medial aspect. The reverse pattern was observed in 4/5 patients with valgus deformity, where medial plate activity exceeded lateral activity. In 5 patients with decreased activity that was symmetric across the plate, there was shortening of the extremity without angulation.

When growth plates are affected by trauma or infection, scintigraphy may be helpful in predicting the eventual outcome. Specific patterns of asymmetry were observed to correlate closely with varus and valgus deformity.

No. 649

THE USE OF GLUCAGON TO IMPROVE Tc-99m-PERTECHNETATE (TcP) ABDOMINAL SCINTIGRAPHY FOR ECTOPIC GASTRIC MUCOSA: CLINICAL EXPERIENCE. G.N. Sfakianakis, A. Gentili, D.M. Buckner, and C. Oiticica. University of Miami School of Medicine, Miami, Florida.

Intravenous (iv) or intramuscular (im) injection of glucagon has an inhibitory effect on gastric wall motion and delays gastric emptying. TcP abdominal scintigraphy for the diagnosis of ectopic gastric mucosa is positive when focal activity appears outside the stomach but gastric content could either cover true abnormalities or produce false positive images. It has been shown that glucagon administration in dogs with experimental ectopic gastric mucosa improved the results of scintigraphy mainly by keeping in the stomach the gastric contents which were rich in TcP.

Glucagon was given iv or im to 21 patients immediately before injection of TcP. Comparing with 19 patients without glucagon an improvement was found (duodenal or jejunal activity was found in 16/19 without and in 12/21 after

glucagon). Although 2 mg were more effective than 1 mg of glucagon appearance of gastric contents in the jejunum was still evident in more than 1/2 of the patients about 40 min from the TcP injection. In 7 patients in whom 1 mg of glucagon (0.5 mg in infants) was injected before and an equal amount at 30 min after the TcP no duodenal or jejunal activity from gastric contents was observed.

We suggest the following protocol as the most effective in keeping the intestine empty of gastric contents: two injections (im or iv) of glucagon (0.5-1mg) one before and the second at 30 min after the injection of TcP.

Monday, 3:30-6:00

Exhibit Hall

PERIPHERAL VASCULAR

No. 650

DEMONSTRATION OF DIFFERENT MUSCLE BLOOD FLOW RESPONSE TO EXERCISE BETWEEN ACTIVE AND RETIRED ATHLETES BY Xe-133 SINGLE DOSE MULTI-STEP METHOD (SDMM). H.Bunko, M.Seto, J.Taki, I.Nanbu, Y.Shiire, K.Nakajima, N.Tonami, K.Hisada, Kanazawa University Hospital, Kanazawa, Japan.

Purpose of this study is to evaluate the difference of muscle blood flow (MBF) response to static and dynamic exercise (Ex) between active (ACT) and retired (RET) athletes by Xe-133 single dose multi-step method (SDMM) which has been developed and reported by us. MBF response of bilateral leg muscles (vastus lateralis [VLM], adductor magnus [AMM] and gastrocnemius [GCM]) are evaluated in 5 young rugby players (2 ACT and 3RET) with single dose of Xe-133 (1-2 mCi/site) and following sequence of study: rest (R1)- static Ex (Ex1)- rest (R2)- dynamic Ex (Ex2)- rest (R3). Every 5 sec. data are acquired for 2.5 min. during R1, R2 and R3 using large field-of-view gamma camera interfaced to a computer. Squatting is used as Ex and continued for 1.5 min. for both Ex1 and Ex2. MBF at R1, Ex1, R2, Ex2 and R3 are calculated by SDMM. There is no significant difference between left and right leg MBF in all muscles both at rest and during Ex. Dynamic Ex (Ex2) induced higher MBF in all muscles than static Ex (Ex1). MBF after static Ex (R2) returned to R1 level in AMM and GCM in both ACT and RET, however MBF in VLM, which is the most stressed muscle, at R2 is higher in RET than ACT (mean MBF: 22.8 v.s. 1.6 ml/min/100g, p<0.005). Although MBF after dynamic Ex (R3) remains high in VLM in both ACT and RET, MBF is higher in RET than ACT (mean MBF : 17.2 v.s. 12.5 ml/min/100g, p<0.1). Teses results indicate low MBF reserve in RET. In conclusion, patterns of MBF response on various Ex evaluated by SDMM is a good indicator of MBF reserve. Continuous training is likely to be important in maintaining MBF reserve on Ex.

No. 651

LEG MUSCLE PERFUSION STUDY USING Tl-201 SINGLE PHOTON EMISSION COMPUTED TOMOGRAPHY(SPECT). M.Oshima, T.Yano, N.Nishikimi, S.Sionoya, H.Akanabe and S.Sakuma. University of Nagoya Medical School, Nagoya, Japan.

The purpose of this study is to evaluate leg muscle perfusion with Tl-201 SPECT. Twenty-three patients with peripheral arterial disease underwent this examination. A cuff was applied above the knee bilaterally and was inflated to 50 mmHg above the brachial systolic pressure. During deflation of the cuff, 3 mCi of Tl-201 was injected intravenously. The lower leg SPECT imaging and whole body imaging were performed by rotating dual type digital gamma cameras(Toshiba GCA-70A) with on-line minicomputer. Transverse images of leg muscle were compared with clinical symptoms and arteriographic findings. For quantitative analysis, each slice counts of lower

leg were normalized by whole body counts.

Results were as follows; 1) Tl-201 SPECT perfusion image of lower leg was obtained satisfactory, 2) SPECT image can be divided into anterior tibial muscle and posterior tibial muscle component, 3) Six out of 8 legs which showed obstructive lesions with adequate collateralization demonstrated normal SPECT image, and 4) Ten out of 13 legs demonstrated abnormal defects correspond with the distribution of arteriograms. In conclusion, SPECT perfusion distribution with quantitative analysis was correlated with arteriographic findings and clinical symptoms.

No. 652

LOWER LIMB PERFUSION WITH 201-THALLIUM BEFORE AND AFTER RECONSTRUCTIVE VASCULAR SURGERY. C.W.J. Schiepers and P.W. Leopold, Albany Medical Center, Albany, New York

Numerous techniques have been used to study lower limb perfusion. Siegel derived an excellent predictive index of healing potential of ulcers. However, timing of reconstructive surgery and changes in perfusion have not been studied extensively. Reconstructive surgery was indicated for limb salvage and consisted of femoral-distal bypass. Tissue perfusion was studied with thallos chloride (55MBq), pre and post-op. Dynamic imaging of the initial phase (build up) and static imaging at equilibrium of calfs, ankles and feet, and as a reference, myocardium and left upper arm, were performed. Five pts were studied, status and results for the affected limb are summarized in the table: age, sex, ankle-to-brachial index (ABI) and pulse volume recording (PVR).

Pt	age	ABI		PVR		c/s/p		post/pre-op ratios			
		pre	post	pre	post	calf	foot	lin	exp	calf	foot
1	65 M	.25	1.50	0	24	.034	.038	.8	.8	1.49	1.80
2	74 F	0	.87	0	14	.044	.026	1.0	2.5	1.05	2.13
3	68 F	.39	.93	13	24	.088	.063	.7	.7	.93	1.12
4	63 F	.35	.70	8	19	.078	.077	1.7	1.0	1.54	1.41
5	63 F	0	.80	0	14	.041	.042	1.3	1.0	1.47	1.37

The build up curve was analyzed using a linear fit of the initial rise (lin) and an exponential fit (exp) of the first 10 minutes. Absolute count rate per pixel (c/s/p) is dose and cardiac output dependent, therefore, ratios are preferable. Myocardial uptake appeared to be a better reference than left arm. All pts were asymptomatic after surgery, showed increased perfusion of all affected limbs, and reached a plateau 3-4 minutes after injection. As expected, a dramatic improvement in flow parameters does not necessarily mean a better perfusion (pts 2,5).

No. 653

FOUR VS TWENTY-FOUR HOUR DELAYED INDIUM-111-PLATELET IMAGES FOR DETECTION OF LOWER EXTREMITY DEEP VEIN THROMBOPHLEBITIS. J.E. Seabold, G.R. Conrad, D.A. Kimball, E.E. Frey, J.D. Coughlan. The University of Iowa, Iowa City, IA.

The purpose of this study was to determine if In-111-platelet scintigraphy (In-PS) performed 4 hours following injection of labeled cells would provide diagnostic information as to the presence of active deep vein thrombophlebitis in the lower extremities.

Seventeen patients clinically suspected of thrombophlebitis underwent In-PS at 4 and 24 hours following injection of autologous labeled platelets as well as lower extremity contrast venography (CV). Eleven of the 17 (65%) patients were found to have one or more intra-luminal filling defects on CV indicative of active thrombophlebitis. Of these 11 patients, 8/11 (73%) had abnormal In-PS at 4 hours and 10/11 (91%) at 24 hours. All studies that were abnormal at 4 hrs remained positive at 24 hrs, but showed greater intensity and/or a greater number of abnormal sites.

In-PS and CV were both negative in 4 cases. Two

patients with a negative CV had abnormal In-PS images in the lower pelvis/upper thigh and were considered to be falsely positive.

Conclusions: In-PS images obtained 4 hours post injection provided diagnostic localization in most patients with active deep vein thrombophlebitis of the lower extremities. Twenty-four hour delayed images are necessary when 4 hour images are negative.

No. 654

THE USE OF INDIUM-111 OXINE LABELLED PLATELETS IN SYMPTOMATIC PATIENTS WITH SUSPECTED DEEP VEIN THROMBOSIS. E. Straus, E.O. Smith, S. Morse, C.V. Sunder Rao, D. Denny, C. Martinez, E. Lerner, M.D. Ezekowitz West Haven VA and Yale University School of Medicine

In-111-oxine labelled platelet scintigraphy (LPS) is uniquely suitable for studying venous thrombosis because the half-life of the isotope and the life span of the injected platelets allow imaging for 5-7 days with a single injection of the labelled material. We and others have shown that LPS is a valuable technique for the surveillance of high risk patients. In this study the accuracy of LPS and the optimum timing of imaging after platelet injection were determined in 23 symptomatic patients who underwent venography. Thirteen of these patients were receiving heparin at the time of study. Venograms were performed 6 ± 8.5 hrs after injection of 333.5 ± 111 uCi of labelled platelets. Platelet scans and venograms were read by single-blinded readers. Analysis was per patient. For images acquired within 4 hrs the sensitivity and specificity for the untreated group were 66% and 86%, and for the treated group were 11 and 75%, respectively. At 24 hrs sensitivity and specificity for the untreated group were 100% and 83%. None of the patients receiving heparin with positive venograms had positive platelet scans at 24 hrs. The specificity in this latter group, however, was 75%. We conclude from this preliminary analysis that LPS is useful in the diagnosis of deep vein thrombosis and that heparin adversely influences the sensitivity of this technique. In non heparinized patients sensitivity is better at 24 vs 4 hrs after injection of the platelet suspension.

No. 655

QUANTITATIVE DEMONSTRATION IN VIVO OF PLATELET ACCUMULATION AFTER BALLOON ANGIOPLASTY IN ATHEROSCLEROTIC RABBIT MODEL: CORRELATION WITH PATHOLOGY C.V. Sunder Rao, S. Morrel, F.J. Wackers, MD Ezekowitz. Yale University School of Medicine, New Haven, CT

Restenosis is the major limitation following balloon angioplasty(A). To investigate the role of platelets(P) in the process of restenosis following A, a rabbit model (New Zealand white males) of focal atherosclerosis was created by air drying a segment of both femoral arteries followed by an alternate day diet of 2% cholesterol and 6% peanut oil for 4.4 ± 0.8 wks. Unilateral (n=6) and bilateral (n=1) femoral artery A were performed using 3 single minute inflations at 4.9 ± 0.9 atmospheres. At A, P derived from a normal donor and labelled with 214 ± 36 uci indium-111 with a labelling efficiency of 89 ± 6% were injected. Images of the femoral arteries were acquired 1.8 ± 1.3 and 21.6 ± 1.3 hrs after A. Images were quantified by outlining an area of interest corresponding to the A site and comparing it with the corresponding atherosclerotic non A side or the aorta in the single animal with bilateral dilations. P uptake was 8.7 ± 12.3 (range 1.3 to 32) times greater at the A site verses control. Histology demonstrated smooth muscle proliferation in the media with foam cells. At the A site denuded endothelium with varying degrees of P deposition and thrombosis was seen. The activity on the P images correlated with the degree of P deposition seen histologically. Thus, from this preliminary study,

quantified indium-111 P imaging may be used to estimate the intensity of P deposition and thrombus formation complicating A and may be correlated successfully with histology.

No. 656

CLINICAL IMAGING OF ARTERIAL AND VENOUS THROMBUS WITH Ga-67-FIBRINOGEN-DAS-DFO, NEWLY DESIGNED BIFUNCTIONAL CHELATING AGENT. T.Suzuki, T.Yamazaki, S.Aoki, K.Masuda and T.Yamazaki. Shiga Medical School, Ohtsu. K.Torizuka, K.Horiuchi and A.Yokoyama. Kyoto University, Kyoto. K. Takahashi and N.Ueda. Nihon Medi-Physics Co., Takarazuka, Japan.

Recently, fibrinogen has been labeled with Ga-67, using a newly designed bifunctional chelating agent, di-aldehyde starch-deferoxamine(DAS-DFO). Successful data gathered with this Ga-67-fibrinogen-DAS-DFO(Ga-67-fibrinogen-DD) in arterial and venous thrombus model in rabbit, stimulated the present study in normal volunteers followed by a clinical evaluation of Ga-67-fibrinogen-DD in 25 patients with arterial or venous thrombus, or bypass graft. Fibrinogen-DD was available as a lyophilized product and easily labeled by simple mixing with Ga-67 Cl₃ solution(2mCi/2ml). The scinti-images were taken by a scintillation camera, 72 hours after the venous injection of Ga-67-fibrinogen-DD(2mCi). Ga-67-fibrinogen-DD well accumulated in the liver and kidney in normal volunteers at the early stage, and the radioactivity in the kidney, lung and heart noticeably decreased after 48 or 72 hours post injection. Ga-67-fibrinogen-DD clearly visualized fresh and old arterial thrombus localized in the thorax or abdomen of all patients suffering aneurysm, and in occlusive bypass graft, contrary to the past observation with the labeled fibrinogen. While in venous thrombus, pulmonary artery included, the visualization was limited to fresh thrombus, up to one month old thrombus. No adverse side effects were not observed in all cases.

Ga-67-fibrinogen-DD method was very simple and indicated good applicability for the diagnosis of active thrombus in most of the organs, except the liver.

No. 657

RELATIONSHIP OF IMPOTENCE TO BENIGN PROSTATIC HYPERTROPHY: ASSESSMENT BY PENILE Xe-133 WASHOUT. S.H. Yeh, R.S. Liu, S.N. Lin, L.C. Wu, Y.K. Chu, M.T. Chen, and S.S. Chang. Veterans General Hospital, Taipei, Taiwan.

We found slow penile Xe-133 washout in a patient of erectile impotence (EI) with benign prostatic hyperplasia (BPH). This led us to study their relationship.

The penile Xe-133 washout study was adopted from Nseyo, et al. (Urology XXIII:31, 1984). Data were acquired in frame mode after subcutaneous injection of 1 to 2 mCi of Xe-133 in 0.1 ml of saline for 20 min. A computer routine was used to calculate clearance half-time (T 1/2) in min and flow rate (Q) in ml/100 gm tissue/min.

Penile Xe-133 washout was performed in 20 patients (pts) with BPH divided into Group 1 in 9 with EI and Group 2 in 11 without EI, 11 age-matched normals (N), and 10 young normals. The results are as follows:

Group	Number	T 1/2*	Q*	BPH Grading**
1	9	9.1 ± 3.1 ⁺ , ^π	5.9 ± 2.0 ⁺ , ^π	1+
2	11	15.2 ± 6.8 ^π	3.7 ± 1.4 ^π	1.83+
Aged N	11	6.1 ± 4.0 [#]	9.4 ± 2.7 [#]	0
Young N	10	5.3 ± 1.0	9.5 ± 1.7	

*mean ± s.d.; **mean; ⁺p < 0.05 vs Group 2;

^πp < 0.005 to 0.05 vs aged N; [#]NS vs young N.

Q and T 1/2 did not differ between young and aged N. Abnormal Q and T 1/2 occurred in 85% (17/20) pts with BPH, but Q, T 1/2 and mean BPH grading were more abnormal in Group 2 than in Group 1. Abnormal Q and T 1/2 occurred in 67% (6/9) in Group 1, but in all of Group 2.

In summary, penile vascular insufficiency (PVI) occurs in the majority of pts with BPH, and will cause EI in pts less tolerable to such an insufficiency. PVI may result

from compression of the internal pudendal artery on each side by the hypertrophic prostate.

Monday, 3:30-6:00

Exhibit Hall

PULMONARY

No. 658

NEUTROPHILS IN OXIDATIVE LUNG INJURY: A FUNCTIONAL ASSESSMENT. D. Bandyopadhyay, D.K. Das*, S. Hoory, and H. Steinberg. Long Island Jewish Medical Center, New Hyde Park, NY and *University of Connecticut Health Center, Farmington, CT.

The present study examines the role of polymorphonuclear leukocytes (PMNs) in hyperoxic lung injury using the nonsteroidal anti-inflammatory drug, ibuprofen. White New Zealand rabbits exposed to 100% O₂ or air for 1 to 4 days were divided in two groups: the treatment group (I) was fed ibuprofen (75 mg/day) with drinking water whereas the control group (C) received water alone. At the end of exposure, all the animals were injected with 60-80 uCi of In-111 oxine labeled PMNs and digitized images were acquired at selected time intervals using a Siemen's Gamma Camera interfaced to a VAX mini-computer. An influx of radioactive PMNs into the lungs was detected only in 72-hr and 96-hr oxygen exposed Group C animals, whereas Group I animals did not exhibit any accumulation of radioactivity into the lung. Quantitative assessment of PMN accumulation was performed both by region of interest studies of images and by counting the vital organs after sacrificing the animals. Although blood gas analysis of all 72-hr oxygen exposed animals did not show any abnormal values, the analysis of dry/wet weight ratios and histopathological examinations of the lungs indicated noncardiogenic edema formation. Severe acidosis, gross cytoplasmic edema and partial destruction of lung endothelium were observed in both I and C groups after 96 hrs of O₂ exposure. The present study clearly demonstrates that although ibuprofen cannot prevent hyperoxic lung injury, it inhibits the influx of PMNs into the injured lung, suggesting that PMNs are not directly involved in the injury process.

No. 659

CLINICAL PATTERNS OF RADIOAEROSOL PENETRATION. M. Colln, R.A. Holmes. Nuclear Medicine, University of Missouri and Harry S Truman Memorial Veterans Hospital, Columbia, MO.

Unlike the radioactive inert gases that readily diffuse throughout the aerated lung and measures regional ventilation radioaerosols, such as Tc-99m-DTPA, penetrates and evaluates the patency of the tracheobronchoalveolar airways and are used clinically to detect endobronchial disease. We have studied more than 150 patients referred to exclude pulmonary embolism (PE) who received a Tc-99m-DTPA radioaerosol instead of radioxenon prior to a Tc-99m-MAA perfusion (Q) image. Nearly 15 percent of the patients had PE documented clinically or with radiologic studies. In practically all the patients where PE was demonstrated, a discordance between the Q and the normal radioaerosol images were seen, however, those with superimposed congestive heart failure, obstructive lung disease or senile emphysema made the interpretation more difficult due to altered patterns of radioaerosol penetration. More than half of the patients studied had some form of airway/parenchymal lung dysfunction that was frequently not appreciated by the referring physician. Patterns of central airway, retention and multifocal peripheral localization could be further characterized and differentiated into several conditions: a) emphysema (pan-lobar); b) bronchitis/bronchiectasis; c), combination of a and b; d) smokers

(small airway disease); e) acute asthma; and f) artificial airway applications. In conclusion, patterns of specific airway disease can be accurately detected with Tc-99m DTPA radioaerosol.

No. 660

RELATIONSHIP OF LUNG VOLUME AND THE PULMONARY CLEARANCE OF TC-99M-DTPA. J.A. Cooper, H. van der Zee, B.R. Line and A.B. Malik. Albany Medical College, Albany, NY.

Clearance of aerosolized Tc-99m-DTPA has been proposed as a measure of pulmonary epithelial permeability, but is affected by increased functional residual capacity (FRC). To examine this further, we studied the dose-response relationship of positive end-expiratory pressure (PEEP) and FRC on the clearance of aerosolized Tc-99m-DTPA (0.44 um). Lung activity was decay corrected, fit to an exponential, and expressed as % decrease per min (%/min). Sheep (n=20) were ventilated with 0, 2.5, 5, 10, 15 or 20 cm H₂O PEEP while clearance was measured. FRC by N₂ washout was measured in 3 sheep while on 0, 2.5, 5, 10, 15 and 20 cm H₂O PEEP ventilation. Data are shown as mean±SEM; *different than next lower step of PEEP (p<0.05):

PEEP (cm H ₂ O)	Clearance (%/min)	FRC (L)
0	0.39±0.05	1.03±0.19
2.5	0.40±0.03	1.26±0.12*
5	1.14±0.19*	1.64±0.19*
10	1.98±0.38*	2.36±0.12*
15	5.98±0.68*	3.44±0.35*
20	5.99±0.39	5.35±0.59*

In 3 sheep ventilated with 20 cm H₂O PEEP, clearance remeasured on 0 cm H₂O PEEP was 0.55±0.07 %/min. Clearance shows a sigmoid relationship with both FRC and PEEP, having threshold and maximal effects. Increased clearance due to increased lung volume is reversible. Lung volume should be controlled in studies examining the pulmonary clearance of aerosolized Tc-99m-DTPA. (P01-HL32418)

No. 661

PULMONARY Tc-99m DTPA CLEARANCE IN PATIENTS WITH RESPIRATORY FAILURE. M. Jacobs, S. Tennenberg, C. Huth, R. Branson, K. Adams. University of Cincinnati Medical Center, Cincinnati, Ohio.

The pulmonary clearance rate of inhaled radioaerosols is thought to be a measure of alveolar capillary permeability (ACP) with a rapid clearance rate associated with increased ACP. Abnormal pulmonary radioaerosol clearance rates (PRCR) have been described in cigarette smokers and various disease states including noncardiogenic pulmonary edema (NPE). Using a readily applicable technique for aerosol delivery we performed clearance studies using Tc-99m diethylenetriamine pentacetate on 27 patients with respiratory failure requiring mechanical ventilation. Our studies were successful regardless of ventilator type (volume-cycled, time-cycled or high-frequency pulse generator) or level of positive end-expiratory pressure used (up to 25 cm H₂O). After blinded retrospective analysis NPE was judged present in 13 patients. One patient was eliminated from analysis due to an underlying lung disease (idiopathic pulmonary fibrosis) associated with abnormal PRCR. Those patients with NPE had a mean PRCR (± SEM) of 6.3 ± 1.0% per minute while those without NPE had a significantly slower PRCR (1.8 ± 0.2% per minute, p < 0.01). Twelve of 13 patients with NPE had PRCR > 3.5%/minute while all 13 patients without NPE had values < 3.5% per minute (χ² = 18.7, p < 0.01). We obtained bronchial secretions and measured the albumin content from 12 patients and found a significant positive correlation between the albumin content and PRCR (r = 0.65, p < 0.01). We conclude that the PRCR is a measure of ACP and can be successfully performed on mechanically ventilated patients. It may be useful in assessing the presence of NPE.

No. 662

RADIONUCLIDE EVALUATION OF LUNG INJURY IN PATIENTS WITH ADULT RESPIRATORY DISTRESS SYNDROME (ARDS). E.E. Kim, G.A. Pjura, P.A. Lowry, and G. Gutierrez, Univ. of Texas Medical School, Houston, TX.

ARDS, a form of acute severe respiratory failure following lung injury at the alveolar-capillary level, is characterized clinically by hypoxemia and decreased pulmonary compliance and radiographically by diffuse alveolar consolidation. Invariably, there is increased pulmonary-capillary endothelial permeability with leaking of fluid and protein into the pulmonary interstitium and airspaces.

We prospectively monitored this change in permeability in acute trauma patients with ARDS utilizing two different techniques. The first method, utilizing Tc-99m aerosol, was employed with 10 patients. Each inhaled aerosol for 2 min., after which whole lung images were acquired at 30-sec. intervals for 10 min. utilizing a computer-equipped portable camera. Clearance rates were then determined for selected, peripheral areas of each lung and converted to mean percent decline per minute. The second method involved injecting 5 patients with 15 mCi of Tc-99m HSA after which images were obtained at 1-min. intervals for 45 min.. Ratios of right lung to heart activity were then plotted vs time and a slope index calculated by a linear least squares fit over the 15-45 min. data.

Changes in both indices over serial studies were well correlated with patient response as judged by clinical, radiographic and pulmonary function studies.

Consequently, we conclude that these radionuclide techniques are of potential value in the diagnosis and monitoring of ARDS patients and, potentially, in prognosis.

No. 663

IMPROVEMENT OF SPECT LUNG PERFUSION PHYSIOLOGY WITH CT HIGH RESOLUTION STRUCTURAL ANATOMY. G.W. Moskowitz, J.C. Vaugeois, R.G. Schiff, and L.M. Levy. Long Island Jewish Medical Center, New Hyde Park, NY 11042.

The application of high resolution structural anatomy of CT to SPECT transaxial images gives the necessary landmarks to yield precise relationships of the vascular abnormalities to the lung and adjacent organs.

A computer program has been created to take the data acquired by SPECT and CT and to combine similar cross-sectional images into one composite image. The SPECT studies are obtained from a Siemens dual-headed ROTA camera using high resolution collimators. The data was acquired in 60 frames of 64 x 64 pixels at angular increments of 6 degrees. SPECT transaxial cross-sections were obtained using a C.D.&A. (VAX 11/750) computer system. The CT cross-sections were obtained on a GE TC/T 9800 with 512 x 512 picture elements. The computer program converts both the SPECT and CT to images of 256 x 256. Slight corrections for orientation and size are required for proper superimposition of corresponding transaxial cross-sections of SPECT upon CT. Adjustment of the CT level and window for mediastinal organ density results in suppression of low density lung tissue leaving an 'empty thoracic cavity' image. A composite image is obtained by superimposing corresponding SPECT and CT cross-sections.

These images provided accurate relationships between the lung perfusion pattern to the adjacent organs. The definition of the boundaries provides a basis for quantifying the size and extent of perfusion changes. In this manner, the configuration and character of each perfusion defect can readily be defined and categorized. These composite images result in improved structural and physiological anatomy of lung vascular perfusion patterns.

No. 664

PULMONARY ACCUMULATION OF 125I-HIPDM STUDIED IN AN ISOLATED PERFUSED RAT LUNG MODEL. D. Slosman,

A.B. Brill and P.O. Alderson. Brookhaven National Lab, Upton, NY and Columbia Univ., New York, NY.

Lung uptake of iodobenzyl-propanediamine (HIPDM) has been reported, but the nature of this process has not yet been fully established. Thus, the mechanism of single-pass 125I-HIPDM accumulation has been studied in rat lung, isolated and perfused with an albumin Krebs-Ringer bicarbonate buffer. HIPDM lung accumulation was monitored by the tissue/medium ratio ($T/M = \text{cpm.gr}^{-1} \text{ lung tissue} / \text{cpm.ml}^{-1} \text{ inflow}$).

As a function of time or concentration, HIPDM accumulation appeared to be a saturable process. During a 2 min perfusion, 97.5% ± 2.5 (n=8) extraction was observed with 2 μM HIPDM, but only 38% ± 1.2 (n=3, p<0.001) was extracted when the concentration was 1mM. Cold (4°C) had little effect on pulmonary accumulation (87.5% ± 2.3, n=5, p<0.01), and the addition of ouabain or the use of sodium-free medium had no effect on pulmonary accumulation. The addition of 1 mM chlorpromazine, propranolol or imipramine significantly reduced the HIPDM accumulation to 42.5% ± 1.3, 51.3% ± 2.0 and 49.3% ± 0.7, respectively (n=4-6 each group, p<0.001). Thus, the pulmonary accumulation of HIPDM does not appear to be energy dependent, but is saturable and inhibited competitively by other basic amines that are known to bind by physico-chemical interactions to pulmonary endothelial cell membranes.

Monday, 3:30-5:00**Exhibit Hall****RADIOASSAY****No. 665**

AN ALTERNATIVE APPROACH TO ON-LINE MONITORING OF ELUTION PROFILES OF Rb-82 FOR RADIOASSAY/RADIATION DOSIMETRY. V. Dhawan* and G.P. Genarro†. *Memorial Sloan-Kettering Cancer Center, New York, NY, and †Squibb Institute for Medical Research, New Brunswick, NJ.

Generator-produced Rubidium-82 has been used with positron emission tomography (PET) to study blood-brain barrier permeability, myocardial imaging and renal perfusion. Static (dose calibrator) assays of Rb-82 bolus yield erroneous estimates of administered activity by ignoring the asymmetric output of Sr-82/Rb-82 generators. Though on-line monitoring of elution profile improves accuracy for quantitative purposes, it requires an elaborately shielded detector and associated electronics at patient-study site. Our alternative approach involving mathematical description of dynamic characteristics of Sr-82/Rb-82 generator based on a set of generator parameters (mCi of Sr-82 and a test elution profile) supplied by the generator manufacturer accurately predicts elution profile at any desired flow rate.

Using a compartmental model with liquid-chromatography "rate theory", we derived a theoretical relationship between eluted activity vs time as a function of elution flow rate. Experimental elution curves were generated at various flow rates (25-75 ml/min) and eluted activity monitored with an appropriately positioned positron detector. Theoretical curves generated by the model were in excellent agreement with experimentally obtained curves.

This proposed model will facilitate the design of Rb-82 infusion protocols for the abovementioned PET studies and also allow an accurate estimate of administered activity without the need for associated on-line monitoring equipment.

No. 666

CARBOHYDRATE ANTIGEN (CA) 19-9 AND LEWIS BLOOD-TYPE; ABSENCE OF CA19-9 AND DEMONSTRATION OF CIRCULATING ANTI-CA19-9 ANTIBODY IN LEWIS NEGATIVE INDIVIDUALS. K.ENDO, H.SAKAHARA, K.NAKAJIMA, T.NAKASHIMA, M.KOIZUMI, Y.KAWAMURA, H.OHTA and K.TORIZUKA. Kyoto University Hospital, Kyoto, Japan.

CA 19-9 is a clinically useful cancer marker for the carcinoma of pancreas and gastrointestinal tract. Recently the structure of CA19-9 is defined as a sialylated monoglycoside, whose sugar sequence also occurs in the human Lewis (Le) blood-group system. This paper describes the relation of serum CA19-9 levels with Lewis blood-types in normal individuals and the presence of circulating antibodies to CA19-9 in some Lewis negative donors.

According to the presence or absence of Lewis antigens, 107 normal individuals were divided into 3 groups: Le(a+b-), Le(a-b+) and Le(a-b-). Serum CA19-9 levels were significantly different among groups they belong. There was more CA19-9 in the serum from normal Le(a+b-) individuals than Le(a-b+) individuals. However, CA19-9 was not detectable in the normal controls and most cancer patients, if not all, who belong to the Le(a-b-) blood-type. Such difference was not observed in other cancer markers such as CA 125 or CEA. Furthermore, autoantibodies directed toward CA19-9 were found in the serum from 10 (19%) of 53 Lewis negative donors, including normals and patients with benign or malignant diseases but not in Le(a+b-) or Le(a-b+) individuals. B lymphocytes from these cases will serve as a good source for the production of human monoclonal antibodies to CA19-9, which have many advantages for the radioimmunoimaging and therapy of cancers.

No. 667

FOUNDATION OF MATHEMATICAL PACKAGE FOR CONSTRUCTION OF LINEAR CURVE FOR IRMA (IMMUNO-RADIOMETRIC ANALYSIS) Z. Kureishy, Dept. of Nuclear Medicine, Kuwait University, Kuwait.

A linear mathematical plot is derived which describes the Irma model and provides a means for plotting data in linear fashion without the use of cumbersome mathematical formulae or special graph paper.

The concept of data reduction in Irma is developed on several assumptions to simplify and explain the system. By using calculus a linear response is generated as illustrated below:

Decreasing function: $y = f(x)$, if $f(x_2) < f(x_1)$ which is differentiable, then $f'(x) < 0$

Increasing function: $y = f(x)$, if $f(x_2) > f(x_1)$ which is differentiable, then $f'(x) > 0$

A linear plot of dose concentration on the X-axis and semi-log plot of normalizing response on Y-axis gives a linear relationship, as indicated below,

$$\text{if } x = \text{linear dose} \quad \frac{B - B_{kg} (B - B_{kg}) - (B_0 - B_{kg})}{B_0 - B_{kg} (B_0 - B_{kg})} = \text{normalizing response}$$

where B = count rate of known or unknown sample
 B = maximum bound count of zero std
 B_{kg} = count rate or non specific binding

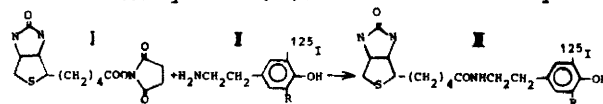
EASE of data acquisition and processing is obtained with the help of calculators and computers.

No. 668

SYNTHESIS OF RADIOIODINATED BIOTIN DERIVATIVES. E. Livaniou*, G.P. Evangelatos*, and D.S. Ithakissios**. N.R.C. Demokritos, Athens*, and University of Patras, Patras**, GREECE.

The importance of biotin in man as well as the usefulness of the avidin-biotin-complex tool has been recently emphasized. Relative investigations would be very much facilitated by a gamma-emitting tracer of the vitamin.

We synthesized the N-[β-(4-OH-3-¹²⁵I-phenyl)ethyl]- and the N-[β-(4-OH-3,5-di-¹²⁵I-phenyl)ethyl]-biotin amides (III) by coupling N-hydroxysuccinimidobiotin (I) to radioiodinated tyramine (II). Radioiodination of tyramine



was performed by a modified Chloramine T method, prior to the coupling in order to protect the biotinyl portions from the oxidative radioiodination conditions. By changing the tyramine amount it was possible to produce the mono- or the di-radioiodinated tyramine derivatives. The final products were separated from the reaction mixture by TLC (n-butanol: 2N NH₄OH: ethanol, 3:1:1). R_f values: 0.46 (I); 0.46 (II, R_H); 0.52 (II, R_H¹²⁵I); 0.67 (III, R_H); 0.70 (III, R_H¹²⁵I); 0.84 for ¹²⁵I.

The radioiodinated derivatives synthesized, with the biotin-ureido group intact, were found to compete for the avidin-binding sites to form complexes with comparable to biotin affinity. Thus they were capable of being used as tracer in biotin radioassays. Their specific activity was high and they were conditionally stable for two months.

No. 669

A NEW TUMOR MARKER, CA15-3, FOR BREAST CARCINOMA. H.Sakahara, K.Endo, K.Nakajima, T.Nakashima, M.Koizumi, Y.Kawamura, H.Ohta, S.Inamoto, and K.Torizuka. Kyoto University Hospital, Kyoto, Japan.

CA15-3 is a new tumor marker measured by immunoradiometric assay using two monoclonal antibodies (115D8, DF3), which react with a circulating antigen expressed by human breast cancer cells. To evaluate the clinical usefulness of CA15-3, we measured serum CA15-3 concentrations in 60 normal subjects and 189 patients with various malignant tumors and benign diseases using a radioimmunoassay kit (CIS, France). Serum CA15-3 levels in normal subjects were 8.8±2.9 U/ml (mean±SD) and all of them were less than 15 U/ml. When the cutoff level was set at 30 U/ml, elevated CA15-3 levels were observed in 39% (15/38) patients with breast carcinoma. Positive rates in primary breast carcinoma were 10% (1/10), 33% (2/6), 25% (2/8) and 100% (1/1) of stage I, II, III, and IV. In patients with recurrent tumor, 9 of 13 (69%) cases had serum CA15-3 levels of over 30 U/ml and 7 cases showed more than 100 U/ml. One patient with stage III whose CA15-3 levels remained elevated after the operation developed bone metastasis and local recurrence. On the other hand, there was no positive case in 37 patients with no evidence of recurrence. In 74 patients with other malignant tumors, increased levels were found in 33%, 11%, 25%, 0%, 7%, 0%, and 43% of sera from patients with gastric, pancreatic, biliary tract, esophageal, lung, uterine cervix, and ovarian carcinomas respectively. Only 3 of 40 patients with benign diseases had elevated CA15-3 levels. In conclusion, the measurement of serum CA15-3 levels would be useful for the management of patients with breast carcinoma.

No. 670

DEVELOPMENT OF A SENSITIVE ASSAY FOR BIOACTIVE PARATHYROID HORMONE. I.Yamamoto, N.Kitamura, J.Aoki and K.Torizuka. Kyoto University School of Medicine, Kyoto, Japan

Most of assays to attempt to measure biologically active parathyroid hormone (PTH) by radioimmunoassay are not sensitive enough to measure values in normal person. We developed relatively simple and sensitive assay for biologically active PTH, employing cyclic AMP measure-

ment, produced in cultured osteoblastic cells (MC3T3-E1), which possess a number of receptors for PTH. First, bioactive PTH was extracted with isopropanol after loading 1 ml of plasma onto C^{18} -silica cartridge (Sepak), lyophilized and stored at $-20^{\circ}C$. Recoveries of PTH, assessed using ^{125}I -labeled (^{34}Try)-human PTH (1-34) and ^{125}I -labeled synthetic human PTH-(1--84) were more than 70 % in this procedure. MC3T3-E1 cells were inoculated in multi-well (96-well) dishes and cultured for a week and medium was changed to the medium which contained 1 mM isobutylmethylxanthine, 1 mM propranolol and materials for the test. MC3T3-E1 cells possess β -adrenergic receptor also and the effect of β -adrenergic stimulants was blocked by addition of 1 mM propranolol. After 10 min incubation at $37^{\circ}C$, reaction was stopped and cyclic AMP produced was measured by a radioimmunoassay. $5 \times 10^{-13}M$ of bioactive PTH was detectable from 1 ml of plasma sample in this assay and thus we could measure bioactive PTH in all of sample from healthy volunteers. Samples from patients with hyperparathyroidism showed higher values than those from normals, while, in patients with hypoparathyroidism, values for bioactive PTH showed lower than the detectable level. Thus, relatively simple and sensitive *in vitro* method, equivalent to nephrogenous cyclic AMP measurement *in vivo*, to evaluate bioactive PTH was demonstrated.

No. 671

CLINICAL EVALUATION OF MEASUREMENT OF SERUM VITAMIN D METABOLITES

I. Yamamoto, N. Kitamura, J. Aoki, S. Dokoh and K. Torizuka
Kyoto University School of Medicine, Kyoto, Japan

1,25-dihydroxyvitamin D is a major steroid hormone, regulating calcium balance. However, clinical evaluation of the measurement of serum 1,25-dihydroxyvitamin D is hampered by its cumbersome purification procedure, including high performance liquid chromatography, before the radioreceptor assay. We developed a sensitive and reproducible radioassay for 1,25-dihydroxyvitamin D and other vitamin D metabolites, and measured serum values in 285 healthy controls, 42 patients with hyperparathyroidism, and more than 505 patients with other metabolic bone diseases. In some of these patients, intestinal calcium absorption was assessed using ^{47}Ca and whole body counting with a human counter, and evaluated for the correlation between serum 1,25-dihydroxyvitamin D values. Values for serum 1,25-dihydroxyvitamin D in normal controls ranged between 15 to 75 pg/ml, showing the highest value at adolescence. Serum values of 1,25-dihydroxyvitamin D are extremely elevated in pregnant women, moderately elevated in patients with primary hyperparathyroidism, and decreased in patients with chronic renal failure, hypoparathyroidism, hypercalcemia with malignancy, hyperthyroidism and liver cirrhosis. Serum values of 1,25-dihydroxyvitamin D correlated well with intestinal calcium absorption both in normal controls and in patients with pathological conditions. Thus, measurements of serum 1,25-dihydroxyvitamin D and other vitamin D metabolites are proved to be essential to understand calcium metabolism.

Monday, 3:30-6:00

Exhibit Hall

RADIOPHARMACEUTICAL: ANTIBODIES**No. 672**

SOLID PHASE AFFINITY BOUND ANTIBODY CONJUGATION FOR SITE DIRECTED RADIOLABELING IN IMMUNOSCINTIGRAPHY. M P Best, PO Box 823, Dunedin, New Zealand.

Selective site directed antibody conjugation is of interest in preservation of binding site immunoreactivity with radiolabeling. Loss of specificity with labeling

results in poor targeting and limits image resolution of many immunoscintigraphic agents. Exposure of the Ab binding site to the conjugation reaction is minimized with an immobilised antigen bound as a protecting group. The antigen covalently attached to CNBr activated gel beads immunoadsorbs specific Abs and provides a heterogeneous reaction system as an affinity bound antibody-antigen gel polymer complex. Spheroidal packing of gel beads allows reaction design in the inefficient conjugation step with simple sequencing of washes and separations in a syringe giving high yields characteristic of solid phase synthesis and methodology. The gel polymer helix provides attachment and allows steric conformation important in antibody-antigen binding. Conjugation is applied to the affinity bound antibody-antigen complex followed by biological perturbation to separate the Ab conjugate from the gel bead otherwise non-specifically conjugated. DTPA anhydride and Bolton Hunter reagent have been used as conjugating agents. Reversible renaturation by ionic extraction is performed using gel filtration or dialysis. Eluted Ab conjugates are instantly labeled with In-111, Tc-99m or iodinated via chloramine-T, with the label substantially directed onto non-binding sites. Immunoreactivity assay utilizes solid phase affinity of labeled Ab with settling times greater than 48 hours for 90% uptake. Instant site directed labeled calcitonin Ab has been useful for inhalation delivery in immunoscintigraphic lung tumour detection studies.

No. 673

Bi-212 LABELED MONOCLONAL ANTIBODIES FOR USE IN RADIO-IMMUNOTHERAPY. W.T. Anderson-Berg*, M. Strand*, M. Brechbiel†, R.W. Atcher†, and O.A. Gansow† *The Johns Hopkins University School of Medicine, Baltimore, MD and National Cancer Institute† Bethesda, MD.

Optimal methods for labeling monoclonal antibodies (MAB) with the alpha particle emitting radionuclide Bi-212 have been developed. In previous studies, Bi-206 labeled cyclic anhydride of DTPA (caDTPA) conjugated to MAB was unstable *in vivo*. We have therefore synthesized 1-(p-isothiocyanatobenzyl)DTPA (SCN-Bz-DTPA); 1-(p-nitrobenzyl)-diethylenetriamine was reacted with $BrCH_2COOH$, reduced to the amine and reacted with thiophosgene to form a chelate which has improved thermodynamic stability for Bi chelation. To radiolabel, $BiCl_3$ was dissolved in HI and adjusted to pH 4.5. DTPA-conjugated-Ab was added; free Bi was separated by HPLC.

By use of Bi-206, caDTPA- and SCN-Bz-DTPA-MABs were evaluated for stability *in vitro* and *in vivo*, targeting to neoplastic spleens, and biodistribution. In serum dialysis at $4^{\circ}C$, the SCN-Bz-DTPA-Ab lost 6% of its radiolabel over 11 days compared to 18% for the caDTPA-Ab. *In vivo*, 89-92% of the radioactivity remained on IgG as determined by affinity chromatography of sera from mice injected 1 hr earlier with the SCN-Bz-DTPA-Ab compared to only 36-38% for the caDTPA-Ab. With caDTPA-Ab only 3% of the injected dose (ID) remained in the blood at 1 hr in normal mice and only 2% reached the tumor in leukemic animals (9% ID/gm). By contrast, 41% of the ID remained in blood at 1 hr with the SCN-Bz-DTPA-Ab and 6-7% reached the tumor (30-36% ID/gm). Biodistribution analysis at 24 hr of SCN-Bz-DTPA-Ab in normal animals showed high levels in kidneys with 25% ID/gm; liver had 16%/gm; bone 4%/gm; and stomach 1%/gm. Experiments to assess the therapeutic efficacy and toxicity using Bi-212 are in progress.

No. 674

IMMUNOREACTIVITY CHANGES IN T-101 MONOCLONAL ANTIBODY DUE TO VARIATIONS IN DTPA CONJUGATION. M.J. Blend, G. Araya, Section of Nuclear Medicine, University of Illinois School of Medicine at Chicago, IL.

Using MoAb T-101* as a model, we evaluated the effects of DTPA conjugation on MoAb immunoreactivity and in addition have established a set of favorable conditions for Indium-111 (In-111) labeling of DTPA-T-101. Briefly, concentrated antibody

solution (8 mg/ml) in 0.1M bicarbonate buffer, pH 8.2, and solid cyclic DTPA anhydride (MoAb to DTPA ratio 1:1, 1:10, 1:20) were incubated for 60 minutes at 24 C. Conjugated products were separated on a Sephadex G-50 column and the protein fraction was then mixed with equal volumes of In-111 Acctate (1.0 mCi/mg) at a final pH of 5.5 for 30 minutes at room temperature. Radiochemical purity of each preparation was determined by ITLC Silica Gel chromatography. Immunoreactivity was measured by comparing the binding of DTPA conjugated MoAb and native MoAb to five serial dilutions of T-8402 lymphocyte cells*. Binding of nine serial dilutions of T-101 and T-101-DTPA with constant cell concentrations (5.0×10^6 cells/ml) was also measured. Antibody to DTPA molar ratio of 1:1 did not significantly alter immunoreactivity but In-111 labeling efficiency was 30-35%. Ratios of 1:10 yielded 80% immunoreactivity with 80-95% labeling efficiency. Ratios of 1:20 also yielded 80% immunoreactivity with 90-95% labeling efficiency. Our results indicate that the MoAb T-101 can be conjugated with DTPA at a molar ratio of 1:20 without significantly altering the immunoreactivity. The final specific activity of In-111-DTPA-T-101 averaged 1 μ Ci/ μ g protein with greater than 80% retained immunoreactivity. These results are ideal for an immunoscintigraphic system.

*Hybritech, Inc., San Diego, CA.

No. 675

COMPARISON OF CARBOHYDRATE DIRECTED VERSUS AMINE DIRECTED ATTACHMENT OF DTPA TO MURINE MONOCLONAL ANTIBODIES. B.A. Brown, C.B. Dearborn, W.P. Neacy, H. Sands, and B.M. Gallagher. Immunopharmaceutical R&D, E.I. duPont de Nemours, Co., Inc. No. Billerica, MA 01862

The attachment of bifunctional chelators to murine monoclonal antibodies (Mab) requires chemical modifications that may result in alteration of their biological behavior. The biochemical, immunological, and biological characteristics of In-111 labeled B6.2 and B72.3 were compared to the appropriate radioiodinated Mab's following either reaction with the cyclic dianhydride of DTPA (cDTPA) (1-3 mg/ml of Mab/ 10-fold molar excess of cDTPA) or periodate oxidation (10 mM) of the carbohydrate moieties of the Mab's and reaction with a bis(1,6-hexanediamine)DTPA derivative (dDTPA). Reaction of Mab's with cDTPA versus dDTPA gave differing forms of crosslinking and aggregation as measured on reducing and non-reducing SDS-PAGE as well as size-exclusion HPLC. Immunoreactivities of the radioiodinated Mab's with either type of DTPA modification were comparable. Biodistributions of both antibodies with I-125 unmodified Mab's, In-111-cDTPA-Mab's, and In-111-dDTPA-Mab's were done in normal CD1 mice. At 1-6 hours both forms of labeled Mab's distributed to the various organs and cleared from the blood at similar rates. However, at 24 hours significant differences were seen in blood clearance (In-111-dDTPA-Mab > In-111-cDTPA-Mab = I-125-Mab) and kidney (In-111-dDTPA-Mab > In-111-cDTPA-Mab > I-125-Mab). Thus, different chemical methods of attachment of bifunctional chelators may provide for a means of selection of the biological distribution to the non-target organs to suit the application.

No. 676

PREPARATION AND CHARACTERIZATION OF BIFUNCTIONAL ANTIBODIES WITH REACTIVITY TO CARCINOEMBRYONIC ANTIGEN AND INDIUM BENZYL EDTA. C.-H. Chang, C. N. Ahlem, B. Wolfert, S. M. Hochschwender, R. Jue, J. M. Frincke, D. J. Carlo. Hybritech Incorporated, San Diego, California.

We report herein on two convenient methods for preparation of bifunctional antibodies (BFA) through chemical combination of two monoclonal antibodies (Mab) Fab' fragments of differing reactivity.

Mab with reactivity to indium benzyl EDTA (IBE) and carcinoembryonic antigen (CEA) have been previously described. Purified Mab were digested with pepsin

to produce F(ab')₂ fragments. The reaction mixture was purified by gel filtration prior to reduction to Fab'. After reduction, Fab' were purified by gel filtration and held for further processing.

BFA were prepared through recombination of two Fab' using protocols which re-generate the disulfide link or, alternatively, join the two fragments through a bis-maleimide bridge. Reformation of a disulfide-linked BFA was achieved through dithionitrobenzoic acid (DTNB) activation of one Fab', purification and reaction with the second Fab', in 25% yield. An alternative disulfide stabilized linkage system was developed using bis-maleimide methylether (BMME). Substituting BMME for DTNB in the aforementioned protocol, a recombined BFA was obtained in 50% yield.

Synthetic BFA titers were similar to those of a biologically produced BFA with the same specificities. The BFA system was designed for two step radioisotope delivery to tumors, bearing CEA.

No. 677

DESIGN OF THERAPEUTIC COPPER-67 LABELED MONOCLONAL ANTIBODIES. S.V. Deshpande, S.J. DeNardo, C.F. Meares, M. Moi, M.J. McCall, G.L. DeNardo. U.C. Davis Medical Center, Sacramento, CA 95817. DOE Grant #DE FG03-84ER60233.

The development of radiopharmaceuticals from monoclonal antibodies has led to the selection of several radiometals as choice nuclides for diagnostics and therapy. Investigators have found radiometal labeled MoAb reached higher tumor levels than their radioiodinated counterparts. However, a parallel increase in hepatic uptake needs to be reduced before these agents can reach their clinical potential. Cu⁶⁷, an optimum therapeutic radionuclide has been chelated into a plasma stable form to MoAb (Lym 1) with TETA. However, various linkages of TETA to Lym 1 have been explored to obtain a blood and tumor stable compound which could be degraded and excreted rapidly if taken up in hepatocytes or R.E. cells. We have conjugated TETA to Lym 1 by two methods. (1) 2-Iminothiolane (2IT) was used to link Lym 1 to p-bromoacetamidobenzyl TETA (BAT) by formation of a thioether link. (2) By using disuccinimidyl suberate (DSS) to conjugate BAT to Lym 1. These conjugates were labeled with Cu⁶⁷ and had immunoreactivity of more than 70%. Mouse biodistributions were performed with Cu⁶⁷-p-nitrobenzyl TETA as a control. The 2IT conjugate has a biological half life of 1 day and shows less organ uptake (liver:3-5% I.D./g) while DSS conjugate showed a biological half life of 4-5 days and high organ uptake (liver:7-9% I.D./g). This may be due to cleavage of thioether link in case of 2IT conjugate. Further studies are needed to prove if this type of linkage design will enhance tumor to nontumor ratio in imaging and therapy.

No. 678

COMPARISON OF IN VITRO AND IN VIVO PROPERTIES OF ANTI-TUMOR MONOCLONAL ANTIBODIES LABELED WITH RADIOIODINE AND METALLIC RADIONUCLIDES; INDIUM-111, GALLIUM-67 AND TECHNETIUM-99M. K.ENDO, H.SAKAHARA, T.NAKASHIMA, M.KOIZUMI, H.OHTA, Y.KAWAMURA, M.KUNIMATSU, Y.OHMOMO, Y.ARANO, T.NAKAMURA, H.TANAKA, Y. KOTOURA, T.YAMAMURO, S.HOSOI, S.TOYAMA, A.YOKOYAMA and K.TORIZUKA. Kyoto University, Kyoto, Japan.

Being aware of the favorable nuclear properties of metallic radionuclides, monoclonal antibody (MoAb) to human osteosarcoma was efficiently labeled with In-111, Ga-67 and Tc-99m by using bifunctional chelating agents; DTPA, Deferoxamine (DFO) and carboxyethyl-phenylglyoxal-dithiosemicarbazone (CE-DTS), respectively. Obtained radiolabels showed similar in vitro and in vivo properties to each other. The number of attached bifunctional chelates to MoAb markedly influenced both in vitro immunoreactivity and in vivo biodistribution. However, under selected conditions we

have used, radiolabeled MoAb was made available with almost full retention of the immunoreactivity and in vivo stability. Transplanted tumors in nude mice were clearly visualized with In-111, Ga-67 and Tc-99m labeled MoAb as well as with I-131 labeled one at 24 and 48 hours after the administration. Tumor-to-blood ratios were higher than that obtained by radioiodinated MoAb in spite of higher nonspecific uptake in the liver and kidney. Tumor was also seen even at 6 hours after the injection of Tc-99m labeled intact MoAb without significant radioactivity in the thyroid. These results provided a good basis for the clinical utility of In-111, Ga-67 and Tc-99m labeled anti-tumor monoclonal antibodies for the radioimmunodiagnosis.

No. 679

RADIOLOCALIZATION OF COLON CARCINOMA XENOGRAFTS IN NUDE MICE WITH IN-111 LABELED B72.3 USING SCN-Bz-DTPA AS LIGAND. J. Esteban, D. Colcher, D. Simpson, O. Gansow, R. Atcher, J. Schlom. Laboratory of Tumor Immunology and Biology, National Cancer Institute, NIH, Bethesda, MD

B72.3 is a murine monoclonal antibody (IgG1) that reacts with a glycoprotein present in 85% of colon carcinomas, but is virtually absent in normal adult tissues. It has been successfully labeled with I-125 and I-131 and injected into mice and patients, providing excellent radiolocalization and images. In-111 has physical properties that make it more suitable for radiolocalization studies. However, the current methodology uses conjugates that are unstable *in vivo* and leak In-111 resulting in accumulation in the liver. We have, therefore, used a new chelating ligand, 1-(p-isothiocyanatobenzyl)-diethylenetriaminopentaacetic acid (SCN-Bz-DTPA), and compared it with the current methodologies, mixed (MA) and cyclic anhydrides (CA) of DTPA. Biodistribution studies performed in athymic mice bearing human colon carcinomas (LS-174T) showed that the uptake of labeled B72.3 by the normal organs, especially the liver, expressed as percent ID/gm was over two times higher with MA and CA-DTPA than with SCN-Bz-DTPA. Tumor to organ ratios rose to 5:1 over 72 h with SCN-Bz-DTPA, while the tumor/liver ratio for the other chelates ranged from 1.3:1 to 2.5:1. The differences in uptake were reflected in the scintigrams where the tumors were visualized with minimal abdominal background in the mice injected with the SCN-Bz-DTPA chelate when compared with the other chelates. SCN-Bz-DTPA chelate could have utility for radiolocalization studies in patients if the uptake of label by normal liver, which could obscure possible metastases, is minimal as in the model system.

No. 680

LABELING ANTIBODIES WITH COPPER-67. S. D. Figard*, J. A. Mercer-Smith*, W. A. Taylor*, and D. K. Lavallee*. *Medical Radioisotope Research Program, Los Alamos National Laboratory, Los Alamos, NM, and †Hunter College, CUNY, New York, NY.

We have developed methods to label antibodies with copper-67, a potentially useful medical radioisotope, using N-benzyl porphyrin chelating agents N-benzyl-5,10,15,20-tetrakis(4-carboxyphenyl) porphine and N-4-nitrobenzyl-5(4-carboxyphenyl)-10,15,20-tris(4-sulfophenyl) porphine. Formation of an activated carboxylate on the porphyrin using either 1-ethyl-3-(3-dimethylaminopropyl) carbodiimide hydrochloride and N-hydroxysuccinimide or 1,1'-carbonyldiimidazole was successful in coupling an average of 2 to 4 porphyrins per antibody molecule, depending on the coupling method. The coupling reactions were optimized as a function of preactivation time, coupling time, coupling pH, and reagent concentrations. Sodium dodecylsulfate polyacrylamide gel electrophoresis was used as an analytical method to determine coupling yields. After removal of non-conjugated porphyrin by gel filtration, the

porphyrin-antibody conjugates can be rapidly labeled by copper-67 chloride in aqueous solution. Studies of antigen binding capacities post-conjugation are in progress. Thus conjugation of N-benzyl porphyrins to antibodies followed by radiometalation is a feasible protocol to radiolabel antibodies with copper-67.

(Research supported by *U.S. Department of Energy and Office of Health and Environmental Research and †NIH Grant CA 25427.

No. 681

PHARMACOKINETICS OF BIFUNCTIONAL ANTIBODY DELIVERED IN-111 BENZYL EDTA TO COLON TUMORS IN NUDE MICE. J.M. Frincke, C.-H. Chang, C.N. Ahlem, G.S. David, R.M. Bartholomew, L.D. Anderson, P.L. Hagan, S.E. Halpern, D.J. Carlo. Hybritech Incorporated and V.A Medical Center, San Diego, California.

In this study we report the pharmacokinetics of bifunctional antibody (BFA) mediated delivery of In-111 benzyl EDTA (IBE) to nude mice bearing carcinoembryonic antigen (CEA) colon tumors (T).

Disulfide-linked and disulfide stabilized BFA F(ab')₂ molecules were synthesized from monoclonal antibodies (MAb) with reactivity to CEA and IBE. BFA doses (14 ug) were injected 4, 24, 48, 72 and 96h before IBE and animals were sacrificed at 1, 2, 4 and 24h post administration.

Maximum T IBE concentration was found at 1-2h post administration and 48-72h post MAB administration. IBE accumulation in T was greatest with stabilized BFA. T to blood (B) and muscle (M) ratios demonstrated the disulfide stabilized BFA was superior (T/B = 21.0, T/M = 88.5) to disulfide BFA at 24h. The radiation dose which remained at the T was found to be greatest for disulfide stabilized BFA 24h post IBE injection. The described BFA delivery system is the first antibody mediated delivery system which permits rapid localization of a radioisotope in tumor subsequent to antibody accumulation, with imaging being theoretically possible within 4h.

No. 682

PREPARATION OF Ga-67 LABELED ANTIBODY ; EFFECT OF COUPLING AGENTS. M. Koizumi, K. Endo, H. Sakahara, H. Ohta, M. Kunimatsu, T. Nakashima, Y. Kawamura, Y. Ohmoto, A. Yokoyama and K. Torizuka. Kyoto University, Kyoto, Japan.

For the application of radioimmunodiagnosis, Ga-67 labeled antibody have been prepared by using deferoxamine(DFO) as a bifunctional chelating agent. In the present study, we have used hCG as a model antigen, monoclonal antibody to hCG as a model antibody and three coupling reagents to the attachment of DFO to antibody; glutaraldehyde, N-succinimidyl 3-(2-pyridyldithio)propionate (SPDP) and succinimidyl 6-maleimidohexanoate (EMCS), introducing Schiff's base, disulphide bond and thioether bond, respectively. The immunoreactivity of obtained radiolabels was determined with the solid-phase radioimmunoassay.

The coupling reagents greatly affected the in vitro properties and in vivo distribution of labeled antibody, although the immunoreactivity, radiochemical purity and in vitro stability were satisfactory. Different from the homocoupling reagent; glutaraldehyde, the formation of polymerized antibody was not detectable in case of heterocoupling reagents; EMCS or SPDP. The radiolabel with disulphide bond showed the fastest clearance from the circulation. However, the liver to blood and spleen to blood ratios of the radioactivity were the lowest when labeled antibody with thioether bond was injected, in spite of showing the similar blood clearance to antibody with Schiff's base. The radiolabel with thioether bond appeared most feasible for the in vivo use due to its low uptake in the liver and the in vivo stability. These coupling methods would be also applied to the antibody labeling with a positron emitter of Ga-68.

No. 683

PREPARATION AND BIODISTRIBUTION OF POLYCHELATE-RADIOLABELLED MONOCLONAL ANTIBODIES. P. Shreve and R.L. Wahl. University of Michigan Medical Center, Ann Arbor, MI.

Chelate molecules covalently linked to monoclonal antibodies (MoAbs) provide a means of labeling antibodies with radioactive metals. Attempts to achieve high levels of specific activity by linking several chelates directly to the antibody at multiple sites may result in a loss of antibody immunoreactivity. We investigated the use of a separate polymeric chelate molecule linked to the antibody at a single site as an alternative means of labeling.

Deferoxamine, a siderophore which forms stable complexes with Ga-67 was linked to a polycarboxylate polymer (polyacrylic or polyglutamic) bearing a free thiol moiety. The resulting polymeric chelate molecule was then covalently linked to antibody at a single site by a heterobifunctional coupling agent. 5C6.4, a murine IgG2ak MoAb was labeled with Ga-67 using a small polychelate (8 chelates, 6K daltons) and a large polychelate (18 chelates, 13.5K daltons). Labeling was also conducted with In-111 DTPA and I-125.

Biodistribution in rats showed rapid hepatic and renal uptake of the MoAbs labeled with the large polychelate. MoAbs labeled with the small polychelate had organ distributions more comparable with that of In-111 DTPA. Hepatic and renal uptake of iodinated antibodies was consistently lower than any of the metal chelate labeled antibodies.

We conclude that small polymeric chelate molecules can be used to label MoAbs. This method of labeling may be useful in achieving increased levels of specific activity for imaging and therapeutic applications of MoAbs labeled with metallic radionuclides.

No. 684

NEW DOUBLE BIFUNCTIONAL CHELATING AGENTS FOR LABELING Fab' FRAGMENTS. T.S.T. Wang, A.M. Gold, R.A. Fawwaz, S. Ferrone, and P.O. Alderson. Columbia Univ. and NY Medical Coll., New York, NY.

To develop new agents that selectively react with the -SH group(s) of the Fab' monomer of the anti-melanoma monoclonal antibody (MAA-MoAb)-763 and with In-111, excess Deferoxamine (DF) was reacted with succinimidyl-4-(p-maleimidophenyl)butyrate (SMPB) or N-succinimidyl-3-(2-pyridyldithio)propionate (SPDP) in 50 M Pi, pH 8.0, 50% acetonitrile at room temperature for 10 min., and then incubated at 37°C for 1 hr. with freshly prepared MAA-MoAb-763-Fab', pH 8.0. Remaining -SH groups were blocked with N-ethylmaleimide. The Fab'-bifunctional chelate conjugate was isolated by using Sephadex G-50 column chromatography, labeled with In-111, and then repurified on Sephadex G-50. Binding of the Ab to melanoma cells (Human Colo-38) and control cells (lymphoma) in tissue culture was evaluated and compared with Fab'-DTPA binding. While labeling of Fab' with DTPA resulted in complete loss of immunoreactivity, almost full immunoreactivity (>95%) was obtained with In-111-DF-SMPB-Fab' and In-111-DF-SPDP-Fab' (n=3 per sample). Binding of the control MAA-MoAb-763-Fab' was found to be 100% and the control lymphoid cell line was less than 3%. These findings indicate that the use of bifunctional chelating agents that bind to the Ab at non-critical sites results in significantly improved immunoreactivity.

No. 685

USE OF HIGH-PERFORMANCE HYDROXYLAPATITE (HPHT) CHROMATOGRAPHY FOR PURIFICATION OF MONOCLONAL ANTIBODY Fab FRAGMENTS. K Yokoyama, JC Reynolds, JA Carrasquillo, P Maloney, SM Larson. National Institutes of Health,

Bethesda, MD. CH Paik, VK Sood, RC Reba. George Washington University Medical Center, Washington, DC.

Development of a purification method for Fab fragments is important because the immunoreactivity of the fragment is very sensitive to chemical modifications. We have developed a simple and fast purification method using a High-Performance Hydroxylapatite (HPHT) chromatography equipped with a 0.8x10cm hydroxylapatite column. This report describes our evaluation of the HPHT chromatographic purification of Fab fragments of monoclonal antibody 96.5 (anti-melanoma p97). HPHT chromatography separated unmodified Fab, I-125-Fab (specific activity 1.3 mCi/mg) or Fab-DTPA (0.6 DTPA/Fab) into two peaks with retention times of 6 and 16 min respectively. The column was eluted with 0.12M phosphate buffer (pH 6.8) at a flow rate of 1 ml/min. The immunoreactivity of each peak from the I-125-Fab purification was determined by a direct cell binding assay (CBA) using FEM X2 skin melanoma cells. For peak 2, 85% of the activity bound to cells whereas for peak 1, 28% was capable of binding to cells. As assessed at 50% inhibition of tracer binding in a competitive CBA, peak 2 from the Fab-DTPA purification was 9 times more potent than peak 1 and also two times that of the unpurified (pre HPHT) Fab-DTPA. Peak 2 from Fab-DTPA and peak 2 from the purification of unmodified Fab had equal potencies. We conclude that HPHT chromatography can be utilized to purify conjugated or unmodified Fab into the higher immunoreactive fraction which has a potential advantage in tumor targeting.

Monday, 3:30-6:00

Exhibit Hall

RADIOPHARMACEUTICAL: GENERAL**No. 686**

UPTAKE OF C-14-LABELED ALICYCLIC α -AMINO ACIDS IN TRANSPLANTED PHEOCHROMOCYTOMAS. B.L. Byrd and J.E. Crook, Medical and Health Sciences Division, Oak Ridge Associated Universities, Oak Ridge, TN.

This study was directed at finding a suitable scanning agent for physiologic studies of pheochromocytomas using positron emission tomography (PET). The biodistributions of C-14-carboxyl-labeled 1-aminocyclopentanecarboxylic acid (ACPC) and two of its analogs, 1-aminocyclobutanecarboxylic acid (ACBC) and 1-aminocyclohexanecarboxylic acid (ACHC), were studied in male New England Deaconess Hospital (NEDH) rats bearing RNC-259 transplanted pheochromocytomas. Tissue uptake was studied at 30 min post-injection, which has been shown to be compatible with the short half life of C-11. The tissue distribution was reasonably uniform with a few exceptions. Uptake in the tumor was relatively high (1.82 percent per gram for ACBC, 1.36 for ACPC, and 1.64 for ACHC). With all three compounds the tumor-to-tissue ratio was above 2:1 for all tissues except the pancreas. The blood had less than 5% of the injected dose remaining at sacrifice and had the lowest tissue concentration of the twelve tissues studied. All three compounds have been labeled with C-11. However, only ACBC and ACPC have been used successfully at our institution for clinical imaging studies of other types of tumors. Based on a comparison of the results of this study with the uptake of these compounds in other tumors which have been scanned successfully using PET, it is felt that they show promise as scanning agents for pheochromocytomas in humans. (This research was supported by contract number DE-AC05-76OR00033 between the U.S. Department of Energy and Oak Ridge Associated Universities.)

No. 687

IMPROVED TUNGSTEN-178/TANTALUM-178 GENERATOR. J.L. Lacy, M.E. Ball, H. Wiles, M.S. Verani, and R. Roberts. Baylor College of Medicine, Houston, TX.

The W-178/Ta-178 generator reported by Neirinckx has a number of unique virtues, including short-lived (9.3 min) low dose daughter, long-lived (22 days) relatively easily produced parent [Ta-181 (p,4n) W-178], high yield and compatibility with the multiwire gamma camera. However, employing the reported eluting solution of .1N HCl and .1% hydrogen peroxide the breakthrough rises rapidly after elution of 25 to 35 column volumes, limiting the number of patient studies and requiring very careful breakthrough monitoring. Accordingly, we attempted to improve the generator's performance by testing changes in eluting solution. With HCl concentration lowered to .03N, the onset of breakthrough did not occur until more than 200 column volumes were eluted, and was very gradual. The eluted activity had a sharp profile, with 98% eluted in .7 column volume. A yield of 30% was achieved at 20°C. A significant inverse relationship was seen between yield and temperature with yield rising to 60% at 5°C with no effect on column chromatography (elution profile), or breakthrough performance. Several units have been used in clinical studies for periods in excess of 30 days, with highly stable performance, Ta-178 yield of up to 120 mCi and breakthrough consistently below .002% of loaded W-178 activity. Thus, with these modifications the W-178/Ta-178 generator is a very practical, low cost clinical system, which provides high doses of Ta-178 for first pass radionuclide angiography with many potential benefits.

No. 688

GADOLINIUM-LABELED PHARMACEUTICALS AS POTENTIAL MRI CONTRAST AGENTS FOR THE LIVER AND BILIARY TRACT. A. NAJAFI, E. C. Amparo, N. Hutchison, R.F. Johnson Jr., University of Texas Medical Branch, Galveston, TX.

Three gadolinium-labeled compounds, potential MRI contrast agents for liver and biliary tract, were studied: 1) Gd-DISIDA, 2) Gd-DTPA-Liposomes, and 3) Gd-DTPA dihexadecylamide. In each case, "Carrier Added" Gd-153 with specific activity of 1.0 uCi/mg was used. Each labeled compound was injected into a rabbit and gamma camera scintiphotos were obtained. The rabbit was imaged in a 0.6T MRI system before and after injection. Pulse sequences were chosen that would yield T1-weighted images, allowing calculation of T1 relaxation times. Gd-DISIDA proved unsatisfactory due to in vivo instability; this was confirmed in our rat biodistribution study. Gd-DTPA-Liposomes showed good uptake in the reticuloendothelial system of the liver and spleen. Gd-DTPA dihexadecylamide showed very good uptake in the hepatocytes with subsequent excretion into the biliary tract. This compound showed very little uptake in the kidneys. Both Gd-DTPA-Liposomes and Gd-DTPA dihexadecylamide produced significant shortening of the T1 relaxation times of the liver and observable increase in intensity on the T1-weighted images. Gd-DTPA-Liposomes and Gd-DTPA dihexadecylamide show promise as potential MRI contrast agents for liver and biliary tract imaging.

No. 689

THE EFFECT OF SERUM CONCENTRATION ON THE LABELING EFFICIENCY OF INDIUM-111 CHELATES. K. Ramberg, R. Connolly, R. Hanson, W. Baur, A. Callow and P. Kahn. Tufts-New England Medical Center, Northeastern University, Boston, MA

The purpose of this study was to determine the effect of serum concentration on the labeling efficiencies of In-111-oxine (In-ox), In-111-tropolone (In-trop), and In-111-mercaptopyridine-n-oxide (In-merc). Bovine endothelial cells in monolayer were used as the cell model.

The cells were grown to confluence in 24 well plates with media (DME) and 10% fetal bovine serum. The media with serum was removed and the cells rinsed once with serum-free media. DME with 0, 2.5, 5 or 10% calf serum was added to the cells. The cells were then incubated at room temperature for 30 minutes with In-ox, In-trop,

or In-merc. The media was removed and the cells harvested with trypsin and assayed for radioactivity.

Results are shown below:

Serum Conc.	Labeling Efficiencies \pm SEM		
	In-ox	In-trop	In-merc
0%	61.7 \pm 0.72	41.0 \pm 1.14	66.6 \pm 0.87
2.5%	34.2 \pm 0.68	4.9 \pm 0.41	6.2 \pm 0.24
5.0%	25.5 \pm 0.58	3.3 \pm 0.25	4.7 \pm 0.14
10%	14.4 \pm 0.70	2.0 \pm 0.11	2.5 \pm 0.12

In this model the addition of serum significantly decreased the labeling efficiency of all three chelates with In-ox the least affected.

No. 690

DIFFERENTIAL INFLUENCE OF GLUCOSE-INSULIN ON CARDIAC TURNOVER OF I-123 PHENYLHEXADECANOIC (IP) AND C-14 PALMITIC ACID (PA). S.N. Reske, W. Schmitt, *F.F. Knapp, Jr. and C. Winkler. Inst. Nuc. Med. Univ. Bonn, FRG and *Nuclear Medicine Group, Oak Ridge National Laboratory (ORNL), Oak Ridge, TN.

Glucose-insulin treatment is known to delay overall cardiac free fatty acid (FFA) oxidation. In this study we compared the effect of this metabolic intervention on the relative oxidation of IP and PA in isolated LANGENDORFF-perfused rat hearts. In total 6 hearts were perfused with an oxygenated Krebs-Henseleit buffer (11 mM glucose, 0.1 IE/ml short acting bovine insulin) at a flow rate of 10 ml/min. An IP/PA mixture, complexed to 3% bovine serum albumin, was injected into the aortic inflow. The production rates of (C-14)CO₂ and (I-123) hydrophilic metabolites (primarily (I-123)benzoic acid) were determined in serial samples of the effluate over 15 min. (C-14)CO₂ production reached a rapid peak at 3 - 4 min p.i. and then declined exponentially. In contrast, (I-123)hydrophilic catabolites showed a similar initial clearance upto 5 min p.i.; however, a second rise or a plateau-phase was observed until about 8 min p.i. Final slopes of both curves were similar. Since IP is known to be converted to phenylated C-1 and C-3 fragment catabolites, these data suggest re-utilisation of IP-metabolites either for FFA-re-synthesis, and/or - more probably - in triglyceride - synthesis due to glucose-insulin mediated increased availability of alpha - glycerol - phosphate. Metabolic interventions thus may have differential effects on cardiac turnover of aliphatic and aromatic FFA. In addition, the data suggest a stringent standardization of dietary state in clinical applications of IP.

ORNL is operated by the U.S. Department of Energy under contract DE-AC05-84OR21400 with Martin Marietta Energy Systems, Inc.

No. 691

IN-VITRO AND IN-VIVO CHARACTERIZATION OF RUTHENIUM-BLEOMYCIN COMPARED TO COBALT- AND COPPER-BLEOMYCIN. H-S. Shao, G.E. Meinken, S.C. Srivastava, D. Slosman, D.F. Sacker, P. Som, and A.B. Brill. Brookhaven National Laboratory, Upton, NY.

Bleomycin (BLM) has undergone extensive investigation both as a cancer chemotherapeutic agent and as a carrier for radionuclides for imaging. In this study we investigated the preparation, chromatographic evaluation and biodistribution in mice of ruthenium (Ru-103, Ru-97)-BLM and compared it with Co-57-BLM and Cu-67-BLM. Ru-103-BLM was obtained in high labeling yields (>60%) using the following conditions: 1.8 mg BLM, 8-20 nmol SnCl₂, pH 6-8, 37°, 3 hr reaction. Purification by CM-25 Sephadex using an ammonium formate gradient (0.05-1.0 M) elution gave three u.v. peaks: BLM B₁, B₂, and A₂, all containing a proportionate amount of Ru-103. Purification on alumina columns eluted with 0.9% NaCl was also effective. TLC (silica gel) using 10% (w/v) ammonium formate/methanol (1:1) gave good separations with R_f values of 0.75, 0.68, 0.40, and 0.25, corresponding to various labeled BLM species. HPLC analysis of Co-57-BLM and Cu-67-BLM using

μ Porasil columns and 0.3% ammonium formate solution in 50% methanol resulted in separation of various forms of labeled BLM. HPLC of Ru-103-BLM, however, gave somewhat ambiguous results. Based on preliminary biodistribution data in adenocarcinoma and melanoma bearing mice, the relative effectiveness for tumor imaging of the three labeled BLM preparations is as follows: Co-57>Cu-67>Ru-97. These results suggest that Co-55 and Cu-67 labeled BLM may warrant evaluation for adjuvant radiation-chemotherapy applications. [Research supported under U.S. DOE Contract No. DE-AC02-76CH00016 and Jiangsu Institute of Nuclear Medicine, Wuxi/Jiangsu, China (P.R.C.)].

No. 692

SAMARIUM-153 TUMOUR UPTAKE IN MELANOTIC AND AMELANOTIC B16 MURINE MELANOMA. J.H. Turner, A.A. Martindale, C. de Witt, J. Webb, P. Sorby and R.E. Boyd. Fremantle Hospital and Murdoch University, Western Australia and the Australian Atomic Energy Commission, NSW, Australia.

Tumour affinity of radiolanthanides prompted investigation of Sm-153 uptake in melanoma. Samarium-153 ($T_{1/2}$ 46.7h, 103 keV γ) was prepared from enriched Sm-152 in the AAEC reactor. Sm-153 chloride, Sm-153 citrate, Sm-153 DTPA, Sm-153 HIDA, Sm-153 PIH (pyridoxal isonicotinoyl hydrazone) and Sm-153 PBH (pyridoxal benzoyl hydrazone) tumour uptake at 1, 6, 24 and 48h in both melanotic (MEL) and amelanotic (AMEL) B16 melanomas of C57 black mice was compared with that of Ga-67 citrate and Se-75 methionine given IV to 5 animals for each time period when the tumour had grown to 1cc. Histopathological examination at each passaging assured comparability of the degree of melanogenesis and absence of necrosis.

The rapid localization of Sm-153 chloride and Sm-153 citrate in liver and spleen was due to in vivo formation of a colloid which on chromatographic and spectroscopic analysis appears to be Sm-153 carbonate. Sm-153 DTPA was rapidly excreted by the kidneys and tumour uptake was negligible. Sm-153 HIDA uptake by the liver made tumour imaging difficult despite relatively high affinity (AMEL 6.82 \pm 1.00% DI/gm at 6h, MEL 6.24 \pm 0.81% DI/gm at 6h). Sm-153 PBH peak tumour uptake (AMEL 3.14 \pm 0.76% DI/gm at 1h, MEL 5.69 \pm 1.20% DI/gm at 6h) and Sm-153 PIH (AMEL 4.23 \pm 0.90% DI/gm at 6h, MEL 4.03 \pm 0.90% DI/gm at 1h) compared unfavourably with that of Ga-67 citrate (AMEL 12.71 \pm 1.98% DI/gm at 24h, MEL 41.45 \pm 12.21% DI/gm at 24h) and Se-75 methionine (AMEL 11.07 \pm 1.55% DI/gm at 24h, MEL 10.55 \pm 1.48% DI/gm at 24h) but images of both AMEL and MEL melanomas were obtained with Sm-153 PBH and Sm-153 PIH.

No. 693

RADIOLABELING OF METALLOPORPHYRINS FOR IMAGING VASCULAR PLAQUES AND LESIONS. Y. Yano, M. Singh, C. Mathis, and T.F. Budinger, Donner Lab, Univ. of Calif., Berkeley, CA

Porphyrins and metalloporphyrins have been shown to accumulate in plaques and atherosclerotic lesions (J Clin Invest 71:395, 1983, Photochem Photobiol 40:59, 1984, SMRM Meeting Aug 1985, Abs p 902). We have studied the radiolabeling of tetrakis(p-methoxyphenyl)porphine (TKMPP), tetra(4-pyridyl)porphine (TPyP), tetraphenylporphine (TPP), protoporphyrin IX di-Na (PP-Na), and hematoporphyrin IX (HP) with generator produced Ga-68 and Tc-99m. Cobalt-57 was used to determine the chemistry of labeling for cyclotron produced Co-55, a positron emitter with an 18 h half-life. The radioisotopes were added to the porphyrins in one of several solvents such as acetic acid-sodium acetate, HCl, pyridine, or CHCl₃. The preparations were heated under reflux or in capped reaction vials with magnetic stirring. Autoclaving the sealed reaction vial was another method which provided the highest radiolabeling yield. Incubation times were from 30-60 min. The radioporphyrins were passed through a 0.45 micron Millipore™ filter with >95% recovery of the labeled compound. Quantitative analysis of the radiolabel was by ITLC in CHCl₃:CH₃OH. The most

successful labeling yields of >95% were obtained with Ga-68-TKMPP and Ga-68-TPyP. The yield of porphyrins labeled with Tc-99m reduced with NaBH₄ was <10%.

The ⁵⁷Co-TKMPP preparation gave 96% labeling at Rf 0.8 and the free ⁵⁷Co²⁺ was about 4% at Rf 0.2.

Monday, 3:30-6:00

Exhibit Hall

RADIOPHARMACEUTICAL: HALOGENS

No. 694

RADIOIODINATION OF 3-QUINUCLIDINYL BENZILATE USING NO-CARRIER-ADDED CONCENTRATION OF I-125/NaI. K.S. Lee, R.E. Gibson, W.C. Eckelman and R.C. Reba. The George Washington University Medical Center, Washington, DC.

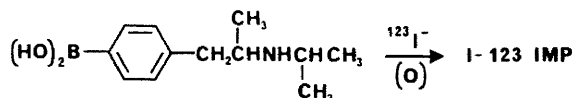
3-Quinuclidinyl benzilate (QNB) is a potent muscarinic antagonist which binds to muscarinic acetylcholine receptors. A radioiodine labeled analogue of QNB is one of the ideal ligands - it can bind to these receptors specifically and may be useful for clinical diagnosis.

A simple method was developed to radioiodinate QNB using milligram or microgram amounts of QNB and thallic trifluoroacetate in trifluoroacetic acid followed by the addition of I-125/NaI, aluminum chloride, and I-127/NaI. Three reaction steps were involved: QNB was reacted with thallic trifluoroacetate at 60°C for 24 hours, then radioactive I-125/NaI and aluminum chloride were added to the reaction mixture and the reaction was allowed to continue at 70°C for 3 or 24 hours; and then non-radioactive I-127/NaI was added to the above mixture at 70°C for another hour. The optimal mole ratio of QNB:aluminum chloride:thallic trifluoroacetate was 2:2:1. The radiochemical yields of [3-I-125]QNB (11 \pm 6% for milligram amounts of QNB and 2 \pm 0.5% for microgram amounts of QNB) and specific activity (8.4 \pm 2.7 Ci/mole) were determined.

No. 695

N-ISOPROPYL p-[I-123]-IODOAMPHETAMINE: A NO-CARRIER-ADDED SYNTHESIS VIA ORGANOBORANES. G. W. Kabalka, R. S. Varma, and Y. Gai. The University of Tennessee, Knoxville, TN

N-Isopropyl p-[I-123]-iodoamphetamine (I-123 IMP) has proven to be a valuable agent for cerebral blood flow measurement. I-123 IMP has also been utilized to evaluate pulmonary endothelial metabolism and enterohepatic absorption. The material is generally prepared via an iodine exchange reaction which can lead to difficult isolation problems when no-carrier-added sodium iodide is utilized. Organoboranes have proven to be useful intermediates for isotope incorporation [Kabalka, *Acct. Chem. Res.*, 17, 215 (1984)]. The borane reagents are unique because they can be prepared containing a variety of physiologically active functional groups. Thus it is often possible to prepare a radio-labeled agent, such as a fatty acid, via a sequence in which the radioisotope is incorporated in the final step. This minimizes synthesis time and maximizes yields. We have developed a synthesis of I-123 IMP via the reaction of the corresponding boronic acid with I-123 sodium iodide as supplied by Medi-Physics, Inc.



The boronic acid precursor is synthesized from the corresponding p-bromo derivative via a reduction-transmetallation sequence developed previously. [Kabalka, et al., *J. Organomet. Chem.*, 259, 269 (1983) and *Synth. Commun.*, 15, 843 (1985).]

No. 696

A TRIGLYCERIDE ESTER OF P-IODOPENTADECANOIC ACID AS A POTENTIAL LIVER IMAGING AGENT. S. Schwendner, J. Weichert, M. Longino, M. Gross, and R. Counsell. The University of Michigan and VA Hospital, Ann Arbor, MI.

A triglyceride analog, glycerol-2-palmitoyl-1,3-di-15-(p-iodophenyl)pentadecanoate (DPPG) was synthesized and radiiodinated for evaluation as a potential functional hepatic scintigraphic agent. This compound was administered in a Tween-saline vehicle to female rats. At 5 m the liver showed accumulation of radioactivity of 7.04 ± 0.26 dose/g (mean \pm SEM, n=4), corresponding to 52.0 ± 1.5 dose/organ. The hepatic activity gradually decreased until at 1 h 2.56 ± 0.26 dose/g remained. DPPG is hydrolysed to the free acid within 5 min as shown by gel electrophoresis ($37.0 \pm 5.1\%$ in the albumin fraction) and lipid extraction of the liver ($55.8 \pm 3.4\%$ remaining as the parent compound). Gamma camera scans were obtained on control rats (C) as well as rats pretreated with ethinyl estradiol (E), streptozotocin (S) or heparin (H). Animals were scanned up to 90 m post-injection. Following this Tc-99m sulphur colloid was injected and an image acquired for comparison of liver uptake. C showed peak accumulation at 15 m with clearance of the radioactivity from the liver apparent by 90 m. E, S, and H all showed more activity in the blood with a less intense liver image at 15 m and delayed clearance with time. Following imaging the animals were sacrificed for tissue distribution studies. Liver DPPG levels were similar (C 1.51, H 1.77, E 1.74 dose/g) except for S with 2.72 dose/g. Blood levels at this time were: C 0.87, H 0.98, D 2.85, and E 5.31 dose/g. Based on differences in uptake and clearance of radioactivity observed in these animal models, DPPG shows potential for in vivo evaluation of liver function.

No. 697

N-(p-iodophenyl)maleimide, A NEW RADIOIODINATED THIOLE REAGENT WITH SELECTIVE EFFECTS ON PLATELET MEMBRANE FUNCTIONS. P. C. Srivastava, F. F. Knapp, Jr., D. W. Karl and D. C. B. Mills. Nuclear Medicine Group, Oak Ridge National Laboratory (ORNL), Oak Ridge, TN, and Departments of ¹Biochemistry and ²Pharmacology and the Thrombosis Research Center, Temple University Hospital, Philadelphia, PA.

N-(p-iodophenyl)maleimide (IPM) was synthesized by condensing maleic anhydride with p-iodoaniline, followed by ring closure of the crystalline intermediate. The corresponding radioactive compound was prepared similarly (radiochemical yield 70%, specific radioactivity 2.5 Ci/mole) from 10 μ mole of iodoaniline, prepared by radiiodination of p-amino-phenylmercuric acetate. When added to washed human platelets, 10 μ M IPM enhanced the stimulation of adenylate cyclase (AC) by prostacyclin, and selectively blocked the inhibition of adenylate cyclase by ADP. At 30 μ M, IPM also blocked the inhibitory effect of epinephrine, but at this concentration it also inhibited in the absence of epinephrine. IPM stimulated platelet uptake of P_i and of adenine by up to 60%. In all of these respects IPM behaved like other lipid-soluble maleimides, e.g., N-phenyl maleimide, N-ethylmaleimide, and cytochalasin A. [¹²⁵I]-IPM combined covalently with many platelet proteins, including the intracellular proteins, actin and myosin.

ORNL research sponsored by the Office of Health and Environmental Research, U.S. Department of Energy, under contract DE-AC05-84OR21400 with Martin Marietta Energy Systems, Inc.

No. 698

ANALYSIS AND QUALITY CONTROL OF RADIOIODINE USING HIGH PERFORMANCE LIQUID CHROMATOGRAPHY (HPLC). S.C. Srivastava,

G.E. Meinken, L.F. Mausner, and T. Prach. Brookhaven National Laboratory, Upton, NY.

High-purity iodine-123 has attracted considerable attention as the ideal radionuclidic label for a variety of diagnostic agents including the brain-localizing lidoamphetamine (IMP) and HIPDM. The chemical nature of iodine has a significant effect on many iodination reactions, for example when using I-123 from different sources. In this study, HPLC methods have been developed for the isolation and characterization of many common inorganic as well as organic forms of iodine. Of the various solvent mixtures and reverse-phase columns (C₂, C₈, C₁₈) evaluated, RP8 Lichrosorb columns and an eluting solution (pH7) containing 0.05 M phosphate, 0.002 M NBU₄OH, and 10% acetonitrile provided the best separations. A procedure was also developed for determining the carrier iodine content of radioiodine solutions by monitoring uv absorption at 225 nm. The curve was linear for 0.01-10 μ g iodide. Using well-characterized standards, HPLC retention factors were established for IO₃⁻, I⁻, I₃⁻, IO₄⁻, I⁺, CH₃I, and CHI₃. A number of unidentified species were also separated using the above system. BLIP-produced (p,5n) I-123 consistently provided >95% I⁻ and almost no iodate. The iodination of IMP (using an exchange method) was more sensitive to iodate impurity, whereas the iodination of HIPDM was not. Labeling conditions and mechanisms can be better optimized from a knowledge of the composition of radioiodine solutions. The HPLC technique developed in this study allows a rapid separation of various iodine species with excellent resolution and appears superior to the routinely used TLC and paper chromatographic methods. (Research supported under U.S. Department of Energy Contract No. DE-AC02-76CH00016.)

No. 699

PREPARATION AND BIODISTRIBUTION OF RADIOIODINATED 1,4-BENZODIAZEPINES, J. L. Wu, D. W. Compton, S. R. Look, R.M. Baldwin, J.F. Lamb, T.H. Lin, Medi-Physics, Inc., Emeryville, California

Benzodiazepines are known to bind to a specific binding site in brain. We have prepared and evaluated two radiiodinated benzodiazepines.

I-125 labeled 5-(2-fluorophenyl)-2,3-dihydro-7-iodo-1-methyl-1H-1,4-benzodiazepine (I) and 5-(2-fluorophenyl)-1,3-dihydro-7-iodo-1-methyl-2H-1,4-benzodiazepine-2-one (II) were prepared from the direct exchange of NaI-125 with I and II in glacial acetic acid in the presence of CuSO₄.

In vivo distribution of I-125-I and I-125-II was determined in rats at 5 min and 2 hr after I.V. injection. The specific activity (SA) was varied from 0.4 Ci/mole to 300 Ci/mole. Both compounds were rapidly taken up by the brain: 1.5% dose/g of I and 0.8% dose/g of II at 5 min. The activity then cleared from the brain with time. Brain to blood ratios were >3 for I at 5 min to 2 hr and >2 for II at 5-10 min, decreasing to 0.9 at 30-60 min. No appreciable activity was found in thyroid. A major fraction of both compounds appeared to be excreted through the hepatobiliary system. Similar brain uptake was observed for I-125-I with SA of 0.4 Ci/mole and 300 Ci/mole. High brain uptake and brain to blood ratio obtained with I-125-I indicated that radiiodinated compound I may be useful for brain imaging.

Monday, 3:30-6:00

Exhibit Hall

RADIOPHARMACEUTICAL: POSITRONS**No. 700**

SYNTHESIS OF C-11 CARBOXYL-LABELLED DOPA. M.J. Adam, J.R. Grierson, T.J. Ruth and B.D. Pate. UBC/TRIUMF Program on Positron Emission Tomography, University of British Columbia, Vancouver, Canada V6T 2A3.

C-11 labelled dopa has been prepared via the Strecker method in order to study the decarboxylation of dopa in patients suffering from movement disorders. The Strecker synthesis has previously been used to prepare a wide variety of amino acids labelled with C-11 [L.C. Washburn et al., *Radiopharmaceuticals II*; Proc. of 2nd Int. Symp. Radiopharm., Seattle, WA, pp 767-777 (1979)] but was never applied to the synthesis of C-11 dopa. The only reported synthesis of C-11 dopa is via the carbonation of an α -lithio-isonitrile precursor [J.M. Bolster et al., *I.J.A.R.I.* 34, 1650 (1983)].

The bisulfate addition complex of 3,4-dimethoxyphenylacetaldehyde is heated in a sealed bomb at 195°C with ammonium carbonate, ammonium chloride and potassium cyanide for 5 min. The bomb was cooled, 1 mL of NaOH (6.25 M) added and the bomb heated again to 195°C for 5 min. The bomb was cooled, the contents were neutralized with 1 mL of H₃PO₄ (6.25 M), diluted with 20 mL H₂O and passed through C-18 Sep Paks. The C-11 dimethoxydopa was eluted from the Sep Paks with 1:1 MeOH/H₂O and the solution evaporated to dryness. HI was added and the mixture heated to 155°C for 5 min. The HI was evaporated and two portions of H₂O (5 mL each) were added and successively evaporated. The residue was dissolved in phosphate buffer and filtered to give C-11 dopa in 60% radiochemical yield (decay corrected to EOB) in an overall synthesis time of ~1 h. The final product was >95% radiochemically and chemically pure.

No. 701

SPECIFIC BINDING OF N-(3-[¹⁸F]FLUOROPROPYL)SPIROPERIDOL TO BABOON BRAIN DOPAMINE RECEPTORS. C. Arnett, C.-Y. Shiu, A. P. Wolf, L.-Q. Bai, and R. Teng. Chem. Dept., Brookhaven National Laboratory, Upton, NY

In a continuing effort to produce positron-emitting radioligands with the appropriate characteristics for PET studies of dopamine receptors, we have synthesized N-(3-[¹⁸F]fluoropropyl)spiroperidol (FPSP) and evaluated its specific distribution and metabolism in the baboon. Following i.v. administration, FPSP localized in those brain regions (striatum) known to contain high concentrations of dopamine receptors. Striatal accumulation of radioactivity was stereospecific, i.e., it was blocked by pretreatment with (+)-butaclamol but not by (-)-butaclamol. The absolute striatal uptake (in % dose per cm³) was intermediate between that of [¹⁸F]-spiroperidol and [¹⁸F]-N-methylspiroperidol. The peripheral metabolism of FPSP followed the same time course as other ¹⁸F-labeled butyrophenones studied. Because 3-[¹⁸F]fluoropropanoic acid, a possible radioactive metabolite of FPSP, would be converted rapidly *in vivo* to ¹⁸F⁻, particular attention was paid to determine the effect, if any, of this metabolite on the utility of FPSP for imaging dopamine receptors *in vivo*. Whereas mouse studies indicated a significant bone accumulation of radioactivity, the brain radioactivity was > 76% unchanged FPSP at 1 h after injection. PET baboon studies demonstrated that peripheral metabolism had little if any effect on the specificity of brain distribution. The ratio of striatum to cerebellum radioactivities at 3 h after injection was 5.9, which is close to the corresponding ratio of 6.1 found for [¹⁸F]-N-methylspiroperidol. Research supported by DOE, OHER and NIH Grant NS-15380.

No. 702

PURIFICATION OF REACTOR-PRODUCED FLUORINE-18 FLUORIDE USING HIGH PRESSURE ION CHROMATOGRAPHY. J.M. Bennett, M.A. Channing, and R.D. Finn. National Institutes of Health, Nuclear Medicine Department, Bethesda, MD.

Reactor-produced ¹⁸F labeled fluoride is an important alternative for facilities which do not have access to a particle accelerator. Fluorine-18 can be prepared via a two-step nuclear reaction:



In our experiments quartz tubes containing 0.4 g of 95.56% enriched ⁶Li₂CO₃ have been irradiated for 2 hours at a thermal flux of 1.3 x 10¹⁴ n cm⁻² sec⁻¹ at the National Bureau of Standards Nuclear Reactor. Typically, 80 mCi of fluorine-18 is produced concurrently with 40 mCi of ³H. A method has been developed utilizing high performance ion chromatography (HPIC) to not only separate, but isolate and purify the fluorine-18 species as its tetramethylammonium salt. Potential sources of cationic and anionic contaminants have been identified and examined by analytical HPIC, while radionuclidic impurities have been determined using gamma spectroscopy and scintillation counting.

The reactivity of the final reagent fluoride was determined by monitoring its incorporation as fluorine-18 labeled 2-fluoro-2-deoxy-D-glucose upon reaction with methyl 4,6-O-benzylidene-2,3-cyclic sulfato-β-D-mannopyranoside.

No. 703

C-11-SCH 23390 FOR THE STUDY OF DOPAMINE D1 RECEPTORS: SYNTHESIS AND BIODISTRIBUTION IN THE MOUSE. O.T. DeJesus, G.J.C. Van Moffaert, and A.M. Friedman. University of Chicago, Chicago, IL and Argonne National Laboratory, Argonne, IL.

We have previously reported the synthesis and evaluation of Br-75 labelled SCH 23390 analog as a selective radioligand for the study of CNS dopamine D1 receptors (*Eur. J. Pharmacol.* 108:327, 1985). The time course of distribution of this drug in the primate brain was found by PET to be rapid which suggested to us that C-11 (t_{1/2} = 20 min) would be the ideal label for this radioligand. Here we report the preparation of C-11-SCH 23390 and its biodistribution in the mouse.

C-11-SCH 23390 was prepared by the reaction of its des-methyl analog in DMF with C-11-CH₃I. Ten minute reaction at 40°C resulted into 60%-80% radiochemical yield based on C-11-CH₃I. HPLC purification gave a product which was found by mass spectrometry to have identical fragmentation pattern as the authentic sample.

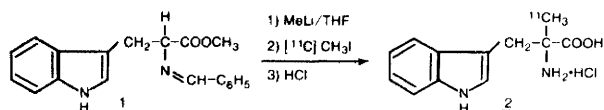
Administration of C-11-SCH 23390 into several sets of mice and analysis of its whole body distribution showed that the critical organs are the liver, kidney, and the G.I. tract. The distribution of the drug in the mouse brain showed a striatum to cerebellum uptake ratio of 23 one hour postinjection. Moreover, the binding in the striatum was found to be saturable. In conclusion, these results show that C-11-SCH 23390 should be the radioligand of choice for PET studies of CNS dopamine D1 receptors.

No. 704

THE SYNTHESIS OF NO-CARRIER-ADDED α-[¹¹C-METHYL]-L-TRYPTOPHAN: M. Diksic and T. Chalv, Brain Imaging Centre, Department of Neurology and Neurosurgery, Montreal Neurological Institute, McGill University, Montreal, Quebec, Canada

The metabolic pathway of α-methyl-L-tryptophan (α-MTry) and its influence on tryptophan metabolism was studied by Sourkes et al (*Neuropharm.* 11 (1972) 197) who found that α-MTry follows the metabolic pathway of tryptophan. We report here the synthesis of α-[¹¹C]MTry, a potential tracer for the measurement of *in vivo* synthesis of the neurotransmitter serotonin. The starting material (I) prepared by reacting tryptophan methyl ester with a mixture of benzaldehyde and triethylamine at about -10°C. The resultant shift base (I) (~1 mmol) was reacted with CH₂Li (~1 mmol) in THF; [¹¹C]CH₂I dissolved in THF was added to the reaction mixture kept in a dry ice-acetone bath. The mixture was then warmed, filtered, and the solvent evaporated under reduced pressure. The protecting group was removed by hydrolysis with 2M HCl for 5 min at 135°C (bath). After hydrolysis, the solution was extracted with ethyl ether. The aqueous layer

was concentrated and passed through a reverse phase Sep Pak column. The synthesis required 25 to 30 min to complete and had a radiochemical yield of about 30%. The specific activity assessed by HPLC was in excess of 1500 Ci/mmol. TLRC on silica gel using $\text{CH}_3\text{OH} - \text{NH}_4\text{OH}$ (3.5:0.05) as the solvent showed one spot with $R_f = 0.85$, the same as an authentic sample identified by MS and $^1\text{H-NMR}$. The work has been supported by the MRC.



No. 705

SYNTHESIS AND EVALUATION OF SOME [C-11]-4-ARYL PIPERAZINIUM SALTS AS MYOCARDIAL IMAGING AGENTS. D.R. Elmaleh, S. Padmanabhan, G.J. Boudreaux, H. Kizuka, E. Livni, M.A. Hassan, J. Cooney, R.N. Hanson and H.W. Strauss, Massachusetts General Hospital, Boston, MA.

The purpose of this work was to synthesize and evaluate a series of [C-11] substituted phenyl piperazinium salts as myocardial imaging agents. Three analogs were synthesized, [C-11]-1-methyl-1-(2-hydroxyethyl)-4-phenyl piperazinium iodide (IIa); [C-11]-1-methyl-1-(2-hydroxyethyl)-4-(2-methylphenyl) piperazinium iodide (IIb) and [C-11]-1-methyl-1-(2-hydroxyethyl)-4-(4-iodophenyl) piperazinium iodide (IIc). The compounds were prepared by the reaction of [C-11]-methyl iodide and the precursor secondary amines. Their radiochemical purity (>99%) was ascertained by HPLC. Biodistribution studies were performed at various time intervals (5, 30, 60 minutes) following intravenous administration of the compounds IIa-IIIc. Two and three dimensional images were obtained in dogs following the i.v. injection of (IIa) (3-5 millicuries).

In rats the concentration of (IIa-IIIc) in the heart varied from 3 to 4% at 5 minutes. For IIIc, the concentration in the heart (%dose/gram) remained essentially the same between 5 and 30 minutes (3.44 and 3.25 respectively). Ratios (% dose/gram) of target (heart) to non-target tissue (blood) were high (12.03-49.14 at 5 minutes to 4.58-28.75 at 60 minutes). Imaging studies of the dog clearly demonstrated activity retention in the myocardium for over 30 minutes. IIIc and [I-125]piperazinium salt were compared for their biodistribution in rats.

These results suggest that some of these agents could be useful as tracers for myocardial imaging studies.

No. 706

SYNTHESIS AND EVALUATION OF [F-18]21-DEOXY-21-FLUORO-PREDNISONE (DFP) AS A POTENTIAL LIGAND FOR NEURO-PET STUDIES. A.L. Feliu and D.A. Rottenberg, Memorial Sloan-Kettering Cancer Center, New York, NY.

Corticosteroids exert a variety of physiological, biochemical and behavioral effects, modulate homeostatic mechanisms and, in high doses, exhibit major anti-inflammatory, anti-neoplastic and anti-edema potency. Because corticosteroid ligands bind specifically to cortical and subcortical receptors, we undertook the synthesis of high specific activity F-18-labeled steroids to study regional brain uptake and disposition. DFP was synthesized in 2-8% radiochemical yield (100 min EOB) from prednisone 21-tosylate and no-carrier-added (NCA) [F-18]tetramethylammonium fluoride. While synthetic steroids typically carry a 9-fluoro group, labeling the 9-position proved impractical with available NCA F-18 reagents. Experiments were conducted in vitro and in vivo to evaluate the pharmacologic effect of altering the 21-position. DFP was unchanged after exposure to cell-free rat plasma, but was biotransformed to the corresponding prednisolone derivative (DFPI) when incubated with rat whole blood at 37° ($t_{1/2}$ 53 + 5 min). In vivo,

conversion of DFP to DFPI appeared to be a "first-pass" process. DFPI rapidly crossed the rat blood-brain barrier (brain/blood activity ratio: 1.1 at 5 min; 0.24 at 30 min; 0.27 at 60 min). Moreover, radio-HPLC analysis of rat blood and brain homogenates suggested that even at 15 min post injection brain tissue was enriched in DFPI compared to blood. Our data demonstrate that DFP exhibits behavior similar to that of prednisone, that the 21-fluorine resists cleavage in vivo, and that [F-18]21-fluoro corticoids are potentially useful probes for neuro-PET regional distribution and binding studies.

No. 707

BIODISTRIBUTION OF ^{11}C -TRANLYCYPROMINE IN RATS: A POTENTIAL BLOOD FLOW AGENT AND MAO INDICATOR IN THE BRAIN. S. Padmanabhan, H. Kizuka and D.R. Elmaleh, Massachusetts General Hospital, Department of Radiology, Boston, MA 02114

We have recently synthesized and evaluated a number of radiolabeled α, α -dimethylphenethylamine analogs (phentermines) as potential brain blood flow agents. In particular, N-[C-11]-methylchlorphentermine (C-11-NMCP) was found to exhibit favorable properties for PET studies; high brain uptake and prolonged retention of radioactivity. A major advantage of using p-halo substituted phentermine analogs is the high level of unchanged compounds in the brain and blood, due to blockage of some metabolic pathways including deamination by MAO and parahydroxylation. As part of the structure-distribution relationship studies, we have prepared the N-[C-11]-methyl analog of a potent MAO inhibitor trans-2-phenylcyclopropylamine (translycypromine) and have studied its tissue distribution in rats. C-11-translycypromine (C-11-TC) was prepared from translycypromine and C-11-labeled methyl iodide in DMF, followed by purification on HPLC. Uptake of C-11-TC in the brain was 1.25, 0.99 and 0.94 of injected dose per organ at 5, 15 and 30 min after injection, respectively, while that of C-11-NMCP was 2.70, 2.67 and 2.67, respectively. Brain-to-blood ratios of C-11-TC were approximately one-third that of C-11-NMCP. Lung uptake of C-11-TC, however was substantially lower than that of C-11-NMCP. The results of the preliminary biodistribution study suggests that C-11-NMCP is superior to C-11-TC as a brain blood flow agent. C-11-TC, however would be a potential MAO indicator in the brain.

No. 708

RADIOSYNTHESIS AND BIODISTRIBUTION OF A POTENT D-1 DOPAMINE RECEPTOR TRACER FOR POSITRON EMISSION TOMOGRAPHY: CARBON-11 SCH 23390. H.T. Ravert, A.A. Wilson, R.F. Dannals, D.F. Wong, and H.N. Wagner Jr. The Johns Hopkins Medical Institutions, Baltimore, MD.

There are at least two dopamine receptor subtypes: D-1 receptors (coupled to adenylate cyclase) and D-2 receptors (independent of adenylate cyclase). SCH 23390 is a selective highly potent antagonist of the dopamine D-1 receptor subtype.

C-11 labeled SCH 23390 was prepared by N-alkylation with C-11 methyl iodide. C-11 methyl iodide prepared from C-11 carbon dioxide was trapped in a cooled solution (-78°C) of the appropriate nor-methyl precursor in dry dimethylformamide (200 μL). The solution was heated to 80°C for 5 min., applied to a semi-preparative C-18 high performance liquid chromatographic column, and eluted with a mixture of acetonitrile and water. The fraction containing C-11 labeled SCH 23390 was collected, evaporated to dryness, and dissolved in sterile saline and sodium bicarbonate. The average specific activity, determined using uv spectroscopy, was 1951 mCi/ μmole at the end-of-synthesis. The radiochemical yield was approx. 28% with a synthesis time of approx. 22 min. from end-of-bombardment.

The striatum-to-cerebellum ratio of i.v. administered C-11 SCH 23390 in mice was in excess of 150 at 1 hour and decreased thereafter. The uptake of the tracer in the striatum was blocked by prior administration of cisflupentixol. Studies in human beings are in progress.

No. 709

L-[N-13]TYROSINE: ENZYMATIC SYNTHESIS AND BIODISTRIBUTION IN TUMOR-BEARING ANIMALS. K.C. Rosenspire, E. Nieves, A.S. Gelbard, S. Filc-DeRicco, M.T. Corbally and G.R. DiResta. Memorial Sloan-Kettering Cancer Center, New York, NY.

L-Tyrosine plays an important role in the formation of catecholamines and melanin. L-Tyrosine labeled with N-13 may prove useful for *in vivo* studies of syndromes associated with aberrant aromatic amino acid metabolism. We synthesized L-[N-13] tyrosine from N-13 ammonia by coupling the glutamate dehydrogenase and glutamate oxaloacetate transaminase reactions, with p-hydroxyphenylpyruvate as the amino acceptor, utilizing enzymes immobilized on CNBr activated Sepharose. After incubation, the reaction mixture contained 57% tyrosine, 39% glutamate and 4% NH₃. N-13 Tyrosine was separated from unreacted N-13 ammonia and glutamate on a Poropak Q column. A yield of 20 mCi of N-13 tyrosine (radiochemical purity >97%) was produced from 400 mCi N-13 ammonia 25 min EOB.

Organ uptake of N-13 tyrosine after retro-orbital injection in tumor-bearing mice was determined. Most of the activity was in liver and pancreas with additional activity in intestines, stomach and tumor. Tumor uptake from N-13 tyrosine was 5.9% at 10 minutes compared to 1.5% from N-13 ammonia, 2.7% from N-13 glutamate and 9.0% from N-13 valine. A rabbit bearing a VX2 tumor on each hind leg was also imaged. Activity was observed in the liver, pancreas, intestine, stomach, kidneys and tumor. Tissue distribution confirmed the results in mice except that the VX2 tumor did not take up as much N-13 activity as the mouse tumor possibly due to extensive necrosis. Our studies demonstrate that N-13 tyrosine can be synthesized and has potential as a tumor localizing agent for studying *in vivo* metabolism.

No. 710

ACCUMULATION OF C-11-LABELED AIB, ACBC, AND ACPC IN THE DUNNING R3327G PROSTATIC ADENOCARCINOMA AND MORRIS 5123C HEPATOMA TUMOR MODELS. B. Schmall,¹ P.S. Conti,¹ and L.C. Washburn.² Memorial Sloan-Kettering Cancer Center, New York, NY¹ and Oak Ridge Associated Universities (ORAU), Oak Ridge, TN.²

C-11-labeled AIB, ACBC, and ACPC have been shown to be useful tumor-imaging agents in clinical trials and are potential tracers of amino acid transport *in vivo*. We have completed a comparative biodistribution study of these agents in the Dunning prostate and Morris hepatoma tumor models (4-5 animals per group; Tsac 30-45 min).

	Relative Concentration (RC)*			Tumor/Blood Ratios		
	AIB	ACBC	ACPC	AIB	ACBC	ACPC
R3327G	1.61	1.15	1.47	1.94	1.42	1.35
5123C	8.45	11.6	8.95	15.9	11.3	8.61
	Tumor/Prostate Ratios			Tumor/Liver Ratios		
R3327G	3.66	2.02	1.60	-	-	-
5123C	-	-	-	8.20	9.35	7.85

*RC=DPM found per g tissue/DPM injected per g animal mass

Although both models accumulate these amino acids in tumor tissue, higher levels were observed in the hepatoma for all three compounds. ACBC showed the highest levels of RC in the hepatoma while the prostate tumor accumulated more AIB. Tumor/blood ratios were highest with AIB in both tumor models. Observation of the accumulation patterns may be important in choosing which of several compounds to use for diagnosing and monitoring malignant disease. Favorable tumor/tissue and tumor/blood ratios

suggest that these agents can be used to visualize tumor present in normal surrounding tissue. (Part of this work was supported by contract number DE-AC05-76OR00033 between the U.S. Department of Energy and ORAU.)

No. 711

L-(1-C-11)TYROSINE FOR THE MEASUREMENT OF PROTEIN SYNTHESIS IN TUMOR AND BRAIN WITH POSITRON EMISSION TOMOGRAPHY. W. Vaalburg, K. Ishiwata, Ph.H. Elsinga, A.M.J. Paans, and M.G. Woldring. Department of Nuclear Medicine, University Hospital, Groningen, The Netherlands.

The feasibility of L-(1-C-11)tyrosine (L-C-11-Tyr) for measuring protein synthesis in tumor and brain tissue with PET was investigated. L-C-11-Tyr was prepared by the lithiated isocyanide method followed by L and D separation using HPLC. Metabolic studies in rats with Walker 256 carcino sarcoma were carried out using L-C-14-Tyr. After i.v. injection the radioactivity was rapidly incorporated into tissue. From 5 to 60 min after injection in many organs the C-14 level remained nearly constant, while in tumor and pancreas the uptake increased. In tumor, pancreas, liver and brain the proportion of protein-bound radioactivity increased with time. In blood the C-14 level decreased rapidly within 5 min, but increased gradually after 15 min. The proportion of protein-bound C-14 in plasma increased to 87% at 60 min after injection. Within 60 min 7.4% of the C-14 was excreted as CO₂. In several rats, lymphnode metastases showed higher uptake than the primary tumors. In PET studies of rats using L-C-11-Tyr the tumors were clearly visualized. Similar kinetic results as with C-14 were obtained. In the metastatic tumors also a higher accumulation of C-11 radioactivity was observed.

Our results show that L-C-11-Tyr is a suitable tracer for measuring protein synthesis by PET and suggest that metastases have a higher ability of protein synthesis compared to primary tumors. The kinetic model of protein synthesis based on these results will be discussed.

Monday, 3:30-6:00

Exhibit Hall

RADIOPHARMACEUTICAL: TECHNETIUM

No. 712

THE HEXAHALOTECHNETATE REAGENTS IN THE SYNTHESIS OF LIPOPHILIC Tc-99m COMPLEXES. J.K. Amarty and W. Wolf. Radiopharmacy Program, University of Southern California, Los Angeles, CA.

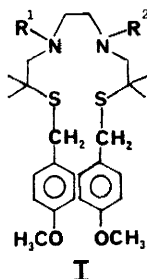
Previous work of this laboratory had defined the conditions under which Tc-VII could be readily reduced to a 'pure' Tc-IV and how one could avoid interfering photoaquations of that reduced technetium species. The method of choice in the preparation of lipophilic Tc-complexes is ligand exchange of the hexahalotechnetate in non-aqueous media. We have prepared a large variety of complexes, whose properties can be tailored to the desired lipophilicities, such as complexes having octanol/water partition coefficients ranging from 20 to 500+. Bidentate ligands yield 2 types of complexes: TcL₂X₂ and TcL₃⁺, where L is the bidentate and X is a monodentate ligand. Tridentate ligands give TcL₂ complexes, either charged or neutral. The complexes obtained were characterized by chromatography and electrophoresis, and could be easily purified by CHCl₃/H₂O partition. Yields of 90% or better have been obtained when using a suitable base to trap the HX produced on ligand exchange. Stability of the complexes under various solvolytic and aqueous conditions have been studied. As an example, the Tc(ox)₂Cl₂ (where ox = 8-hydroxyquinoline) and Tc(ox)₃⁺ have been obtained in 92% yields when

using acetonitrile as the reaction solvent. Such complexes exhibited a stability of better than 95% over a 24 hr. period, when redissolved in an aqueous medium containing 5% ethanol.

No. 713

SYNTHESIS OF Tc-99m-N₂S₂ COMPLEXES VIA THE p-METHOXYBENZYL PROTECTED THIOL LIGAND. K.E. Baidoo, S.Z. Lever, A.V. Kramer, L.A. Epps, H.D. Burns, and H.N. Wagner Jr. The Johns Hopkins Medical Institutions, Baltimore, MD.

The preparation of Tc-99m diaminodithiol (Tc-99m-N₂S₂) complexes via the p-methoxybenzyl (MBz) protected dithiol ligand (I) obviates several problems associated with direct use of the unprotected ligand. The protected thiols resist oxidation and are more easily purified and handled. They also permit the synthesis of symmetrical and unsymmetrical N, N'-disubstituted N₂S₂ ligands which cannot be prepared directly from the macrocyclic disulfide, the usual precursor. Furthermore, they provide a means for attaching functional groups which do not tolerate typical disulfide reduction conditions.



In a typical reaction, thiol deprotection is carried out in situ by treating I with trifluoroacetic acid at 70° for 10-30 minutes. The reaction mixture is then neutralized with phosphate buffer and filtered. Addition of Tc-99m pertechnetate and stannous chloride yields the expected Tc-99m N₂S₂ complex in > 98% yield as determined by TLC and HPLC. Use of anisole scavenger favors cleaner deprotection, but has little effect on complex yield.

No. 714

METAL ISONITRILE COMPOUNDS FOR THE CONVENIENT PREPARATION OF HEXAKIS (ISONITRILE) Tc(I) COMPLEXES. A. Carpenter, Jr., L. Maheu, K. Linder, T. Tulip, J. Thompson*, M. Doshi, M. Matthew, M. Patz and V. Subramanyam*; E.I. DuPont de Nemours, NEN Medical Products, N. Billerica, MA and *Central Research and Development, Wilmington, DE

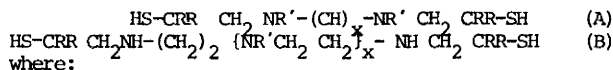
The unipositive cationic complex ^{99m}Tc(TBI)₆⁺ (TBI = tertiary butyl isonitrile) reported by Jones et. al. has interesting pharmacological properties including retention in the human heart (Holman, et al). Past syntheses of ^{99m}Tc-isonitriles have been based on the use of the free ligand in aqueous ethanol containing sodium dithionite as the reductant or from an aqueous solution of the zinc adduct (e.g. Zn(TBI)₂Br₂) using stannous glucoheptonate as the reducing agent. Due to the nature of the starting materials, these methods are not convenient for the preparation of ^{99m}Tc-isonitriles in the clinical setting.

We undertook the preparation and evaluation of several transition metal TBI complexes in combination with a variety of reductants for making ^{99m}Tc(TBI)₆⁺. Optimal radiochemical yields were obtained from complexes of Cu(I), Ag(I), Ni(II) and Co(I). Little or no ^{99m}Tc(TBI)₆⁺ was obtained when using d⁰ metal complexes as the source of isonitrile (e.g. Mn^I, Fe^{II}, Ru^{II}). Best yields of ^{99m}Tc-isonitrile were generally achieved at elevated temperature (~ 100°C) with a stannous or sulfur compound as the reductant. Although many of the transition metal TBI complexes evaluated were found to be convenient, stable, non-volatile sources of TBI, the best overall results were exhibited by the tetrakis (TBI) Cu(I) complex. This result was successfully extended to the preparation of other Tc-isonitrile complexes starting from Cu(CNR)₄X as the source of isonitrile.

No. 715

COMPARATIVE BIODISTRIBUTION OF 99m Tc-LABELED POLYAMINO-DITHIOL DERIVATIVES. E. Chiotellis, A. Varvarigou, N.R.C. "Demokritos", Athens, GREECE.

Bis-aminoethane-dithiol (BAT) has proved to be an interesting molecule in preparing 99m-Tc complexes capable to cross the BBB. In the present study new polyaminodithiol ligands of 99m Tc were prepared and evaluated in mice comparatively to BAT moiety. The compounds studied were of the following types:



- A (I) x=2. R=R'=H (1), R=H R'=C₂H₅ (2), R=CH₃ R'=H (3)
- (II) x=3. R=CH₃ R'=H (4)
- B(III) x=1. R=CH₃ R'=H (5), R=C₂H₅ R'=H (6), R=CH₃ R'=C₃H₇ (7)
- (IV) x=2. R=CH₃ R'=H (8), R=C₂H₅ R'=H (9)

The compounds were labeled with 99m-Tc, using sodium borohydride. The complexes were administered in mice in dilute alcohol. Partition coefficient (p.c.) was determined in octanol/phosphate buffer. Biological data are expressed as % dose/gr. The values of brain uptake are listed below:

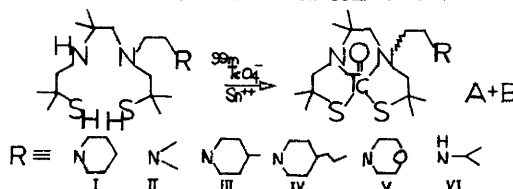
COMPOUND	1	2	3	4	5	6	7	8	9
p.c.	2.04	3.41	12.8	2.18	2.46	7.05	3.06	0.23	4.24
2min	2.55	3.87	3.82	1.04	1.07	0.66	0.52	0.34	0.38
15min	2.03	2.56	1.14	0.57	0.48	0.27	0.22	0.13	0.16

Compounds 1-3 showed comparatively the greatest brain uptake. By increasing the chain length between the nitrogens of BAT moiety (compounds 4-9) brain accumulation decreased significantly.

No. 716

COMPARISON OF Tc-99m AMINOETHYL DIAMINODITHIOL ANALOGUES FOR BRAIN BLOOD FLOW IMAGING. H.W. Goldfarb, U. Scheffel, S.Z. Lever, H.D. Burns, H.N. Wagner Jr. The Johns Hopkins Medical Institutions, Baltimore, MD.

We recently developed the Tc-99m complex of N-piperidinylethyl diaminodithiol (NEPDADT) (IA) for measurement of regional brain blood flow by SPECT(+). We have now synthesized and tested 10 new N-aminoethyl derivatives (II-VI, A+B) to compare their uptake and retention in the mouse brain with complex IA.



The reaction of Tc-99m pertechnetate with each ligand in the presence of stannous ion produces two complexes, which were isolated by normal phase HPLC and reconstituted with saline for injection. Biodistributions at 5min after injection showed that complexes IA, IIA and IIIA had the highest uptake of tracer in the brain. Biodistributions of these three complexes at times up to 2hr showed that retention of complex IIIA was nearly twice that of IA and IIA after 30min. These studies suggest that perturbation of the aminoethyl moiety produces significant differences in the biodistribution in mice. In particular, the addition of a methyl group to the 4-position of the piperidine ring increases the retention of tracer in the brain.
 †) J Nucl Med 26: 1287-1294, 1985

No. 717

VALIDATION OF Tc-99m-d,1-HEXAMETHYL PROPYLENE AMINE OXIME (Tc-99m-d,1-HM-PAO) AS A REGIONAL CEREBRAL BLOOD FLOW

AGENT: A MICROSPHERE STUDY. T.J. Hoffman, E.H. McKenzie, W.A. Volkert, M.H. Laughlin, and R.A. Holmes. Harry S. Truman Memorial Veterans Hospital and the University of Missouri, Columbia, MO.

Tc-99m-d,l-hexamethylpropylene amine oxime (Tc-99m-d,l-HM-PAO) was validated as a regional cerebral blood flow (rCBF) agent by comparing its cerebral uptake and retention to Sn-113 microspheres in rabbit brain.

Two groups of New Zealand White rabbits (4 per group) were studied. Sixteen discrete cerebral tissue areas were dissected from each animal. The samples included cortical grey matter, white matter, midbrain, diencephalon, pons, medulla, and spinal cord. The first group of rabbits sacrificed 4 min. post injection (p.i.), gave a Tc-99m-d,l-HM-PAO/Sn-113m microsphere (Tc/Sn) ratio of 1.082 ± 0.300 (N = 60) over a range of rCBF values (28 - 134 ml/min/100g). The second group sacrificed one hour p.i. gave a Tc/Sn ratio of 1.024 ± 0.169 (N = 64) over an rCBF range of (24 - 202 ml/min/100g). Linear regression analysis of the Tc/Sn ratio vs. rCBF for early and delay studies gave slopes of -0.0063 ± 0.0015 and -0.0015 ± 0.0005 respectively. This excellent correlation confirms that Tc-99m-d,l-HM-PAO distribution reflects cerebral blood flow and should be readily amenable to study human cerebral blood flow disorders.

No. 718

EVALUATION OF ISCHEMIC DAMAGE OF GASTRONEMIIUS MUSCLES OF MICE BY Tc-99m PYROPHOSPHATE: A POSSIBLE MODEL FOR MYOCARDIAL ISCHEMIC INJURY. P.V. Kulkarni, M. Bennett, R.W. Parkey. The University of Texas Health Science Center at Dallas, TX

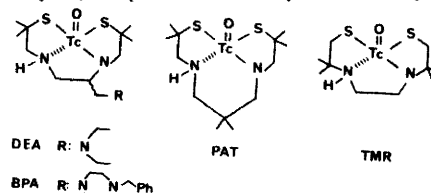
Among various models of myocardial infarction and ischemic damage, dog models with permanent or temporary ligation of coronary arteries are used extensively. However, studies with these models are involved, extensive, and expensive. Facilities, personnel, etc. may not be readily available to carry out these types of studies. Thus we are exploring the possibility of utilizing small animal models, viz., mice. In this study one hind leg of the animal was tied with a suture string for various time intervals from 15 min to 5 days; then the tie was released. Tc-99m PPI [an indicator of muscle injury] $10\text{-}30\mu\text{Ci}$, was injected into tail veins at various time intervals (30 min to 2 wks) after the release of the tie. The animals were killed at 1 hr post-injection of the radiotracer. Calf muscle from control leg (untied calf) and from injured leg (tied calf) were weighed and counted in a gamma well counter. Sternum and blood samples were also taken for counting. In a separate group of animals CK and LDH enzyme measurements were obtained to verify the muscular damage by the calf tying process. The ratio of radioactivity in unit mass of damaged muscle to that in control calf muscle was calculated for each group of animals (6 in each group). The muscle sections were observed with a regular microscope for gross histology. Muscular damage was not apparent by gross histology or by enzyme measurements at early time intervals. The uptake of Tc-PPI in tied calf muscle was noticeable in animals tied only for 15 min and reperused for 24 hrs. The ratios were 4.1 ± 2.0 (mean \pm SD) and increased to 35.9 ± 4.5 when the tie was for 6 hrs and reperfusion for 24 hrs. The ratios returned to 2.8 ± 0.3 when the tie was for 5 hrs and reperfusion was for 2 wks. These results parallel those reported for uptake of Tc-PPI in myocardial infarcts in dogs. Thus, our study shows that the mouse model may be useful in studies of ischemic muscle damage.

No. 719

NEW Tc-99 COMPLEXES BASED ON N_2S_2 LIGANDS. H.F. Kung, Y-Z. Guo, C-C. Yu, R.H. Mach, S.M.N. Efang, and M. Blau. Department of Nuclear Medicine, SUNY at Buffalo, NY.

In developing new Tc-99m labeled brain imaging agents, several lipid-soluble and neutral Tc-99 complexes based on the N_2S_2 ligand were prepared to determine the chemical structure and radiochemical stability. The complexes can be prepared by reducing Tc-99m or Tc-99 pertechnetate with Sn(II) glucoheptonate or sodium dithionite in the presence of a ligand. The complexes were extracted with chloroform and purified further by silica gel column chromatography and re-

crystallization. The structure of the complexes were determined by IR, NMR, elemental analysis and x-ray crystallography.



Both DEA and BPA showed two distinctive isomers, depending on whether the unsymmetrically substituted side chain is in a *syn*- or *anti*- position to the pyrimidal Tc complex. The *syn*- and *anti*- structures have been confirmed by x-ray crystallography. As expected, TMR and PAT gave only one form of complex. All of the complexes showed high *in vitro* and *in vivo* stability, an essential property making these ligands attractive as a basis for future structural modification to develop new Tc-99m radiopharmaceuticals. Acknowledgment: Authors thank Dr. V. Subramanian of DuPont for providing NMR and x-ray crystallography data.

No. 720

SERUM STABILITY AND NON-SPECIFIC BINDING OF TECHNETIUM-99m LABELED DIAMINODITHIOL FOR PROTEIN LABELING. F. Liang, R.L. Childs and D.J. Hnatowich. University of Massachusetts Medical Center, Worcester, MA.

Previously we investigated the use of DTPA-coupled proteins to simplify labeling with technetium-99m (Tc) but especially to improve the stability of the label. These investigations have now been extended to include diaminodithiol (N,N'-bis(2-methyl-2-mercaptoethyl)ethylenediamine, DADT) originally reported by Epps et al. (J. Nucl. Med. 24 (1983) P 10). The conditions of labeling of free ligand (pH, DADT buffer and tin concentration) were optimized to provide 100% chelation with Tc at reasonable DADT concentrations (100 $\mu\text{g/ml}$ or less) and under non-denaturing conditions. Labeling was determined by paper chromatography, reversed-phase and size exclusion HPLC. After incubation in 80% fresh serum, 37°C for 24 hrs, repeat analysis showed only 5% dissociation of the chelate. By contrast, the DTPA chelate shows instability towards oxidation during this period. DADT derivatized on an ethylene carbon showed almost identical serum stability as DADT itself whereas when derivatized on a nitrogen greater instabilities were apparent. Using identical labeling conditions, free DADT was chelated in the presence of IgG at different ligand:protein molar ratios. Non-specific binding of Tc to IgG at a 10:1 DADT:IgG molar ratio was as little as 5%. However, non-specific binding was essentially zero at a 2:1 molar ratio when labeling was by trans-complexation from Tc-EDTA. In conclusion, DADT forms more stable chelates with Tc than does DTPA with reduced non-specific binding and may therefore represent an attractive alternative for labeling proteins with Tc by the bifunctional chelate approach.

No. 721

SQ 30217, A TECHNETIUM 99m LABELLED MYOCARDIAL IMAGING AGENT WHICH SHOWS NO INTERSPECIES DIFFERENCES IN UPTAKE. R.K. Narra, T. Feld, P. Wedeking, J. Matyas, A.D. Num. Squibb Institute for Medical Research, New Brunswick, NJ.

SQ 30217 (Chloro (Methylboron(1-)-tris[1,2-Cyclohexanedione)dioxime(1-)]-N,N',N'',N''',N''''',N''''''')Technetium is a promising myocardial imaging agent. We have tested Tc-99m SQ 30217 in animals and found that it has proportionate myocardial uptake in all animals tested. In particular, the guinea pig does not show a drop in heart uptake relative to the rat which is a characteristic of those technetium compounds that perform well in most animals but poorly in man.

	Poor Human		Good Human	
	Myocardial Uptake TcD2Cl2*	TcD3	TcBIN	SQ 30217
Rat	2.83†	1.55	2.10	1.81
Guinea Pig	0.48	0.80	1.88	1.59

*D=DMPPE, BIN=(CN tButyl)6, †%I.D. in heart @ 5 m.

The washout of activity from the heart is biexponential with t1/2 of 2 and 44 m in rats and 3.4 and 42 m in dogs. The major organ for excretion is the liver. There is rapid blood clearance and no appreciable lung uptake. These characteristics are duplicated in all animals and species tested.

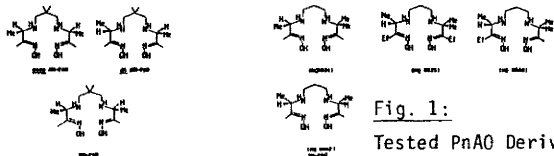
The dependence of heart uptake on perfusion was demonstrated in the pig with dipyridamole where uptake increased 40% and faster washout was observed: an acute myocardial infarct was seen in dogs as an area of decreased activity which upon reperfusion, appeared normal with a second dose of Tc-99m SQ 30217 1 hour later.

A stable preparation of Tc-99m SQ 30217 is made using a lyophilized kit reconstituted with saline. It is essentially non toxic at >200 times the expected human dose.

No. 722

COMPARATIVE TISSUE UPTAKE OF Tc-99m-d, 1-HMPAO AND OTHER PNAO ANALOGUES IN BABOONS. K. Reichmann*, H.-J. Biersack*, L. Basso*, A. Hartmann*, L.T.W. Matthews**, R.D. Neirinckx, R.D. Pickett** and C. Windkler*, Inst. for Clin. and Exp. Nucl. Med. and Neurology Dept., Univ. Bonn, Germany, and Amersham International**, Amersham, England.

To optimize the brain (Br) uptake and retention of analogues of propyleneamine oxime (PNAO), five Tc-99m-labeled derivatives were studied in normal adult baboons. Following i. v. injection, both planar and tomographic (SPECT) images were obtained with a rotating gamma camera (Gammatome T9000), equipped with a high resolution collimator. Time-activity curves were generated and evaluated over a 30 min. period for the brain, liver and neck (soft tissue and bone). HMPAO showed the best results which were dependent upon stereochemistry, dl- to dl+meso-, and this agent was chosen for further study. The dl- form showed rapid cerebral extraction (apprx. 1 min) and essentially no clearance over the 23 min period, with Br uptake of 4.3% (whole Br counts/whole body counts). The clearance was <8% over 23 min. The best of the other analogues showed a Br uptake of 3.6% after 1 min but a rapid clearance to 2.1% within 10 min. Because of the excellent properties of Tc-99m for SPECT, the ready availability of freeze-dried kits of dl-HMPAO, and the minimal clearance, the Tc-99m-dl-HMPAO may be an excellent agent for measurement of regional cerebral perfusion by SPECT.



No. 723

STANNOUS GLUCOHEPTONATE: AN EFFECTIVE TINNING AGENT FOR Tc-99m LABELING OF BLOOD CELLS. R.F. Straub, G.E. Meinken, and S.C. Srivastava. Brookhaven National Laboratory, Upton, NY.

Various tin complexes have been used as vehicles for introducing stannous (Sn⁺⁺) ions into blood cells for in-situ reduction of pertechnetate as a Tc-99m cell labeling technique. Since reduced Tc-99m species do not cross the cell membrane, and since only a fraction of the added tin is taken up into the cells, it is necessary to quantitatively remove extra-cellular Sn⁺⁺ before adding Tc-99m pertechnetate to the "tinned" cells. Using Sn-113 labeled complexes, we have studied the effect of the following ligands on the cellular uptake of tin: pyrophosphate (PYP), citrate (cit), EDTA, and glucoheptonate (GH). Of these ligands, GH gave the greatest Sn⁺⁺ uptake in all blood cells (RBC, lymphocytes, granulocytes, platelets). The order of

effectiveness was GH>Cit>>PYP>EDTA. The increased uptake is particularly advantageous with leukocytes, since tinned cells acquire a greater reduction capability and less extra-cellular Sn⁺⁺ remains to be washed off. The effect of the nature and volume of suspending media, time, temperature, etc., has been investigated. From a stannous cit kit containing 50 µg Sn, only 0.8 µg Sn is taken up by WBC (from 4 ml blood) whereas 1.1 µg Sn is taken up using a stannous GH kit with 10 µg Sn. This results in an increase in Tc-99m labeling efficiency from 50 ± 10% to 80 ± 10% for mixed leukocytes. Similar effects are observed for separated lymphocytes, granulocytes, and platelets. Results from these studies demonstrate that stannous glucoheptonate is a superior tinning agent for high-yield Tc-99m labeling of RBC, leukocytes, and platelets. (Research supported under U.S. Department of Energy Contract No. DE-AC02-76CH00016.)

Monday, 3:30-6:00

Exhibit Hall

RENAL

No. 724

EVALUATION OF ACUTE TUBULAR NECROSIS BY FACTORIAL ANALYSIS OF RENAL PERFUSION IN KIDNEY TRANSPLANTS. J.Darcourt, I.G.Mena, M.Koyle, L.Philippe, C.S.Marcus. Division of Nuclear Medicine, Harbor-UCLA Medical Center, Torrance, Ca.

The classical complications of allograft renal transplants are acute tubular necrosis (ATN), rejection and drug toxicity. We report on quantitation of ATN by performing factor analysis to the flow (FAF) component of Tc-99m DTPA renography. We studied 13 patients within 24 hrs. post cadaveric transplantation, assuming that they represented a relatively pure form of ATN. The control group was 9 patients with normal renography studied 2 months or more after transplantation. 20 mCi were injected intravenously and images acquired in anterior projection at 1 sec/frame. We limited the 4 factors FAF to the first 50 sec. after appearance of the bolus in the abdominal aorta. The area analyzed was transplant and corresponding iliac artery (IA). This provided 4 images and corresponding curves: background, IA, and 2 kidney images. The corresponding kidney curves were: one with a bell shape (K1), and the other with an ascending slope only (K2). K1 corresponds to parenchymal perfusion, it is shaped after the IA curve, while K2 represents DTPA retained by filtration.

During the 50 sec. of observation the total transplant activity is K1+K2. The relative contribution of K2 was .47±.19* in control patients and .18±.13 in ATN (p<.001), and K1 was .53±.19 and .82±.13 respectively (p<.001). These results confirm the loss of filtration function in ATN, while the flow is well preserved. It demonstrates that quantitative information on clinical entities like ATN can be derived from the flow segment of the DTPA renogram. *m±sd

No. 725

COMPARISON OF TRIAMIDE MERCAPTIDE (N3S) COMPLEXES AS POTENTIAL RENAL TUBULAR FUNCTION AGENTS. D. Eshima, A. Taylor, A. R. Fritzberg and S. Kasina. University of Utah Health Sciences Center, Salt Lake City, UT

Tc-99m Mercaptoacetylglycylglycylglycine (Tc-99m MAG3), a triamide mercaptide (N3S) ligand, has been shown to have biological properties similar to I-131 o-iodohippuric acid (OIH). Substitutions were made at the terminal amino acid to determine the effect this would have on the biological behavior of the complex. Ten new N3S complexes were screened in mice with the most promising ones being Tc-99m mercaptoacetylglycylglycine-R (Tc-99m MAG2-R), where R was: Ala, Asn and Gln (both complexes).

These complexes were further evaluated in rats utilizing constant infusion clearances, extraction efficiencies and plasma binding. The results show:

	Cl (ml/min/100g)	Plasma Binding	Extraction Efficiency
I-131 OIH	2.01	35%	63%
Tc-99m MAG ₃	2.84	77%	85%
Tc-99m MAG ₂ -Ala	2.33	78%	85%
Tc-99m MAG ₂ -Asn	2.01	24%	69%
Tc-99m MAG ₂ -Gln-A	1.96	36%	66%
Tc-99m MAG ₂ -Gln-B	1.89	52%	56%

HPLC analysis of urine showed no metabolism for any of the complexes.

In summary, these four triamide mercaptide complexes all compared favorably to simultaneously administered I-131 OIH in normal rodents and represent a new ligand class for Tc-99m which may provide a variety of complexes for the evaluation of renal tubular function.

No. 726

QUANTITATIVE ASSESSMENT OF THE DIURESIS RENOGRAM
K.Kletter, N.Nürnbergger, R.Dudczak
1st Med.Dept. and Dept. of Urology, Univ. of Vienna

Recently there have been numerous critical reports concerning the ability of diuresis renography (DRG) to distinguish between nonobstructive and obstructive urinary tract dilation. So far mainly qualitative criteria were used for the interpretation of the data, and this is why we tried to quantify the DRG.

40 patients with urinary tract dilation were studied by DRG as well as by the invasive pyeloureterometry (PUM-Whitaker Test). The DRG (0.5 mg frusemide/kgBW) was performed immediately following standard renography (15uCi I123-OIH/kgBW) in hydrated patients (10 ml/kgBW). Upper urinary tract volume was estimated from i.v.urography in all patients and in some patients directly measured using the nephrostomy. Assuming an approximately sigmoidal shape for the renal curve after frusemide application, the maximal elimination rate (Emax) of the tracer was determined. This value, closely related to the maximal urinary flow rate after frusemide, is calculated using the slope in the turning point of the curve. For grouping the pressure-flow values from the PUM, the scheme proposed by Whitaker was used.

Considering the Emax values alone, 33 patients could be attached to the same group as by the PUM. The remaining 7 patients were classified to adjacent groups by the different methods. In no case a complete mismatch (obstr. vs. nonobstr.) was obtained. A further improvement was gained in patients with considerable urinary tract dilation (up to 250 ml) by normalizing the Emax values using the measured urinary tract volumes. Using this quantification, the DRG seems to be suitable to save the invasive PUM except in cases of extremely reduced renal function.

No. 727

THREE-PHASE EVALUATION OF SCINTIGRAPHIC FINDINGS IN TESTICULAR TORSION. G.A. Kraslcky, J.H. Thrall, D.A. Parker, J.W. Froelich, R. Moore and J. Cerny. Henry Ford Hospital, Detroit, MI

To further evaluate the spectrum of findings in testicular torsion, Tc-99m pertechnetate flow studies and scintigrams of 16 surgically proven cases were reviewed. Three phases of each study were assessed: spermatic cord flow (SCF) in the early dynamic phase, hemiscrotal flow (HSF) in the late dynamic phase, and hemiscrotal static (HSS) activity. All examinations were performed preoperatively in the clinical setting of the acute hemiscrotum.

Five patients had viable testicles following detorsion and eight required orchiectomy for non-viability. Three patients had torsion of the testicular appendages. Decreased flow to the involved hemiscrotum (decreased HSF) was present in only 1 of 13 patients with torsion

of the spermatic cord. SCF was symmetric in all but one case, where it was increased to the side of a non-viable testicle. HSS activity was asymmetric (decreased) in all cases of viable torsion. In the non-viable group, HSF activity was symmetric in 2 cases, but increased in 6/8. Five of these six patients demonstrated a "halo sign" on the HSS images. Flow parameters were normal in all 3 cases of testicular appendage torsion. HSS images showed normal, decreased, or increased uptake, respectively.

We conclude that the finding of decreased flow by dynamic scintigraphy has low sensitivity and is therefore not a reliable marker of testicular torsion. Increased HSF and HSS activity and the "halo sign" are predictors of non-viability. Findings in torsion of the testicular appendages may be variable.

No. 728

RENAL FUNCTIONAL CHANGES AFTER CONVERTING ENZYME (CE) INHIBITION OR NITROPRUSSIDE (NP) IN HYPERTENSIVE RATS. H.B. Lee and M.D. Blaurock. Albert Einstein College of Medicine, Bronx, NY

Converting enzyme inhibition may enhance Nuclear Medicine diagnosis of Renovascular Hypertension (RVH). However, its effect on differing models of RVH needs further study. RVH was induced in rats by clamping the renal artery (RA) and measuring GFR and RPF pre and post CE or NP. The groups studied were: 1) 2K 1RA clamped for 1 week; 2) 2K 1RA clamped for 6 weeks; 3) 2K 2RA clamped for 1 week; 4) 1K 1RA clamped for 1 week; 5) SHR no RA clamped; 6) 2K 1RA clamped for 1 week; Group 6 was studied using NP to lower mean arterial pressure (MAP) to a similar degree as CE.

GROUP	% CHANGE AFTER ANTIHYPERTENSIVE DRUG					N
	N GFR	C GFR	N RPF	C RPF	BP	
1	- 3.2	-46.8*	17.3*	-39.4*	-13.0*	10
2	14.0	-72.6*	41.9*	-62.7*	-14.6*	10
3	--	-29.7*	--	-19.3	-14.7*	10
	--	-18.6	--	- 4.7		
4	--	-38.6*	--	-18.3*	-11.4*	10
5	26.1*	--	32.1*	--	- 7.4*	6
	26.2*	--	32.4*	--		
6	2.4	6.5	- 7.1*	1.7	-16.6*	5

*p<0.05 N=unclamped RA C=clamped RA
Changes in renal function with CE were qualitatively similar in all the models with clamped kidneys. In SHR rats GFR and RPF changes were related to vasodilatation. The effect on the unclamped kidney of rats with RVH was similar. NP changed the BP with little change in renal function. These data support a potential role for CE in enhancing the diagnosis of RVH.

No. 729

DYNAMICS OF RUBIDIUM-82 IN THE KIDNEYS: MEASUREMENT OF EXTRACTION FRACTION AND FLOW. N.A. Mullani, R. Ekas, S. Marani and K.L. Gould. University of Texas Health Science Center, Houston, TX.

Rubidium-82, a potassium analog and generator produced positron emitter, has been investigated in a preliminary study as a tracer for measuring renal plasma flow. Seven acute dogs were studied with beta probes to understand the dynamics of Rubidium-82 in the kidneys. Four dogs had arterial, venous and ureter catheters placed to measure the extraction and excretion of Rb-82 in the kidneys. Intra arterial injections were also carried out to obtain the washout rate constants. Three dogs were studied for renal plasma blood flow by comparing Rubidium-82 obtained flows with microspheres obtained flows. PET studies with Rb-82 were carried out in two dogs and one patient. First pass extraction fraction for Rb-82 ranges from 80-95% with an average of 89%. Majority of the excretion of Rubidium is to the venous side rather than the ureter with the rate of washout being flow dependent. Flow measurements with Rubidium and microspheres correlated well with the average control

flow of 5.0 ml/min/gm measured by microspheres and 4.5 ml/min/gm of flow measured by Rb-82. Reduction in renal flow was observed by both techniques when arterial flow was reduced by constricting the renal artery. PET studies of the dogs were obtained every two seconds for the evaluation of the dynamics of the renal artery input function and renal uptake. Kidneys of a patient were also imaged with Rb-82 and demonstrate the feasibility of using this technique in man. Due to its short half-life and high extraction in the kidneys, the potential use of Rubidium-82 for renal plasma flow measurements with PET needs to be further investigated.

No. 730

RENAL TRANSPLANT (RT) EVALUATION WITH Tc-99m DTPA (DTPA) - THE ROLE OF FACTOR ANALYSIS. Z.H. Oster, J.P. Bazin, C. Raynaud, D. Anais, M. Di Paola, R. Di Paola, F. Rapaport and H.L. Atkins. SUNY at Stony Brook, NY U.S.A. Service Hospitalier F. Joliot, CEA, Orsay and Inst. G. Roussy, Villejuif, France.

The etiological diagnosis of renal allograft dysfunction although very important has not yet been resolved. Determination of the perfusion index (PI) improves the accuracy of DTPA studies, but not to optimum.

FA was performed on 87 DTPA studies of 35 RT patients, by the now standard routine using a 64 x 64 matrix, acquisition of 1 frame/1 sec for 40 sec and 1 frame 20 sec for 17 min. A diagnosis was established within 24 hrs of each DTPA study mostly by biopsy and in some cases by surgery or other modalities. The global, cortical and medullary PI was calculated by ROI drawing, as described earlier.

The FA was restricted to a square containing the kidney and blood vessels supplying it. In the first min an arterial and a parenchymal factor are found. In the second group of images (2-20 min p.i.) factors representing parenchymal washout, accumulation in the collecting system and bladder become evident. The weight of these factors, their curves and pictorial outlines are obtained without the need of empirical ROI drawing. In addition, unsuspected findings such as peri-graft inflammation, infarcts, intrarenal venous congestion and urinary obstruction were detected.

This method seems to provide new information not available otherwise. Its value in diagnosing rejection vs. immunosuppressive-induced nephropathy is still under investigation.

No. 731

TOTAL AND SPLIT RENAL FUNCTION IN PATIENTS WITH RENO-VASCULAR HYPERTENSION. A. Singh, G. Reams, K.W. Logan, R.A. Holmes, J. Bauer. University of Missouri and Harry S. Truman Memorial Hospital, Columbia, MO.

Quantitative split renal function studies were performed in 8 patients with renovascular hypertension on therapy with angiotension converting enzyme inhibitors (ACEI). Effective renal plasma (ERPF) was measured using I-131 hippuran and a 44 minute plasma sample. Glomerular filtration rate (GFR) was measured from the renal uptake (2-3 min post-injection) of Tc-99m DTPA. All individuals had their total ERPF estimated by p-aminohippurate (Cpah) and total GFR estimated by inulin (Cinulin) clearance techniques. The results are shown below.

	Total Function, ml/min/1.73m ²	Split Function (ml/min/1.73m ²)		P
		Ipsilateral	Contralateral	
DTPA	67±10	31±7	36±4	NS
Cinulin	74±13			
Hippuran	396±44	164±33	232±20	<0.05
Cpah	312±56			

Conclusions: 1) Total GFR by DTPA closely parallels the GFR by inulin clearance. 2) Total ERPF by Hippuran was

higher than the total ERPF by Cpah. 3) Split function measuring ERPF may be more valuable than GFR measurements in patients with renovascular hypertension.

No. 732

RENAL BLOOD FLOW IN RENOVASCULAR HYPERTENSION ASSESSED BY POSITRON TOMOGRAPHY WITH Rb-82; EFFECT OF CAPTOPRIL. N. Tamaki, C.A. Rabito, N.M. Alpert, M. Barlai-Kovach, J.A. Correia, M.A. Nedelman, S. Dragotakes, H.W. Strauss. Massachusetts General Hospital, Boston, MA.

Serial measurements of renal perfusion were recorded with positron emission tomography (PET) and rubidium-82 (Rb-82) in a canine model of renovascular hypertension. Rb-82 calculated perfusion was compared to that determined by left atrial injection of microspheres. Renal perfusion images and microsphere injections were recorded in each of 7 dogs at: (a) control, (b) during renal artery stenosis and (c) stenosis with intravenous injection of captopril (1.2mg/kg). The tissue concentration of Rb-82 (Ct) in each PET transverse section of the kidney was determined and arterial blood activity of Rb-82 (Ca) measured by well counting during the equilibrium scan. Ct/Ca was correlated with microsphere renal blood flow according to a steady state single compartment model (r=0.90). Mean blood pressure was 115±15 (mean±sd) at control, significantly increased to 130±10 and went down to 98±15 after captopril infusion. Rb-82 determined flow and microsphere (ϕ) flow in each step were:

	Stenotic Kidney		Contralateral Kidney	
	Rb-82 flow	ϕ flow	Rb-82 flow	ϕ flow
Control	3.12±1.36	3.03±1.07	4.00±1.02	3.84±0.86
Stenosis	0.99±0.65*	1.09±0.55*	3.57±1.36*	2.97±0.79*
Captopril	0.67±0.59*	0.63±0.65*	4.49±1.13**	3.98±0.91**

(*p<0.05 vs control; **p<0.05 vs stenosis) These data indicate that captopril infusion resulted in a significant increase in flow to the contralateral kidney while flow to the stenosed kidney slightly (p=ns) decreased. These changes were associated with a decrease in blood pressure.

Monday, 3:30-6:00

Exhibit Hall

RADIOPHARMACEUTICAL CHEMISTRY: MISCELLANEOUS

No. 732.2

SYNTHESIS AND EVALUATION OF RADIOIODINATED 2-DEOXY-2- IODOVINYL ALTROSE DERIVATIVES AS POTENTIAL BRAIN IMAGING AGENTS. M. M. Goodman, F. F. Knapp, Jr., and A. P. Callahan, Nuclear Medicine Group, Oak Ridge National Laboratory, Oak Ridge, Tennessee 37831

Single photon tomography of the brain using iodine-123-labeled glucose analogues may enable the *in vivo* study of transport and utilization of glucose in patients with pathological disorders. This study was undertaken to design and evaluate 2-deoxy-2-(E)-iodo-vinyl-D-altrose derivatives as agents for monitoring glucose metabolism in the brain. The synthetic approach involved the scission of an anhydro sugar with a Grignard reagent. The starting material methyl 4,6-O-benzylidene-2-deoxy-2-ethynyl-β-D-altropyranoside (II) was prepared by treating methyl 2,3-anhydro-4,6-O-benzylidene-β-D-altropyranoside (I) with ethynyl-magnesium chloride. Hydrostannylation of (II) with (n-Bu)₃SnH gave the key intermediate, methyl 4,6-O-benzylidene-2-deoxy-2-(E)-(n-Bu)₃SnHC=CH-β-D-altropyranoside (III). Iododestannylation of (III) followed by hydrolysis (40% CH₃SO₃H) gave 3-deoxy-3-(E)-iodo-vinyl-D-altrose (V) whereas hydrolysis (20% CF₃COOH) followed by treatment with pyridine-Ac₂O gave methyl-2-deoxy-2-(E)-iodovinyl-2,4,6-O-triacetyl β-D-altropyranoside (VII). ¹²⁵I-labeled (V) and (VII) were evaluated in rats. Iodovinyl (VII) showed good brain

uptake (1.65% dose/gm at 5 min) and good retention (0.89% dose/gm at 30 min) with brain/blood values varying from 1.6:1 (5 min) to 1.1:1 (30 min).

Research sponsored by the Office of Health and Environmental Research, U.S. Department of Energy, under contract DE-AC05-84OR21400 with Martin Marietta Energy Systems, Inc.

No. 732.4

SYNTHESIS AND HIGH MYOCARDIAL SPECIFICITY OF A NEW OLEIC ACID TYPE RADIOIODINATED TELLURIUM FATTY ACID. P.C. Srivastava, F.F. Knapp, Jr., and A.P. Callahan, Nuclear Medicine Group, Oak Ridge National Laboratory (ORNL), Oak Ridge, TN 37831, and M. Varma and G.W. Kabalka, Chemistry Dept., University of Tennessee, Knoxville, TN 37996-1600

A new tellurium fatty acid, 9(10)-[¹²⁵I]iodo-5-tellura-9-hexadecenoic acid ([¹²⁵I]I), with a double bond between C-9 and C-10 similar to oleic acid and iodine stabilized at C-9(10), has been prepared and evaluated in rats. The boronic acid intermediate, H₃C-(CH₂)₅-CH=C[B(OH)₂](CH₂)₃-I (2) was prepared as a 4,5 mixture from the precursor, HC≡C-(CH₂)₃OH involving a series of chemical manipulations. Na[¹²⁵I]-chloramine-T iodination of (2) gave a 4,5 mixture of H₃C-(CH₂)₅-CH=C[¹²⁵I](CH₂)₃-I which after condensation with Na-Te-(CH₂)₃COOC₂H₅ followed by hydrolysis of the ethyl ester yielded H₃C-(CH₂)₅-CH=C[¹²⁵I](CH₂)₃-Te-(CH₂)₃-COOH ([¹²⁵I]I). The ([¹²⁵I]I) shows prolonged and high myocardial uptake (mean % dose/gm of 5 rats) and is a candidate for further evaluation with ¹²³I.

T, min	Heart	Blood	Liver	Lungs	Thyroid
5	5.11	0.33	14.23	0.67	10.44
30	5.76	0.48	11.51	0.57	17.19
60	6.52	0.32	9.24	0.50	28.78

ORNL research supported by the Office of Health and Environmental Research, U.S. Department of Energy, under contract DE-AC05-84OR21400 with Martin Marietta Energy Systems, Inc. and grant HL-27012 with National Institutes of Health.

No. 732.6

[I-123]-15-(p-IODOPHENYL)-3,3-DIMETHYLPENTADECANOIC ACID (DMIPP) - A NEW AGENT TO EVALUATE REGIONAL MYOCARDIAL FATTY ACID UPTAKE. F. F. Knapp, Jr.,¹ S.N. Reske,² M. M. Goodman,¹ J. Nitsch,³ K. R. Ambrose,¹ H.-J. Biersack² and C. Winkler,² ¹Nucl. Med. Group, Oak Ridge National Laboratory (ORNL), Oak Ridge, TN, ²Inst. for Clin. and Exp. Nucl. Med. and ³Dept. Card. Univ. of Bonn, FRG.

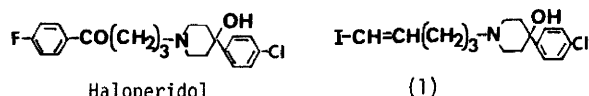
Studies with DMIPP, the 3,3-dimethyl analogue of 15-(p-iodophenyl)pentadecanoic acid (IPP), have shown the inhibitory effect of β-dimethyl-substitution on β-oxidation. DMIPP shows high heart uptake in fasted rats and prolonged myocardial retention (T_{1/2} IPP, 5-10 min; T_{1/2} DMIPP, 5-7 h). Lipid analyses of heart extracts show high levels of free fatty acid and slow conversion to triglycerides. A fatty acid CoA synthetase-CoA oxidase system demonstrates significant oxidation of straight-chain fatty acids (IPP, etc.), but no oxidation of DMIPP and the 3-monomethyl analogue (BMIPP). The prolonged myocardial retention of DMIPP thus appears to result from inhibition of β-oxidation. Studies in patients with [I-123]DMIPP also demonstrate this unique "trapping" and high heart:blood ratios with excellent SPECT images. These results suggest that [I-123]DMIPP may be useful for the evaluation of aberrations in regional fatty acid uptake that may occur in chronic hypertension and cardiomyopathies.

ORNL is operated by the U.S. Department of Energy under contract DE-AC05-84OR21400 with Martin Marietta Energy Systems, Inc.

No. 732.8

A RADIOIODINATED HALOPERIDOL ANALOGUE: CONVENIENT PREPARATION OF AN ATTRACTIVE BRAIN IMAGING AGENT P.C. Srivastava and F.F. Knapp, Jr., Nuclear Medicine Group, Oak Ridge National Laboratory, Oak Ridge, TN 37831

[⁷⁷Br]Bromperidol shows high brain uptake in rats (S. M. Morriein and G. L. Stocklin, J. Med. Chem., 28, 1319, 1985) and meperidines show interesting CNS properties suggesting the design and evaluation of similar ¹²³I-analogues for brain imaging studies by SPECT. For preliminary studies the radioiodinated haloperidol analogue, 1-(E-1-[¹²⁵I]iodo-1-penten-5-yl)-4-(4-chlorophenyl)-4-hydroxypiperidine (1) has been prepared (250 mCi/mole, 70% yield) by condensing E-1-borono-5-iodo-1-pentene with 4-(4-chlorophenyl)-4-hydroxypiperidine followed by Na[¹²⁵I]-chloramine-T iodination of the borono intermediate. ¹²⁵I-(1) shows good brain uptake (% dose/gm; range of 5 rats) and high brain:blood ratios (10, 5 min). The data suggest that similar ¹²³I-labeled agents may be attractive for evaluation as potential brain imaging agents.



T, min	Brain	Blood	Liver	Lungs
5	2.18-2.73	0.22-0.29	1.80-2.68	11.03-13.51
30	1.13-1.44	0.34-0.42	1.36-1.92	2.91-4.24
60	0.50-0.70	0.38-0.53	1.85-2.07	1.35-1.93

Research supported by the Office of Health and Environmental Research, U.S. Department of Energy, under contract DE-AC05-84OR21400 with Martin Marietta Energy Systems, Inc.

Author Index: Scientific Papers and Posters

- Abbott, J. 989
Abdel-Dayem, HM. 965, 1033
Abdel-Razzak, M. 1013
Abe, O. 1022
Abitol, C. 918
Abou-Khalil, BW. 902
Abrams, P. 1022
Abreau, C. 909
Abubacker, KC. 965
Aburano, T. 957, 1011, 1033
Ackerman, RH. 969
Ackermann, R. 950
Ackery, DM. 1030
Adachi, H. 1013
Adam, MJ. 936, 972, 1046
Adam, WE. 892
Adams, K. 1037
Adams, MD. 984
Adams, R. 881
Addonizio, LJ. 910
Adler, LP. 981
Adler, S. 918, 973
Agranoff, BW. 936
Ahlem, CN. 1041, 1042
Ahmad, M. 886
Ahmann, FR. 1020
Ahmann, ME. 1020
Akanabe, H. 1035
Alavi, A. 887, 889, 901, 919, 945, 952, 969, 988, 1010
Alavi, JB. 889
Alderson, PO. 896, 907, 910, 923, 970, 1038, 1043
Aldridge, J. 994
Alfano, B. 1024
Al-Huda, F. 1033
Aliabadi, P. 978
Allen, EW. 999
Allen-Mersh, T. 1023
Alpert, NM. 941, 969, 1054
Al-Rashed, AA. 965
Alyea, K. 892
Amartey, JK. 1049
Ambrose, KR. 1055
Ammar, IA. 975, 1011
Amor, M. 996, 1005
Amox, D. 1020
Amparo, EG. 986, 1044
Anais, D. 1054
Anderson, LD. 1042
Anderson-Berg, WT. 1040
Andrews, V. 978
Angelberger, P. 878
Angello, DA. 953
Angrist, B. 901
Anh-Le. 995
Ansari, AN. 929
Antar, MA. 891
Antman, KH. 971
Aoki, E. 1013
Aoki, J. 1039, 1040
Aoki, S. 1036
Apicella, A. 1025
Appledorn, CR. 906
Arano, Y. 1041
Araya, G. 1040
Armstrong, PW. 997
Arnbjarnarson, O. 970
Arndt, JW. 975
Arnett, C. 880, 1047
Arnett, CD. 906, 982
Arnstein, NB. 886
Arost, C. 1028
Ashburn, WL. 876
Aspey, BS. 905
Atcher, R. 1042
Atcher, RW. 897, 898, 1040
Atkins, HL. 1054
Atsumi, H. 987
Aubert, B. 1008
Aug, F. 996, 1005
Aujard, Y. 985
Austin, AR. 883
Avigad, I. 963
Axel, L. 952
Axelsson, B. 884
Babaian, R. 1021
Babich, JW. 1030
Babikian, V. 969
Badger, CC. 983
Badimon, JJ. 995
Bading, JR. 1030
Bagchi, A. 918
Bagchi, A. 928
Bai, L-Q. 906, 1047
Baidoo, KE. 1050
Bailey, DL. 884, 1005
Bairamian, D. 901
Balatoni, JA. 972
Baldwin, RM. 940, 1046
Ball, ME. 911, 1043
Ballance, C. 1016
Bamberger, J. 985
Bandyopadhyay, D. 1037
Banham, SW. 950, 1032
Bank, S. 876
Banna, G. 890
Banner, H. 914
Bard, R. 1034
Barker, W. 1025
Barkon, A. 910
Barlai-Kovach, M. 910, 916, 941, 950, 966, 1054
Baron, JC. 888
Barreto, ACP. 990
Barrio, JR. 879
Barrio, JR. 955
Bartholomew, R. 902, 942, 958, 1015, 1042
Bartynski, B. 962
Basmadjian, GP. 906
Bassingthwaighte, JB. 966
Basso, L. 1052
Bateman, T. 926, 953
Bateman, TM. 933
Bateson, B. 882
Bauer, J. 1054
Baulieu, F. 1009
Baulieu, JL. 1009
Baum, RP. 948, 1019, 1032
Baumgartner, W. 910
Baur, W. 1044
Bautovich, GJ. 1005
Baxter, LR. 920
Bazin, JP. 1054
Beatty, BG. 1023
Beatty, JD. 1023
Beaumont, W. T000
Beck, T. 898
Becker, GJ. 956
Becker, L. 967
Beckers, J. 891
Beerman, R. 961
Behal, R. 935, 955, 1027
Beierwaltes, WH. 886, 908
Belhobek, G. 952
Beller, GA. 926, 967, 998
Bellet, D. 1022
Belliveau, P. 1010
Bellotti, G. 994
Belzer, FO. 984
Bemis, CE. 934
Ben-Dov, D. 1032
Benedetto, AR. 883, 991
Benko, H. 1012
Bennett, JM. 936, 1047
Bennett, M. 1051
Benua, RS. 947, 1023, 1030
Berberich, A. 888
Berent, S. 901, 902, 920
Berg, GW. 895
Berg, J. 1002
Berger, H. 967
Berger, HJ. 900, 997, 1005
Berger, N. 881
Bergman, D. 886
Bergmann, H. II. 1019
Bergmann, JF. 1022
Bergsland, J. 966
Berk, PD. 938
Berlin, F. 1027
Berman, DS. 899, 926, 933, 934, 943, 944, 953, 954, 968, 985, 997, 998, 999
Bermond, A. T000
Bernier, S. 954
Berridge, MS. 971
Berry, JM. 994
Berthold, F. 1019
Bertrand, A. 996, 1005
Besnard, JC. 1009
Best, MP. 1040
Betley, A. 920
Bettinardi, V. 884
Bhayana, JN. 966
Bia, M. 983
Bice, AN. 898, 945, 1002, 1005, 1016, 1026
Bida, GT. 879
Bieber, K. 981
Biello, DR. 974, 990
Biersack, H-J. 1052
Bietendorf, J. 899
Bigler, RE. 898
Bilezikian, JP. 907
Billings, JB. 906, 972
Bingham, L. 881
Bischof-Delaloye, A. 880, 1019
Blake, GM. 963, 1030
Blake, JS. 1008
Blanchet, M. 919
Blasberg, RG. 936
Blau, M. 1051
Blaufox, MD. 984, 1034, 1053
Blend, MJ. 1040
Block, CH. 1028
Block, D. 982
Bocchi, E. 994
Bockisch, A. 948, 1028
Boddaert, A. 987
Boddie, AW. 1015
Bogaerts, M. 1014
Bohuon, C. 1022
Bol, A. 946, 974
Bolomey, L. 976
Bolton, RW. 932
Bomanji, J. 881, 929
Boothe, T. 982
Borow, KM. 992
Botti, J. 898
Botvinick, E. 949, 976, 989, 993
Boucher, CA. 911, 944
Boudreaux, GJ. 1048
Bouffard, JA. 908
Boullais, C. 949, 950
Bourdoiseau, M. 888
Bourgoignie, J. 961
Bourguignon, M. 888, 985
Bouzglou, A. 971

Bowsher, P. 886
 Boyd, G. 950
 Boyd, RE. 1045
 Boyd, ST. 943
 Brachman, MB. 1030
 Brackett, DJ. 999
 Bradley, E. 902
 Bradley, WG. 985
 Brady, LW. 1028
 Braestrup, C. 1027
 Branson, R. 1037
 Braun, J. 910
 Braun, S. 886
 Braunstein, P. 998
 Braverman, L. 909
 Brechbiel, M. 898
 Brechbiel, M. 1040
 Brechner, R. 931
 Brem, H. 890
 Brennan, K. 897, 976
 Brennan, KM. 955
 Brennan, MF. 1031
 Breton, G. 988
 Bricker, JA. 915, 943
 Bridges, R. 998
 Brill, AB. 933, 957, 1038, 1044
 Bristow, D. 973
 Brittain, HG. 915
 Britton, KE. 881, 929
 Brodack, JW. 879
 Brodie, JD. 880, 889, 901
 Brooks, KM. 932
 Brooks, RA. 901, 920
 Broussolle, E. 880, 1010
 Brown, BA. 1020, 1023, 1041
 Brown, G. 927
 Brown, K. 1017
 Brown, ML. 1011, 1014
 Brown, PH. 937
 Brown, RKJ. 924, 925
 Broyer, M. 985
 Bruch, PM. 943
 Brücke, Th. 887
 Brunetti, JC. 924
 Brunken, RC. 967
 Bryant, G. 902
 Buchegger, F. 880, 1019
 Buchpiguel, C. 994
 Buckner, DM. 1034
 Buda, AJ. 935
 Budinger, TF. 955, 976, 996, 1045
 Buell, U. 888
 Bufalini, M. 881
 Buja, LM. 891
 Bunko, H. 911, 993, 1035
 Bunn, PA. 903, 1022
 Burchiel, SW. 896
 Burns, HD. 1050
 Burow, RD. 996, 999
 Burt, RW. 964, 968
 Busemann-Sokole, E. 961
 Busuttill, RW. 925
 Butler, TA. 1008
 Butler, WF. 1004
 Buxton, RB. 969
 Buyschaert, M. 1009
 Byrd, BL. 1043

Cabanis, E. 888
 Cacciaguerra, G. 881
 Caldwell, JH. 939
 Callahan, AP. 1054, 1055
 Callahan, RJ. 915, 916, 946
 Callegaro, L. 1023
 Callow, A. 1044
 Calmette, C. 1009
 Calne, DB. 936
 Camargo, EE. 990, 994, 1015
 Camin, LL. 878
 Camli, U. 936
 Camp, VM. 893
 Campbell, D. 1013

Campbell, S. 878
 Cance, WG. 958
 Cancro, R. 901
 Canning, L. 905
 Cannon, P. 967
 Cannon, PJ. 910
 Cantineau, R. 995
 Carey, JE. 886
 Caride, V. 877
 Carlo, DJ. 902, 942, 958, 1015, 1021, 1041, 1042
 Carlyle, D. 950
 Carpenter, A. Jr. 1050
 Carr, EA, Jr. 966
 Carrasquillo, JA. 902, 903, 922, 1021, 1022, 1043
 Carrera, GF. 952
 Carrier, L. 988
 Carroll, LR. 1018
 Carroll, M. 966
 Carroll, MJ. 929
 Carroll, S. 982
 Carroll, TR. 877
 Carson, RE. 895
 Carson, RE. 936
 Carter, S. 948
 Casset, D. 992
 Cayla, J. 949
 Cendron, J. 985
 Cerny, J. 1053
 Cerqueira, M. 989
 Chadwick, B. 993
 Chaly, T. 1047
 Chamberlain, GW. 882
 Chamberlain, MJ. 942
 Chan, SM. 922
 Chandraratna, PAN. 985
 Chang, C-H. 1041, 1042
 Chang, JY. 1025
 Chang, LT. 1004, 1007
 Chang, SL. 888
 Chang, SS. 929, 1036
 Chang, W. 1017, 1018
 Channing, MA. 936, 1047
 Chaovapong, W. 938
 Chaplin, SB. 905
 Charbonneau, P. 949, 950
 Charkes, ND. 903, 904, 951, 981
 Chartrand, R. 988
 Charuzi, Y. 933
 Chatal, JF. 1019
 Chaudhuri, TK. 905
 Chawluk, J. 945, 969
 Chen, C. 935
 Chen, C-J. 1006
 Chen, CT. 899
 Chen, DCP. 988, 1031
 Chen, I-W. 892
 Chen, IW. 948
 Chen, KK. 929
 Chen, MT. 929, 1036
 Chen, O. 988
 Chestnut, C. 908
 Cheung, NK. 881
 Chey, WY. 882
 Chi, DY. 879
 Childs, RL. 1051
 Chin, M. 949
 Chinol, M. 959
 Chiotellois, E. 1050
 Chiou, R. 922
 Chittenden, S. 1030
 Chiueh, CC. 879
 Choi, H. 943
 Chowdhury, SC. 1011
 Christ, F. 948
 Christian, PE. 904, 914, 956, 962, 1015
 Christiansen, C. 885
 Christie, JH. 896
 Christie, MJ. 977
 Christin, A. 890, 909
 Christman, DR. 889
 Chu, FL. 888

Chu, YK. 989, 1036
 Chugani, HT. 901
 Churchley, S. 964
 Cios, KJ. 928
 Civelek, AC. 1031
 Clanton, JA. 986
 Clark, O. 963
 Clarke, HS. 961
 Clarke, LP. 1017
 Clausen, M. 1002, 1005, 1016
 Claverie, JG. 915
 Cleynhens, B. 894
 Clinthorne, NH. 896, 960
 Cloninger, KG. 900, 997
 Clutter, M. 1020
 Cobb, FR. 893
 Coenen, HH. 982
 Cogneau, M. 946
 Cohen, A. 998
 Cohen, I. 926
 Cohen, RM. 936
 Cohn, K. 1023
 Colcher, D. 902, 922, 1019, 1021, 1023, 1042
 Cole, P. 910, 937, 1009, 1031
 Cole, PJ. 950
 Coleman, RE. 893, 895, 930, 960
 Collier, BS. 923
 Collier, BD. 952, 984
 Collin, M. 1037
 Compton, DW. 1046
 Conforti, P. 1024
 Conklin, CM. 933
 Connolly, R. 1044
 Connors, D. 929
 Conrad, GR. 915, 1006, 1035
 Conti, PS. 1031, 1049
 Cook, SA. 1001
 Cool, SL. 884
 Cooley, LA. 1034
 Cooney, J. 1048
 Coonrod, DV. 1033
 Cooper, JA. 924, 1000, 1037
 Cooper, M. 899
 Cooper, MD. 1026
 Coornaert, S. 947
 Corbally, MT. 1049
 Corbett, JR. 891, 918
 Cordero, S. 968
 Corn, CR. 996, 999
 Cornelius, E. 1019
 Corpuz, SW. 963
 Correia, JA. 912, 941, 969, 1054
 Corwin, LA, Jr. 986
 Cosma, M. 898
 Cosnay, P. 992
 Costa, DC. 905
 Coughlan, JD. 1035
 Counsell, R. 1046
 Coupal, JJ. 1008
 Courtecuisse, V. 985
 Courtenay-Luck, N. 975
 Coutris, G. 1009
 Covell, D. 896
 Coveney, JR. 894
 Craddock, TD. 960
 Crawley, JCW. 990
 Creasey, H. 1024
 Creutzig, H. 876, 953
 Crook, JE. 1043
 Crouzel, C. 949, 950
 Cruces, J. 985
 Cruces, JV. 1008
 Cullen, J. 1017
 Cullum, I. 905
 Curchod, S. 880
 Currie, DC. 950
 Curtis, G. 901
 Czer, LSC. 933
 Czerniak, A. 963

DaCosta, M. 886, 907
 Dadparvar, S. 1028

- Dae, M. 949, 976, 989, 993
 DaFoe, D. 996
 Dahl, CM. 884, 917
 Dalakas, MC. 920
 Daly, J. 1023
 D'Amato, R. 936
 D'Amour, P. 988
 Danchin, N. 996
 Dann, R. 945
 Dannals, RF. 880, 898, 935, 945, 954, 955, 983, 1010, 1026, 1027, 1048
 Danskin, S. 902
 Darcourt, J. 927, 968, 984, 991, 1052
 Das, DK. 1037
 Datz, FL. 904, 914, 956, 977, 1015
 Daube-Witherspoon, ME. 917
 David, GS. 959, 1042
 Davidson, JT. 1004
 Davie, JM. 958
 Davis, J. 949, 989
 Davis, L. 993
 Davison, A. 878, 894, 967
 Day, PA. 896
 Dean, RT. 894
 Dearborn, CB. 1041
 De Bakker, C. 1014
 Dec, W. 910
 Deconinck, F. 927
 DeCosse, J. 1023
 Deecke, L. 887, 1029
 De Gautard, R. 890
 DeGrado, TR. 949, 966
 DeGraff, W. 898
 Deierhoi, MH. 909, 984
 De Jesus, OT. 1026, 1047
 Dekempencer, P. 894
 Delaloye, B. 880, 1019
 DeLand, FH. 1008
 De Landsheere, C. 891
 DeLaney, M. 886, 907, 1002
 Delepine, N. 1009
 Delfiore, G. 891
 Delisle, MJ. 1009
 Del Negro, G. 1015
 Del Rio, M. 1020
 Del Vecchio, G. 1024
 Del Vecchio, S. 1022
 Demer, L. 943, 977
 DeNardo, GL. 903, 958, 1041
 DeNardo, SJ. 903, 958, 1041
 Dence, CS. 982
 Denham, JS. 956
 Dennecke, H. 880
 Denny, D. 1036
 DePasquale, EE. 997
 DePuey, EG. 900, 956, 963, 997, 1005
 DeQuattro, V. 929
 Derbekyan, V. 1010
 Derenzo, S. 976
 DeRidder, P. 882
 De Roo, M. 894, 1014
 Deshpande, SV. 1041
 Desir, G. 983
 DeSombre, ER. 972
 Desreux, JF. 915
 Deutsch, E. 894, 948
 DeVito, RP. 960, 988
 Devous, MD, Sr. 997
 Dewanjee, MK. 947, 1011, 1014
 de Witt, C. 1045
 Dhawan, V. 1024, 1038
 Diamond, GA. 926, 934
 Di Chiro, G. 901, 920
 Dickinson, CZ. 978
 Diemer, H. 888
 Dighero, HR. 944
 Diksic, M. 889, 999, 1047
 Dilley, WG. 958
 Dillman, J. 1020
 Dillman, RO. 1020
 Di Paola, M. 1008, 1054
 Di Paola, R. 1008, 1054
 DiResta, GR. 1049
 Dmurchowski, C. 886, 908
 Doherty, PW. 881, 959, 1003
 Dokoh, S. 1040
 Dolher, W. 910
 Dommergues, JP. 985
 Donath, A. 890, 909
 Don Michael, TA. 953
 Dorf, B. 876
 Dornfest, DJ. 986
 Doshi, M. 1050
 Doss, JK. 918
 Douglass, K. 1027
 Douglass, KH. 955
 Dowdey, JE. 1006
 Dragotakes, S. 1054
 Dragotakes, SC. 916
 Dreesen, RG. 956
 Drew, H. 890, 928
 Drinkwater, B. 908
 Drozynski, CA. 896, 1015
 Drubach, L. 1009
 Drum, DE. 892, 893
 Drury, H. 978
 Duara, R. 1025
 Dubé, S. 1010
 Dudczak, R. 878, 1053
 Duhaime, T. 919
 Dunn, WL. 964
 Duray, P. 922
 Early, MY. 994
 Eary, JF. 983
 Ebina, A. 951
 Eckelman, W. 937
 Eckerman, K. 979
 Eder, JP. 971
 Edgerton, ER. 1002
 Edwards, B. 915
 Edwards, C. 929
 Efang, SMN. 1051
 Egeci, R. 890
 Eggi, D. 931
 Eggi, K. 931
 Ehrenkauf, R. 901
 Ehrhardt, JC. 1018
 Ehrhardt, JE. 1017
 Ehsani, AA. 990
 Eilles, A. 888
 Eisenberg, B. 887
 Eisner, RL. 961
 Ekas, R. 1053
 El-Aggan, A. 1013
 El-Aini, K. 1013
 Elgazzar, A. 988
 Ell, PJ. 905
 Ellery, S. 881
 Ellison, EC. 937
 Elmaleh, D. 966
 El-Sayed, M. 1033
 Elsinga, PH. 1049
 Emeis, JJ. 975
 Emran, A. 982
 Emrich, J. 1029
 Endo, K. 921, 1021, 1033, 1039, 1041, 1042
 Endo, M. 940
 Engelbretson, D. 907
 Engelman, K. 1010
 Engelstad, B. 1020
 English, RJ. 889, 971
 Entine, G. 1017
 Epps, LA. 1050
 Epstein, AL. 903
 Ergin, MT. 970
 Ernstoff, M. 922, 1019
 Eshima, D. 898, 962, 1052
 Esser, PD. 907, 910
 Esteban, J. 902, 1019, 1042
 Esterhai, J. 988
 Ethevenot, G. 1005
 Ettinger, M. 885
 Evangelatos, GP. 1039
 Evans, AC. 889, 1024
 Evans, AE. 931
 Evans, DG. 876
 Evans, H. 907
 Evans, ML. 979
 Ezekowitz, MD. 946, 983, 1036
 Ezquerro, NF. 1005
 Faber, TL. 918
 Fabre, G. 1014
 Fajman, W. 961
 Fallon, FT. 910
 Fanaras, G. 880, 1027
 Faraj, BA. 893
 Farde, L. 879
 Fassbender, D. 934
 Fauchier, JP. 992
 Faulhaber, P. 899
 Faulkner, DB. 963, 989
 Fawwaz, RA. 896, 970, 1043
 Fazekas, F. 919, 969
 Fazio, F. 884, 894, 1024
 Feiglin, DHI. 882, 952, 985
 Feindel, W. 889
 Feinendegen, LE. 891
 Feitsma, RIJ. 975
 Feld, T. 893, 1051
 Feldman, MJ. 966
 Feldman, N. 932
 Feliu, AL. 1048
 Ferbert, A. 888
 Ferguson, R. 964
 Ferguson, WR. 951
 Ferrant, A. 946
 Ferreira, NL. 916
 Ferrone, S. 1043
 Fielding, S. 1030
 Fieschi, C. 1024
 Figard, SD. 1042
 Filc-DeRico, S. 1049
 Fine, EJ. 984
 Fink, S. 905
 Fink-Bennett, D. 882
 Finkelstein, M. 1034
 Finn, RD. 936, 982
 Finney, C. 1017
 Firna, G. 879
 Fischer, K. 974
 Fischman, AJ. 993
 Fishbein, DS. 901, 936
 Fisher, J. 1027
 Fisher, RS. 903, 904, 981, 1011
 Flamm, E. 889
 Fletcher, JW. 938
 Flower, MA. 1030
 Floyd, CE. 895, 930, 960
 Flye, W. 983
 Foon, KA. 903, 1022
 Ford, EH. 897
 Forstrom, LA. 1014
 Fortune, JB. 924
 Fountos, A. 990
 Fowler, JS. 880, 889, 982
 Fox, PT. 1025
 Frackowiak, RSJ. 912, 913
 Francis, B. 937
 Francis, IR. 908
 Franke, LA. 939
 Fraser, I. 937
 Frazer, JW. 1015
 Freed, SZ. 1034
 Freedman, R. 942
 Freeland, DS. 986
 Freeman, LM. 1034
 Freeman, MR. 997
 French, WJ. 991
 Frenkel, TL. 895, 1003, 1007
 Frey, EE. 1035
 Frey, KA. 936
 Frey, P. 890, 909
 Friedland, RP. 955
 Friedman, AM. 897, 972, 1026, 1047
 Friedman, J. 899, 943, 944, 999

- Friel, HT, 941, 1028
 Frincke, JM, 902, 942, 1015, 1041, 1042
 Fritsch, S, 886
 Fritzbeg, AR, 957, 959, 962, 1052
 Froelich, JW, 1053
 Froncisz, W, 952
 Front, A, 1032
 Frost, JJ, 935, 936, 945, 955, 969, 983, 1027
 Fudo, T, 999
 Fuentes, F, 943, 976, 977
 Fugate, K, 914
 Fujibayashi, Y, 1013
 Fujimi, K, 1012
 Fujisawa, I, 1026
 Fujita, T, 1001
 Fukunaga, M, 987
 Fukuyama, H, 1026
 Fulton, RR, 1005
 Fung, A, 950
 Fung, D, 916
 Furlan, AR, 1028
 Fuster, V, 995
- Gaab, MR, 890
 Gaddis, PJ, 992
 Gagliardi, P, 883
 Gai, Y, 1045
 Gal, R, 912
 Gala, K, 971
 Galante, M, 963
 Gallagher, BM, 896, 922, 958, 1023, 1041
 Gamhbir, SS, 913
 Ganatra, R, 1019
 Gansow, O, 898, 1042
 Ganz, WI, 974
 Garay, S, 914
 Garcia, E, 953
 Garcia, EV, 900, 997, 1005
 Garcia, V, 931
 Gardet, D, 1009
 Gardner, J, 946
 Gasthuisberg, UZ, 1014
 Gatley, SJ, 966
 Gaughan, GT, 915
 Gebarski, S, 901
 Gefter, WB, 887
 Gelbard, AS, 1030, 1049
 Genarro, GP, 1038
 Gentili, A, 974, 1034
 George, EA, 938
 Gerald, K, 1012
 Gerhards, W, 888
 Gerich, B, 922
 Gertz, E, 890
 Gerundini, P, 884, 894
 Gheorghide, M, 926
 Gibson, R, 937
 Gibson, RE, 913, 916, 1045
 Gibson, RS, 926, 967, 998
 Gil, MC, 946
 Gilardi, MC, 884
 Gilbert, B, 908
 Gilgenkrantz, JM, 996
 Gilis, F, 995
 Gill, CC, 985
 Gill, JB, 911, 966, 1002
 Gilland, DR, 1002
 Gilman, S, 902, 920
 Gingrass, D, 952
 Ginsberg, HN, 995
 Gionet, M, 881, 909
 Giorgi, MCP, 990, 1015
 Gjedde, A, 888, 954, 1027
 Glassman, M, 931
 Glazer, G, 898, 908
 Gleichmann, U, 934
 Glenn, HJ, 942, 1016, 1021
 Glick, SJ, 1003
 Glicklick, D, 984
 Glickman, S, 925
 Go, RT, 882, 985
 Gober, AM, 963
- Goble, JC, 1000
 Godoy, N, 946
 Goeckeler, WF, 915, 986
 Goetsch, RA, 905
 Gokan, T, 1032
 Gold, AM, 1043
 Gold, HK, 909, 910, 911, 923, 950, 992
 Goldberg, DS, 954, 1010
 Golden, JA, 914
 Golden, RN, 916
 Goldenberg, DM, 897, 943, 1016
 Goldenberg, G, 887
 Goldenberg, H, 897
 Goldfarb, HW, 1050
 Goldman-Leiken, RE, 903
 Goldsmith, SJ, 886, 907, 918, 923, 938, 995, 1002
 Goldstein, RA, 918, 943, 977
 Goll, S, 988
 Gomes, A, 924
 Gona, JM, 994
 Goodenday, LS, 928
 Goodgold, HM, 919
 Goodman, MM, 916, 933, 1054, 1055
 Goodwin, DA, 938, 959
 Gordon, R, 882
 Gordon-Cardo, C, 1023
 Goris, ML, 954
 Gotfredsen, A, 885
 Gould, KL, 918, 921, 943, 973, 976, 977, 1053
 Goveltz, G, 897
 Grace, DM, 882
 Grafström, G, 1007
 Graham, MM, 979, 1033
 Graham, TO, 877
 Granowska, M, 881
 Gratz, K, 876
 Gray, LL, 937
 Gray, RJ, 933
 Grecos, GP, 961
 Green, AM, 925
 Green, KA, 1020
 Green, MV, 895
 Greenberg, JH, 1028
 Greene, J, 914
 Greenspan, B, 886, 918
 Greer, KL, 895, 930, 960
 Gregorio, SN, 896
 Grenier, R, 912
 Grierson, JR, 1046
 Griese, J, 948
 Griffin, T, 881
 Griffin, J, 989
 Grochow, L, 1031
 Grochowski, EW, 1003
 Gross, M, 908, 1046
 Gross, ML, 961
 Grossman, SJ, 990
 Grossman, ZD, 941
 Grover, M, 980
 Grover-McKay, M, 890, 932, 933, 967, 976
 Growcock, GW, 883
 Grunbaum, Z, 916
 Gryboski, J, 904
 Guermazi, F, 947
 Guiltarte, TR, 969, 1026
 Guillebeau, D, 1009
 Guo, Y-Z, 906, 972, 1051
 Gupta, BK, 961
 Gur, RC, 901
 Gur, RE, 901
 Gurewitz, J, 899, 926, 953, 999
 Gutierrez, G, 1038
 Gutman, S, 994
 Guzzetta, PC, 962
- Haber, E, 909, 910, 923, 950, 967, 993
 Hackney, D, 889
 Hadjian, RA, 896, 1015
 Hagan, PL, 876, 902, 942, 1015, 1020, 1042
 Hakki, A-H, 926, 934, 968
- Halama, JR, 917
 Halkar, RK, 965
 Hall, LD, 972
 Hall, T, 910
 Hall, TR, 1034
 Halldin, C, 879
 Halpern, SE, 902, 942, 1015, 1020, 1042
 Hamil, D, 889
 Hammersley, PAG, 1031
 Hanada, J, 953
 Handa, H, 1026
 Hanelin, LG, 925
 Hanish, BL, 906
 Hansen, CL, 891
 Hanson, RN, 939, 1048
 Happ, J, 948, 1019, 1032
 Harcke, HT, 932, 1034
 Hardoff, R, 1032
 Hardy, M, 896, 970
 Harp, G, 989
 Harper, A, 921
 Harris, CC, 960
 Harris, J, 1027
 Harris, R, 1016
 Harrison, RC, 905
 Harrison, RH, 1000
 Hartley, G, 994
 Hartman, MT, 876
 Hartmann, A, 1052
 Hartmann, O, 947
 Hartz, RK, 973
 Hasegawa, B, 899
 Hashimoto, S, 987, 1022, 1032
 Hashimoto, T, 987
 Hassan, MA, 1048
 Hatazawa, J, 901, 920
 Hattner, R, 993, 1020
 Haucknewman, A, 936
 Hawkins, RA, 879, 913, 924, 925, 940, 955, 1004
 Hawkins, WG, 895, 1003, 1007
 Hawman, EG, 896, 930
 Haxby, J, 1024
 Hayashi, N, 1013
 Hayden, PW, 932
 Hayes, D, 1012
 Haynie, TP, 942, 1016, 1021
 Hazue, M, 965
 Heilbrun, LK, 885
 Heim, M, 987
 Heitner, D, 882
 Hellman, RS, 952, 984
 Hellwig, B, 962
 Helson, L, 947
 Helus, F, 970
 Heminger, LA, 892
 Henderson, JM, 956
 Henderson, R, 985
 Henderson, RG, 978
 Hendry, GO, 1018
 Henkin, RE, 917
 Henry, M, 964
 Henry, RE, 1020
 Henze, E, 892
 Heo, J, 926, 934, 954
 Heppell, J, 1010
 Herbold, D, 952
 Herbst, CP, 999
 Herda, S, 890
 Herholz, K, 1012
 Herr, J, 949, 989
 Hersh, EM, 1021
 Herzog, H, 891
 Herzzentrum, NRW, 934
 Heyman, S, 931, 932
 Heyns, A du P, 965
 Hiatt, J, 925
 Hichwa, R, 920
 Hiesiger, E, 889
 Higuchi, ML, 994
 Hilsom, A, 948
 Hines, HH, 1004, 1007
 Hines, JJ, 897

- Hinkle, G. 937, 964
Hino, M. 1012
Hinshelwood, L. 1017
Hiraga, S. 937
Hirano, T. 951
Hirasa, M. 1012
Hiroe, M. 965
Hirohashi, S. 1022
Hironaka, FH. 990
Hirth, W. 894
Hisada, K. 911, 957, 993, 1010, 1011, 1033, 1035
Hladik, WB. 896
Hnatowich, DJ. 881, 939, 959, 1051
Hochschwender, SM. 1041
Hoffer, PB. 922
Hoffman, EJ. 879, 976, 980
Hoffman, TJ. 905, 1051
Hoffmann, RG. 984
Hogg, N. 975
Holburn, GE. 986
Holcomb, H. 890
Holden, JE. 940, 949, 966
Holden, RW. 956
Holly, A. 887
Holm, S. 888
Holman, BG. 878
Holman, BL. 878, 889, 895, 913, 930, 967, 971, 1009
Holmes, RA. 905, 915, 986, 1028, 1037, 1051, 1054
Hoogmartens, M. 894
Hook, P. 1016
Hoory, S. 1037
Hör, G. 948, 1019, 1032
Horiuchi, K. 1036
Horn, B. 1017
Horne, C. 883, 931
Horosowsky, H. 987
Hosain, F. 1007
Hosoi, S. 921, 1021, 1041
Hsieh, J. 896, 930
Hu, HH. 888
Hu, SC. 1011
Huang, JC. 888
Huang, SC. 879, 912, 913, 920
Huber, O. 890
Huberty, J. 949
Hubner, PJB. 994
Huesman, RH. 955, 980
Hughes, A. 972
Hundeshagen, H. 876, 890, 953
Hünemann, B. 948, 1028
Hung, GL. 1031
Hunter, R. 881
Hurford, W. 916
Hurtig, H. 945
Hurwitz, RA. 919
Hutchins, G. 910
Hutchins, GD. 902, 940, 941, 973, 1003
Hutchison, N. 916, 1044
Huth, C. 1037
Hutter, AM. 911
Hutton, BF. 884, 1005
Hutton, J. 934
Hutton, LC. 882
Hyams, D. 922
Hyde, JS. 952
- Iannotti, F. 1024
Ibuki, Y. 1012
Ichise, M. 889, 971
Ido, T. 983
Iida, H. 976
Iinuma, T. 940
Iio, M. 970, 1029
Ikekubo, K. 1012
Imahori, Y. 983
Inamoto, S. 1039
Inoue, M. 990
Isawa, T. 951
Ishida, H. 1033
Ishida, Y. 990
- Ishikawa, M. 1026
Ishimori, T. 953
Ishiwata, K. 983, 1049
Isitman, AT. 952, 984
Iskandrian, AS. 926, 934, 954, 968
Ithakissios, DS. 1039
Ito, H. 1012
Itoh, M. 970
Itti, R. 992, 1009
Iwa, T. 993
Iwata, R. 983
- Jackson, AL. 913
Jacobs, M. 1037
Jacobus, W. 910
Jaeger, A. 888
Jaeger, J. 901
Jaffe, D. 961
Jäger, N. 948
Jagust, WJ. 955
Jain, A. 911, 944
Jakowatz, JG. 1023
James, C. 967
Jansen, DE. 891, 918
Jass, JR. 881
Jaszczak, RJ. 895, 930, 960
Jatenc, A. 994
Jay, T. 955
Jayasinghe, MAC. 1005
Jeavons, A. 890, 909
Jerabek, PA. 969
Jesmanowicz, A. 952
Jewett, D. 920
Jewkes, RF. 905
Jhingran, S. 907
Jih, F. 981
Johner, B. 880
Johnes, J. 950
Johns, MF. 942
Johnson, JA. 977
Johnson, KA. 889
Johnson, LL. 910
Johnson, MW. 983
Johnson, P. 907
Johnson, RF, Jr. 986, 1044
Joliot, F. 1054
Jones, AG. 878, 894, 967
Jones, BE. 905
Jones, DS. 959
Jones, PL. 922, 1020
Jones, RH. 992
Jones, SC. 941, 1028
Jones, T. 912, 913
Jonson, B. 1004
Jönsson, B-A. 1007
Jordan, B. 901
Jovkar, S. 999
Jue, R. 1041
Junck, L. 920
Juni, J. 927, 1013
Juri, PN. 893
Justice, T. 902
- Kabalka, G. 982
Kahn, C. 991
Kahn, P. 1044
Kalaras, KI. 1013
Kalifa, C. 987
Kalish, R. 946
Kallick, S. 881
Kaltovich, FA. 897
Kamada, T. 990
Kameyama, M. 1026
Kan, SH. 964
Kane-Marsch, S. 954
Kangaroo, H. 925
Kanis, JA. 963
Kanke, M. 910, 923, 941, 950
Kanno, I. 976
Kanwar, N. 997
Kao, J. 1015
Kaplan, M. 939
- Kaplan, WD. 971
Karatzas, ND. 1013
Karcher, G. 996, 1005
Karimeddini, MK. 975, 1007
Kariyone, S. 1014
Karl, DW. 1046
Kasecamp, W. 937, 1009
Kashgarian, M. 983
Kashida, H. 1012
Kashima, H. 1009
Kasi, LP. 942, 1015, 1016
Kasina, S. 957, 962, 1052
Kato, K. 900
Katzenellenbogen, JA. 879
Katzmann, JA. 1014
Kauffman, HM. 984
Kawabata, S. 1010, 1033
Kawamura, Y. 921, 1021, 1039, 1041, 1042
Kawasaki, Y. 965
Kaye, JJ. 977
Kaye, MP. 947
Kazikiewicz, JM. 903
Keane-Chuda, M. 922
Keeffe, EB. 1012
Keeling, F. 1030
Keen, RE. 879, 955
Keenan, AM. 903, 1022
Keery, RJ. 975
Kelley, E. 1016
Kelly, K. 931
Kelly, TA. 998
Kememy, N. 1023
Kemeny, MM. 1023
Kennedy, C. 955
Kennedy, P. 971
Kennedy, PL. 891
Keshavarzian, A. 978
Ketring, AR. 986
Khalil, MN. 994
Khalkhali, I. 974
Khan, AR. 994
Khaw, BA. 909, 910, 915, 923, 950, 993
Khentigan, A. 1020
Kijewski, MF. 895, 930
Kilbanov, AL. 909
Kilbourn, MR. 879, 982
Kim, BH. 990
Kim, CK. 984
Kim, EE. 1038
Kim, KI. 930, 981
Kimball, DA. 1035
Kimbiris, D. 934
Kimura, K. 990
King, MA. 884, 1000, 1003
King, SB. 900
King, W. 924
Kiraly, T. 946
Kirchner, PT. 943, 1006, 1017, 1018
Kirkeide, R. 943, 976, 977
Kirkwood, J. 922, 1019
Kishore, R. 983
Kitamura, N. 1039, 1040
Kizuka, H. 1048
Klatte, EC. 956
Kleba, C. 953
Klein, HA. 877
Kleinert, EL. 1031
Kletter, K. 1053
Klingensmith, WC. 925
Knapp, FF. 916, 1028
Knapp, FF, Jr. 933, 1044, 1046, 1054, 1055
Knapp, WH. 934, 970, 1029
Kneeland, JB. 952
Knight, LC. 975, 1011
Knittel, BL. 955
Knoll, GF. 896
Knop, J. 981
Knopp, R. 948
Knust, EJ. 934
Kodaira, S. 1022
Koeppel, RA. 920, 936, 940, 941, 973, 1003
Koide, H. 933, 995, 999
Koizumi, K. 1010

- Koizumi, M. 921, 1021, 1039, 1041, 1042
 Kokal, W.A. 1023
 Kolb, F.O. 886
 Kölbl, C. 1012
 Koller, D. 910, 937, 1009
 Kolodny, G.M. 1000
 Kolozsi, W. 882
 Kolstad, K. 971
 Komatani, A. 1018
 Komatsumoto, S. 1028
 Komori, H. 1012
 Konishi, I. 1011
 Konishi, Y. 933, 999
 Konno, K. 951
 Kopecky, R.T. 962
 Koprowski, C. 1028
 Koral, K.F. 896, 898, 960
 Körfer, R. 934
 Kornguth, M.L. 966
 Kosaka, N. 1029
 Koslow, S.H. 944
 Kosuda, S. 987, 1032
 Kothari, P. 982
 Kotler, J.A. 1020
 Kotler, T.S. 926, 934
 Kotoura, Y. 921, 1021, 1041
 Kotze, H. 965
 Kovacs, C.A. 936
 Kovandi, S. 902
 Koyle, M.A. 980, 984
 Kozak, R.W. 897
 Kozuka, T. 990
 Krajewski, K.J. 921
 Kraly, C. 881
 Kramer, A.V. 1050
 Kramer, E.L. 914
 Krappel, W. 888
 Krasicky, G.A. 1053
 Krasnow, A.Z. 952
 Kremer, P.A. 939
 Krepshaw, J.D. 980
 Kressel, H.Y. 887, 1010
 Krevsky, B. 903, 904, 981, 1011
 Krishnaiah, P.R. 918, 928
 Krishnamurthy, G.T. 937, 1012
 Krishnamurthy, S. 1012
 Krivokapich, J. 933
 Krohn, K.A. 916, 939, 969, 983, 1026, 1033
 Kroiss, A. 1012
 Kronauge, J.F. 878, 894, 9675
 Kruntz, T. 945
 Kübler, W.K. 1029
 Kubo, A. 987, 1022, 1032
 Kubota, K. 933, 957
 Kudo, M. 1012
 Kuge, Y. 972, 1013
 Kuhl, D.E. 920
 Kuhnen, K. 1028
 Kulbertus, H. 891
 Kulkarni, P.V. 891
 Kundel, H. 952
 Kung, H.F. 906, 972, 1051
 Kunieda, E. 987
 Kunimatsu, M. 921, 1021, 1041, 1042
 Kureishy, Z. 1039
 Kurtzman, S. 898
 Kusakabe, K. 965
 Kyriakides, G. 961
- Lacy, J.L. 911, 1043
 Ladenheim, M. 954
 LaFrance, N.D. 890, 910, 928, 937, 967, 994, 1009, 1031
 Lahiri, A. 990
 Lai, Z.Y. 888
 Laird, J.D. 951
 Lairmore, T.A. 1028
 Lallo, C. 1015
 Lamb, J.F. 1046
 Lamki, L.M. 942, 1016, 1021
 Lammertsma, A.A. 912, 913
 Lamotte, D. 891
- Lan, J.L. 989
 Landmeier, B. 881
 Landrieu, P. 985
 Lange, P.H. 922
 Lange, R.C. 877, 904, 983
 Langfitt, T. 919
 Langstrom, B. 982
 Lanza, M. 985
 Lapenta, L. 1022
 Larson, S.M. 895, 902, 903, 922, 936, 937, 1021, 1022, 1023, 1043
 Larsson, S.A. 884, 917
 Lassen, N.A. 888
 Lastoria, S. 1023
 Latimer, S. 931
 Lattimer, J.C. 986
 Laubenstein, L. 914
 Laufer, P. 982
 Laughlin, M.H. 1051
 Lavallee, D.K. 1042
 Lavender, J.P. 950, 975, 978
 Layer, K. 970
 Lear, J.L. 913, 956, 1000, 1018
 LeBlanc, A. 907
 Lecklitner, M.L. 883
 Leclere, J. 947
 Lecomte, R. 974
 Lee, H.B. 1053
 Lee, K.H. 988
 Lee, K.S. 1045
 Lee, M.C. 945, 994, 1026
 Lee, M.E. 925, 933
 Lee, S.R. 893
 Lechner, P.K. 895, 1003, 1007
 Leinbach, R.C. 910, 950, 992
 Lemerle, J. 947
 Lenton, J.D. 893
 Lenzi, G.L. 1024
 Leopold, P.W. 1035
 Leppo, J.A. 965
 Lerner, E. 1036
 Lesch, O. 1029
 Lesser, M. 1006
 Leung, F.Y. 942
 Leutzinger, E.E. 971
 Lever, S.Z. 1050
 Levine, A. 1031
 Levine, M. 876, 952
 Levy, H.A. 1032
 Levy, L.M. 1038
 Lewellen, T.K. 1000, 1033
 Lewis, C. 948
 Li, S. 1017, 1018
 Liang, F. 1051
 Liao, S.Q. 989
 Liberatore, F.A. 958
 Libson, K. 894, 948
 Lieberman, D.A. 1012
 Lieberman, H. 967
 Lieberman, K. 918
 Lieberman, L.M. 987
 Liebert, M. 996
 Lim, C.B. 930, 981
 Lin, H.Y. 989
 Lin, S.N. 1036
 Lin, T.H. 940, 1046
 Linder, K. 1050
 Lindsley, H. 1012
 Linc, B.R. 924, 1000, 1037
 Ling, M. 887, 963
 Link, J.M. 939, 983, 1033
 Links, J. 890, 935, 954, 1027
 Links, J.M. 880, 898, 955, 1000, 1002, 1010, 1027
 Liprandi, A.S. 878
 Lipszyc, H. 995
 Lister-James, J. 878, 894
 Little, J.R. 1028
 Little, S.E. 966
 Littlefield, J.L. 938
 Liu, J. 981
 Liu, R.S. 888, 929, 989, 1011, 1036
 Livanou, E. 1039
- Livesey, J.C. 916
 Livni, E. 966, 1048
 Ljungberg, M. 1004
 Lloyd, K. 1023
 Lloyd, R.V. 908
 Lo, Y.K. 888
 Lockhart, J. 918
 Logan, J. 880, 889
 Logan, K.W. 1028, 1054
 Loncaric, S. 1005, 1016
 Long, A. 909
 Long, D. 890
 Longino, M. 1046
 Loo, D. 1017
 Look, S.R. 1046
 Loose-Wagenbach, I. 1032
 Lopez, I. 946
 Lopez-Berestein, G. 1016
 Lora, M.E. 1022
 Losse, B. 891
 Lotter, M.G. 965
 Loudenslager, D.M. 895, 1003, 1007
 Lowry, P.A. 1038
 Loy, P. 1006
 Lu, D. 941, 1028
 Lucignani, G. 955
 Luckey, M. 907
 Ludbrook, P.A. 990
 Luk, K. 1017
 Lukes, S. 948
 Lumbroso, J. 947, 987, 1008, 1022
 Lumley, P. 975
 Luxenberg, J. 1024
- MacDonald, C. 883
 MacEwen, G.D. 932
 Macey, D.J. 903
 MacGregor, R. 880
 MacGregor, R.R. 889, 982
 Mach, J.P. 880, 1019
 Mach, R.H. 1051
 Machac, J. 907
 Machulla, H.-J. 891, 934
 MacIntyre, W.J. 882, 952, 985
 Mackey, S.T. 947
 Maddahi, J. 899, 926, 933, 943, 944, 953, 968, 985, 997, 998, 999
 Madden, V. 935
 Magill, G.B. 1030
 Mahaux, V. 891
 Maher, J.M. 923
 Maheu, L. 1050
 Maheu, L.J. 877
 Mahler, P.A. 979
 Mahmarian, J.J. 911, 944
 Mahoney, D.K. 1004
 Mail, J.T. 956
 Majd, M. 931, 962
 Majdalani, A. 888
 Mak, H. 1017
 Maki, M. 965
 Makler, T. 952
 Malagelada, J. 1011
 Malech, H. 946
 Malik, A.B. 1037
 Mallett, S. 950
 Malmin, R.E. 930
 Malmud, L.S. 903, 904, 981, 1011
 Malone, M.E. 1015
 Maloney, P. 1043
 Mamoli, B. 1029
 Mancini, D. 993
 Mandell, G.A. 932, 988, 1034
 Manegold, K. 1019
 Manegold, K.H. 948
 Mangios, S.H. 895, 930, 960
 Manil, L. 1022
 Manner, S. 892
 Manning, R.G. 939
 Mansi, L. 1022, 1023, 1024
 Manspeaker, H.F. 925
 Marani, S. 921, 973, 1053

- Marboe, C. 910
 Marciano, D. 924, 925
 Marcus, CS. 974, 980, 984, 1052
 Marcus, ML. 943
 Margouleff, D. 1006
 Maric, N. 922
 Markel, DS. 920
 Markham, CH. 920
 Marshall, R. 891
 Martiat, P. 946
 Martin, NL. 1012
 Martin, W. 934
 Martin, WRW. 936
 Martindale, AA. 1045
 Martinez, C. 1036
 Martinowitz, U. 987
 Masoli, O. 878
 Masuda, K. 987, 1036
 Masuda, Y. 940
 Mathias, CJ. 879, 969
 Mathieu, H. 985
 Mathis, C. 1045
 Mathis, CA. 955
 Matloff, JM. 933
 Matsubara, N. 990
 Matsuda, H. 1033
 Matsuda, S. 1014
 Matsudaira, M. 1011
 Matsueda, G. 910, 923
 Matsumae, M. 1025
 Matthew, M. 1050
 Matthews, LTW. 1052
 Mattis, J. 967
 Mattis, JA. 975
 Maturi, M. 893
 Matyas, J. 1051
 Maul, FD. 948, 1032
 Maurer, AH. 903, 904, 975, 981, 1011
 Maurin, P. 996, 1005
 Mausner, LF. 1046
 Maxon, HR. 892, 948
 Mayaud, C. 951
 Mayberg, H. 935, 1027
 Mayberg, HS. 955, 1027
 Mayfield, G. 935
 Mayfield, PG. 979, 1016
 Mayr, N. 1029
 Mazess, RB. 885
 Mazoyer, BM. 955, 980
 Mazziotto, JC. 879, 901, 920, 940, 944, 955
 McAfee, JG. 941, 962
 McCall, MJ. 938, 959, 1041
 McCallum, RW. 877, 904
 McCarthy, E. 988
 McCarthy, K. 969
 McCartney, WH. 1002
 McCready, VR. 1030, 1031
 McDermott, R. 1017
 McEwan, A. 908
 McEwan, AJ. 1030
 McGahan, JP. 903
 McGarity, WC. 963
 McGhie, I. 934
 McGuire, A. 919
 McGuire, AH. 938
 McKenna, RJ. 971
 McKenzie, EH. 905, 1051
 McKillop, JH. 950, 1032, 1033
 McKusick, KA. 878, 911, 946, 992
 McLellan, CA. 936
 McNeil, BJ. 978
 McPherson, D. 889
 McTigue, M. 938, 959
 Meaney, T. 882
 Meares, CF. 938, 959, 1041
 Mease, RC. 972
 Meekin, GK. 938
 Mehlinger, M. 974
 Mehta, RC. 984
 Meier, D. 907
 Meier, KA. 886
 Meignan, M. 951
 Meinken, GE. 957, 958, 1044, 1046, 1052
 Melin, Y. 985
 Melton, LJ. III. 964
 Mena, IG. 927, 968, 991, 1052
 Mena, P. 946
 Meneguetti, JC. 990, 994
 Mercer-Smith, JA. 1042
 Merchant, EB. 902, 942
 Merhige, M. 943, 977
 Mericle, J. 985
 Messiah, O. 1014
 Meyer, G-Y. 890
 Meyer, KE. 963
 Meyers, B. 909
 Meyers, L. 898, 950, 957
 Michel, CH. 946, 974
 Michler, RE. 910
 Mido, K. 1018
 Mies, C. 1023
 Miller, C. 926
 Miller, DD. 966
 Miller, J. 961
 Miller, JH. 923, 1034
 Miller, M. 1006
 Miller, RI. 923
 Miller, T. 1006
 Miller, TR. 990
 Millet, D. 989
 Milligan, FD. 937
 Millikan, WJ. 956
 Mills, DCB. 1046
 Mills, SL. 903, 958
 Milroy, R. 1032
 Minato, K. 1001
 Minelli, MF. 1019
 Minnaar, PC. 965
 Mintun, MA. 1025
 Mintz, GS. 934
 Miraldi, F. 881
 Misaki, T. 993
 Mitchell, J. 898
 Mitchell, M. 952
 Mitchell, ME. 919
 Mitta, A. 878
 Mitta, AEA. 878
 Mitty, H. 923
 Miura, S. 976
 Miura, Y. 983
 Miyazaki, I. 1011
 Mobarak, L. 1033
 Mock, BH. 964, 968
 Moeller, JR. 945
 Moffett, TC. 966
 Moi, M. 1041
 Momose, T. 1029
 Montz, R. 981
 Moodie, DS. 985
 Moore, JA. 904
 Moore, R. 1053
 Moore, RH. 911, 1002
 Moore, SC. 895, 930
 Moran, D. 923
 Moretti, GJ. 878
 Morgan, AC. 959
 Morgan, AC, Jr. 957
 Morgan, C. 1022
 Morgan, RA. 877
 Mori, K. 955
 Morin, M. 922
 Moring, AF. 965
 Morita, R. 987
 Mornex, F. 1019
 Morrel, S. 1036
 Morse, S. 1036
 Mortelmans, L. 1014
 Moscatelli, G. 881
 Moser, E. 880, 886, 888
 Moser, H. 1027
 Mosimann, F. 880
 Moskowitz, GW. 876, 1038
 Moulart, M. 1009
 Mountz, J. 901
 Mousa, SA. 877, 894, 994, 995
 Msakikarolinska, P. 884
 Mselati, JC. 985
 Muehlechner, G. 917
 Mueller, SP. 889, 895, 930
 Mukai, K. 1033
 Mukai, T. 999, 1001
 Mukherji, B. 970
 Mullani, N. 921, 976, 977
 Mullani, NA. 918, 943, 973, 977, 1053
 Muller, AF. 991
 Müller, CH. 887, 1029
 Müller, JA. 890
 Mulshine, JL. 903, 1022, 1023
 Munz, D. 1022
 Murakami, M. 976
 Murakami, T. 1025
 Muranaka, A. 987
 Murray, JL. 1021
 Murtagh, R. 1017
 Muswick, G. 928
 Muth, RA. 1018
 Muto, T. 900
 Nagai, K. 987
 Nagel, JS. 913, 971
 Nagel, SJ. 889
 Naidu, S. 1027
 Najafi, A. 916, 1044
 Najpauer, K. 893
 Nakai, H. 999
 Nakajima, K. 911, 957, 993, 1010, 1035, 1039
 Nakamura, T. 921, 1021, 1041
 Nakashima, T. 921, 1021, 1033, 1039, 1041, 1042
 Nakatsuka, I. 972
 Nally, JV. 961
 Nanbu, I. 911, 993, 1035
 Nance, EP. 977
 Nancy-Brabois, CHU. 1005
 Napychank, P. 946
 Narra, RK. 1051
 Nasef, A. 1013
 Natarajan, TK. 945
 Navarro, DA. 913
 Neacy, WP. 902, 1041
 Nedelman, MA. 915, 941, 966, 1054
 Needham, SG. 950, 975, 978
 Neely, HR. 892
 Neese, R. 890
 Neirinckx, RD. 905, 1009, 1052
 Nelp, WB. 983
 Nelson, AD. 881
 Nelson, T. 955
 Nepola, JV. 915
 Nestico, PF. 968
 Neumann, A. 992
 Neumann, RD. 1019, 1022
 Neumayr, A. 1012
 Newell, JB. 992
 Ng, CK. 949, 966
 Nickles, RJ. 941, 981
 Nieuwenhuizen, W. 975
 Nieves, E. 1049
 Nilas, L. 885
 Nimmon, CC. 881, 929
 Nishikawa, A. 943, 976, 977
 Nishikawa, J. 1029
 Nishikimi, N. 1035
 Nishimura, K. 1026
 Nishizawa, S. 928, 1001, 1026
 Nitsch, J. 1055
 Nitz, C. 948
 Nody, A. 997
 Noel, L. 1014
 Nofal, M. 1019
 Nohara, R. 933
 Noll, R. 935
 Norris, S. 910
 Northover, JMA. 881
 Nosco, DL. 894, 939
 Notohamprodo, G. 934
 Noujaim, AA. 947
 Nowak, DJ. 961, 1002
 Nowotnik, DP. 905

- Nunes, R. 938
 Nunn, AD. 893, 1051
 Nürnberger, N. 1053
 Nusynowitz, ML. 991
 Nygaard, TS. 967
 Nyhan, W. 1027
- O'Byrne, GT. 943, 944
 O'Connell, W. 949, 963, 989
 O'Donnell, J. 952
 O'Donnell, JK. 882, 985
 O'Donoghue, N. 948
 Ody, B. 890
 Oettgen, H. 1023
 O'Grady, LF. 903
 Ohishi, T. 1022
 Ohmomo, Y. 1021, 1041, 1042
 Ohta, H. 921, 1021, 1033, 1039, 1041, 1042
 Ohta, Y. 965
 Ohtake, T. 1029
 Oiticica, C. 1034
 Okabe, A. 900
 Okada, RD. 944
 Okerlund, M. 887, 963, 1020
 Okerlund, MD. 963
 Okuda, H. 938
 Okuno, M. 972
 Okuzumi, I. 900
 Old, L. 1023
 Olea, E. 927, 991, 1006
 Olive, WH. 1028
 Olsen, J. 937, 964
 Olson, DO. 964
 Omar, YT. 1033
 Ono, Y. 976
 Oppenheim, BE. 978, 980
 Orino, A. 1012
 Orlin, JA. 1000
 Ortega, C. 1026
 Osher, AB. 923
 Oshima, M. 1035
 Oster, ZH. 933, 1054
 Ostertag, H. 970, 1029
 Otsuka, FL. 921, 958
 Otsuka, N. 987
 Ott, S. 908
 O'Tuama, L. 880, 954, 1010, 1027
 O'Tuama, LA. 969, 1026
 Owunwanne, A. 965
 Oyog, SS. 986
- Paans, AMJ. 1049
 Padmanabhan, S. 1048
 Paganelli, G. 881
 Pahl, J. 920
 Paidi, M. 995
 Paik, CH. 959, 1043
 Palac, RT. 953
 Palace, F. 882
 Palacios, IF. 910
 Palembo, E. 955
 Palme, D. 922
 Palmer, MR. 1003
 Pantalone, C. 884
 Panzer, M. 970
 Pappas, D. 918
 Paradis, RL. 882
 Parikh, A. 906
 Park, CH. 947, 1032
 Park, HM. 887, 956, 964, 978
 Parker, DA. 1053
 Parker, JA. 1000
 Parkey, RW. 891, 918, 1051
 Parmentier, C. 947, 1008, 1022
 Partain, CL. 978
 Pate, BD. 936, 1003, 1046
 Patel, H. 971
 Patel, KM. 994
 Patel, NM. 990
 Patlak, C. 937
 Patrone, VJ. 998
 Patt, YZ. 1021
- Patz, M. 1050
 Pauly, MP. 924
 Pauwels, EKJ. 975
 Pauwels, S. 904, 1009
 Pavel, DG. 927, 991, 1006
 Paxton, RJ. 1023
 Payne, JK. 997
 Pearlson, G. 880
 Pedersen, F. 888
 Pelletier, S. 1003
 Peng, J-S. 903, 958
 Penikas, VT. 1007
 Penin, H. 1028
 Penney, BC. 1003
 Penney, JB. 920
 Percival, RC. 963
 Perentesis, P. 903, 922
 Perez-Balino, N. 878
 Perez-Stable, E. 961
 Perlman, SB. 909, 984
 Perri, JL. 903, 904, 981
 Perry, JR. 1002
 Peschl, L. 1012
 Peters, AM. 950, 975, 978
 Peters, JM. 891
 Peters, T. 1001
 Petersen, JM. 877
 Peterson, CJ. 886
 Pettavel, J. 880
 Pettigrew, K. 937
 Pettigrew, RI. 961
 Pflanze, W. 952
 Phelps, ME. 879, 890, 901, 912, 913, 920, 924, 925, 932, 933, 940, 955, 967, 976, 980, 1004
 Philben, VJ. 1023
 Philippe, L. 927, 968, 991, 992, 1052
 Philippsen, L. 978
 Phillips, P. 945
 Picard, C. 951
 Picard, D. 988
 Pickering, CA. 892
 Pickett, RD. 905, 1052
 Picozzi, P. 1024
 Pidick, G. 1017
 Pierson, R. 996
 Pileggi, F. 990, 994
 Pino, S. 909
 Pinto, WP. 1015
 Pitt, S. 957
 Piwnica-Worms, D. 9675
 Pjura, GA. 1038
 Plotnick, JP. 1018
 Plotnick, JS. 1000
 Podreka, I. 887, 1029
 Poggenburg, JK. 902, 942, 1015
 Pohost, GM. 996
 Politano, V. 918
 Pollock, BH. 926
 Pollock, RR. 1023
 Popp, AJ. 924
 Port, S. 912
 Porter, BA. 964
 Porter, C. 963
 Poss, R. 908
 Potter, BM. 962
 Potvin, WJ. 961
 Pourcelet, L. 1009
 Powe, J. 889
 Powell, G. 899
 Powell, MR. 886
 Powelson, SW. 900
 Pozzilli, C. 1024
 Prach, T. 1046
 Prasad, UR. 912
 Pratt, G. 908
 Presant, CA. 971
 Preston, DF. 1012
 Prevost, WJ. 986
 Price, RR. 986
 Price, RW. 945
 Prigent, F. 899, 968, 997, 999
 Primus, FJ. 897, 943, 1016
- Pring, TJ. 978
 Proffitt, RT. 971
 Prokoff, E. 877
 Punzo, A. 1024
 Purut, CM. 992
 Pusey, E. 924, 925
- Quackenbush, RC. 1033
 Quadri, SM. 959
 Quaglia, L. 891
- Rabanni, R. 886
 Rabarison, Y. 947, 987
 Rabhani, R. 908
 Rabito, C. 993
 Rabito, CA. 941, 946, 1054
 Raffel, DM. 949, 966
 Raftery, EB. 990
 Raichle, ME. 1025
 Ramanna, L. 1030
 Ramberg, K. 1044
 Ramos, E. 1020
 Ramsdale, D. 943, 944
 Ramsey, FA. 1018
 Rancurel, G. 888
 Ranganath, MV. 918
 Rao, SA. 984
 Rapaport, F. 1054
 Rapoport, SI. 1024
 Rapp, J. 882
 Rasey, JS. 969, 979, 1026
 Ratib, O. 991
 Rauf, G. 935
 Ravert, H. 890, 935, 955, 983, 994, 1027, 1048
 Ray, CK. 918
 Raymond, MJ. 933
 Raynaud, C. 888, 985, 1054
 Reams, G. 1054
 Reba, RC. 916, 937, 959, 1043, 1045
 Reddy, RV. 968
 Reich, G. 890, 909
 Reich, RH. 953
 Reichle, R. 957, 1013
 Reichmann, K. 1028, 1052
 Reinhold, C. 1020
 Reisman, S. 953, 954, 998
 Reitz, B. 910
 Reivich, M. 889, 901, 919, 945
 Remley, K. 956
 Renda, A. 1023
 Reno, JM. 957
 Repetto, L. 1030
 Reske, SN. 1044, 1055
 Resnick, S. 901
 Revuz, J. 951
 Reynolds, JC. 902, 903, 922, 1022, 1043
 Reynolds, JR. 1021
 Rezaei, K. 943, 1017, 1018
 Ricard, M. 1008
 Ricard, S. 888
 Rice, DE. 916
 Rice, K. 936
 Riceputi, G. 881
 Richards, TL. 916
 Richards, WO. 956
 Richter, KY. 983
 Riege, W. 920
 Riehle, R. 929
 Riggs, BL. 964
 Righetti, A. 991
 Rigo, P. 878, 891, 995
 Riihimaki, DU. 1023
 Riis, BJ. 885
 Ritchie, J. 989
 Ritter-Hrncirik, CA. 941
 Riva, P. 881
 Robbins, WL. 900, 997, 1005
 Roberts, R. 911, 944, 1043
 Roberts, RK. 1004
 Robeson, W. 1006
 Robinson, GR. 1028

- Robinson, RG, 1012
 Robuschi, G, 909
 Rogers, MP, 956
 Rogers, WL, 896, 960, 973
 Rohner, A, 890
 Rose, EA, 910
 Rosebrough, SF, 941
 Rosen, ST, 903
 Rosendorf, L, 1020
 Rosenspire, KC, 1049
 Rosenthal, R, 925
 Roskopf, M, 962
 Ross, C, 880
 Ross, PD, 885
 Rossing, N, 888
 Rossleigh, M, 1030
 Rosso, J, 951
 Roth, J, 1023
 Rothenberg, J, 882
 Rothley, J, 920
 Roti, E, 909
 Rotrosen, J, 880, 901
 Rottenberg, DA, 945, 1048
 Roubin, GS, 900, 997
 Rougier, P, 1022
 Rowe, B, 909
 Royal, HD, 1000
 Rozanski, A, 934, 944, 998
 Rubertone, J, 1029
 Rubin, RH, 915
 Ruddy, TD, 944
 Rudolfstiftung, KA, 1012
 Ruley, EJ, 962
 Rumley, S, 1000
 Ruszkowski, M, 881, 939
 Russell, JAG, 880
 Russo, A, 898
 Ruth, TJ, 936, 1046
 Ryan, DE, 952
 Ryan, JW, 992
 Rycoff, KM, 882
 Rzeszutarski, WJ, 916
- Saccavini, JC, 1019, 1022
 Sackellaes, JC, 902
 Sacker, DF, 957, 1044
 Saenger, EL, 892
 Saha, GB, 882, 1028
 Sahweil, A, 1033
 Saiga, A, 972
 Saiki, Y, 1012
 Saint-Blancard, J, 1014
 Saint-Paul, B, 1014
 Saitoh, H, 970
 Saji, H, 928, 933, 972, 995, 1001, 1013
 Sakahara, H, 921, 1021, 1033, 1039, 1041, 1042
 Sakamoto, J, 1023
 Sakulsky, SB, 971
 Sakuma, S, 1035
 Salimi, Z, 952
 Salvatore, M, 1022, 1023, 1024
 Samson, Y, 888
 Samuels, LD, 919
 Sanchez, N, 958
 Sandler, MP, 977, 978, 986
 Sands, H, 902, 922, 1015, 1020, 1023, 1041
 Sanger, JJ, 914
 Santa, C, 901
 Sarkar, S, 928, 931
 Sato, O, 1025
 Satter, MR, 981
 Satyamurthy, N, 879
 Savant, V, 907, 1002
 Savi, A, 894
 Sayre, SL, 926
 Scannon, P, 1020
 Schaefer, DJ, 1008
 Schalber, E, 876
 Schaller, G, 890, 909
 Scharff, MD, 1023
 Schauwecker, DS, 887, 956, 964, 968, 978
- Schechtman, KB, 990
 Scheffel, U, 994, 1027, 1050
 Scheidhauer, K, 880
 Scheiner, SJ, 913
 Scheinman, M, 989, 993
 Schelbert, HR, 890, 891, 932, 933, 967, 976, 980
 Schenkenfelder, R, 919
 Schiepers, CWJ, 1035
 Schiff, RG, 876, 1038
 Schlom, J, 902, 922, 1019, 1021, 1023, 1042
 Schlumberger, M, 1008
 Schlüsselberg, SS, 917
 Schlyer, DS, 982
 Schmall, B, 1049
 Schmid, L, 880
 Schmidt, DH, 912
 Schmidt, K, 955
 Schmitt, W, 1044
 Schmitt-Bylandt, T, 1032
 Schmitz, H-G, 948
 Schmoliner, R, 878
 Schneider, C, 981
 Schneider, RF, 962
 Schneider, V, 907
 Schnitzlein, N, 1017
 Schober, O, 890
 Schroeder, G, 953
 Schroff, RW, 903, 957, 1022
 Schulz, E, 885
 Schwabe, D, 948
 Schwaiger, M, 890, 891, 932, 933, 967
 Schwartzkopf, B, 891
 Schwendner, S, 1046
 Schwinger, RB, 884, 1003
 Scott, JA, 993
 Seabold, JE, 915, 1035
 Sedvall, G, 879
 Seevers, RH, 972
 Seki, H, 1033
 Seki, Y, 1010
 Seldin, DW, 907, 910, 967
 Selin, C, 920
 Sell, TL, 992
 Seltzer, SE, 978
 Semeraro, LA, 904
 Senda, M, 928, 933, 995, 1001, 1026
 Senekowitsch, R, 1019
 Serafini, A, 918, 974
 Seto, M, 949, 957, 1035
 Sewall, S, 952
 Sfakianakis, GN, 918, 961, 1034
 Shaffer, P, 937, 964
 Shah, DM, 924
 Shah, P, 948
 Shah, SA, 922, 1015, 1023
 Shanes, J, 991
 Shao, H-S, 1044
 Shapiro, B, 908, 950
 Sharkey, CA, 932, 1034
 Sharkey, RM, 897, 943, 1016
 Shaw, DW, 969, 1026
 Shealy, DJ, 975
 Sheiöani, K, 1023
 Sherlock, FG, 1008
 Shen, SW, 949
 Shepard, M, 970
 Shibui, S, 970
 Shields, AF, 964, 1033
 Shigeta, A, 965
 Shih, LB, 897
 Shiire, Y, 911, 993, 1010, 1035
 Shimizu, T, 1029
 Shimosato, Y, 1022
 Shiplett, CA, 956
 Shiue, C-Y, 880, 906, 982, 1047
 Shively, JE, 1023
 Shochat, D, 943
 Shook, MA, 916
 Shreve, P, 1043
 Shuke, N, 1010
 Shuler, SE, 892
 Shulkin, B, 950
- Sia, BST, 878
 Siddhivarn, N, 951
 Siddiqui, AR, 887, 919, 923, 956
 Siegel, GJ, 902
 Siegel, JA, 903, 904, 981, 1011
 Siegel, ME, 929, 960, 988, 1031
 Silberstein, EB, 885, 892, 935, 979, 988, 1016
 Silbiger, M, 1017
 Silverstein, EA, 903
 Simmons, GH, 1008
 Simon, J, 915, 986
 Simon, TR, 917, 1006
 Simpson, D, 922, 1042
 Sindelar, W, 898
 Singh, A, 1028, 1054
 Singh, M, 883, 931, 1045
 Sinn, H-J, 970
 Sionoya, S, 1035
 Sirna, S, 943
 Sisson, JC, 886, 898, 908, 950
 Slosman, D, 1038, 1044
 Smalling, RW, 943, 976, 977
 Smid, A, 908
 Smirnov, VN, 909
 Smith, A, 909
 Smith, E, 983
 Smith, EO, 946, 1036
 Smith, JD, 971
 Smith, LM, 942
 Smith, M, 880
 Smith, MA, 1012
 Smith, ML, 1032
 Smith, R, 923
 Smith, T, 990
 Smith, WK, 917
 Snook, D, 975
 Snow, BW, 919
 Snyder, D, 1006
 Snyder, EL, 946
 Soares, J, Jr, 990, 994
 Soberman, R, 984
 Sodee, DB, 1001
 Sokal, G, 946
 Sokoloff, L, 955
 Sole, MJ, 933
 Solis, E, 947
 Sollinger, HW, 909, 984
 Solomon, H, 998
 Som, P, 933, 957, 1044
 Sommer, B, 964
 Sone, T, 987
 Sood, VK, 1043
 Sorby, P, 1045
 Sordillo, PP, 1030
 Sosa-Liprandi, A, 878
 Souchkewitch, G, 1019
 Soucy, JP, 888
 Spaulding, SA, 886
 Spence, AM, 1026
 Spencer, RP, 970, 971, 975, 1007
 Sperling, M, 1016
 Spies, SM, 903
 Spies, WG, 903
 Spitzer, L, 1020
 Spitznagle, LA, 970, 971, 975, 1007
 Spivak, W, 931
 Spohr, G, 891
 Sporn, BV, 878
 Sporn, V, 878
 Spritzer, CE, 887
 Srinivasan, A, 957
 Srivastava, PC, 1046, 1055
 Srivastava, SC, 946, 957, 958, 1044, 1046, 1052
 Stabin, MG, 979, 1008
 Stadalnik, RC, 924
 Stammers, TW, 893
 Stamos, JA, 896
 Stanford, CF, 951
 Staniloff, HM, 926, 954
 Stapleton, J, 986
 Starling, MR, 991
 Starnes, HF, 1031

- Starosta-Rubinstein, S. 920
 Staubus, A. 937
 Stefan, H. 1028
 Stein, SM. 978
 Steinbach, JJ. 994
 Steinberg, H. 1037
 Steinberg, M. 952
 Steiner, M. 887, 1029
 Steiner, TJ. 905
 Steinhardt, GF. 919
 Steis, RG. 903
 Ste-Marie, L-G. 988
 Stephenson, JA. 942
 Steplewski, Z. 1028
 Sterba, R. 985
 Sterling, FH. 887
 Stevens, SJ. 994
 Stewart, SL. 903
 Stoecklin, G. 982
 Stoessl, AJ. 936
 Stokely, EM. 918
 Stolf, N. 994
 Stone, P. 1034
 Stone-Elander, S. 879
 Stoub, EW. 960
 Straatmann, MG. 1018
 Strand, M. 1040
 Strand, S-E. 1004, 1007
 Strashun, A. 886, 918, 922, 938
 Straub, RF. 946, 1052
 Straus, E. 1036
 Strauss, HW. 909, 910, 911, 915, 916, 923, 941, 944, 946, 950, 966, 992, 993, 1002, 1048, 1054
 Strauss, J. 918
 Strauss, W. 967
 Strich, G. 998
 Stringham, L. 986
 Stritzke, P. 981
 Strother, SC. 945, 1001, 1024
 Stucki, V. 991
 Stulbarg, M. 993
 Stulberg, B. 952
 Stump, D. 1017
 Stumpf, MJ. 1002
 Sty, JR. 1034
 Suarez, J. 944
 Subramanian, G. 941, 962
 Subramanyam, V. 1050
 Suess, E. 887, 1029
 Sugarbaker, P. 902, 1021, 1022
 Sulzer, J. 883
 Sumida, R. 920
 Sumiya, H. 1033
 Sundaram, M. 1024
 Sunderland, JJ. 981
 Sunder Rao, CV. 1036
 Sung, BH. 999
 Suzuki, A. 911, 1002
 Suzuki, MN. 911, 1002
 Suzuki, T. 1036
 Suzuki, Y. 1025
 Swayne, L. 882
 Sychra, J. 927, 991, 1006
 Syrota, A. 888, 949, 950, 985
- Tada, A. 1011
 Tagge, E. 1013
 Taillefer, R. 1010
 Tainturier, C. 987
 Takagi, Y. 1014
 Takahashi, A. 976
 Takahashi, K. 965, 976, 1036
 Takahashi, T. 983
 Takakuwa, H. 1012
 Takayama, T. 957
 Takeda, H. 990
 Takeda, K. 994
 Takeshita, Y. 1011
 Taki, J. 911, 957, 993, 1035
 Taki, W. 1026
 Tal, I. 1000
- Tamaki, N. 911, 941, 992, 995, 999, 1002, 1054
 Tammaing, C. 954
 Tamura, K. 1032
 Tanada, S. 994, 1001
 Tanaka, H. 921, 1021, 1041
 Tanasescu, DE. 1030
 Taniguchi, M. 911, 993
 Tarver, RD. 887
 Tateno, Y. 940
 Tatum, JL. 912
 Tauxe, WN. 918, 928
 Taylor, A. 914, 977, 1052
 Taylor, A. Jr. 898, 962
 Taylor, DN. 994
 Taylor, WA. 1042
 Teates, CD. 998
 Teng, R. 906, 1047
 Tennenberg, S. 1037
 Tepe, PG. 918, 928
 Teresinska, A. 960
 Terz, JJ. 1023
 Teshima, T. 951
 Tewson, TJ. 949, 971, 976
 Thakur, ML. 947, 979
 Thaler, HT. 945
 Thiagarajan, P. 947
 Thomas, FD. 962
 Thomas, S. 948
 Thomforde, G. 1011
 Thompson, CJ. 1001, 1024
 Thompson, J. 1050
 Thompson, JT. 912
 Thompson, N. 908
 Thomsen, K. 885
 Thornback, JV. 994
 Thorne, DA. 914, 956, 977, 1015
 Thrall, JH. 925, 1053
 Tian, C. 1017
 Tiernan, T. 1017
 Tillapaugh-Fay, G. 941, 962
 Tillisch, JH. 891, 932, 967
 Tisdale, PL. 984
 Tison, V. 881
 Tiu, S. 914
 Tobolski, MM. 964
 Tochon, H. 890
 Todd, IP. 881
 Todd-Pokropek, A. 884
 Todo, A. 1012
 Tokars, M. 899
 Tokui, I. 972
 Tolbert, MEM. 906
 Tolman, GL. 896, 1015
 Tomashefsky, P. 970
 Tomita, S. 1012
 Tomomitsu, T. 987
 Tonami, N. 911, 957, 993, 1010, 1011, 1033, 1035
 Torchilin, VP. 909
 Torizuka, K. 921, 928, 933, 972, 987, 995, 999, 1001, 1013, 1021, 1026, 1033, 1036, 1039, 1040, 1041, 1042
 Townsend, D. 890, 909
 Toyama, S. 921, 1021, 1041
 Traill, T. 910
 Tran-Dinh, S. 985
 Treher, EN. 893
 Trembath, LA. 984
 Triebel, J. 1006
 Trinchieri, G. 947
 Trivino, J. 882
 Troutner, D. 905
 Troutner, DE. 915
 Trudeau, WL. 924
 Tsen, O. 928
 Tsui, BMW. 1002, 1017
 Tsuneoka, Y. 990
 Tucker, J. 931
 Tulip, T. 1050
 Tumeih, SS. 978
 Tune, L. 954
 Turner, AF. 971
- Turner, JH. 1045
 Tuttle, S. 937
 Tweddel, AC. 934
 Tweedle, MF. 915
 Twitchell, J. 976
 Tyler, JL. 889
 Tymm, R. 994
- Uchida, T. 1014
 Ueda, M. 1025
 Ueda, N. 965, 1036
 Ueno, T. 900
 Ugolini, V. 891
 Unger, MW. 942, 1019, 1020, 1021
 Urbain, JL. 904, 1009
 Urrutia, E. 941
- Vaalburg, W. 1049
 Vahlensieck, W. 948
 Valayer, J. 985
 Vallabhajosula, S. 938, 995
 Valle, D. 1026
 Vallois, JM. 949
 Vanderheyden, J-L. 894, 957
 van der Vusse, GJ. 966
 van der Zee, H. 1037
 Van Heertum, RL. 924
 Van Moflaert, GJC. 1026, 1047
 Van Train, KF. 899, 943, 944, 953, 968, 999
 Varga, D. 1016
 Varma, M. 1055
 Varma, RS. 1045
 Varvarigou, A. 1050
 Vasquez, P. 958
 Vasquez, TE. 876
 Vaitay, A. 943
 Vaugeois, JC. 1038
 Velchik, MG. 887, 952, 988, 1010
 Vera, DR. 924
 Verani, MS. 911, 944, 1043
 Verbruggen, A. 894, 1014
 Vessella, R. 922
 Vester, E. 891
 Vezina, WC. 882
 Vikydal, R. 878
 Villanueva-Meyer, J. 968
 Villemure, J-G. 889
 Virzi, F. 959
 Vitti, RA. 903, 904, 981
 Vlahos, WG. 1023
 Vogel, JM. 885
 Volant, JC. 880
 Volkert, WA. 905, 915, 986, 1028, 1051
 Volkow, ND. 918, 921
 Volle, CP. 892
 Von Eschenback, AC. 1021
 von Fliedner, V. 1019
 von Kummer, R. 1029
 Von Moll, L. 908
 Vora, M. 982
 Vosberg, AH. 878
 Votaw, JR. 981
 Vyska, K. 934
- Wackers, FJ. 1036
 Wade, RA. 916, 939
 Wagner, HN, Jr. 880, 890, 898, 910, 935, 936, 937, 945, 954, 955, 969, 983, 994, 1000, 1002, 1005, 1009, 1010, 1016, 1026, 1027, 1048, 1050
 Wahl, RL. 921, 988, 996, 1043
 Wahner, HW. 964
 Wald, A. 877
 Waldmann, TA. 897
 Walker, BS. 1006
 Walker, PJ. 884
 Walker, RD. 989
 Wallis, JW. 935, 988
 Walser, M. 928
 Walsh, RA. 991
 Wand, G. 1010

- Wang, C-I, 923
 Wang, SJ, 888, 989
 Wang, TST, 896, 970, 1043
 Wang, X, 960
 Wapenski, J, 920
 Warber, SL, 1013
 Warren, GL, 939
 Washburn, LC, 1049
 Wasnich, RD, 885
 Watanabe, N, 957, 1010, 1022, 1033
 Watson, DD, 926, 967, 998
 Watson, EE, 979, 1008
 Watts, NB, 963
 Waxman, A, 899
 Waxman, K, 998, 1030
 Weaver, A, 906
 Webb, J, 1045
 Weber, J, 1002
 Wedeking, P, 1051
 Wegst, AV, 1012, 1019
 Wehmeyer, G, 880
 Wehr, CJ, 986
 Weichert, J, 1046
 Weiss, S, 969
 Weissman, BN, 978
 Welch, MJ, 879, 921, 958, 969, 982
 Wellman, HN, 906, 919, 923, 964, 968
 Wells, SA, Jr, 958
 Welt, S, 1023
 Werner, JL, 971, 1023
 Wernz, J, 914
 Wesolowski, CA, 1006
 Wessels, BW, 902
 Wessels, P, 965
 Wester, DW, 894
 Wexler, J, 993
 White, F, III, 947
 Whitfield, HN, 929
 Whitton, A, 1030
 Wieland, B, 1018
 Wijns, W, 890
 Wilbur, DS, 957, 959
 Wiles, H, 911, 1043
 Wilkinson, R, 915
 Willerson, JT, 891, 918
 Williams, C, 948
 Williams, J, 880, 890, 954, 1010, 1026, 1027
 Williams, JJ, 1017
 Williams, KA, 992
 Williams, LE, 971, 1023
 Williams, SJ, 877, 894, 994, 995
 Wilson, A, 890, 935, 1027
 Wilson, AA, 955, 969, 983, 1027, 1048
 Wilson, D, 915
 Wilson, MA, 909, 984
 Wilson, MF, 999
 Wilson, PD, 1004
 Wilson, R, 978
 Wilson, RA, 953
 Wilson, WW, 967
 Wimberger, D, 1029
 Winckler, C, 1052
 Windham, JP, 961
 Winkler, C, 948, 1028, 1044, 1055
 Winsor, D, 971
 Winter, D, 931
 Wiseman, C, 971
 Wisneski, J, 890
 Witanowski, LS, 941
 Witherspoon, LR, 892
 Witt, RM, 906, 968
 Witzum, K, 938
 Woldring, MG, 1049
 Wolenski, PE, 992
 Wolf, AP, 880, 889, 901, 906, 982, 1047
 Wolf, E, 937
 Wolf, W, 1049
 Wolfe, O, 978
 Wolfert, B, 1041
 Wolfert, R, 958
 Wolfstein, I, 963
 Wolkin, A, 880, 901
 Wong, C, 899, 943, 944, 999
 Wong, D, 890
 Wong, DF, 880, 888, 898, 954, 1010, 1027, 1048
 Wong, W, 976
 Wong, WH, 883, 973
 Wong, WJ, 888
 Woo, DV, 1028, 1029
 Woodward, DJ, 917
 Woolverton, WL, 1026
 Wooten, WW, 898
 Work, JW, 926, 934
 Wright, JR, 966
 Wu, JL, 940, 1046
 Wu, LC, 929, 989, 1011, 1036
 Wurtman, RJ, 913
 Wutz, W, 982
 Yamaguchi, K, 1018
 Yamamoto, I, 1039, 1040
 Yamamoto, K, 928, 933, 1001, 1013
 Yamamoto, YL, 889, 999
 Yamamuro, T, 921, 1021, 1041
 Yamaoka, N, 1018
 Yamazaki, T, 1036
 Yanagimoto, S, 987
 Yanai, K, 983
 Yang, NC, 895, 1003, 1007
 Yankelevitz, D, 928
 Yano, T, 1035
 Yano, Y, 955, 976, 1045
 Yasillo, NJ, 1026
 Yasuda, T, 910, 911, 923, 941, 950, 967, 992, 1002
 Yeh, SDJ, 947, 1023
 Yeh, SH, 888, 929, 989, 1011, 1036
 Yen, TC, 929, 1011
 Yokoyama, A, 972, 1021, 1036, 1041, 1042
 Yokoyama, K, 957, 959, 1010, 1033, 1043
 Yonekura, Y, 928, 933, 995, 999, 1001, 1013, 1026
 Yoshida, K, 940
 Yoshii, F, 1025
 Yoshikawa, K, 970, 1029
 Yoshitake, A, 972
 Young, AB, 920
 Young, WC, 958
 Yu, C-C, 1051
 Yudd, AP, 924
 Yui, T, 1014
 Zabel, PL, 942
 Zacur, H, 1010
 Zanelli, GD, 990
 Zannad, F, 996, 1005
 Zanzi, I, 1006
 Zanzonico, PB, 898, 928
 Zecca, L, 894
 Zhu, Y, 993
 Ziada, G, 1033
 Ziessman, HA, 938
 Zillereulo, G, 918
 Zimmer, AM, 903
 Zimmer, RA, 882
 Zimmerman, RA, 919, 969
 Zimmerman, RE, 1009
 Zivanovic, MA, 1030
 Zoghbi, S, 922, 1019
 Zolnierczyk, K, 991, 1006
 Zuckier, LS, 1034
 Zwas, ST, 963, 989

Abstracts in this section pertain to papers as Works-in-Progress at the 33rd Annual Meeting of the SNM, June 22-25, 1986 at the Washington Convention Center, Washington, D.C. Scientific Program Chairman: Philip O. Alderson, MD

BONE/JOINT

No. 820

TECHNETIUM-99M MDP 4-H AND 24-H WHOLE BODY RETENTION MEASUREMENTS IN SKELETAL DISEASE. F.P. Castronovo, K.A. McKusick and H.W. Strauss. Massachusetts General Hospital, Boston, MA.

A simple technique for determining the whole body retention of Tc-99m labeled methylene diphosphonate (MDP) has been utilized for the 4-h and 24-h time periods. Twenty eight adult patients (22 prostate cancer, 6 osteoporosis) were administered 20 mCi (740 MBq) Tc-99m MDP and thereafter a qualitative scintigram was performed as well as whole body retention measurements at 4h and 24h. The prostate cancer patients all had positive bone scintigrams, and of this group, 7 were in relapse and 15 in remission on chemotherapy. All the osteoporotic patients had active disease.

Mean percent whole body retention values were significantly greater at 4h and 24h for the cancer patients in relapse relative to both the prostate cancer patients in remission and the osteoporotics: 4-h/24-h; 74.3/60.2, 57.5/33.5, and 48.0/30.3, respectively. The whole body retention values of the latter two groups, however, were only significantly different at 4-hours.

An additional index of skeletal pathology was developed by combining the 4-h/24-h values to calculate the T 1/2 b for this time period. Again the cancer patients in relapse exhibited a significantly longer half time relative to those in remission and the osteoporotics (70.4 hr vs. 25.7 hr and 29.2 hr, respectively).

The combination of 4-h and 24-h whole body retention values with the associated T 1/2 b has potential for following and classifying patients during the course of their skeletal disease.

No. 821

DEGRADED BONE IMAGE QUALITY FROM TC-99M GENERATOR ELUATE CONTAMINANT(S). J.J. Coupal and W.J. Shih, Veterans Administration and University of Kentucky Medical Centers, Lexington, KY.

Beginning mid-November 1985, a rash of Tc-99m-oxidronate (Tc-99m-HMDP) bone images showing diffuse liver (and sometimes gallbladder) radioactivity was experienced throughout the United States. In 12 (including ours) of 13 complaints to radiopharmaceutical manufacturer B, the Tc-99m was derived from a generator of manufacturer A to label Sn-HMDP kits from manufacturer B. Since we encountered degraded images sporadically and unpredictably, we attempted to resolve the problem. In all cases, aluminum ion in generator eluate was less than 1 ug/ml. Miniaturized chromatography of affected Tc-99m-HMDP radiopharmaceuticals revealed 2.31% - 6.86% hydrolyzed reduced Tc-99m ("colloid") (normal <1.5%) and 3.06% - 10.02% free pertechnetate (normal <1.1%). However, since neither thyroid nor stomach was seen on total body or spot films, at least some of the measured free pertechnetate was a radiochemical specie that migrates chromatographically like pertechnetate. Since findings suggest presence of unknown oxidant(s) in the generator eluate, we prospectively employed normal saline containing less than 5 ppm dissolved oxygen (LDO saline) from manufacturer C to dilute pertechnetate

eluate to 5.0 ml to make Tc-99m-HMDP. That has led to absence of liver and/or gallbladder radioactivity from most Tc-99m-HMDP preparations. Until the putative contaminant(s) can be identified and eliminated, we suggest employing LDO saline routinely to prepare Tc-99m-HMDP bone agent.

No. 822

DUAL PHOTON ABSORPTIOMETRY (DPA): QUALITY CONTROL. K. Wilkins, F.S. Prato, L. Reese, A. Hodson. St. Joseph's Health Centre and University of Western Ontario, London, Canada.

The value of DPA bone mineral density (BMD) for diagnosis of diseases such as osteoporosis and evaluation of treatment is established. Good reproducibility (precision) is necessary for the repeated measurements made during the evaluation of therapy. A large nuclear medicine department must develop an effective quality control programme to maintain precision since repeat measurements, or even data acquisition and subsequent analysis of the same study, may be performed by different technologists.

Bone mineral density in g/cm² was determined for the 2nd to 4th vertebrae using a commercially available DPA scanner (Lunar Radiation Corp) employing a Gd-153 1Ci source. All new technologists are initially required to analyse the same set of 10 studies. These 10 studies represent 5 different patient studies which are duplicated and their order for analysis randomised. Any technologist with a correlation coefficient less than 0.98 for the duplicate pairs must re-analyse the data and repeat this until the desired intra-technologist precision is achieved. These data are then used to determine the inter-technologist precision, and new technologists are accepted only when comparison to each established technologist exceeds a correlation coefficient of 0.96.

In order to determine that this quality control programme was successful, we scanned 28 patients twice, each repeat within a 2 hour period. Between the two scans, the patient walked around and was then repositioned. Data collection and analysis were performed by the technologist on duty and no attempt was made to restrict one patient to the same technologist. Analysis of these data gave a correlation coefficient of 0.98 with a 95% confidence interval of 0.08g/cm². It should be stressed that repeat measurements for evaluation of reproducibility must be performed within as short a period as possible. Thirty patients scanned twice with an average of 35 days between scans gave a correlation coefficient of only 0.89 and a 95% confidence interval of 0.17g/cm².

Adequate precision for BMD determinations made by a number of different technologists can be achieved if an appropriate quality control programme is implemented.

No. 823

EVALUATION OF GADOLINIUM-153 SEALED SOURCES USED IN DUAL-PHOTON BONE MINERAL SCANNERS. R.M. Witt, C.R. Appledorn, H.N. Wellman, and C.C. Johnston. R.L. Roudebush Veterans Administration Medical Center and Indiana University Medical Center, Indianapolis, Indiana 46202

Four Gd-153 sources fabricated as sealed point sources for use with dual-photon bone mineral scanners have been evaluated for radioactive contaminants and their effects on bone mineral measurements. All sources were prepared from material originating from Oak Ridge National Laboratory. The source material spans approximately 8 years of production and the latest source is 6 months old. All sources were evaluated with a high resolution detector (Ge(Li)) connected to a computer based spectrum analysis system. The latest source was evaluated one month after calibration and again three months later.

All gadolinium sources examined, qualitatively have the same spectra and all principal peaks can be identified. The primary contaminants are Eu-152 and Eu-154 with 12 and 8.6 year half-lives respectively. Spectra from

the most recent source indicates that there are no short-lived contaminants with half-lives of about 30 days. The observed background count rates range from 3 to 20 cps in the 44-keV and 100-keV windows and are a function of the thickness of the overlying soft tissue thickness. Improper correction for "true" background produced a 50% decrease in the measured crossover fraction at a soft-tissue thickness of 25-cm.

The usual gadolinium sources used for bone mineral determinations contain high energy and long-lived contaminants and improper correction of their background radiation can produce large errors in the determinations of the count correction factors used in the analysis of bone mineral data.

CARDIOVASCULAR

No. 824

MEASUREMENT OF LEFT VENTRICULAR DIASTOLIC FUNCTION: EFFECT OF CYCLE-LENGTH WINDOWING C.C. Chen, J.E. Juni
University of Michigan Medical Center, Ann Arbor, MI.

Variations in cardiac cycle length during ECG-gated blood pool studies cause errors in measurement of left ventricular diastolic function. This study evaluated the effects of different cycle-length windows on the measurement of peak filling rate (PFR) and time to PFR during forward gated blood pool studies. In addition, errors contributed by malpositioning the center of cycle-length windows were studied. To model normal variations in cycle length, simulated time-activity curves with cycle lengths varied in a Gaussian distribution were used to create 25 sets of 300 cycles. With the variation of one standard deviation (SD) set at 20% of the mean cycle length (MCL), forward gating had the following results: With cycle-length windows centered around the MCL, rms error in PFR using a 5% window was 0.2% compared to 0.7% with a 20% window ($P < 0.001$); 5% and 20% windows were more accurate than using no windowing which had rms error of 3.6% ($P < 0.001$); 30% and 40% windows had 1.79% and 1.81% rms errors, respectively. Using a 5% window, setting the window center at 94% MCL versus 106% MCL produced rms errors of 4.7% versus 1.7% ($P < 0.001$). 20% windows centered at 94% MCL and 106% MCL produced 4.5% and 1.6% rms errors, respectively ($P < 0.001$). Similar results were obtained when cycle lengths were varied with one SD set at 10% MCL, as found in normal hearts. (1) Windowing significantly improved the accuracy of forward ECG-gated blood pool studies. (2) When the windows are centered at the true mean cycle length, the narrower the window widths the more accurate are the measurements; narrowing windows less than 20% MCL did little to increase accuracy. (3) Malpositioning the center of the window produced additional errors in measurement of PFR. Overestimating the MCL produced more accurate measurements than underestimating the MCL.

No. 825

DISCRETE SUB-AORTIC STENOSIS: NEW CONCEPTS ON PATHOGENESIS AND DIAGNOSIS GAINED BY ECG-GATED Tl-201 MYOCARDIAL SCINTIGRAPHY. I. Garty, A.A. Shem-Tov and H.N. Neufeld. Afula and Chaim Sheba Hospitals, Israel.

This work-in-progress was undertaken to support our previously suggested new hypothesis concerning the dynamic features of discrete sub-aortic stenosis (DSS).

19 Patients suffering from DSS, diagnosed by echocardiography, heart catheterization and angiocardiography (Group A) were further evaluated by ECG-gated Tl-201 myocardial scintigraphy. The results were compared with 20 patients suffering from idiopathic hypertrophic sub-aortic stenosis (IHSS) (Group B) and 28 patients with no previous history of heart disease (Group C); all of whom were studied by the same method.

The following combination of scintigraphic signs were found typical in both DSS and IHSS patients: 1) End systolic left ventricular cavity obliteration; 2) Hypertrophy of septal myocardium; 3) Hypokinesis of the septal myocardium. The latter combination of "perfusion/wall

motion" mismatch has already been suggested by us as a new specific diagnostic sign for IHSS and was demonstrated in 100% Group A and B patients and none in Group C.

The close similarity of DSS and IHSS, as introduced by this work-in-progress, serves as additional proof in support of our previously expressed hypothesis that most of the cases of DSS involve dynamic features similar to those of hypertrophic obstructive cardiomyopathy. Accordingly, ECG-gated Tl-201 study seems to provide an additional sensitive method for the early diagnosis and evaluation of DSS patients, in a similar way to that of IHSS patients. The value of this method for the post surgical follow-up of DSS patients is now prospectively investigated.

No. 826

IMPAIRED MYOCARDIAL RETENTION OF I-131 METAIODOBENZYL-GUANIDINE (MIBG) IN CHRONIC VOLUME-OVERLOAD HEART FAILURE. M.A. Rabinovitch, C.P. Rose, G. Chartrand, J.L. Rouleau, D.M. Weiland, J.H. Burgess, and L. Rosenthal. Montreal General Hospital, Montreal, P.Q.

In heart failure, the function of cardiac sympathetic nerve endings is grossly disturbed. To assess the potential of sympathetic neuronal imaging for early detection of myocardial failure, scintigrams were acquired at 0.5, 2, 4, and 13 hours after intravenous administration of I-131 MIBG to 11 normal dogs, 3 auto-transplanted (denervated) dogs, 3 dogs with left (L) ventricular (LV) failure and 4 dogs with compensated LV hypertrophy (LVH) due to surgical arteriovenous shunt. Nine dogs were sacrificed at +14 hours for determination of I-131 MIBG and norepinephrine (NE) content in L atrium, LV septum, LV free wall, liver, and spleen.

There was a good correlation between I-131 MIBG and NE tissue content ($r = 0.74$, $p < 0.001$). The best scintigraphic discriminator between the subsets was the 0.5 - 2 hour LV efflux rate (LVER) in % per hour:

	Normal(NL)	Denervated	LV failure	LVH
LVER(M \pm SD)	13.9 \pm 3.1	20.3 \pm 3.4	26.4 \pm 4.7	16.7 \pm 2.9
P vs NL		0.05	0.01	NS

Thus, the I-131 MIBG myocardial retention characteristics of LV failure dogs are similar to denervated dogs, whereas LVH dogs behave like NLs. Qualitatively, splenic sequestration of I-131 MIBG was preserved in LV failure dogs, correctly reflecting the fact that sympathetic neuronal dysfunction in cardiac failure is not a generalized phenomenon. I-123 MIBG scintigraphy should be explored as a means of early detection of myocardial failure in patients.

No. 827

REVERSIBLE STRESS-INDUCED INHIBITION OF CARDIAC [I-123]PHENYL FATTY ACID (IP) METABOLISM IN CAD SHOWN BY SPECT. S. N. Reske, F. F. Knapp, Jr.*, K. Reichmann, J. Nitsch** and C. Winkler, Inst. for Clin. and Exp. Nucl. Med. and **Dept. Card., Univ. Bonn, FRG, and *Nucl. Med. Group, Oak Ridge Nat. Lab. (ORNL), Oak Ridge, TN.

Ischemia is a potent inhibitor of cardiac FFA utilization and degradation. IPSPECT has now been used in conjunction with sub-maximal exercise (SME) in 15 patients (pts) with CAD as follows: SME (6 min), IP injection and SPECT (I) followed by SME and SPECT (II) to increase regional differences of IP turnover. In 14/15 patients, segments with reduced IP uptake were observed after (I). Filling-in of these defects in (II) was observed in 11/15 pts. Infarctions showed clear uptake defects in both images (4 pts). Five pts without CAD (controls) showed homogeneous uptake and radioactivity release of 40-50%. Circumferential profiles showed inhomogeneous IP metabolic release in all 15 CAD pts. In one case, where a filling-in of the defect was clearly observed after the second SME with IP, Tl-201 imaging and ventriculography at the same

level of SME did not define the extent of exercise-induced ischemia. IP-SPECT and repeated SME may be a useful tool for the definition of stress-induced early ischemic changes in CAD.

ORNL is operated by the U.S. Department of Energy under contract DE-AC05-84OR21400 with Martin Marietta Energy Systems, Inc.

No. 828

SERIAL RESTING RADIONUCLIDE ANGIOCARDIOGRAPHY PERMITS SAFE ADMINISTRATION OF HIGH DOSE DOXORUBICIN THERAPY IN PATIENTS WITH NORMAL OR ABNORMAL BASELINE VENTRICULAR FUNCTION. R.G. Schwartz, J. Alexander, P.T. Sager, J. Setaro, W.B. McKenzie, F.J. Wackers, and E.L. Zaret; U. of Rochester, Rochester, NY; Yale U., New Haven, CT.

High dose doxorubicin (D) therapy has been reported to cause severe, irreversible and frequently fatal congestive heart failure (CHF). To assess the efficacy of serial resting radionuclide angiocardiotherapy (RNA) with technetium-99m-pertechnetate using first pass or multigated techniques for monitoring cardiotoxicity, we analyzed left ventricular ejection fraction (LVEF) and CHF incidence, severity and reversibility in 176 patients (pts) who had serial studies (1 RNA) and high dose (>450 mg/m²) D. CHF developed in 34 (19%) of this group, and was mild in 13 (7%), moderate in 17 (10%) and severe in 4 (2%) pts. Of 19 pts with abnormal baseline LVEF (<50%), CHF developed in 3 pts (16%). Despite identical baseline LVEF in both groups (62 ± 9%), pts developing CHF had a greater decline in LVEF (28 ± 11%) vs pts without CHF (14 ± 10%, P<0.001) and received more D (624 ± 135 vs 566 ± 84 mg/m², P<0.002). Routine treatment of CHF improved CHF in 30/34 pts (88%), including all 3 pts with abnormal baseline LVEF and CHF. No CHF death occurred in pts managed by RNA guidelines.

Thus, in pts with normal or abnormal baseline LVEF monitored with serial resting RNA who receive high dose D: (1) CHF is associated with greater decline in LVEF and with higher total dosage; (2) the incidence, severity and reversibility of CHF are favorable. Serial resting RNA can be effectively utilized with appropriate guidelines to monitor high dose D therapy with either normal or abnormal baseline ventricular function.

No. 829

COMPARISON OF INFARCT IMAGING MODALITIES: VALUE OF MONOCLONAL ANTIMYOSIN. H. Sochor, E. Ogris, O. Pachinger, D. Glogar, P. Probst, H. Weber, F. Kaindl. Dept. of Cardiology, University of Vienna, Austria

Current infarct seeking methods have conceptual limitations: Overestimation by TI-201 by imaging of residual ischemia, late imaging possibilities of Tc-99m PYP, which also may accumulate in only partially necrotic tissue. To assess myocardial infarct size and location we applied In-111 labelled monoclonal antimyosin Fab (mAM) and Tc-99m PYP in 12 pts with recent myocardial infarction. Infarct size (IS) was estimated semiquantitatively from planar 3 views scans for both compounds and compared to TI-201 perfusion images in the same pts. mAM was injected within 18 hrs (as early as 8 hrs post MI in 2 pts), PYP between 24 and 72 hrs. Target to non-target ratios for mAM were: infarct/control myocardium = 2.5-1.8, infarct/lung = 1.9±0.4, infarct/liver = 0.8±0.2. Location of mAM and PYP-defined infarcts was concordant in all cases, IS correlated significantly (r=0.72, p < 0.01) but mAM-IS was systematically smaller than PYP-IS. TI-201 was equivocal in 2 smaller posterior MIs, picked up by both other tracers. IS by mAM and PYP both correlated with CK-maximum enzyme release (r=0.64, r=0.62). In 2 pts following successful reperfusion IS was significantly smaller than area-of-risk outlined by TI-201. We conclude that infarct imaging with Fab mAM provides reliable information regarding infarct size and location with the advantage of being more confined to the "true" area of necrosis. However, TI-201 as an additional reference

tracer may facilitate assessment of the precise area-of-risk. Thus, this technique might contribute to the assessment of reversibly compromised myocardium.

No. 830

SERIAL RADIONUCLIDIC ASSESSMENT OF SPECIFIC HEMODYNAMIC CONSEQUENCES OF SURGICALLY INDUCED LEFT TO RIGHT SHUNTS IN MATURING MINISWINE. R. Stratbucker, R. Kelly, K. Kilzer, E. Robertson, M. Quaife, and L. Latson. University of Nebraska Medical Center, Omaha, NE.

Comprehensive, non-invasive definition of the hemodynamic status of left to right (L/R) cardiac shunts in an animal model during maturation may yield useful criteria in the clinical management and/or intervention in affected children. Serial Nuclear Medicine (NM) measurements, i.e., pulmonary to systemic flow ratio (Qp:Qs), left & right ventricular ejection fractions (EF's), stroke counts (SC's), and ventricular time activity curves with slope parameters (SP's), were performed. An average of 5 studies each were done on 26 anesthetized miniswine. Animals were followed from infancy to full maturity at 9 months. Eight had surgically created neonatal L/R shunts and the balance were sham operated controls. One in three had parallel invasive studies. The NM measurement of Qp:Qs (gamma variate analysis) tracked the invasive measurement (O₂ saturation analysis) with a correlation coefficient of 0.75. Qp:Qs's ranged from 1.27 to 3.02 with a mean of 2.5 and remained surprisingly constant. Control Qp:Qs's averaged 1.11 (SEM 0.031). Heart rate dropped more for shunts (30%) than controls (20%) during the maturation period. RVEF nearly doubled in shunts (.35 to .57) but changed little in controls. LVEF changed little in either case. These findings may assist in assessment of the physiologic status of recirculatory lesions in the young.

CDA

No. 831

HUMAN FACTORS ENGINEERING IN A NETWORKED NUCLEAR MEDICINE FACILITY. Brown GS, Feldt DA, Juni JE. University of Michigan Medical Center, University Hospital Ann Arbor, MI

Implementation of Picture Archiving Computer Systems are hindered by a lack of perceived value by physicians and technologists. We are implementing a distributed system which is unique in providing 1) "instant" quality control during scan acquisition; 2) automatic flow of images to reading areas and image archives; 3) rapid personnel management and electronic communication.

Scans are acquired at 15 workstations on several floors all feeding into the networked system. Without leaving the patient, the technologist can electronically forward images to the scan reading room where a physician can determine the scan's quality and request additional views if needed. Physicians and technologists are automatically located by the system for real-time communications. Images acquired during the day are automatically forwarded to high-resolution workstations for interpretation. Images are automatically archived onto magnetic disk (short-term) and/or optical disk (long-term). This allows rapid access to all images acquired from any camera at any time.

This network supports clinical image processing, distributing clinical patient reports through the hospital information network, receiving lab reports, maintenance of all clinical protocols, maintaining service logs on all equipment, word processing as well electronic mail and message services.

No. 832

BACKGROUND CORRECTION FOR QUANTITATIVE ANALYSIS OF DTPA RENAL STUDIES. E. Byrom. Michael Reese Hospital, Chicago, Illinois

The usefulness of dynamic renal studies with Tc-99m DTPA for measurements of glomerular filtration (GFR) is limited by underlying spatially inhomogeneous nonrenal activity, or 'background'. A new method is proposed to correct for the major inhomogeneities while grouping pixels to minimize statistical fluctuations. Successive 'annuli' one pixel wide are constructed inwards and outwards from the renal ROI boundary, and divided into 3 sectors for the liver (or spleen), the lower lateral renal boundary, and the lower medial boundary. In each sector, the outer annular arcs establish a background count density and a radial count density gradient, for biquadratic interpolation across the inner arcs. This method was compared in 10 consecutive studies to the correction used in the Gates regression equation (sampling background by a ROI drawn around the lower part of the kidney). By including liver and spleen activities, the regression is modified to eliminate the intercept term. The method also revises differential GFR by more than 5 percentage points in 5 of the 10 cases, and eliminates the unphysiological negative initial slope of the kidney time-activity curve found in 4/10 cases with the older technique. This new method provides an accurate starting point for improved measurements of glomerular function from radionuclide renal studies.

No. 833

NONUNIFORM ATTENUATION CORRECTION IN SPECT USING ITERATIVE RECONSTRUCTION ALGORITHMS. E.R. Edgerton¹, B.M.W. Tsui¹, G.T. Gullberg², D.R. Gilland¹, J.R. Perry¹, W.H. McCartney¹ and J. Berg³. ¹Univ. of North Carolina, Chapel Hill, NC; ²Univ. of Utah, Salt Lake City, UT; ³General Electric Medical Systems Group, Milwaukee, WI.

Conventional attenuation correction methods used in SPECT assume uniform attenuation throughout the body. In body regions such as the chest, however, the various tissue types have very different attenuation coefficients and the resulting nonuniform attenuation affects the quality of the reconstructed image. We evaluated the use of iterative reconstruction algorithms for correcting the nonuniform attenuation distribution with phantom and clinical studies. The correction method involved the acquisition of transmission projection data using a collimated flood source mounted opposite the camera on the rotating gantry of a SPECT system. The transmission CT images provided the attenuation distribution of the body and were incorporated into the reconstruction of the emission data. The algorithms under evaluation included the conjugate gradient and the maximum likelihood methods. A phantom consisting of separate chambers to simulate the chest region was constructed. Results from the phantom studies demonstrated that the iterative reconstruction methods gave less image artifact, more accurate quantitative information and decreased image noise when compared to the conventional reconstruction methods. The maximum likelihood algorithm provided the best image quality and quantitative accuracy. The nonuniform attenuation correction method were applied to liver, cardiac and lung studies. The results demonstrated improved image quality and confirmed clinical utility of the correction method.

No. 834

MONTE CARLO SIMULATION OF DATA WITH POISSON NOISE FOR GAMMA CAMERA BASED SPECT SYSTEMS.

L.J. Hahn, C.E. Floyd, R.J. Jaszczak, S.H. Manglos, K.L. Greer, R.E. Coleman.
Duke University Medical Center, Durham, NC.

It is desirable to simulate projections with noise for evaluating properties of scintillation camera based

SPECT systems. For example a Monte Carlo model of the SPECT system simulating scattering, attenuation and noise allows a quantitative evaluation of noise propagation in the case when scatter and attenuation effects are compensated.

In our Monte Carlo code variance reduction methods are used. As a result, the statistics of the calculated projections are not generally Poisson. We have simulated projections with a large number of histories (5 million or more). These projections are essentially noise free. Then the calculated data are modified to obtain projections with the desired level of noise, with proper Poisson statistics.

Simulated data were compared with experimental measurements of a physical phantom (disk source in water filled cylinder). Calculated values of %rms noise in the reconstructed images were 3.4 (3.2), 6.8 (7.8) and 19.6 (20.11) for experimental (simulated) data for 10, 1.5 and 0.1 million total counts, respectively.

As a further step a similar procedure for cone beam collimators is being developed, allowing comparison of different collimator geometries.

No. 835

COMPARISON OF RAPID PARAMETER ESTIMATION TECHNIQUES FOR QUANTITATING LOCAL METABOLIC RATE AND INDIVIDUAL RATE PARAMETERS FROM DYNAMIC PET USING 2-FDG. R.A. Koeppel, G.D. Hutchins, J.E. Holden*. Cyclotron/PET Facility, University of Michigan, Ann Arbor, MI and *Department of Medical Physics, University of Wisconsin, Madison, WI.

Local cerebral metabolic rate (LCMRGlc) can be estimated from single scan or dynamic protocols. Single scan methods are simpler, but often less accurate. Dynamic techniques provide estimates of the individual model parameters in addition to more accurate estimation of LCMRGlc. However, acquisition time is lengthened and computational requirements are far greater. The use of rapid estimation techniques for pixel-by-pixel calculations can effectively eliminate the computational problems.

We have developed three techniques for rapid pixel-by-pixel estimation in 2-FDG studies, each adapted from an existing blood flow estimation technique. The first method utilizes a least squares search scheme. The other two methods involve the use of weighted integrals of data, one using a lookup table, the other using matrix inversion. For comparison, we examined two other rapid techniques, one calculating multiple integrals of data over various time periods (1), the other involving a slope and intercept determination (2).

Theoretical studies of statistical uncertainties were carried out for each technique. Errors differed by as much as a factor of three between methods. Images of LCMRGlc and the individual rate constants were calculated from dynamic PET data. Computation time varied by a factor of five. The optimal technique to use depends on the relative importance of speed versus accuracy.

1. Blomqvist (1984) J Cereb Blood Flow Metabol 4:629.
2. Gjedde et al (1985) J Cereb Blood Flow Metabol 5:163.

No. 836

QUANTIFICATION OF RADIONUCLIDE CONCENTRATIONS WITH SPECT. L.G. Strauss, T. Fleiner, E. Wetzel, J.H. Clorius, M. Georgi. Klinikum Mannheim and German Cancer Research Center, Heidelberg, West-Germany.

The quantitative determination of radionuclide concentrations was assessed in phantom studies. The pancreas and the surrounding abdominal region of the Alderson Remcal phantom were filled with different concentrations of Tc-99m pertechnetate. A rotating gamma camera connected to a computer system was used for SPECT data acquisition. The radionuclide concentrations of the pancreas were varied from 35.8 MBq/l to 552.3 MBq/l, and in the abdomen from 1.76

MBq/l to 109.7 MBq/l. Cross sections were reconstructed using two different filters (Ramp-Hanning, Butterworth), and three different cut-off frequencies (0.25, 0.5, 1 Pixel). Then ROIs were placed over the two areas with different radionuclide concentrations. The mean ROI values were transformed, and compared to corresponding logarithms for the radionuclide concentrations.

We were able to demonstrate a high correlation between the transformed mean ROI values, and the radionuclide concentrations ($r=0.9929$). Furthermore, scatter correction was applied to the cross sections using the double energy method of Jaszczak et al. Scatter correction did not improve the correlation coefficient ($r=0.9931$) or reduce the standard deviation, but reduced the offset error. The non-scatter corrected SPECT cross sections are reliable for determining low and high radionuclide concentrations. The Butterworth filter with a cut-off frequency of 0.5 gave best results.

DOSIMETRY

No. 837

EVALUATION OF EXTERNAL MONITORING VS. URINE ASSAY FOR DETERMINING POST-THERAPY I-131 RETENTION. J.A. Ponto, L.L.B. Ponto, and J.A. Bricker. University of Iowa, Iowa City, IA.

External exposure-rate monitoring with energy-compensated (comp) and uncompensated (uncomp) probe detectors was compared with the traditional urine assay method for the determination of I-131 body retention following thyroid cancer treatment. Preliminary theoretical calculations and modified isoresponse measurements indicated that exposure-rate monitoring should be performed at a minimum distance of 106 cm from the midpoint of the patient's torso. Body retention in each of 17 patients with thyroid cancer treated with 66-208 mCi I-131 was periodically determined using the urine assay method until body retention fell below 30 mCi (total number of determinations = 25). Determination of body retention using external monitoring with both comp and uncomp probes was performed by comparing exposure-rates at the time of administration and at the time of subsequent urine assay. Linear regressions between body retention determined from urine assay and from comp and uncomp probe measurements were: urine = $0.77 + 0.961 \text{ comp}$ ($r^2 = 0.812$) and urine = $4.73 + 0.672 \text{ uncomp}$ ($r^2 = 0.747$). Predictive distributions fit to this data indicate that body retention determined by external monitoring with comp and uncomp probes must be less than 20 mCi and 16 mCi, respectively, to be 95% confident that body retention determined by urine assay is less than 30 mCi. Advantages of external monitoring methods include simplicity and low exposure to hospital personnel. A comp probe is preferred because its uniformity in response to primary and scattered photons provides greater accuracy.

ENDOCRINE

No. 838

IN VITRO UPTAKE OF I-131 MIBG BY MEDULLARY CELL CARCINOMA OF THE THYROID. G.J. Poston, E. James, H.D. Fawcett, C.M. Townsend, J.C. Thompson, M.L. Nusynowitz, University of Texas Medical Branch, Galveston, TX.

Controversy exists as to whether or not medullary thyroid cancer (MTC) takes up I-131 metaiodobenzylguanidine (MIBG). We studied rat MTC (6-23), rat pheochromocytoma (PC-12), rat small bowel (RIE-1), and mouse colon cancer (MC-26) cells in tissue culture incubated for 24 hours in either 1 microcurie of I-131 MIBG or 1 microcurie of I-131 NaI. After decantation of culture medium and washing

of cells, retained radioactivity of the cells was measured. Results are expressed as mean counts per million cells \pm S.D.; $n=6$ for each group.

Cell type	I-131 NaI	I-131 MIBG
6-23	24 \pm 15	196 \pm 9
PC-12	2001 \pm 333	42,412 \pm 6755
RIE-1	134 \pm 24	372 \pm 67
MC-26	30 \pm 26	55 \pm 19

MIBG significantly increases I-131 uptake by MTC cells but this is still less than 0.5% of the uptake of MIBG seen in pheochromocytoma cells. I-131 MIBG is probably not a useful agent to localize or treat MTC.

GASTROENTEROLOGY

No. 839

ASSESSMENT OF LIVER PRESERVATION BY ^{31}P NMR: EFFECT OF ISCHEMIA, ANOXIA AND REPERFUSION. RG Lee, ME Clouse, A Lanir, P Kasulis. Department of Radiology, New England Deaconess Hospital, and Harvard Medical School, Boston.

Human liver transplantation is a major advance in medical science, but its application is hampered by limited preservation techniques for the donor liver. We hypothesized that donor livers could be preserved longer if the liver energy charge could be maintained.

ATP decay, inorganic phosphate appearance and phosphate chemical shift in mouse livers were studied by ^{31}P NMR spectroscopy. Cold flush followed by cold preservation in Collins solution resulted in slower ATP decay than preservation in Krebs-Henseleit buffer or saline. ATP decay was much slower at cold temperatures (factor of 1.81 ± 0.06 for every 10°C). Injection of chlorpromazine into the mouse 3 hr before sacrifice markedly decreased ATP decay rate and inorganic phosphate appearance.

In perfusion experiments with oxygenated Krebs-Henseleit buffer, ATP/Pi remained constant for 3 hr at 37°C and for more than 6 hr at 20°C .

During ischemia produced by reduced perfusate flow, ATP rapidly fell to undetectable levels with concomitant rises in inorganic phosphate and sugar phosphate. Intracellular pH fell continuously during ischemia (10-60 min at 20°C). With reperfusion, ATP concentration was higher than baseline within 5-7 min and then fell back to baseline; pH was rapidly restored. After warm ischemia for 10-30 min, the ATP level recovered only partially. During anoxia at 37°C , ATP/Pi decreased slowly but constantly to complete decay at 60 min and only partially returned with restoration of oxygen. Reoxygenation resulted in massive liver enzyme release and broadening of the ^{31}P spectra, suggesting free radical formation.

No. 840

INDIUM III LABELLED LEUKOCYTES IN THE DETECTION OF TUBERCULOUS ENTERITIS. KE Pettengell, A Houlder, M Garb, AE Simjee, Dept. of Medicine, University of Natal & Dept. Radiology, Addington Hospital, Durban, South Africa.

INTRODUCTION: Indium III labelled leukocyte scanning is now an established technique for the detection of sepsis and has been used in the imaging of inflammatory bowel disease. We know of no reported series in which the technique has been applied to tuberculous enteritis (TE). **PATIENTS:** 5 Patients in whom a diagnosis of TE was made and confirmed by histology were studied. 4 of the 5 patients were on anti-TB treatment for periods up to 1 month before investigation.

METHOD: The extent of the disease was determined by a combination of upper and lower GI endoscopy and radiology. **Scanning:** this was performed within 2 weeks of the diagnosis. Leukocytes were labelled in saline with Indium III oxine and abdominal scans were performed at 4 hrs and 24 hrs. Results were assessed by a radiologist unaware of the endoscopic or radiological assessment.

RESULTS: All scans were positive at 3 hours and remained so at 24 hours.

PATIENT AGE SEX	LOCALISATION		Rx BEFORE SCAN	KEY
	INDIUM	ENDO/XRAY		
23 M	2,3,4	2,3,5	18 days	1-Upper small bowel
15 F	2	2	-	2-Ileocaecal region
27 F	2,3	2,3,4	2 days	3-Ascending colon
24 F	2,3,4	2,3,4	31 days	4-Transverse colon
30 M	1	1	18 days	5-Descending colon

CONCLUSION: Indium III leukocyte scanning appears to be able to detect tuberculous enteritis and provide information as to its extent. This information may be obtainable up to 4 weeks after the initiation of treatment for tuberculosis and may provide a non-invasive means of follow-up.

No. 841

RADIONUCLIDE GASTRIC EMPTYING STUDY IN PATIENTS WITH ANOREXIA NERVOSA, BULIMIA, OR ANOREXIA NERVOSA/BULIMIA. W.J. Shih, L. Humphries, P.A. Domstad, F.X. Castellanos, F.H. Deland. University of Kentucky and Veterans Administration Medical Centers, Lexington, KY.

To evaluate gastric emptying in patients with anorexia nervosa (Abulimia (B), or AN/B, 48 patients (46 females, 2 males) with upper G-I symptoms ingested 150 uCi Tc-99m triethelene tetraamine polyesterene resin in cereal and were imaged in the supine position. Data were accumulated at 5 min intervals to obtain the gastric emptying time (GET). In four patients GET was normal (40-85 min), in 19 rapid GET, and in 25 prolonged GET. Twenty-four of 25 with prolonged GET were given 10 mg metoclopramide (MP) IV, with good response in 18 and no response in 6. Among 19 with AN, 10 had prolonged GET, 8 had rapid GET, and 2 were normal. In 18 with B, 9 had prolonged GET, 7 rapid GET, and 1 normal GET. In the 11 patients with AN/B, 6 had prolonged GET, 4 rapid GET, and 1 normal GET. Eight patients with prolonged GET underwent MP therapy and 6 of the 8 showed benefit from the therapy; 2 patients discontinued MP because of somnolence. Although all patients had subjective symptoms of gastric dysfunction, our results indicate only 52% had objectively prolonged GET, and 48% showed normal or even rapid GET. Therefore, this radionuclide study enables (1) objective measurement of gastric emptying to separate those patients with rapid or normal GET from those with prolonged GET, avoiding possible side effects from MP medication, (2) prediction of the effectiveness of MP therapy in patients with prolonged GET.

No. 842

A NEW CHOLESCINTIGRAPHIC AGENT: RUTHENIUM-97-DISIDA. I. Zanzi, S.C. Srivastava, G.E. Meinken, W. Robeson, L.F. Mausner, R.G. Fairchild, and D. Margouloff. North Shore University Hospital, Cornell University Medical College, Manhasset, NY; and Brookhaven National Laboratory, Upton, NY, USA.

Previous studies in experimental animals suggested that the radiopharmaceutical Ru-97-iminodiacetic acid might be useful as an alternative to I-131 Rose Bengal when delayed hepatobiliary studies are needed. The advantages of Ru-97 are based on a relatively long half life ($T_{1/2} = 2.9$ d), a convenient primary gamma photon (216 KeV), and similar biological behavior as Tc-99m labelled hepatobiliary agents (demonstrated by similar blood clearance and biodistribution studies in animals). Ru-97 was prepared at the BNL BLIP by proton spallation of rhodium foil. A DISIDA commercial kit with 10% ethanol was utilized in 9 patients (age 6 weeks -84 years). Hepatobiliary images obtained were of excellent quality. Prompt blood clearance was noted. The cholecystograms correlated well with other imaging procedures and clinical

findings. Biliary atresia was ruled out in an infant. Combined with Tc-99m-Sulfur Colloid the agent was utilized in the concomitant quantification of entero-gastric reflux and delayed gastric emptying in 3 patients. We believe that Ru-97-DISIDA may be particularly useful in patients in whom delayed hepatobiliary views are desirable and in subjects in whom dual isotope quantification of enterogastric reflux is required. Further study of more patients is in order to confirm the clinical utility of this agent.

HEMATOLOGY

No. 843

DEPENDENCE OF Tc-99m RED BLOOD CELL LABELING EFFICIENCY ON RED CELL SURFACE CHARGE. D.W. Seldin, S. Simchon, K.M. Jan, S. Chien, and P.O. Alderson. Columbia University, New York, NY.

The mechanism by which Tc-99m pertechnetate (Tc) labels stannous primed red blood cells (RBC) is controversial. We studied the effect of altering the surface charge of the RBC on the efficiency with which Tc would label the cells. RBC surface charge was reduced by removing the terminal sialic acid moiety of membrane glycoprotein with neuraminidase. Thirty-nine blood samples from 5 volunteers were incubated with neuraminidase for varying lengths of time, resulting in reductions of surface charge to from 89% to 1% of normal negative values. Surface charge was determined from electrophoretic mobility measurements (EPM). The treated blood samples then were labeled with Tc using a standard protocol. Following labeling, the blood samples were centrifuged and the cells and supernatant were counted separately to determine the percent of the Tc bound to the RBC. For those samples with EPM > 20%, there was an excellent correlation ($r=0.90$) between EPM and percent bound, i.e. as cell surface charge was reduced the Tc labeling efficiency decreased in direct linear proportion. When EMP was < 20%, the percent bound showed little variation from a mean value of 35%. The findings suggest that surface charge is a significant factor in the labeling of RBCs with Tc.

IMMUNOLOGY

No. 844

ALTERATION OF RADIOANTIBODY CLEARANCE PATTERNS AND BIODISTRIBUTION BY HUMAN ANTI-MOUSE ANTIBODY (HAMA). E.H. Ford, F.J. Primus, B. Greenspan, R. DeJager, K. Brennan, and D.M. Goldenberg. Dept. of Radiology, and Center for Molecular Medicine and Immunology, UMDNJ, Newark, NJ.

Vascular clearance patterns, HAMA formation, and scintigraphic biodistribution imaging were used to measure patient response to radioimmunotherapy. Eight of 14 patients developed HAMA prior to or during treatment with 4 injections of 25-60 mCi of I-131(anti-CEA) NP-2. Only 2 patients were skin test positive. The appearance of circulating plasma protein aggregates indicating complexes between HAMA and radioantibody was revealed by gel filtration chromatography. This was associated with spleen visualization on scintigraphy. NP-2 did not combine with circulating CEA, demonstrating negligible contribution to the formation of the immune complexes detected. Progressive shortening of blood clearance rates of radioantibody paralleled rising HAMA titers as measured by enzyme immunoassay. A shift of circulating antibody-associated radioiodine to free iodine followed the formation of complexes with HAMA, suggesting splenic dehalogenation of radioantibody. Higher HAMA titers accelerated the conversion of circulating radioactivity to mostly free iodine within a few hours after injection. In patients without HAMA, the circulating

radioactivity was entirely associated with antibody up to 8 days after injection, during which time the spleen was not visualized by scintigraphy. Evaluation of splenic uptake on diagnostic studies combined with peripheral immune complex assay can be used as an assessment of immune complex formation and injected antibody integrity. (Supported in part by NIH grant 39841).

INSTRUMENTATION

No. 845

EVALUATION OF SCATTER CORRECTION FOR In-111 LABELED CARDIAC AGENTS ON A SPECT SYSTEM. P.D. Esser, A.M. Keller, D.W. Seldin, L.L. Johnson, P.J. Cannon, and P.O. Alderson. Columbia University, New York, NY.

A SPECT system for imaging In-111 labeled anti-cardiac myosin Fab fragments and other In-111 agents was investigated. The all-digital system consisted of dual heads, rotating gantry, body contouring, medium energy collimation (10.3 mm FWHM at 10.2 cm), and acquisition photopeaks (PP) at 172 + 247 keV (15% windows) and in the Compton scatter (CS) region, 120 keV (25% window). System performance was evaluated with a 22.2 cm diam. phantom containing line sources (LS) or a 6 cm diam. sphere. Line spread functions (LSF) were calculated from a 1 pixel slice of the LS (radius of rotation=17.5 cm). LSF showed:

Energy	FWHM/air	FWHM/Water	FWTM/Air	FWTM/Water
120	26.0 mm	27.6	55.1	79.0
172	18.3	19.2	36.3	39.2
247	18.0	18.5	35.4	36.6

Slices of LS in air and water, with attenuation correction (AC), were compared and showed a 55% scatter contribution. For a cold ball in a hot background the CS component was evaluated from SPECT image profiles. Scatter contributed 59% of the counts. If AC was ignored, this decreased to 22%, indicating that AC is necessary. We conclude that scatter is a major component of In-111 images and that In-111 activity quantitation with SPECT will require both attenuation and scatter corrections. The latter seems readily obtainable from data collected simultaneously through a Compton window.

No. 846

A FAST GAMMA RAY DETECTION SYSTEM FOR IN-VIVO MEASUREMENT OF BODY CARBON. J.J. Kehayias, K.J. Ellis and S.H. Cohn, Medical Research Center, Brookhaven National Laboratory, Upton, NY.*

A miniature 14 MeV neutron generator is used for in-vivo carbon, oxygen and hydrogen measurements for the determination and monitoring of body fat. The neutron generator is pulsed at a rate of 10KHz and delivers 10^3 neutrons/pulse. A target-current feedback system regulates the source of the accelerator to assure constant neutron output.

Carbon is measured by detecting the 4.44 MeV γ -rays from inelastic scattering. The short half-life of the 4.44 MeV state of carbon requires detection of the γ -rays during the 7 μ s neutron pulse. Generators with low pulsing rate were found inappropriate for carbon measurements because of their low duty-cycle (high neutron output during pulse).

The detection system consists of NaI(Tl) detectors and fast electronics for handling the high event rate during the neutron pulse. Fast ADCs with a constant conversion time of 1.5 μ s are used for counting. A buffer based micro-multichannel analyzer designed for maximum data throughput is used for data acquisition. A microcomputer controls the micro-multichannel analyzer and stores the data. This independent fast data acquisition system is operating at counting rates

of 100 KHz per detector and can be easily interfaced with a mainframe computer.

*Work supported by DOE No. DE-AC-02-76CH00016.

No. 847

INSTALLATION OF A HIDAC POSITRON CAMERA. S. Kuijk¹, G. Bennett¹, Y-N Tang¹, D. Townsend², M. Defrise³, F. Deconinck³, A. Jeavons⁴, A.B. Brill¹, A. Donath².
¹Brookhaven National Laboratory, Upton, NY.; ²Cantonal Hospital, Geneva, Switzerland; ³VUB, Brussel, Belgium; ⁴CERN, Geneva, Switzerland.

A positron camera based on the High Density Avalanche Chamber (HIDAC) detector has been installed in the Med. Dept. of BNL. Each detector has a sensitive area of 31 cm x 31 cm, an intrinsic spatial resolution of 2mm, (3mm in reconstructed images), and a detection efficiency of 12% for 511 keV photons. The positron camera consists of a pair of HIDAC detectors operated in coincidence with a 20 nsecs resolving time. A similar pair of detectors has been undergoing clinical evaluation in Geneva for the past eighteen months. The detectors were mounted on the same gantry as that used for the UNICON, a dual-headed Anger camera at BNL. The HIDAC detectors are mounted orthogonally to the UNICON heads, in order to conduct simultaneous PETT and SPECT studies with the system.

The detectors are interfaced through CAMAC to a PDP 11/34 which is linked over DECNET to a host VAX 11/780. A typical study is performed in step-and-shoot mode with 20 angular positions of the detectors and the data stored in list mode.

To date, the system has been used for a number of phantom studies, and system performance factors have been established. Clinical trials have begun and are expected to last for a period of 8-10 months.

Work supported by Swiss National Science Foundation, NFWO (Belgium) and U.S. Department of Energy.

NEUROLOGY

No. 848

DOPPLER-SONOGRAPHY (DS) & IMP SPECT IN PATIENTS WITH ISCHEMIC CEREBROVASCULAR DISEASES. E. Deisenhammer, K. Höll, F. Migl, Ch. Luft, Wagner-Jauregg-KH, Linz, AUSTRIA.

The purpose of this study was to investigate the influence of neck vessels pathology proved by DS on IMP accumulation measured with SPECT. In DS hemodynamic relevant stenosis was assumed when flow reversal, oscillating flow or amplitude attenuation of more than 50% was observed in ophthalmic collaterals. SPECT System: 30 min post i.v. inj. of 5mCi IMP a dual head rota camera (25 cm diameter of rotation, LEAP-collimators) acquired 64 projections in 50 min with a linear sampling distance of 3mm. After the weighted subtraction of scatter using multiple energy windows the projections are smoothed with a variable filter to suppress noise prior to reconstruction. Bellini's method is used to correct for attenuation, axial slices are reconstructed after Shepp, Logan. 12mm resolution was found in the 21mm thick final tomograms. Semiquantitative rCBF was estimated by taking the ratio of local tracer uptake to the mean uptake of the contralateral grey matter. Values are defined as abnormal when exceeding more than 2 stand.dev. from the mean. 60 patients with reversible or irreversible ischemic disease have been examined (mean age 45 y, 25 males). Decreased IMP-uptake was observed in all cases with infarction, in 1/3 of those larger than the infarcted region defined by TCT. In all patients without infarction IMP distribution was normal when DS was normal; whereas in all cases with abnormal DS IMP SPECT revealed abnormal regions on the same side, even when excellent compensatory circulation was seen in angiography.

Therefore, IMP SPECT distribution correlates better with flow measured by DS than with angiography and/or the morphological information given by TCT. Current work on absolute rCBF-values will increase application of SPECT.

No. 849

STUDY OF METABOLIC AND HAEMODYNAMIC ASPECTS OF HUNTINGTON'S DISEASE BY POSITRON EMISSION TOMOGRAPHY. A.C. Evans, C. Redies, S. Gauthier, J.L. Tyler, M. Diksic, E. Meyer, Y.L. Yamamoto, A. Hakim, Montreal Neurological Institute

PET was used to provide regional measurements in 7 HD subjects, with minimal caudate atrophy, for oxygen metabolism (rCMRO₂), oxygen extraction fraction (rOEF), blood volume (rCBV), blood flow (rCBF), pH (rCpH) and glucose metabolism (rCMRGlc). In addition regional rate constants for the transport and phosphorylation of F-18 labelled deoxyglucose (FDG) were measured. Results were compared with similar data from a control group of 6 older normal patients. rCMRO₂, rCMRGlc, and rCBF in the caudate nucleus exhibited a coupled depression. Transverse profiles through the head of the caudate body were analyzed with the caudate/cortex index of Kuhl et al. For the control group the index for each parameter was 20% while in the HD group the indices were 40-50%. Metabolic and haemodynamic measurements in the cortex of the HD patients were not significantly different from those of the control group. The caudate/putamen region showed a 35% reduction in rCMRGlc while rCMRO₂ and rCBF were reduced by 20%. The FDG rate constants are similar for the HD and control groups except for k₂, expressing FDG backflow, in the caudate/putamen. The ratio of k₂ in the cortex to k₂ in the caudate/putamen is a factor of two smaller in HD patients than in controls.

- 1) Kuhl DE, Phelps ME, Markham CH, Metter EJ, Riege WH, Winter J (1982) Cerebral metabolism and atrophy in Huntington's disease determined by FDG and computer tomographic scan. *Ann Neurol* 12: 425-434.

No. 850

EVALUATION OF Tc-99m HM-PAO AS A CEREBRAL BLOOD FLOW TRACER USING QUANTITATIVE MULTIPLE-RADIONUCLIDE AUTORADIOGRAPHY J. L. Lear, K. Mido, D. Navarro, and T. Martinez. Stanford University and V. A. Medical Center, Palo Alto, CA

Tc-99m hexamethylpropyleneamineoxime (HM-PAO) has been proposed as a potential tracer for cerebral blood flow (CBF) based upon observations of high cerebral uptake after intravenous administration. The purpose of this investigation was to evaluate the local cerebral distribution of HM-PAO as compared to that of a reference CBF tracer, C-14 iodoantipyrine (IAP).

Mixtures of 15-20 mCi of HM-PAO and 60-70 µCi of IAP were administered by intravenous infusion to a series of awake and anesthetized rats. Arterial samples were obtained during the infusion and the rats were killed by KCl injection after approximately 45 seconds. Autoradiographs of brain sections were first made from 18 hour exposures and therefore primarily represented HM-PAO. The sections were removed from the film for 2 days to allow the Tc-99m to decay, and second exposures of 7 days duration were made which represented IAP. The images were analyzed using a digital autoradiographic scanner and the slight amount of C-14 exposure in the first set of images was subtracted. CBF values for both tracers were computed using a standard diffusible tracer model, and CBF images were generated and compared on a pixel by pixel basis.

We found that the distribution of HM-PAO was different between the awake and anesthetized rats, with a more heterogeneous pattern occurring in the awake animals. This caused both over- and underestimation of CBF by HM-PAO compared to IAP, which was most likely secondary to violation of the assumption of well-mixed tissue compartments in the diffusible tracer model with HM-PAO. These differences occurred over very small areas and would not be detectable with the resolution of SPECT in human studies.

No. 851

QUANTITATIVE ASSESSMENT OF BLOOD-BRAIN-BARRIER (BBB) IN DEMENTIA WITH Ga-68 EDTA AND POSITRON EMISSION TOMOGRAPHY (PET). G. Smith, K.F. Hubner, E. Buonocore, J. Daugherty, Dept. Radiol., U.T. Hospital, Knoxville, TN and J.E. Crook, W. Byrd, S. Holloway, Med. Health Sci. Div. of Oak Ridge Ass. Univer., Oak Ridge, TN.

The purpose of this study was to determine whether areas of low density on CT or high signal intensity on MRI scans represent changes of the BBB in patients with Alzheimer type (1), multi-infarct (2), depressive dementia (1) or stroke (1). These patients had PET scans as a measure of BBB permeability to Ga-68 EDTA. Serial images were obtained 6.5 cm above the O.M. line, and arterialized venous blood was used to quantitate the plasma input function. The multiple time/graphical analysis method of Patlak, et al. (*J Cereb Blood Flow Metab* 1983; 3:1-7) was used to determine the unidirectional transport constant, K_i, for the blood to brain transport of Ga-68 EDTA. This was done by finding the linear least squares slope of the Ci(t)/Cp(t) versus $\int_0^t Cp(t)dt/Cp(t)$ curve. Time t was assumed to be the start time of the scan. Vascular volume, V_i, was estimated by the intercept of the least squares line. Each pixel was treated as a separate ROI to generate K_i and V_i maps. Results showed average K_i and V_i values in all patients of 0.000286 and 0.0249, respectively, both within the reported normal range (Iannotti et al. *Acta Neurol Scand* 1985; 72(1):104). The K_i maps showed no distinguishing features for any disorder tested, and the V_i maps were nearly uniform, indicating no focal areas of increased intravascular volume. This study showed no differences between the BBB transfer constant or intra-vascular volume for various clinical types of dementia and normal brain.

No. 852

S2 SEROTONIN RECEPTOR BINDING OF C-11-3-N-METHYLSPERONE (NMSP) IN PATIENTS WITH DEPRESSION FOLLOWING STROKE. DF Wong, H Mayberg, RG Robinson, E Broussolle, R Parker, D Danashvar, J Links, J Lipsey, RF Dannals, H.N. Wagner, Jr. Johns Hopkins Medical Institutions, Baltimore, MD.

Persistent depression following stroke has been shown to correlate with lesions in the left hemisphere. Animal studies have shown right sided ischemic lesions to decrease biogenic amines in the ipsilateral cortex to a greater degree than left sided lesions (*Science*, 205:707-710, 1976). We carried out C-11-methylspiperone PET scans in 11 subjects with varying strokes and depression. Five had left-sided and six had right-sided strokes. The early images indicated that there was a reduction in blood flow ipsilateral to the lesion in all studies, regardless of side. To estimate the degree of binding remaining in a stroke-involved region, we examined the ratio of the S2 binding in the cortex to the cerebellum late in the scan in both the affected and unaffected hemisphere. The cortex/cerebellar ratios in the late scans were higher in the ipsilateral cortex in right-sided lesions compared to left lesions (p=0.05). These results support the observation that right and left sided ischemic lesions have different effects on endogenous biogenic amines and their receptors. The ipsilateral increase in receptor binding in the right sided lesions may suggest an asymmetry in compensatory receptor up-regulation mechanisms in the two hemispheres following stroke. An additional 4 patients are being studied with a focus on unilateral cortical strokes and kinetic modelling.

No. 853

THE EFFECT OF IV COCAINE ON THE KINETICS OF C11-3-N-METHYLSPERONE BINDING IN THE HUMAN CAUDATE D.F. Wong, C. Ross, H.N. Wagner, Jr., G. Pearlson, J.M. Links, E. Broussolle, G. Fanaras, M. Fischman,

D. Danashvar, A. Wilson, H. Ravert, R.F. Dannals. The Johns Hopkins Medical Institutions, Baltimore, MD.

A goal of positron emission tomography is the measurement of the rate of secretion of neurotransmitters by their effect on the kinetics of injected radioligands. High affinity ligands such as C11-3-N-methylspiperone (NMSP) may bind so tightly that the much lower affinity of endogenously secreted dopamine may not affect the rate of binding of the tracer. Cocaine, a potent dopamine uptake inhibitor, was administered intravenously in order to increase synaptic dopamine concentrations; subjective effects were observed almost instantly. Three subjects received cocaine (48mg IV) 30 min. after the NMSP injection. Since we have previously observed a linear relationship of the caudate/cerebellum over time, we used this measure of the rate of binding to the receptor to monitor possible competition of NMSP with cocaine. We observed a change in the slope (SL) of the caudate/cerebellum (CA/CB) vs time of only -.003, -.009 and .0074/min. which was within the 95% tolerance limits of 23 normal subjects (-0.0553 to 0.0473/min.) for SL. A fourth subject received a control NMSP PET followed the next day by a 2nd scan in which the same cocaine IV dose was given 4 min. prior to NMSP. The change in slope was only 2% which is within our observed reproducibility (5-10%). All subjects had physiological evidence of a substantial response to the cocaine. Our preliminary data suggest that endogenous dopamine release does not have a significant effect on NMSP binding in normal PET scan conditions. Studies with amphetamine are in progress.

ONCOLOGY

No. 854

PRELIMINARY STUDIES OF IN-111-LABELED ZCE 025 MONOCLONAL ANTIBODY (MoAB) IMMUNOSCINTIGRAPHY IN METASTATIC COLORECTAL CARCINOMA. H. Abdel-Nabi, C.S. Higano, A.N. Schwartz, M.D. Cerqueira, VA Medical Center and University of Washington, Seattle, WA, and M.W. Unger, Hybritech, Inc., San Diego, CA.

We have performed an investigation to determine the utility of Indium-111-labeled (In-111) anticarcinogenic embryonic antigen (CEA) monoclonal antibody (MoAB) scanning in the detection of metastatic colorectal carcinoma (Ca). 6 patients (pts) with confirmed metastases (mets) and 2 pts with suspected mets based on raising serial CEA serum levels were studied. Each received 5.5 mCi of In-111-labeled MoAB ZCE 025 (anti-CEA murine MoAB of the IgG₁ class produced by Hybritech, Inc.). The MoAB was infused over 2 hours at doses of 2.5 mg (2 pts), 10 mg (4 pts) and 20 mg (2 pts). Total body scans with region of interest analysis were performed at 3 and 6 days post-infusion. 15 tumor sites were demonstrated by surgery and conventional diagnostic x-ray methods in 6 pts. 2 pts were free of tumor. ZCE 025 MoAB visualized 12 of these 15 tumor sites (80% detectability rate). With respect to tumor sites, MoAB visualized 8/8 lymph node mets, 2/2 lung mets greater than 1cm in diameter, and 2/2 local recurrence. All lesions were seen at day 3, but more easily seen at day 6. MoAB visualized 2 sites of recent surgery, not shown to harbor recurrence by CT and needle biopsy.

The high detectability of mets from colorectal carcinoma with In-111-labeled ZCE 025 MoAB demonstrates the potential of this antibody as a diagnostic agent as well as a therapeutic agent.

PERIPHERAL VASCULAR

No. 855

VENOUS DOPPLER DIRECTED INTERPRETATION OF Tc 99m RBC VENOGRAPHY. Frank M. Grund, Robert P. Miller, Rex B. Shafer. V.A. Medical Center, Minneapolis, MN

Accurate non-invasive tests are required by clinicians to diagnose deep venous thrombosis. We propose to improve the accuracy of Tc 99m RBC venograms by examining venous blood flow with doppler ultrasound. Tc 99m RBC venograms are not widely used because of the difficulties presented in interpretation. Doppler ultrasound allows physiologic assessment of the venous blood flow and may help resolve indeterminate RBC venograms. We studied 12 patients after contrast venography was performed because of symptoms and signs of deep venous thrombosis. Tc 99m RBC venography was performed using an in vivo labeling technique with the injection of 30 mc Tc 99m pertechnetate in a forearm vein 15 minutes after the injection of stannous pyrophosphate. The nuclear medicine physician responsible for interpretation of the RBC venogram performed venous doppler exams using a 5.3 MHz ultrasound stethoscope. Thus far, 6 patients with negative contrast venograms and 4 patients found to have proximal deep venous disease were correctly diagnosed with these non-invasive studies. As expected, this approach did not diagnose small calf vein thrombi in 2 patients. Knowledge of the anatomical and physiological information from Tc 99m RBC venograms and venous doppler analysis allowed accurate assessment of proximal deep venous thrombosis in 12 patients. Based on these early results, we plan to continue this research to determine the predictive accuracy of each test individually and when used conjointly.

PULMONARY

No. 856

A SIMPLE METHOD TO OPTIMIZE Tc-99m DTPA RADIOAEROSOL (RA) CONTRIBUTION TO Tc-99m MAA (MAA) LUNG PERFUSION (Q) IMAGES. C.K. Kim, E.J. Fine, K.J. Chun, and L.M. Freeman. Montefiore Medical Center, Bronx, NY.

Ventilation (V) imaging with RA is convenient and cost effective. In our institution, patients (pts) inhale nebulized Tc-99m DTPA (30 mCi in 3 ml saline and 9L O₂/min) for approx. 3-5 min, before the Q scan. The amount of RA deposited in the lungs varies widely depending on pts' pulmonary status and effort. Inhalation of 2-3 mCi of RA may obscure Q (3 mCi MAA) findings. We have developed a simple way of monitoring V studies to minimize excessive RA deposition. 25 RA and MAA studies were obtained using 1 gamma camera (camera A). 500K Q posterior images required 40-95 sec [mean=64±19(SD)]. To limit RA's contribution to approx. 15% of Q image, one must deposit 0.5-0.6 mCi of RA. Since 64 sec were spent for 500K Q images [7810 cts/sec(cps)], one should obtain approx. 1170 cps from RA. This is done conveniently by determining counts during sequential 5 sec (or less) intervals while pt is inhaling RA until the requisite 1170 cps rate is obtained in a given interval. Another 21 pts were studied with camera B and 5 with camera C. Applying the same procedure, we noted different detection efficiencies for cameras B&C during Q imaging. Camera B required 970 cps for appropriate V imaging and C required 500 cps. Considering all pts, the V time varied from less than 1 min to 7 min. Conversely, if all pts had breathed for the same time (e.g. 4 min), RA deposited in the lungs would have been approx. 0.2-3.0 mCi. In conclusion, prospective determination of Q rates allows calculation of proper V rates (15% of Q rates). During subsequent pt studies, repeat short intervals (45 sec) during V monitoring is key to optimizing examinations.

No. 857

SINGLE PHOTON EMISSION COMPUTED TOMOGRAPHY VERSUS PLANAR IMAGING IN PULMONARY PERFUSION DEFECTS. A. Palla, S.S. Tume, R.J. English, S.Z. Goldhaber, B.L. Holman. Harvard Medical School, Boston, MA.

To assess the role of emission tomography (SPECT) in the evaluation of pulmonary embolism (PE), we compare planar

(P) and SPECT imaging after the injection of Tc-99m MAA (3mCi) in 19 patients. Pulmonary angiography (PA) was done in all patients except 6 with normal perfusion scan. All images were acquired on a large field of view gamma-camera (GE 400/AT). 64 projections encompassing 360°, 64x64 matrix and 20"/projection were used. Segmental and non segmental defects were determined on each modality independently, and then assigned as high (HP), moderate (MP), low (LP), indeterminate (IP), or nil (NP) probability of PE. The defects in each modality were outlined as follows:

		HP	MP	LP	IP	NP
SEG DEF	P	37	1	0	2	0
	SPECT	92	2	11	8	0
NON SEG DEF	P	19	2	3	17	0
	SPECT	14	0	0	18	6

Comparison between our impression and PA was as follows:

	P	PA+	PA-	SPECT	PA+	PA-
HP	8	7	1	10	8	2
MP	1		1	2	1	1
LP	1	1		2		
IP	3	1	2	1		1
NP	6			4		

SPECT showed segmental defects in all patients with positive PA, while P failed to show segmental defects in 2. SPECT and P showed 15 and 5 segmental defects, respectively, in 4 with negative PA. In conclusion, SPECT detected all cases with positive PA but overestimated the presence of segmental perfusion defects.

No. 858

PULMONARY ACCUMULATION OF ^{131}I -MIBG IN THE ISOLATED PERFUSED RAT LUNG. D. Slosman, D. Davidson, A.B. Brill, and P.O. Alderson. Columbia-Presbyterian Medical Center, New York, NY and Brookhaven National Lab, Upton, NY.

The lung is responsible for the active uptake of biogenic amines such as serotonin and norepinephrine. MIBG is taken up by adrenomedullary cells by an energy-requiring, sodium-dependent active process. To determine if MIBG might be useful for evaluation of pulmonary endothelial cell function, the mechanism of single-pass ^{131}I -MIBG accumulation was studied in rat lungs, isolated and perfused with an albumin Krebs-Ringer bicarbonate buffer. ^{131}I -MIBG lung accumulation was measured by the percent lung extraction per gram of lung tissue after 2 minutes of perfusion with ^{131}I -MIBG under the experimental conditions below:

EXPERIMENTAL CONDITIONS	N	%extractions.d.
Control 0.01 μM MIBG (37° celcius)	8	19.72±2.34
+ Serotonin (0.7 μM)	5	15.25±2.29†
+ Imipramine (10 μM)	5	5.87±0.82*
+4° celcius	5	2.95±0.64*
+ ouabain (0.5mM)	7	7.93±1.21*
2.0 μM MIBG	5	7.31±1.29*

* p<0.001, † p<0.01

The addition of 0.5 μM norepinephrine to the medium containing ^{131}I -MIBG (0.1 to 0.5 μM) also demonstrated significant (24%, p<.005) inhibition of MIBG lung extraction. Thus, the pulmonary accumulation of MIBG appears to be energy-requiring and sodium-dependent, with characteristics very similar to norepinephrine uptake. Studies of MIBG lung extraction may be useful for clinical investigations of lung endothelial cell function.

RADIOPHARMACEUTICAL CHEMISTRY

No. 859

SYNTHESIS AND MELANOMA-AVIDITIES OF I-125 DERIVATIVES OF ELLIPTICINE AND AMSA. N.D. Heindel#, J.G. Emrich#, D.V. Woo#, K. Ganes*, S.W. Landvatter*, A.A. Wilson+, and H.D. Burns+, #Hahnemann Univ., Philadelphia, PA 19102, and *SKF, Philadelphia, PA 19102, +Johns Hopkins Univ., Baltimore, MD 21205.

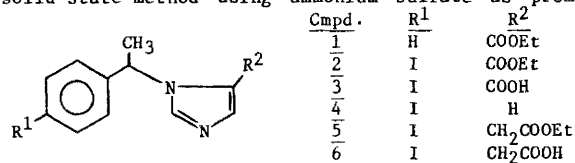
Polycyclic nitrogenous antitumor agents such as AMSA and ellipticine demonstrate high affinity binding to both DNA and uveal melanin. In search of a melanoma imaging agent we have developed syntheses of three I-125 analogs of these classes. 2-Iodo-AMSA was prepared from the corresponding acridone precursor and labeled by melt exchange with I-125 NaI in a 30% radiochemical yield and a specific activity of 1.6 mCi/mmole. However, in both the 1- and 2-p-iodobenzylellipticines, melt exchange occurred in radiochemical yields <5% and alternative radioiodinated products were formed. 2-p-Tri-methylsilylbenzylellipticinium was prepared as a precursor but an electrophilic substitution by I-125 NaI/N-chlorosuccinimide yielded none of the desired I-125 2-p-iodobenzylellipticinium. The latter was obtained by first preparing I-125 p-iodobenzyl bromide through reaction of p-trimethylsilylbenzyl bromide, I-125 NaI, and N-chlorosuccinimide and alkylating ellipticine directly with the radioiodinated benzyl halide. The product was isolated by preparative HPLC in >99% radiochemical purity, SA 1.4 mCi/mmole. Both the I-125 iodo-AMSA and the I-125 iodo-benzylellipticinium showed significant eye/blood (8/1 and 24/1 respectively) and melanoma/blood ratios (4/1 and 12/1 respectively) in the Fortner malignant melanoma of the Syrian Golden hamster.

No. 860

RADIOLABELED ENZYME INHIBITORS: EVALUATION OF ANALOGS OF ETOMIDATE. T-Y. Lin, D.M. Wieland, J.C. Sisson, S.J. Fisher, P.S. Sherman and H. Lee. University of Michigan Medical Center, Ann Arbor, MI

Etomidate (1) an intravenous anesthetic used widely in Europe, has been implicated in the death of patients due to marked lowering of plasma cortisol. Recent studies have shown that etomidate is a selective inhibitor of two adrenocortical cytochrome P-450 enzymes, P-450-sec and P-450-11. The goal of this work was to synthesize and evaluate radioiodinated etomidate and structurally related imidazoles as possible rapid imaging agents for the adrenal cortex.

Starting with 4-iodoacetophenone, compounds 2-6 were synthesized in 5-8 steps by literature methods. Exchange labeling with NaI-125 was achieved in high yield by a solid-state method using ammonium sulfate as promoter.



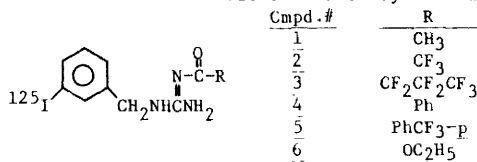
The in vivo affinities of 2-4 for the whole adrenal were determined in rats following intravenous injection: only compound 4 showed significant adrenal localization at 5 and 30 min. Further evaluation of 4 showed peak adrenal uptake at 0.5-2.0h with complete washout at 24h. Maximum adrenal-to-kidney (20) and adrenal-to-blood (42) concentration ratios occurred at 0.5 h. Similar results were obtained in dogs. Compounds 5 and 6 have been synthesized and are under evaluation in hopes that they will show high adrenal affinity as well as rapid hepatic clearance.

No. 861

PROTRACERS FOR MAPPING CENTRAL CATECHOLAMINE STORES. D.M. Wieland, T-Y. Lin, P. Arjunan, H. Lee, P.S. Sherman and S.J. Fisher. University of Michigan Medical School, Ann Arbor, MI

Although radioiodinated meta-iodobenzylguanidine (MIBG) has been used to image peripheral organs and tumors based on its affinity for adrenergic neurons, application of MIBG to mapping central catecholamine stores is limited by its failure to pass the blood-brain barrier (BBB). We report here the synthesis of derivatives of MIBG that have lower pKa's and higher lipophilicities than MIBG

itself. The goal was to have these derivatives serve as protracer forms that would enter the brain following i.v. injection and be quickly hydrolyzed to the parent tracer MIBG. I-125-MIBG in free base form was acylated with the



appropriate anhydride, acid chloride or ester to give 1-6. Tracers 2 and 4 exhibited 10-20 fold higher concentrations in the rat brain than MIBG 1-30 min after i.v. injection. In contrast to 4, compound 2 showed virtually no washout from the brain over the first 30 min suggesting hydrolysis to MIBG and subsequent trapping. The hydrolytic stability in phosphate (pH 7.1) buffered ethanol is $4 \gg 2$. Tracers 3 and 5, though highly lipophilic, gave low brain uptakes due likely to enhanced blood binding. These initial experiments show that a protracer form of MIBG can penetrate the BBB and that in certain cases (ie., 2) intra-brain hydrolysis may occur.

RENAL/ELECTROLYTE/ HYPERTENSION

No. 862

EVALUATION OF PLASMA RENIN ACTIVITY (PRA) AND PLASMA VOLUME (PV) DURING THE FOLLOW-UP OF ADRENOCORTICAL FAILURE. J.L. Urbain, A.

Ferrant, J. Crabbé, J.F. De Plaen & C. Beckers. University of Louvain Medical School, B-1200 Brussels (Belgium).

Eleven patients with adrenocortical failure were studied to assess the respective value of the measurements of PRA and PV during substitutive therapy. Seven patients suffered from primary adrenocortical failure and 4 had undergone bilateral adrenalectomy for Cushing's disease. Patients were studied whilst receiving cortisone and/or fludrocortisone. Two patients had 2 measurements and another was evaluated on 3 occasions. Plasma volume was measured using I-125 labelled albumin and PRA was determined by radioimmunoassay of angiotensin I generated. Results of PRA (ng/ml/h), PV (% of normal) and blood pressure (BP, mm Hg) are summarized below.

PAT.	BP	PRA	PV	PAT.	BP	PRA	PV
1	130/80	11	62	7	115/80	10	79
2	170/80	8.5	82		130/90	9.5	81
	150/100	1.4	94		130/100	20	64
3	150/110	8.8	77	8	170/85	12.5	70
4	135/80	14	80		130/90	33	71
	155/85	1.6	76	9	160/110	2.4	99
5	140/80	7.1	87	10	180/115	3.4	94
6	130/90	2.6	81	11	170/60	6.6	88

In 12 of the 16 measurements PV was inversely correlated with PRA; 2 patients had a low PRA despite a low PV and 1 patient had a high PRA with a high PV. The reason of this discrepancy could be the fact renin release depends of multiple factors. Despite these 3 discordant measurements, a statistically significant inverse relationship was found between PRA and PV ($r=-0.65; p<0.01$). Our results suggest that PRA in patients with adrenocortical failure is most often related to plasma volume. Further studies are needed to precise the specific value of each test in the followup of these patients.

Categorical Seminars

SATURDAY

CARDIOVASCULAR NUCLEAR MEDICINE 1986

(sponsored by the SNM Cardiovascular Council)

8:00-3:30

Room 40

Educational Objective:

To highlight controversies and new areas of development in cardiovascular nuclear medicine

TOPICS:

1. New Tc-99m perfusion tracers
2. Dipyridamole stress imaging
3. Prognosis in coronary artery disease
4. Exercise left ventricular functions
5. Imaging artifacts
6. Tl-201 washout
7. Tl-201 SPECT
8. Artificial intelligence
9. Thrombolysis
10. Infarct-avid scintigraphy

Summary: This year's categorical course in cardiovascular nuclear medicine is divided into six topics, each of which includes several speakers presenting either opposing viewpoints or complementary subjects. The orientation is heavily clinical, and the course is designed for clinicians practicing advanced nuclear cardiology. Topics to be discussed include the following: 1) imaging artifacts and the need for quality control in equilibrium radionuclide angiography and myocardial perfusion imaging with thallium-201. 2) the differentiation of myocardial ischemia from myocardial infarction and assessment of myocardial viability. The utilization of radionuclide techniques for assessment of thrombolysis will be included. 3) the potential clinical utility of positron emission tomography. The emphasis will be on the potential problems associated with implementing a PET laboratory in a non-research hospital setting. 4) new advances in myocardial perfusion imaging, such as radiopharmaceuticals labeled with technetium-99m and alternatives to dynamic exercise, specifically pharmacologic stress intervention. 5) new developments in computer techniques applicable to nuclear cardiology. The pitfalls associated with assessment of thallium-201 washout from planar studies will be addressed. Single photon emission computed tomography and quantification of thallium-201 will be updated. Lastly, the potential role of artificial intelligence and smart expert systems for image interpretation will be addressed. 6) the role of exercise radionuclide angiography, in establishing prognosis in coronary artery disease. The clinician's perspective in decision making also will be included.

Chairmen: Harvey J. Berger, M.D., Centocor, Inc., Malvern, PA; Elias H. Botvinick, M.D., University of California, San Francisco, CA

8:00 Introductions. Harvey J. Berger, M.D., Centocor, Inc., Malvern, PA

Infarct vs Ischemia: How Can They be Differentiated?

8:05 Evaluation of Coronary Thrombolysis with Myocardial Perfusion Imaging and Radionuclide Angiography. Daniel S. Berman, M.D., Cedars-Sinai Medical Center, Los Angeles, CA

8:30 Infarct-Avid Scintigraphy—New and Old Tracers. Harvey J. Berger, M.D., Centocor, Inc., Malvern, PA

What is the Role of PET Imaging in Clinical Cardiology?

8:55 Panel Discussion/Debate

Protagonists: Lance Gould, M.D., University of Texas, Houston, TX; Ed Geltman, M.D., Washington University, St. Louis, MO; Heinrich Schelbert, M.D., University of California, Los Angeles, CA

Moderators: Elias H. Botvinick, M.D., University of California, San Francisco, CA; Daniel S. Berman, M.D., Cedars-Sinai Medical Center, Los Angeles, CA

9:45 Break

Imaging Artifacts and Quality Control: How Do They Affect Clinical Interpretation?

10:00 Thallium-201 Perfusion Imaging. Michael Dae, M.D., University of California, San Francisco, CA

10:25 Equilibrium Radionuclide Angiography. E. Gordon DePuey, M.D., Emory University Hospital, Atlanta, GA

Efficacy of Cardiovascular Nuclear Medicine Procedures

10:55 Systematic Approach to Decision-Making in Patients with Coronary Artery Disease: A Clinician's Appraisal. Bernard Siegal, M.D., Hahnemann University, Philadelphia, PA

11:40 Use of Exercise Radionuclide Angiography to Define Prognosis in Coronary Artery Disease. Robert H. Jones, M.D., Duke University, Durham, NC

12:00 Lunch

New Approaches to Myocardial Perfusion Imaging

1:15 Technetium-99m Tracers: Thallium Replacements? B. Leonard Holman, M.D., Brigham and Women's Hospital, Boston, MA

1:40 Dipyridamole Pharmacologic Stress: When Should It Be Used Instead of Exercise? Jeffrey Leppo, M.D., University of Massachusetts, Worcester, MA

2:05 Pitfalls in Washout Analysis of Exercise Thallium-201 Scintigrams. Denny Watson, Ph.D., University of Virginia, Charlottesville, VA

2:30 Quantification of Thallium-201 Images: How Important are Evaluation of Washout and Use of Tomography? Jamshid Maddahi, M.D., Cedars-Sinai Medical Center, Los Angeles, CA

3:05 Artificial Intelligence: Can Cardiac Images Be Interpreted by Computers? Ernest V. Garcia, Ph.D., Emory University School of Medicine, Atlanta, GA

NUCLEAR MEDICINE: THE NEXT FIVE YEARS

(sponsored by the SNM Correlative Imaging Council)

9:00-3:30

Room 39

Educational objective:

To educate constituents regarding state of the art and promising developments which may impact their clinical practice through 1990.

Summary: The purpose of the course is to inform the practitioners of nuclear medicine of many new and exciting developments which will impact the clinical practice of nuclear medicine over the next five years. New developments in radiopharmaceuticals, brain imaging with single photon agents, positron tomography and its impact on the clinical practice of nuclear medicine, monoclonal antibodies including diagnostic and therapeutic implications, cardiac imaging including newer radiopharmaceuticals and quantitative tomographic techniques, new modes of therapy using non-sealed sources, the impact of nuclear magnetic resonance, computers including important characteristics for individual departments ranging from the one camera practice to a multi-modality large department and newer and evolving forms of instrumentation will all be discussed by leading experts in the field. Emphasis will be placed on the clinical importance to the field of nuclear medicine.

By the completion of the course, attendees will have had exposure to state of the art and emerging technologies and be made aware of new advances which would impact their clinical practices within the next few years.

Moderators: Alan D. Waxman, M.D., James Fletcher, M.D., Jamshid Maddahi, M.D., C. Leon Partain, M.D., Ph.D.

TOPICS:

1. Radiopharmaceuticals
2. Brain imaging with single photon agents
3. Positron tomography
4. Monoclonal antibodies
5. Cardiac imaging
6. Therapy
7. Magnetic resonance
8. Computers
9. Instrumentation

9:00 **Advances in Radiopharmaceuticals.** Maria Liteplo, Ph.D., E.I. DuPont Diagnostic Imaging Division, Billerica, MA

9:45 **Single Photon Imaging of the Brain.** Richard Holmes, M.D., University of Missouri, Columbia, MO

10:15 **Positron Emission Tomography: (The Impact on Clinical Decision Making).** Michael Phelps, Ph.D., University of California, Los Angeles, CA

11:00 **Monoclonal Antibodies: Diagnostic Imaging and Therapeutic Implications.** Brian Gallagher, Ph.D., E.I. DuPont, Billerica, MA

11:30 **New Frontiers in Nuclear Therapy.** Richard Holmes, M.D., University of Missouri, Columbia, MO

1:00 **Cardiac Imaging: The Role of Nuclear Medicine in a Multi-Modality World.** Daniel S. Berman, M.D., Cedars-Sinai Medical Center, Los Angeles, CA

1:40 **The Future Role of Computer Technology in Nuclear Medicine.** Ernest Garcia, Ph.D., Emory University, Atlanta, GA

2:20 **Instrumentation of the 80's and Beyond.** Gerd Muehllehner, Ph.D., University of Pennsylvania, Philadelphia, PA

2:55 **The Potential Impact of NMR on the Clinical Practice of Nuclear Medicine.** John Crues, M.D., Cedars-Sinai Medical Center, Los Angeles, CA

3:30 **Session ends**

THE CHEMISTRY OF RADIOPHARMACEUTICALS *IN VIVO*:

Methods and State of Characterization
(Sponsored by the SNM Radiopharmaceutical Science Council)

8:10-4:30

Room 30

Educational objective:

The objective of the seminar is to present the chemical state of radiopharmaceuticals *in vivo*; metabolism, tissue binding at the molecular level, and methodology of characterization

Topics:

1. Brain perfusion agent
2. Brain receptor agents
3. Uptake of cations by the heart
4. Organic cations
5. Tc-99m cations
6. Liver metabolism and binding
7. Misonidazole and analogs
8. Antibody metabolism
9. Labeled fatty metabolism

Summary: Recently developed radiopharmaceuticals have been designed to interact with biological systems in a specific manner. Organ specific transport, as well as intracellular binding and metabolism, are involved. Thus, it is important that the *in vivo* behavior of these radiopharmaceuticals be characterized in order to understand the chemical form the nuclear medicine image reflects. The faculty will review the methodology of metabolic and tissue binding characterization and the state of *in vivo* chemical characterization at the molecular level for different organs of interest to nuclear medicine. These include brain perfusion and receptor agents, cationic agents for the heart, and agents that are acted upon by the liver. In addition, metabolism of labeled antibodies by tumor and liver will be discussed.

Program Chairman: Alan R. Fritzberg, Ph.D., NeoRx Corporation, Seattle, WA

Moderator: William C. Eckelman, Ph.D., E.R. Squibb & Sons, New Brunswick, NJ

8:10 **Introduction.** Alan R. Fritzberg, Ph.D., NeoRx Corporation, Seattle, WA

8:20 **The Characterization of the *In Vivo* Chemistry of Brain Perfusion Radiopharmaceuticals.** Ronald Blasberg, Ph.D., National Institutes of Health, Bethesda, MD

- 9:00 The *In Vivo* Chemistry of Iodoamphetamine (IMP).** Ronald Baldwin, Ph.D., Medipysics, Inc., Richmond, CA
- 9:30 The Characterization of the *In Vivo* Chemistry of Brain Receptor Radiopharmaceuticals.** Kirk Frey, Ph.D., M.D., University of Michigan, Ann Arbor, MI
- 10:00 *In Vivo* Binding to Opiate Receptors.** James Frost, M.D., Johns Hopkins University, Baltimore, MD
- 10:30 Break**
- Moderator:** Brian Gallagher, Ph.D., Dupont de Nemours & Co., N. Billerica, MA
- 10:45 The Characterization of the *In Vivo* Chemistry of Cations in the Heart.** Shakar Mousa, Ph.D., E.I. Dupont De Nemours & Co., N. Billerica, MA
- 11:15 The *In Vivo* Chemistry of Organic Cations.** Donald Wieland, Ph.D., University of Michigan, Ann Arbor, MI
- 11:45 The *In Vivo* Inorganic Chemistry of Technetium Cations.** Edward Deutsch, Ph.D., University of Cincinnati, Cincinnati, OH
- 12:10 Lunch**
- Moderator:** Donald Wieland, Ph.D., University of Michigan, Ann Arbor, MI
- 1:30 Metabolism of Radiolabeled Fatty Acids by Heart and Liver.** L.E. Feinendegen, M.D., Kernforschungsanlage, Julich, FRG
- 2:00 The Characterization of *In Vivo* Chemistry of Compounds Interacting with the Liver.** Gerald Miwa, Ph.D., Merck, Sharp and Dohme, Rahway, NJ
- 2:40 Characterization of the Metabolism of Misonidazole and Radiolabeled Analogs.** Kenneth Krohn, Ph.D., University of Washington, Seattle, WA
- 3:10 Characterization of the Metabolism of Radiolabeled Monoclonal Antibodies by Tumor and Liver.** Howard Sands, Ph.D., E.I. Dupont De Nemours & Co., N. Billerica, MA
- 3:40 Discussion of Methods, Approaches, and State of *In Vivo* Characterization of Radiopharmaceuticals.** Donald Wieland, Ph.D., Moderator. Invited Speakers and Categorical Seminar Attendees
- 4:30 Adjourn and Reception for Seminar Participants**

CURRENT ISSUES IN NUCLEAR MEDICINE:

Categorical Seminar on Marketing Nuclear Medicine Services and Update on Low-Level Waste (sponsored by the American College of Nuclear Physicians)

- 9:00-3:00 Room 38**
- Sponsor: American College of Nuclear Physicians (ACNP) Professional and Public Information Program**
- 9:00-9:10 Introduction and Objectives.** Ralph G. Robinson, M.D., Kansas University Medical Center, Kansas City, KS
- 9:10-9:30 The Importance of Marketing.** Stuart J. Somerville, President, Medi-Physics, Inc., Richmond, CA
- 9:30-9:50 Identifying Market Segments.** Jerome M. Smith, DuPont Diagnostic Imaging Division, Boston, MA
- 9:50-10:10 Describing Your Product.** Orlin Yenerich, Manager, Nuclear Diagnostics Products, General Electric Co., Milwaukee, WI
- 10:10-10:30 Break**
- 10:30-11:00 Marketing to the Referring Physician.** Ralph G. Robinson, M.D., Kansas University Medical Center, Kansas City, KS
- 11:00-11:30 Marketing Strategies That Work for Nuclear Physicians.** Conrad E. Nagle, M.D., William Beaumont Hospital, Troy, MI
- 11:30-12:00 Cost Analysis: The Real Cost of Nuclear Medicine Procedures.** Larry L. Heck, M.D., Methodist Hospital of Indiana, Indianapolis, IN
- 12:00-1:15 Lunch**
- 1:15-1:45 The Low-Level Waste Policy Act Amendments of 1985: Implications for Clinical Practice. Where We Are Now, Where Should We Go, and the Regional Siting Process.** G. John Weir, Jr., M.D., Marshfield Clinic, Marshfield, WI
- 1:45-2:15 Volume Reduction as an Approach to Low-Level Waste Management.** Kerry Bennet, DuPont Diagnostic Imaging Division, Boston, MA
- 2:15-2:45 Alternative Technologies to Shallow Land Burial for Low-Level Waste.** USCEA Representative
- 2:45-3:00 Discussion (Faculty)**

NUCLEAR MEDICINE REVIEW COURSE

Sunday–Wednesday **Room 29**
(Refreshments compliments of Amersham Corporation.) This four day course is a review of selected topics for candidates for examination by the American Board of Nuclear Medicine, as well as for practicing nuclear medicine physicians and technologists. Residents in nuclear medicine or allied training programs should find these in-depth reviews helpful. The program is scheduled during the same time periods as the scientific sessions and categorical courses. Attendees are invited to participate in this course in its entirety, or in part. The faculty is composed of nuclear medicine physicians and scientists who are renown educators. They have donated their time and expertise to this review course. There is no additional fee for this course.

Chairmen:

Robert J. Lull, M.D., Letterman Army Medical Center, San Francisco, CA; Michael F. Hartshorne, M.D., Brooke Army Medical Center, San Antonio, TX.

Sunday June 22

- 10:30 Development Administration, Psychometrics, and Evaluation of the American Board of Nuclear Medicine Certifying Examination.** Joseph F. Ross, M.D., President, and I. Ross McDougall, M.B., Ch.B., Ph.D., Chairman, American Board of Nuclear Medicine, Los Angeles, CA
- 11:30 Thirty Things That They Didn't Teach You During Residency.** Myron L. Lecklitner, M.D., University of South Alabama, Mobile, AL
- 12:00 Lunch**
- 1:30 Review of Rules and Regulations Governing the Practice of Nuclear Medicine:** Paul J. Early, B.S., Nuclear Medicine Associates, Cleveland, OH

Monday, June 23

- 8:30 Quality Assurance I: Radiopharmaceuticals.** Richard E. Stotler, LTC, MS, Letterman Army Medical Center, San Francisco, CA
- 10:00 Break**
- 10:30 Quality Assurance II: Instrumentation.** L. Stephen Graham, Ph.D., V.A. Hospital, Sepulveda, CA
- 12:00 Lunch**
- 1:30 Quality Assurance III: Radioassay.** Martin L. Nusynowitz, M.D., University of Texas Medical Branch, Galveston, TX
- 3:00 Break**
- 3:30 Nuclear Accident Management.** Eugene L. Saenger, M.D., University of Cincinnati Medical Center, Cincinnati, OH
- 5:00 Session ends.**

Tuesday, June 24

- 8:30 Review of Procedures for Evaluation of the Thyroid.** N. David Charkes, M.D., Temple University Hospital, Philadelphia, PA
- 10:00 Break**
- 10:30 Review of Procedures for Evaluation of the Gastrointestinal Tract.** Leon S. Malmud, M.D., Temple University Hospital, Philadelphia, PA
- 12:00 Lunch**
- 1:30 Radionuclide Therapy.** William H. Blahd, M.D., V.A. Wadsworth Medical Center, Los Angeles, CA
- 3:00 Break**
- 3:30 Radionuclide Evaluation of Renal Structure and Function.** Eva V. Dubovsky, M.D., Ph.D., University of Alabama, Birmingham, AL

Wednesday, June 25

- 8:30 Radionuclide Evaluation Bone Abnormalities.** Lawrence E. Holder, M.D., Baltimore, MD
- 10:00 Break**
- 10:30 Radionuclide Evaluation of the Lung.** William G. Spies, M.D., Northwestern Memorial Hospital, Chicago, IL
- 12:00 Lunch**
- 1:30 Useful But Uncommonly Performed Procedures in Nuclear Imaging.** George A. Wilson, M.D., University of Rochester Medical Center, School of Medicine, Rochester, NY
- 3:00 1986 Scientific Meeting Highlights.** Henry N. Wagner, Jr., M.D., Johns Hopkins Medical Institutions, Baltimore, MD (Room 40)

SUNDAY

ENDOCRINE EVALUATION USING RADIOASSAY & MULTIPLE IMAGING MODALITIES

10:30–12:00 Room 38

Educational Objective:

Review of current status of endocrine evaluation.

TOPICS:

1. Radioimmunoassay
2. Advances in endocrine imaging

Summary:

Clinical and laboratory evaluation of the endocrine system

has continued to evolve rapidly in the past ten years. Radioimmunoassay has provided new insights into metabolism, hormone synthesis and endocrine physiology, providing a new spectrum of diagnostic in vitro procedures. Nuclear imaging has evolved from thyroid scanning to the recently developed methods for radionuclide imaging of the parathyroid and adrenal glands. At the same time, ultrasound, CT and NMR imaging have improved identification of these organs in health and disease. This session will review these developments and discuss the current status, and future potential of specific radioligand assays and organ imaging techniques.

Moderator: Stanley J. Goldsmith, M.D.

Faculty:

Stanley J. Goldsmith, M.D., Mount Sinai Medical Center, New York, NY; Rosalyn S. Yalow, Ph.D., Veterans Administration Hospital, Bronx, NY; Martin P. Sandler, M.D., Vanderbilt University, Nashville, TN

SPECT vs. PET vs. MRI: RELATIVE ROLES, COST, AND CAPABILITY

10:30-12:00

Room 40

Educational Objective:

To review the current and potential clinical capability of SPECT, PET, MRI and NMR Spectroscopy and their relative independent, correlative or competitive roles in clinical diagnosis.

Topics:

1. Single photon emission computed tomography
2. Positron emission tomography
3. Magnetic resonance imaging
4. NMR spectroscopy

Summary:

The current and potential capability, cost, and relative clinical roles of single photon emission computed tomography (SPECT), positron emission tomography (PET), magnetic resonance imaging (MRI), and nuclear magnetic resonance (NMR) in vivo spectroscopy will be compared and evaluated. Correlative, competitive, and independent roles will be identified and discussed. Presentation will include an open panel discussion in order to encourage audience participation.

Moderator: C. Leon Partain, M.D., Ph.D.

Faculty:

R. Edward Coleman, M.D., Duke University, Durham, NC; Robert Kessler, M.D., Vanderbilt University, Nashville, TN; Thomas Brady, M.D., Harvard University, Boston, MA; John C. Gore, Ph.D., Yale University, New Haven, CT

PICTURE ARCHIVING AND COMMUNICATION SYSTEM (PACS)—ALL DIGITAL NUCLEAR MEDICINE DEPARTMENT

10:30-12:00

Room 39

Educational objective:

These presentations will discuss the hardware and software requirements for an all digital nuclear medicine department, including image perception, displays, networks and storage

needs. Cost and clinical advantages will be addressed in functioning PACS departments.

Topics:

1. Theoretical requirements for nuclear medicine all digital departments
2. Descriptions of currently functioning and developing all digital nuclear medicine departments

Summary:

The use of digital Picture Archiving and Communications Systems (PACS) in radiology departments provides three principal advantages over their analog counterparts. First by acquiring and viewing diagnostic images digitally, one can use a computer to manipulate the images, thus extending the diagnostic potential of the acquired data. Examples of computer enhancement are background subtraction, modifying the gray scale of the image, and creating movies, or "cines". For instance, by expanding a portion of the gray scale, small differences can be accentuated revealing structures which otherwise might not have been visualized. Cines are particularly useful when viewing flow studies as they present the frames sequentially at a rate up to sixty frames/second. A second advantage of digital PAC systems arises from storing the data in a digital format. As a result of this, the ability to analyze images with a computer is retained. This means that at a later date, a study can be recalled either for comparison to a current study, or so that a new analysis algorithm can be applied. Finally, digital storage of the studies in a central archive prevents loss of studies and reduces the time to locate studies as compared to conventional filing systems. The ninety minute session will be divided into two sections.

The first section with two 15 minute presentations will deal with some theoretical aspects and requirements of an all digital nuclear medicine department. Harold Kundel, M.D. of the University of Pennsylvania Hospital Department of Radiology will lead off with a discussion of image perception and diagnostic requirements of nuclear medicine. Samuel Dwyer, Ph.D. from the University of Kansas Hospital Department of Radiology will next present theoretical software and hardware requirements including display, bus and storage needs. The second section of the program will present a series of current clinically functioning all digital nuclear medicine departments each with an evaluation of diagnostic, administrative and cost benefits. The presentors will emphasize from their experience practical, functional, and clinical systems solutions they have developed.

Moderator: Gerald M. Kolodny, M.D.

Faculty:

Harold Kundel, M.D., University of Pennsylvania Hospital, Philadelphia, PA; Samuel Dwyer, Ph.D., University of Kansas Hospital, Kansas City, KS; John A. Parker, M.D., Ph.D., Beth Israel Hospital, Boston, MA; Jack Juni, M.D., University of Michigan Hospital, Ann Arbor, MI; Theodore J. Stahl, M.D., Middlesex General University Hospital, New Brunswick, NJ; Stephen Bacharach, Ph.D., National Institutes of Health, Bethesda, MD; Jason Zielonka, M.D., Veterans Administration Medical Center, Milwaukee, WI

Background of the Kinetic Approach

10:30-12:00

Room 31

Educational objective:

Fundamental and basic ideas underlying kinetic modeling are presented with actual examples of progressively more com-

plex systems starting with the microsphere model and including the method for calculating the rate of constant and lumped contrast for the fluorodeoxyglucose model. The specific topics to be discussed are:

Topics:

1. Types of flow tracers
2. Models appropriate for emission data
3. Method for quantitating receptors
4. Power and pitfalls of inferring metabolism of glucose, amino acids and fatty acids using emission tomography.

Moderator: Thomas F. Budinger, M.D., Ph.D., University of California, Berkeley, CA; Albert Gjedde, Ph.D., Panum Institute, Copenhagen, Denmark

Societal Considerations in Nuclear Medicine

1:30-3:00

Room 31

Educational objective:

To review a variety of current societal concerns impacting medicine in general and nuclear medicine in particular.

Topics:

1. Preserving the biomedical research establishment
2. Legislative initiative/AAMC
3. Antitrust and organized medicine
4. Cost of imaging technology
5. Effect of DRG's on imaging procedures

Summary:

Multiple societal stress points are impacting with increasing significance on the evolution of health care in this country. Sources of stress include governmental control, legislative initiatives, increasing frequency of litigation, and cost of medical care (including imaging technology). Special attention will be paid to the impact of these societal concerns on the practice of medical imaging.

FUNCTIONAL BRAIN IMAGING: NEW RADIOPHARMACEUTICALS

10:30-12:00

Room 33

Educational objective:

To review the history of radionuclide brain imaging techniques for the detection of blood-brain-barrier abnormalities, brain blood flow and cerebral metabolism and receptor distribution with SPECT and PET, with special attention to the chemical development, in vitro and in vivo testing and preliminary clinical experience with the new I-123 and Tc-99m labeled agents for rCBF including HM-PAO.

Topics:

1. Early radionuclide brain imaging techniques, Xe-133 for detection of BBB abnormalities, the need for rCBF measurements, and the use of I-123 IMP.
2. Development and testing of HM-PAO.
3. Current and potential clinical utility of rCBF measurement, receptor binding, and metabolic radionuclide studies.

Summary:

This session will summarize the history of nuclear medicine, brain scanning techniques, namely Xe-133 washout technique for detection of blood-brain-barrier abnormalities and the new techniques to measure brain function through evaluation

of blood flow, cerebral metabolism, and receptor distribution using PET and SPECT. Special attention will be paid to I-123 and Tc-99m labeled agents for rCBF measurements. The chemical development, in vivo and in vitro evaluation of preliminary clinical experience with HM-PAO will be described. The potential applicability of these agents will be discussed.

Moderator: R.D. Neirinckx, PhD

Faculty:

Neils Lassen, MD, Bisbebjerg Hospitalet, Copenhagen, Denmark; R.D. Neirinckx, PhD, Amersham, Buckinghamshire, England; Peter Ell, MD, Middlesex Hospital, London, England.

Moderator: A. Everette James, Jr., J.D., M.D.

Faculty:

A. Everette James, Jr., J.D., M.D., Vanderbilt University, Nashville, TN; Otha Linton, M.S., American College of Radiology, Reston, VA; Terry Calvani, J.D., Federal Trade Commission, Washington, DC; Seymour Perry, M.D., Georgetown Institute for Health Care Policy, Washington, DC; Caroline Davis, M.D., Health Care Financing Administration (HCFA), Washington, DC

PRESENTATION OF AWARDS, SNM BUSINESS MEETING AND WINE & CHEESE RECEPTION

5:00-6:00

Room 40

Presentation of Awards by Leonard M. Freeman, M.D., Chairman, Awards Committee and Walter Wolf, Ph.D., President, Education and Research Foundation.

COMPUTERS FOR THE COMPUTER-SHY WORKSHOP

6:00

Location to be announced

(Buses leave from front entrance of the Convention Center after the SNM Business Meeting.)

Purpose:

To educate the computer novice in some basic aspects of computer usage and how to use some practical nuclear medicine programs.

Presented by:

The SNM Computer Council and Barbara Y. Croft, Ph.D. (Limited audience, register early on registration form.)

MONDAY

CONSIDERATION OF IMAGING MODALITIES TO EVALUATE MYOCARDIAL ISCHEMIA DURING STRESS: THE POTENTIAL IMPACT OF EXERCISE ECHOCARDIOGRAPHY

8:30-10:00

Room 40

Educational objective:

We seek simply to familiarize the nuclear physician with the growing body of work supporting the advantages of the

application of echo-Doppler methods for the identification and quantitation of stress-induced myocardial ischemia. These methods will be described and their capabilities noted. Scintigraphic methods will be briefly summarized and a comparison drawn between echocardiographic and scintigraphic methods. The relative clinical utility and specific applications of each technique will be considered.

Topics:

1. Stress echocardiography and Doppler methods
2. Scintigraphic methods for the evaluation of stress-induced myocardial ischemia
3. A comparison of echocardiographic and scintigraphic methods and a consideration of their relative clinical benefits

Summary:

We seek here to familiarize the audience with the current and potential advantages, as well as disadvantages, of stress echocardiography and Doppler techniques for the evaluation of stress-induced myocardial ischemia. A comparison will be made with other imaging modalities currently employed for this purpose and the relative clinical advantages will be discussed. The specific benefits of application of individual modalities to specific patient subgroups will be considered, and the potential interaction of modalities sought. Finally, issues of cost-effectiveness, diagnostic accuracy and overall clinical utility will be considered as speculation and is given to the developing and future role, as well as the breadth of clinical application, for each modality.

Moderator: Elias H. Botvinick, M.D.

Faculty:

William F. Armstrong, M.D., Indiana University, Indianapolis, IN; Miguel Quinones, M.D., Baylor University, Houston, TX; Alan Rozanski, M.D., Cedars-Sinai Medical Center, Los Angeles, CA

Panelist:

Robert Jones, M.D., Duke University, Durham, NC

An evaluation of noninvasive modalities for the assessment of myocardial ischemia during dynamic stress

MONOCLONAL ANTIBODIES IN THE MANAGEMENT OF THE CANCER PATIENT

8:30-10:00

Room 39

Educational objective:

At the completion of the session the attendee should be able to outline the major characteristics of antibody structure and function, define the steps involved in the antigen-antibody reaction and list the major areas of antibody imaging as applied to patient evaluation.

Topics:

1. Introduction to immunology—basic concepts
2. Clinical imaging with monoclonal antibodies
3. Appropriate radiolabels
4. Routes of administration

Summary:

This session is directed to the clinician and technologist interested in expanding their knowledge of immunology and the application of antibodies to patient evaluation. An in-depth

presentation at the introductory level will cover basic concepts of immunology, fundamentals of nomenclature, antibody-antigen reactions and a look at future uses. The session will also include a review of monoclonal imaging applications emphasizing clinical results as function of radiolabel, routes of administration, injected doses, and antibody specificity.

Moderator: William D. Kaplan, M.D.

Faculty:

Jeffrey Schlom, Ph.D., National Institutes of Health, Bethesda, MD; Ronald D. Neumann, M.D., National Institutes of Health, Bethesda, MD; William D. Kaplan, M.D., Dana Farber Cancer Institute, Boston, MA

ACCEPTANCE TESTING AND QUALITY CONTROL OF CAMERAS (INCLUDING SPECT)

8:30-10:00

Educational objective:

To review the performance parameters of scintillation cameras that are appropriate for routine quality and acceptance testings.

Topics:

1. Acceptance testing
2. Quality control of scintillation cameras
3. Quality control of SPECT systems

Summary:

The performance characteristics of a scintillation camera should be checked upon receipt and periodically thereafter to ensure appropriate performance. The acceptance testing criteria are generally more extensive than those for routine quality control. Quality control on cameras that are used for SPECT imaging include all of those appropriate for planar imaging in addition to those that are unique to SPECT data acquisition. Recommendations for acceptance and QC testing will be presented.

MODERATOR: Paul Murphy, M.D.

Faculty:

L. Stephen Graham, Ph.D., University of California, Los Angeles, CA; Anthony R. Benedetto, Ph.D., University of Texas Medical Branch, Galveston, TX; Jon J. Erickson, Ph.D., Vanderbilt University, Nashville, TN

KINETICS WITH SINGLE PHOTON EMITTING RADIOTRACERS: I

8:30-10:00

Room 31

Educational objective:

To review the kinetic approach to analyzing images using ^{123}I -HIPDM and ^{123}I -IQNB.

Topics:

1. The critical analysis of a "chemical microsphere"—HIPDM
2. The effect of the critical analysis of HIPDM on clinical studies
3. The analysis of IQNB data

Summary:

HIPDM, an iodinated diamine, has been suggested as a

"chemical microsphere" to measure cerebral perfusion. Other investigators have shown that the constant retention of HIPDM is a result of various balancing factors and is not indicative of a pure "chemical microsphere." This information

will be reviewed and the effect of these complications on clinical studies will be addressed.

Recently, an iodinated ligand that binds to the muscarinic cholinergic receptor has been developed. The pharmacokinetics of 3-quinoclidinyl 4-iodobenzilate (IQNB) will be discussed and estimates made of the binding parameters. These two single photon-emitting radiotracers, one for the measurement of flow (HIPDM) and one for the measurement of a biochemical reaction (IQNB) can both be used with SPECT.

Moderator: William C. Eckelman, Ph.D.

Faculty:

Giovanni Luciquani, M.D., Ospedale S. Raffaele, Milano, Italy; B. Leonard Holman, M.D., Brigham and Women's Hospital, Boston, MA; Ronald Blasberg, M.D., National Institutes of Health, Bethesda, MD

PEDIATRIC NUCLEAR MEDICINE UPDATE

10:30-12:00

Room 33

Educational objective:

Update on pediatric nuclear medicine techniques, urinary tract and skeletal scintigraphy.

Topics:

1. Techniques in pediatric nuclear medicine
2. Urinary tract updates
3. Skeletal scintigraphy update

Summary:

Pediatric nuclear medicine techniques differ in many aspects from adult routine techniques. Not only immobilization of the patient and resolution play a vital role in obtaining meaningful results but the spectrum of diseases and many protocols are different. The nuclear medicine physician has to be familiar with the techniques and the interpretation of the results.

Renal scintigraphy provides regional functional information with sufficient resolution to achieve specific diagnosis. The use of multiple radiopharmaceuticals, pharmacologic interventions and quantitation amplifies the usefulness of renal scintigraphy in pediatrics. The function and pathology of the ureters is studied during renal scintigraphy and by retrograde methods. Factors such as pressure and volume, which influence the function and pathology of ureters and bladder may be monitored with nuclear medicine techniques.

Bone scintigraphy remains a useful imaging approach for the study of the pediatric patient with musculoskeletal problems. New modalities influence the spectrum and the specific indications of bone scintigraphy. Quantitation techniques, the three phase approach and high resolution skeletal scintigraphy help in making the specific diagnosis of diseases and in studying the normal and abnormal functional characteristics of the growing skeleton.

Moderator: George Sfakianakis, M.D.

Faculty:

James J. Conway, Children's Memorial Hospital, Chicago, IL; George N. Sfakianakis, M.D., University of Miami, Miami, FL; Howard T. Harcke, M.D., Alfred I. DuPont Institute, Wilmington, DE

Note: The Pediatric Nuclear Medicine Club will convene immediately following this session. Room 33, 12:00-1:30.

IMPACT OF GRADUATE MEDICAL EDUCATION FUNDING CHANGES AND PRIMARY BOARD STATUS ON NUCLEAR

MEDICINE RESIDENCY TRAINING PROGRAMS

(sponsored by the SNM Academic Council and the American Association of Nuclear Medicine Program Directors)

12:00-1:30

Room 27

IN VIVO APPLICATIONS OF MULTINUCLEAR NMR SPECTROSCOPY AND IMAGING

1:30-3:00

Room 32

Educational objective:

To inform the participants of the basic principles of MR spectroscopy. The objective of this session will be to evaluate the *in vivo* applications of nuclei other than hydrogen in their application to diagnosis of disease states. Specific attention will be applied to the advantages and limitations of MR spectroscopy when applied to the diagnosis and management of disease states.

Topics:

1. Basic principles of MR spectroscopy
2. P-31 spectroscopy as a monitor of tissue metabolism
3. Imaging and spectroscopy of nuclei other than hydrogen—their potential applications and limitations

Summary:

Nuclear magnetic resonance has shown strong potential as an imaging modality for the basic screening of patients. The basic principles upon which NMR is based are rooted deeply in chemistry. The use of NMR techniques for spectroscopic evaluations have recently been applied in the *in vivo* diagnosis of disease states and monitoring of therapy. Phosphorus-31 spectroscopy provides a sensitive, direct look at the metabolic processes at the cellular level. The potential for characterizing disease, monitoring ischemia, and therapy will be discussed. Other nuclei exhibit NMR characteristics which allow potential uses for spectroscopy and imaging. These nuclei include sodium and fluorine characterization of disease states, however, each has its specific limitations.

Moderator: Robert J. Herfkens, M.D.

Faculty:

Tom Perkins, Ph.D., General Electric Co., Milwaukee, WI; Robert J. Herfkens, M.D., Duke University, Durham, NC

TUESDAY

STRATEGIES FOR A SUCCESSFUL NUCLEAR MEDICINE PRACTICE: VIEWPOINT OF CLINICAL PRACTICE

3:30-5:00

Room 40

Educational objective:

Provide information to the practitioner with regard to organizing an office, its financial structure and marketing approaches to allow for a successful practice.

Topics:

1. How to be a successful nuclear medicine physician
2. How to develop a nuclear medicine product
3. Organization of practice finances

Summary:

In order to be a successful nuclear medicine consultant, certain factors must be included as follows: 1) Provide imaging excellence. 2) Be available. 3) Be courteous. 4) Be visible. 5) Give prompt service. 6) Be relevant in your reports. 7) Provide personal contact. 8) Practice cost and price containment. 9) Provide diagnostic accuracy.

Nuclear medicine services should be regarded as a product. Consideration will be given to the development of a quality product, the establishment of the clinical value of that product, and the integration of that product into clinical practice. Such factors as quality control, quality assurance, the nuclear medicine physician as a consultant and an imaging specialist, the non-imaging nuclear medicine services, and the involvement and education of the referring physician will be reviewed. Lastly, certain elements of financial management of the nuclear medicine office will be presented.

Moderator: Howard J. Dworkin, M.D.

Faculty:

Philip Matin, M.D., Sierra Nuclear Medicine Group, Roseville, CA; Lawrence E. Holder, M.D.; Donald L. Holmquest, M.D., Houston, TX

NEW CARDIOVASCULAR TRACERS AND TECHNIQUES ON THE HORIZON

8:30–10:00

Room 29

Educational objective:

To update status of new radiopharmaceuticals suitable for cardiac imaging.

Topics:

1. Clot imaging (antifibrin, anti-platelet antibody)
2. Myocardial damage (antimyosin)
3. Myocardial perfusion (Tc-99m isonitriles)
4. Fatty acids
5. Cardiac SPECT

Summary:

This course is designed to update the current status of new radiopharmaceuticals suitable for cardiac imaging. The emphasis will be on assessment of:

1. Intravascular thrombosis with monoclonal antibodies,
2. Myocardial damage in myocardial infarction, cardiac transplantation, and inflammatory myocarditis with monoclonal antibodies,
3. Myocardial perfusion with technetium-99m isonitrile analogs,
4. Myocardial metabolism with single photon emitting labeled fatty acids.

The goals of this course will be to define the clinical utility of these agents and the feasibility of new clinical applications. Cardiac single photon emission computed tomography, with these agents as well as with more conventional agents such as thallium-201, will also be addressed.

Moderator: Harvey J. Berger, M.D.

Faculty:

Harvey J. Berger, M.D., Centocor, Inc., Malvern, PA; H.

William Strauss, M.D., Massachusetts General Hospital, Boston, MA; John McAfee, M.D., Update Medical Center, Syracuse, NY; B. Leonard Holman, M.D., Brigham and Women's Hospital, Boston, MA

BONE DENSITOMETRY INSTRUMENTATION

8:30–10:00

Room 38

Educational objective:

To summarize the physical principles of bone mineral quantification by photon absorptiometry and to review the available instrumentation with regard to clinical efficacy.

Topics:

1. Summary of absorptiometry modalities
2. Principles of absorptiometry
3. Comparison of instrumentation
4. Discussion of requisite instrumentation specifications with regard to clinical applications

Summary:

Bone mineral density may be measured by planar imaging instruments utilizing either single photon absorptiometry (SPA) or dual photon absorptiometry (DPA) and by CT scanners equipped with appropriate reference standards. SPA is generally applied to appendicular bone sites having minimal interposed soft tissue whereas DPA provides direct access to sites such as the lumbar spine and the proximal femur. The various modalities differ in their inherent precision (reproducibility), accuracy, radiation exposure, and cost. These and other factors, which are reviewed in depth in this session, are particularly relevant to the needs of screening and therapy monitoring and in the selection of appropriate instrumentation.

Moderator: Stuart G. Mirell, Ph.D.

Faculty:

Stuart G. Mirell, Ph.D., Nuclear Medicine Service/UCLA School of Medicine, Los Angeles, CA; Richard B. Mazess, Ph.D., Lunar Radiation Corporation and University of Wisconsin, Madison, WI; William L. Dunn, M.S., Mayo Clinic, Rochester, MN; Heinz W. Wahner, M.D., Mayo Clinic, Rochester, MN

SIMULTANEOUS IMAGING MEASUREMENTS OF BLOOD FLOW AND RECEPTOR CONCENTRATION

8:30–10:00

Room 31

Educational objective:

To demonstrate the potential of receptor radioligands for simultaneously measuring flow and receptor concentration. To emphasize the importance of separating flow and biochemical effects when analyzing receptor-based images.

Topics:

1. Goals for kinetic models of receptor-based tracers
2. Models need to account for known molecular biopsy
3. Simultaneous measurements of flow & receptor concentration are useful in the clinic
4. New biochemical radiopharmaceuticals require new models that describe dynamic bimolecular processes

Summary:

Radiopharmaceutical design has graduated to a new level of sophistication in exploiting biochemical mechanisms for localization. These new tracers need kinetic models that derive maximum information from their imaging pharmacokinetics. The presentations in this session will demonstrate the potential of receptor radioligands for simultaneously measuring blood flow and receptor concentration. This emphasizes the importance of separating flow and binding effects when analyzing receptor-based images. Particular attention will be given to understanding the reaction volume for ligand-receptor interactions, which are inherently biomolecular, and to appropriate methods for analyzing and minimizing errors in parameter estimates.

Our experience with pharmacokinetic measurements of Tc-galactosyl neoglycoalbumin (TcNGA) binding to its receptor will be used to demonstrate the practical application of the principles of receptor kinetic analysis. TcNGA has been used to simultaneously measure flow and receptor concentration and these measurements have been independently validated. The clinical measurement of both flow and receptor concentration provide a quantitative prognostic index; receptor concentration correlates with a standard measure of parenchymal mass. The discussion will focus on the extension of these principles of kinetic analysis to other receptor-based radiopharmaceuticals

Moderator: Kenneth A. Krohn, Ph.D.

Faculty:

David R. Vera, Ph.D., University of California Davis, Sacramento, CA; Robert C. Stadalnik, M.D., University of California, Davis, Sacramento, CA; Kenneth A. Krohn, Ph.D., University of Washington, Seattle, WA

FEDERAL REGULATORY ASPECTS REGARDING THE USE OF INVESTIGATIONAL RADIOPHARMACEUTICALS

10:30-12:00

Room 40

Summary:

The presentation will inform the participant of the various FDA regulatory differences between labeled monoclonals and labeled drugs. Further, the presentation will include instructions and requirements (including preclinical) regarding IND submissions and studies carried out under the Radioactive Drug Research Committee. Comments from the NRC and a discussion will be included.

Topics:

1. Introduction, overview, timeframes, unapproved uses
2. Requirements regarding INDs (for drugs)
3. Requirements regarding INDs (for antibodies)
4. Preclinical requirements and clinical protocols
5. Studies carried out under the Radioactive Drug Research Committee
6. The NRC's requirements regarding radioactive investigational drugs
7. Panel discussion and questions

Moderator: Neil M. Abel

Faculty:

Neil M. Abel, Robert West, M.S., Samuel K. Ackerman, M.D., Alfred E. Jones, M.D., Norman L. McElroy, Food and Drug Administration, Rockville, MD

PET AND SPECT: WHAT ARE THE THINGS THAT WILL MAKE A DIFFERENCE?

1:30-3:00

Room 40

Educational objective:

To define the rate-limiting steps in producing significant advances in the clinical utility and value of PET and SPECT.

Topics:

1. Design of SPECT and PET systems
2. The effect of new tracers on tomograph design
3. The use of generators vs kits for PET radiopharmaceuticals

Summary:

The course will examine the issues in tomographs and tracers to identify those that will make a real difference in the growth of nuclear medicine. Points of focus will be: 1) Were existing SPECT systems properly designed for SPECT or not? If not, what would optimally designed SPECT systems provide and what would they cost? 2) What tracers and studies, when combined with SPECT, would provide new opportunities? 3) What is the present performance of PET tomographs and will advances make a difference? If so, to what degree and at what cost? 4) Should positron planar imaging systems be developed? 5) What are the technical, practical and cost issues involved in clinical accelerator-based generators and should tracers be prepared by semi-automated module techniques or should accelerators simply produce isotopes with compounds being prepared by commercially supplied kits?

Moderator: Michael E. Phelps, Ph.D.

Faculty:

Michael E. Phelps, Ph.D., University of California, Los Angeles, CA; Ronald Jaszczak, Ph.D., Duke University, Durham, NC; Edward J. Hoffman, Ph.D. University of California, Los Angeles, CA; William C. Eckelman, Ph.D., E.R. Squibb & Son, Inc., New Brunswick, NJ; Maria Straatman, M.A., CTI, Inc., Berkeley, CA

STRATEGIES FOR A SUCCESSFUL NUCLEAR MEDICINE PRACTICE THE CUSTOMER'S PERSPECTIVE

3:30-5:00

Room 38

Educational objective:

To have participants understand and appreciate the needs of the people they serve. By understanding and working to meet these needs, practices will improve and grow.

Topics:

1. What the hospital wants from nuclear medicine
2. What referring physicians want from nuclear medicine

Summary:

Almost every book on contemporary management practice stresses the importance of knowing the customer and his or her needs. This presentation is designed to increase your insight into the real needs of the individuals whose decisions result in the growth or decline in the utilization of nuclear medicine services.

Presentations by the panelists will express their needs and expectations of nuclear medicine. Subjects addressed will include service, clinical support and financial components.

Moderator: Henry L. Ernstthal, CAE, Society of Nuclear Medicine, New York, NY

Faculty: will include a hospital administrator, a physician from a department of medicine, a physician from a department of surgery.

Please Note

The Education and Research Foundation of the Society of Nuclear Medicine Technologist Section has presented an award to Gordon E. Wynant, CNMT for his paper "Experimental and Clinical Validation of a Radio-nuclide Angiographic Method for Assessing Myocardial Dyskenesis."

Mr. Wynant will make a special presentation of the paper on Tuesday, June 24 at 2:30 in Room 13-14.

Moderator: Richard A. Holmes, M.D.

Faculty:

Michael D. Devous, Ph.D., University of Texas, Dallas, TX; David B. Collier, M.D., Milwaukee County Medical Complex, Milwaukee, WI; Richard A. Holmes, M.D., University of Missouri, Columbia, MO; R.D. Neirinckx, Ph.D., Amersham, Buckinghamshire, England

CLINICAL APPLICATIONS OF BONE MINERAL ESTIMATION BY SINGLE AND DUAL PHOTON ABSORPTIOMETRY

8:30-10:00

Room 40

Educational objective:

To provide a sound basis for clinical use of bone mineral measurements to detect bone disease and measure bone response to therapy and disease.

Topics:

1. Peripheral extremity measurements
2. Lumbar spine measurements
3. Hip and femur measurements
4. Epidemiologic inferences
5. Whole body measurements

Summary:

This course is intended to compliment a preceding session on the physical and technical aspects of bone absorptiometry. Succinct discussions of the applications of bone mineral measurement by planar absorptiometry technique will be given by speakers who have long experience with peripheral extremity measurements, lumbar spine measurements, and hip and femur measurements. Site to site correlations will be presented and the bone mineral at each site will be related to osteoporotic fracture prevalence. For the purposes of this discussion, osteoporotic fractures will be defined as fractures occurring in the wrist, spine, hip and ribs with no or limited trauma in individuals who have bone demineralization. Epidemiologic studies offer some insight into the significance of these correlations, the appropriate definition of fracture thresholds, and even the distinction of abnormal from normal. Last, although whole body measurements have not yet enjoyed widespread utilization, early data on the clinical relevance will be discussed with the thought that whole body bone mineral measurements by absorptiometry technique which can be accomplished with one percent precision are as close to a gold standard as can be approached in the study of human biology. Since there is thought to be more need for absorptiometry bone mineral measurement procedures in the U.S. population at any time than there is need for the sum of all scintillation camera studies, it is important that members proceed to rapidly implement and utilize this new technique.

Moderator: Malcolm R. Powell, M.D.

Faculty:

John M. Vogel, M.D., University of California Davis Medical Center, Sacramento, CA; Malcolm R. Powell, M.D., F.A.C.P., Nuclear Medicine Consultants, San Francisco, CA; Eloy E. Schulz, M.D., Loma Linda University Medical Center, Loma Linda, CA; Heinz W. Wahner, M.D., Mayo Clinic, Rochester, MI; J. Chris Gallagher, M.D., Creighton University School of Medicine, Omaha, NE

WEDNESDAY

RADIONUCLIDE FUNCTIONAL BRAIN IMAGING

8:30-10:00

Room 39

Educational objective:

To review the techniques and radiopharmaceuticals used in development for SPECT imaging of the brain and the data it reveals and adds to the diagnosis of several neurologic diseases (e.g., cerebrovascular disease, dementia, psychiatric disease, seizure disorder).

Topics:

1. The method and use of radioxenon tomographic imaging in cerebrovascular accidents (CVA) and neuropsychiatric disorders.
2. Application of iodoamphetamine SPECT imaging in CVA, seizure disorders and dementia
3. Assessment of the new Tc-99m-labeled amine for cerebral blood flow (CBF) imaging in CVA, and other neurologic diseases

Summary:

Radionuclide conventional brain imaging has all but been replaced by x-ray computed tomography (CT) and NMRI but studies employing positron labeled radiopharmaceuticals and PET imaging has served as a catalyst in developing new gamma-emitting radiopharmaceuticals that normally cross the intact BBB and are readily imaged by SPECT. Xenon-133 has long been used to evaluate rCBF but recent tomographic instrumentation has improved its detection accuracy. The redistribution of the iodoamphetamines may be useful in determining the selection of shunt surgery patients with extracranial carotid occlusion and in differing various forms of organic dementia. The new Tc-99m labeled tetraamine hexamethyl-propyleneamine oxime can be used to monitor the course of infarction and compare its functional changes to the anatomical lesions detected on the CT.

KINETICS WITH POSITRON EMITTING RADIOTRACERS

8:30-10:00

Room 38

Educational objective:

An understanding of methods for the kinetic analysis of neuroreceptor binding studies and their application.

Topics:

1. Modeling of kinetic studies
2. Implementation of kinetic studies
3. Results

Summary:

Kinetic modeling of neuroreceptor binding using positron emitting radionuclides will be discussed. Several different methods requiring different assumptions have been proposed for analysis of these positron emission tomographic (PET) data. These different approaches will be presented and compared. The potential advantages and disadvantages of the different analysis methods will be addressed. Results of studies with these methods in humans will be demonstrated.

Moderator: Martin Reivich, M.D.

Faculty:

Henry Wagner, M.D., Johns Hopkins University, Baltimore,

MD; Joel S. Perlmutter, M.D., Washington University, St. Louis, MO

NUCLEAR MEDICINE MILESTONES

10:30-12:00

Room 13

The Historian of The Society of Nuclear Medicine will present a lecture and an interesting collection of historical slides. William G. Myers, Ph.D., M.D., Ohio State University, Columbus, OH

He plans to emphasize the impact of the discovery of radioactivity in Paris, just 90 years ago, and to interrelate it with the discussion of a dozen and a half Nobel Laureates on the emergence of nuclear medicine.

SCIENTIFIC MEETING HIGHLIGHTS

3:00-4:30

Room 40

For the ninth consecutive year, Henry N. Wagner, Jr., M.D., of the Johns Hopkins Medical Institutions, will present his views of papers at the Annual meeting. As in the past, he will relate current advances to previous work and future directions of the field of nuclear medicine.

Scientific Exhibits

All Scientific Exhibits to be presented at the 33rd Annual Meeting of the Society are listed by the title and author. Exhibits will be on display in the Washington Convention Center in Washington, D.C. For full abstracts, exhibit numbers and locations, and times for viewing, please consult the *Show Directory*, which will be distributed on site.

BONE JOINT

Posterboard No. 733

INTERNAL DERANGEMENT OF THE TEMPOROMANDIBULAR JOINT: CLINICAL IMPORTANCE AND DIAGNOSTIC EVALUATION. J. Diaz, C. Nagle, S. Noujaim, and W. Cheslin. William Beaumont Hospital. Troy, MI.

Viewbox No. 734

OPTIMIZATION OF MR IMAGING OF THE KNEE JOINT. M. Mesgarzadeh, C.D. Schneck, A. Bonakdarpour, A.H. Maurer, L.S. Maimud. Temple University Hospital, Philadelphia, PA.

Viewbox No. 735

ANATOMY OF THE WRIST AND CARPAL TUNNEL SHOWN BY MRI. M. Mesgarzadeh, C.D. Schneck, A. Bonakdarpour, A.H. Maurer, L.S. Maimud. Temple University Hospital, Philadelphia, PA.

Posterboard No. 736

GASTRIC ACTIVITY ON Tc-99m OXIDRONATE BONE SCANS CAN BE CAUSED BY ISOPROPYL ALCOHOL. E.M. Peterson, J.W. Ryan, and W.B. Martin. University of Chicago, Chicago, IL.

Posterboard No. 737

SCINTIGRAPHIC EVOLUTION OF TOTAL KNEE REPLACEMENTS (TKR). A. Ramos-Gabatin, J. Orzel, W. Montgomery, Wilford Hall USAF Medical Center, San Antonio, TX.

Viewbox No. 738

SKELETAL TUMORS AND INFECTIONS: A COMPARISON BETWEEN MRI AND OTHER MODALITIES. S. Rindsberg, M. Mesgarzadeh, A. Bonakdarpour, A.H. Maurer, L.S. Maimud. Temple University Hospital, Philadelphia, PA.

Viewbox No. 739

GALLIUM UPTAKE IN MYOSITIS OSSIFICANS: POTENTIAL PITFALLS IN DIAGNOSIS. L. Salzman, V.W. Lee, and P. Grant. Lahey Clinic Medical Center, Burlington, MA and Boston City Hospital, Boston, MA.

Viewbox No. 740

OS CALCIS BONE MINERAL MEASUREMENTS: AN EVALUATION OF THEIR CLINICAL UTILITY. J.M. Vogel, P.D. Ross, and R.D. Wasnich. Kuakini Medical Center, John A. Burns School of Medicine, Honolulu, HI and U.C. Davis, Sacramento, CA.

Posterboard No. 741

SKELETAL PHOTOPENIC LESIONS IN IN-111 LABELED LEUKOCYTE IMAGING OF PAGET'S DISEASE. William T. C. Yuh, Joan M. Hartnell, Theodore J. Hahn, William H. Bland. West Los Angeles V. A. Medical Center, Wadsworth Division, Los Angeles, CA.

CARDIOVASCULAR

Booth No. 742

RUBIDIUM-82 AND PET FOR EVALUATION AND MEASUREMENT OF REGIONAL MYOCARDIAL BLOOD FLOW AND NONINVASIVE DETECTION OF CORONARY ARTERY DISEASE. M. Grover-McKay, E.J. Hoffman, S.C. Huang, M.E. Phelps, H.R. Schelbert, UCLA School of Medicine, Los Angeles, CA.

Posterboard No. 743

FIVE-SEGMENT DISPLAY FORMAT FOR MYOCARDIAL THALLIUM SPECT ANALYSIS. A. Hamid I. Hakki, Robert G. Carroll, Pamela J. Goldner, Carroll A. Johnson and Steven J. Harwood. University of South Florida, VAMC at Bay Pines, FL.

Posterboard No. 744

A NEW METHOD FOR "INFARCT MAP". K. Imai, S. Yumikura, T. Ando, S. Saito, Y. Ozawa, M. Hatano, T. Takemoto, H. Abe, R. Kamata. Nihon University, Tokyo, Japan

Posterboard No. 745

SINGLE PHOTON EMISSION COMPUTERIZED TOMOGRAPHY WITH THALLIUM-201 DURING EXERCISE IN THE DIAGNOSIS OF CORONARY ARTERY DISEASE: COMPARISON WITH QUANTITATIVE PLANAR IMAGING. J.J. Mahmarian, A. Jain, R. Roberts, and M.S. Verani. Baylor College of Medicine, Houston, TX.

Viewbox No. 746

CARDIAC REJECTION MONITORED BY RADIOISOTOPE BIVENTRICULAR EJECTION FRACTIONS AND WALL MOTION STUDIES. N.L. Martin, D.F. Preston, R.G. Robinson, and M.P. Huntrakoon. The University of Kansas College of Health Sciences and Hospital, Kansas City, KS.

Booth No. 747

TISSUE MANGANESE LEVEL AS AN INDICATOR OF BIOCHEMICAL DERANGEMENT OF METABOLISM IN MYOCARDIAL ISCHEMIA AND INFARCTION. M.A. Quaife, R.A. Quaife, J.W. Dirksen, R.S. Markin, S.C. Augustine, R.A. Stratbucker. Univ. Nebraska Medical Center, Omaha, NE.

COMPUTER AND DATA ANALYSIS

Booth No. 748

A MATHEMATICAL LIVER PHANTOM AND ITS APPLICATION TO SYSTEM EVALUATION. E. B. Cargill, R. D. Fiete, H. H. Barrett, W. E. Smith, A. V. Clough. University of Arizona, Optical Sciences Center, and University Medical Center, Tucson, AZ.

Posterboard No. 749

A MICROCOMPUTER IMAGE ANALYSIS SYSTEM: DEVELOPMENT AND APPLICATION TO QUANTITATIVE AUTORADIOGRAPHY. T.J. Hoffman, W.A. Volkert, and R.A. Holmes. Research Service—Harry S. Truman Memorial Veterans Hospital and Nuclear Medicine—University of Missouri, Columbia, MO.

Booth No. 750

ORGAN PERFUSION MAPS OF BRAIN AND HEART DISPLAYED AS THREE-DIMENSIONAL SHADED SURFACE MAPS FROM SPECT IMAGES. S.P. Mueller, D.J. Nowak, K.A. Johnson, R.J. English, B.L. Holman. Harvard Medical School, Boston, MA and General Electric Medical Systems, Milwaukee, WI.

Posterboard No. 751

OPTIMIZED DISPLAY FOR EVALUATION OF PLANAR EXERCISE TL-201 WASHOUT AND REDISTRIBUTION. D.G. Pavel, E. Olea, G. Kondos, P. Briandet, M. Goris. Univ. of Illinois Hospital, Chicago, IL and Stanford Univ. Hosp., Stanford CA.

Viewbox No. 752

LONG-TERM DIGITAL ARCHIVING REQUIREMENTS AND THROUGH-PUT ANALYSIS FOR A NUCLEAR MEDICINE FACILITY. D.F. Preston, S.J. Dwyer, III, L.T. Cook, A.V. Wegst, N.L. Martin, R.G. Robinson. University of Kansas Medical Center, Kansas City, KS.

DOSIMETRY/RADIOBIOLOGY

Posterboard No. 753

RADIATION DOSIMETRY OF Sm-153-EDTMP IN HUMANS. K.W. Logan, W.A. Volkert, R.A. Holmes, University of Missouri, and H. S. Truman Memorial Veterans Hospital, Columbia, MO.

ENDOCRINE

Posterboard No. 754

ASSESSMENT OF THYROID MASS FROM SCINTIGRAPHIC THYROIDAL DIMENSIONS. R.E. Choi, R.P. duCret, S. Roe, H.M. Park. Indiana University, Indianapolis, IN.

Posterboard No. 755

THYROID ABNORMALITIES DETECTED IN PATIENTS WITH PARATHYROID DISEASE: HISTOPATHOLOGICAL CORRELATION WITH DUAL ISOTOPIC PARATHYROID STUDIES. S. Lottenberg, R.C. Brunken, M.E. Phelps, R.A. Hawkins, K.H. Anders, R.K.J. Brown. UCLA School of Medicine, Los Angeles, CA.

GASTROENTEROLOGY

Posterboard No. 756

Tc-99m-RBC BLEEDING SCANS IN NOMRAL SUBJECTS: CONFUSION WITH GI BLEEDING SITES. C.M. Boyd, M.R. Williamson, S. Balachandran, T.L. Angtuaco, H.R. Shah, and S. Tucker. University of Arkansas for Medical Sciences and Veteran's Administration Medical Center, Little Rock, AR.

Viewbox No. 757

SCINTIGRAPHIC SIGNS AND PITFALLS IN LOWER GASTROINTESTINAL HEMORRHAGE: THE CONTINUED NECESSITY OF ANGIOGRAPHY. G.S. Dorfman, J.J. Cronan, and K.M. Staudinger. Rhode Island Hospital, Providence, RI.

Booth No. 758

NUCLEAR HEPATOLOGY. S. Krishnamurthy, F.E. Turner, G.T. Krishnamurthy. VA Medical Center and Oregon Health Sciences University, Portland, OR.

Posterboard No. 759

HEPATOMA: EVALUATION BY MULTI-TRACER SCINTIGRAPHY, COMPUTED TOMOGRAPHY AND SONOGRAPHY. V.W. Lee, E. Kuligowska, B. Leiter, T.T. Peng, and L. Zollars. Boston City Hospital, Boston, MA.

Posterboard No. 760

SCINTIGRAPHIC EVALUATION OF AMYLOIDOSIS. V.W. Lee, L. Salzman, T.T. Peng, M. Skinner, and A.S. Cohen. Boston City Hospital, Boston, MA.

IMMUNOLOGY

Viewbox No. 761

IMAGING OF FRESH VENOUS THROMBI IN THE DOG WITH I-131 AND IN-111 LABELED MONOCLONAL ANTIBODY AND ANTIBODY FRAGMENTS. Z.D. Grossman, S.F. Rosebrough, J.G. McAfee, G. Subramanian, C.A. Ritter-Hrncinc, L.S. Witanowski, G. Tillapaugh-Fay, and E. Urrutia. SUNY Health Science Center, Syracuse, NY.

INFECTIOUS DISEASE

Posterboard No. 762

CLINICAL UTILITY OF INDIUM LABELED WHITE BLOOD CELL SCANNING IN PROSTHETIC GRAFT INFECTIONS. M.R. Williamson, C.M. Boyd, T.L. Angtuaco, S. Balachandran, and H.R. Shah. University of Arkansas for Medical Sciences and Veterans Administration Medical Center, Little Rock, AR.

INSTRUMENTATION

Posterboard No. 763

EFFECT OF RADIATION SOURCE STRENGTH ON DUAL PHOTON ABSORPTIOMETRY (DPA) MEASUREMENTS. W.L. Dunn, H.W. Wahner. Mayo Clinic/Foundation, Rochester, MN.

Viewbox No. 764

FACTORS INFLUENCING THE ACCURACY OF

TL-201 SPECT IMAGING. R.L. Eisner, W.A. Fajman, T. Noever, D. Nowak, A. Churchwell, J. Oates, R.I. Pettigrew, D. Dunn, K. Cloning, R.E. Patterson. Dpts of Radiology-EU and Medicine-Carlyle Fraser Heart Ctr/Crawford W. Long Hsp. of Emory Univ., Atlanta, GA; G.E. Medical Sys. Grp., Milwaukee, WI.

Posterboard No. 765

ASPECT: A THREE-DIMENSIONAL SINGLE-CRYSTAL ANNULAR SPECT BRAIN CAMERA WITH A HIGH EFFICIENCY ROTATING MULTIFIELD COLLIMATOR. S. Genna, A.P. Smith. Digital Scintigraphics, Inc., Belmont, MA.

Posterboard No. 766

A DUAL-DETECTOR PROBE FOR SURGICAL TUMOR STAGING. T.S. Hickemell, H.B. Barber, H.H. Barrett, J.M. Woolfenden. University of Arizona, Tucson, AZ.

Posterboard No. 767

COMPARISON OF XE-PRODUCED AND TE-PRODUCED I-123: EFFECT ON MTF OVER TIME. A.G. Howell, A.V. Wegst, D.F. Preston, R.G. Robinson, J.A. Spicer. University of Kansas Medical Center, Kansas City, KS.

Posterboard No. 768

MUMPI BRAIN IMAGING SYSTEM: PERFORMANCE SPECIFICATIONS. K.W. Logan, R.A. Holmes, W.D. McFarland. University of Missouri, and Harry S. Truman Memorial Veterans Hospital, Columbia, MO.

Viewboxes No. 769-770

TECHNIQUES, PITFALLS, AND ARTIFACTS IN MAGNETIC RESONANCE IMAGING. J.A. Patton, M.V. Kulkarni, O.H. Wolfe, J.K. Craig, R.R. Price, C.L. Partain, and A.E. James, Jr.

Viewbox No. 771

OPTIMIZATION OF SPECT IMAGING FOR GALLIUM-67 STUDIES. D.F. Preston, A.V. Wegst, N.L. Martin and D. Ryan. University of Kansas Medical Center, Kansas City, KS.

Booth No. 772

A MODULAR DETECTOR SYSTEM FOR SPECT. W.L. Rogers, N.H. Clinthorne L. Shao, K.F. Koraf. Division of Nuclear Medicine, University of Michigan Medical Center, Ann Arbor, MI.

Posterboard No. 773

SPECT-ACULAR ARTIFACTS. K. Sorgentoni, M.G. Velchik, and A. Alavi. Hospital of the University of Pennsylvania, Philadelphia, PA.

Posterboard No. 774

SPECT-IMAGING WITH 123-I PRODUCED VIA VARIOUS ROUTES. F.H. van Weeren, District Hospital Het Nieuwe Spitaal, Warnsveld, Netherlands.

Viewbox No. 775

DESIGN OF SCINTILLATION CAMERA ACCEPTANCE TESTING AND QUALITY CONTROL PROGRAM. D.A. Weber, M. Ivanovic, G.A. Wilson, L. Decker, and R.E. O'Mara. University of Rochester School of Medicine and Dentistry, Rochester, NY.

NEUROLOGY

Booth No. 776

APPLICATION OF HM-PAO IN ACUTE HEAD INJURY (AHI) AND COMPARISON WITH X-RAY

COMPUTERISED TOMOGRAPHY (CT). H.M. Abdel-Dayem, S. Sadek, K. Kouris, R. Bahar, E. Higazi, S. Ericksson, S. Englesson, L. Bermtmas, G. Sigurdsson, M. Foad and H. Olivecrona. Depts. of Nucl. Med. Surgery and Radiology, Fac. of Medicine, Kuwait Univ. & Mubarak Al-Kabeer Hospital, Kuwait.

Posterboard No. 777

CLINICAL PHARMACOKINETICS AND APPLICATION OF Tc-99m-d,1-HM-PAO. R.A. Holmes, K.W. Logan, W.A. Volkert, A. Singh. Nuclear Medicine, University of Missouri and Harry S. Truman Memorial Veterans Hospital, Columbia, MO.

Posterboard No. 778

POSITRON EMISSION TOMOGRAPHY AND FRONTAL CORTEX ACTIVATION IN PSYCHIATRIC PATIENTS AND NORMAL SUBJECTS. J.T. Metz, H.Y. Meltzer, N.J. Yasillo, C.J. Ortega, C.T. Chen and M.D. Cooper, The University of Chicago and Illinois State Psychiatric Institute, Chicago, IL.

Posterboard No. 779

THE DETERMINATION OF DEATH AND THE CHANGING ROLE OF MEDICAL IMAGING. S.J. Morayati and C.E. Nagel. William Beaumont Hospitals, Royal Oak and Troy, MI.

Posterboard No. 780

THE EFFECT OF EXTERNAL STIMULI ON THE DISTRIBUTION OF Tc99m-HM-PAO IN THE BRAINS OF NORMAL SUBJECTS. B. Murby, S. Edwards, J. Gregg, C.R. Lazarus and M.N. Maisey, Depts. of Clinical Physics and Nuclear Medicine, Guy's Hospital, London SE1 9RT

Posterboard No. 781

PERFUSAMINE™ BRAIN SCANNING IN STROKE—A COMPARISON WITH TRANSMISSION CT. Chan H. Park, Mark Madsen, Toni McLellan and Robert Schwartzman. Thomas Jefferson University Hospital, Philadelphia, PA.

Posterboard No. 782

GLUCOSE METABOLIC ALTERATIONS IN STURGE-WEBER SYNDROME. M.E. Phelps, H.T. Chugani and J.C. Mazziotta. UCLA School of Medicine, Los Angeles, CA.

Posterboard No. 783

RELATIVE CEREBRAL GLUCOSE METABOLIC PATTERNS DURING PERFORMANCE OF A VISUAL MONITORING TASK. N. Wagner, J. Levy, M.P. Grattan, M. Edelman, C.T. Chen and M. Cooper. The University of Chicago, Chicago, IL.

ONCOLOGY

Posterboard No. 784

IMPROVED TUMOR SPECIFICITY OF MONOCLONAL RADIOIMMUNOIMAGING USING DUAL PARAMETER COLOR FUNCTIONAL MAPS. B.L. Engelstad, E.C. Ramos, J. Stoudemire, J.W. O'Connell, J. Villaneuva, D.B. Faulkner, R.S. Hattner, L.E. Spitzer, and P. Scannon. Nuclear Medicine Section, Department of Radiology, University of California, San Francisco, CA and XOMA Corporation, Berkeley, CA.

Viewbox No. 785

IMPACT OF LYMPHOSCINTIGRAPHY IN PATIENTS WITH STAGE I MALIGNANT

MELANOMA. E.L. Kramer, A. Postel, J. Sanger, F. Golomb. Bellevue Hospital/NYU Medical Center, NY, NY.

Posterboard No. 786

RESPONSE TO STEREOTACTIC TREATMENT OF 14 PATIENTS WITH BRAIN TUMORS WITH Na Cr PO-4—P-32. V.C. Taasan, J.A. Taren, W.H. Beierwaltes, P. McKeever, T.W. Hood, B. Shapiro, R.C. Wahl, C. Dmuchowski, R. Rabbani. University of Michigan Hospitals, Ann Arbor, MI.

PEDIATRICS

Booth No. 787

PLANAR AND SPECT IMAGING OF NEUROFIBROMATOSIS WITH TECHNETIUM-99m DIETHYLENE TRIAMINE PENTAACETIC ACID. G.A. Mandell, H.T. Harkke, C.A. Sharkey, K.M. Brooks, G.D. MacEwen. A.I. duPont Institute, Wilmington, DE.

Posterboard No. 789

NUCLEAR MEDICINE IMAGING OF CO-JOINED TWINS STUDIED AT THE HOSPITAL FOR SICK CHILDREN, TORONTO, CANADA. R. Puntillo, D.L. Gilday, M. Green, J. Ash

Viewbox No. 790

AN APPROACH TO INFECTIONS OF THE EXTREMITIES IN CHILDREN (OSTEOMYELITIS OR NOT?). L.E. Swischuk, C.K. Hayden, Jr., H.D. Fawcett, University of Texas Medical Branch, Galveston, TX.

PULMONARY

Posterboard No. 791

RENAL SCINTIGRAPHY ROLE IN THE DIAGNOSIS AND MANAGEMENT OF COMPLICATIONS OF PERCUTANEOUS NEPHROLITHOTOMY: BASED ON THE EXPERIENCE OF 529 CASES. G.W. Moskowitz, R.G. Schiff, W.J. Lee, L.M. Levy and A.D. Smith. Long Island Jewish-Hillside Medical Center, New Hyde Park, NY 11042.

Posterboard No. 792

THE COMPLEMENTARY ROLES OF

RADIONUCLIDE SPECT LUNG PERFUSION AND CT OF THE CHEST. G.W. Moskowitz, J.C. Vaugeois, R.G. Schiff, and L.M. Levy. Long Island Jewish-Hillside Medical Center, New Hyde Park, NY 11042

RADIATION SAFETY

Posterboard No. 793

A GUIDE TO BETTER NRC INSPECTIONS. R.E. Burgin and C.C. Casey. United States Nuclear Regulatory Commission, Glen Ellyn, IL.

RADIOPHARMACEUTICAL CHEMISTRY

Posterboard No. 794

A NEW GENERATOR FOR THE PRODUCTION OF PB-212 AND ITS ALPHA-EMITTING DAUGHTERS. R. Atcher, A. Friedman, J. Hines. National Cancer Institute, Bethesda, MD and Argonne National Laboratory, Argonne, IL.

Posterboard No. 795

VOLATILITY OF THERAPEUTIC I-131 SODIUM IODIDE SOLUTIONS FOR ORAL ADMINISTRATION. J. Clanton, J. Seibert and D. Sneed. Vanderbilt University, Nashville, TN.

Booth No. 796

SM-153-EDTMP: A POTENTIAL THERAPEUTIC BONE AGENT. W.F. Goeckeler, W.A. Volkert, D.E. Troutner, L.A. Corwin, J.C. Lattimer, and J. Simon. University of Missouri-Columbia, Depts. of Chemistry, Radiology and Veterinary Medicine, Columbia, MO and The Dow Chemical Company, Freeport, TX.

Posterboard No. 797

Tc-99m-d,1-HEXAMETHYL PROPYLENE AMINE OXIME (Tc-99m-d,1-HM-PAO) VS. I-125- IODOAMPHETAMINE (I-125-IMP): A DIRECT AUTORADIOGRAPHIC COMPARISON. T.J. Hoffman, E.H. McKenzie D.P. Nowotnik, W.A. Volkert, and R.A. Holmes. Research Service—Harry S. Truman Memorial Veterans Hospital and Nuclear Medicine—University of Missouri, Columbia, MO and Amersham International, UK.

Posterboard No. 798

THE PHARMACOKINETICS OF A NEW NEUTRAL TECHNETIUM HEART AGENT IN ANIMALS AND MAN. A.D. Nunn, J. Matyas, B. Kuczynski, R.K. Narra, W.C. Eckelman. Squibb Institute for Medical Research, New Brunswick, NJ.

Viewbox No. 799

SYNTHESIS AND IN VIVO IMAGING OF ESTROGEN RECEPTORS BY EXTREMELY HIGH SPECIFIC ACTIVITY 16 ALPHA I-123 IODOESTRADIOL-17 BETA. D.F. Preston, J.A. Spicer, R.A. Baranczuk, W.R. Jewell, R.G. Robinson. University of Kansas Medical Center, Kansas City, KS.

Posterboard No. 800

INHIBITION OF PLATELET DEPOSITION BY ASPIRIN (ASA) OR HEPARIN (HEP). K. Ramberg, J. Eldrup-Jorgensen, R. Connolly, W. Mackey, N. Shoenfeld, A.D. Callow, and P.C. Kahn. Tufts-New England Medical Center, Boston, MA.

RENAL/ELECTROLYTE/ HYPERTENSION

Viewbox No. 801

THE SENSITIVITY AND SPECIFICITY OF THE MONOEXPONENTIAL FIRST PASS WASHOUT PARAMETER IN DIFFERENTIATING RENAL TRANSPLANT REJECTION FROM NONREJECTION. D.F. Preston, D.G. Pauls, L. Wetzel, K. Baxter, A.V. Wegst, N.L. Martin, R.G. Robinson. University of Kansas Medical Center, Kansas City, KS.

Viewbox No. 802

THE ROLE OF RENAL SCINTIGRAPHY IN URINARY LEAKS. C.R. Wall, R.E. O'Mara, and G.A. Wilson. University of Rochester Medical Center, Rochester, NY.

Viewbox No. 803

PRINCIPLES AND PITFALLS OF PERITONEAL SCINTIGRAPHY. L.S. Witanowski, E.J. Urrutia, F.D. Thomas, M.P. Bartlett, R. Kopecky and D. Ewing. Department of Radiology, Division of Nuclear Medicine and Department of Medicine, SUNY Health Science Center at Syracuse, NY.